Synthesis and Reactivity Studies of Zirconium and Hafnium Borylimido Compounds

Bowen Xie

MChem, AMRSC

St Edmund Hall



Thesis submitted to the University of Oxford for the degree of Doctor of Philosophy in Inorganic Chemistry, September 2017.

The work described in this Thesis was carried out in the Chemistry Research Laboratory, University of Oxford from October 2014 to September 2017 under the supervision of Professor Philip Mountford. All work is my own unless stated to the contrary, and has not previously been submitted for any degree at this or any other university.



Bowen Xie

September 2017

Abstract

Bowen Xie Trinity 2017
St Edmund Hall D.Phil. Thesis

This Thesis reports the synthesis and reactivity of zirconium and hafnium borylimides. Synthetic routes to such complexes of these two metals and corresponding novel borylamines were targeted. Their reactions with small polar and non-polar compounds were explored.

Chapter One provides a background on Group 4 imido and hydrazido complexes. Group 4 alkoxyimides are also reviewed, as well as the recently developed titanium and scandium borylimides. The Chapter focuses on the synthesis, structure, and stoichiometric and catalytic reactions of these complexes with unsaturated substrates.

Chapter Two describes the synthesis and structures of new zirconium and hafnium borylimides and their reactions with C–H and H–H bonds. The electronic structures of these complexes are analysed by DFT and QTAIM studies.

Chapter Three describes the reactions of Group 4 metallocene borylimides with terminal alkynes. The principal reaction outcomes are [2+2] cycloadditions and C–H bond activations, and attempts to catalyse the hydro-borylamination reaction are also described. Kinetic studies of some reactions are presented, and are supported by DFT, QTAIM and NBO studies.

Chapter Four describes the reactions of $Cp_2Zr\{NB(NAr'CH_2)\}(py)$ with polar compounds, with a particular focus being the reactivity of esters and their analogues with this complex, eliminating and self-trapping ketene. Kinetic studies of some reactions are presented, and are supported by further DFT studies.

Chapter Five presents full experimental procedures and characterising data for the new complexes reported.

CD Appendix contains CIF files for all new crystallographically characterised complexes.

Acknowledgements

First and foremost, I would like to extend my sincere thanks to Prof. Philip Mountford for his support, advice and DFT calculations for this project. Thanks for your patience in our discussions about kinetics (even on the weekend!) – I really do appreciate it. I am very grateful to have worked on this project and to work with you.

Some particular thanks go to Dr Benjamin Clough for this involvement in discussion about my projects and his generous help towards everything! Thanks for tolerating with endless crystal samples of mine for crystallography and running them on weekends! I cannot finish without acknowledging Theresa Scharbert and Ben for proofreading this Thesis. Thanks also to the members of "open-market team": Martin Slusarczyk and Archibald McNeillis, for open discussions about chemistry, and having proper lunches outside. Further thanks to Dr Insun Yu and Ben (again) for their hard work maintaining order in the lab and their kind support for the group, as well as Dr Andrey Protchenko for his "How to grow crystals" tutorials, which enabled me to crystallise everything! I have truly appreciated the other group members, Dr Matt Blake, Dr Laura Stevenson, Dr Richard Collins, Dr Xinning Yin, Dr Simona Mellino, Ross Green, Adan Reyes, Karen Gamero, Nichabha Diteepeng, Natalia Vieira, David Ryan for sharing an enjoyable time in the group.

Thanks also go to Dr Nick Rees for maintenance of the NMR facilities, as well as Dr Amber Thompson and Dr Kirsten Christensen for assistance with X-ray crystallography, and lastly to all of the support staff of the CRL for keeping it running.

This Thesis is dedicated to my parents and my love Yijia Zhang. The "personal acknowledgements" will be in Chinese. 感谢我的父母对我留学7年的资助和对我选择的支持。感谢我的爷爷奶奶和外婆从小对我的照顾。感谢嘉嘉3年的陪伴和支持，让我成为更好的自己。

Contents

	Declaration	i
	Abstract	ii
	Acknowledgements	iii
	Contents	iv
	Abbreviations	vii
	Notes	xiii

Chapter One: Introduction

1.1	General introduction	1
1.2	The imido ligand	1
1.3	Group 4 imido complexes	3
1.3.1	Synthesis of titanium imido complexes	3
1.3.2	Synthesis of zirconium and hafnium imido complexes	6
1.3.3	Stoichiometric reactions of imido titanium complexes	8
1.3.4	Stoichiometric reactions of imido zirconium complexes	10
1.3.5	Catalytic hydroamination	13
1.4	The hydrazido ligand	15
1.5	Group 4 hydrazido complexes	16
1.5.1	Synthesis of titanium hydrazido complexes	16
1.5.2	Synthesis of zirconium and hafnium hydrazido complexes	18
1.5.3	Stoichiometric reactions involving the $M=N_\alpha$ bond	19
1.5.4	Stoichiometric reactions involving N_α–N_β bond cleavage	22
1.5.5	Catalytic reactions	24
1.6	Group 4 alkoxyimido complexes	27
1.7	Transition metal borylimido complexes	29
1.8	References	37

Chapter Two: Zirconocene and hafnocene borylimides: synthesis, structure, bonding and reactivity

2.1	Overview	47
2.2	Synthesis and selection of borylamines	48

2.3	Synthesis of $Cp_2M\{NHB(NAr'CH)_2\}(Me)$ and $Cp_2M\{NB(NAr'CH)_2\}$-(L) (M = Zr or Hf)	59
2.4	C–H bond activation of benzene by transient $Cp_2Zr\{NB(NAr'CH)_2\}$	70
2.5	H–H bond activation by $Cp_2Zr\{NB(NAr'CH)_2\}(py)$ (**11**)	74
2.6	Synthesis of $Ind_2Zr\{NHB(NAr'CH)_2\}(Me)$ (**21**) and $Ind_2Zr\{NB$-$(NAr'CH)_2\}(L)$	78
2.7	Computational studies of bonding in zirconocene borylimides	85
2.8	Conclusions and Outlook	95
2.9	References	96

Chapter Three: Reactions of Group 4 metallocene borylimides with terminal alkynes

3.1	Overview	103
3.2	DFT studies of the reactions of model organo- and boryl-imides with alkynes	106
3.2.1	Structural trends and electronic structure of the cycloaddition products of $Cp_2Zr\{NB(NMeCH)_2\}$ (**1Q_B(NMeCH)$_2$**)	107
3.2.2	Thermodynamic preferences: C–H bond activation *vs* 1,2- or 2,1-cycloaddition for Group 4 metallocene imido compounds	111
3.3	Reactions of $Cp_2Zr\{NB(NAr'CH)_2\}(py)$ (**11**) with the electron rich alkyne ^{t}BuCCH	114
3.4	Reactions of Group 4 metallocene borylimide complexes with electron deficient terminal aryl alkynes	124
3.4.1	Reactions of $Cp_2Zr\{NB(NAr'CH)_2\}(py)$ (**11**) with aryl alkynes	124
3.4.2	Kinetic study of the C–H bond activation reactions of $Cp_2Zr\{NB$-$(NAr'CH)_2\}(L)$ (L = py (**11**) or DMAP (**14**)) with Ar^FCCH	143
3.4.3	Reactions and kinetic study of $Cp_2M\{NB(NAr'CH)_2\}(py)$ (M = Ti (**1.117**) or Hf (**12**)) with electron deficient terminal alkynes	158
3.4.4	Mechanistic discussion	167
3.5	Hydro-borylamination reactions	169
3.6	Conclusions and Outlook	172
3.7	References	174

Chapter Four: Reactions of zirconium borylimides with polar substrates

4.1	Overview	180

4.2	Reactions of $Cp_2Zr\{NB(NAr'CH)_2\}(py)$ (**11**) with CO_2, CS_2 and PhNCE (E = O or S)	182
4.3	Reactions of $Cp_2Zr\{NB(NAr'CH)_2\}(py)$ (**11**) with organic carbonyl compounds	186
4.3.1	Reactions of $Cp_2Zr\{NB(NAr'CH)_2\}(py)$ (**11**) with tolylaldehyde and acetophenone	186
4.3.2	Reactions of $Cp_2Zr\{NB(NAr'CH)_2\}(py)$ (**11**) with esters	189
4.3.2.1	Reactions of $Cp_2Zr\{NB(NAr'CH)_2\}(py)$ (**11**) with $MeCO_2R$ (R = ^{i}Pr, Et, Me)	189
4.3.2.2	Reactions of $Cp_2Zr\{NB(NAr'CH)_2\}(py)$ (**11**) with MeC(O)SR (R = Et, Me)	201
4.3.2.3	Reactions of $Cp_2Zr\{NB(NAr'CH)_2\}(py)$ (**11**) with MeC(O)Cl and $MeC(O)NMe_2$	205
4.3.2.4	Reactions of enolate zirconocene complexes with $Me_3Si(H)CCO$	210
4.3.3	Kinetic study of the ketene elimination and trapping reactions of $Cp_2Zr\{NHB(NAr'CH)_2\}\{OC(CH_2)EEt\}$ (E= O (**54**), S (**61**))	216
4.4	Reactions of $Cp_2Zr\{NB(NAr'CH)_2\}(py)$ (**11**) with strained heterocycles	231
4.4.1	Reactions of $Cp_2Zr\{NB(NAr'CH)_2\}(py)$ (**11**) with epoxides	231
4.4.2	Reactions of $Cp_2Zr\{NB(NAr'CH)_2\}(py)$ (**11**) with episulfides	237
4.5	Conclusions and Outlook	241
4.6	References	243

Chapter Five: Experimental details and characterising data

5.1	General methods and implemenation	250
5.2	Literature preparations	250
5.3	X-ray data collection and processing parameters	251
5.4	Computational details	251
5.5	Experimental details and characterising data for Chapter Two	252
5.6	Experimental details and characterising data for Chapter Three	266
5.7	Experimental details and characterising data for Chapter Four	284
5.8	References	302

Appendix 306

CD Appendix

Abbreviations

General

Å	Ångstrom
atm	atmosphere(s)
avg.	average
ca.	*circa*, about
cf.	*confer*, compared to
CSD	Cambridge Structural Database
^{o}	degrees
^{o}C	degrees Celsius
d	day(s)
e	elementary charge
FA	fold angles
g	grams
h	hour(s)
HA	hinge angles
η	hapticity
K	Kelvin
kcal mol^{-1}	kilocalorie(s) per mole
M	molarity, mol dm^{-3}
mbar	millibar(s)
min	minute(s)
mL	millilitre(s)
mmol	millimole(s)
RDS	rate determining step
RT	room temperature
s	second(s)
$t_{1/2}$	half-life
μ	bridging
vs	versus

Chemical

9-BBN	9-borabicyclo[3.3.1]nonane
Ad	adamantyl
Ar	aryl group
Ar'	2,6-$C_6H_3{}^{i}Pr_2$
Ar^{CF_3}	3,5-$C_6H_3(CF_3)_2$
Ar^{F}	C_6F_5
Bn	benzyl
bipy	2,2'-bipyridine
^{n}Bu	*n*-butyl
Cat	1,2-benzenediol
CCC^{Bu}	2-(1,3-bis(N-butylimidazol-2-ylidene)-phenylene
cent	ring centroid
Cp	C_5H_5
Cp*	C_5Me_5
Cp'	C_5H_4Me
Cp^{Me4}	C_5HMe_4
Cp^{ipr}	$C_5H_4{}^{i}Pr$
Cp"	1,3-$C_5H_3(SiMe_3)_2$
Cy	Cyclohexyl
DMAP	4-dimethylaminopyridine
E	generic chalcogen atom
ebthi	ethylenebis(tetrahydroindenyl)
EIE	equilibrium isotope effect
Et	Ethyl
Fc	ferrocenyl
H_2Me_4taa	tetramethyl dibenzotetraaza[14]annulene
H-hpp	1,3,4,6,7,8-hexaydro-2*H*-pyrimido[1,2-*a*]pyrimidine
Hpypyr	2-(2′-pyridyl)-3,5-dimethylpyrrole
IDipp	*N*,*N*'-bis(2,6-diisopropylphenyl)imidazol-2-ylidene
^{i}Pr	*iso*-propyl
Ind	C_9H_7
Ind^{Me3}	$C_9H_4Me_3$
KIE	kinetic isotope effect(s)

L	a supporting ligand (set)
Me	methyl
Me_2pz	3,5-dimethylpyrazolyl
$Me_3[6]aneN_3$	1,3,5-trimethyltriazacyclohexane
$Me_3[9]aneN_3$	1,4,7-trimethyltriazacyclononane
Mes	2,4,6-$C_6H_2Me_3$
$NacNac^{NMe_2}$	Ar'NC(Me)CHC(Me)N$CH_2CH_2NMe_2$
N_2NN'	(2-C_5H_4N)$CH_2N(CH_2CH_2NSiMe_3)_2$
N_2N^R	generic diamide-amine ligand
N_2N^{py}	MeC(2-C_5H_4N)$(CH_2NSiMe_3)_2$
$N_2{}^{SiMe_3}N^{Me}$	$MeN(CH_2CH_2NSiMe_3)_2$
$N_2{}^{ArF}N^{Me}$	$MeN(CH_2CH_2NAr^F)_2$
$N_2N^{SiMe_3}$	$Me_3SiN(CH_2CH_2NSiMe_3)_2$
$N_2{}^{iPr}N^{Me}$	$MeN(CH_2CH_2N^iPr)_2$
$N_2{}^{TBS}N^{py}$	MeC(2-C_5H_4N)$\{CH_2N(Si^tBuMe_2)\}_2$
$N_2{}^{TFAP}N^{py}$	MeC(2-C_5H_4N)$\{CH_2NH(2\text{-}C_6F_4NMe_2)\}_2$
$N_2{}^{3,5\text{-}Xyl}N^{py}$	MeC(2-C_5H_4N)$\{CH_2NH(3,5\text{-}C_6H_3Me_2)\}_2$
$N^{3,5\text{-}Xyl}N^{pyr}$	2-(3,5-dimethylphenylamino)pyrrolinato
$N_2{}^{pyr}N^{Me}$	*N*,*N*-di(pyrrolyl-α-methyl)-*N*-methylamine
$N_2{}^{SiMe3}O$	O-$(CH_2CH_2NSiMe_3)_2$
$N_2{}^{Ar}O$	O-$(2\text{-}C_6H_4NSiMe_3)_2$
$N^{pyr}N^{Me_2}$	$Me_2NCH_2(2\text{-}NC_4H_3)$
Ph	phenyl
Pin	2,3-dimethyl-2,3-butanediol
PN	*N*-(2-(diisopropylphosphino)-4-methylphenyl)-2,4,6-trimethylanilide
PNP	$N\{2\text{-}P^iPr_2\text{-}4\text{-}C_6H_3Me\}_2$
py	pyridine
py'	4-pyrrolidinopyridine
R	generic aryl or alkyl
^tBu	*tert*-butyl
^tBu-bipy	4,4'-di-*tert*-butyl-2,2'-bipyridine
$^{tBu}NacNac$	$HC\{C(^tBu)NAr'\}_2$
Tex	*Tert*-hexyl
THF	tetrahydrofuran
TMEDA	N,N,N',N'-tetramethylethylenediamine

Tol	4-C_6H_4Me
$Tp^{tBu,Me}$	tris(3-methyl-5-*tert*-butylpyrazolyl)borate
TTP	*meso*-tetra-*p*-tolylporphyrinato dianion
X	generic anionic ligand
Xyl	2,6-$C_6H_3Me_2$
‡	transition state or activation parameter

Calculations

BCP	bond critical point
BD	bond dissociation
DFT	density functional theory
δ	delocalisation index
ε	ellipticity
HOMO	highest occupied molecular orbital
k	bond force constant
LUMO	lowest unoccupied molecular orbital
MO	molecular orbital
NBO	natural bonding orbital
NLMO	natural localised molecular orbital
TS	transition state
ρ	electron density
Q	charge
QTAIM	Quantum Theory of Atoms in Molecules
$\nabla^2\rho$	electron density Laplacian

Mass Spectrometry

EI	electron impact
FI	field impact
HR	high-resolution
m/z	mass to charge ratio
MS	mass spectrometry

Nuclear Magnetic Resonance Spectroscopy

$^{13}C\{^{1}H\}$	proton-decoupled ^{13}C
$^{11}B\{^{1}H\}$	proton-decoupled ^{11}B
$^{19}F\{^{1}H\}$	proton-decoupled ^{19}F
br.	broad
COSY	correlation spectrocopy
d	doublet
HMBC	heteronuclear multiple-bond correlation
HSQC	heteronuclear single quantum correlation
Hz	Hertz
i	*ipso*
J	coupling constant
m	*meta*
m	multiplet
MHz	Megahertz
NMR	nuclear magnetic resonance
NOE	nuclear Overhauser effect
o	*ortho*
p	*para*
ppm	parts per million
q	quartet
ROESY	Rotating-frame nuclear Overhauser Effect spectroscopy
s	singlet
sept.	septet
t	triplet
VT	variable temperature
δ	chemical shift in ppm

Infrared Spectroscopy

br.	broad
FT-IR	fourier transform infrared
IR	infrared
cm^{-1}	wavenumber
m	medium

s	strong
w	weak
ν	frequency

Notes

Literature compounds described in this Thesis are numbered **1.x**, **2.x**, **3.x**, **4.x** according to the Chapter in which they first occur. The new compounds described in this Thesis are numbered **1** – **79**. Density functional theory (DFT) calculated compounds are clearly stated in the text.

X-ray crystallography data was collected, solved and refined by the Author with the help and guidance of Prof. Philip Mountford. For compounds **2**, **6**, **7**, **9 – 12**, **18**, **19**, **21**, **23**, **24**, **31**, **50**, **53**, **56**, **59**, **60** and **67** data was collected by Dr Benjamin Clough, and for compounds **32**, **74** and **79** data was collected by Dr Matthew Blake. For compound **26** data was collected and solved by Dr Amber Thompson. Molecular drawings were produced by Prof. Philip Mountford.

DFT calculations were performed by Prof. Philip Mountford of the University of Oxford.

Chapter One

Introduction

1.1 General introduction

Complexes containing transition metal-ligand multiple bonds have been of interest to researchers for about forty years, and have been applied to a range of important organic and inorganic transformations.[1] Of particular relevance to this Thesis are Group 4 imido and hydrazido complexes, M=NR and $M=NNR_2$ (R = alkyl or aryl) respectively, the structure and bonding of which have been studied in details. Both exhibit a wide range of stoichiometric and catalytic reactions with small molecules, as well as other applications, for example the stoichiometric and catalytic reduction of dinitrogen,[2–7] carbodiimide metathesis,[8] olefin polymerisation,[9–13] Metal-Organic Chemical Vapour Deposition[10,14,15] and new C–N bond forming reactions including hydroamination and hydrohydrazination (N–H bond addition across the multiple bonds of alkenes, alkynes, allenes and carbodiimides).[16–29]

This Thesis describes the synthesis and reactivity of the first terminal borylimido complexes of zirconium and hafnium, i.e., of the type $(L)_nM=NBR_2$. Before the successful establishment of the synthetic route to the borylimido titanium compounds and the studies on the relevant reactivity in our research group, the synthesis of borylimido complexes were almost undeveloped with only a handful of examples reported without reactivity for all the metals. The development of novel cyclic borylamines and the synthesis of corresponding zirconocene and hafnocene borylimides are described in Chapter Two, their initial reactivity towards C–H and H–H bonds is also explored. Chapter Three focuses on the reactions of titanocene, zirconocene and hafnocene borylimides with alkynes, accompanied by detailed kinetic studies and some DFT calculations. Novel reactions between a borylimido zirconocene complex and oxygen- or sulfur- containing small polar molecules, namely epoxides, carbonyls and heteroallenes, are investigated in Chapter Four.

1.2 The imido ligand

The first class of transition metal–nitrogen multiple bonded complexes to be extensively studied since the 1950s were the imido complexes, of the type $(L)_nM=NR$ (R = alkyl or aryl). The imido ligand can either function as an unreactive ancillary ligand, especially in late transition metals, or as a reacting centre for early transition metals (Group 3 – 5), attributed to the increased $M–N_{im}$ bond polarity.[1,30–34] Later in this Chapter, the bonding

modes and reactivity of Group 4 imido, hydrizido and alkoxyimido complexes are presented, and compared with recently developed borylimido complexes.

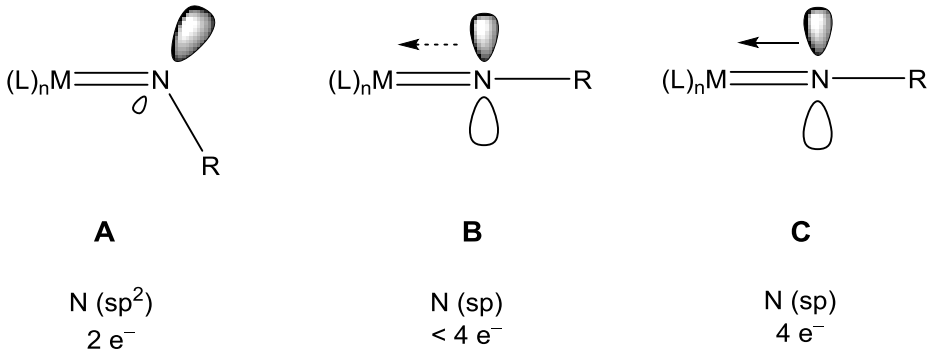

Figure 1.1. Bonding modes of the terminal imido ligand, along with orbital hybridisation of the N atom, and the neutral valence electron count of the ligand.[32]

The bonding of imido complexes is well understood. For the terminal imido ligand N–R (R = alkyl or aryl), the interaction to the transition metal is considered to be one σ-bond and either one or two π-bonds.[32] The three possible bonding modes are depicted in Figure 1.1. In structure **A**, a formally bent M=N–R linkage is depicted in which the lone pair resides in an sp^2-hybridised nitrogen atomic orbital which gives a formal metal nitrogen double bond ($\sigma^2\pi^2$). This rare bonding situation is found in the compound $Mo(NPh)_2(S_2CNEt_2)_2$ (**1.1**, Figure 1.2), where one of the Mo–N–Ph linkage is significantly bent (Mo–N–C = 139.4(4)°).[35] In contrast, most of the M–N–R linkages are approximately linear reflecting an sp-hybridised nitrogen atom as depicted in structures **B** and **C** with M–N–R angle being greater than *ca.* 155°. Structure **B** shows the bonding situation where the sp-hybridised nitrogen lone pair in a 2p orbital cannot effectively donate to the metal centre due to symmetry, energy restrictions or a lack of an acceptor orbital at the metal. This type of bonding ($\sigma^2\pi^n$, $2 < n < 4$) is seen in the compound $Os(NAr')_3$ (**1.2**, Ar' = 2,6-$C_6H_3{}^iPr_2$), in which all the three M–N–R linkages are linear. Each imido ligand is considered to formally donate 3⅓ electrons to osmium due to the unmatched symmetry.[36] It also arises in metallocene based imido complexes, such as $Cp_2Ti(N^tBu)(py)$ (**1.3**) and $Cp_2Zr(N^tBu)(THF)$ (**1.4**), in which full donation from imido π-component to the metal gives rise to a formal electron count of twenty at metal centre (Ti, **1.3**; Zr, **1.4**). Therefore, the lone pair donation from this sp-hybridised nitrogen orbital is in competition with π-donation from the Cp ligands.[37,38] However, the most common mode is structure **C**, where the dianionic imido ligand functions as a four electron donor,

forming a formal triple bond ($\sigma^2\pi^4$), but conveniently drawn as M=N throughout this Thesis.

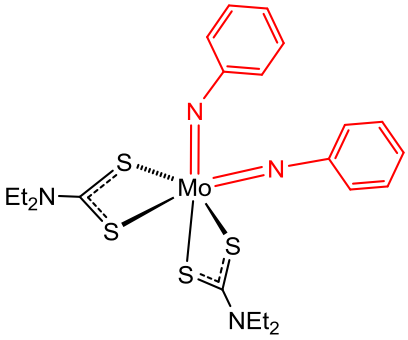

1.1

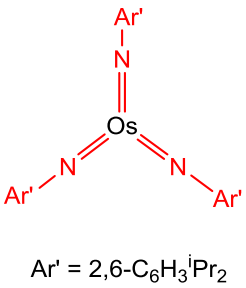

Ar' = 2,6-$C_6H_3{}^iPr_2$

1.2

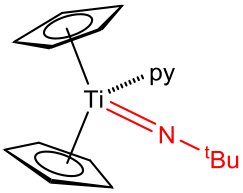

1.3

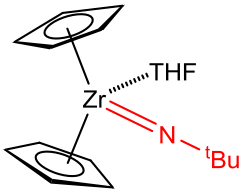

1.4

Figure 1.2. Examples of bent (**1.1**) and linear **(1.2**, **1.3** and **1.4**) imido complexes.[35–38]

1.3 Group 4 imido complexes

1.3.1 Synthesis of titanium imido complexes

The first structurally authenticated imido titanium complexes Ti{NP(S)Ph_2}$Cl_2(py)_3$ (**1.5**) and Ti(NPh)(Ar'O)$_2$(py')$_2$ (**1.6**, py' = 4-pyrrolidinopyridine) were reported by Roesky and Rothwell, respectively, in 1990.[39,40] Later, Wolczanski reported the synthesis of a transient imido titanium complex Ti(NSi^{t}Bu$_3$)(NHSi^{t}Bu$_3$)$_2$ (**1.7**) through thermolysis of Ti(NHSi^{t}Bu$_3$)$_3$(Me).[41] More examples have been published either from reacting Ti(II) complexes with azide through an oxidative route, or reaction between (L)$TiCl_2$ and 2 equivalents of LiNHR.[8,42–44]

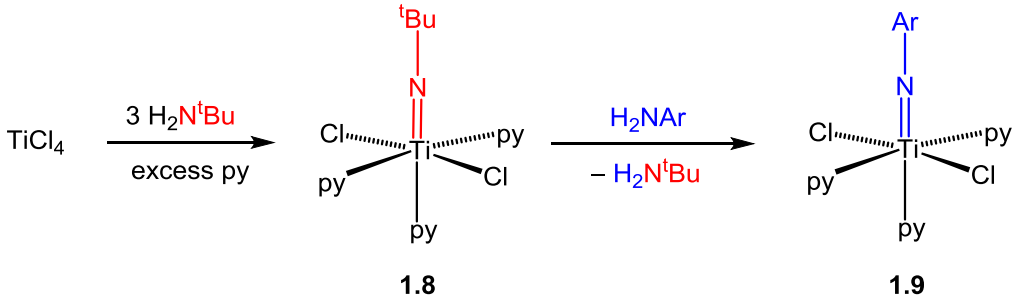

1.8 **1.9**

Scheme 1.1. Synthesis of complexes of the type $Ti(NR)Cl_2(py)_3$ (R = ^{t}Bu (**1.8**) or aryl (**1.9**)).[45]

In 1994, the discovery of a convenient multigram scaled synthesis of $Ti(N^tBu)Cl_2(py)_3$ (**1.8**) was published by Mountford and co-workers *via* the reaction of readily available $TiCl_4$ with H_2N^tBu and pyridine.[45] Attempts to synthesis $Ti(NAr)Cl_2(py)_3$ (**1.9**), by reacting with anilines ($ArNH_2$) were unsuccessful. However, synthesis of arylimido titanium compounds **1.9** was achieved in high yield by reacting corresponding aniline with **1.8** though aniline/*tert*-butylimide exchange (Scheme 1.1).[34,45–47] Then the synthesis of a wide range of alkyl/aryl-imido titanium compounds, by addition of lithiated ancillary ligands through a salt metathesis methodology, was rapidly developed by using **1.8** or **1.9** as precursors.[8,34,37,47–50] This methodology allows the half sandwich complex $Cp^*Ti(N^tBu)Cl(py)$ (**1.10**) and sandwich complex $Cp_2Ti(N^tBu)(py)$ (**1.3**) to be obtained simply by reacting **1.8** with $M\{C_5R_5\}$ (M = Li or Na, R = H or Me).[37] Tridentate and tetradentate supporting ligands installed with titanium imides were similarly synthesised and fully studied in our research group (Scheme 1.2).[51,52]

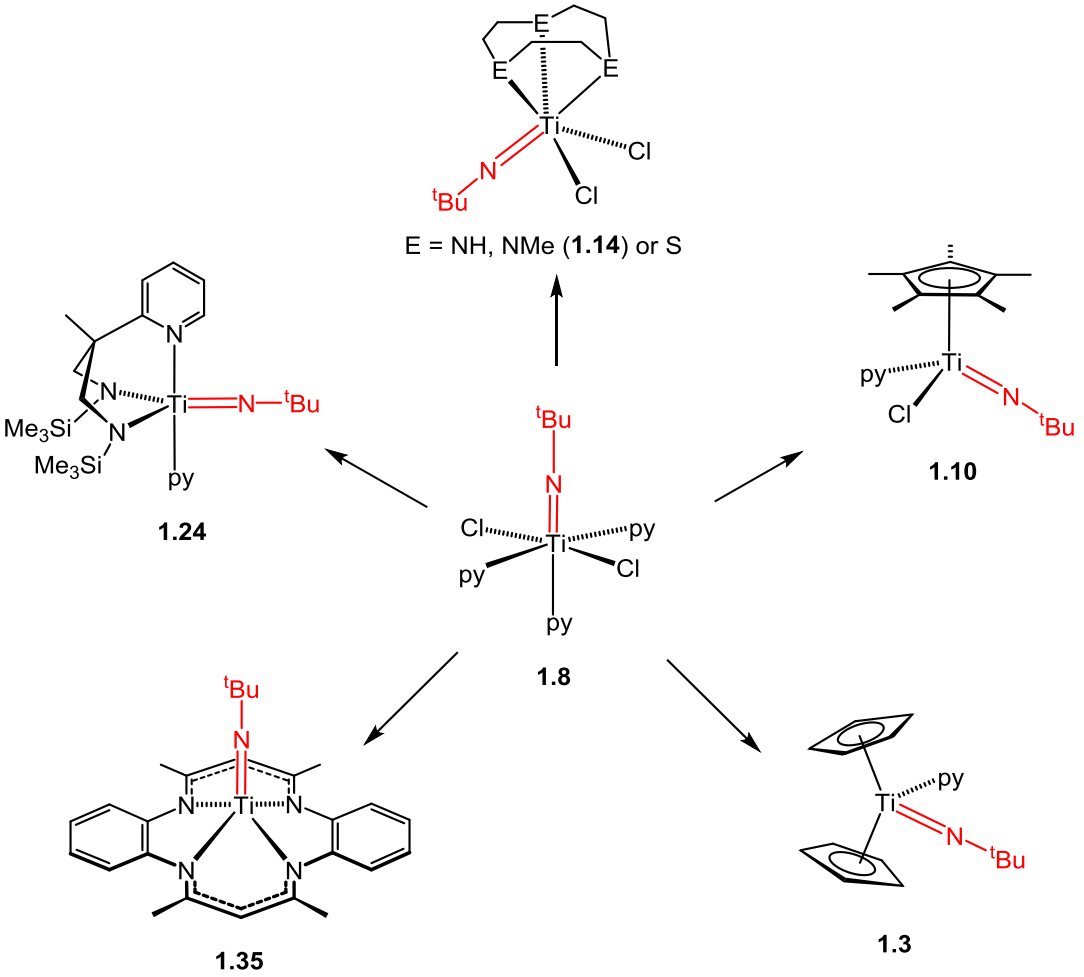

Scheme 1.2. Examples of titanium *tert*-butylimido complexes synthesised from $Ti(N^tBu)Cl_2(py)_3$ (**1.8**).[8,34,37,47–52]

In 2005, the compound $Ti(NMe_2)_2Cl_2$ (**1.11**) synthesised from the redistribution reaction between $Ti(NMe_2)_4$ and $TiCl_4$,[53] was also found to be a good entry point for making imido titanium compounds, of the type $Ti(NR)Cl_2(NHMe_2)_2$ (R = alkyl (**1.12**) or aryl (**1.13**)) through proton transfer by reacting with corresponding anilines or alkylamines.[54] Subsequently, ancillary ligands can be readily installed, especially using neutral tridentate supporting ligands; e.g. reacting with $Me_3[9]aneN_3$ (1,4,7-trimethyltriazacyclononane) yields the dichloride imido compounds $Ti(NR)Cl_2(Me_3[9]aneN_3)$ (R = alkyl (**1.14**) or aryl (**1.15**)).[9] In a number of cases, the tris(pyridine) imido complexes (**1.8**) and (**1.9**) can be alternatively synthesised from **1.11** by replacing the amine ligands in neat pyridine (Scheme 1.3).[39,45] This developed synthetic route allows some previously unknown imido synthons, of the type **1.9**, to be accessible**.**

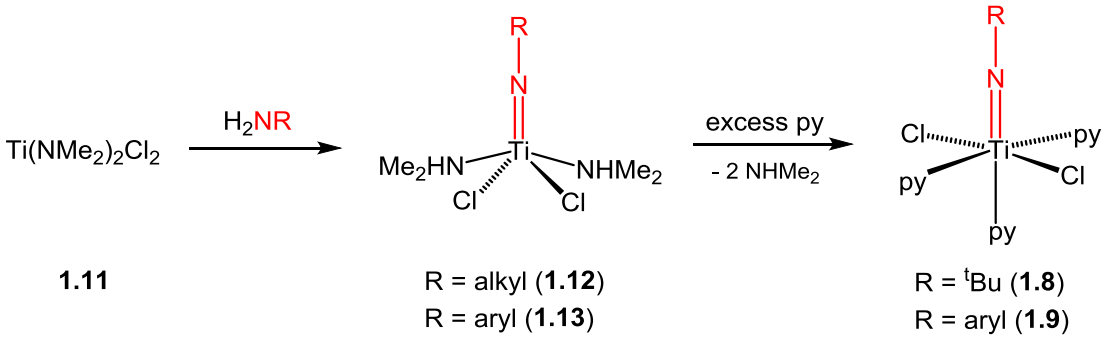

Scheme 1.3. Synthesis of $Ti(NR)Cl_2(NHMe_2)_2$ (R = alkyl (**1.12**) or aryl (**1.13**)), and reactions with pyridine.[45]

1.3.2 Synthesis of zirconium and hafnium imido complexes

Despite the success in the development of titanium imido compounds, the first Group 4 examples, of the type $[Cp_2Zr(NR)]$ (R = ^{t}Bu (**1.16**), Xyl (**1.17**), 4-$C_6H_4{}^t$Bu (**1.18**)), were reported by Bergman in 1988 (Figure 1.3).[55] These series of transient base free imido complexes were synthesised though thermolysis of alkyl-amido precursors $Cp_2Zr(NHR)(R')$ (R' = alkyl). In the absence of a Lewis base trapping reagent, these transient compounds spontaneously dimerised to give imido-bridged complexes $Cp_4Zr_2(\mu\text{-}NR)_2$. However, by performing the thermolysis of **1.16** in the presence of THF, the monomeric terminal imido complex $Cp_2Zr(N^tBu)(THF)$ (**1.4**) was isolated and structurally authenticated.[38] Shortly afterwards, a non-metallocene transient zirconium imido, $Zr(NSi^tBu_3)(NHSi^tBu_3)_2$ (**1.19**), was prepared by Wolczanski and co-workers *via* thermolysis. Isolable compound $Zr(NSi^tBu_3)(NHSi^tBu_3)_2(THF)$ was obtained by trapping with THF.[56] Therefore, thermolytic methods were found to be a successful approach to prepare zirconium imides. A similar methodology can be applied for readily available zirconium and hafnium dichloride precursors. For example, marcrocycle-supported imido compounds M(TTP)(NAr') (M = Zr (**1.20**) or Hf, TTP^{2-} = *meso*-tetra-*p*-tolylporphyrinato dianion) were isolated though the thermolysis of $M(NHAr')_2(TTP)$ which were prepared by reacting $M(TTP)Cl_2$ with two equivalents of LiNHAr'.[57] A tridentate ligand supported imido zirconium compound $Zr(N_2NN')(N^tBu)(py)$ (N_2NN' = $(2\text{-}C_5H_4N)CH_2N(CH_2CH_2NSiMe_3)_2$) was reported in our research group from the analogous reaction of $Zr(N_2NN')Cl_2$ with $LiCH_2SiMe_3$, H_2N^tBu and pyridine.[58]

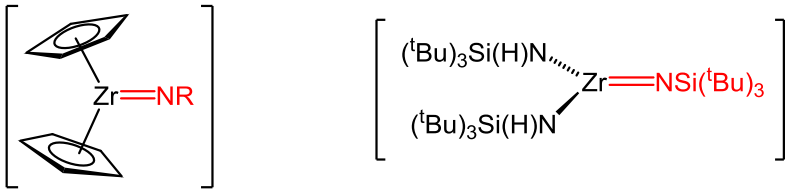

R = ^{t}Bu (**1.16**)
R = Xyl (**1.17**)
R = 4-$C_6H_4{}^t$Bu (**1.18**)

1.19

Figure 1.3. Early examples of transient zirconium imido complexes.[55,56]

Wigley and co-workers reported the preparation of the first zirconium and hafnium synthons $Zr(NAr')Cl_2(THF)_2$ (**1.21**) and $Hf(NAr')Cl_2(THF)_2$ in 1992, by reacting $MCl_4(THF)_2$ (M = Zr or Hf) with LiNHAr', Me_3SiCl and THF. In the presence of pyridine, another synthon, $Zr(NAr')Cl_2(py)_3$ (**1.22**) was formed.[59] However, the extension to a wider range of alkyl- or aryl-imido functionalities was limited. Compound **1.21** was alternatively prepared by Mountford and co-workers, and structurally authenticated as a dimeric species containing bridging imido ligands $Zr_2(\mu\text{-}NAr')_2Cl_4(THF)_4$ (**1.21**), as depicted in Figure 1.4.[60] Complex **1.22** was found to be a precursor to make dimeric zirconium imido complexes $[(\eta^8\text{-}C_8H_8)Zr(\mu\text{-}NAr')]_2$ and $[Cp'ZrCl(\mu\text{-}NAr')]_2$ (Cp' = η^5-C_5H_4Me).[59] Dimeric zirconium and hafnium imido complexes containing bridging imido ligands are commonly formed due to larger radius of zirconium and hafnium compared to titanium renders, in the case of which, the monomeric terminal imido compounds require steric protection from ancillary ligands to prevent dimerization. Further examples are dimeric imido zirconium and hafnium complexes previously observed by Nugent and Harlow in 1979 from the reaction of $M(NMe_2)_4$ (M = Zr or Hf) with H_2N^tBu.[61]

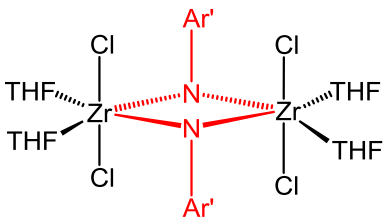

1.21

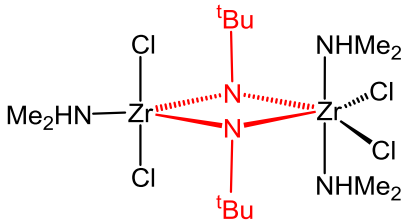

1.23

Figure 1.4. Examples of zirconium synthons containing bridging supported imido ligands.[60]

Later in our research group, a wider range of alkyl- and aryl-imido zirconium complexes were obtained *via* protonolysis of $Zr(CH_2SiMe_3)_2Cl_2(Et_2O)_2$ and $Zr(NMe_2)_2Cl_2(THF)_2$ with a range of primary alkylamines and substituted anilines. They were found to provide general entry points to the synthesis of dimeric imido zirconium dichloride complexes, such as $Zr_2(\mu\text{-}N^tBu)_2Cl_4(NHMe_2)_3$ (**1.23**) shown in Figure 1.4.[60] Addition of pyridine to these compounds resulted only in the replacement of THF forming pyridine-bound dimeric zirconium complexes. However, several further 2,6-diisopropylphenylimido complexes were synthesised in our research group by using **1.22**.[52,62]

1.3.3 Stoichiometric reactions of imido titanium complexes

Compound $Ti(N_2N^{py})(N^tBu)(py)$ (**1.24**) provides fruitful reactivity towards unsaturated molecules, and selected transformations are shown in Scheme 1.4.[8,47,63–67] Compound **1.24** reacted with acetonitrile or *tert*-butyl phosphaalkyne through [2+2] cycloaddition intermediates before the ancillary ligand changes to the κ^2-bound compound **1.25** and **1.26** respectively. Moving to isocyanides (XylNC and RCH_2NC, R = Me or Ph), highly selective coupling with the imido linkage of **1.24** formed **1.27** and **1.28**. Reaction with terminal alkynes led to the formation of azatitanacyclobutenes (**1.29**) proceeding through anti-Markovnikov type addition, while reaction with allenes or methyl-substituted internal alkynes (RCCMe, R = Me or Ph) yielded titanaazetidines (**1.30**).

Reactions between terminal alkynes and the half-sandwich arylimido compounds $Cp^*Ti(N^{3,5\text{-}Xyl}N^{pyr})(NAr)$ (Ar = Xyl (**1.31**) or Mes (**1.32**), $N^{3,5\text{-}Xyl}N^{pyr}$ = 2-(3,5-dimethylphenylamino)pyrrolinato) also yielded azatitanacyclobutene products. However, C–H bond activation of HCCAr (Ar = Ph or Tol) was found upon reaction with the *tert*-butylimide $Cp^*Ti(N^{3,5\text{-}Xyl}N^{pyr})(N^tBu)(^tBuNH_2)$ (**1.33**), yielding the acetylide products $Cp^*Ti(N^{3,5\text{-}Xyl}N^{pyr})(NH^tBu)(CCAr)$.[29] In contrast, C–H bond activation of the less active benzene by the transient titanium imido compound $Ti(NSi^tBu_3)(NHSi^tBu_3)_2$ (**1.7**) was reported by Wolczanski in 1991.[41]

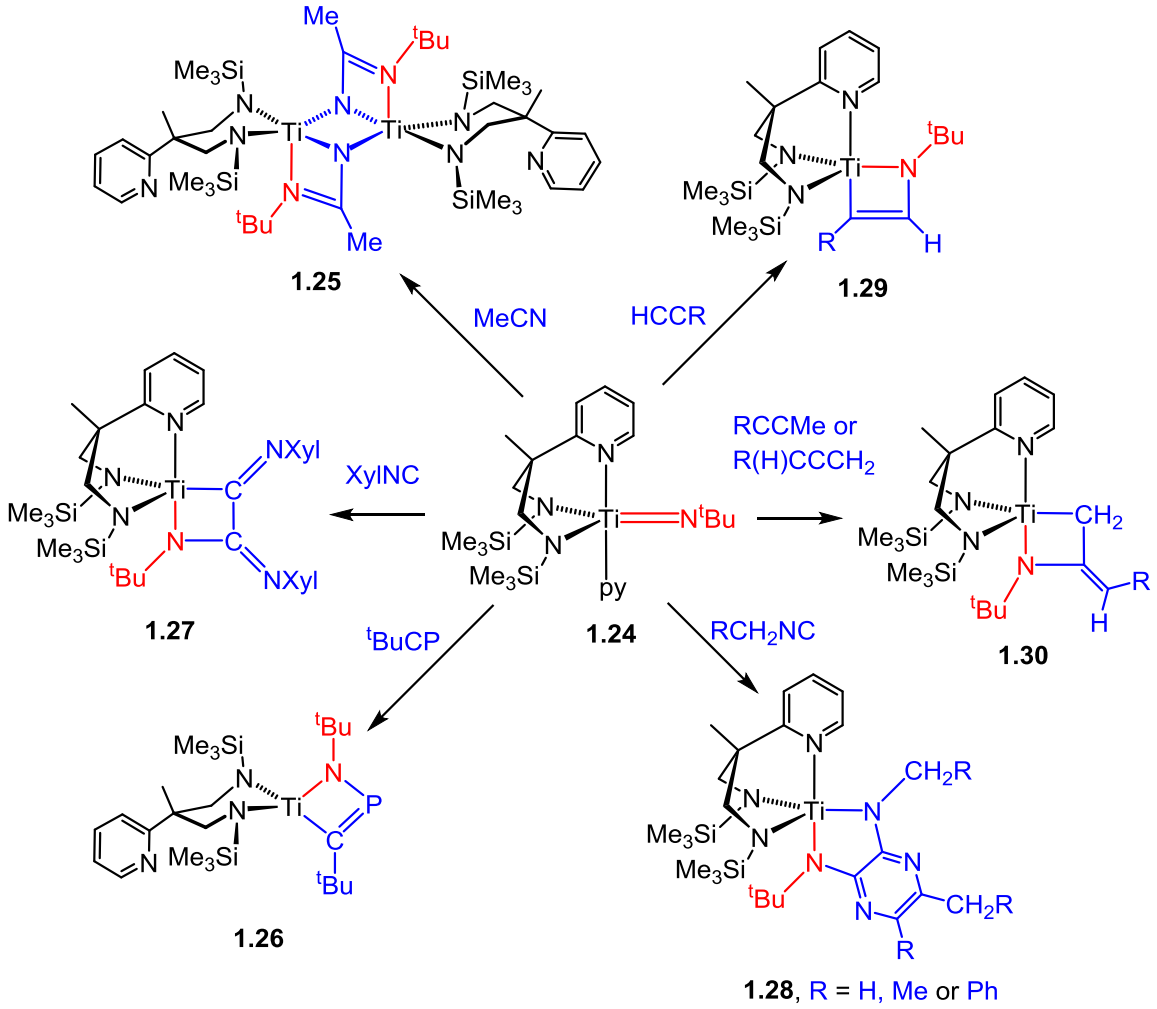

Scheme 1.4. Selected reactions of Ti(N_2N^{py})(N^tBu)(py) (**1.24**) with unsaturated compounds.[63–67]

In contrast to C–H bond activation, titanium imido complexes, particularly titanocene and its derivatives, have also been shown to be capable of activating H–H and S–H bonds. When exposed to H_2, the compounds $\{\eta^5\text{-}1,3\text{-}C_5H_3(SiMe_3)_2\}_2Ti(NR)$ (R = $SiMe_3$ or Mes) reacts through a 1,2-addition across the metal–nitrogen multiple bond, yielding hydrido-amido products,[44] and reversible H_2 1,2-addition was reported for the compound Cp_2*Ti(NPh).[68,69] Whereas titanium imides react with S–H compounds, sulfide abstraction was commonly observed accompanied by amine elimination. For example, $Cp_2Ti(N^tBu)(py)$ (**1.3**) reacts with MeSH yielding $Cp_2Ti(SMe)_2$, and with H_2S yielding the monomer $Cp_2Ti(SH)_2$ and dimer $Cp_2Ti(\mu\text{-}S)_2TiCp_2$.[70] In contrast, the non-metallocene titanium imido complex $Ti(N^tBu)(Me_4taa)$ (**1.35**, H_2Me_4taa = tetramethyl dibenzotetraaza[14]-annulene) reacts with H_2S producing the terminal sulfide compound $Ti(N^tBu)(Me_4taa)(S)$.[49] Other interesting reactions were observed for the

cyclopentadienyl-amidinate supported compound Cp*Ti{MeC(N^{i}Pr)$_2$}(NTol) with H_2BTex, 9-BBN, and HBAr$^F_2$ (Tex = *tert*-hexyl; Ar^F = C_6F_5), resulted in the hydride-bridged adducts Cp*Ti{MeC(N^{i}Pr$_2$)$_2$}{N(Tol)HBRR'} without B–H bond cleavage.[71]

1.3.4 Stoichiometric reactions of imido zirconium complexes

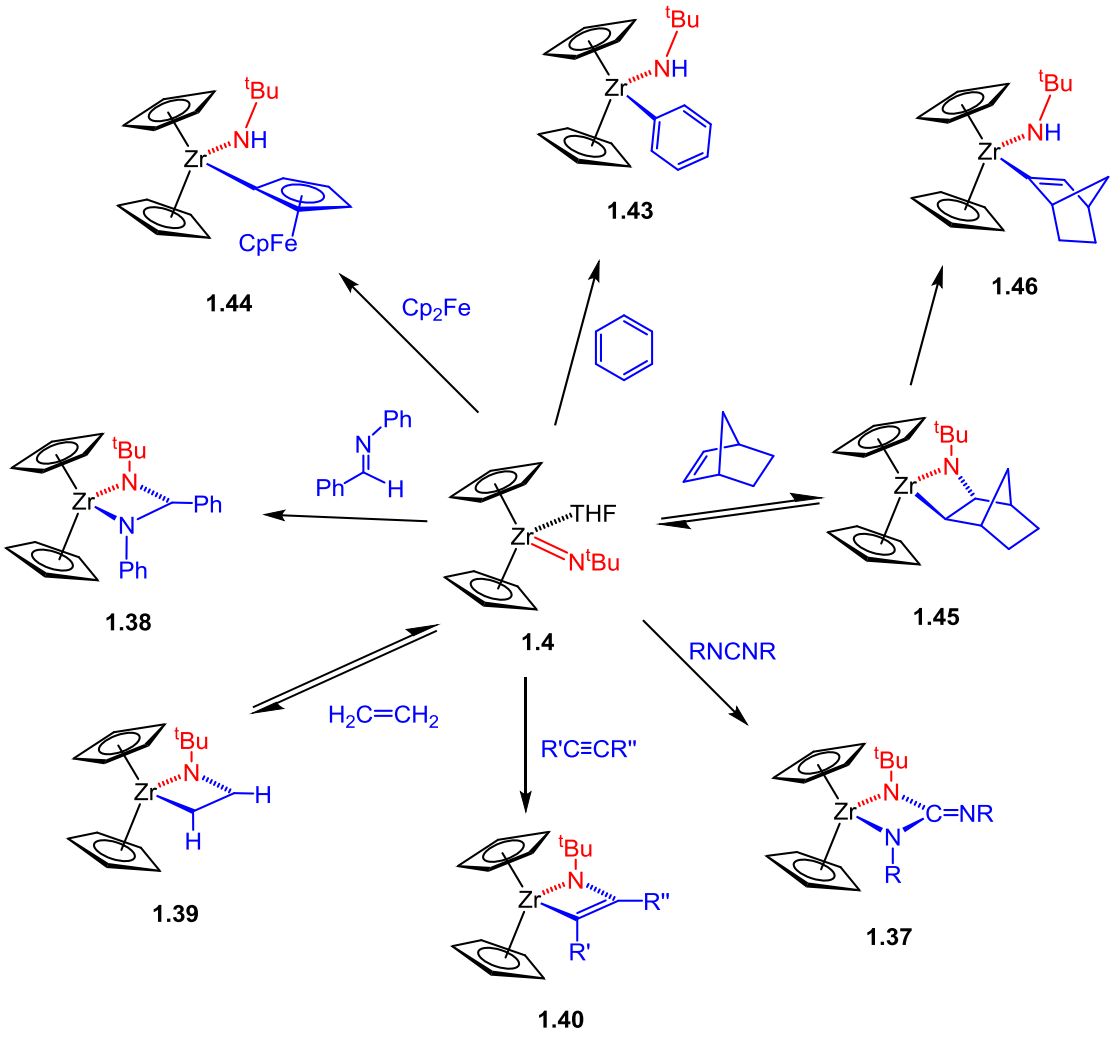

Scheme 1.5. Cycloaddition and C–H bond activation reactions of Cp$_2$Zr(N^{t}Bu)(THF) (**1.4**).[38,72–74]

The hallmark of the majority of Group 4 imido chemistry is [2+2] cycloaddition of substrates to the metal-nitrogen multiple bond. As for titanium imido compounds, the main point of interest for the zirconium imido analogues is the reactivity of the unsaturated Zr=NR linkage. Bergman's zirconocene imido compound Cp$_2$Zr(N^{t}Bu)(THF) (**1.4**) and its transient analogue Cp$_2$Zr(N^{t}Bu) (**1.16**) show extensive [2+2] cycloaddition reactions with a range of unsaturated small molecules as shown in Scheme 1.5. Carbodiimides react with Cp$_2$Zr(NR)(THF) (R = ^{t}Bu (**1.4**), 2,6-$C_6H_3Me_2$ (**1.36**) or 2,6-

$C_6H_3{}^iPr$), yielding β-iminodiazazirconacyclobutanes $Cp_2Zr\{N(R)C(NR')N(R')\}$ (R = ^{t}Bu, R' = Ph (**1.37**)).[38] Stoichiometric reaction with one equivalent of imine PhC(H)=NPh provides the diazazirconacyclobutane complex (**1.38**). Interestingly, by adding an excess of imine to **1.38** at elevated temperatures, imine metathesis was observed to yield PhC(H)=N^{t}Bu and the symmetrically substituted compound $Cp_2Zr\{N(Ph)C(Ph)N(Ph)\}$.[38] Compounds **1.4** and **1.36** gave [2+2] cycloaddition products $Cp_2Zr\{N(R)C(R'')C(R')\}$ (**1.40**, R = ^{t}Bu; R', R'' = H, Me or aryl) with both internal and terminal alkynes R'CCR''. The complex **1.4** also gave reversible cycloaddition products with alkenes, such as ethylene (**1.39**), but in equilibrium with the starting material.[38]

In contrast to the cycloaddition reactions between **1.4** and alkynes, C–H bond activation of ^{t}BuCCH by the homologous Cp*CpZr(N^{t}Bu)(THF) (**1.41**) was reported by Bergman, forming an acetylide-amido compound Cp*CpZr(NH^{t}Bu)(CC^{t}Bu) (**1.42**).[73] Studies of the sp^2 C–H bond activation reaction of **1.4** have been expanded to a great extent. For instance, reaction with benzene led to the phenyl-amido zirconocene complex $Cp_2Zr(NH^tBu)Ph$ (**1.43**), proceeding through the reactive base free transient intermediate [$Cp_2Zr(N^tBu)$] (**1.16**). In contrast, the arylimido analogue [$Cp_2Zr(NXyl)$] (**1.17**) fails to react with benzene under any conditions.[72] Thermolysis of **1.4** in the presence of ferrocene or other metallocene compounds $CpM(CO)_3$ (M = Re, Mn), results in activation of one cyclopentadienyl C–H bond, yielding bimetallic complexes, such as $Cp_2Zr(NH^tBu)(\eta^1{:}\eta^5\text{-}\mu\text{-}C_5H_4)FeCp$ (**1.44**). The norbornene underwent reversible cycloaddition with **1.4** at RT giving **1.45**, similar to the reaction with ethylene; however, elevating the reaction temperature to 45 °C yielded the C–H bond activated product **1.46** (Scheme 1.5).[74] Wolczanski reported a similar reaction between the monomeric zirconium imido compound $Zr(NSi^tBu_3)(NHSi^tBu_3)_2$ (**1.19**) and benzene, yielding a phenyl-amido zirconium analogue $Zr(NHSi^tBu_3)_3Ph$. In this case, activation of one of the sp^3 C–H bonds in CH_4 was also observed, probably due to the greater coordinative and electronic unsaturation of **1.19**.[56]

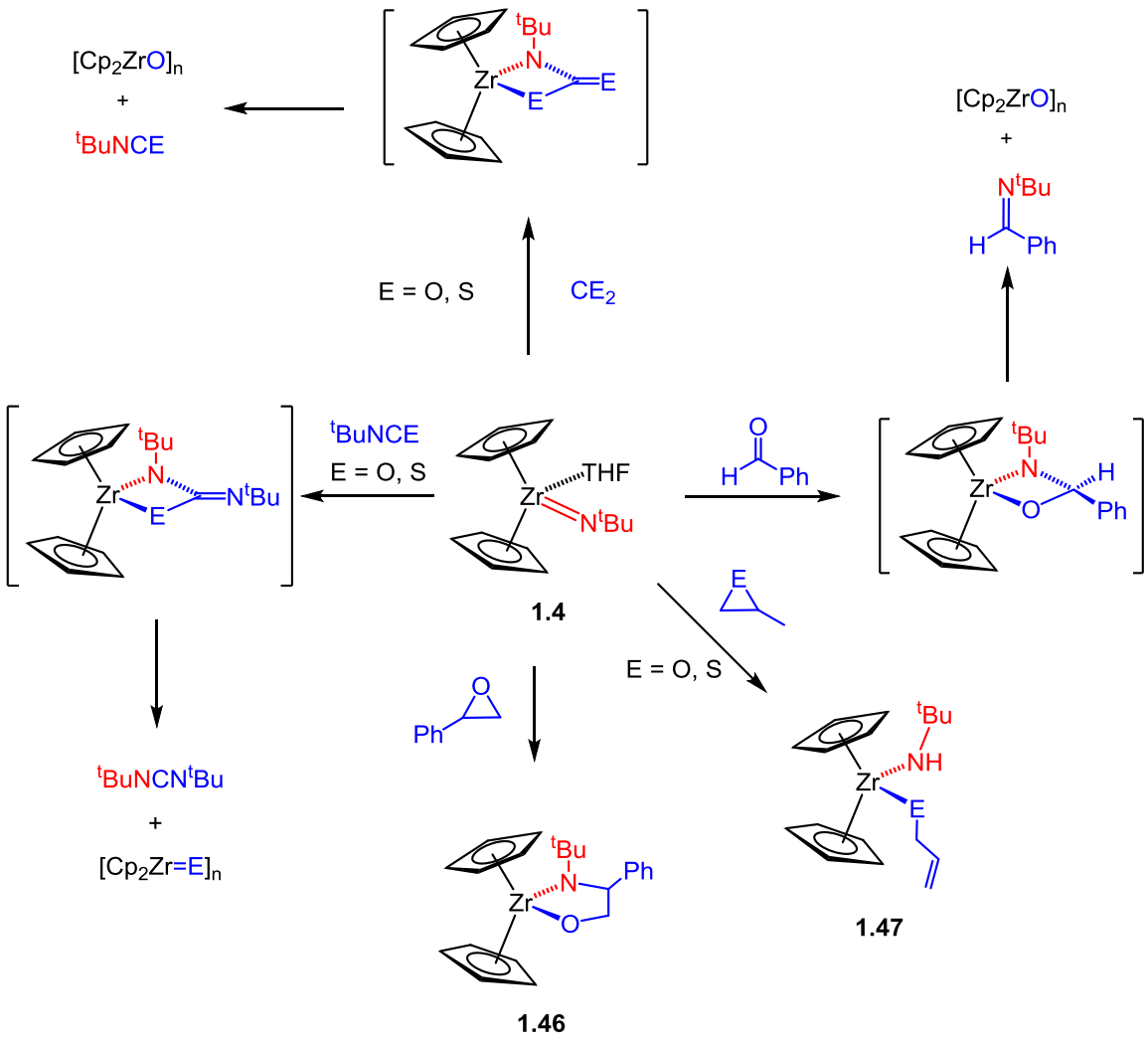

Scheme 1.6. Other selected reactions of $Cp_2Zr(N^tBu)(THF)$ (**1.4**).[38,75–77]

In 1996, the [2+2] cycloaddition of ^{t}BuNCO to Zr(Me$_4$taa)(NAr')(py) giving the ureate complex Zr(Me$_4$taa){(NAr')C(O)N(^{t}Bu)} was reported by Mountford and co-workers. Later, Woo and co-workers reported a similar reaction between isocyanates and Zr(NAr')(TTP) (**1.20**) proceeding through a [2+2] cycloaddition reaction, but followed by isomerisation and subsequent extrusion to generate carbodiimides.[57] Bergman's zirconocene imido complex **1.4** also behaves in the same way with isocyanate, ultimately extruding carbodiimides. Additionally other selected functional group transfer reactions of **1.4** are shown in Scheme 1.6, which allow the synthesis of a large range of organo-nitrogen ligands *via* novel methods proceeding through a [2+2] cycloaddition with isocyanates, heteroallenes and carbonyls,[63,72,74–79] and the insoluble $[Cp_2ZrO]_n$ allows simple purification of the extruded organic compounds.[76] The studies indicated that elimination of the carbodiimide (and related products) was significantly favoured for the

alkylimide, and the observation had been mirrored in titanium imido and hydrazido chemistry.[80] In addition, compound **1.4** presents interesting reactions towards epoxides and episulfides. For example, reaction of heterocycles without accessible β-hydrogens undergoes ring opening insertion, giving azaoxazirconacyclopentane **1.46**, whereas the reaction of heterocycles with accessible β-hydrogens undergo elimination reaction producing allylic oxide/sulfide complexes **1.47**.[75]

1.3.5 Catalytic hydroamination

Hydroamination is the addition of an N–H bond across an unsaturated C–C bond, and is an atom-economical method for the efficient formation of new C–N bonds. Group 4 metal complexes have been widely studied as such catalysts, through a series of mechanistic studies and three general mechanisms have been established.[17–19,72,81–88] The Group 4 imido complexes have been found as catalysts in the hydroamination of alkynes, and the "imido route" was found to be the most common mechanism, proceeding through a [2+2] cycloaddition reaction at the metal–nitrogen multiple bond. The imido catalyst can be subsequently regenerated through protonolysis with an equivalent of amine to continue the catalytic cycle, releasing an enamine which may tautomerise to the more stable imine isomer.[21,89–92] Some examples are discussed below.

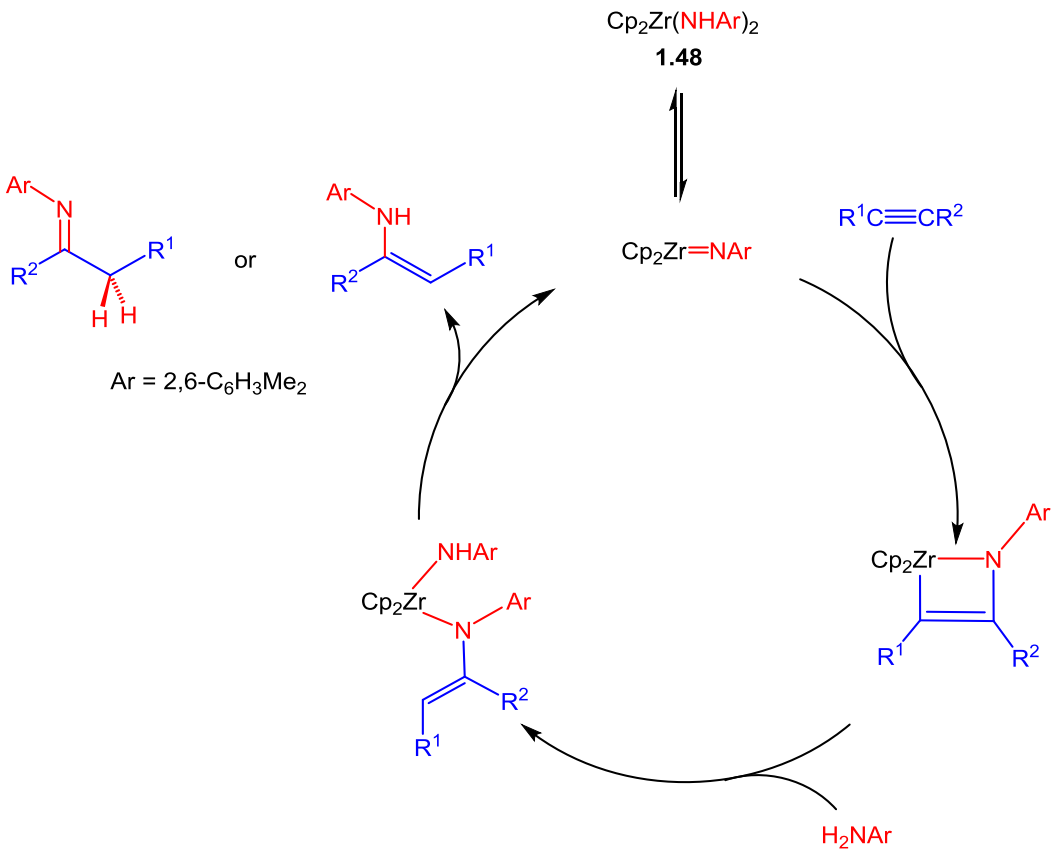

Scheme 1.7. Hydroamination catalytic cycle using exemplar $Cp_2Zr(NHXyl)_2$ (**1.48**) as a pre-catalyst.

Bergman and co-workers reported an effective zirconium pre-catalyst $Cp_2Zr(NHXyl)_2$ (**1.48**) in 1992, which can catalyse the coupling of alkynes, e.g. diphenylacetylene, 2-butyne, and allenes with H_2NXyl (Scheme 1.7) at 3 mol% catalyst loading at relatively high temperature (95 – 120 °C). The reversible α-elimination of enamine and generation of the transient imido complex $Cp_2Zr(NXyl)$ (**1.17**) was found to be the rate-determining step.[78,89,90] More recently, $Zr(NMe_2)_4$, $Cp_2Zr(NMe_2)_2$ and sulfonamide-supported zirconium complexes have also been shown to be effective hydroamination catalysts for allenes.[93] Only a few reports on the use of hafnium complexes as hydroamination catalysts have been reported recently.[94–96] An example is the NHC-supported diiodide complex $(CCC^{Bu})Hf(NMe_2)I_2$ (**1.49**, CCC^{Bu} = 2-(1,3-bis(N-butylimidazol-2-ylidene)-phenylene, Figure 1.5),[96] which is able to catalyse the intramolecular hydroamination/cyclisation of a range of aminoalkene substrates. However, in all of these reports, the hafnium catalysts were much less active than their zirconium congeners, presumably due to the stronger metal–ligand bonds in the former.

The titanium complexes, Cp*Ti($N^{3,5\text{-Xyl}}N^{pyr}$)(NXyl) (**1.31**) and Cp*Ti($N^{3,5\text{-Xyl}}N^{pyr}$)($N^{t}$Bu)(^{t}BuNH$_2$) (**1.33**), were also reported to catalyse the hydroamination of both terminal and internal alkynes over a period of 24 h at 5 mol% catalyst loading, and again similar to the zirconium analogues, high temperatures (105 °C) were required, and mixtures of linear and branched enamines were isolated.[29] The dimethyl compound Cp*Ti($N^{3,5\text{-Xyl}}N^{pyr}$)Me$_2$ was also found to be an active (intramolecular) hydroamination catalyst, whereby the imido species **1.31** and **1.33** are generated *in situ* upon addition of amine. Other active catalysts reported in the literature include Cp$_2$Ti(η^2-Me$_3$SiC$_2$SiMe$_3$),[82] Ti($N_2^{pyr}N^{Me}$)(NMe$_2$)$_2$ ($N_2^{pyr}N^{Me}$ = *N*,*N*-di(pyrrolyl-α-methyl)-*N*-methylamine)[20] and Ti(NMe$_2$)$_4$,[93,97,98] with the proposed catalytic cycles proceeding *via* imido intermediates in all cases.

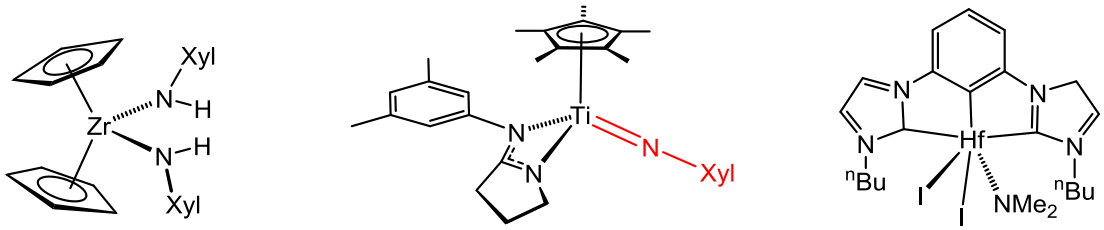

1.48 **1.31** **1.49**

Figure 1.5. Examples of Group 4 metal hydroamination catalysts.[29,89,96]

1.4 The hydrazido ligand

The terminal hydrazido complexes of transition metals have been known for as long as their imido counterparts. The initial research focused on the Group 6 hydrazido compounds, of the type (L)M=NNR$_2$, with a view to understand the fixation of nitrogen in biology.[99–103] Nevertheless, the chemistry of Group 4 terminal hydrazido complexes remained remarkably understudied until relatively recently.[20,27,80,104–125]

Hydrazido ligands can bind to transition metal centres through different coordinating modes which can be correlated with the variations of the formal ligand charge from –1 to –2, and the presence of an N$_\beta$R$_2$ group may also coordinate to a metal centre, as shown in Figure 1.6.[20] The favoured coordination mode is found to be influenced by several factors, including the identity of the metal, the N$_\beta$ substituents and the metal supporting ancillary ligand set. All the hydrazido(2-) ligands mentioned in the Thesis refer to the η^1-hydrazido(2-) variety, which are four-electron donors in the neutral ligand formalism and

isoelectronic with the imido ligand.[80,120] The nitrogen atoms are described as $M=N_{\alpha}\text{-}N_{\beta}R_2$ in all cases.

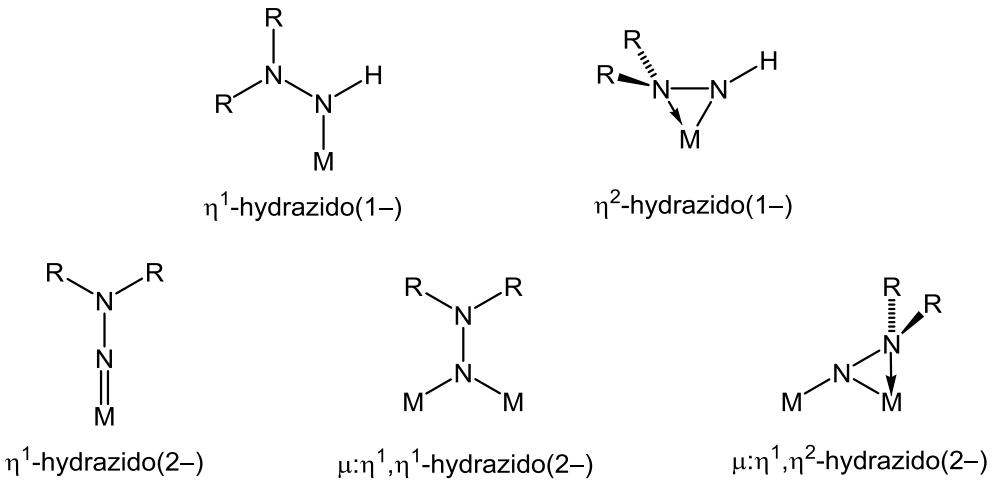

Figure 1.6. Coordinating modes of hydrazido ligands.

1.5 Group 4 hydrazido complexes

1.5.1 Synthesis of titanium hydrazido complexes

The first monomeric terminal hydrazido complex of titanium was reported in 1978 by Wiberg. It was synthesised through a silyl-transfer reaction between $CpTiCl_2$ and two equivalents of $Me_3SiN{=}NSiMe_3$.[126] However, due to the thermal instability of $Me_3SiN{=}NSiMe_3$, further studies and full characterisation were not carried out. In 1999, the first fully characterised terminal titanium hydrazide $Ti(NNPh_2)(Me_4taa)$ (**1.51**) was reported by our research group, *via* simple imido/hydrazine exchange from the imido compound $Ti(N^tBu)(Me_4taa)$ (**1.35**).[48] It was not until 2004 that the first structurally characterised terminal hydrazide, $Ti(N_2{}^{pyr}N^{Me})(NNMe_2)(^tBu\text{-bipy})$ (^tBu-bipy = 4,4'-di-*tert*-butyl-2,2'-bipyridine), was reported by Odom and co-workers.[20]

Mountford and co-workers reported the synthesis of hydrazido synthons $Ti(NNPh_2)Cl_2(py)_3$ (**1.52**) through imido/hydrazine exchange from $Ti(N^tBu)Cl_2(py)_3$ (**1.8**). The successful synthesis of the diphenylhydrazido synthon **1.52** allowed access to a wide range of diphenylhydrazido complexes.[114] However, attempts to synthesise the dimethylhydrazido analogue of **1.52** using H_2NNMe_2 resulted in the formation of dimeric complexes containing bridging dimethylhydrazido ligands.[114,120] For the diphenylhydrazido synthon **1.52**, subsequent salt metathesis reactions with lithiated

supporting ligands resulted in the formation of new hydrazide compounds. Selected examples, **1.53** – **1.56**, are shown in Scheme 1.8.[114]

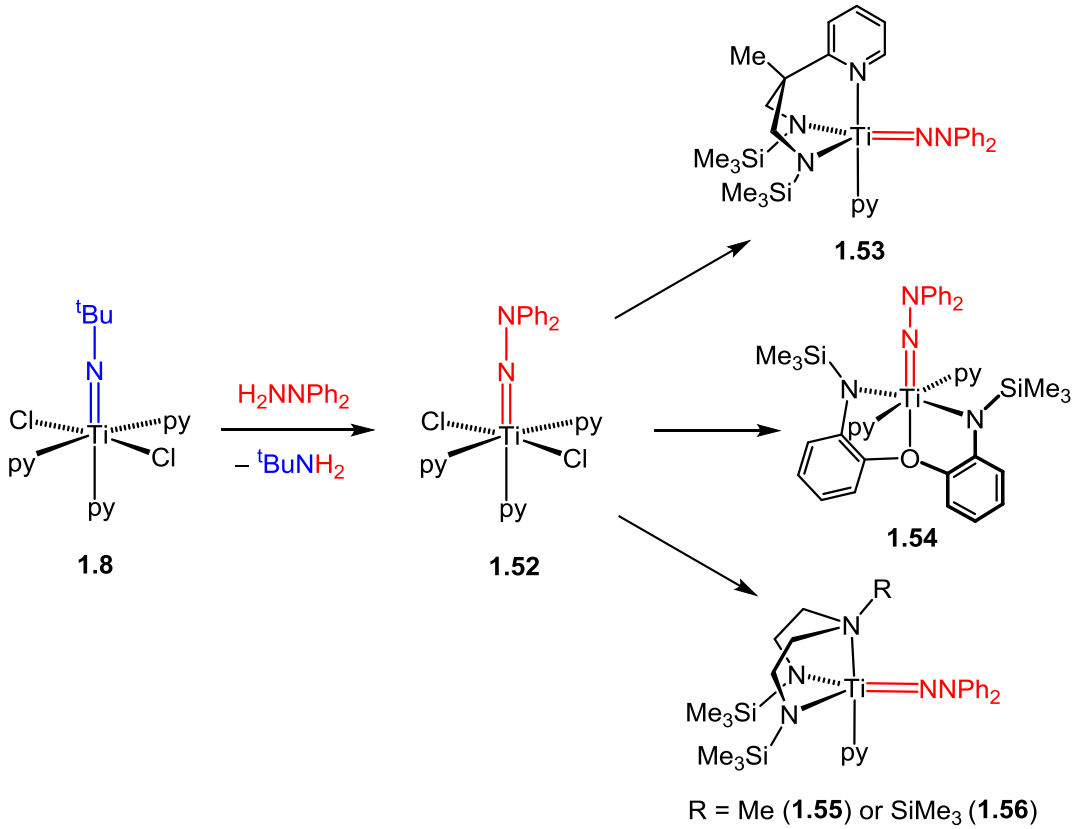

Scheme 1.8. Synthesis of $Ti(NNPh_2)Cl_2(py)_3$ (**1.52**) and examples of its salt metathesis reactions with lithiated ligands.[114]

In addition, cyclopentadienyl-amidinate-supported titanium hydrazido complexes have been developed and continue to be the focus of attention in our research group, due to the richness in reactivity of the hydrazido ligand and the relatively robust supporting ligands. Complexes with different substituents at N_β, namely $Cp^*Ti\{MeC(N^iPr)_2\}(NNRR')$ (R = R' = Me (**1.57**) or Ph (**1.58**); R = Me, R' = Ph (**1.59**) were synthesised by reacting the *tert*-butylimido compound **1.10** with the corresponding hydrazine. Other examples of cyclopentadienyl ligand-supported hydrazides including $Cp_2Ti(NNPh_2)(py)$ (**1.60**) and $Cp^*Ti(NNPh_2)Cl(py)$ (**1.61**) are shown in Figure 1.7, which are all prepared *via* the imido/hydrazine exchange route.[113]

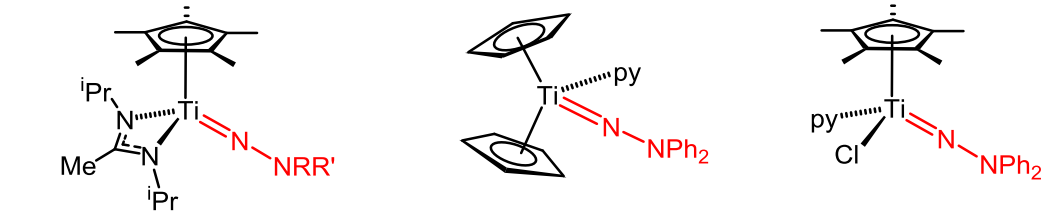

R = R' = Me (**1.57**) or Ph (**1.58**);
R = Me, R' = Ph (**1.59**)

1.60

1.61

Figure 1.7. Examples of Cp-supported titanium hydrazides.[80,113]

1.5.2 Synthesis of zirconium and hafnium hydrazido complexes

The first structurally characterised monomeric terminal zirconium hydrazido compound was reported by Bergman and co-workers in 1991.[121] The transient complex $Cp_2Zr(NNPh_2)$ (**1.62**) was generated *via* thermolysis of alkyl-hydrazido(1-) compound $Cp_2Zr(NHNPh_2)(CH_2CH_2{}^tBu)$ with concomitant loss of 2,2-dimethylbutane at relatively high temperature. In the presence of DMAP, the monomeric terminal product $Cp_2Zr(NNPh_2)$(DMAP) (**1.63**) was successfully isolated. However, in the absence of DMAP, **1.62** rapidly dimerises in solution to form a complex with bridging hydrazido ligands. However unlike the titanium hydrazide bridged dimers, the zirconium dimer can be cleaved to regenerate compound **1.63** by using excess DMAP and elevated temperatures. Compound **1.63** contains a short $Zr{=}N_\alpha$ bond of 1.873(7) Å, which is similar to that in the arylimido complex $Cp_2Zr(NAr')$(THF) (**1.50**, Zr=N = 1.888(2) Å).[72] It is consistent with the hydrazide group bonding in the same way to the imido ligands, donating up to four electrons to the metal centre, in competition with the cyclopentadienyl rings.

In 2007, Gade and co-workers reported the synthesis of the diamide-pyridine-supported hydrazide $Zr(N_2{}^{TBS}N^{py})(NNPh_2)(py)$ (**1.64**, $N_2{}^{TBS}N^{py}$ = MeC(2-$C_5H_4N)(CH_2NSiMe_2{}^tBu)_2$) from the reaction between $Zr(N_2{}^{TBS}N^{py})Cl_2$ and $LiNHNPh_2$, followed by dehydrohalogenation with $LiN(SiMe_3)_2$.[111] One year later, the first hafnium hydrazido compound $Hf(N_2{}^{TBS}N^{py})(NNPh_2)(py)$ (**1.65**) was prepared using the same method.[108] In contrast to titanium hydrazido synthons, for which a number of supporting ligands can be installed, corresponding zirconium and hafnium hydrazido synthons, of the type $Zr(NNPh_2)Cl_2(L)_x$, have not been reported. As for the synthesis of zirconium and hafnium imido analogues (Section 1.3.2), the desired ancillary ligands are usually added to the zirconium or hafnium prior to incorporation of the hydrazido ligand. For example,

$Zr(N_2^{3,5\text{-}Xyl}N^{py})(NMe_2)_2$ ($N_2^{3,5\text{-}Xyl}N^{py}$ = $MeC(2\text{-}C_5H_4N)(CH_2N\text{-}3,5\text{-}C_6H_3Me_2)_2$) was firstly prepared from the reaction between $Zr(NMe_2)_4$ and protioligand $H_2N_2^{3,5\text{-}Xyl}N^{py}$ *via* protonolysis. The second protonolysis reaction with two equivalents of cyclic hydrazines H_2NNR_2 in the presence of DMAP yielded the hydrazido compounds $Zr(N_2^{3,5\text{-}Xyl}N^{py})(NNR_2)(DMAP)_2$ (R = C_9H_{10} (**1.66**, Figure 1.8) or $C_{12}H_8$).[127] Modifying the ancillary ligand to $N_2^{ArF}N^{py}$ ($MeC(2\text{-}C_5H_4N)(CH_2NAr^F)_2$), with electron-withdrawing aryl substituents at the N_{amide} atoms, interestingly led to the formation of the difluoride compound $Zr(N_2^{TFAP}N^{py})F_2$ (**1.67**, $N_2^{TFAP}N^{py}$ = $MeC(2\text{-}C_5H_4N)\{CH_2N(2\text{-}C_6F_4NMe_2)\}_2$) at 90 °C.[128] Compound **1.67** is formed from the exchange of one of the *ortho*-fluorine substituents on both aryl rings with a dimethylamido group. However, the zirconium hydrazido compound, $Zr(N_2^{TFAP}N^{py})(NNPh_2)$, can be still obtained from the reaction between **1.67** and $LiNHNPh_2$ and then $LiN(SiMe_3)_2$.

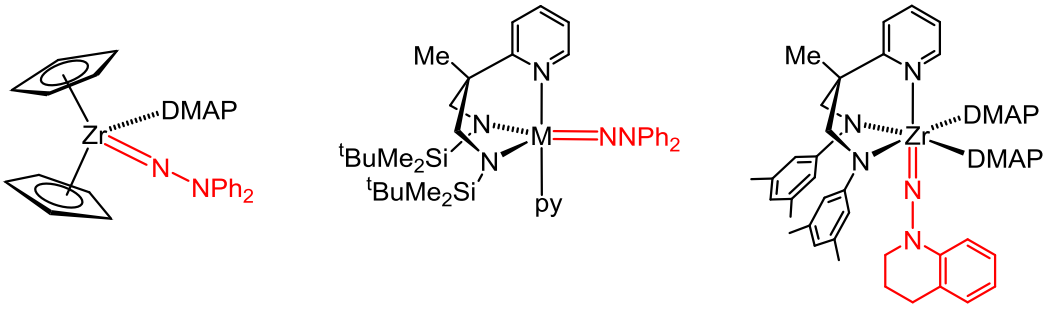

1.63 M = Zr (**1.64**), Hf (**1.65**) **1.66**

Figure 1.8. Examples of zirconium and hafnium hydrazido complexes.[108,111,121,127]

1.5.3 Stoichiometric reactions involving the M=N_α bond

Group 4 hydrazido compounds show fruitful reactivity with small molecules. The first step commonly happens at the M=N_α multiple bond through a [2+2] cycloaddition, as the reaction for Group 4 imides, and the products of this initial cycloaddition can be isolated and characterised in many cases. Subsequent reactions can also occur, for example, insertion of a second substrate into the now single M–N_α bond, or extrusion of an organic compound.

Mountford and co-workers reported the first example of isolable [2+2] cycloaddition addition products resulting from the reactions between the macrocycle-supported complex $Ti(NNPh_2)(Me_4taa)$ (**1.51**) and CO_2 or TolNCO, albeit, without authenticated structures.[48] The first structurally authenticated metallacyclic product $Cp_2Ti\{N(NPh_2)PC(^tBu)\}$ was isolated by reacting the sandwich compound

$Cp_2Ti(NNPh_2)(py)$ (**1.60**) with ^tBuCP *via* [2+2] cycloaddition, and it is the first reported reaction of a hydrazido compound with a phosphaalkyne.[115]

Shortly after the early study, the stoichiometric reactivity of titanium hydrazido compounds was developed rapidly. The cyclopentadienyl-amidinate-supported hydrazido compounds $Cp^*Ti\{MeC(N^iPr)_2\}(NNR_2)$ (R = Me (**1.57**) or Ph (**1.58**)) exhibit rich reactivity with small unsaturated molecules, as for the imido analogues. Selected reactions and their products are shown in Scheme 1.9. The carbamate-type compounds **1.68** were formed first by reacting with CE_2 (E = O or S) *via* [2+2] cycloaddition. For E = O, "double insertion" complexes **1.69** were eventually formed, resulting from the second insertion of CO_2 into the now single Ti–N_α bond.[80] Compound **1.57** and **1.58** also reacted with RNCE (R = alkyl or aryl, E = O or S) to give [2+2] cycloaddition products, resulting, however, in different reaction outcomes. The reaction between the diphenylhydrazido compound **1.58** and either alkyl or aryl isocyanates yielded isolable cycloaddition products **1.74**. However, for **1.57** elimination of the carbodiimide $^tBuNCNNMe_2$ (**1.70**) or cyclic $N(Me)_2NC(NAr')N(Ar')C(O)$ (**1.71**), from the inherently unstable cycloaddition intermediates, occurred more readily, forming the oxo-bridged dimer $[Cp^*Ti\{MeC(N^iPr)_2\}(\mu\text{-}O)]_2$ (**1.72**) as the organometallic product. The higher propensity of alkyl substituted hydrazides to eliminate organic fragments mirrors the trend found in imido chemistry. Interestingly, reacting **1.57** with two equivalents of TolNCO yielded $Cp^*Ti\{MeC(N^iPr)_2\}\{OC(NNMe_2)N(Tol)C(NTol)O\}$ (**1.73**), which followed the same cycloadditon-extrusion pathway as with Ar'NCO and ^tBuNCO. However, in this case, rapid cycloaddition of the extruded organic fragment to Ti=O (instead of dimerization) formed $Cp^*Ti\{MeC(N^iPr)_2\}\{N(Tol)C(NNMe_2)O\}$ (not observed), which then gave **1.73** by reacting with a second equivalent of TolNCO.

Corresponding [2+2] cycloaddition reactions of the zirconium hydrazido compound $Zr(N_2{}^{TBS}N^{py})(NNPh_2)(py)$ (**1.64**) with MesNCS and PhNCS were described by Gade and co-workers. The products were isolated with the new ligands bound in a κ^2-N,S-fashion.[122] The cycloaddition reaction of compound **1.64** and the hafnium congener **1.65** with alkyl- or aryl-substituted allenes were also reported, proceeding through Markovnikov regioselectivity in both cases. In addition, compound **1.64** gave [2+3] cycloaddition with organic azides forming azazirconacyclopentene-type complexes, which are the first compounds of any metal containing that functional group.[106]

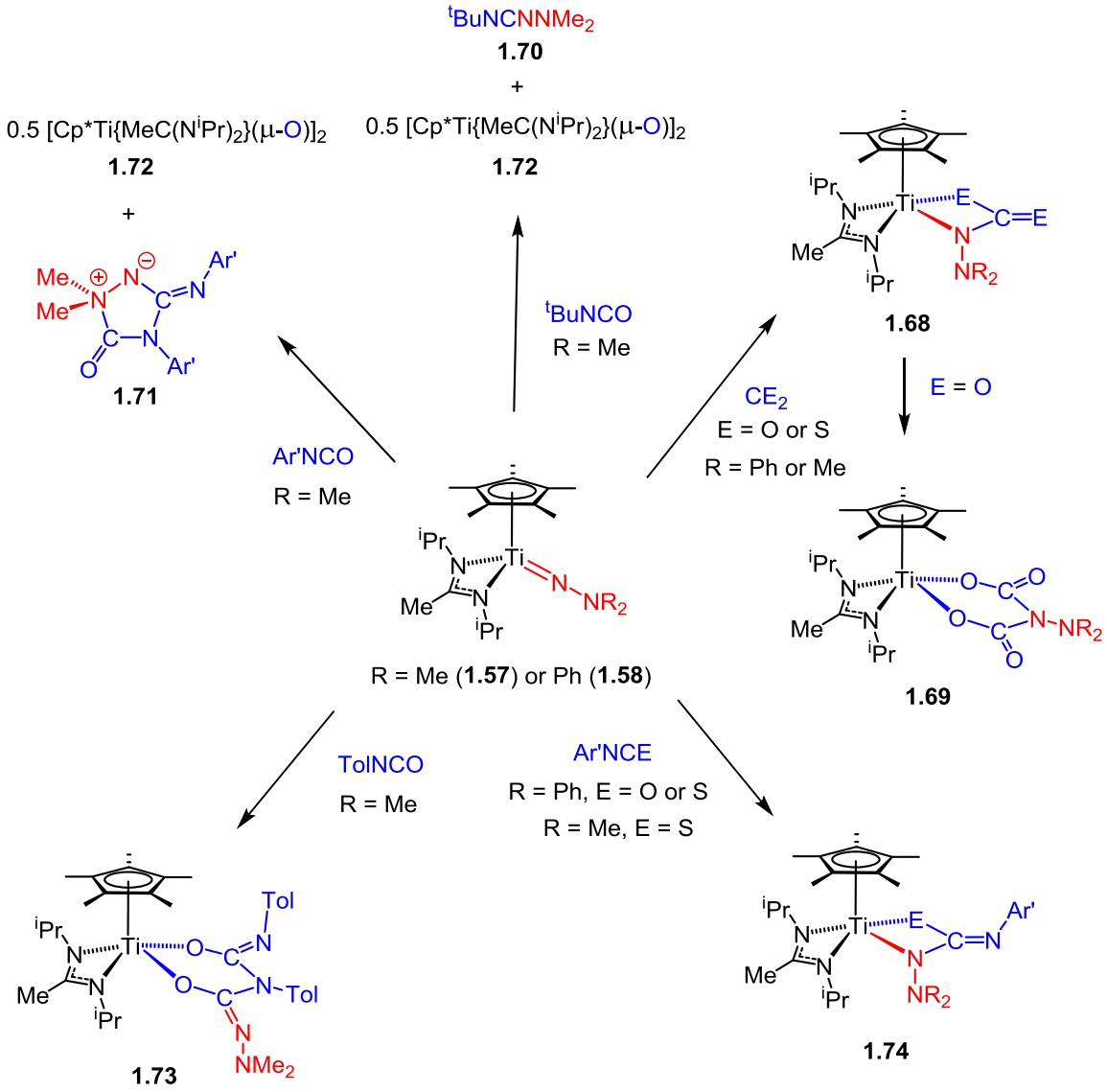

Scheme 1.9. Reactions of Cp*Ti{MeC(N^{i}Pr)$_2$}(NNR$_2$) (R = Me (**1.57**) or Ph (**1.58**) with unsaturated substrates.[80]

The half-sandwich compounds **1.57** and **1.58** showed no reactions with alkynes. In contrast, the more open cyclopentadienyl-amidinate-supported compound Cp*Ti(N$^{3,5\text{-Xyl}}$N^{pyr})(NNMe$_2$)(DMAP), reported by Gade, reacted with HCCPh yielding Cp*Ti(N$^{3,5\text{-Xyl}}$N^{pyr}){N(NMe$_2$)C(Ph)C(H)} stoichiometrically, in which the C(H) carbon is bound to titanium as the Markovnikov type regioisomer. This is due to the steric bulk of the Cp*-amidinate supporting ligand set preventing the alkyne from approaching from the other orientation (anti-Markovnikov).[27] However, the anti-Markovnikov regioisomer was calculated to be the electronically favoured product with the C(Ph) bound to titanium. This was found for the diamide-pyridine-supported analogue Ti(N$_2$N^{py})(NNPh$_2$)(py) (**1.53**), which exclusively yielded anti-Markovnikov regioisomers, of the type

Ti(N_2N^{py}){N(NPh_2)C(R)C(Ar)} (**1.75**, Ar = phenyl or substituted phenyl; R = H or Me, Equation 1.1), upon reaction with either terminal or internal alkynes.[129]

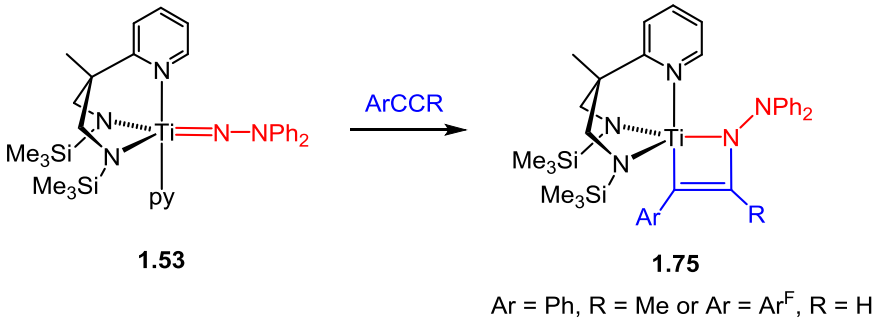

1.53 **1.75**

Ar = Ph, R = Me or Ar = Ar^F, R = H

Equation 1.1[129]

1.5.4 Stoichiometric reactions involving N_α–N_β bond cleavage

As well as the rich reactivity at the M=N_α bond being exhibited above, Group 4 hydrazido compounds also undergo reductive cleavage of the relatively weak N_α–N_β bond with oxidisable substrates such as isonitriles. These types of reactions are obviously inaccessible for the analogous imido complexes. For example, N_α–N_β bond cleavage reactions were observed during the reaction of diamide-donor-supported compounds Ti(N_2N^{py})($NNPh_2$)(py) (**1.53**) or Ti($N_2^{SiMe_3}N^{Me}$)($NNPh_2$)(py) (**1.55**) with one equivalent of XylNC, yielding Ti(N_2N^{py})(NPh_2)(NCNXyl) and Ti($N_2^{SiMe_3}N^{Me}$)(NPh_2)(NCNXyl) (**1.76**, Figure 1.9), respectively.[130] DFT calculations indicated that the first step was the loss of pyridine, followed by the formation of an isonitrile adduct prior to the formation of a three-membered intermediate which is supported by coordination of the N_β atom to the metal centre, and subsequently resulted in facile N_α–N_β bond cleavage to form the final product.[130] This isonitrile insertion reaction had previously been reported for analogous zirconium hydrazido compound Zr($N_2^{TBS}N^{py}$)($NNPh_2$)(py) (**1.64**) with ^{t}BuNC, and was later reported for the reaction of Ti($N_2^{SiMe_3}O$)($NNPh_2$)($py)_2$ (**1.77**, $N_2^{SiMe_3}O$ = $O(CH_2CH_2NSiMe_3)_2$) with ^{t}BuNC.[131] Compound **1.77** also reacted with XylNC, but this reaction required two equivalents of substrates. The first equivalent XylNC resulted in N_α–N_β bond cleavage as above, and the second equivalent inserted in a Ti–N_{amide} bond of the supporting ligand, eventually affording the final product **1.78** after $SiMe_3$ group migration (Figure 1.9). Compound **1.64** also underwent N_α–N_β bond cleavage reaction with propylene sulfide or Ph_3PSe,

forming the dimeric compounds {Zr($N_2^{TBS}N^{py}$)(NPh_2)}$_2$(μ-N_2E) (E = S (**1.79**) or Se (**1.80**), Figure 1.9).[111]

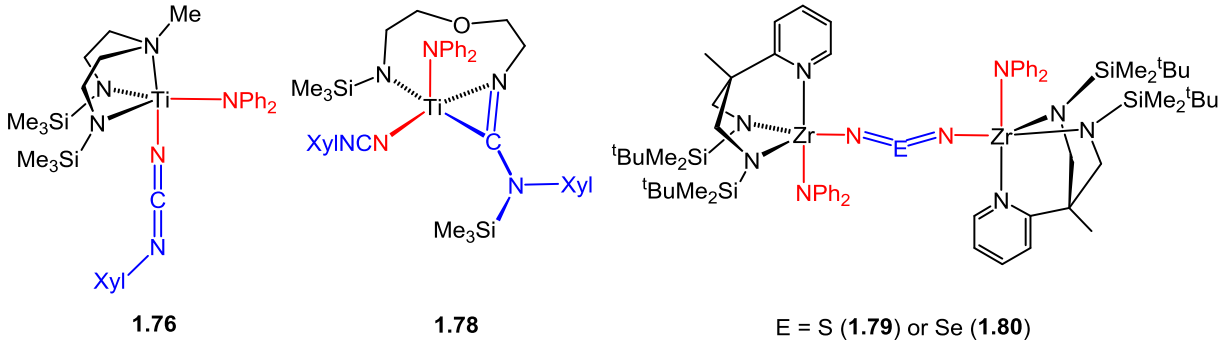

Figure 1.9. N_α–N_β bond cleavage products of Group 4 hydrazido compounds.[111,130,131]

These isonitrile-induced N_α–N_β bond cleavage reactions are reminiscent of an early example of zirconium hydrazide reactivity reported by Bergman and co-workers in 1991. The *in situ*-generated transient intermediate $Cp_2Zr(NNPh_2)$ (**1.62**) reacted with CO, proceeding through N_α–N_β bond cleavage, forming the mixed amide/metallated isocyanate $Cp_2Zr(NCO)(NPh_2)$ (**1.81**, Scheme 1.10) which could be prepared independently by reacting $Cp_2Zr(NPh_2)Cl$ with AgNCO.[121] The transient intermediate **1.62** also underwent N_α–N_β bond cleavage upon reaction with symmetrical internal alkynes RCCR (R = Et, Ph or Tol), followed by C–H bond activation to yield the 7-membered ring complexes $Cp_2Zr(N(H)C(R)C(R)$-1,2-$C_6H_4N(Ph)\}$(**1.82 – 1.84**), and upon treatment with aqueous HCl, the corresponding *N*-phenylindoles were formed. Similar seven-membered metallacycles were reported from the reaction between the diamide-pyridine-supported zirconium hydrazide **1.64** and internal alkynes. However, when MeCCMe was used, the vinylimido compound Zr($N_2^{TBS}N^{py}$)\{NC(Me)C(Me)NPh_2\}(py) was formed (which represents insertion of the alkyne into the N_α–N_β bond), alongside the seven-membered cyclic species in equal amounts.[104]

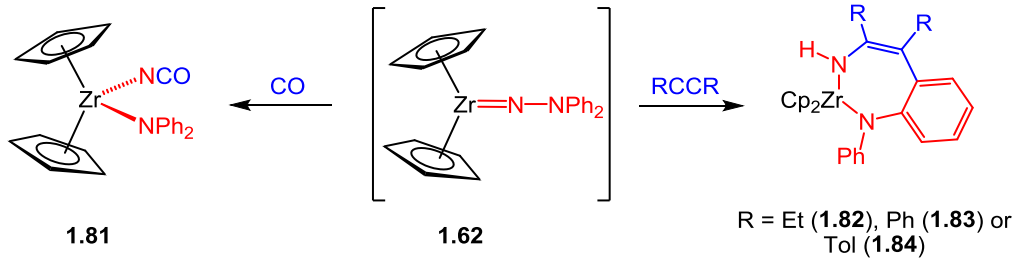

Scheme 1.10. Reactions of $Cp_2Zr(NNPh_2)$ (**1.62**) with CO and internal alkynes.[121]

Following on from the cycloaddition reactions of alkynes with Ti(N_2N^{py})($NNPh_2$)(py) (**1.53**) to give metallacycles **1.75** as described in the previous Section 1.5.3, the azametallacyclic product Ti(N_2N^{py}){N(NPh_2)C(Me)C(Ph)} (**1.75**) further converted to the vinylimido compound Ti(N_2N^{py}){NC(Ph)C(Me)NPh_2}(py), in the presence of pyridine after 3 days at RT.[115] Similar reactions were reported between Ti($N_2^{SiMe_3}N^{Me}$)($NNPh_2$)(py) (**1.55**) and a range of internal alkynes to yield analogous vinylimido products Ti($N_2^{SiMe_3}N^{Me}$){NC(R)C(Me)NPh_2} (**1.85**, R = alkyl or aryl).[129] However, when compound **1.55** reacted with diarylalkynes ArCCAr (Ar = Ph or 4-C_6H_4OMe), the products Ti{MeN($CH_2CH_2NSiMe_3$)(CH_2CH_2NH)}-{N($SiMe_3$)C(Ar)C(Ar)-1,2-C_6H_4N(Ph)} (Ar = Ph (**1.88**) or 4-C_6H_4OMe (**1.89**)) were observed alongside the expected vinylimido compounds Ti($N_2^{SiMe_3}N^{Me}$){NC(Ar)C(Ar)NPh_2}(py) (Ar = Ph (**1.86**) or 4-C_6H_4OMe (**1.87**)). The compounds **1.88** and **1.89** are expected to follow the same mechanism as **1.82 – 1.84** described above, followed by a 1,3-$SiMe_3$ sigmatropic shift (Figure 1.10).

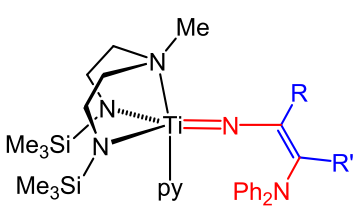

R = alkyl or aryl, R' = Me (**1.85**)

R = R' = Ph (**1.86**) or 4-C_6H_4OMe (**1.87**)

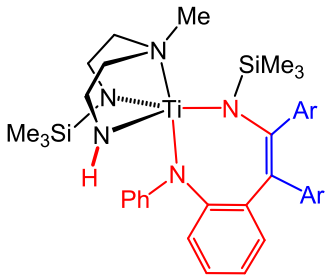

Ar = Ph (**1.88**) or 4-C_6H_4OMe (**1.89**)

Figure 1.10. Reaction products of Ti($N_2^{SiMe_3}N^{Me}$)($NNPh_2$)(py) (**1.55**) with alkynes.[129]

1.5.5 Catalytic reactions

As the Group 4 imido compounds have been widely used as effective catalysts for the hydroamination of alkynes, described in Section 1.3.5, naturally a substantial body of work has evolved studying the possible catalytic reactions of terminal Group 4 hydrazido compounds. Firstly, a direct extension of hydroamination catalysis known as hydrohydrazination, in which the N–H bonds of an N,N-disubstituted hydrazine add across the C≡C bond of an alkyne to form hydrazones, has received much attention, and several examples have been reported.[20–22,26,27,81,82] Similar to hydroamination, hydrohydrazination is postulated to proceed *via* metallacycles of the type **1.90** which can then undergo protonolysis of the Ti–C and Ti–N bonds to form hydrazones (**1.91**) upon

addition of an equivalent of hydrazine (Scheme 1.11). The second step of this catalytic cycle is proposed to proceed through a transient mixed bis(hydrazido(1-)) intermediate, in analogous to the mechanism for hydroamination shown in Scheme 1.7.

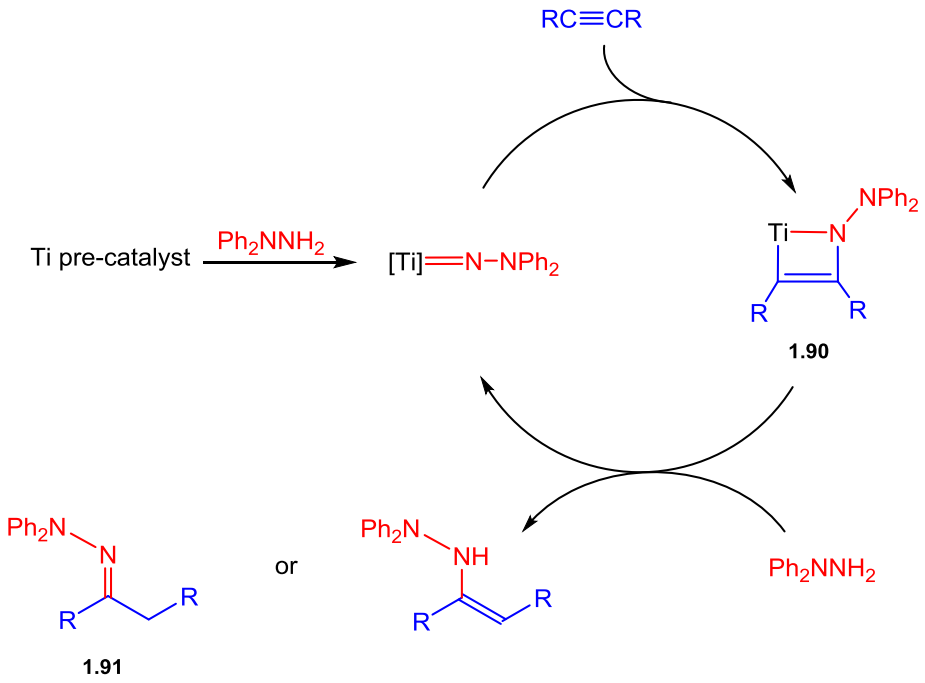

Scheme 1.11. Titanium catalysed hydrohydrazination using 1,2-diphenylhydrazine and an alkyne.

Elevated temperatures (> 75 °C) and long reaction times (2 – 75 h) have been typically found to be necessary for these catalytic reactions, in which harsher conditions are required for internal alkynes. In many cases, the active hydrazido catalysts are synthesised *in situ* from the reaction between the corresponding diamide pre-catalyst (L)Ti(NMe_2)$_2$ and hydrazine.[21,22,26,81] The compounds Cp*Ti($N^{3,5\text{-}Xyl}N^{pyr}$)(NNRR')(L) (R = R' = Ph or Me; R = Ph, R' = Me; L = py, DMAP or H_2N^tBu), reported by Gade in 2011, were found to catalytically produce hydrazones *via* the hydrohydrazination reaction with a range of alkynes. The reactions were quantitative within 1 h with a catalyst loading of 5 mol% at ambient temperature, the products exhibiting Markovnikov regioselectivities of > 99%.[27] In some cases, other small nitrogen containing molecules can be catalytically produced from further reaction of the hydrazones. For example indoles,[20,22,23,81,82] pyrroles[81] and tryptamines[24] have been described *via* cyclisation reaction, which usually require the addition of an external Lewis acid, such as $ZnCl_2$.

Furthermore, an iminohydrazination reaction has been developed by Odom using the pre-catalysts **1.92** and **1.93** (Figure 1.11), where an alkyne, a hydrazine and an isocyanide are coupled in a single reaction through *in situ* generated titanium hydrazido compound forming a 1,3-iminohydrazone.[25,119] This catalytic progress was further developed by using the pre-catalyst $Ti(NMe_2)_2(pypyr)_2$ (**1.94**, Hpypyr = 2-(2'-pyridyl)-3,5-dimethylpyrrole, Figure 1.11), which is employed in the multicomponent coupling of alkynes, isonitriles and monosubstituted hydrazines to yield pyrazoles in a single step without the need for an external Lewis acid.[132]

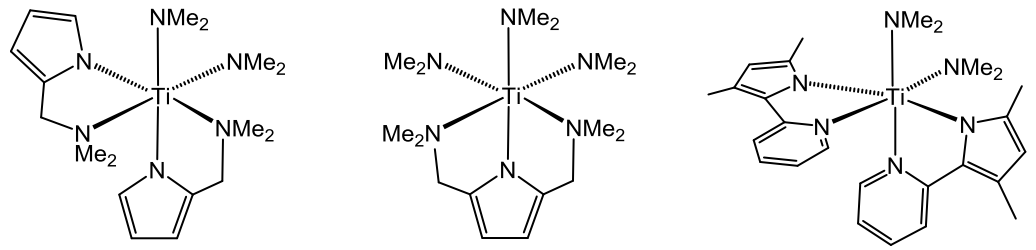

1.92 **1.93** **1.94**

Figure 1.11. Titanium pre-catalysts for iminohydrazination process.[25,119,132]

As discussed in Section 1.5.4, the diamide-amine supported titanium hydrazido compound of $Ti(N_2^{SiMe_3}N^{Me})(NNPh_2)(py)$ (**1.55**) reacted with a range of internal alkynes *via* N_α–N_β bond insertion to yield vinylimido compounds of the type **1.85**.[129] Subsequently, the starting hydrazide can be regenerated by addition of one equivalent of Ph_2NNH_2, along with the organic product $RC(NH_2)C(Me)NPh_2$ (Equation 1.2). This was the first example of such transformation of alkynes and hydrazines, and the reactions can be performed catalytically from either **1.55** or **1.85** with the overall result being the 1,2-diamination of alkynes, which is a previously unknown reaction.

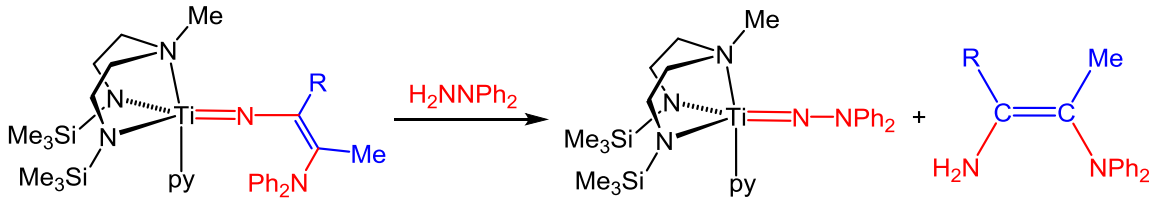

1.85
R = alkyl or aryl

1.55

Equation 1.2[129]

Subsequent work has been carried out in our research group to elucidate the full mechanism of this novel 1,2-diamination, and extension of the scope of alkynes and hydrazines is found to be successful.[133,134] Recent work has also shown that replacing the $-SiMe_3$ substituents on the N_{amide} atoms of the ancillary ligand in **1.55** with the less sterically demanding $-^{i}Pr$ substituents resulted in a switch in the type of catalysis of alkynes and hydrazines, back to the more usual hydrohydrazination.[135]

1.6 Group 4 alkoxyimido complexes

A wide range of Group 4 imido and hydrazido compounds with a variety of different supporting ligands have been prepared, which exhibit rich reactivity with small molecules, including catalytic C–N bond formation. These prompted recent work in our research group investigating new imido-type functionalities with different heteroatoms bound to N_α. The work then was focused on the use of oxygen as the heteroatom to prepare alkoxyimido complexes, of the type M=NOR, with the aim in this case to discover novel C–O bond forming processes.

In 2011, the first Group 4 alkoxyimide $Ti(NO^{t}Bu)Cl_2(NHMe_2)_2$ (**1.95**) was successfully prepared from the reaction between $Ti(NMe_2)_2Cl_2$ and $H_2NO^{t}Bu$, which is analogous to its imido and hydrazido counterparts.[136,137] Installation of a range of neutral tridentate ligands resulted in the corresponding dichloride compounds $Ti(NO^{t}Bu)Cl_2(L)$ (L = $Me_3[9]aneN_3$, $HC(Me_2pz)_3$ (Me_2pz = 3,5-dimethylpyrazolyl) and $Me_3[6]aneN_3$ (trimethyl-1,3,5-triazacyclohexane, **1.96**). In an attempt to add $H_2NO^{t}Bu$ into $Ti(N^{t}Bu)Cl_2(py)_3$, proceeding through *tert*-butylimide/alkoxyamine exchange, did not clearly give the desired alkoxylimido analogue $Ti(NO^{t}Bu)Cl_2(py)_3$ (**1.97**), and neither could this be formed through direct addition of pyridine to **1.95**. However, compound **1.97** could be obtained by reaction of **1.96** with neat pyridine, releasing the free neutral tridentate ligand (Scheme 1.12).

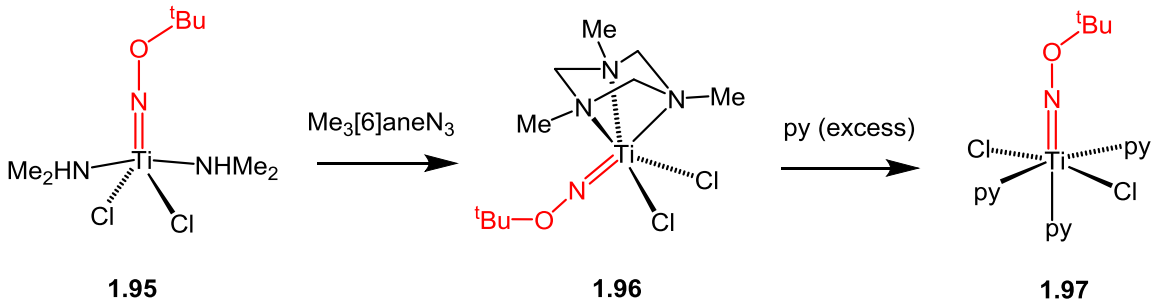

1.95 **1.96** **1.97**

Scheme 1.12. Synthesis of the titanium alkoxyimido synthon $Ti(NO^tBu)Cl_2(py)_3$ (**1.97**).[137]

As discussed previously for the imido and hydrazido analogues, compound **1.97** was found to be a useful synthon for the installation of a range of lithiated ligand sets *via* salt metathesis reactions, and several titanium alkoxyimides were successfully synthesised. The diamide-amine-supported complex $Ti(N_2^{SiMe_3}N^{Me})(NO^tBu)(py)$ (**1.98**) formed in such way, reacted with PhCCMe to give N–O bond cleavage yielding **1.99**, but this also accompanied by ligand degradation (Equation 1.3).[136] Unfortunately, this activation of the supporting ligand of **1.98** (and its homologues) prevented the possibility of developing catalytic processes based on this reaction.

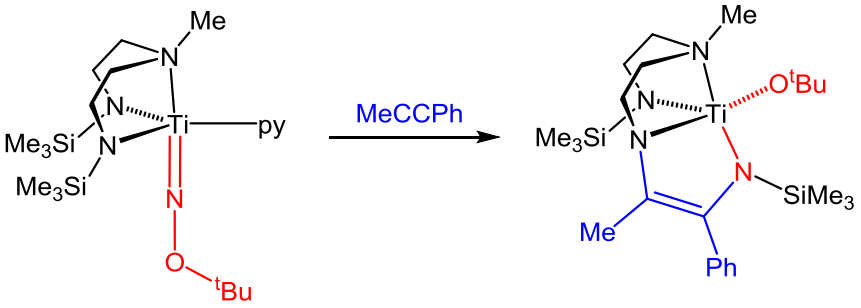

1.98 **1.99**

Equation 1.3[136]

Encouraged by the wealth of reactivity exhibited with both the imido and hydrazido cyclopentadienyl-amidinate supported compounds, the preparation of an alkoxyimido analogue was targeted, in order to further investigate the reactivity of this functional group. By analogy with the preparation of hydrazido analogue **1.58** in Section 1.5.1, the titanium alkoxyimide $Cp^*Ti\{PhC(N^iPr)_2\}(NO^tBu)$ (**1.100**) was synthesised *via* a *tert*-butoxyamine/*tert*-butylimide exchange reaction from the corresponding imido compound.[138] The reaction of compound **1.100** with CS_2, isocyanates, aldehydes, ketones and nitriles have been reported, and is the only detailed reactivity study of an

alkoxyimido compound to date. However, the reactivity of **1.100** was generally not found to differ substantially from that of its imido and hydrazido analogues.

Interestingly, however, the reaction of compound **1.100** with the terminal alkyne $HCCAr^F$ gave quantitative formation of the seven-membered cyclic product $Cp^*Ti(O^tBu)\{NC(Ar^F)C(H)N(^iPr)C(Ph)N(^iPr)\}$ (**1.101**, Equation 1.4).[138] The mechanism of formation of **1.101** involves an initial [2+2] cycloaddition across $Ti=N_\alpha$, prior to the N–O bond cleavage to form an azirinyl intermediate, which in turn undergoes nucleophilic attack by one of the amidinate nitrogens to give the final product **1.101**. Unfortunately, attempts to react **1.100** with internal alkynes, such as MeCCPh and $MeCC\text{-}4\text{-}C_6H_4CF_3$, resulted only in complicated mixtures of products.[138]

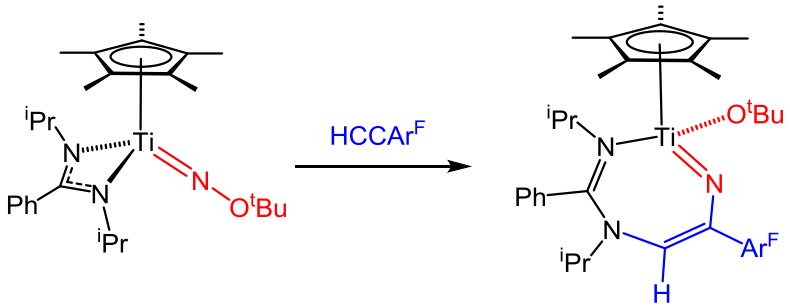

1.100 **1.101**

Equation 1.4[138]

1.7 Transition metal borylimido complexes

The substitution of boron as the heteroatom, of the type BR_2, at the N_α atom of a metal–nitrogen multiple bonded functional group forms a borylimido moiety. Until recent work in our research group,[139,140] only a handful of transition metal complexes containing a terminal borylimido ligand have been reported. These reported borylimido complexes were sometimes prepared through serendipitous N–B couplings, or (more rationally) through an oxidative route using a borylazide, and there had been no reported reactivity of any borylimido complex with small molecules.

In 1993, Wilkinson and co-workers reported the first borylimido complex, namely $W\{NB(Mes)_2\}_2Cl_2(PMe_3)_2$ (**1.102**, Figure 1.12), from the reaction between the tungsten (+2) complex $WCl_2(PMe_3)_4$ and two equivalents of Mes_2BN_3 *via* an oxidative process, along with formation of two equivalents of N_2.[141] In 2003, two further borylimido complexes, reported by Sundermeyer and co-workers, were prepared using the same

oxidative methodology. The reaction between the bis(imide) $W(NMes)_2(PMe_3)_3$ and Mes_2BN_3 yielded the mixed borylimido-bis(arylimido) complex $W\{NB(Mes)_2\}(NMes)_2(PMe_3)_2$ (**1.103**, Figure 1.12), and the reaction between the vanadium(+3) complex $VMes_3(THF)$ and Mes_2BN_3 yielded the vanadium(+5) borylimide $V\{NB(Mes)_2\}(Mes)_3$ (**1.104**, Figure 1.12).[142]

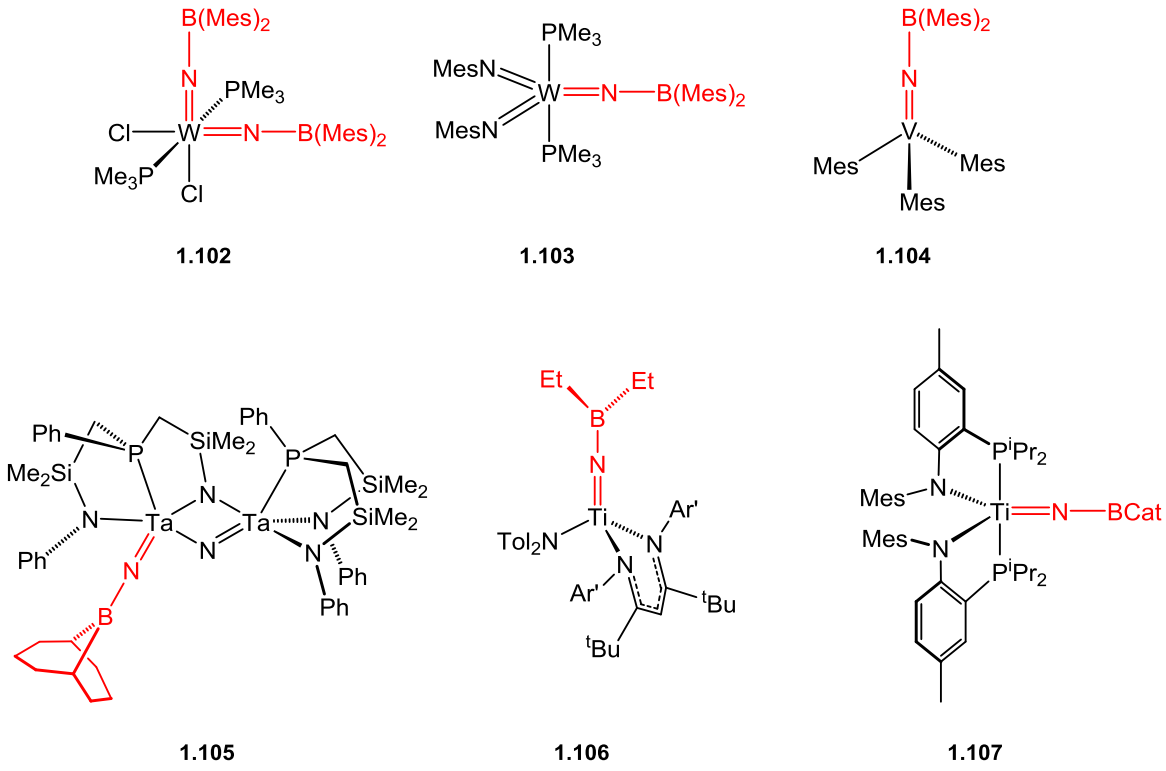

Figure 1.12. Previously reported terminal borylimido complexes.[141–144]

Two further terminal borylimido complexes were reported through investigations of dinitrogen reactivity with organoboranes. Fryzuk and co-workers reported the formation of the "BBN-imido" complex **1.105** from the rearrangement of a 9-BBN adduct of a tantalum dinitrogen complex (Figure 1.12).[143] This borylimido ligand of **1.105** remained intact with further addition of another equivalent of 9-BBN monomer. However, its bridging nitride atom reacted with the 9-BBN monomer to form a Lewis acid-base adduct. Similarly, Semproni and Chirik reported the formation of bridging borylimido bimetallic zirconocene and hafnocene complexes through the rearrangement of a BPin (Pin = $O_2C_2Me_4$) adduct of the respective bridging-dinitrogen complex.[145]

The first Group 4 terminal borylimido complex (^{tBu}NacNac)Ti($NBEt_2$)($NTol_2$) (**1.106**, Figure 1.12) was reported by Mindiola and co-workers in 2014, through a serendipitous

reaction of the parent imido (terminal NH) compound with two equivalents of $NaHBEt_3$.[144] Three years later, they reported another titanium borylimido complex $(PN)_2Ti(NBCat)$ (**1.107**, Cat = $O_2C_6H_4$, PN = *N*-(2-(diisopropylphosphino)-4-methylphenyl)-2,4,6-trimethylanilide) from the salt metathesis reaction of a dinuclear nitride complex with ClBCat.[146] In 2015, our research group communicated the preparation of a second terminal titanium borylimido complex through the reaction of a diphenyl- or dimethylhydrazide (**1.57** or **1.58**, respectively) with one equivalent of 9-BBN dimer (Equation 1.5).[71,147] A computational study of **1.108** has been performed, confirming the presence of a Ti–N triple bond ($\sigma^2\pi^4$), in which two Ti–N π interactions were found by MO and NBO analyses, and one of the π interaction is significantly stabilised by delocalisation into the otherwise vacant 2p AO of boron.[147]

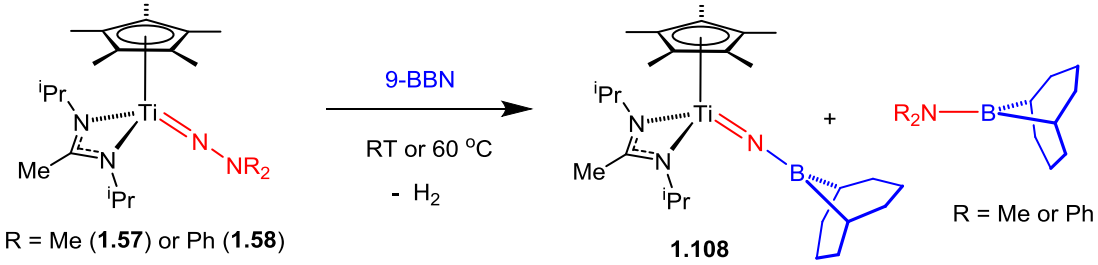

Equation 1.5[147]

More recently, our research group focused on the preparation of titanium borylimido complexes, in particular, using an imide/amine exchange reaction as discussed above. Preliminary attempts between a *tert*-butylimide and conventional dialkyl- or diarylborylamines, such as H_2NBMes_2 and $H_2NBC_8H_{14}$, using protonolysis methodologies did not give the desired borylimido products.[148] However, the preparation of the half-sandwich borylimido compound Cp*Ti{NB(NAr'CH)$_2$}Cl(py) (**1.109**) *via* a *tert*-butylimido/borylamine ($H_2NB(NAr'CH)_2$ (**1.110**)[149]) exchange reaction was ultimately achieved through a reaction in the melt, assisted by removal of H_2N^tBu by dynamic vacuum (Equation 1.6).[140,148] DFT calculations find that Ti–N_{im} bonds for borylimides are stronger and more covalent than in their organoimido or hydrazido analogues, and are strongest for alkyl- and arylborylimides. Borylamine/*tert*-butylimide exchange reactions fail for H_2NBR_2 (R = hydrocarbyl) but not for $H_2NB(NAr'CH)_2$ (**1.110**) because the increased strength of the new Ti–N_{im} bond for the former is outweighed by the increased net H–N bond strengths in the borylamine. Meanwhile, variation of the Ti–N_{im} bond length over short distances is dominated by π-bonding with

any suitable orbital on the N_{im} atom substituent. However, over the full range of imides and hydrazides studied, overall bond energies do not correlate with bond length but with the Ti–N_{im} σ-bond character and the orthogonal π-interaction, which is dominated by the electron-donating or –withdrawing ability of the N_{im} substituent.[140]

The installation of the amidinate [MeC($N^{i}Pr$)$_2$] into the coordination sphere of **1.109**, which has been used in the hydrazido analogues **1.57** and **1.58**, was unsuccessful here. This is ascribed to insurmountable steric constraints of this borylimido species. However, the employment of less bulky Li[hpp] (Hhpp = 1,3,4,6,7,8-hexahydro-pyrimido[1,2-*a*]pyrimidine) and Li$N^{pyr}N^{Me_2}$ ($N^{pyr}N^{Me_2}$ = Me_2NCH_2(2-NC_4H_3)) yielded Cp*Ti(hpp){NB(NAr'CH)$_2$} and Cp*Ti($N^{pyr}N^{Me_2}$){NB(NAr'CH)$_2$}, respectively.[140]

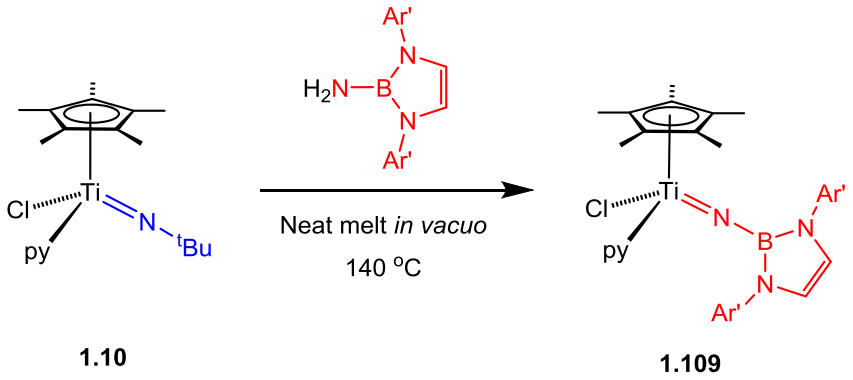

1.10 **1.109**

Equation 1.6[140]

As was found in the failed borylamine/*tert*-butylimide exchange reactions, the double-deprotonation reactions of H_2NBMes_2 and $H_2NBC_8H_{24}$ with various reagents also appeared experimentally unfeasible. However, successful preparation of the first non-cyclopentadienyl titanium borylimido synthon Ti{NB(NAr'CH)$_2$}Cl_2($NHMe_2$)$_2$ (**1.111**) was found from the reaction of **1.110** with Ti(NMe_2)$_2Cl_2$ (**1.11**), by analogy with the reactions with anilines described in Section 1.3.1. The DFT reactions of Ti(NMe_2)$_2Cl_2$ with H_2NPh, $H_2N^{t}Bu$, H_2NB(NAr'CH)$_2$ (**1.110**), H_2NBMes_2 and monomeric $H_2NBC_8H_{14}$ showed a much reduced tendency on electronic grounds for this transformation, where the reaction with $H_2NBC_8H_{14}$ is fairly endergonic and the reaction with H_2NBMes_2 may undergo more feasible and deleterious alternative pathways.[140]

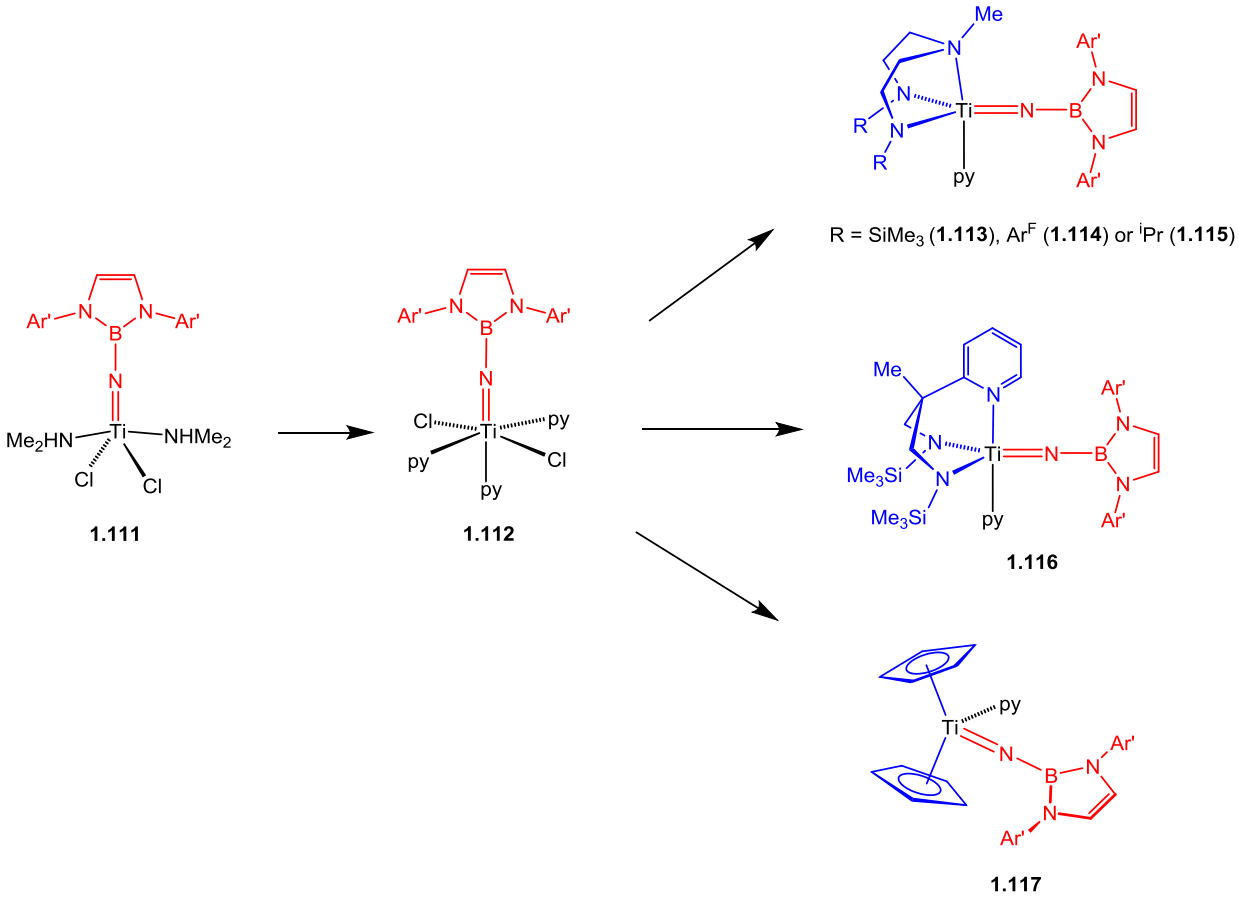

Scheme 1.13. Synthesis of Ti{NB(NAr'CH)$_2$}Cl$_2$(py)$_3$ (**1.112**) and examples of its salt metathesis reactions with lithiated ligands.[140]

A subsequent ligand exchange reaction in neat pyridine replaced acidic HNMe$_2$ and yielded the compound Ti{NB(NAr'CH)$_2$}Cl$_2$(py)$_3$ (**1.112**). Structural analysis showed that the borylimido ligand exerts a very strong *trans* influence, as a consequence being a very strong σ donor. Crystallographic characterisation of **1.111** and **1.112** demonstrated that the Ti–N$_{im}$ linkage is best described as a triple bond, as in titanium imido, hydrazido or alkoxyimido analogues, and its bond metrics are particularly comparable to those in analogous arylimido complexes. The reaction between **1.112** and Li$_2$N$_2$^{R}N^{Me} resulted in the respective diamide-amine supported titanium borylimido compounds Ti(N$_2$^{R}N^{Me}){NB(NAr'CH)$_2$}(py) (R = SiMe$_3$ (**1.113**), Ar^F (**1.114**), ^{i}Pr (**1.115**)). The diamide-pyridine-supported complex Ti(N$_2$N^{py}){NB(NAr'CH)$_2$}(py) (**1.116**) was prepared in the same way, and the reactions of compounds **1.113** –**1.116**, in particular, with terminal alkynes have been studied (Scheme 1.13).

The first sandwich titanium borylimide Cp$_2$Ti{NB(NAr'CH)$_2$}(py) (**1.117**) was prepared by reacting **1.112** with two equivalents of NaCp (Scheme 1.13).[140] As described above,

neither of imide/borylamine exchange nor double deprotonation protocols are thermodynamically feasible for dialkyl- or diarylborylamines. However, an oxidative method seems to be suitable for appropriate precursors. The reaction of the dinitrogen compound $(Cp''_2Ti)_2(\mu_2{:}\eta^1,\eta^1\text{-}N_2)$ (**1.118**, Cp" = 1,3-$C_5H_3(SiMe_3)_2$) with the borylazide N_3BMes_2 yielded the base-free titanocene borylimido complex $Cp''_2Ti(NBMes_2)$ (**1.119**, Equation 1.7).

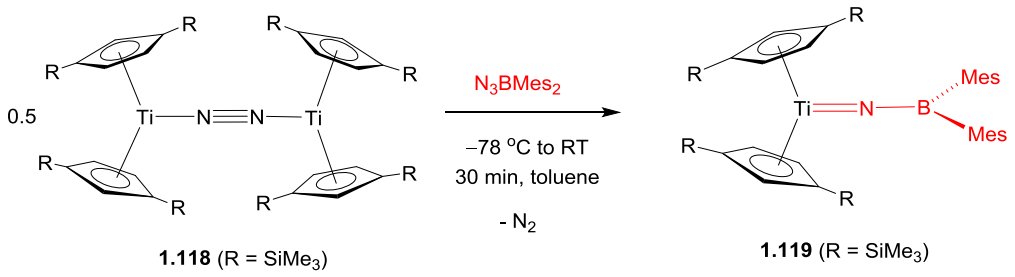

1.118 (R = $SiMe_3$) **1.119** (R = $SiMe_3$)

Equation 1.7[140]

The Ti–N_{im} distance of **1.119** (1.8069(7) Å) is significantly longer than the corresponding value in **1.117** (1.7549(13) Å), and the N_{im}–B distance of 1.3782(12) Å is significantly shorter than that of **1.117** of 1.426(2) Å. These features suggest significantly more multiple (π-) bond character in the N_{im}–B bond, as well as less multiple (π-) bond character in the Ti–N_{im} bond (*cf.* **1.117**). Figure 1.13 shows the principal bonding and non-bonding π-type Ti–N_{im} MOs of $Cp_2Ti(NBMe_2)$ (**1.120**). The HOMO-1 is the Ti–N_{im} π_h interaction. The corresponding π_v interaction is found in HOMO-5 which also contains significant Cp-Ti bonding character, whilst the HOMO (π_{nb}) is wholly ligand-based. As in the half-sandwich systems mentioned above, the Ti–N_{im} bond length of **1.120** is dominated by Ti–N_{im} π_v bonding effects (bond energies correlates to σ- and π_h interactions). This is further amplified by the π-loaded nature of these metallocene derivatives, giving longer Ti–N_{im} bonds.

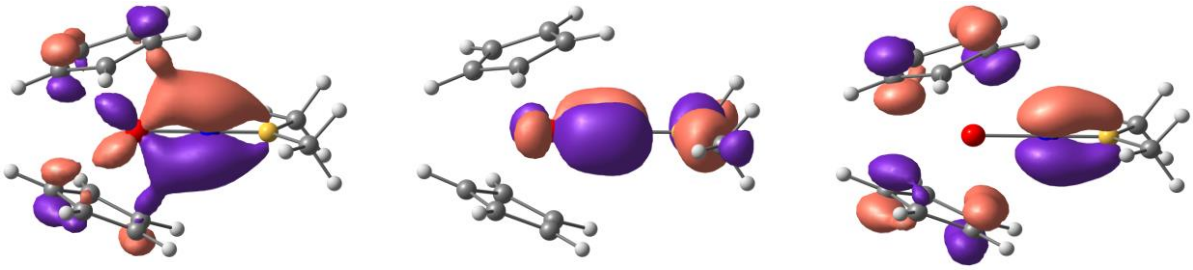

HOMO-5 (π_v) **HOMO-1 (π_h)** **HOMO (π_{nb})**

Figure 1.13. Selected molecular orbitals of $Cp_2Ti(NBMe_2)$ (**1.120**).

The first borylimido (albeit transient) complex of a rare earth metal ($NacNac^{NMe_2}$)Sc{NB(NAr'CH)$_2$} (**1.121**, $NacNac^{NMe_2}$ = Ar'NC(Me)CHC(Me)NCH$_2$CH$_2$NMe$_2$)) was reported by our research group this year, from thermolysis of the methyl-borylamide ($NacNac^{NMe_2}$)Sc(Me){NHB(NAr'CH)$_2$} (**1.122**) *via* methane elimination.[139] The reaction of **1.121** with internal alkyne PhCCMe gave the azascandacyclobutene product ($NacNac^{NMe_2}$)Sc{N{B(NAr'CH)$_2$}C(Me)C(Ph)} (**1.123**) *via* [2+2] cycloaddition. The reaction with TolCCH gave the terminal acetylide $NacNac^{NMe_2}$)Sc{NHB(NAr'CH)$_2$}(CCTol) (**1.124**) *via* C–H bond activation. DFT calculations found that both the formation of **1.123** and **1.124** are strongly thermodynamically favoured. However, **1.124** is found not to be the thermodynamic product, and the [2+2] cycloaddition product with TolCCH is the most stable isomer. The formation of **1.124** is therefore under kinetic control as confirmed by the higher transition state of cycloaddition compared to C–H bond activation. Additionally, the high stability of **1.124** ensures that even at elevated temperatures, **1.124** remains the only product formed (Scheme 1.14).[139]

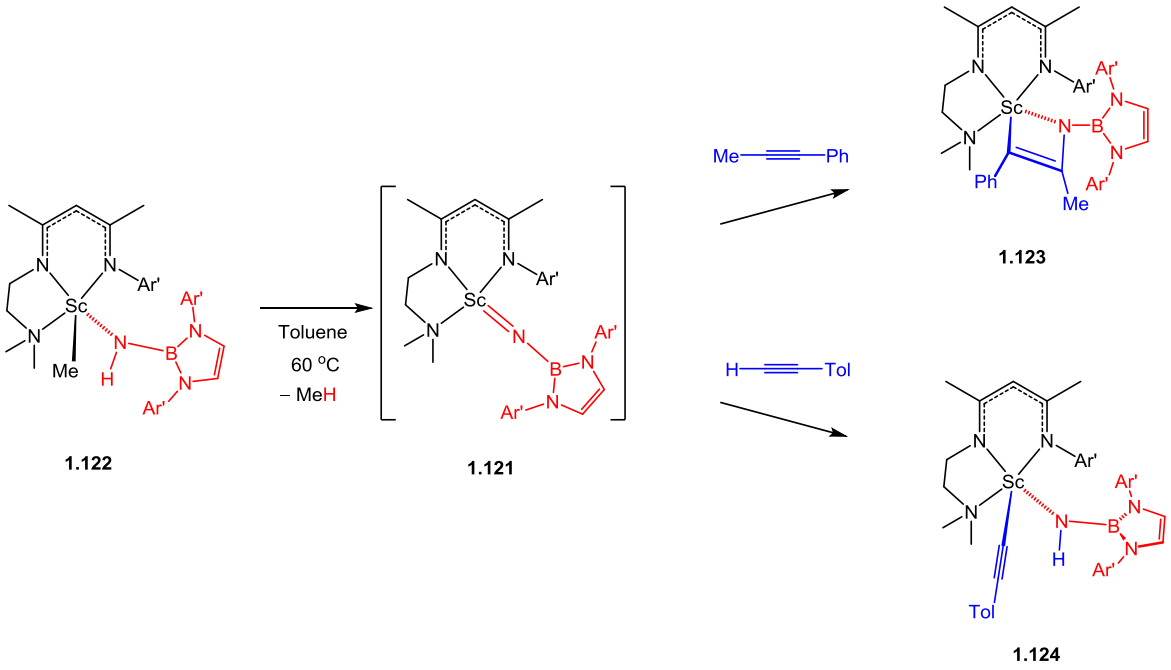

Scheme 1.14. Preparation of (NacNac^{NMe_2})Sc{NB(NAr'CH)$_2$} (**1.121**) and [2+2] and C–H bond activation with alkynes.[139]

Figure 1.14 shows the σ- and π-type three highest energy frontier orbitals of the $[NB(NHCH)_2]^{2-}$ dianion. It was found that although aromatic $[NB(NHCH)_2]^{2-}$ is isoelectronic with $[NPh]^{2-}$, the electropositive nature of boron atom makes MOs containing contributions from this element less stable, and thus the larger HOMO-HOMO-1 separation in $[NPh]^{2-}$compared to that in $[NB(NHCH)_2]^{2-}$ indicates the Ph ring better stabilises π_v. Due to the electropositive nature of boron compared to carbon, the average energy of the HOMO and HOMO-1 of the borylimide dianion is higher (less stable), suggesting that this borylimide is a better π-donor than phenylimide. This effect is amplified in the HOMO-2 of the anions which are the σ-donor orbitals where the borylimide orbital is *ca.* 2 eV less stable, suggesting an even greater improvement in σ-donor ability. Thus, the C–H bond activations are more favourable in the borylimido case (*cf.* arylimido), due to the higher strength of the newly formed N–H bond formed from a borylimido ligand compared with an arylimido ligand, where the same effect is found with the N–C bond in a metallacycle.[139]

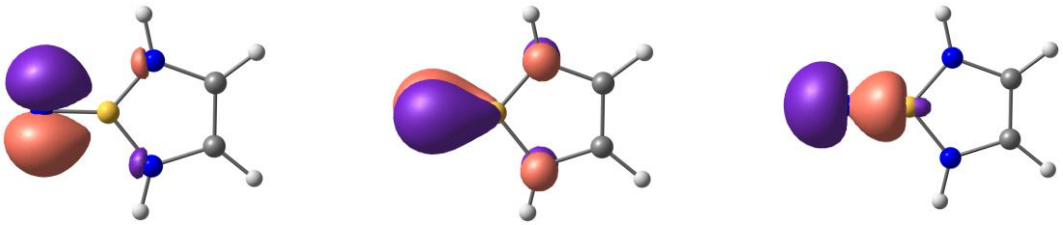

HOMO (π_h)	**HOMO-1 (π_v)**	**HOMO-2 (σ)**
7.38 (6.91) eV	7.06 (6.23) eV	5.00 (2.99) eV

Figure 1.14. DFT computed σ- and π-type fragment molecular orbitals of the borylimido dianion $[NB(NHCH)_2]^{2-}$ with the values for $[NPh]^{2-}$ in parentheses.

Summary and objectives

This Chapter has described the well-established chemistry of Group 4 imido and hydrazido complexes, including their synthesis, bonding, structure and reactivity, as well as practical application in catalysis. The current effort is looking into the investigation of new heteroatoms bonded at the N_{im} group and exploring resultant reactivity and bonding. In contrast, until recent work by our research group, only a handful of terminal borylimido compounds have been reported to date, and the systematic synthesis and reactivity of titanium borylimido compounds were just developed in our research group recently during the early stages of this Thesis.

One aim of this Thesis is to develop new borylamines with different steric profiles, and target the synthesis of first terminal zirconium and hafnium borylimides. Secondly, as imido and hydrazido Group 4 compounds provide catalytic C–N bond-forming reactions, another aim of this Thesis is to investigate the reactivity of zirconium and hafnium borylimides, particularly with alkynes to explore the analogous catalytic processes, and to compare them with the zirconium and hafnium imides and hydrazide analogues. Finally, the third aim of this Thesis is to study the reactions and potential functional group transfer processes with small polar molecules, in particular those containing C–O or C–S single and multiple bonds.

1.8 References

1 W. A. Nugent and J. M. Mayer, *Metal-Ligand Multiple Bonds*, Wiley-Interscience, New York, 1988.

2 J. Chatt, A. J. Pearman and R. L. Richards, *J. Chem. Soc. Dalton. Trans.*, 1977, 2139–2142.

3 M. Hidai, *Coord. Chem. Rev.*, 1999, **185**–**186**, 99–108.

4 R. R. Schrock, *Angew. Chem. Int. Ed.*, 2008, **47**, 5512–5522.

5 R. R. Schrock, *Acc. Chem. Res.*, 2005, **38**, 955–962.

6 W. W. Weare, X. Dai, M. J. Byrnes, J. M. Chin, R. R. Schrock and P. Muller, *Proc. Natl. Acad. Sci.*, 2006, **103**, 17099–17106.

7 D. V Yandulov and R. R. Schrock, *Inorg. Chem.*, 2005, **44**, 1103–1117.

8 N. Hazari and P. Mountford, *Acc. Chem. Res.*, 2005, **38**, 839–849.

9 N. Adams, H. J. Arts, P. D. Bolton, D. Cowell, S. R. Dubberley, N. Friederichs, C. M. Grant, M. Kranenburg, A. J. Sealey, B. Wang, P. J. Wilson, A. R. Cowley, P. Mountford and M. Schröder, *Chem. Commun.*, 2004, 434–435.

10 P. D. Bolton and P. Mountford, *Adv. Synth. Catal.*, 2005, **347**, 355–366.

11 H. R. Bigmore, S. R. Dubberley, M. Kranenburg, S. C. Lawrence, A. J. Sealey, J. D. Selby, M. A. Zuideveld, A. R. Cowley and P. Mountford, *Chem. Commun.*, 2006, 436–438.

12 H. R. Bigmore, M. A. Zuideveld, A. M. Kowalczyk, A. R. Cowley, M. Kranenburg, E. J. L. McInnes and P. Mountford, *Inorg. Chem.*, 2006, **45**, 6411–6423.

13 P. J. Wilson, A. J. Blake, P. Mountford and M. Schröder, *Chem. Commun.*, 1998, 1007–1008.

14 C. H. Winter, P. H. Sheridan, T. S. Lewkebandara, M. J. Heeg and J. W. Proscia, *J. Am. Chem. Soc.*, 1992, **114**, 1095–1097.

15 T. S. Lewkebandara, P. H. Sheridan, M. J. Heeg, A. L. Rheingold and C. H. Winter, *Inorg. Chem.*, 1994, **33**, 5879–5889.

16 I. Bytschkov and S. Doye, *Eur. J. Org. Chem.*, 2003, **2003**, 935–946.

17 S. Doye, *Synlett*, 2004, **2004**, 1653–1672.

18 A. V Lee and L. L. Schafer, *Eur. J. Inorg. Chem.*, 2007, 2243–2255.

19 T. E. Müller, K. C. Hultzsch, M. Yus, F. Foubelo and M. Tada, *Chem. Rev.*, 2008, **108**, 3795–3892.

20 Y. Li, Y. Shi and A. L. Odom, *J. Am. Chem. Soc.*, 2004, **126**, 1794–1803.

21 J. S. Johnson and R. G. Bergman, *J. Am. Chem. Soc.*, 2001, **123**, 2923–2924.

22 C. Cao, Y. Shi and A. L. Odom, *Org. Lett.*, 2002, **4**, 2853–2856.

23 L. Ackermann and R. Born, *Tetrahedron Lett.*, 2004, **45**, 9541–9544.

24 V. Khedkar, A. Tillack, M. Michalik and M. Beller, *Tetrahedron Lett.*, 2004, **45**, 3123–3126.

25 S. Banerjee, Y. Shi, C. Cao and A. L. Odom, *J. Organomet. Chem.*, 2005, **690**, 5066–5077.

26 S. Banerjee, E. Barnea and A. L. Odom, *Organometallics*, 2008, **27**, 1005–1014.

27 K. Weitershaus, H. Wadepohl and L. H. Gade, *Organometallics*, 2009, **28**, 3381–3389.

28 P. D. Schweizer, H. Wadepohl and L. H. Gade, *Organometallics*, 2013, **32**, 3697–3709.

29 K. Weitershaus, B. D. Ward, R. Kubiak, C. Müller, H. Wadepohl, S. Doye and L. H. Gade, *Dalton Trans.*, 2009, 4586–4602.

30 G. R. Giesbrecht and J. C. Gordon, *Dalton Trans.*, 2004, 2387–2393.

31 W. A. Nugent and B. L. Haymore, *Coord. Chem. Rev.*, 1980, **31**, 123–175.

32 D. E. Wigley, in *Prog. Inorg. Chem.*, ed. K. D. Karlin, Wiley-Interscience, New York, 1994, vol. 42, pp. 239–482.

33 M. H. Chisholm and I. P. Rothwell, in *Comprehensive Coordination Chemistry*, Pergamon Press, Oxford, 1987, vol. 2, pp. 161–184.

34 P. Mountford, *Chem. Commun.*, 1997, 2127–2134.

35 B. L. Haymore, E. A. Maatta and R. A. D. Wentworth, *J. Am. Chem. Soc.*, 1979, **101**, 2063–2068.

36 J. T. Anhaus, T. P. Kee, M. H. Schofield and R. R. Schrock, *J. Am. Chem. Soc.*, 1990, **112**, 1642–1643.

37 S. C. Dunn, P. Mountford and D. A. Robson, *J. Chem. Soc. Dalton. Trans.*, 1997, **2**, 293–304.

38 P. J. Walsh, F. J. Hollander and R. G. Bergman, *Organometallics*, 1993, **12**, 3705–3723.

39 H. W. Roesky, H. Voelker, M. Witt and M. Noltemeyer, *Angew. Chem. Int. Ed. English*, 1990, **29**, 669–670.

40 J. E. Hill, R. D. Profilet, P. E. Fanwick and I. P. Rothwell, *Angew. Chem. Int. Ed. English*, 1990, **29**, 664–665.

41 C. C. Cummins, C. P. Schaller, G. D. Van Duyne, P. T. Wolczanski, A. W. E. Chan and R. Hoffmann, *J. Am. Chem. Soc.*, 1991, **113**, 2985–2994.

42 A. R. Fout, U. J. Kilgore and D. J. Mindiola, *Chem. - Eur. J.*, 2007, **13**, 9428–9440.

43 R. Duchateau, A. J. Williams, S. Gambarotta and M. Y. Chiang, *Inorg. Chem.*, 1991, **30**, 4863–4866.

44 T. E. Hanna, I. Keresztes, E. Lobkovsky, W. H. Bernskoetter and P. J. Chirik, *Organometallics*, 2004, **23**, 3448–3458.

45 A. J. Blake, P. E. Collier, S. C. Dunn, W. Li, P. Mountford and O. V Shishkin, *J. Chem. Soc. Dalton. Trans.*, 1997, 1549–1558.

46 S. C. Dunn, A. S. Batsanov and P. Mountford, *J. Chem. Soc. Chem. Commun.*, 1994, **724**, 2007–2008.

47 L. H. Gade and P. Mountford, *Coord. Chem. Rev.*, 2001, **216**–**217**, 65–97.

48 A. J. Blake, J. M. McInnes, P. Mountford, G. I. Nikonov, D. Swallow and D. J. Watkin, *J. Chem. Soc. Dalton. Trans.*, 1999, 379–392.

49 D. Swallow, J. M. McInnes and P. Mountford, *J. Chem. Soc. Dalton. Trans.*, 1998, 2253–2260.

50 E. Müller, J. Müller, F. Olbrich, W. Brüser, W. Knapp, D. Abeln and F. T. Edelmann, *Eur. J. Inorg. Chem.*, 1998, 87–91.

51 P. E. Collier, S. M. Pugh, H. S. C. Clark, J. B. Love, A. J. Blake, F. G. N. Cloke and P. Mountford, *Inorg. Chem.*, 2000, **39**, 2001–2005.

52 A. J. Blake, P. E. Collier, L. H. Gade, P. Mountford, J. Lloyd, S. M. Pugh, M. Schubart, M. E. G. Skinner and D. J. M. Trösch, *Inorg. Chem.*, 2001, **40**, 870–877.

53 M. Froneman, D. L. Cheney and T. A. Modro, *Phosphorus. Sulfur. Silicon Relat. Elem.*, 1990, **47**, 273–281.

54 N. Adams, H. R. Bigmore, T. L. Blundell, C. L. Boyd, S. R. Dubberley, A. J. Sealey, A. R. Cowley, M. E. G. Skinner and P. Mountford, *Inorg. Chem.*, 2005, **44**, 2882–2894.

55 P. J. Walsh, F. J. Hollander and R. G. Bergman, *J. Am. Chem. Soc.*, 1988, **110**, 8729–8731.

56 C. C. Cummins, S. M. Baxter and P. T. Wolczanski, *J. Am. Chem. Soc.*, 1988, **110**, 8731–8733.

57 J. L. Thorman, I. A. Guzei, Young and L. K. Woo, *Inorg. Chem.*, 1999, **38**, 3814–3824.

58 M. E. G. Skinner, T. Toupance, D. A. Cowhig, B. R. Tyrrell and P. Mountford, *Organometallics*, 2005, **24**, 5586–5603.

59 D. J. Arney, M. A. Bruck, S. R. Huber and D. E. Wigley, *Inorg. Chem.*, 1992, **31**, 3749–3755.

60 S. R. Dubberley, S. Evans, C. L. Boyd and P. Mountford, *Dalton Trans.*, 2005, 1448–1458.

61 W. A. Nugent and R. L. Harlow, *Inorg. Chem.*, 1979, **18**, 2030–2032.

62 A. J. Blake, P. Mountford, G. I. Nikonov and D. Swallow, *Chem. Commun.*, 1996, 1835–1836.

63 D. J. M. Trösch, P. E. Collier, A. Bashall, L. H. Gade, M. McPartlin, P. Mountford and S. Radojevic, *Organometallics*, 2001, **20**, 3308–3313.

64 B. D. Ward, A. Maisse-Francois, P. Mountford and L. H. Gade, *Chem. Commun.*, 2004, 704–705.

65 A. Bashall, P. E. Collier, L. H. Gade, M. McPartlin, P. Mountford, S. M. Pugh, S. Radojevic, M. Schubart, I. J. Scowen and D. J. M. Trösch, *Organometallics*, 2000, **19**, 4784–4794.

66 S. M. Pugh, D. J. M. Trösch, D. J. Wilson, A. Bashall, F. G. N. Cloke, L. H. Gade, P. B. Hitchcock, M. McPartlin, J. F. Nixon and P. Mountford, *Organometallics*, 2000, **19**, 3205–3210.

67 A. Bashall, P. E. Collier, L. H. Gade, M. McPartlin, P. Mountford and D. J. M. Trösch, *Chem. Commun.*, 1998, 2555–2556.

68 J. L. Polse, R. A. Andersen and R. G. Bergman, *J. Am. Chem. Soc.*, 1998, **120**, 13405–13414.

69 T. L. Gianetti, H. S. La Pierre and J. Arnold, *Eur. J. Inorg. Chem.*, 2013, 3771–3783.

70 P. Mountford, *J. Organomet. Chem.*, 1997, **528**, 15–18.

71 S. Mellino, L. C. Stevenson, E. Clot and P. Mountford, *Organometallics*, 2017, **36**, 3329–3342.

72 A. P. Duncan and R. G. Bergman, *Chem. Rec.*, 2002, **2**, 431–445.

73 H. M. Hoyt and R. G. Bergman, *Angew. Chem. Int. Ed. Engl.*, 2007, **46**, 5580–5582.

74 S. Y. Lee and R. G. Bergman, *J. Am. Chem. Soc.*, 1995, **117**, 5877–5878.

75 S. A. Blum, V. A. Rivera, R. T. Ruck, F. E. Michael and R. G. Bergman, *Organometallics*, 2005, **24**, 1647–1659.

76 R. L. Zuckerman and R. G. Bergman, *Organometallics*, 2000, **19**, 4795–4809.

77 S. Y. Lee and R. G. Bergman, *J. Am. Chem. Soc.*, 1996, **118**, 6396–6406.

78 S. Y. Lee and R. G. Bergman, *Tetrahedron*, 1995, **51**, 4255–4276.

79 K. E. Meyer, P. J. Walsh and R. G. Bergman, *J. Am. Chem. Soc.*, 1995, **117**, 974–985.

80 P. J. Tiong, A. Nova, L. R. Groom, A. D. Schwarz, J. D. Selby, A. D. Schofield, E.

Clot and P. Mountford, *Organometallics*, 2011, **30**, 1182–1201.

81 A. L. Odom, *Dalton Trans.*, 2005, 225–233.

82 A. Tillack, H. Jiao, I. G. Castro, C. G. Hartung and M. Beller, *Chem. - Eur. J.*, 2004, **10**, 2409–2420.

83 B. F. Straub and R. G. Bergman, *Angew. Chem. Int. Ed.*, 2001, **40**, 4632–4635.

84 S. Tobisch, *Dalton. Trans.*, 2006, **13**, 4277.

85 S. Tobisch, *Chem. - Eur. J.*, 2007, **13**, 4884–4894.

86 C. Müller, R. Koch and S. Doye, *Chem. - Eur. J.*, 2008, **14**, 10430–10436.

87 S. Tobisch, *Chem. - Eur. J.*, 2008, **14**, 8590–8602.

88 K. C. Hultzsch, *Adv. Synth. Catal.*, 2005, **347**, 367–391.

89 P. J. Walsh, A. M. Baranger and R. G. Bergman, *J. Am. Chem. Soc.*, 1992, **114**, 1708–1719.

90 A. M. Baranger, P. J. Walsh and R. G. Bergman, *J. Am. Chem. Soc.*, 1993, **115**, 2753–2763.

91 F. Pohlki and S. Doye, *Angew. Chem. Int. Ed.*, 2001, **113**, 2361–2364.

92 L. E. N. Allan, G. J. Clarkson, D. J. Fox, A. L. Gott and P. Scott, *J. Am. Chem. Soc.*, 2010, **132**, 15308–15320.

93 L. Ackermann, R. G. Bergman and R. N. Loy, *J. Am. Chem. Soc.*, 2003, **125**, 11956–11963.

94 K. Manna, W. C. Everett, G. Schoendorff, A. Ellern, T. L. Windus and A. D. Sadow, *J. Am. Chem. Soc.*, 2013, **135**, 7235–7250.

95 L. Luconi, A. Rossin, G. Tuci, S. Germain, E. Schulz, J. Hannedouche and G. Giambastiani, *ChemCatChem*, 2013, **5**, 1142–1151.

96 J. Cho, T. K. Hollis, E. J. Valente and J. M. Trate, *J. Organomet. Chem.*, 2011, **696**, 373–377.

97 D. Duncan and T. Livinghouse, *Organometallics*, 1999, **18**, 4421–4428.

98 L. Ackermann and R. G. Bergman, *Org. Lett.*, 2002, **4**, 1475–1478.

99 M. D. Fryzuk and S. A. Johnson, *Coord. Chem. Rev.*, 2000, **200**–**202**, 379–409.

100 R. F. Munhá, L. F. Veiros, M. T. Duarte, M. D. Fryzuk and A. M. Martins, *Dalton Trans.*, 2009, 7494–7508.

101 B. A. MacKay and M. D. Fryzuk, *Chem. Rev.*, 2004, **104**, 385–402.

102 J. Chatt, J. R. Dilworth and R. L. Richards, *Chem. Rev.*, 1978, **78**, 589–625.

103 J. R. Dilworth, *Coord. Chem. Rev.*, 2017, **330**, 53–94.

104 T. Gehrmann, S. A. Scholl, J. L. Fillol, H. Wadepohl and L. H. Gade, *Chem. - Eur.*

J., 2012, **18**, 3925–3941.

105 T. Gehrmann, J. L. Fillol, H. Wadepohl and L. H. Gade, *Organometallics*, 2010, **29**, 28–31.

106 T. Gehrmann, J. L. Fillol, H. Wadepohl and L. H. Gade, *Angew. Chem. Int. Ed.*, 2009, **48**, 2152–2156.

107 K. Weitershaus, J. Lloret Fillol, H. Wadepohl and L. H. Gade, *Organometallics*, 2009, **28**, 4747–4757.

108 H. Herrmann, J. L. Fillol, T. Gehrmann, M. Enders, H. Wadepohl and L. H. Gade, *Chem. - Eur. J.*, 2008, **14**, 8131–8146.

109 H. Herrmann, J. L. Fillol, H. Wadepohl and L. H. Gade, *Organometallics*, 2008, **27**, 173–174.

110 H. Herrmann, T. Gehrmann, H. Wadepohl and L. H. Gade, *Dalton Trans.*, 2008, 6231–6241.

111 H. Herrmann, J. L. Fillol, H. Wadepohl and L. H. Gade, *Angew. Chem. Int. Ed.*, 2007, **46**, 8426–8430.

112 P. J. Tiong, A. Nova, A. D. Schwarz, J. D. Selby, E. Clot and P. Mountford, *Dalton Trans.*, 2012, **41**, 2277–2288.

113 J. D. Selby, M. Feliz, A. D. Schwarz, E. Clot and P. Mountford, *Organometallics*, 2011, **30**, 2295–2307.

114 J. D. Selby, C. D. Manley, A. D. Schwarz, E. Clot and P. Mountford, *Organometallics*, 2008, **27**, 6479–6494.

115 J. D. Selby, C. Schulten, A. D. Schwarz, A. Stasch, E. Clot, C. Jones and P. Mountford, *Chem. Commun.*, 2008, 5101–5103.

116 J. D. Selby, C. D. Manley, M. Feliz, A. D. Schwarz, E. Clot and P. Mountford, *Chem. Commun.*, 2007, **733**, 4937–4939.

117 D. J. Mindiola, *Angew. Chem. Int. Ed.*, 2008, **47**, 1557–1559.

118 S. Patel, Y. Li and A. L. Odom, *Inorg. Chem.*, 2007, **46**, 6373–6381.

119 S. Banerjee and A. L. Odom, *Organometallics*, 2006, **25**, 3099–3101.

120 T. B. Parsons, N. Hazari, A. R. Cowley, J. C. Green and P. Mountford, *Inorg. Chem.*, 2005, **44**, 8442–8458.

121 P. J. Walsh, M. J. Carney and R. G. Bergman, *J. Am. Chem. Soc.*, 1991, **113**, 6343–6345.

122 T. Gehrmann, G. T. Plundrich, H. Wadepohl and L. H. Gade, *Organometallics*, 2012, **31**, 3346−3354.

123 T. Gehrmann, J. Lloret Fillol, S. A. Scholl, H. Wadepohl and L. H. Gade, *Angew. Chem. Int. Ed.*, 2011, **50**, 5757–5761.

124 H. Herrmann, H. Wadepohl and L. H. Gade, *Dalton. Trans.*, 2008, 2111–2119.

125 A. J. Clulow, J. D. Selby, M. G. Cushion, A. D. Schwarz and P. Mountford, *Inorg. Chem.*, 2008, **47**, 12049–12062.

126 N. Wiberg, H.-W. Häring, G. Huttner and P. Friedrich, *Chem. Ber.*, 1978, **111**, 2708–2715.

127 S. A. Scholl, H. Wadepohl and L. H. Gade, *Organometallics*, 2013, **32**, 937–940.

128 S. A. Scholl, G. T. Plundrich, H. Wadepohl and L. H. Gade, *Inorg. Chem.*, 2013, **52**, 10158–10166.

129 A. D. Schofield, A. Nova, J. D. Selby, C. D. Manley, A. D. Schwarz, E. Clot and P. Mountford, *J. Am. Chem. Soc.*, 2010, **132**, 10484–10497.

130 A. D. Schofield, A. Nova, J. D. Selby, A. D. Schwarz, E. Clot and P. Mountford, *Chem. - Eur. J.*, 2011, **17**, 265–285.

131 J. Unruangsri, H. Morgan, A. D. Schwarz, A. D. Schofield and P. Mountford, *Organometallics*, 2013, **32**, 3091–3107.

132 A. A. Dissanayake and A. L. Odom, *Chem. Commun.*, 2012, **48**, 440–442.

133 A. D. Schofield, DPhil Thesis, University of Oxford, 2012.

134 L. R. Groom, DPhil Thesis, University of Oxford, 2014.

135 A. D. Schwarz, C. S. Onn and P. Mountford, *Angew. Chem. Int. Ed.*, 2012, **51**, 12298–12302.

136 A. D. Schwarz, A. Nova, E. Clot and P. Mountford, *Chem. Commun.*, 2011, **47**, 4926–4928.

137 A. D. Schwarz, A. Nova, E. Clot and P. Mountford, *Inorg. Chem.*, 2011, **50**, 12155–12171.

138 L. R. Groom, A. D. Schwarz, A. Nova, E. Clot and P. Mountford, *Organometallics*, 2013, **32**, 7520–7539.

139 B. A. Clough, S. Mellino, E. Clot and P. Mountford, *J. Am. Chem. Soc.*, 2017, **139**, 11165–11183.

140 B. A. Clough, S. Mellino, A. V Protchenko, M. Slusarczyk, L. C. Stevenson, M. P. Blake, B. Xie, E. Clot and P. Mountford, *Inorg. Chem.*, 2017, **56**, 10794–10814.

141 A. A. Danopoulos, C. Redshaw, A. Vaniche, G. Wilkinson, B. Hussain-Bates and M. B. Hursthouse, *Polyhedron*, 1993, **12**, 1061–1071.

142 K. Weber, K. Korn, A. Schorm, J. Kipke, M. Lemke, A. Khvorost, K. Harms and J.

Sundermeyer, *Z. Anorg. Allg. Chem.*, 2003, **629**, 744–754.

143 M. D. Fryzuk, B. A. MacKay, S. A. Johnson and B. O. Patrick, *Angew. Chem. Int. Ed.*, 2002, **41**, 3709–3712.

144 R. Thompson, C.-H. Chen, M. Pink, G. Wu and D. J. Mindiola, *J. Am. Chem. Soc.*, 2014, **136**, 8197–8200.

145 S. P. Semproni and P. J. Chirik, *Eur. J. Inorg. Chem.*, 2013, **2**, 3907–3915.

146 L. N. Grant, B. Pinter, T. Kurogi, M. E. Carrikk, G. Wu, B. C. Manor, P. J. Carroll and D. J. Mindiola, *Chem. Sci.*, 2017, **8**, 1209–1224.

147 L. C. Stevenson, S. Mellino, E. Clot and P. Mountford, *J. Am. Chem. Soc.*, 2015, **137**, 10140–10143.

148 B. Clough, DPhil Thesis, University of Oxford, 2016.

149 T. J. Hadlington, J. A. B. Abdalla, R. Tirfoin, S. Aldridge and C. Jones, *Chem. Commun.*, 2016, **52**, 1717–1720.

Chapter Two

Zirconocene and hafnocene borylimides: synthesis, structure, bonding and reactivity

2.1 Overview

As described in Chapter One, the synthesis, characterisation and reactivity of Group 4 metal–nitrogen multiple bonded complexes, of the type $(L)_nM{=}N{-}X$ (X = R or NR_2), have been widely studied over the last forty years.[1–15] The first class of transition metal–nitrogen multiple bond complexes to be extensively studied were the imido complexes, $L_nM{=}N{-}R$ (R = alkyl or aryl), which formally contain a metal–nitrogen triple bond ($\sigma^2\pi^4$).[13,16–22] The structures and reactivities of the Group 4 imides with a wide range of ancillary ligands have been studied in detail, especially for titanium.[7,11–13,23–27] However, the first Group 4 imides to be prepared and crystallographically characterised was the zirconium compound $Cp_2Zr(N^tBu)(THF)$ (**1.4**), described by Bergman.[28,29] For this 20 VE metallocene system, competition between the Cp-supporting ligands and imido ligand for the metal accepter orbitals promotes the reactivity of the Zr=N multiple bond. The examples of reactivity provided by this compound demonstrate a fruitful area of research, including C–H bond activation, cycloaddition with a range of unsaturated small molecules and catalytic hydroamination of alkynes.[29,30] The Group 4 hydrazides have also undergone rapid development over the last decade, with a number of synthesis, bonding and reactivity studies reported.[7,31–33] The first structurally characterised terminal zirconium hydrazide, $Cp_2Zr(NNPh_2)(DMAP)$ (**1.63**) again synthesised *via* thermolysis was also reported by Bergman.[33] By introducing this electron-donating β-atom (N) its reactivity differed, commonly resulting in $N_\alpha{-}N_\beta$ cleavage, for example in reactions with CO and alkynes.[33]

Changing the β-atom from carbon or nitrogen to electropositive boron gives a borylimido functional group. However, Group 4 borylimido compounds are still virtually unknown. Related studies which attempted to access borylimides on titanium from non-heteroatom functionalised borylamines, for example H_2NBMes_2 and $H_2NBC_8H_{14}$ (abbreviated as H_2NBBN), were unsuccessful.[34] It was speculated that the nitrogen lone pair would have significant donation to the empty 2p orbital of boron in these amines, and thus the ability of the aminoborane to pre-coordinate to the metal would be reduced.[34] Therefore, we focused on H_2NBR_2 systems where R_2 is an N_2-donor moiety. Such $H_2NB(NR'CH)_2$ and related borylamines are accessible for a number of R'-groups and backbone substituents, allowing for variation of the steric profiles. Borylamines of this type can be electronically analogues to anilines H_2NAr (Ar = 2,6-C_6H_3R, R = Me (Xyl) or ^{i}Pr (Ar')), which were extensively used as entry points to the corresponding arylimido compounds (L)M=NAr.[10]

This Chapter will focus on the synthesis of borylimido complexes of the type $Cp_2M(NBR_2)(L)$, making comparisons to the extensive zirconocene chemistry reported by Bergman. DFT and Quantum Theory of Atoms in Molecules (QTAIM) calculations are used to assess the underlying electronic structure of these complexes, and also the associated thermodynamic trends associated with H–H bond and C–H bond activation reactions.

2.2 Synthesis and selection of borylamines

The borylamines used in this study are shown in Figure 2.1. Generally, these borylamines incorporate a 1,3,2-diazaborole moiety, and the boron atom is a part of a five-membered heterocycle, flanked by two nitrogen atoms in this ring.

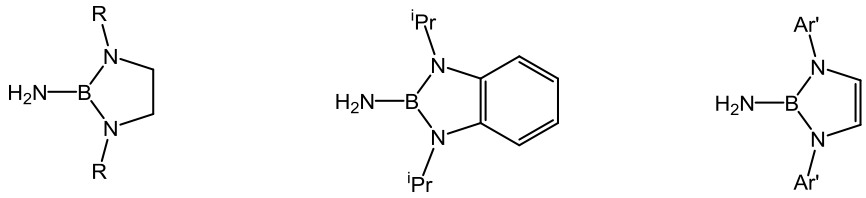

Figure 2.1. Borylamines used in this study. Ar' = 2,6-$C_6H_3{}^{i}Pr$

Initial studies centered on the saturated-backbone borylamines $H_2NB(N^{i}PrCH_2)_2$ (**1**) and $H_2NB(N^{t}BuCH_2)_2$ (**2.1**), where the synthesis of **2.1** has been previously reported by reacting $BrB(N^{t}BuCH_2)_2$ with gaseous ammonia, which is accompanied by formation of NH_4Br.[35] However, by reacting the less bulky $BrB(N^{i}PrCH_2)_2$ with gaseous ammonia, an unexpected bis(boryl)amine $HN\{B(N^{i}PrCH_2)_2\}_2$ (**2**), as well as the desired borylamine $H_2NB(N^{i}PrCH_2)_2$ (**1**), showing resonances at 26.6 and 24.8 ppm, respectively, in their ^{11}B NMR spectrum, were formed in a *ca* 1:1 ratio at RT. This result is attributed to the steric bulk of the substituent R, where the less bulky isopropyl substituents result in **1** reacting further with unreacted $BrB(N^{i}PrCH_2)_2$ in the presence of NH_3, yielding **2** (Scheme 2.1). However, the mixture of mono- and bis(boryl)amine can be separated and further purified by distillation (60 – 70 °C, 10^{-1} bar) yielding **1** as a clear oil and colourless crystalline **2**.

An unsaturated-backbone bis(boryl)amine analogue $HN\{B(N^{t}BuCH)_2\}_2$ (**2.2**) was previously reported, but under slightly more forcing conditions, from the reaction between $BrB(N^{t}BuCH)_2$ and $HN(SiMe_3)B(N^{t}BuCH)_2$ at 68 °C.[36]

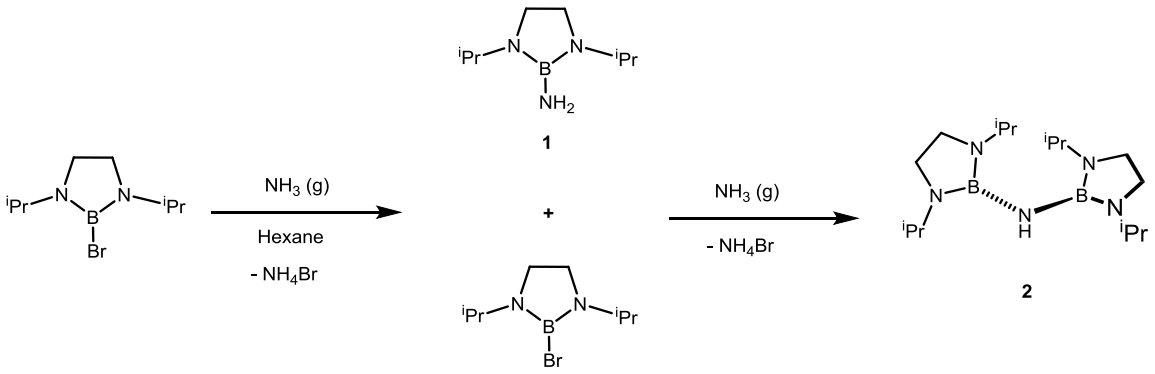

Scheme 2.1. Formation of borylamine $H_2NB(N^iPrCH_2)_2$ (**1**) and bis(boryl)amine $HN\{B(N^iPrCH_2)_2\}_2$ (**2**).

In order to synthesis **2** solely, $BrB(N^iPrCH_2)_2$ was reacted with $H_2NB(N^iPrCH_2)_2$ (**1**) in the presence of one equivalent of NEt_3 at RT. Immediate precipitation of $[NEt_3H]Br$ was observed, and the bis(boryl)amine **2** was formed exclusively in 81% isolated yield. The ^1H NMR spectrum in C_6D_6 solution displays a singlet at 3.03 ppm for the CH_2CH_2 backbone and a broad singlet at 1.89 ppm for the NH group in an 8:1 ratio by integration, as well as the expected resonances for the isopropyl groups. Additionally, there was only one ν(N–H) band at 3398 $cm^{-1}$was observed in the solid state IR spectrum (Nujol mull), indicating a secondary amine.

Since the first-formed less bulky borylamine can further react with unreacted bromoborane generating the bis(boryl)amine compound, slow addition of $BrB(N^iPrCH_2)_2$ into a saturated ammonia solution in hexane was initially attempted to maximise the concentration of NH_3 during the reaction. In this case, proportionately more **1** was formed, but still with a significant amount of the bis(boryl)amine **2** (25%). To increase the concentration of NH_3 further, liquid ammonia was employed. Slow addition of a hexane solution containing $BrB(N^iPrCH_2)_2$ into liquid ammonia at –78 °C effectively suppresses the generation of bis(boryl)amine **2**, and **1** was formed almost exclusively (95%) without requiring further purification (Equation 2.1).

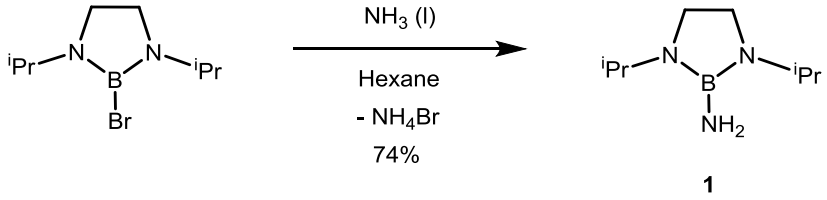

Equation 2.1

As mentioned in Chapter One, the zirconocene imido compound $Cp_2Zr(N^tBu)(THF)$ (**1.4**) and the hydrazido(2-) compound $Cp_2Zr(NNPh_2)(DMAP)$ (**1.63**) were successfully synthesised by Bergman *via* thermolytic alkane elimination of the corresponding alkyl zirconocene amide $Cp_2Zr(NH^tBu)(Me)$ (**2.3**) or hydrazide(1-) $Cp_2Zr(NHNPh_2)(CH_2CH_2{}^tBu)$ (**2.4**) precursors, respectively.[10,28,29,33] Given the success of the synthesis of **1.4** and **1.63**, analogous attempts to synthesise the first borylimido zirconocene compounds *via* thermolysis were carried out.

The borylamines **2.1** and **1** were lithiated *in situ* with one equivalent of ^{n}BuLi to give $LiNHB(N^iPrCH_2)_2$ and $LiNHB(N^tBuCH_2)_2$, respectively. Following salt metathesis with $Cp_2Zr(Me)Cl$, compounds $Cp_2Zr\{NHB(N^iPrCH_2)_2\}(Me)$ (**3**) and $Cp_2Zr\{NHB(N^tBuCH_2)_2\}(Me)$ (**4**) were cleanly formed on the NMR tube scale in C_6D_6. On the preparative scale, **3** was isolated as a pale red oil in 61% yield. The ^{11}B NMR spectrum of **3** in C_6D_6 solution shows a signal at 28.9 ppm. The ^{1}H NMR spectrum displays resonances for a C_s symmetric species containing one borylamido moiety ($NHB(N^iPrCH_2)_2$), one CH_3 and two C_5H_5 ligands. The resonances attributed to the borylamido moiety include a broad singlet at 4.81 ppm for the NH unit, and a resonance at 0.17 ppm is attributed to the methyl group bound to zirconium, indicating formation of the desired compound **3**. However, upon heating **3** on the NMR tube scale, in the presence of DMAP in toluene-d_8 at 80 – 120 °C, only decomposition to borylamine **1** and several unidentified species were observed, and no CH_4 formation was noted in the ^{1}H NMR spectrum. In an attempt to enhance the stability of the borylamido compound during the thermolysis at high temperature, increased steric bulk using *tert*-butyl substituted **4** was employed. Unfortunately similar decomposition was again observed (Scheme 2.2).

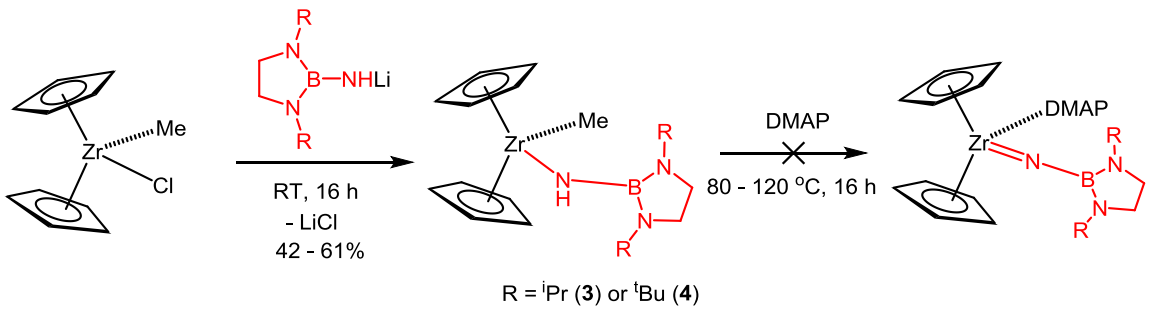

Scheme 2.2. Synthesis of borylamides $Cp_2Zr\{NHB(N^iPrCH_2)_2\}(Me)$ (**3**) and $Cp_2Zr\{NHB(N^tBuCH_2)_2\}(Me)$ (**4**), and attempts to access the corresponding borylimides.

Since attempts to make the zirconocene borylimides using the saturated-backbone borylamine **2.1** and **1** were unsuccessful, unsaturated analogues were next investigated. These species are more analogous to arylamines due to the 6π–aromatic character of the boryl ring $B(NRCH)_2$.[36] The synthesis of unsaturated-backbone borylamines with less bulky alkyl substituent requires harsh condition and very long reaction times.[37] Given the difficulty of the synthesis, the more conveniently prepared phenylene-backbone borylamine $H_2NB(N^iPr)_2C_6H_4$ (**5**), from *o*-phenylene diamine, was targeted.

The bromoborane starting material, $BrB(N^iPr)_2C_6H_4$, was prepared from $(HN^iPr)_2C_6H_4$ and BBr_3, according to the literature method.[38] However, on reaction of $BrB(N^iPr)_2C_6H_4$ with gaseous NH_3 in hexane an appreciable amount of formation of the bis(boryl)amine $H\{NB(N^iPr)_2C_6H_4\}_2$ (**6**) and desired **5** were again observed in a *ca* 1:1 ratio, the same as the preparation for **1** (Scheme 2.3). The formation of **6** can again be minimised by using liquid ammonia, giving pure borylamine **5** without further purification.

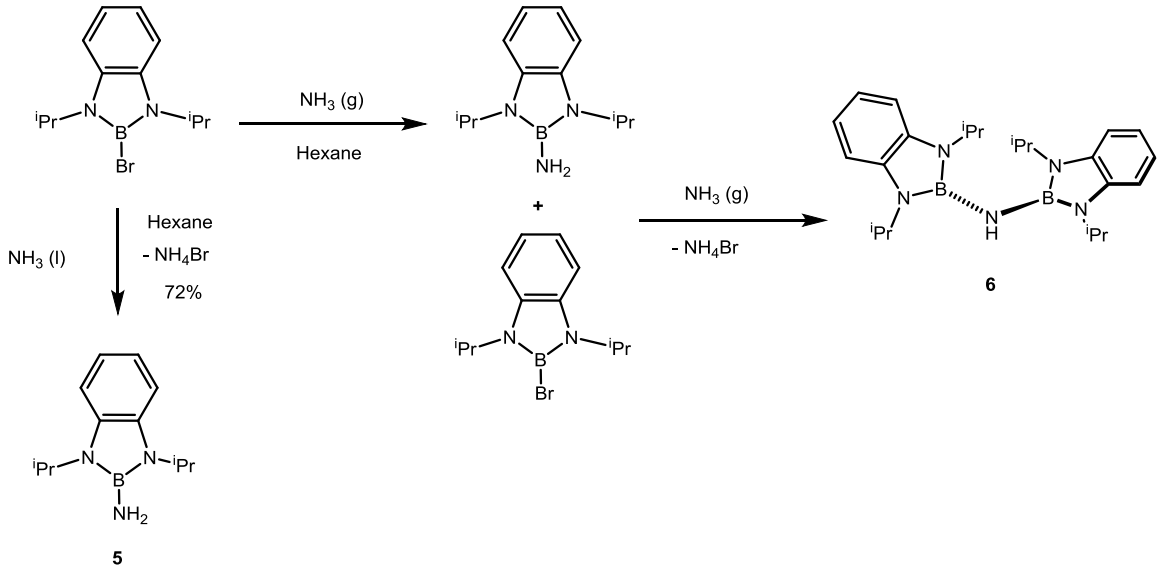

Scheme 2.3. Synthesis of borylamine $H_2NB(N^iPr)_2C_6H_4$ (**5**) and formation of $H\{NB(N^iPr)_2C_6H_4\}_2$ (**6**).

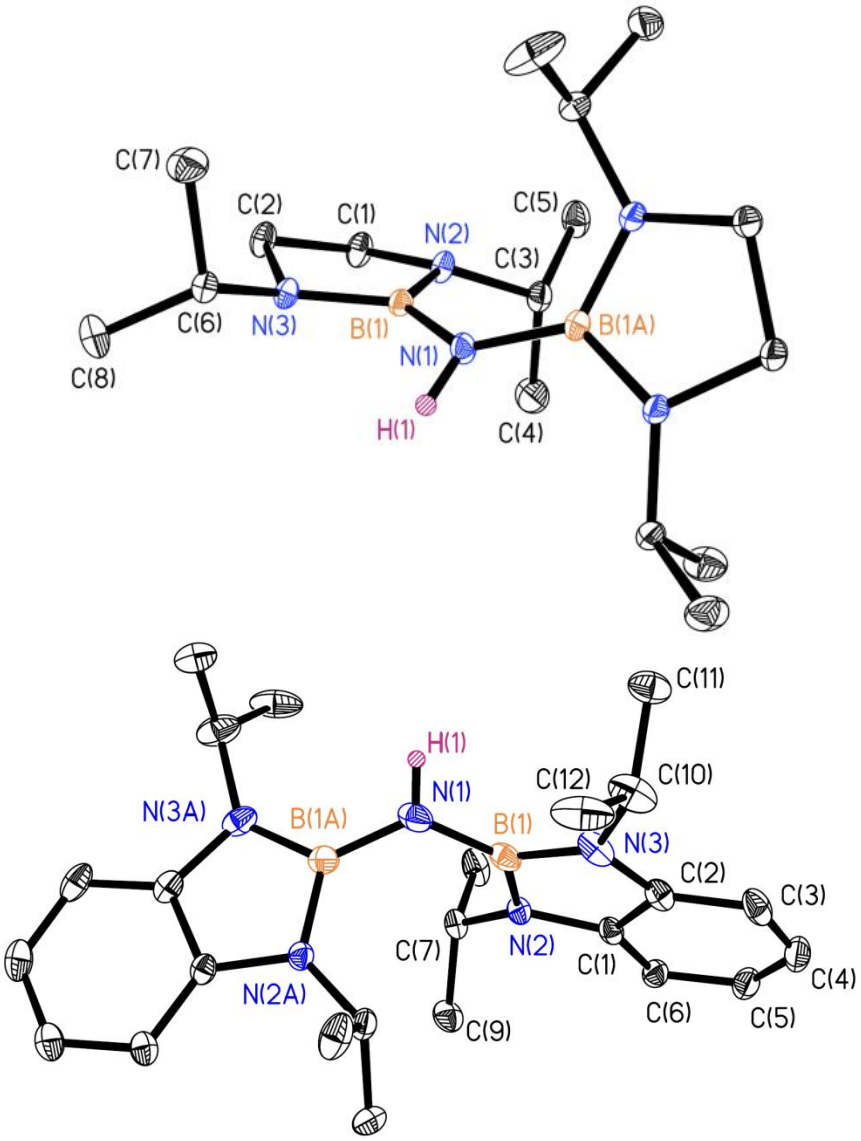

Figure 2.2. Displacement ellipsoid plots (20% probability) of $HN\{B(N^iPrCH_2)_2\}_2$ (**2**, top) and $HN\{B(N^iPr)_2C_6H_4\}_2$ (**6**, bottom). C–bound H atoms omitted for clarity.

Diffraction-quality crystals of **2** and **6** were grown from hexane solutions at 4 °C. The molecular structures of **2** and **6** as determined by X-ray crystallography are presented in Figure 2.2 with selected distances and angles in Table 2.1. The N(1)–B(1) bond distances of the two bis(boryl)amines are identical within error (1.4409(11) Å (**2**) and 1.443(5) Å (**6**)), showing no significant influence on this bond length by changing the backbone. The coordination about each of N(1), N(2) and N(3) within **6** is trigonal planar, with the angles subtended calculated to be 359.9(5), 359.0(5) and 359.9(6)° respectively. The angle subtended at N(1) within **2** is also planar (359.97(11)°), but the sums of the angles subtended at N(2) (352.16(13) ° and N(3) (353.64(12)°) deviate slightly from the

expected trigonal planar geometry, possibly due to puckering of the ring caused by the saturated backbone.

The N(2)–C(1)···C(2)–N(3) torsion angle in **6** is negligible (0.11°), demonstrating an planar and aromatic (6π electrons) boryl ring. In comparison, the torsion angle in **2** is 22.30°, due to the sp^3 hybridized C(1) and C(2). The B(1)–N(3) lengths in **2** and **6** are 1.4290(11) and 1.430(6) Å, respectively, and thus shows no differences within error.

Table 2.1. Selected bond lengths (Å) and angles (°) for $HN\{B(N^iPrCH_2)_2\}_2$ (**2**) and $HN\{B(N^iPr)_2C_6H_4\}_2$ (**6**).

	2	**6**
B(1)–N(1)	1.4409(11)	1.443(5)
B(1)–N(2)	1.4285(13)	1.450(5)
B(1)–N(3)	1.4290(11)	1.430(6)
N(2)–C(1)	1.4609(11)	1.410(4)
N(3)–C(2)	1.4629(11)	1.397(5)
C(1)–C(2)	1.5273(13)	1.396(5)
N(2)–C(1)–C(2)	104.54(7)	108.9(3)
N(3)–C(2)–C(1)	104.47(7)	108.8(3)
B(1)–N(1)–B(1A)	132.17(11)	129.1(5)
B(1)–N(2)–$C_{iPr}(1)^a$	125.43(8)	126.5(3)
B(1)–N(2)–$C_{iPr}(2)^b$	126.65(7)	131.8(4)
N(2)–B(1)···B(1A)–$N(2A)^c$	54.83	72.06
N(2)–C(1)···C(2)–$N(3)^c$	22.30	0.11

a. "$C_{iPr}(1)$" = C(3) **2**, C(7) **6**. *b*. "$C_{iPr}(2)$" = C(6) **2**, C(10) **6**. *c*. Torsion angle for this linkage.

The new borylamido zirconocene compound $Cp_2Zr\{NHB(N^iPr)_2C_6H_4\}(Me)$ (**7**) was synthesised on the preparative scale in benzene solution at RT, using the aforementioned methodology, reacting $Cp_2Zr(Me)Cl$ with $LiNHB(N^iPr)_2C_6H_4$ which was previously prepared by reacting $H_2NB(N^iPr)_2C_6H_4$ with one equivalent ^{n}BuLi. Compound **7** was isolated as a yellow-green solid in 85% yield.

Upon heating **7** at 120 °C in the presence of DMAP, a major new species was formed with multiple unidentified byproducts on the NMR tube scale in toluene-d_8, as judged by ^{1}H NMR spectroscopy. Although the ^{1}H NMR spectrum shows that there was no significant shift on the (coordinated) DMAP resonances, a low intensity singlet at 0.17 ppm (attributed to CH_4) was observed which indicates the successful thermolysis, forming $Cp_2Zr\{NB(N^iPr)_2C_6H_4\}$(DMAP) (**8**). On the preparative scale in toluene solution at 120 °C for 23 hours, **8** was isolated as yellow crystals in 37% yield, after multiple fractional recrystallisations (Scheme 2.4). Attempts to employ the weaker Lewis base pyridine, rather than DMAP, resulted in mixtures with a high amount of impurities, including borylamine **5** on the NMR tube scale.

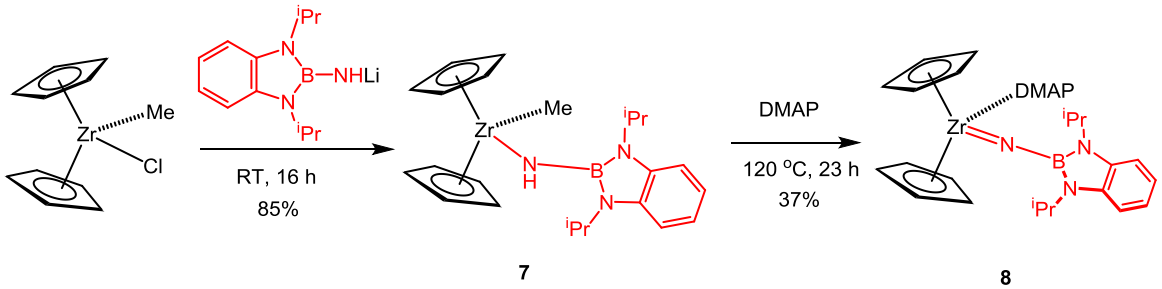

7 **8**

Scheme 2.4. Synthesis of $Cp_2Zr\{NHB(N^iPr)_2C_6H_4\}$(Me) (**7**) and $Cp_2Zr\{NB(N^iPr)_2C_6H_4\}$(DMAP) (**8**).

Compound **8** displays an upfield shifted ^{11}B signal of 20.7 ppm, compared to that of **7** of 27.5 ppm. The ^{1}H NMR spectra of the borylamide **7** and the borylimide **8** indicate that they have C_s symmetric structures in the solution phase where the chemically equivalent but diastereotopic isopropyl groups appear as a septet and a doublet resonance. Compound **7** displays an NH resonance at 4.93 ppm and a ZrMe resonance at 0.22 ppm, while **8** shows DMAP resonances at 8.29, 5.75 and 2.03 ppm instead, with relative intensity 6 H for N$\underline{Me}_2$. All the ^{1}H NMR resonances, except the H atoms on the *o*-phenylene backbone, of **8** are slightly downfield shifted relative to those of **7** (Figure 2.3).

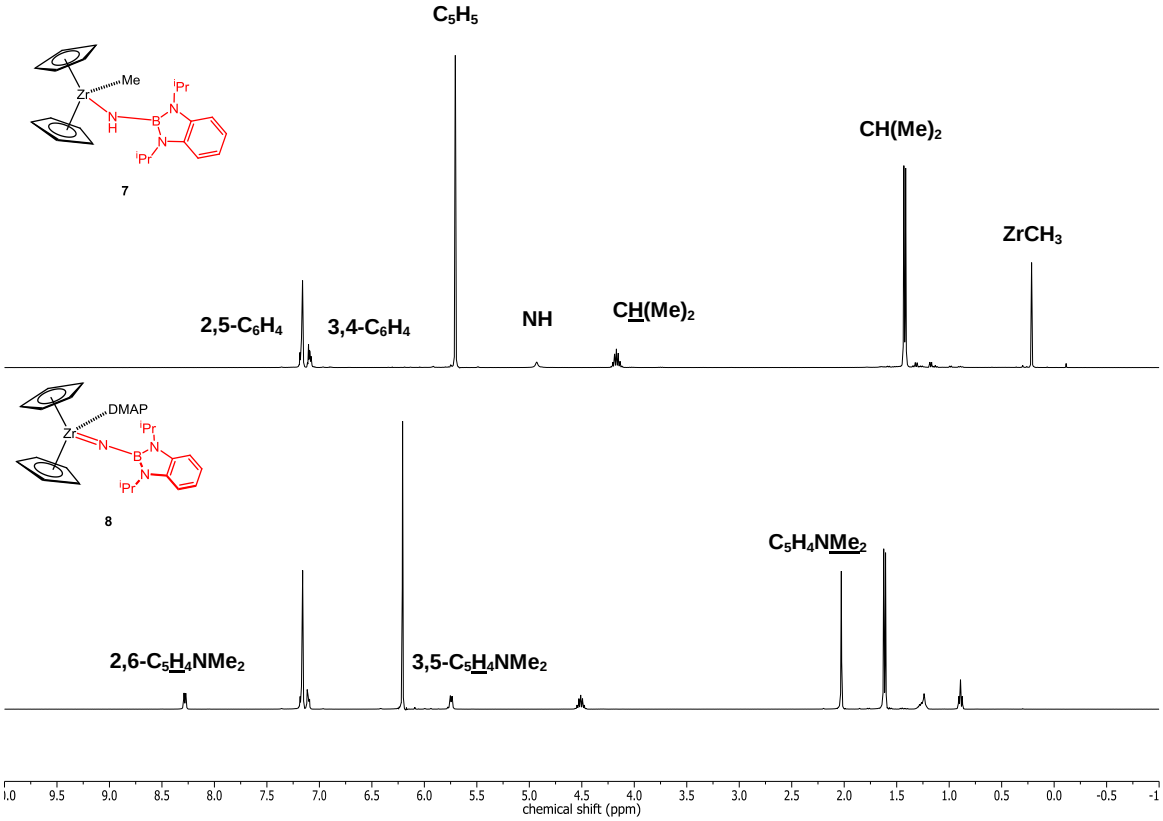

Figure 2.3. ^{1}H NMR spectra (400.1 MHz) of $Cp_2Zr\{NHB(N^iPr)_2C_6H_4\}(Me)$ (**7**, top) and $Cp_2Zr\{NB(N^iPr)_2C_6H_4\}(DMAP)$ (**8**, bottom) in C_6D_6 at 298 K.

Diffraction-quality crystals of **7** and **8** were grown from a hexane solution and a toluene solution layered with hexane at 4 °C, respectively. The structures of **7** and **8** are shown in Figure 2.4, and selected distances and angles are given in Table 2.2. In both compounds, the metal centres have a pseudo tetrahedral environment, with two sites occupied by the cyclopentadienyl rings and the other two by the borylimido and DMAP ligands (**8**) or borylamido and methyl ligands (**7**). The cyclopentadienyl rings are mutually staggered in both cases. The Zr(1)–N(1) bond length in **7** (2.0811(7) Å) is comparable with those in a number of zirconocene alkyl- and aryl-amides complexes (avg. Zr–N_{im} = 2.085 Å, range 2.060(3) – 2.122(3) Å),[30,39–45] and the sum of angles subtended at N(1) is 360(11)°, indicating a single Zr(1)–N(1) bond and sp^2 hybridised N(1).[30,42,44,46] The plane of the boryl ring and the equatorial plane of Cp_2Zr are perpendicular to the Zr(1)–N(1)–B(1) plane in order to maximise the interaction between the lone pair on N(1) and the equatorial non-bonding orbital on Zr(1), which also minimise the backbonding between N(1) and B(1) to avoid the competition with N(2) and N(3).

At first sight, **8** would be a twenty valence electron species as well as its imido and hydrazido analogues,[10,23,28,33,47,48] where the zirconium centre provides four electrons, the

two Cp rings provide ten electrons, DMAP provides two electrons and the borylimido (as well as imido and hydrazido) ligand is considered to donate four electrons, by using the neutral counting method. Therefore, competition between the Cp ligand set and the borylimido (imido and hydrazido) ligand would be expected, giving the characteristically long Zr–N_{im}, Cp_{cent}–Zr lengths.[49,50] The Zr–N_{im} bond length in **8** is 1.895(3) Å, which is significantly longer than that found in the alkyl imide $Cp_2Zr(N^tBu)(THF)$ (**1.4**, Zr–N_{im} of 1.826(4) Å), and also than that in $Cp_2Zr(NNPh_2)(DMAP)$ (**1.63**, Zr–N_α = 1.878(7) Å).[28,33] The Zr(1)–N(1)–B(1) angle (166.6(2)°) in **8** deviates somewhat from the linearity in **1.4** (174.4(3)°).[28] Both of these structural features imply a lower Zr–N_{im} bond order in **8** than in **1.4**. This may be the consequence of both steric and electronic factors, the latter of which reduces the extent of π-donation from the borylimido lone pair to the metal-centered acceptor orbital.[49] This lengthening is also observed in the complex $Cp_2Zr(NAr')(THF)$ (**1.50**), where Ar' is isoelectronic with and sterically similar to the $B(N^iPr)_2C_6H_4$ moiety. In this case, the Zr–N_{im} bond length is 1.8882(2) Å and the Zr–N_{im}–C angle is 159.1(2)°.[51] The bond length is comparable to that of **1.50**. However, as described in Section 1.7, the aromatic boryl ring does not stabilise π-backdonation from N_{im} as well as the aryl counterpart,[49,52] which should expect to give rise to a shorter Zr–N_{im} bond in **8** (*cf.* **1.50**). However, it is possible that the more strongly donating DMAP ligand in **8** has a greater lengthening effect on Zr–N_{im} than the THF ligand in **1.50**. DFT studies of the bonding in zirconocene imido systems are discussed later in this Chapter.

On the basis of the orientation of the boryl moiety in solid state, the equatorial Zr–Cp non-bonding orbital interacts with the equatorial N(1) lone pair forming a π-bond, and another π-bond (perpendicular to the equatorial plane), which may only feasibly take place using the Zr–Cp anti-bonding orbital, which could have backdonation to the boron elongating the Zr–N_{im} bond as mentioned above. As a result of donation from N(1) to B(1), the degree of donation from N(2) and N(3) to B(1) would be decreased by competition with N(1), and consequently increase the bond length of B(1)–N(2)/N(3). These are in line with marginally longer B(1)–N(2) and B(1)–N(3) bond lengths for **8** (1.469(4) and 1.465(4) Å respectively) than those in borylamide **7** (1.4444(11) and 1.4520(12) Å respectively).

The two Zr–Cp_{cent} distances in **7** are nearly identical to each other, as are those in **8**. However, the individual Zr-Cp_{cent} distances in **8** (2.285 and 2.306 Å) are marginally longer than those in **7** (2.238 and 2.231 Å). This again reflects the π-bond competition

between the Cp and borylimido ligands (*vide supra*). The Zr–Cp_{cent} lengths in **8** are also significantly longer than in other examples (e.g. Cp_2ZrCl_2, avg. Zr–Cp_{cent} = 2.194 Å) due to the π-loaded nature of this complex (as are the organoimido and hydrazido compounds).[53] The Cp_{cent}–Zr–Cp_{cent} angle of **7** is 130.7°, which is comparable to that reported elsewhere (e.g. Cp_2ZrCl_2; Cp_{cent}–Zr–Cp_{cent} = 129.03°). In contrast, the Cp_{cent}–Zr–Cp_{cent} angle in **8** is slightly more acute, being 127.9°, similar to those in imido and hydrazido analogues **1.50** (Cp_{cent}–Zr–Cp_{cent} = 127.22°) and **1.63** (Cp_{cent}–Zr–Cp_{cent} = 125.5°), again reflecting the π-loaded nature of this borylimido complex.[49]

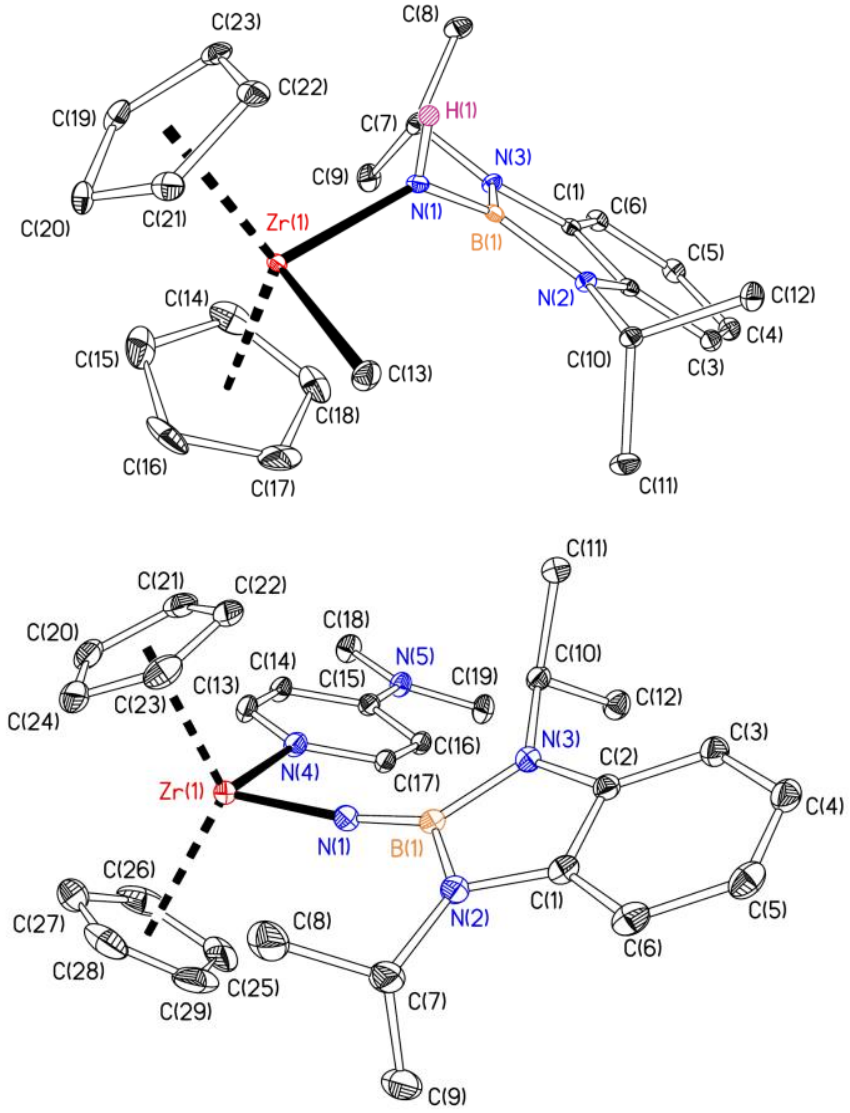

Figure 2.4. Displacement ellipsoid plots (20% probability) of $Cp_2Zr\{NHB(N^iPr)C_6H_4\}(Me)$ (**7**, top) and $Cp_2Zr\{NB(N^iPr)C_6H_4\}(DMAP)$ (**8**, bottom). C–bound H atoms omitted for clarity.

Table 2.2. Selected bond lengths (Å) and angles (°) for $Cp_2Zr\{NHB(N^iPr)C_6H_4\}(Me)$ (**7**) and $Cp_2Zr\{NB\text{-}(N^iPr)C_6H_4\}(DMAP)$ (**8**). $Cp_{cent(1)}$ and $Cp_{cent(2)}$ refer to the computed Cp ring centroids for "upper" and "lower" Cp rings, respectively, as depicted in Figure 2.4.

	7	**8**
Zr(1)–N(1)	2.0811(7)	1.895(3)
Zr(1)–N(4)/C(13)	2.2971(9)	2.313(2)
Zr(1)– $Cp_{cent(1)}$	2.238	2.285
Zr(1)–$Cp_{cent(2)}$	2.231	2.306
N(1)–B(1)	1.4394(12)	1.404(4)
B(1)–N(2)	1.4444(11)	1.469(4)
B(1)–N(3)	1.4520(12)	1.465(4)
$Cp_{cent(1)}$–Zr(1)–$Cp_{cent(2)}$	130.7	125.9
N(1)–Zr(1)–$Cp_{cent(1)}$	108.2	109.7
N(1)–Zr(1)–$Cp_{cent(2)}$	108.3	112.8
N(4)/C(13)–Zr(1)–$Cp_{cent(1)}$	102.4	104.1
N(4)/C(13)–Zr(1)–$Cp_{cent(2)}$	103.5	101.9
N(1)–Zr(1)–N(4)/C(13)	98.87(3)	97.60(10)
Zr(1)–N(1)–B(1)	134.90(5)	166.6(2)
N(1)–B(1)–N(2)	126.89(8)	130.5(3)
N(1)–B(1)–N(3)	128.06(8)	125.9(3)

This first terminal zirconium borylimide **8** was successfully synthesised. However given the low yielding, difficult purification steps required and the non-volatile DMAP base, further reactivity studies of **8** were not explored. Nonetheless, the installation of this borylimide group using borylamine **5** on titanium was recently achieved by other group members, and the reactivity studies of these titanium borylimido complexes are ongoing.[54] In the case of zirconium, the difficulty for the synthesis of **8** led us to search for a more readily prepared borylimido complexes of this metal, which could be extended to future reactivity studies.

2.3 Synthesis of $Cp_2M\{NHB(NAr'CH)_2\}(Me)$ and $Cp_2M\{NB(NAr'CH)_2\}(L)$ (M = Zr or Hf)

We have previously found that the bulky borylamine $H_2NB(NAr'CH)_2$ (**1.110**) was a good entry point to scandium and titanium borylimido compounds.[49,52] Like $H_2NB(N^iPr)C_6H_4$ (**5**), **1.110** also has a 6π-aromatic character, contributed from the unsaturated C_2H_2 backbone, though has much more bulky Ar' substituents. This borylamine **1.110**, recently reported by Jones and co-workers has been prepared in high yield on a multi-gram scale. Thus bubbling of ammonia though a hexane solution of $BrB(NAr'CH)_2$ yields **1.110** and NH_4Br (Equation 2.2), where, in this instance, no bis(boryl)amine is obtained due to the bulky Ar' substituents.[55] With such convenient access, this bulky borylamine **1.110** became the focus of study.

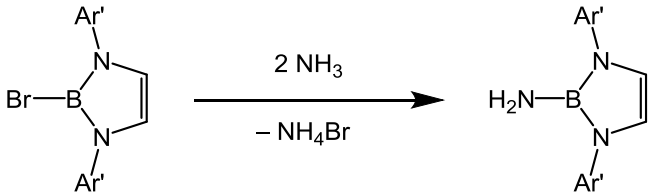

1.110

Equation 2.2[55]

Compound $LiNHB(NAr'CH)_2$ (**2.5**) was firstly prepared by lithiation using ^nBuLi.[55] Subsequently, the salt metathesis reaction between **2.5** and $Cp_2M(Me)Cl$ (M = Zr or Hf) produced $Cp_2M\{NHB(NAr'CH)_2\}(Me)$ (M = Zr (**9**) or Hf (**10**)) after stirring at RT for 16 h (Equation 2.3). Complexes **9** and **10** were isolated in 49% and 41% yield, respectively, by filtration and washing with hexane at 0 °C. The ^1H and ^{13}C NMR spectra of **9** and **10** indicate C_s symmetric structures in the solution phase. The resonances observed include one metal-bound methyl, two equivalent C_5H_5, and one borylamido ligands. The ^{11}B chemical shifts of the borylamido ligand in **9** and **10** are 24.8 and 25.8 ppm, respectively, which can be compared to 23.0 ppm for $H_2NB(NAr'CH)_2$ (**1.110**) and 28.6 ppm for $LiNHB(NAr'CH)_2$ (**2.5**). In addition, an improved synthesis of $Cp_2Hf(Me)Cl$ was developed here, based on the reported selective halodemethylation reactions for other Group 4 metallocenes.[56,57] Thus the readily available Cp_2HfMe_2 reacts with Ph_3CCl at 95 °C for 22 h, yielding $Cp_2HfMeCl$ in 80% isolated yield by simple recrystallisation from hexane at –30 °C.

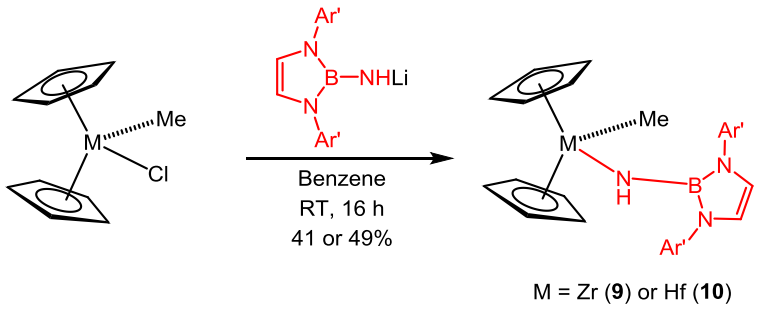

Equation 2.3

Diffraction–quality crystals of compounds **9** and **10** were grown from hexane solutions at 4 °C, and the solid state structures are shown in Figure 2.5 along with selected bond lengths and angles in Table 2.3. The structures of **9** and **10** are fully consistent with the NMR data, possessing a pseudo tetrahedral, C_s geometries. Both contain a borylamido ligand, where the sum of subtended angles at N(1) are 357.97(30) [357.39(31)] and 352.8(3) [359.1(3)]°, respectively, for two crystallographically independent molecules in each cases, indicating sp^2 hybridisation. The average M–C(27) and M–N(1) bond lengths within the zirconium complex **9** are marginally longer than those in **10** (*avg*. 2.324(2) and 2.0875(12) Å (**9**) compared to *avg*. 2.294(2) and 2.074(2) Å (**10**)), due to the lanthanide contraction.

The boryl rings in **9** and **10** are all twisted significantly out of the Cp_2Zr equatorial plane (torsion angle of M(1)–N(1)···B(1)–N(3) = 43.9 [49.8]° (**9**) and 49.9 [45.5]° (**10**)). This is presumably to minimise the steric clash between the bulky boryl group and one of the Cp rings. This can be also reflected by the slightly wider angle of N(1)–M(1)–$Cp_{cen(1)}$ (108.6 [109.0]° (**9**) and 109.5 [108.7]° (**10**)) compared to the N(1)–M(1)–$Cp_{cen(2)}$ angles (106.8 [106.5]° (**9**) and 105.9 [106.5]° (**10**)). In both cases the borylamido ligand bends towards the $Cp_{(1)}$ (as depicted in Figure 2.5) resulting in the perturbed position of $Cp_{(1)}$ ligand, and consequently causing the M(1)–N(1)–B(1) angles (151.37(15) [148.39(16)]° (**9**) and 146.8(2) [151.1(2)]° (**10**)) to become less acute. These M(1)–N(1)–B(1) angles are significantly wider compared to that found in **7** (134.90(5)°). Similarly, these wide angles are observed in previously reported sterically encumbered zirconium amido compounds.[58–62] In compound **9**, the Zr(1)–N(1) bond length is comparable to that in **7**, and the $Cp_{cent(1)}$–M(1)–$Cp_{cent(2)}$ (M = Zr (**9**) and Hf (**10**)) angles are similar to that found in **7**.

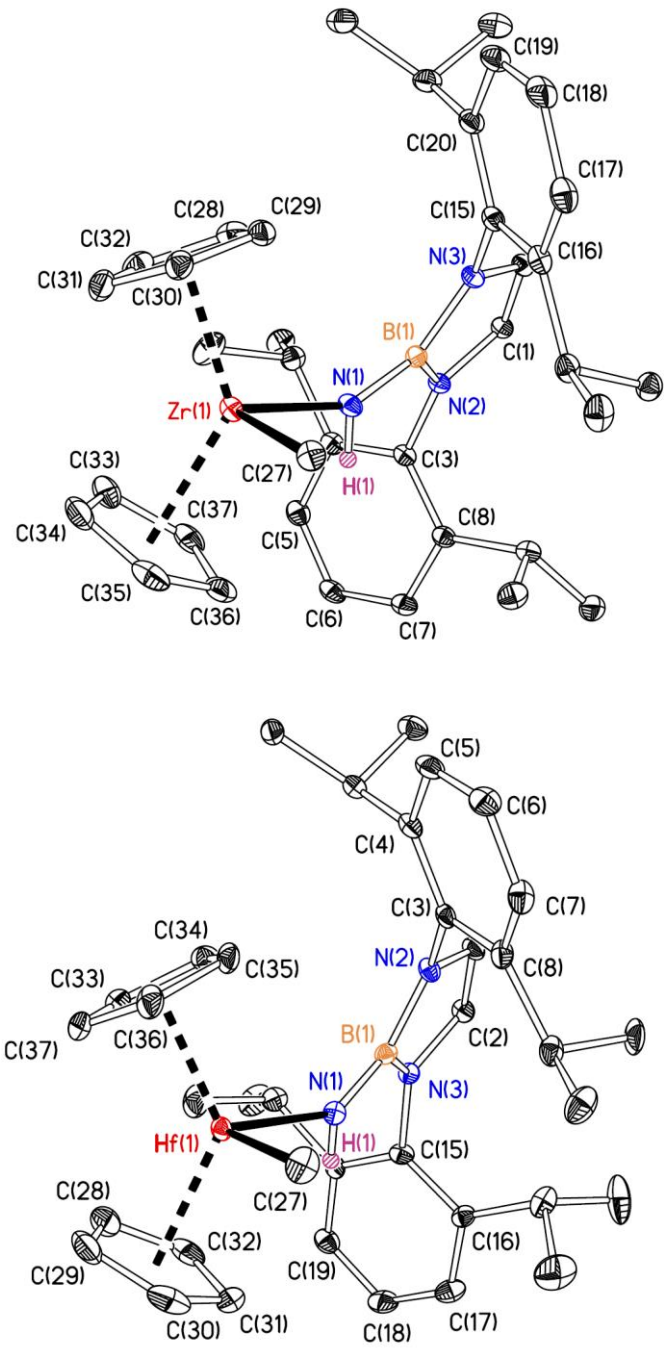

Figure 2.5. Displacement ellipsoid plots (20% probability) of $Cp_2M\{NHB(NAr'CH)_2\}(Me)$ (M = Zr (**9**, top) or Hf (**10**, bottom)). C–bound H atoms omitted for clarity.

Table 2.3. Selected bond lengths (Å) and angles (°) for $Cp_2M\{NHB(NAr'CH)_2\}(Me)$ (M = Zr (**9**) or Hf (**10**)). Values in brackets are for the second crystallographically independent molecule. $Cp_{cent(1)}$ and $Cp_{cent(2)}$ refer to the computed Cp ring centroids for "upper" and "lower" Cp rings, respectively, as depicted in Figure 2.5.

	9	**10**
M(1)–N(1)	2.0780(17) [2.0950(17)]	2.090(3) [2.058(3)]
M(1)–C(27)	2.336(2) [2.312(3)]	2.313(2) [2.275(3)]
$M(1)–Cp_{cent(1)}$	2.22 [2.21]	2.19 [2.19]
$M(1)–Cp_{cent(2)}$	2.25 [2.25]	2.22 [2.23]
N(1)–B(1)	1.433(3) [1.436(3)]	1.434(5) [1.430(4)]
B(1)–N(2)	1.441(3) [1.451(3)]	1.444(4) [1.468(4)]
B(1)–N(3)	1.451(3) [1.454(3)]	1.445(5) [1.427(4)]
$Cp_{cent(1)}–M(1)–Cp_{cent(2)}$	131.3 [130.2]	130.2 [131.3]
$N(1)–M(1)–Cp_{cent(1)}$	108.6 [109.0]	109.5 [108.7]
$N(1)–M(1)–Cp_{cent(2)}$	106.8 [106.5]	105.9 [106.5]
M(1)–N(1)–B(1)	151.37(15) [148.39(16)]	146.8(2) [151.1(2)]
N(1)–B(1)–N(2)	123.24(18) [124.69(19)]	131.7(3) [132.2(3)]
N(1)–B(1)–N(3)	132.64(19) [131.2(2)]	123.8(3) [124.3(3)]

By mixing **9** and pyridine on the NMR tube scale in toluene-d_8, the zirconocene borylimide $Cp_2Zr\{NB(NAr'CH)_2\}(py)$ (**11**) was slowly formed at 120 °C after 16 h, similar to the formation of **8** *via* thermolysis (*vide supra*). This route also enabled the formation of the first hafnium congener $Cp_2Hf\{NB(NAr'CH)_2\}(py)$ (**12**), but requiring an extended reaction time of 72 h to reach completion, as monitored by ^1H NMR spectroscopy. In both cases, a low intensity singlet resonance at 0.17 ppm attributed to CH_4 and diagnostic upfield shifted pyridine resonances for a coordinated pyridine ligand were observed in ^1H NMR spectrum.

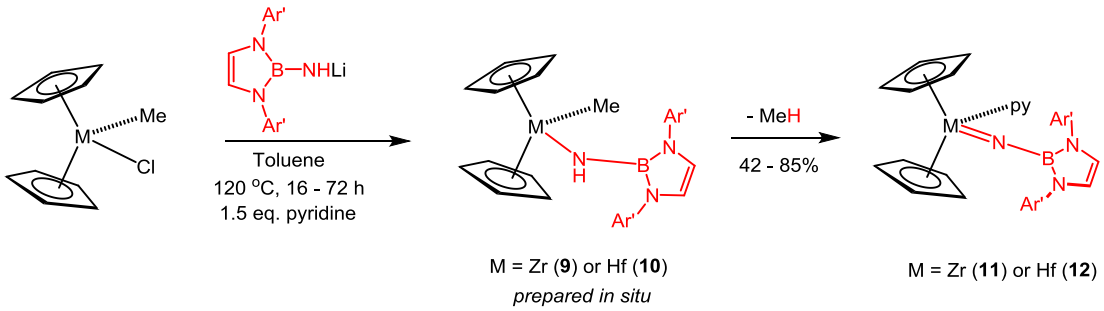

Scheme 2.5. Synthesis of $Cp_2M\{NB(NAr'CH)_2\}(py)$ (M = Zr (**11**) or Hf (**12**)) proceeding through *in situ*-generated borylamides $Cp_2M\{NHB(NAr'CH)_2\}(Me)$ (M = Zr (**9**) or Hf (**10**)).

Given the low isolated yields of the borylamido precursor compounds (49% (**9**) and 41% (**10**)), these borylimides were synthesised directly on the preparative scale by reacting $Cp_2M(Me)Cl$ (M = Zr or Hf) with **2.5**, in the presence of pyridine, under the same reaction condition as for the NMR tube scale, forming the corresponding borylamides *in situ* (Scheme 2.5). Compound **11** was isolated on a multi-gram (3.0 g) scale in 85% overall yield. In contrast, only 42% yield was obtained for the hafnium congener **12** due to higher degree of decomposition to borylamine **1.110** caused by extended reaction time at 120 °C, and subsequent purification by extra washing with hexane to separate the major impurity **1.110**. In the preparation of imido zirconocene compounds, this "one pot" synthesis was found to be unsuccessful, where the presence of lithium inhibits the thermolysis completely giving a complex mixture. However, this is not the case for this borylamide, presumably due to the steric protection of the boryl moiety preventing the coordination with lithium and formation of "ate" species.

For the reactions between imido or hydrazido zirconocene complexes and organic substrates, the formation of a reactive base-free intermediate is believed to be the common first step of the mechanism, thus providing a vacant coordination site for incoming substrates. Therefore, the weaker Lewis base THF was employed to potentially enhance the reactivity of the zirconium borylimide for the later reactivity studies described in Chapter Three. Compound $Cp_2Zr\{NB(NAr'CH)_2\}(THF)$ (**13**) was formed under the same reaction conditions as **11**. However, the yield and scale are limited by a relatively high amounts of impurities and the increased amounts of THF required (20 equivalents) at high temperature, compared to the synthesis of **11**. In comparison, in the presence of the stronger Lewis base DMAP at the same reaction conditions, both of the

complexes $Cp_2M\{NB(NAr'CH)_2\}(DMAP)$ (M = Zr (**14**) and Hf (**15**)) formed cleanly and were successfully isolated in relatively high yields (73% (**14**) and 55% (**15**), Scheme 2.6).

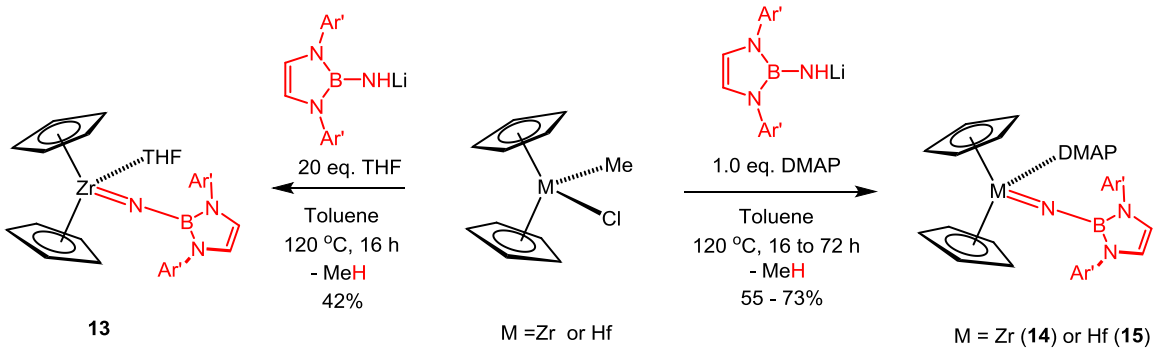

Scheme 2.6. Synthesis of $Cp_2Zr\{NB(NAr'CH)_2\}(THF)$ (**13**) and $Cp_2M\{NB(NAr'CH)_2\}(DMAP)$ (M = Zr (**14**) or Hf (**15**)).

The ^1H and ^{13}C NMR spectra of $Cp_2M\{NB(NAr'CH)_2\}(L)$ (M = Zr, L = THF (**13**), py (**11**) or DMAP (**14**); M = Hf, L = py (**12**) or L = DMAP (**15**)) indicate that they have C_s symmetric structures, which include cyclopentadienyl ligands, a borylimido ligand containing diastereotopic isopropyl methyl groups, and the corresponding coordinated Lewis bases (THF, py or DMAP) in the solution phase. The ^{11}B chemical shifts of the borylimido ligand in zirconium borylimido compounds **11**, **13** and **14** are 20.2, 19.9 and 19.7 ppm, respectively, comparable to 20.7 ppm for **8**, showing no significant difference in ^{11}B chemical shift by changing the boryl substituents and backbone on the boryl moiety, as well as the coordinated Lewis bases. Additionally, the ^{11}B chemical shift for hafnium compounds **12** and **15** are 23.8 and 22.9 ppm respectively, again showing no significant difference by changing the Lewis base. In contrast, the titanium conger $Cp_2Ti\{NB(NAr'CH)_2\}(py)$ (**1.117**) shows a upfield shifted ^{11}B signal at 18.0 ppm,[49] giving an overall trend for the borylimido metallocene complexes that the ^{11}B signal shifts downfield along with the coordinated metal going down the group (Ti, Zr and Hf). These ^{11}B chemical shifts are consistent with the values calculated by DFT for the model compounds $Cp_2M\{NB(NMeCH)_2\}$ (M = Ti (18.6 ppm), Zr (19.5 ppm) or Hf (20.5 ppm) and $Cp_2Ti\{NB(NMeCH)_2\}(py)$ (18.6 ppm).

For a given metal, varying the Lewis bases, no effect on the rate of borylimido complex formation was observed. In contrast employing hafnium, rather than zirconium, significantly extended reaction time for forming the corresponding borylimide was required (16 h for zirconium borylimides and 72 h for hafnium congener). This implies

that the rate-determining step (RDS) involves some degree of metal-ligand bond breaking, since the Hf–X bonds are stronger than Zr–X bonds. Thus, it suggests that the RDS is thermolysis of the parent borylamides forming corresponding base free intermediates, followed by fast Lewis base trapping, which was also found to be the case for the synthesis of zirconocene imido compounds.[10,28,29,59] Further studies will be discussed later (*vide infra*), and the difference in reactivities of $Cp_2Zr\{NB(NAr'CH)_2\}(L)$ (L = THF (**13**), py (**11**) or DMAP (**14**)) is discussed in Chapter Three.

An alternative method of synthesising **14** was also developed, proceeding in one step from the readily available Cp_2ZrCl_2, $LiN(SiMe_3)_2$ and $LiNHB(NAr'CH_2)$ (**2.5**), giving an slightly improved yield 78% (Scheme 2.7). However, an attempt to employ pyridine, rather than DMAP, was unsuccessful giving many unidentified species. The *in situ* generated chloride-borylamido zirconocene compound $Cp_2Zr\{NHB(NAr'CH)_2\}Cl$ (**16**) can be isolated independently in 75% yield from the reaction between Cp_2ZrCl_2 and **2.5**. The ^1H NMR spectrum of **16** is comparable to that of the methyl analogue **9**, apart from the absent methyl resonance, and the ^{11}B NMR spectrum shows a similar resonance at 24.9 ppm. Subsequent salt metathesis with excess **2.5** did not yield bis(borylamido) zirconocene complex $Cp_2Zr\{NHB(NAr'CH)_2\}_2$ presumably due to steric reasons. In contrast, the bis(amido) zirconocene analogue $Cp_2Zr(NHXyl)_2$ (Xyl = 2,6-dimethylphenyl) has been previously reported, which was found to be an effective pre-catalyst for the hydroamination of alkynes *via in situ* generated base free imido compound $[Cp_2Zr(NXyl)]$ (**1.17**).[63] Thus, catalysing hydro-borylamination reactions of alkynes using the borylimido complex **11** were attempted which is described in Chapter Three. The chloride-borylamido hafnium congener $Cp_2Hf\{NHB(NAr'CH)_2\}Cl$ (**17**) was also isolated in 72% yield, using the same method, and the ^1H and ^{13}C NMR spectra are nearly identical to those of **16**. However, this alternative method was unsuccessful for the synthesis of hafnium borylimides from **17**, even using DMAP, giving incompletion and several unidentified species.

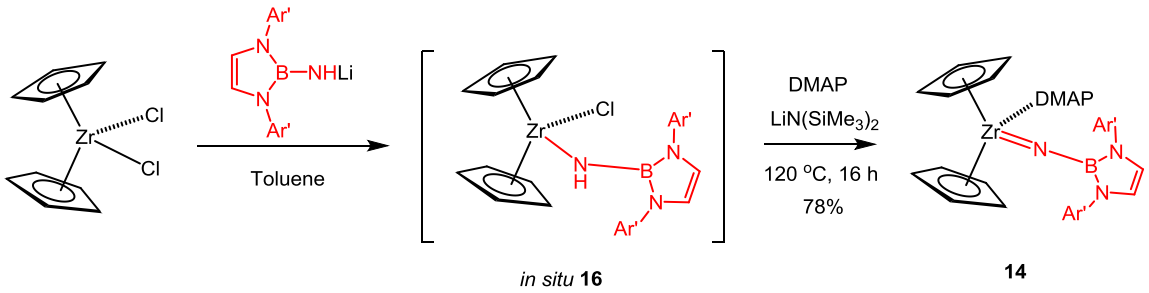

in situ **16** **14**

Scheme 2.7. Alternative synthesis of $Cp_2Zr\{NB(NAr'CH)_2\}(DMAP)$ (**14**).

Diffraction-quality crystals of **11** and **12** were grown from saturated hexane solutions at 4 °C and the solid state structures are shown in Figure 2.6. Selected bond length and angles are given in Table 2.4. Both complexes have pseudo tetrahedral geometries, in which the cyclopentadienyl ligands are mutually staggered and eclipsed, respectively. The $M–N_{im}$ bond lengths are the same within error (**11**, 1.891(3) – 1.902(3) Å for four crystallographically independent molecules; **12**, 1.889(4) [1.898(5)] Å for two crystallographically independent molecules) and also equal to that of $Cp_2Zr\{NB(N^iPr)C_6H_4\}(DMAP)$ (**8**, $Zr–N_{im}$ of 1.895(3) Å), showing that increasing the bulk of substituents on the boryl ligands from ^{i}Pr to Ar' group has no significant influence on the Zr–N bond length.

As in **8** ($Zr–N_{im}$ = 1.895(3) Å), the bond length of $Zr–N_{im}$ bond in **11** is comparable within error to that in $Cp_2Zr(NAr')(THF)$ (**1.50**, $Zr–N_{im}$ = 1.888(2) Å). However, while comparing with a range of zirconium and hafnium arylimides (except **1.50**), the $M–N_{im}$ distances appear significantly shorter (M = Zr, range 1.844(9) – 1.868(3) Å, 4 examples; M = Hf, range 1.822 – 1.859(2) Å, 4 examples).[62,64–66] The long Hf–N bond of **12** reflects the π back-donation from N(1) to the aromatic boryl ring, decreasing the bond order of $Hf–N_{im}$ by reducing the extent of π-donation, as also observed here for the zirconium analogue **11** and previously discussed for **8** (*vide supra*). This is also illustrated by comparing the depicted boryl ring orientation of borylimide and borylamide in the solid state. As previously discussed for the parent borylamides **9** and **10**, the borylamido ligand twisted significantly due to the steric requirement to minimise the steric clash with the Cp ligands. In contrast, for the borylimides **11** and **12**, the boryl ring (plane of N(2)–B(1)–N(3)) is approximately parallel to the Cp_2Zr equatorial plane, which enables the backbonding to the boryl ring from N(1), minimising the π-bonding competition with the Cp ligands. Consequently, this electronically preferred orientation of the borylimido ligand, in both **11** and **12**, perturbed the positions of the Cp rings resulting in a more acute

$Cp_{cent(1)}$–M(1)–$Cp_{cent(2)}$ angle (125.8 – 128.1° (**11**) and 125.6 [126.8]° (**12**)) in contrast to that in the parent borylamides (131.3 [130.2]° (**9**) and 130.2 [131.3]° (**10**)), reflecting the π-loaded nature of borylimido zirconocene complex, like in **8**.[50] Other distances in **12** are slightly shorter than those in **11** due to the lanthanide contraction (e.g. Zr(1)–N(4) = 2.347(3) – 2.356(3) Å, avg. Zr(1)–Cp_{cent} = 2.29 Å (**11**); Hf(1)–N(4) = 2.309(5) [2.316(5)] Å, avg. Hf(1)–Cp_{cent} = 2.26 Å, (**12**)). The terminal hafnium borylimido compound $Cp_2Hf\{NB(NAr'CH)_2\}(py)$ (**12**) possesses a Hf(1)–N(1)–B(1) angle of 157.9(4) [161.1(4)]° which is comparable within error to that in the zirconium congener **11** (Zr(1)–N(1)–B(1) = 158.2(3) – 165.2(3)°).

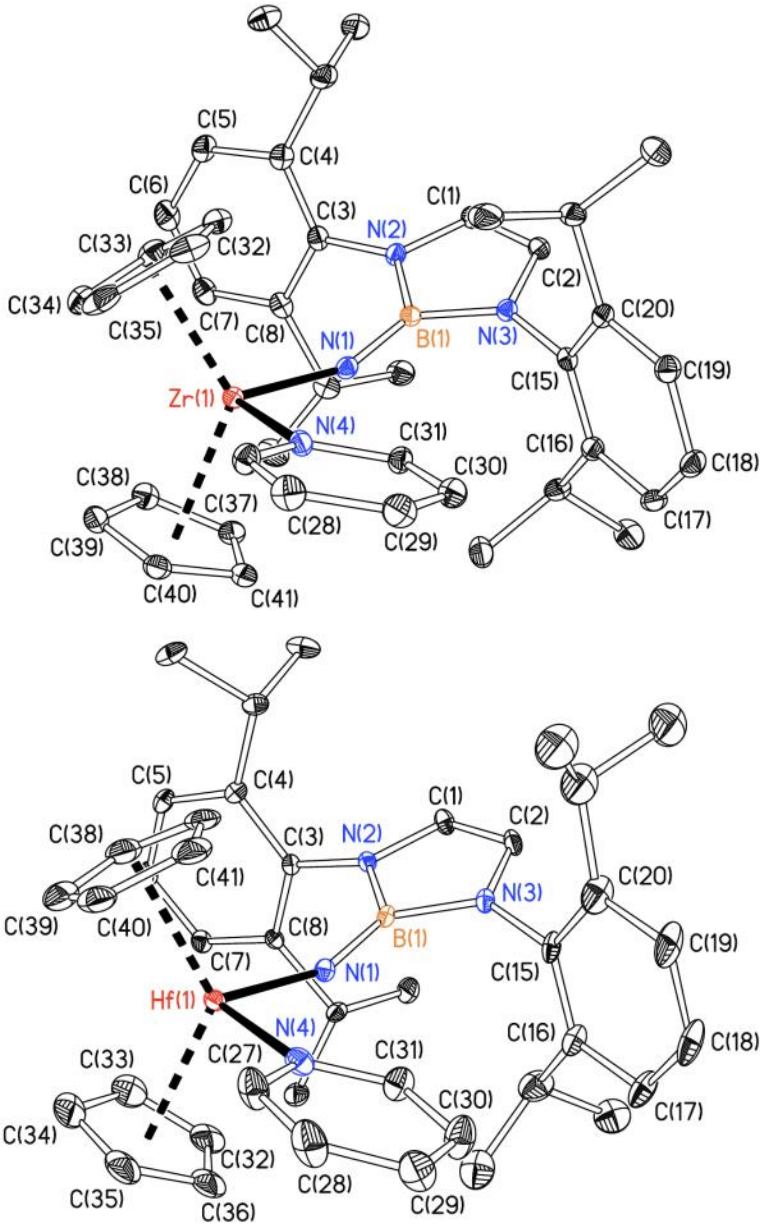

Figure 2.6. Displacement ellipsoid plots (20% probability) of $Cp_2M\{NB(NAr'CH)_2\}(py)$ (M = Zr (**11**, top) or Hf (**12**, bottom)). H atoms omitted for clarity.

Table 2.4. Selected bond lengths (Å) and angles (°) for $Cp_2M\{NB(NAr'CH)_2\}(py)$ (M = Zr (**11**) or Hf (**12**)). Values in brackets are for the second, third and fourth crystallographically independent molecules. $Cp_{cent(1)}$ and $Cp_{cent(2)}$ refer to the computed Cp ring centroids for "upper" and "lower" Cp rings, respectively, as depicted in Figure 2.6.

	11	**12**
M(1)–N(1)	1.902(3) [1.899(3)] [1.891(3)] [1.895(3)]	1.889(4) [1.898(5)]
M(1)–N(4)	2.347(3) [2.350(3)] [2.356(3)] [2.351(3)]	2.309(5) [2.316(5)]
M(1)– $Cp_{cent(1)}$	2.27 [2.29] [2.29] [2.26]	2.24 [2.26]
M(1)–$Cp_{cent(2)}$	2.31 [2.28] [2.28] [2.31]	2.28 [2.25]
N(1)–B(1)	1.400(4) [1.389(5)] [1.395(4)] [1.401(5)]	1.391(8) [1.401(8)]
B(1)–N(2)	1.477(4) [1.467(5)] [1.464(4)] [1.460(5)]	1.477(7) [1.462(8)]
B(1)–N(3)	1.453(4) [1.451(4)] [1.466(4)] [1.461(4)]	1.469(7) [1.467(8)]
$Cp_{cent(1)}$–M(1)–$Cp_{cent(2)}$	126.3 [125.8] [128.1] [126.1]	126.8 [125.6]
N(1)–M(1)–$Cp_{cent(1)}$	110.3 [112.9] [111.7] [111.6]	111.1 [112.9]
N(1)–M(1)–$Cp_{cent(2)}$	112.9 [110.2] [110.6] [112.0]	111.0 [110.7]
M(1)–N(1)–B(1)	158.6(2) [162.1(3)] [165.2(3)] [158.2(3)]	157.9(4) [161.1(4)]
N(1)–B(1)–N(2)	128.8(3) [129.2(3)] [128.6(3)] [128.4(3)]	128.9(5) [129.5(6)]
N(1)–B(1)–N(3)	129.0(3) [128.6(3)] [128.6(3)] [129.0(3)]	129.4(5) [127.8(6)]

The Cp rings of **11** and **12** are both η^5-coordinated to the metal, and the difference in distances between the "top" and "bottom" M–Cp_{cent} for **11** and **12** is 0.011 – 0.053 and 0.018 [0.042] Å, respectively. This is in contrast to the hydrazido analogues $Cp_2Zr(NNPh_2)(DMAP)$ (**1.63**) and $Cp_2Hf(NNPh_2)(DMAP)$ (**2.6**), where the M–Cp_{cent} length are nearly identical.[67] However, in the titanium congener $Cp_2Ti\{NB(NAr'CH)_2\}(py)$ (**1.117**),[49] one of the Cp rings has a considerable tilt away from the borylimido ligand giving 0.08 Å in length difference between Ti–$Cp_{cent(1)}$ and Ti–$Cp_{cent(2)}$. Therefore, the bonding situation of one of the Cp for **1.117** may be moving towards an η^3-coordination mode. Similarly, this is also observed for $Cp_2Ti(NNPh_2)(DMAP)$ (**2.7**) in which the difference between M–$Cp_{cent(1)}$ and M–$Cp_{cent(2)}$ is 0.052 Å. This tilting effect could be caused by both electronic (20 VE) and steric effects, as in general, the titanium is smaller than zirconium and hafnium, thus having a more crowded coordination environment around the metal center.

2.4 C–H bond activation of benzene by transient $Cp_2Zr\{NB(NAr'CH)_2\}$

When $Cp_2Zr\{NB(NAr'CH)_2\}(py)$ (**11**) was synthesised on the preparative scale, trace amounts of impurities were observed in the ^{1}H NMR spectrum. The amounts of impurities were increased when the weaker Lewis base, THF, was employed for generating $Cp_2Zr\{NB(NAr'CH)_2\}(THF)$ (**13**), whereas they were barely observed using the stronger Lewis base DMAP. To investigate the identity of these impurities, a reaction of $Cp_2Zr\{NHB(NAr'CH)_2\}(Me)$ (**9**) in toluene was performed at 120 °C for 16 h, in the absence of Lewis base on the preparative scale. In the ^{1}H NMR spectrum, three major C_5H_5 resonances were observed, as well as three singlets at 2.35, 2.32 and 1.98 ppm possibly attributed to the methyl protons on the tolyl functional group which are absent for the NMR tube scale reaction in toluene-d_8. These suggest the formation of putative $Cp_2Zr\{NHB(NAr'CH)_2\}(Tol)$ regioisomers by C–H bond activation at the *o*-, *m*- and *p*-positions of toluene. This is also supported by the ^{11}B NMR spectrum showing a broad resonance at 24.7 ppm which is consistent with the characteristic chemical shift for a zirconocene borylamide (e.g. 24.8 ppm for **9**). Unfortunately, in an attempt to isolate a single regioisomer by crystallisation was unsuccessful.

To give an analogous product without regioisomers, benzene was similarly employed. On the preparative scale at 90 °C for 7 days, exclusive formation of

$Cp_2Zr\{NHB(NAr'CH)_2\}(Ph)$ (**18**) resulted, and this was isolated in 40% yield as a pale yellow solid. The ^1H NMR spectrum of isolated **18** shows a broad NH singlet resonance at 5.45 ppm, and the ^{11}B NMR spectrum gives the resonance at 24.8 ppm, both indicating the formation of a borylamide. An HSQC correlation is found between *o*-$C_6\underline{H}_5$ resonances at 7.12 ppm and a ^{13}C resonance at 126.9 ppm, as well as an HMBC correlation being observed to a ^{13}C resonance at 178.9 ppm. The latter downfield resonance is diagnostic of the carbon (*i*-$\underline{C}_6H_5$) which is directly bonded to the zirconium center.

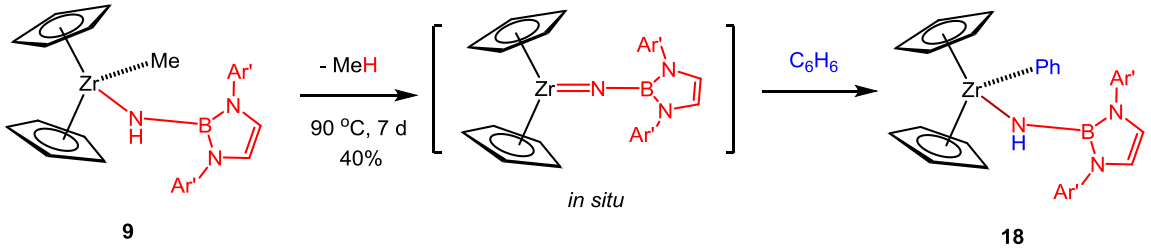

9 **18**

Scheme 2.8. C–H bond activation of benzene and the synthesis of $Cp_2Zr\{NHB(NAr'CH)_2\}(Ph)$ (**18**).

In order to investigate the mechanism, a similar reaction was performed on the NMR tube scale in C_6D_6 at 90 °C, and the formation of $Cp_2Zr\{NDB(NAr'CH)_2\}(C_6D_5)$ (**18-*d*$_6$**) was monitored by ^1H NMR spectroscopy. In this instance, the NH resonance at 5.45 ppm was absent in the ^1H NMR spectrum and a corresponding signal was observed in the ^2H NMR spectrum. Additionally, a triplet resonance of CH_3D was not observed by ^1H NMR spectroscopy, which reveals that the direct sigma-bond metathesis between Zr–Me and C_6D_6 did not occur. Instead a low intensity singlet resonance at 0.17 ppm attributing to CH_4 was observed showing that the thermolysis takes place forming the base free intermediate $Cp_2Zr\{NB(NAr'CH)_2\}$, followed by C–H bond activation on benzene (Scheme 2.8).

To further support this proposed mechanism, the C–H bond activation reaction of benzene was also performed by heating isolated $Cp_2Zr\{NB(NAr'CH)_2\}(L)$ (L = py (**11**) or THF (**13**)) at 90 °C in C_6D_6 on the NMR tube scale. Compound **18-*d*$_6$** was formed in 87% NMR yield after 16 h from the reaction of **13**, in which the THF is weakly coordinated to the zirconium centre, whereas only 5% **18-*d*$_6$** was formed when **11** was employed under the same reaction condition. On standing for 7 days at this temperature, the C–H bond activation were both significantly slowed down, giving only extra 5% conversion of **18-*d*$_6$** from the reactions of both **13** (92% overall) and **11** (10% overall). The retarded C–H bond activations of **11** and **13**, in the late stage, are possibly due to overall equilibria that

the formed **18-d_6** undergoes slow thermolysis at this high temperature to reform the base free intermediate followed by Lewis base (THF or pyridine) trapping, where the formation of **11** is more thermodynamically favoured than that of **13**. Additionally, the increased amount of free Lewis base also slows down the base dissociation pathway. The much faster formation of **18-d_6** from **13** (*cf.* **11**) confirms that the C–H bond activation proceeds through the base free intermediate.

This thermolysis mechanism proceeding through a base free intermediate was found to be the case for all of the previously reported C–H bond activations by zirconium imido complexes. Reactions with benzene and more unreactive sp^3 C–H bonds (e.g. CH_4) by a transient bis(amido)imido zirconium complex was reported by Wolczanski and co-workers, where the elevated reactivity is likely due to the greater coordinative and electronic unsaturation compared to a metallocene system.[68] For the zirconocene system, the sp^2 C–H bond activation of benzene and other substrates (e.g. indene, ferrocene and norbornene) by the alkylimido zirconocene complex $Cp_2Zr(N^tBu)(THF)$ (**1.4**) was also previously reported by Bergmam.[10,30] More recently, selective primary sp^3 C–H bond activation of hexane and other saturated hydrocarbons has been achieved by using the base free racemic ethylenebis(tetrahydro)indenyl supported $Zr{=}N^tBu$ intermediate.[59] However, no reaction was observed between the arylimido zirconocene complex $Cp_2Zr(NXyl)(THF)$ (**2.8**) and benzene under any conditions. This lack of reactivity was proposed to be ascribed to the stabilization of the imide lone pair by the aryl substituent.[10,29] Although similar stabilisation was observed in the borylimido zirconocene complexes (**1.50**) where the boryl ring is also aromatic, the reactivity based on the Zr=N multiple bond is more like the alkylimido zirconocene complexes. The more reactive borylimide (*cf.* arylimide) is likely arisen from the higher strength of the newly formed N–H bond in the product (thermodynamically favoured),[52] as described in Section 1.7. To probe the electronic origin of this difference further, DFT calculation were carried out for the model reaction of $Cp_2Zr(NR)$ with C_6H_6 forming $Cp_2Zr(NHR)(Ph)$. The ΔE (gas phase electronic energy exchange) became less negative in the order R = Me (–21.0 kcal mol^{-1}) < $B(NMeCH)_2$ (–18.0 kcal mol^{-1}) < Xyl (–11.6 kcal mol^{-1}), consistent with experimental observations.

Diffraction-quality crystals of **18** were grown from a hexane solution at 4 °C, and the compound was then structurally characterised. The molecular solid state structure is shown in Figure 2.7, and selected bond distances and angles are listed in Table 2.5.

Molecules of the compound **18** possess a pseudo tetrahedral environment, with staggered cyclopentadienyl rings. The Zr(1)–N(1)–B(1) linkage of **18** shows Zr(1)–N(1) and N(1)–B(1) single bonds distances of 2.0877(11) Å and 1.4417(18) Å, respectively, and the Zr(1)–N(1)–B(1) bond angle is 142.46(9)°, which are comparable with those in the analogous borylamido compound $Cp_2Zr\{NHB(NAr'CH)_2\}(Me)$ (**9**). Additionally, the phenyl ring is bound to Zr(1) with the Zr(1)–C(27) distance being 2.3022(13) Å (*cf.* 2.336(2) [2.312(3)] Å in **9**).

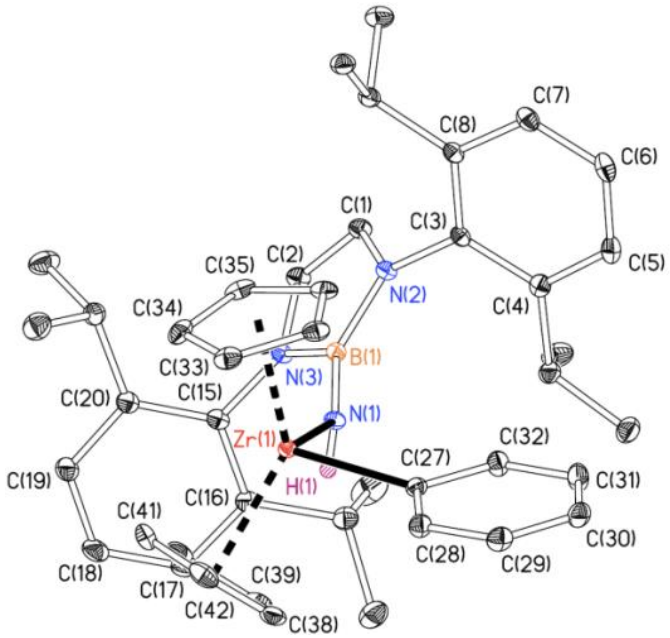

Figure 2.7. Displacement ellipsoid plot (20% probability) of $Cp_2Zr\{NHB(NAr'CH)_2\}(Ph)$ (**18**). C–bound H atoms omitted for clarity.

Table 2.5. Selected bond lengths (Å) and angles (°) for $Cp_2Zr\{NHB(NAr'CH)_2\}(Ph)$ (**18**). $Cp_{cent(1)}$ and $Cp_{cent(2)}$ refer to the computed Cp ring centroids for "upper" and "lower" Cp rings, respectively, as depicted in Figure 2.7.

Zr(1)–N(1)	2.0877(11)	$Cp_{cent(1)}$–Zr(1)–$Cp_{cent(2)}$	132.5
Zr(1)–C(27)	2.3022(13)	N(1)–Zr(1)–$Cp_{cent(1)}$	106.7
Zr(1)–$Cp_{cent(1)}$	2.210	N(1)–Zr(1)–$Cp_{cent(2)}$	107.5
Zr(1)–$Cp_{cent(2)}$	2.245	Zr(1)–N(1)–B(1)	142.46(9)
N(1)–B(1)	1.4417(18)	N(1)–B(1)–N(2)	132.60(12)
B(1)–N(2)	1.4505(18)	N(1)–B(1)–N(3)	123.83(12)
B(1)–N(3)	1.4450(18)		

2.5 H–H bond activation by $Cp_2Zr\{NB(NAr'CH)_2\}(py)$ (11)

Given the relative ease with which the base free borylimido complex $Cp_2Zr\{NB(NAr'CH)_2\}$ activates the C–H bond of benzene, the reactions of the borylimido complexes $Cp_2Zr\{NB(NAr'CH)_2\}(L)$ (L = py (**11**) or DMAP (**14**)) with H_2 were next investigated. Exposure of a C_6D_6 solution of **11** in an NMR tube to 1.2 bar of H_2 at 60 °C resulted in slow conversion to a single zirconium-containing product and free pyridine after 16 h (Equation 2.5). The ^1H NMR spectrum of the reaction mixture shows that the borylamido-hydrido product $Cp_2Zr\{NHB(NAr'CH)_2\}(H)$ (**19**) was formed, where diagnostic N–H and Zr–H resonances at 5.22 and 4.71 ppm, respectively, as well as other functional groups including a singlet C_5H_5 resonance at 5.47 ppm, and a septet (4 H), two doublets (12 H each) and a singlet (2 H) attributed to the boryl moiety. Additionally, infrared resonances at 3289 and 1582 cm^{-1} attributable to ν(N–H) and ν(Zr–H), respectively, are consistent with the ^1H NMR data, indicating the formation of a borylamido-hydrido complex. Again, this is also supported by the ^{11}B NMR spectrum showing a diagnostic borylamide resonance at 24.5 ppm. Upon continued heating the solution at 60 °C for another 16 h did not yield further hydrogenolysis forming $Cp_2Zr(H)_2$ and $H_2NB(NAr'CH)_2$ (**1.110**). Meanwhile, the reaction of **14** with H_2 gave no reaction at all after 16 h under the same reaction condition. DFT calculation (full systems) suggests the lack of reactivity of **14** may be due to thermodynamic limitation. Thus the formation of **19** from **11** was computed to be exergonic (Δ_rG = –3.3 kcal mol^{-1}) and slightly endothermic (Δ_rH = 1.9 kcal mol^{-1}), whereas formation of **19** from **14** was only slightly exergonic (Δ_rG = –0.8 kcal mol^{-1}) and significantly endothermic (Δ_rH = 6.3 kcal mol^{-1}). In addition, formation of Cp_2ZrH_2 and **1.110** from **19** and H_2 was highly endergonic (Δ_rG = 15.1 kcal mol^{-1}). The mechanism is proposed to be the initial formation of the base free intermediate followed by 1,2-addition of H_2 across the Zr=N multiple bond.

Compound **19** can be alternatively synthesised *via* salt metathesis on the preparative scale by reacting Schwartz's reagent $Cp_2Zr(H)Cl$ with $LiNHB(NAr'CH)_2$ (**2.5**) in benzene at RT (Equation 2.4). After 16 h stirring, complex **19** was isolated in 38% yield as pale yellow crystals.

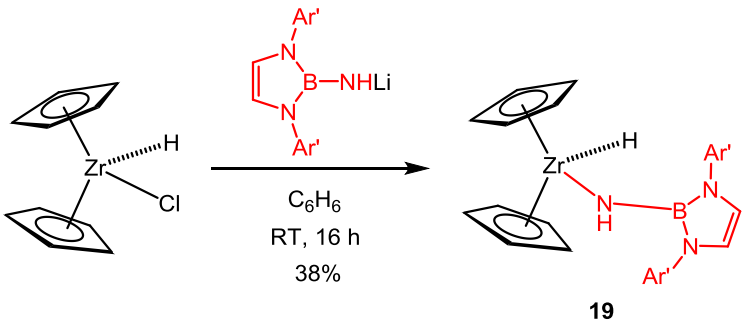

19

Equation 2.4

Since the reaction between $Cp_2Zr(N^tBu)(THF)$ (**1.4**) and H_2 has not been reported previously, the reaction between **1.4** and H_2 was performed at RT in C_6D_6 on the NMR tube scale for comparison with borylimido analogues. Fast formation of the analogous amido-hydrido product $Cp_2Zr(NH^tBu)(H)$ (**20**) was observed, accompanied by free THF. Similarly, the diagnostic N–H and Zr–H resonances at 5.72 and 4.29 ppm, respectively, were found in the ^1H NMR spectrum. The shifted ^{13}C signal of the quaternary carbon $\underline{C}Me_3$ of the amido ligand at 57.1 ppm is comparable with that of the $Cp_2Zr(NH^tBu)(Me)$ at 56.5 ppm.[29] Unfortunately, attempts to synthesis **20** on the preparative scale were unsuccessful.

Similar 1,2-additions of H_2 across M=NR multiple bonded compounds have been previously reported, especially in metallocene based systems. The first Group 4 imido complexes undergoing 1,2-addition with H_2 forming amido-hydride zirconium and titanium complexes were reported by Wolczanski and co-workers.[69–73] Later, Bercaw reported a similar reaction by reacting a cationic Group 5 species $[Cp^*_2Ta(N^tBu)(THF)][B(C_6F_5)_4]$ (**2.9**) with H_2 at RT forming $[Cp^*_2Ta(NH^tBu)(H)][B(C_6F_5)_4]$ (**2.10**), which was structurally authenticated.[74] Chirik and co-workers reported the study and synthesis of the first neutral amido-hydride complexes $Cp^{Me4}Zr(NHR)(H)$ (R = ^{t}Bu, NMe_2, Ph and Me) by reacting the corresponding primary amine or hydrazine with $[Cp^{Me4}Zr(H)_2]_2$.[75] Detailed mechanistic studies of the D_2 isotopic exchange supported by computational calculations were discussed by comparing the rate constants of the N–H and Zr–H isotopic exchange, which reveals a 1,2-elimination pathway (thermolysis). This proposed mechanism for the fast intramolecular isotopic exchange also clearly suggests the formation of a d^0 η^2-dihydrogen imido transient intermediate $Cp^{Me4}Zr(NR)(\eta^2\text{-}H_2)$.

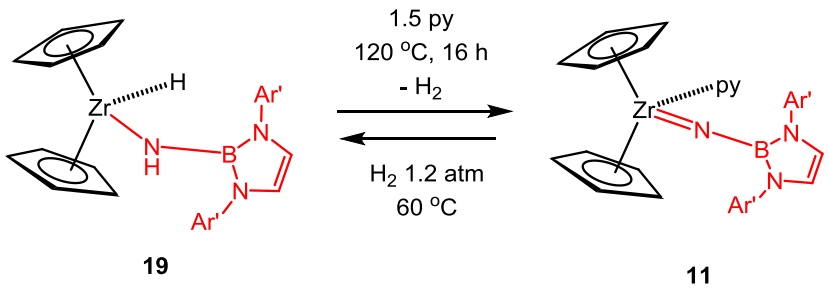

Equation 2.5

When a toluene-d_8 solution of **19** and one equivalent of pyridine was heated at 120 °C, formation of $Cp_2Zr\{NB(NAr'CH)_2\}(py)$ (**11**) was achieved in *ca.* 70% NMR yield (*ca.* 30% **19**) after 16 h (Equation 2.5), along with liberated H_2, as observed by NMR spectroscopy (singlet at 4.47 ppm). The reaction was found to reach equilibrium and continued heating of the reaction solution gave no further conversion to **11**. A similar thermolysis process occurred for the imido analogue **20**, however, with more unidentified impurities. These imply that the thermolysis took place, producing the base free intermediate $Cp_2Zr\{NB(NAr'CH)_2\}$ followed by pyridine trapping. The formation of this base free borylimido intermediate is consistent with the previously reported base free imido intermediate of $Cp^{Me4}Zr(N^tBu)(H)$ **(2.10)** for D_2 exchange.[75] However, it is not clear whether dihydrogen is η^2-coordinated on the base free borylimido intermediate $Cp_2Zr\{NB(NAr'CH)_2\}$, prior to the pyridine trapping. Reversible H_2 addition and elimination has been reported for the titanium imido complex $Cp^*_2Ti(NPh)$ (**2.11**), but under milder condition.[76]

Diffraction-quality crystals of **19** were grown from a hexane solution at 4 °C. The molecular solid state structure is shown in Figure 2.8, and selected bond distances and angles are listed in Table 2.6. Molecules of compound **19** possess a pseudo tetrahedral environment, with staggered cyclopentadienyl rings. The Zr(1)–N(1)–B(1) linkage of **19** shows Zr(1)–N(1) and N(1)–B(1) single bonds of 2.0753(15) [2.0703(16)] Å and 1.437(3) [1.442(3)] Å, respectively, and Zr(1)–N(1)–B(1) bond angle of 147.86(13) [149.74(13)]°, which are consistent with those in the analogous borylamido compound **9** and **18**. The Zr–H bond distance of 1.903(9) [1.892(10)] Å is comparable to those reported zirconocene hydride complexes (e.g. $Cp_2Zr(H)\{N(SiHMe_2)\}_2$, Zr–H = 1.90(3) Å).[77]

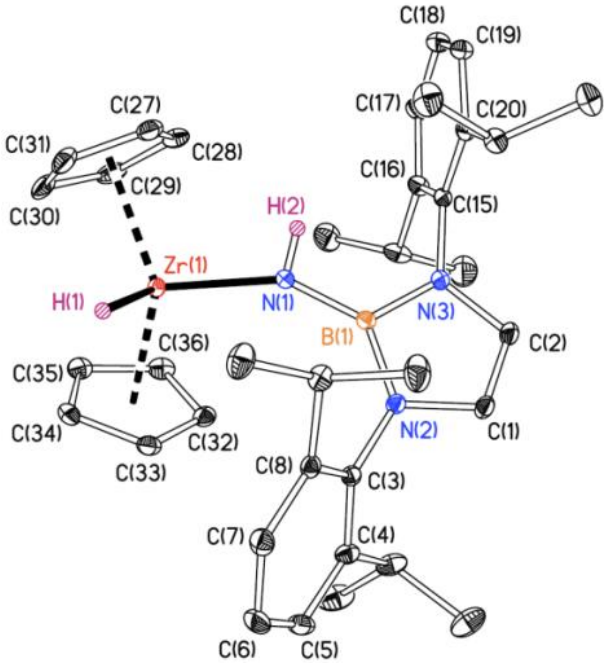

Figure 2.8. Displacement ellipsoid plot (20% probability) of $Cp_2Zr\{NHB(NAr'CH)_2\}(H)$ (**19**). C–bound H atoms omitted for clarity.

Table 2.6. Selected bond lengths (Å) and angles (°) for $Cp_2Zr\{NHB(NAr'CH)_2\}(H)$ (**19**). Values in brackets are for the second crystallographically independent molecules. $Cp_{cent(1)}$ and $Cp_{cent(2)}$ refer to the computed Cp ring centroids for "upper" and "lower" Cp rings, respectively, as depicted in Figure 2.8.

Zr(1)–N(1)	2.0753(15) [2.0703(16)]
Zr(1)–H(1)	1.903(9) [1.892(10)]
$Zr(1)–Cp_{cent(1)}$	2.22 [2.21]
$Zr(1)–Cp_{cent(2)}$	2.21 [2.22]
N(1)–B(1)	1.437(3) [1.442(3)]
B(1)–N(2)	1.448(2) [1.446(2)]
B(1)–N(3)	1.443(2) [1.434(3)]
$Cp_{cent(1)}–Zr(1)–Cp_{cent(2)}$	132.7 [134.2]
$N(1)–Zr(1)–Cp_{cent(1)}$	111.7 [109.8]
$N(1)–Zr(1)–Cp_{cent(2)}$	109.5 [107.9]
Zr(1)–N(1)–B(1)	147.86(13) [149.74(13)]
N(1)–B(1)–N(2)	132.45(17) [132.17(17)]
N(1)–B(1)–N(3)	123.33(17) [123.54(17)]

2.6 Synthesis of $Ind_2Zr\{NHB(NAr'CH)_2\}(Me)$ (21) and $Ind_2Zr\{NB(NAr'CH)_2\}(L)$

To explore the binding situation for these π-loaded borylimido zirconocene compounds, indenyl ligands are employed here, in which the fused benzene ring results in more facile η^5 to η^3 ring isomerisation than for cyclopentadienyl ligands.[78,79] In this instance, η^3-coordination could be invoked to avoid the formation of 20 VE species. Examples of both an η^3-indenyl imido complex Ti(η^5-Cp)(η^3-Ind)(N^{t}Bu)(py) (18 VE) and an η^5-indenyl imido complex Ti(η^5-Ind^{Me_3})(N^{t}Bu)Cl($NC_5H_4{}^t$Bu) (16 VE) have been previously reported by Mountford and co-workers, where the variation in the bonding situation is due to the electron-count.[23] Similar observation has been found in the sandwich molybdenum *tert*-butylimido complexes, in which employing an indenyl ligand gives the ring-slipped complex (η^5-Cp^{ipr})(η^3-Ind)Mo(N^{t}Bu) (18 VE), in contrast to (η^5-Cp^R)$_2$Mo(N^{t}Bu) (20 VE).[80] Given the successful synthesis of the borylimido zirconocene complex **11** and the analogous ethylenebis(tetrahydroindenyl) supported zirconium imido analogue *rac*-(η^5-ebthi)Zr(N^{t}Bu)(py) (**2.12**) reported by Bergman,[59] the synthesis of $Ind_2Zr\{NHB(NAr'CH)_2\}(Me)$ (**21**) and $Ind_2Zr\{NB(NAr'CH)_2\}(L)$ (L = THF (**22**), py (**23**) or DMAP (**24**)) were targeted.

On the preparative scale, mixing $Ind_2Zr(Me)Cl$ and $LiNHB(NAr'CH)_2$ (**2.5**) in benzene, followed by 16 h stirring at RT produced the bis(indenyl) ligand supported zirconium borylamide $Ind_2Zr\{NHB(NAr'CH)_2\}(Me)$ (**21**) in 66% yield as yellow solids. Performing the thermolysis reaction in the presence of the corresponding Lewis base at 120°C on the NMR tube scale, fast formation of the indenyl-supported borylimido compounds **22**, **23** and **24** were observed by ^{1}H NMR spectroscopy. As found for the synthesis of zirconium analogues **11** and **12**, compounds **22**, **23** and **24** can also be synthesised in "one pot" proceeding through *in situ*-generated **21** on the preparative scale, giving improved overall yields 65 – 76% (Scheme 2.9).

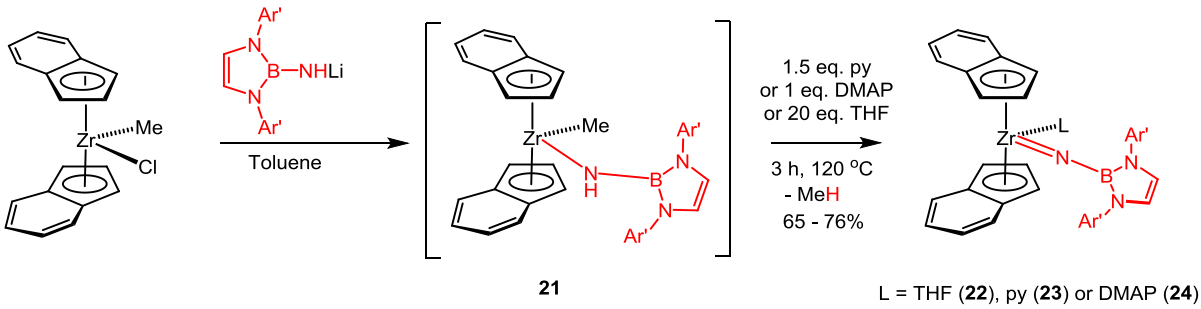

Scheme 2.9. Synthesis of $Ind_2Zr\{NB(NAr'CH)_2\}(L)$ (L = THF (**22**), py (**23**) or DMAP (**24**)).

Diffraction-quality crystals of **21** and **23** were grown from saturated hexane or toluene solutions, respectively at 4 °C, and the solid state structures are shown in Figure 2.9 along with selected bond lengths and angles in Table 2.7. Both of **21** and **23** have pseudo tetrahedral geometries, in which the indenyl ligands are *anti* and *syn* orientated, respectively, in the solid state, with the arrangement of ligands about the zirconium being analogous to the zirconocene compounds **9** and **11**. For example, the Zr(1)–N(4)/C(27) bond length of 2.338(3) and 2.306(4) [2.315(5)] Å in **23** and **21**, respectively, are comparable to those of the metallocene compounds **11** and **9** and the bond length of Zr(1)–N(1) in borylamide **21** (2.076(3) [2.077(3)] Å) is the same as that in **9** within error. The Ind_{cent}–Zr distances in both **23** and **21** are generally slightly longer than the Cp_{cent}–Zr distances in **11** and **9**. The Zr–N_{im} bond length in borylimide **23** (1.872(3) Å) is marginally shorter than what found in **11** and **8**, which may reflect stronger Zr–N_{im} bond. DFT studies of the bonding in bis(indenyl) ligand supported zirconium borylimide are discussed later in this Chapter.

The Zr(1)–Ind_{cent} distances in **23** of 2.33 and 2.35 Å are comparable to those in *rac*-(η^5-ebthi)Zr(N^tBu)(py) (**2.12**, 2.32 and 2.33 Å). The individual Zr–C(Ind) distances are substantially different with a wide range (2.501(5) – 2.790(3) Å), in contrast to other bis(indenyl) zirconium compounds (e.g. Ind_2ZrR_2; 2.457(7) – 2.587(7) Å (R = CO), 2.478(8) – 2.616(8) Å (R = Cl), 2.508(2) – 2.691(3) Å (R = NC_3H_6)).[81–83] Furthermore, the slip parameters, which is defined in the literature,[84] $\Delta_{Zr–C\text{-}Ind}$ of 0.169(8) and 0.208(8) Å for Ind(1) and Ind(2), respectively, in **23**, are relatively longer than those measured in the borylamide **21** ($\Delta_{Zr–C\text{-}Ind(1)}$ = 0.122(8) [0.128(8)] Å and $\Delta_{Zr–C\text{-}Ind(2)}$ = 0.127(8) [0.111(9)] Å), and they are at the high end of the range observed for $IndRhL_2$ complexes generally, e.g. $\Delta_{M–C\text{-}Ind}$ = 0.112(2) – 0.227(3) Å, indicating some degree of ring slippage.[85] The hinge angles ($HA_{(1)/(2)}$ = 3.25 and 7.17 °) and fold angles ($FA_{(1)/(2)}$ = 8.01

and 9.18 °) of **23**, which again are slightly higher than those in **21**, are comparable with those for Ind_2Co (distorted η^5-bonding mode) and lower than those in Ind_2Ni (*ca*. half-way to η^3-bonding mode),[84] demonstrating the η^5-bonding mode for indenyl ligands in **23**, but slightly distorted.

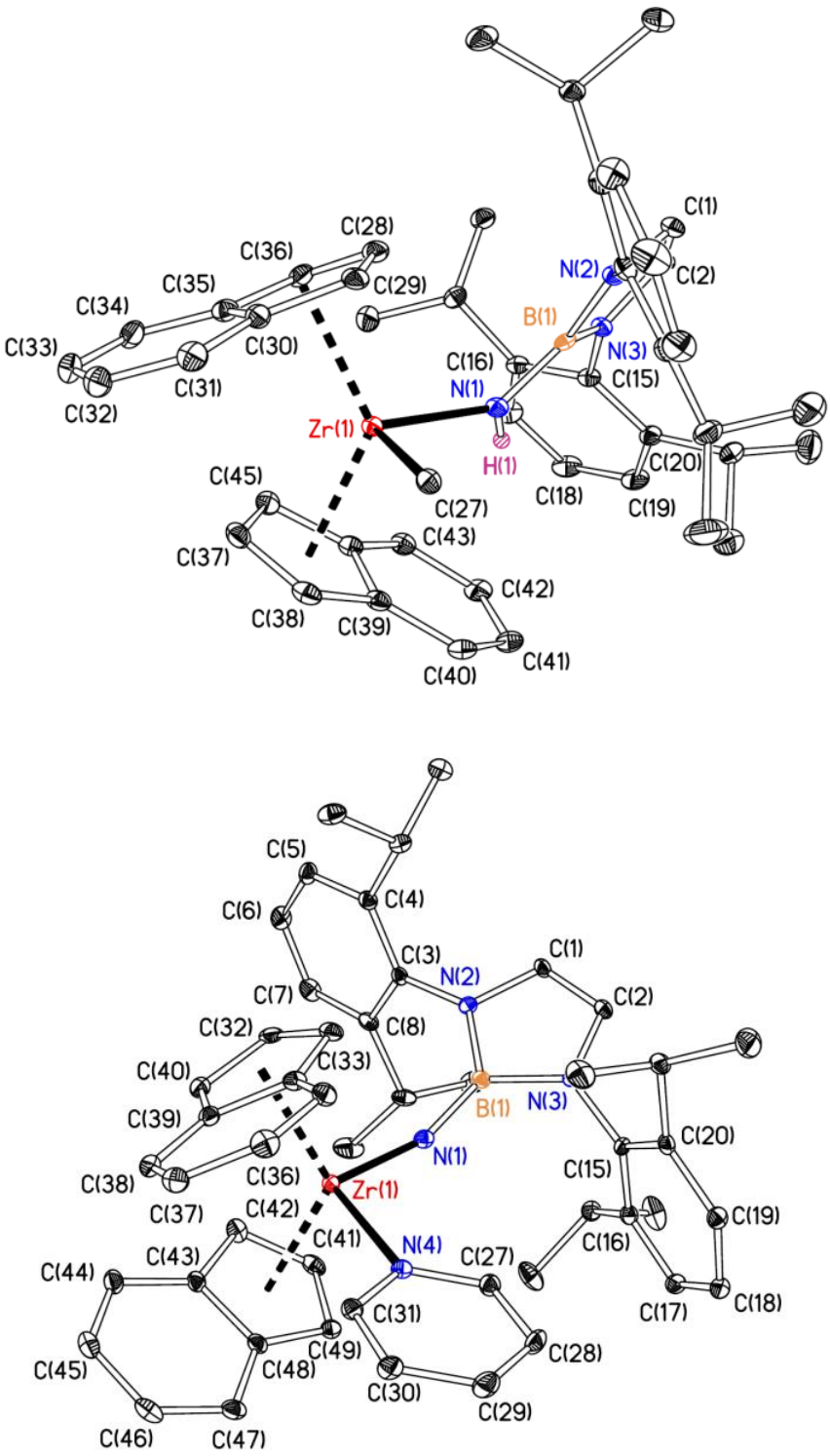

Figure 2.9. Displacement ellipsoid plots (20% probability) of $Ind_2Zr\{NHB(NAr'CH)_2\}(Me)$ (**21,** top) and $Ind_2Zr\{NB(NAr'CH)_2\}(py)$ (**23**, bottom). C–bound H atoms omitted for clarity.

Table 2.7. Selected bond lengths (Å) and angles (°) for $Ind_2Zr\{NHB(NAr'CH)_2\}(Me)$ (**21**) and $Ind_2Zr\{NB(NAr'CH)_2\}(py)$ (**23**). Values in brackets are for the second crystallographically independent molecule. $Ind_{cent(1)}$ and $Ind_{cent(2)}$ refer to the computed centroids for "upper" and "lower" indenyl five-membered rings, respectively, as depicted in Figure 2.9.

	21	**23**
Zr(1)–N(1)	2.076(3) [2.077(3)]	1.872(3)
Zr(1)–N(4)/C(27)	2.306(4) [2.315(5)]	2.338(3)
$Zr(1)–Ind_{cent(1)}$	2.257 [2.244]	2.331
$Zr(1)–Ind_{cent(2)}$	2.269 [2.277]	2.346
N(1)–B(1)	1.434(5) [1.437(5)]	1.410(5)
B(1)–N(2)	1.453(5) [1.457(5)]	1.474(5)
B(1)–N(3)	1.453(5) [1.447(5)]	1.469(5)
$Ind_{cent(1)}–Zr(1)–Ind_{cent(2)}$	128.8 [130.5]	127.0
$N(1)–Zr(1)–Ind_{cent(1)}$	111.4 [110.3]	108.3
$N(1)–Zr(1)–Ind_{cent(2)}$	107.5 [106.7]	112.0
Zr(1)–N(1)–B(1)	142.3(3) [143.3(3)]	157.4(3)
$\Delta_{Zr–C\text{-}ind(1)}{}^{a}$	0.122(8) [0.128(8)]	0.169(8)
$\Delta_{Zr–C\text{-}ind(2)}{}^{a}$	0.127(8) [0.111(9)]	0.208(8)
$HA_{ind(1)}{}^{b}$	4.99 [3.81]	3.25
$HA_{ind(2)}{}^{b}$	4.38 [4.96]	7.12
$FA_{ind(1)}{}^{c}$	7.30 [6.24]	8.01
$FA_{ind(2)}{}^{c}$	4.76 [6.02]	9.18

a. slippage parameter, *b*. hinge angle, *c*. fold angle for the "upper" Ind(1) and "lower" Ind(2), respectively, as depicted in Figure 2.9.[84]

The ^{1}H and ^{13}C NMR spectra of **21** and **23** indicate that those complexes have C_s symmetric structures in the solution phase, similar to the metallocene analogues **9** and **11**. However, in this case, the prochiral indenyl ligands give rise to seven individual

resonances due to reduced symmetry of the indenyl rings. The ^{11}B chemical shifts of **21** and **23** are 24.7 and 17.7 ppm, respectively, showing the same trend as in the analogous borylamido and borylimido zirconocene compounds (*vide supra*). It was reported that the ^{13}C chemical shift for the bridgehead quaternary carbon atoms of Group 4 η^5-indenyl (and ring-methylated indenyl) transition metals commonly appear in the 127 – 136 ppm region, giving an indication of the degree of folding of the indenyl ligand.[86,87] For **23**, the bridgehead atom ^{13}C chemical shifts are 128.5 and 128.7 ppm, being again consistent with the η^5-bonding mode, as previously discussed for the solid state structure.

Attention is now given to the mechanism of formation of the borylimido zirconium compounds **23** and **11**. The reaction time for the formation of **23** (3 h) is significantly shorter than that for **11** (16 h) at the same temperature (120 °C) on the NMR tube and preparative scales. Thus, in contrast to the cyclopentadienyl ligands, the indenyl ancillary ligands appear to accelerate the reaction rate significantly. The indenyl ligand acceleration effect is commonly observed for associative reactions due to facile $\eta^5 \rightarrow \eta^3$ ring slippage.[88–91] Therefore, at first sight, this may reflect an associative thermolysis mechanism, in which the Lewis base coordinates to the metal centre accompanied by an η^5-η^3 ring slippage, prior to the thermolysis eliminating alkane and forming a metal–nitrogen multiple bond. An associative thermolysis mechanism has been reported by Chen *et al* for the formation of a scandium arylimido complex.[92] But this is very unlikely for these electron rich η^5-coordinated metallocene borylimide systems, and sterically, the associative pathway is also disfavoured by the bulky boryl moiety. In contrast, the dissociative thermolysis pathway, reported by Bergman, is found to be the case for the formation of zirconocene imido and hydrazido(2-) complexes from the parent amide or hydrazide(1-); e.g. the formation of $Cp_2Zr(NR)(THF)$ (R = ^{t}Bu (**1.4**) or Ar' (**1.50**), $Cp_2Zr(NNPh_2)(DMAP)$ (**1.63**) and *rac*-(η^5-ebthi)Zr(N^{t}Bu)(py) (**2.12**). In all cases, the alkane elimination is prior to the Lewis base coordination for metallocene compounds.

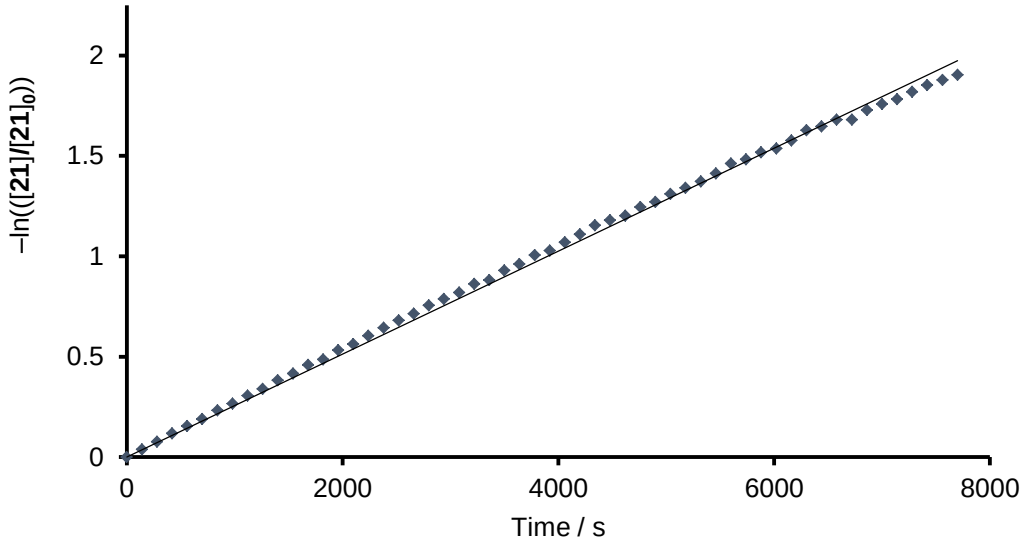

Figure 2.10. First order semi-logarithmic plots for decay of $Ind_2Zr\{NHB(NAr'CH)_2\}(Me)$ (**21**) at 90 °C in toluene-d_8 (r^2 = 0.997).

To distinguish between an associative or dissociative pathway, the reaction between $Ind_2Zr\{NHB(NAr'CH)_2\}(Me)$ (**21**) and 2 equivalents of pyridine in toluene-d_8 was monitored by a ^{1}H NMR array at 90 °C, and the decay of **21** was found to follow first order kinetics as judged by a linear semi-logarithmic plot of $-\ln([\mathbf{21}]/[\mathbf{21}]_0)$ *vs* time. The plot is shown to at least 85% conversion (approximately three half-lives) in the Figure 2.10. The first order kinetic reflects an intramolecular RDS, while no pyridine-coordinated intermediate was observed by ^{1}H NMR spectroscopy. These indicate the base free intermediate was primarily formed *via* thermolysis, followed by fast pyridine trapping, this being consistent with the dissociative pathway. The reactions of **21** with 1 or 5 equivalents of pyridine were also performed at 100 °C in toluene-d_8. The half-life was measured to be 22 mins (*cf.* 30 mins with 1 equivalent of pyridine), thus significant rate acceleration was not observed. This is consistent with previously discussed syntheses of $Cp_2Zr\{NB(NAr'CH)_2\}(L)$ (L = THF (**13**), py (**11**) or DMAP (**14**)) and $Cp_2Hf\{NB(NAr'CH)_2\}(L)$ (L = py (**12**) or DMAP (**15**)) suggesting that the RDS in all cases follow a dissociative pathway rather than Lewis base pre-coordination pathway. The rate acceleration through a dissociative pathway was previously reported for the reaction of $IndFe(CO)_2$ with $P(OR)_3$ (R = Et or Ph), which was explained as a loss of planarity of the indenyl ligand, with the six-membered ring bending toward the metal.[93–95] However, this should be very unlikely to happen for these sterically encumbered borylimido compounds.

DFT calculations on the model base-free systems $Cp_2Zr\{NB(NMeCH)_2\}$ (**1Q_B(NMeCH)$_2$**), $Ind_2Zr\{NB(NMeCH)_2\}$ (**2Q_B(NMeCH)$_2$**) and their methyl-amide precursors $(L)_2Zr\{NHB(NMeCH)_2\}(Me)$ (L = Cp or Ind) shed light on why the methane elimination reaction of **21** occurs at lower temperature than that of **9**. Thus, addition of CH_4 to the bis(cyclopentadienyl) model was found to have Δ_rE = –18.7 kcal mol^{-1}, whereas for the bis(indenyl) counterpart Δ_rE was 5.6 kcal mol^{-1} less exergonic. Assuming similar transition states, this would correspond to a significantly lower activation energy for CH_4 elimination in the case of **21**. The difference in Δ_rE is attributed to the stronger Zr–N_{im} interaction in the bis(indenyl) borylimide system **2Q_B(NMeCH)$_2$**, as indicated by the shorter Zr(1)–N(1) bond length in **23** compared to **11**, and the DFT calculations discussed below.

2.7 Computational studies of bonding in zirconocene borylimides

As mentioned above and in Section 1.2, the bis(cyclopentadienyl) transition metal imides are interesting particularly from a bonding point of view, being so-called "π-loaded" complexes.[17] These have more π-donor ligand orbitals than the metal has acceptor orbitals of correct symmetry, resulting in non-bonding ligand-base molecular orbitals (MOs). These complexes, such as $Cp_2Zr(N^tBu)(THF)$ (**1.4**), have previously displayed high reactivity towards a range of substrates, and the reactivity of the borylimido analogue $Cp_2Zr\{NB(NAr'CH)_2\}(py)$ (**11**) is described in later Chapters.

Recently, in the bonding models of the analogous titanium (boryl)imido complexes, $Cp_2Ti(NR)$ (R = BMe_2, $B(NMeCH)_2$, Me, Ph, ^{t}Bu and BMe_2NH_3), were analysed by DFT and QTAIM methods.[49] It was found that the Ti–N_{im} bond distance and bond dissociation energy are separable and arise from distinct electronic factors, where the Ti–N_{im} bond distance is dominated by the π-bonding with any suitable orbital on the N_{im} atom substituent, while the bond dissociation energy correlates with the Ti–N_{im} σ-bond character and the orthogonal π-interaction. In other words, the borylimides have the strongest and most covalent Ti–N_{im} bonds because of the electronpositive boron atom, as discussed fully in Section 1.7.[49]

To gain insight into the bonding of zirconocene borylimido complexes, similar DFT and QTAIM calculations were carried out on the model systems $Cp_2Zr(NR)$ (R = Xyl (**1Q_Xyl**), Me (**1Q_Me**), $B(NMeCH)_2$ (**1Q_B(NMeCH)$_2$**)) and $Ind_2Zr\{NB(NMeCH)_2\}$ (**2Q_B(NMeCH)$_2$**) by Prof. Philip Mountford (Figure 2.11), using the B3PW91

functional and Def2TZVP basis set. The smaller $B(NMeCH)_2$ group, rather than the real $NB(NAr'CH)_2$, was used here in order to study the underlying electronic interactions without contribution from steric effects. Calculations were also carried out on the pyridine adducts $Cp_2Zr(NR)(py)$, which gave analogous results but for which the analysis was less straightforward in the lower symmetry of these adducts.

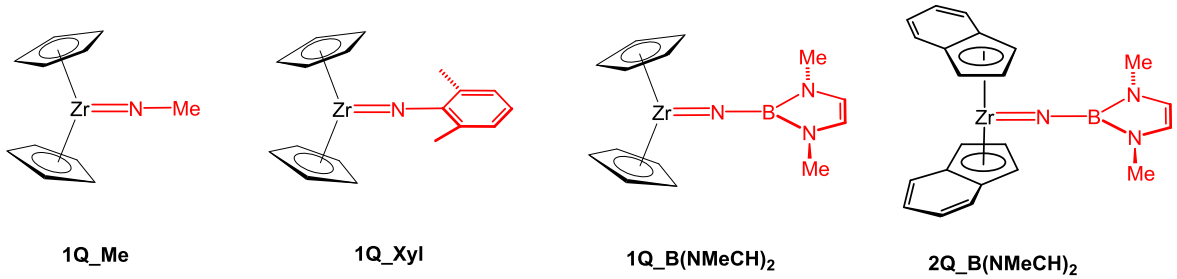

Figure 2.11. Model bis(cyclopentadienyl) and bis(indenyl) (boryl)imido complexes.

The bonding in these zirconocene imides can be approached by considering the interactions of the frontier molecular orbitals (FMOs) of the bent Cp_2Zr moiety with an imido ligand. The former are well-known from previous studies.[50,96] and the latter have been previously calculated from analogous titanium systems (the three highest occupied MOs are shown in Figure 2.12.[49] The σ- and π-donor FMOs, as well as the ring-based MOs of isoelectronic $[NPh]^{2-}$ and $[NB(NMeCH)_2]^{2-}$ are also shown in the Appendix A1, which are fairly similar, showing the 6π electrons of the aromatic boryl and phenyl rings. The HOMO and HOMO–1 are the π_h- (π orbital in aromatic plane) and π_v-orbitals (π orbital perpendicular to the aromatic plane), respectively, in $[NPh]^{2-}$ and $[NB(NMeCH)_2]^{2-}$. As described in Section 1.7, although $[NPh]^{2-}$ and $[NB(NMeCH)_2]^{2-}$ are isoelectronic to each other, $[NB(NMeCH)_2]^{2-}$ appears to be a weaker π_v-acceptor, as the HOMO–HOMO–1 separation is significantly smaller than that of $[NPh]^{2-}$ (0.20 eV *vs* 0.65 eV). Meanwhile, $[NB(NMeCH)_2]^{2-}$ was found to be a much stronger π_h- and σ-donor, because of the electropositive nature of the boron atom compared to carbon.

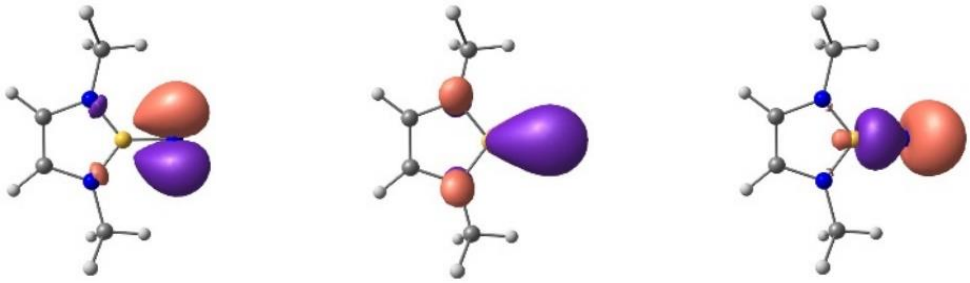

HOMO (π_h, 6.81 eV) **HOMO-1 (π_v, 6.61 eV)** **HOMO-2 (σ, 4.50 eV)**

Figure 2.12. σ- and π-type frontier molecular orbitals of the borylimido dianion $[NB(NMeCH)_2]^{2-}$ in the geometry of the model Cp*Ti(hpp){$NB(NAr'CH)_2$}.[49]

The FMOs for d^0 C_s-$[Cp_2Zr]^{2+}$ (cyclopentadienyl rings are mutually staggered) were calculated at a Cp_{cent}–Zr–Cp_{cent} angle of 129.9°, which is the angle in the optimised geometry of **1Q_B(NMeCH)$_2$**. Selected FMOs are depicted in Figure 2.13. $[Cp_2Zr]^{2+}$ contains three vacant, predominantly non-bonding orbitals (mainly metal d-orbitals), LUMO+2 (a' (σ) symmetry), LUMO (a' (σ)) and LUMO+1 (a" (π)). The HOMO and HOMO–1 are also depicted here, these being the occupied bonding orbitals with a' and a" symmetry, respectively. The higher energy 3a' FMO, interacts best with the σ-donor orbital of the imido-type ligand, such as $[NR]^{2-}$.[50,96] The relative lower energy 2a" FMO lies in the equatorial plane, and can interact with the π_h donor orbital of $[NR]^{2-}$. There is no vacant non-bonding π-orbital in $[Cp_2Zr]^{2+}$ to interact with the π_v donor orbital of $[NR]^{2-}$. Nonetheless, the "fourth frontier orbital",[96] 4a', is known to be available for such a π_v interaction to take place. This 4a' FMO is formally Cp_2–Zr antibonding, and is slightly in higher energy than 3a', and the counterpart of the Cp_2–Zr bonding HOMO (1a', Figure 2.13). This is consistent with the borylimido ligand orientation in the solid-state structure of **11**, where the aromatic boryl ring is parallel to the equatorial plane of Cp_2Zr group. This allows full π_h-donation from N_{im} atom to the zirconium centre, and partial π_v-backdonation to the unoccupied boryl-ring π-orbital to minimise the interaction with high energy lying LUMO+3 (4a'). It is noted in this discussion that the FMO energies for both $[NR]^{2-}$ and $[Cp_2Zr]^{2+}$ are artificially raised and lowered, respectively, by imposition of the formal 2– and 2+ charges.

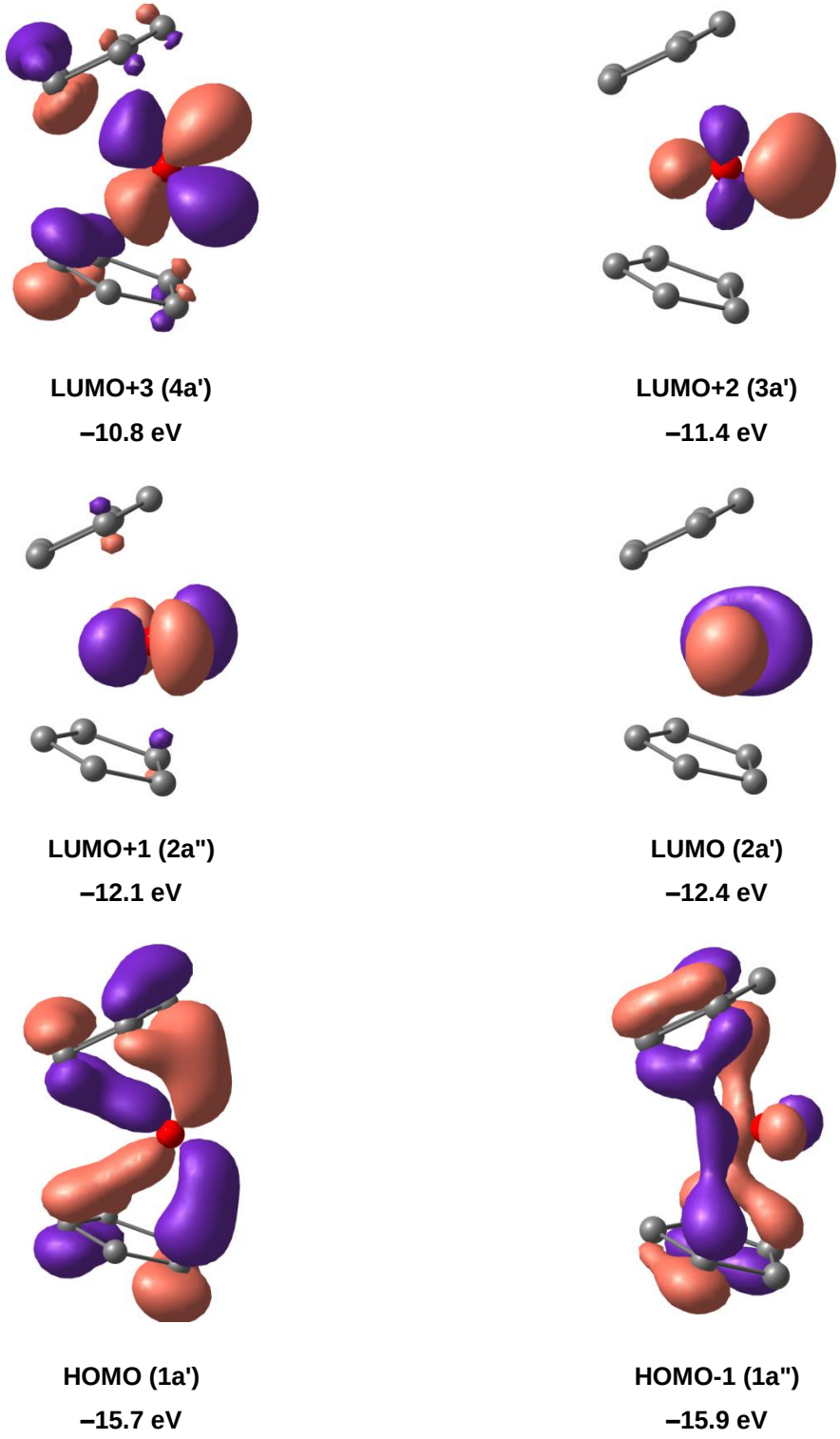

Figure 2.13. Isosurfaces and energies of frontier molecular orbitals in the model dicationic fragment $[Cp_2Zr]^{2+}$. The energies are given for Cp_{cent}–Zr–Cp_{cent} = 129.9°.

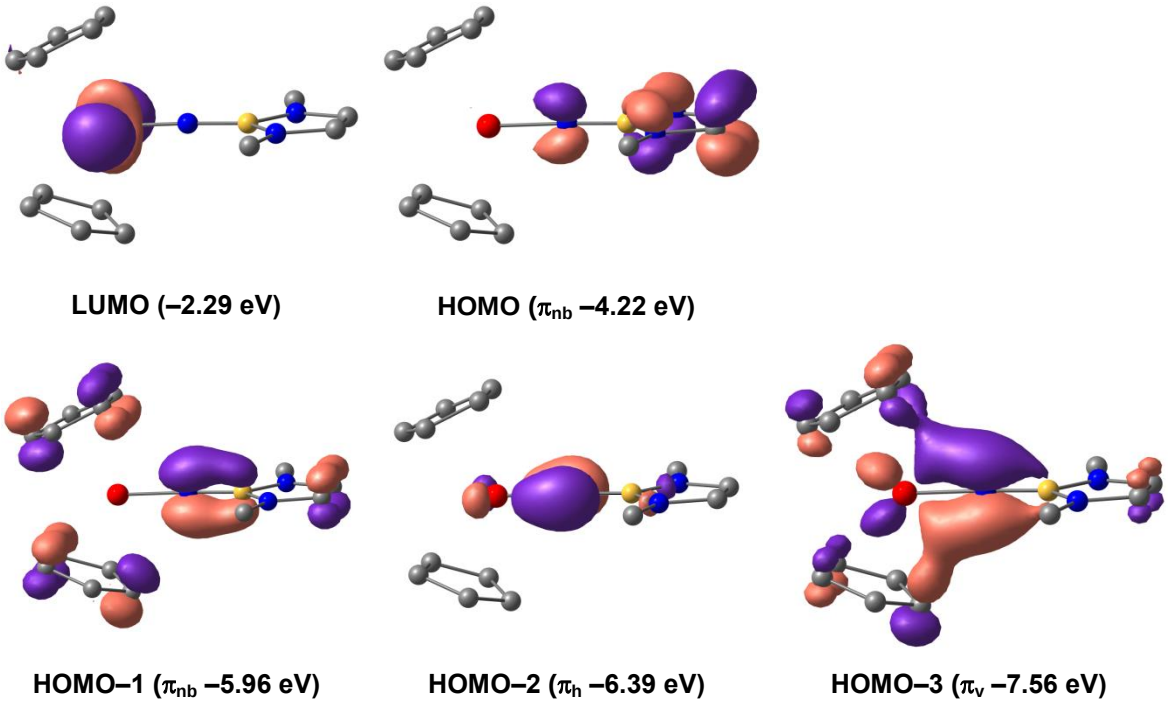

Figure 2.14. DFT model compound $Cp_2Zr\{B(NMeCH)_2\}$ (**1Q_B(NMeCH)$_2$**), and associated isosurfaces and energies of selected MOs.

With the FMOs of both the dicationic $[Cp_2Zr]^{2+}$ fragment and the imido-type dianions having been considered, the electronic structure of the model base-free compound **1Q_B(NMeCH)$_2$** will next be described (Figure 2.14). The HOMO (π_{nb}) is mostly borylimido ligand based (79% in character). The HOMO–1 is also predominantly ligand based, with $NB(NMeCH)_2$ and Cp_2 characters of 44% and 47%, respectively. HOMO–2 is the Zr–N_{im} π_h interaction, whilst HOMO–3 is the corresponding π_v interaction which also contains significant Cp_2–Zr bonding character. The HOMO–1 and HOMO–3 arise from the three-centre/four-electron-like interaction between the π_v donor of $[NB(NMeCH)_2]^{2-}$ and the 4a' (LUMO+3) and 1a' (HOMO) FMOs of $[Cp_2Zr]^{2+}$. The non-bonding LUMO has also been illustrated, which is based on the 2a' FMO of $[Cp_2Zr]^{2+}$, this being capable of σ-interaction with a Lewis base, such as THF, pyridine or DMAP, forming base-coordinated adducts (e.g. **11**).

Table 2.8. Zr–N_{im} and Zr–Cp_{cent}/Ind_{cent} distances, Cp_{cent}–Zr–Cp_{cent}/Ind_{cent}–Zr–Ind_{cent} angles, and Zr–N_{im} bond dissociation energy ($\Delta E_{Zr–N(R)}$) to relaxed *S* = 1 fragments for optimised $Cp_2Zr(NR)$ (**1Q_R**; R = Xyl, Me and $B(NMeCH)_2$) and $Ind_2Zr\{NB(NMeCH)_2\}$ (**2Q_B(NMeCH)$_2$**). Values for geometrically frozen fragments (*S* = 1) in parentheses.

Compound	*d*(Zr–N_{im}) (Å)	*d*(Zr–Cp) /*d*(Zr–Ind) (av., Å)	Cp-Zr-Cp/ Ind-Zr-Ind (°)	$\Delta E_{Zr–N(R)}$ (kcal mol^{-1})
1Q_Xyl	1.861	2.270	130.1	95.0 (106.2)
1Q_Me	1.835	2.292	128.2	97.8 (109.9)
1Q_B(NMeCH)$_2$	1.854	2.277	129.9	109.3 (120.2)
2Q_B(NMeCH)$_2$	1.847	2.290	128.7	107.8 (123.8)

In order to shed light on the origin of trends in bond strengths (Zr–N_{im}, Zr–Cp/Ind), bond distances and Ind_2/Cp_2Zr angles in model compounds **1Q_R** and **2Q_B(NMeCH)$_2$**, a combined DFT and QTAIM study was performed, and selected parameters are shown in Tables 2.8 and 2.9. In the family of model complexes **1Q_R**, the Zr–N_{im} bond distance of **1Q_Me** (1.835 Å) was calculated to be the shortest, and it was longest in **1Q_Xyl** (1.861 Å). This correlates with the π_v-backdonation abilities of $[NR]^{2-}$ ($[NXyl]^{2-}$ > $[N(BNMeCH)_2]^{2-}$ > $[NMe]^{2-}$), being also consistent with the previously calculations on models of the titanocene congeners, where the Ti–N_{im} bond distance correlates with the extent of Ti–N_{im} π_v-interaction.[49] In addition, the Zr–N_{im} bond distance in **2Q_B(NMeCH)$_2$** (1.847 Å) is considerably shorter than that in **1Q_B(NMeCH)$_2$** (1.854 Å), thus reflecting a stronger Zr–N_{im} π_v-interaction in the indenyl supported systems, because of the greater degree of ring slippages for indenyl rings. However, the calculated $\Delta E_{Zr–N(R)}$ bond dissociation energies of the family of model complexes **1Q_R** did not show a correlation with *d*(Zr–N_{im}). Instead, the Zr–N_{im} bond of **1Q_B(NMeCH)$_2$** appeared to be stronger than that in both **1Q_Me** and **1Q_Xyl**, which correlates with the σ- and π_h-donation ability, again consistent with the calculated titanocene congener systems.[49] In addition, for comparison with **1Q_B(NMeCH)$_2$**, the $\Delta E_{Zr–N(R)}$ values of titanium and hafnium congener models were also calculated to be 85.8 and 126.6 kcal mol^{-1}, respectively, following the trend, as expected, that the M–X bond gets stronger

going down the group. Interestingly, it was found that the $\Delta E_{Zr-N(R)}$ value of **2Q_B(NMeCH)$_2$** (109.3 kcal mol^{-1}) was slightly lower than that of **1Q_B(NMeCH)$_2$** (107.8 kcal mol^{-1}). This unexpected low value is due to the different relaxation degree in the Cp_2Zr and Ind_2Zr fragments after bond-breaking. It was found that the relaxation of the more highly distorted indenyl rings in **2Q_B(NMeCH)$_2$** has a significantly greater contribution to the corresponding $\Delta E_{Zr-N(R)}$ values, compared to the cyclopentadienyl rings in **1Q_B(NMeCH)$_2$**. In this instance, the $\Delta E_{Zr-N(R)}$ values were recalculated with geometrically frozen Cp_2Zr/Ind_2Zr and NR fragments. The resulting values are relatively higher than the former as expected, giving the lack of exoergic relaxation, and give the same trend in the **1Q_R** family. In contrast, the $\Delta E_{Zr-N(R)}$ value of **2Q_B(NMeCH)$_2$** (123.8 kcal mol^{-1}) is now significantly higher than that in **1Q_B(NMeCH)$_2$** (120.2 kcal mol^{-1}). Thus, **2Q_B(NMeCH)$_2$** has an overall shorter and stronger $Zr–N_{im}$ bond, compared to its bis(cyclopentadienyl) counterpart **1Q_B(NMeCH)$_2$**.

Hoffmann showed that decreasing the $Cp_{cent}–M–Cp_{cent}$ angle of Cp_2M stabilizes 4a' and destabilizes 1a'. Therefore, stronger π_v-donation should favor a smaller Cp_2M bend angle to enhance interaction between the various FMOs involved (Figure 2.13).[50] In addition, formal π_v-donation into 4a' should also lead to longer $M–Cp_{cent}$ distances.[96] It was also found that 3a' and 2a'' are destabilized with bending,[50] therefore a large $Cp_{cent}–Zr–Cp_{cent}$ angle are expected to be favoured for good σ- and π-donors. These correlations have also been found in the previously calculated titanocene congeners.[49] The same trend was observed here (Table 2.8), where the $d(Zr–N_{im})$ values are correlated to $Cp_{cent}–Zr–Cp_{cent}$ ($Ind_{cent}–Zr–Ind_{cent}$) angles and anti-correlated to $Zr–Cp_{cent}$ ($Zr–Ind_{cent}$) distances. **1Q_Me**, which contains the shortest $Zr–N_{im}$ bond (1.835 Å), shows the smallest $Cp_{cent}–Zr–Cp_{cent}$ angle (128.2°) and longest $Zr–Cp_{cent}$ distance (2.292 Å), whilst **1Q_Xyl** shows the largest $Cp_{cent}–Zr–Cp_{cent}$ angle (130.1°) and shortest $Zr–Cp_{cent}$ distance (2.270 Å), while the values for **1Q_B(NMeCH)$_2$** were intermediate. This also holds true when comparing those values between **1Q_B(NMeCH)$_2$** and **2Q_B(NMeCH)$_2$**, where the latter showed a shorter $Zr–N_{im}$ distance (1.847 Å), a smaller $Ind_{cent}–Zr–Ind_{cent}$ angle (128.7°) and a longer $Zr–Ind_{cent}$ distance (2.290 Å), these reflecting again a stronger $Zr–N_{im}$ π_v-interaction. This "push-pull" or buffering effect between the Zr–Cp and $Zr–N_{im}$ interactions is also confirmed by the anti-correlation between $Q(Cp_2/Ind_2)$ and Q(NR) (Table 2.9). For an anionic ligand, a less negative Q value reflects greater covalent interaction with the metal centre as its negative charge is partially donated to the metal centre.

Turning now to relationships with QTAIM parameters, the delocalization index, δ(A–B), of a bond A–B is a measure of the number of electron pairs delocalized or shared between the two atoms and can relate to formal bond order.[97] For example, δ(C–C) values calculated for ethane, ethylene and acetylene are 1.02, 1.93 and 2.88, respectively. The correlation between δ and formal bond does not hold for bonds between heteroatoms, but trends can be extracted from a family of compounds containing the same pair of bonded atoms. Thus the variation in δ(Zr–N_{im}) with the change of R or Cp/Ind groups may be considered, and related to the relative bond orders (bond distances) in these four complex models. The largest and smallest values of 1.517 and 1.370 were found in **1Q_Me** and **1Q_Xyl** respectively. The value of 1.462 (**1Q_B(NMeCH)$_2$**) is intermediate between these two, and slightly lower than the value of **2Q_B(NMeCH)$_2$** (1.488). These indicate that the bond order of the Zr–N_{im} multiple bonds in **1Q_R** and **2Q_B(NMeCH)$_2$** are in the order of **1Q_Me** > **2Q_B(NMeCH)$_2$** > **1Q_B(NMeCH)$_2$** > **1Q_Xyl**, which is the reverse of the trend in Zr–N_{im} distances in Table 2.8.

The ellipticity (ε) of a bond is a measure of the asymmetry of π bonding in that bond.[97] For example, the C–C bonds of ethane and acetylene have ε value of 0, representing their cylindrical nature, whilst that of ethylene (one π component) has a value of 0.22. Among the **1Q_R** complex models, the lowest ε value (0.089) was found in **1Q_Me**. Since the NMe group is cylindrical, this clearly reflects asymmetric π bonding components (π_v and π_h) which arise from the different orientations and energies of the π-acceptor orbitals in these bent metallocene systems (4a' and 2a", Figure 2.13). The largest ε value (0.179) was observed in **1Q_Xyl**, where a less cylindrical symmetry was caused by available π_v backbonding from N_{im} into unoccupied orbitals of the xylyl ring, which further weakens the Zr–N_{im} π_v interaction to a greater extent. Again, an intermediate ε value was found in **1Q_B(NMeCH)$_2$**, since the Xyl ring is a better π_v acceptor than B(NMeCH)$_2$. This disruption of a π component of the multiple bond is reflected in the calculated Zr–N_{im} distances, in which **1Q_Xyl** with the largest ε value (0.179) has the longest Zr–N_{im} distance (1.861 Å), and **1Q_Me** with the smallest ε value (0.089) has the shortest Zr–N_{im} distance (1.835 Å). In addition, **2Q_B(NMeCH)$_2$**, has an ε value of 0.088, which is significantly lower than that in **1Q_B(NMeCH)$_2$**, reflecting a significantly stronger Zr–N_{im} π_v interaction.

Correlations between binding energy and electron density at the bond critical point (BCP), ρ, are known for a number of different types of bond, and can be used as a measure of bond covalency.[98] In the previous study of the titanium congeners,[49] ρ was found to correlate strongly with the $\Delta E_{Ti–N(R)}$ values, and reflected increasing covalency of the Ti–N_{im} bond with more electron-releasing NR fragments. The same observation is found here, showing ρ(Zr–N_{im}) increases with $\Delta E_{Zr–N(R)}$ values. In the **1Q_R** systems, the highest value (0.176) was found in **1Q_B(NMeCH)$_2$**, larger than the values in **1Q_Me** (0.173) and **1Q_Xyl** (0.165), these values being consistent with the downward trend in $\Delta E_{Zr–N(R)}$. These also reflect the decrease in Zr–N_{im} covalency, in the order **1Q_B(NMeCH)$_2$** > **1Q_Me** > **1Q_**Xyl. For **2Q_B(NMeCH)$_2$**, an even larger ρ value (0.179) was observed, consistent with a stronger and more covalent Zr–N_{im} bond (*cf.* **1Q_B(NMeCH)$_2$**) in the bis(indenyl) system.

The electron density Laplacian, $\nabla^2\rho$, is defined as the sum of three curvatures of electron density at the BCP: λ_1 and λ_2 are negative and lie in two coordinates perpendicular to the bond path, while λ_3 is positive and lie along the bond path.[98] It is the two negative components of the Laplacian which measure the concentration of electron density along the bond path. Thus, a trend was noted between $\Delta E_{Zr–N(R)}$ and the magnitude of $\lambda_{1+}\lambda_2$. The most negative value was found in **2Q_B(NMeCH)$_2$** (–0.466), while the least was found in **1Q_Xyl** (–0.394). The values of **1Q_Me** and **1Q_B(NMeCH)$_2$** are intermediate, being –0.400 and –0.455, respectively. Therefore, these reflect the greatest degree of electron density concentration along the bond path for the strongest bond.

Table 2.9. Selected QTAIM data (atomic units) for optimised $Cp_2Zr(NR)$ (**1Q_R**; R = Xyl, Me and $B(NMeCH)_2$) and $Ind_2Zr\{NB(NMeCH)_2\}$ (**2Q_B(NMeCH)$_2$**) at the bond critical points: $\delta(Zr–N_{im})$, ε (ellipticity), ρ (electron density), $\nabla^2\rho$ (electron density Laplacian), Q(NR) and $Q(Cp_2)$, along with $Zr–N_{im}$ bond dissociation energy ($\Delta E_{Zr–N(R)}$) to frozen S = 1 fragments. λ_1 and λ_2 are curvatures of the electron density in two coordinates perpendicular to the bond path, while λ_3 is the curvature of the electron density along the bond path.

Compound	$\Delta E_{Zr–N(R)}$ (kcal mol^{-1})	$\delta(Zr–N_{im})$	$\varepsilon(Zr–N_{im})$	$\rho(Zr–N_{im})$	$\nabla^2\rho(Zr–N_{im})$	Q(NR)	$Q(Cp_2/Ind_2)$	λ_1	λ_2	$\lambda_1+\lambda_2$	λ_3
1Q_Xyl	106.2	1.370	0.179	0.165	0.633	-1.043	-1.099	-0.213	-0.181	-0.394	1.027
1Q_Me	109.9	1.517	0.089	0.173	0.675	-0.959	-1.168	-0.209	-0.192	-0.400	1.076
1Q_B(NMeCH)$_2$	120.2	1.462	0.110	0.176	0.587	-1.025	-1.124	-0.240	-0.216	-0.455	1.043
2Q_B(NMeCH)$_2$	123.8	1.488	0.088	0.179	0.590	-0.984	-1.136	-0.243	-0.223	-0.466	1.056

2.8 Conclusions and Outlook

This Chapter has described the synthesis and characterisation of new borylamines, and a number of borylamido and borylimido complexes of zirconium and hafnium. Firstly, a new route to synthesise the novel borylamines $H_2NB(N^iPr)C_6H_4$ (**5**) and $H_2NB(N^iPrCH_2)$ (**1**) was developed by using liquid ammonia, preventing the subsequent reaction to form bis(boryl)amines $HN\{B(N^iPrCH_2)_2\}_2$ (**2**) and $HN\{B(N^iPr)_2C_6H_4\}_2$ (**6**) in the presence of base (NH_3 or NEt_3). Thermolysis of $Cp_2Zr\{NHB(N^iPr)C_6H_4\}(Me)$ (**7**) with DMAP produced the first zirconium borylimido compound $Cp_2Zr\{NB(N^iPr)C_6H_4\}(DMAP)$ (**8**). Crystallographic characterisation of **8** demonstrated that the $Zr–N_{im}$ bond distance is significantly longer than those in alkylimido zirconocene complexes, but comparable to those in arylimido analogues.

Next, borylamido precursors $Cp_2M\{NHB(NAr'CH)_2\}(Me)$ (M = Zr (**9**) or Hf (**10**)) were produced by using the bulky, unsaturated-backbone lithium borylamide $LiNHB(NAr'CH)_2$ (**2.5**). Subsequent thermolysis gave the zirconium borylimido complex and the first hafnium borylimido compound $Cp_2M\{NB(NAr'CH)_2\}(py)$ (M = Zr (**11**) or Hf (**12**)), which have entirely analogous structures to **8**. THF- and DMAP-coordinated borylimido zirconocene compounds were also successfully isolated. However, an attempt to synthesis the THF-coordinated hafnium borylimide was failed. A new method of synthesising $Cp_2Zr\{NB(NAr'CH)_2\}(DMAP)$ (**14**) was developed using readily available Cp_2ZrCl_2. The C–H bond activation of toluene solvent was observed with the *in situ* generated base-free intermediate $Cp_2Zr\{NB(NAr'CH)_2\}$ during the synthesis of zirconocene borylimides. Performing the same reaction in benzene, the C–H bond activation product $Cp_2Zr\{NHB(NAr'CH)_2\}(Ph)$ (**18**) was synthesised and characterised. Further reaction between **11** and H_2 presented a H–H bond cleavage reaction forming the borylamido-hydrido complex $Cp_2Zr\{NHB(NAr'CH)_2\}(H)$ (**19**), and reversible formation of **11** and H–H bond *via* thermolysis from **19**.

Indenyl ligand-supported zirconium borylimido complexes $Ind_2Zr\{NB(NAr'CH)_2\}(L)$ (L = THF (**22**), py (**23**) or DMAP (**24**)) were synthesised using the same methodology. Kinetic studies for the formation of **23** showed that the rate-determining thermolysis of $Ind_2Zr\{NHB(NAr'CH)_2\}(Me)$ (**21**) undergoes a dissociative pathway, which is significantly faster than that for the Cp-analogue **9**. DFT calculations performed on the model reaction of $Ind_2Zr\{NB(NMeCH)_2\}$ (**2Q_NB(NMeCH)$_2$**) with CH_4 was found to be

less exergonic than that of $Cp_2Zr\{NB(NMeCH)_2\}$ (**1Q_NB(NMeCH)$_2$**), which was attributed to a stronger Zr–N_{im} interaction in the bis(indenyl) borylimide systems.

DFT and QTAIM studies investigated the "push-pull" (buffering) effect between the Zr–Cp and Zr–N_{im} interactions in these π-loaded zirconocene (boryl)imido systems. The variation in the Zr–N_{im} distance is determined by the π_v interaction involved in this bonding, which is enhanced in the bis(indenyl) system. The Zr–N_{im} bond energy is instead correlated to the σ- and π_h-donation ability of the respective NR group in the bis(cyclopentadienyl) systems. The bis(indenyl) supported system gave both a stronger and shorter Zr–N_{im} bond, compared to bis(cyclopentadienyl) systems, which was attributed to the significantly stronger π_v interaction.

The preparation of titanium borylimides using $H_2NB(N^iPr)_2C_6H_4$ (**5**) were found to be more successful (*cf.* zirconium borylimide **8**), and installation of different supporting ligands have been achieved in our research group.[54] Further reducing the steric profile of the borylamine **5** by using an NMe substituent is the current focus, and the synthesis of the corresponding titanium borylimides are under investigation.[48]

2.9 References

1 M. J. Carney, P. J. Walsh, F. J. Hollander and R. G. Bergman, *J. Am. Chem. Soc.*, 1989, **111**, 8751–8753.

2 M. J. Carney, P. J. Walsh and R. G. Bergman, *J. Am. Chem. Soc.*, 1990, **112**, 6426–6428.

3 M. J. Carney, P. J. Walsh, F. J. Hollander and R. G. Bergman, *Organometallics*, 1992, **11**, 761–777.

4 M. R. Smith, P. T. Matsunaga and R. A. Andersen, *J. Am. Chem. Soc.*, 1993, **115**, 7049–7050.

5 J. L. Polse, R. A. Andersen and R. G. Bergman, *J. Am. Chem. Soc.*, 1995, **117**, 5393–5394.

6 W. A. Howard, T. M. Trnka, M. Waters and G. Parkin, *J. Organomet. Chem.*, 1997, **528**, 95–121.

7 A. J. Blake, J. M. McInnes, P. Mountford, G. I. Nikonov, D. Swallow and D. J. Watkin, *J. Chem. Soc. Dalton. Trans.*, 1999, 379–392.

8 I. Pappas and P. J. Chirik, *Angew. Chem. Int. Ed.*, 2014, **53**, 6241–6244.

9 D. E. Wigley, in *Prog. Inorg. Chem.*, ed. K. D. Karlin, Wiley-Interscience, New

York, 1994, vol. 42, pp. 239–482.

10 A. P. Duncan and R. G. Bergman, *Chem. Rec.*, 2002, **2**, 431–445.

11 P. Mountford, *Chem. Commun.*, 1997, 2127–2134.

12 L. H. Gade and P. Mountford, *Coord. Chem. Rev.*, 2001, **216**–**217**, 65–97.

13 N. Hazari and P. Mountford, *Acc. Chem. Res.*, 2005, **38**, 839–849.

14 A. R. Fout, U. J. Kilgore and D. J. Mindiola, *Chem. - Eur. J.*, 2007, **13**, 9428–9440.

15 C. M. Kozak and P. Mountford, *Angew. Chem. Int. Ed.*, 2004, **43**, 1186–1189.

16 T. R. Cundari, *J. Am. Chem. Soc.*, 1992, **114**, 7879–7888.

17 Z. Lin and M. B. Hall, *Coord. Chem. Rev.*, 1993, **123**, 149–167.

18 P. Mountford and D. Swallow, *J. Chem. Soc., Chem. Commun.*, 1995, 2357–2359.

19 N. Kaltsoyannis and P. Mountford, *J. Chem. Soc., Dalton. Trans.*, 1999, 781–789.

20 T. R. Cundari, *Chem. Rev.*, 2000, **100**, 807–818.

21 A. D. Schwarz, A. J. Nielson, N. Kaltsoyannis and P. Mountford, *Chem. Sci.*, 2012, **3**, 819–824.

22 S. C. Dunn, N. Hazari, N. M. Jones, A. G. Moody, A. J. Blake, A. R. Cowley, J. C. Green and P. Mountford, *Chem. Eur. J.*, 2005, **11**, 2111–2124.

23 S. C. Dunn, P. Mountford and D. A. Robson, *J. Chem. Soc. Dalton. Trans.*, 1997, **2**, 293–304.

24 D. Swallow, J. M. McInnes and P. Mountford, *J. Chem. Soc. Dalton. Trans.*, 1998, 2253–2260.

25 E. Müller, J. Müller, F. Olbrich, W. Brüser, W. Knapp, D. Abeln and F. T. Edelmann, *Eur. J. Inorg. Chem.*, 1998, 87–91.

26 A. J. Blake, P. E. Collier, L. H. Gade, P. Mountford, J. Lloyd, S. M. Pugh, M. Schubart, M. E. G. Skinner and D. J. M. Trösch, *Inorg. Chem.*, 2001, **40**, 870–877.

27 P. E. Collier, S. M. Pugh, H. S. C. Clark, J. B. Love, A. J. Blake, F. G. N. Cloke and P. Mountford, *Inorg. Chem.*, 2000, **39**, 2001–2005.

28 P. J. Walsh, F. J. Hollander and R. G. Bergman, *J. Am. Chem. Soc.*, 1988, **110**, 8729–8731.

29 P. J. Walsh, F. J. Hollander and R. G. Bergman, *Organometallics*, 1993, **12**, 3705–3723.

30 S. Y. Lee and R. G. Bergman, *J. Am. Chem. Soc.*, 1995, **117**, 5877–5878.

31 N. Wiberg, H.-W. Häring, G. Huttner and P. Friedrich, *Chem. Ber.*, 1978, **111**, 2708–2715.

32 J. L. Thorman and L. K. Woo, *Inorg. Chem.*, 2000, **39**, 1301–1304.

33 P. J. Walsh, M. J. Carney and R. G. Bergman, *J. Am. Chem. Soc.*, 1991, **113**, 6343–6345.

34 B. Clough, DPhil Thesis, University of Oxford, 2016.

35 L. Weber, I. Domke, W. Greschner, K. Miqueu, A. Chrostowska and P. Baylère, *Organometallics*, 2005, **24**, 5455–5463.

36 L. Weber, *Coord. Chem. Rev.*, 2001, **215**, 39–77.

37 L. Weber, E. Dobbert, H.-G. Stammler, B. Neumann, R. Boese and D. Bläser, *Chem. Ber.*, 1997, **130**, 705–710.

38 L. Weber, J. Kahlert, L. Böhling, A. Brockhinke, H.-G. Stammler, B. Neumann, R. A. Harder, P. J. Low and M. A. Fox, *Dalton. Trans.*, 2013, **42**, 2266–2281.

39 J. Feldman and J. C. Calabrese, *J. Chem. Soc. Chem. Commun.*, 1991, 134–136.

40 R. Fandos, M. Martínez-Ripoll, A. Otero, M. J. Ruiz, A. Rodríguez and P. Terreros, *Organometallics*, 1998, **17**, 1465–1470.

41 S. Y. Lee and R. G. Bergman, *J. Am. Chem. Soc.*, 1996, **118**, 6396–6406.

42 T. L. Breen and D. W. Stephan, *Organometallics*, 1996, **15**, 4223–4227.

43 C. J. Harlan, J. A. Tunge, B. M. Bridgewater and J. R. Norton, 2000, 2365–2372.

44 W. J. Grigsby, M. M. Olmstead and P. P. Power, *J. Organomet. Chem.*, 1996, **513**, 173–180.

45 C. Lefeber, P. Arndt, A. Tillack, W. Baumann, R. Kempe, V. V Burlakov and U. Rosenthal, *Organometallics*, 1995, **14**, 3090–3093.

46 R. L. Zuckerman, S. W. Krska and R. G. Bergman, *J. Am. Chem. Soc.*, 2000, **122**, 751–761.

47 J. D. Selby, M. Feliz, A. D. Schwarz, E. Clot and P. Mountford, *Organometallics*, 2011, **30**, 2295–2307.

48 B. Clough and P. Mountford, Unpublished results.

49 B. A. Clough, S. Mellino, A. V Protchenko, M. Slusarczyk, L. C. Stevenson, M. P. Blake, B. Xie, E. Clot and P. Mountford, *Inorg. Chem.*, 2017, **56**, 10794–10814.

50 J. W. Lauher and R. Hoffmann, *J. Am. Chem. Soc.*, 1976, **98**, 1729–1742.

51 R. L. Zuckerman and R. G. Bergman, *Organometallics*, 2000, **19**, 4795–4809.

52 B. A. Clough, S. Mellino, E. Clot and P. Mountford, *J. Am. Chem. Soc.*, 2017, **139**, 11165–11183.

53 K. Prout, T. S. Cameron, R. A. Forder, S. R. Critchley, B. Denton and G. V Rees, *Acta Crystallogr. Sect. B*, 1974, **30**, 2290–2304.

54 H. Barrett, M. Slusarczyk and P. Mountford, Unpublished results.

55 T. J. Hadlington, J. A. B. Abdalla, R. Tirfoin, S. Aldridge and C. Jones, *Chem. Commun.*, 2016, **52**, 1717–1720.

56 K. C. Jantunen, B. L. Scott and J. L. Kiplinger, *J. Alloys Compd.*, 2007, **444**–**445**, 363–368.

57 E. J. Hawrelak and P. A. Deck, *Organometallics*, 2004, **23**, 9–11.

58 A. Havlik, M. Lamac, J. Pinkas, A. Ruzicka and M. Horacek, *RSC Adv.*, 2015, **5**, 59154–59166.

59 H. M. Hoyt, F. E. Michael and R. G. Bergman, *J. Am. Chem. Soc.*, 2004, **126**, 1018–1019.

60 E. Hollink, P. Wei and D. W. Stephan, *Can. J. Chem.*, 2004, **82**, 1634–1639.

61 R. D. Profilet, C. H. Zambrano, P. E. Fanwick, J. J. Nash and I. P. Rothwell, *Inorg. Chem.*, 1990, **29**, 4362–4364.

62 C. H. Zambrano, R. D. Profilet, J. E. Hill, P. E. Fanwick and I. P. Rothwell, *Polyhedron*, 1993, **12**, 689–708.

63 P. J. Walsh, A. M. Baranger and R. G. Bergman, *J. Am. Chem. Soc.*, 1992, **114**, 1708–1719.

64 J. L. Thorman, I. A. Guzei, Young and L. K. Woo, *Inorg. Chem.*, 1999, **38**, 3814–3824.

65 H. Hamaki, N. Takeda and N. Tokitoh, *Organometallics*, 2006, **25**, 2457–2464.

66 I. Castillo and T. Don Tilley, *J. Organomet. Chem.*, 2002, **643**–**644**, 431–440.

67 A. D. Schofield, DPhil Thesis, University of Oxford, 2012.

68 C. C. Cummins, S. M. Baxter and P. T. Wolczanski, *J. Am. Chem. Soc.*, 1988, **110**, 8731–8733.

69 C. C. Cummins, C. P. Schaller, G. D. Van Duyne, P. T. Wolczanski, A. W. E. Chan and R. Hoffmann, *J. Am. Chem. Soc.*, 1991, **113**, 2985–2994.

70 J. L. Bennett and P. T. Wolczanski, *J. Am. Chem. Soc.*, 1994, **116**, 2179–2180.

71 J. L. Bennett and P. T. Wolczanski, *J. Am. Chem. Soc.*, 1997, **119**, 10696–10719.

72 C. P. Schaller, C. C. Cummins, P. T. Wolczanski and N. York, *J. Am. Chem. Soc.*, 1996, **118**, 591–611.

73 T. R. Cundari, T. R. Klinckman and P. T. Wolczanski, *J. Am. Chem. Soc.*, 2002, **124**, 1481–1487.

74 R. E. Blake, D. M. Antonelli, L. M. Henling, W. P. Schaefer, K. I. Hardcastle and J. E. Bercaw, *Organometallics*, 1998, **17**, 718–725.

75 H. E. Toomey, D. Pun, L. F. Veiros and P. J. Chirik, *Organometallics*, 2008, **27**, 872–879.

76 J. L. Polse, R. A. Andersen and R. G. Bergman, *J. Am. Chem. Soc.*, 1998, **120**, 13405–13414.

77 K. Yan, A. Ellern and A. D. Sadow, *J. Am. Chem. Soc.*, 2012, **134**, 9154–9156.

78 M. E. Rerek, L.-N. Ji and F. Basolo, *J. Chem. Soc. Chem. Commun.*, 1983, 1208–1209.

79 J. M. O'Connor and C. P. Casey, *Chem. Rev.*, 1987, **87**, 307–318.

80 J. C. Green, M. L. H. Green, J. T. James, P. C. Konidaris, G. H. Maunder and P. Mountford, *J. Chem. Soc., Chem. Commun.*, 1992, 1361–1365.

81 M. D. Rausch, K. J. Moriarty, J. L. Atwood, W. E. Hunter and E. Samuel, *J. Organomet. Chem.*, 1987, **327**, 39–54.

82 T. Repo, M. Klinga, I. Mutikainen, Y. Su, M. Leskelä, M. Polamo, M. N. Homsi, F. K. H. Kuske, M. Haugg, N. Trabesinger-Rüf and E. G. Weinhold, *Acta Chem. Scand.*, 1996, 50, 1116–1120.

83 R. Ascenso, C. G. De Azevedo, M. J. Correia, A. R. Dias, M. T. Duarte, L. Ferreira, P. T. Gomes, F. Lourenc, A. M. Martins and S. S. Rodrigues, *J. Organomet. Chem.*, 2001, **632**, 58–66.

84 S. A. Westcott, A. K. Kakkar, G. Stringer, N. J. Taylor and T. B. Marder, *J. Organomet. Chem.*, 1990, **394**, 777–794.

85 A. K. Kakkar, S. F. Jones, N. J. Taylor, S. Collins and T. B. Marder, *J. Chem. Soc. Chem. Commun.*, 1989, 1454–1456.

86 J. Okuda, P. König, I. L. Rushkin, H.-C. Kang and W. Massa, *J. Organomet. Chem.*, 1995, **501**, 37–39.

87 D. O'Hare, V. Murphy, G. M. Diamond, P. Arnold and P. Mountford, *Organometallics*, 1994, **13**, 4689–4694.

88 A. J. Hart-Davis and R. J. Mawby, *J. Chem. Soc. A*, 1969, 2403–2407.

89 P. Caddy, M. Green, E. O'Brien, L. E. Smart and P. Woodward, *Angew. Chem.*, 1977, **89**, 671–672.

90 P. Caddy, M. Green, E. O'brien, L. E. Smart and P. Woodward, *J. Chem. Soc. Dalton. Trans.*, 1980, 962–972.

91 P. Caddy, M. Green, J. A. K. Howard, J. M. Squire and N. J. White, *J. Chem. Soc. Dalton. Trans.*, 1981, 400–406.

92 E. Lu, Y. Li and Y. Chen, *Chem. Commun.*, 2010, **46**, 4469–4471.

93 A. J. Hart-Davis, C. White and R. J. Mawby, *Inorg. Chim. Acta*, 1970, **4**, 441–446.

94 C. White and R. J. Mawby, *Inorg. Chim. Acta*, 1970, **4**, 261–266.

95 D. J. Jones and R. J. Mawby, *Inorg.Chim. Acta*, 1972, **6**, 157–160.

96 J. C. Green, *Chem. Soc. Rev.*, 1998, **27**, 263–271.

97 X. Fradera, M. A. Austen and R. F. W. Bader, *J. Phys. Chem. A*, 1999, **103**, 304–314.

98 C. F. Matta and R. J. Boyd, *The Quantum Theory of Atoms in Molecules*, Wiley-VCH, Weinheim, 2007.

Chapter Three

Reactions of Group 4 metallocene borylimides with terminal alkynes

3.1 Overview

As introduced in Chapter One, Group 4 imido complexes can undergo new C–N bond-forming processes that arise from the reactions of the electron-rich metal–nitrogen multiple bond and the electrophilic multiple bond of the incoming unsaturated substrate. In particular, stoichiometric and catalytic hydroamination has drawn great attention over 30 years, in which an azametallacyclobutene complex is firstly formed *via* a [2+2] cycloaddition of the alkynes, alkenes or allenes across the metal–nitrogen multiple bond.[1–5] The imido catalyst can be subsequently regenerated through protonolysis by adding an equivalent of corresponding amine to continue the catalytic cycle, accompanied by the generation of enamines, as a result of the net addition of an N–H bond across an unsaturated C–C bond. This area of interest has been expanded to the hydrazido complexes, which can react with alkynes catalytically giving hydrohydrazination, iminohydrohydrazination or diamination processes.[6–19] In addition, competitive 1,2-C–H bond activations across the metal–nitrogen multiple bond may also take place when terminal alkynes are employed.[20–25]

A range of stoichiometric and catalytic reactions of titanium imides and hydrazides have been studied within our research group,[10,18,19,26–32] and different catalytic reactions (hydrohydrazination or diamination) of titanium hydrazido complexes have been studied in detail and found to be controlled by the steric and electronic demands of the supporting ligands. The exemplar diamide-amine ligand supported titanium hydrazido complex $Ti(N_2^{SiMe_3}N^{Me})(NNPh_2)(py)$ (**1.55**) was found to catalyse the diamination reaction with internal alkynes by generating vinylimido species of the type $Ti(N_2^{SiMe_3}N^{Me})\{NC(R)=C(Me)NPh_2\}$ (R = alkyl or aryl), through N_α–N_β insertion.[18,19] Modifying the diamide-amine ligand by incorporating isopropyl rather than trimethylsilyl groups as the N_{amide}-substituents results in more usual catalytic hydrohydrazination with internal alkynes, by forming vinylhydrazide-acetylide species of the type $Ti(N_2^{iPr}N^{Me})\{N(NPh_2)C(H)C(H)(R)\}(CCR)$ (R = Tol, 4-$C_6H_4CF_3$, 4-C_6H_4OMe, Ar^F (C_6F_5), $SiMe_3$).[10]

In the case of the transient bis(cyclopentadienyl) zirconium hydrazide complex $Cp_2Zr(NNPh_2)$ (**1.62**) reported by Bergman and co-workers, it also underwent N_α–N_β bond cleavage upon reaction with symmetrical internal alkynes RCCR (R = Et, Ph or Tol), but this was followed by C–H bond activation of one of the phenyl rings to yield

the 7-membered metallacyclic complexes $Cp_2Zr\{N(H)C(R)C(R)\text{-}1,2\text{-}C_6H_4N(Ph)\}$ (**1.82 – 1.84**, Equation 3.1).[33] This results in stoichiometric formation of the corresponding *N*-phenylindoles upon treatment with aqueous HCl.

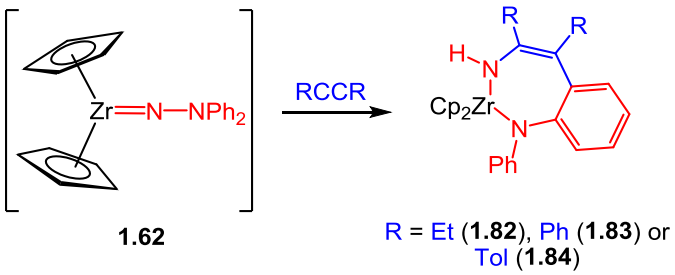

Equation 3.1[33]

In contrast, the bis(amide) $Cp_2Zr(NHXyl)_2$ (**1.48**), also reported by Bergman *et al.*, was an effective hydroamination pre-catalyst, *via in situ* formation of the transient base-free imido complex $Cp_2Zr(NXyl)$ (**1.17**). This compound can catalyse the hydroamination of internal alkynes, e.g. diphenylacetylene and 2-butyne, in which reversible α-elimination of enamine and regeneration of the transient imide **1.17** is the rate-determining step (RDS).[1,34,35] Meanwhile, those authors also reported the rapid and exclusive C–H bond activation by the zirconocene imido complex Cp*CpZr(N^{t}Bu)(THF) (**1.41**) when the terminal alkyne, ^{t}BuCCH, was employed. The small and inverse kinetic isotope effect (KIE; k_H/k_D) value of 0.8 suggests that the reaction proceeds *via* a rate-determining 2,1-cycloaddition (Markovnikov type) between ^{t}BuCCH and the base free transient intermediate Cp*CpZr(N^{t}Bu) (**3.1**) to form an azazirconacyclobutene complex Cp*CpZr{(N^{t}Bu)C(^{t}Bu)C(H)} (**1.42_int**), before C–H bond activation takes place to generate the amide-acetylide zirconocene complex Cp*CpZr(NH^{t}Bu)(CC^{t}Bu) (**1.42**, Scheme 3.1).[25]

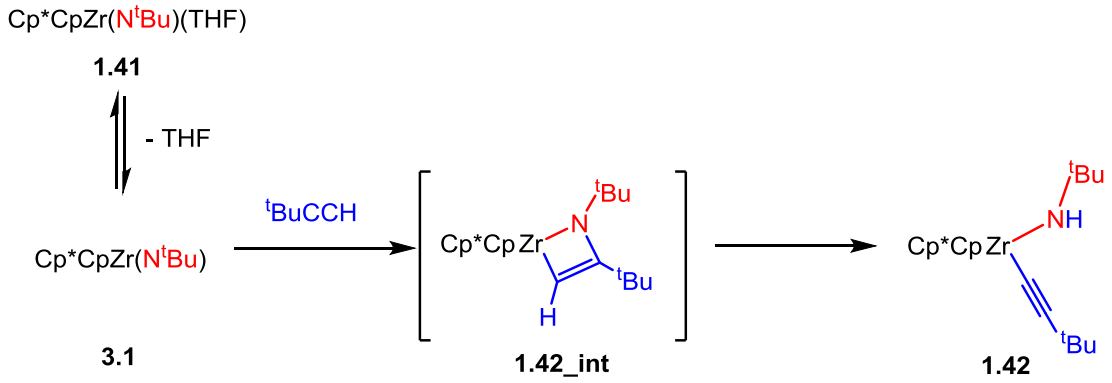

Scheme 3.1. Mechanism of the C–H bond activation of ^{t}BuCCH by Cp*CpZr(N^{t}Bu)(THF) (**1.41**).[25]

The 2,1-cycloaddition (Markovnikov type) products have been isolated[21,36], but are less commonly reported on steric grounds compared to 1,2-cycloaddition. On some occasions equilibria between C–H bond activation and cycloaddition products, or the conversion of one to the other, have been observed,[36,37] and proposals of kinetic factors controlling reaction outcomes despite thermodynamic preferences have been advanced based on experimental data,[23,38] and supported by computational studies.[38]

It has also been shown experimentally (supported by DFT studies in some instances) that [2+2] cycloaddition products formed from oxo and imido or related compounds and alkynes or nitriles can be thermodynamically stabilised by electron-withdrawing groups.[19] In other literature,[39–42] it has also been shown that the C–H bond activation products of alkynes with metal complexes become more thermodynamically stable with electron-withdrawing R-groups (i.e. as the alkynes become more 'acidic'). However, it is not clear from the literature how relatively important these stabilisation effects are in azametallacyle and acetylide derivatives: *a priori* one would expect more acidic alkynes to favour the formation of amide- or hydroxide-acetylide species. Finally, very little is yet known about the relative thermodynamic features of borylimides in comparison with the widely-studied organoimido counterparts, and the interplay between the imide N-substituents and the types of reaction products formed with alkynes.

The work described in this Chapter concerns principally the reactions of terminal alkynes RCCH (R = ^{t}Bu or aryl) with the borylimides $Cp_2M\{NB(NAr'CH)_2\}(L)$ (M = Ti, Zr or Hf; L = THF, py or DMAP) and the bis(indenyl) analogues $Ind_2Zr\{NB(NAr'CH)_2\}(L)$. Kinetic analyses of these reactions will be presented, and the preparation of

borylenamines from corresponding azazirconacyclobutene complexes, and attempts to catalyse the hydro-borylamination reaction will also be discussed.

3.2 DFT studies of the reactions of model organo- and boryl-imides with alkynes

This Section describes DFT calculations performed by Prof. Philip Mountford using the B3PW91 functional and Def2TZVP basis set, supported by Quantum Theory of Atoms in Molecules (QTAIM)[43] and Natural Bond Orbital (NBO) analyses,[44] on the reactions of the model zirconocene borylimido complexes, $Cp_2Zr\{B(NMeCH)_2\}$ (**1Q_B(NMeCH)$_2$**), R = Xyl (**1Q_Xyl**), Me (**1Q_Me**)) and $Ind_2Zr\{NB(NMeCH)_2\}$ (**2Q_B(NMeCH)$_2$**), introduced in Section 2.7 of the previous Chapter, with the alkynes RCCH (R = H, Me, ^{t}Bu, Ph, Ar^{CF_3} (Ar^{CF_3} = 3,5-$C_6H_3(CF_3)_2$), Ar^F (Ar^F = C_6F_5) and PhCCMe. Comparison is made with the titanocene congener $Cp_2Ti\{NB(NMeCH)_2\}$ (**3Q_B(NMeCH)$_2$**). By way of example, Figure 3.1 illustrates the model reaction products formed between $Cp_2Zr(NR)$ (**1Q_R′**) and the alkynes RCCH, namely C–H bond activation (**4Q_R′,R)** or 1,2- or 2,1-cycloaddition (**5Q_R′,R** or **6Q_R′,R**). Further calculations on the full experimental systems, incorporating corrections for dispersion and solvent effects, and for enthalpy and Gibbs free energy, are described later in the Chapter alongside the relevant experimental results.

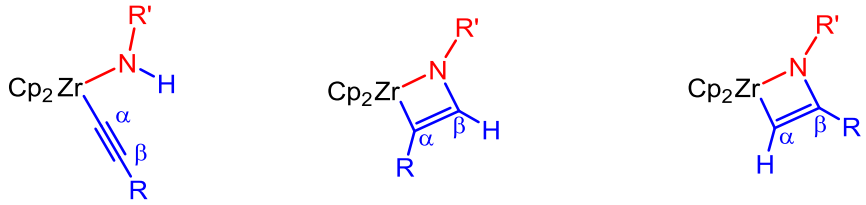

Figure 3.1. Examples of model reaction products studied by DFT: C–H bond activation (**4Q_R′,R**), 1,2-cycloaddition (**5Q_R′,R**) and 2,1-cycloaddition (**6Q_R′,R**). R′ = $B(NMeCH)_2$, Me or Xyl; R = H, Me, ^{t}Bu, Ph, Ar^{CF_3} or Ar^F (Ar^{CF_3} = 3,5-$C_6H_3(CF_3)_2$; Ar^F = C_6F_5).

3.2.1 Structural trends and electronic structure of the cycloaddition products of $Cp_2Zr\{NB(NMeCH)_2\}$ (**1Q_B(NMeCH)$_2$**)

The HCCH cycloaddition product $Cp_2Zr\{N\{B(NMeCH)_2\}C(H)C(H)\}$ (**5Q_B(NMeCH)$_2$,H**) serves as a benchmark for the other homologues studied (*vide infra*). The geometric data (Table 3.1) are in agreement with those of previous cycloaddition species reported by Bergman, and in this Thesis in the following Sections. A molecular orbital (MO) analysis established **5Q_B(NMeCH)$_2$,H** as a formally 16 valence electron Cp_2ZrX_2 species. Selected MOs are shown in Figure 3.2. The non-bonding LUMO is Zr-based and essentially the 2a' MO of $[Cp_2Zr]^{2+}$ as discussed in Chapter 2 (Section 2.7, Figure 2.13). The N_{im} out-of-plane $2p_v$ AO interacts with the alkyne fragment π-bonding MO to form predominantly ligand-based MO68 and its antibonding partner, MO76 which is the HOMO-1. The HOMO (not shown) is mainly based on the boryl ring (the HOMO of $Cp_2Zr\{B(NMeCH)_2\}$ itself (Chapter Two, Figure 2.14). Mulliken population analysis of MO68 shows a small (4%) contribution from zirconium (mixing with the 1a′ MO of $[Cp_2Zr]^{2+}$ (*cf.* Figure 2.13)) suggesting that π-donation is present but relatively limited because of the delocalised nature of the $N_{im}+C_\alpha+C_\beta$ π-LCAO (Linear Combination of Atomic Orbital) and the significantly lengthened Zr–N_{im} bond (2.114 Å *cf.* 1.854 Å in **1Q_B(NMeCH)$_2$**).

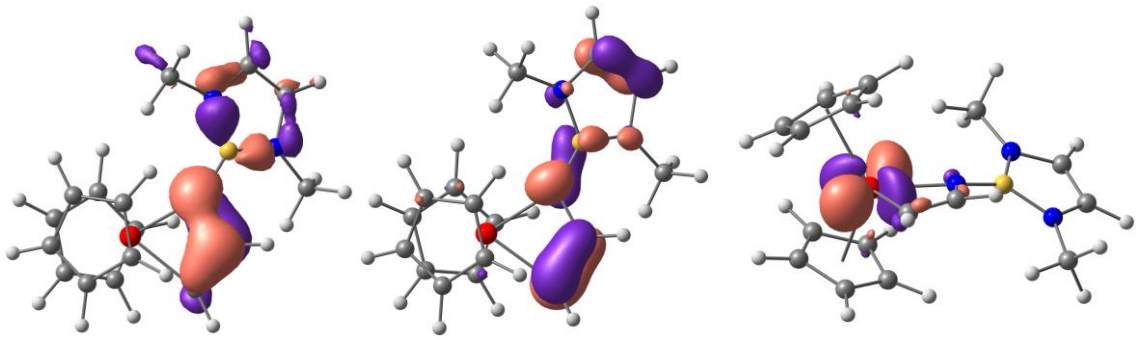

Figure 3.2. DFT computed MO68 (left, E = –9.14 eV) MO76 (HOMO-1, centre, E = –5.61 eV), and MO78 (LUMO, right, E = –1.52 eV) of $Cp_2Zr\{N\{B(NMeCH)_2\}C(H)C(H)\}$ (**5Q_B(NMeCH)$_2$,H**).

The net QTAIM charge of –1.113 of the $\{N\{B(NMeCH)_2\}C(H)C(H)\}$ fragment in **5Q_B(NMeCH)$_2$,H** (Table 3.1) is larger in magnitude than that of the $NB(NMeCH)_2$ ligand in **1Q_B(NMeCH)$_2$** (–0.903), with the HCCH moiety having a charge of –0.210. The *Q*(Zr) stays effectively the same on cycloaddition, but Σ*Q*$(Cp)_2$ decreases in

magnitude from –1.124 in the imide to –1.039 in the metallacycle. Therefore, both the imido and Cp fragments of the π-loaded **1Q_B(NMeCH)$_2$** are stabilised as ligand-based charge is transferred to the alkyne fragment. The accumulated charge on HCCH is unevenly distributed: $Q(C_\alpha) = –0.532$ and $Q(C_\beta) = 0.238$. π-acceptor substituents such as aryl groups should in principle stablisise the net alkyne charge and may interact best with HOMO-1 (N_{im}–C_β π* antibonding, C_α–C_β π-bonding) as this is closer in energy to the vacant π∗ aryl MOs. Since $Q(C_\alpha)$ is negative, and the HOMO-1 has 22% weighting on C_α but only 12% on C_β, aryl group should be electronically preferred to attachment at C_α. Electron-releasing groups would be destabilising, especially at C_α.

The electronic structure of **5Q_B(NMeCH)$_2$,H** was also analysed using the NBO method. NBOs closely correspond to the picture of localised bonds and lone pairs, so that is possible to interpret conveniently *ab initio* wave-functions in terms of Lewis structure concepts. In molecules such as **5Q_B(NMeCH)$_2$,H** expression of delocalisation from a chosen Lewis structure is important and this can be interrogated by consideration of the NBO occupancies. An NBO occupancy should be 2 or 0 for a Lewis ('L') or non-Lewis ('NL') orbital, respectively, if the Lewis structure is totally appropriate. Deviations from these extremes reflect delocalisation (interactions between NBOs); in this case the NBO analysis is extended to include combinations of the relevant NBOs so as to form Natural Localized Molecular Orbitals (NLMOs). The interactions (L→NL) between NBOs can be expressed as second order perturbation energies $\Delta E_{(L\rightarrow NL)}$.

Table 3.1. Selected bond distances (*d*, Å) and angles (°) and QTAIM (entries 9 – 16) and NBO (entries 17 – 24) parameters for $Cp_2Zr\{N\{B(NMeCH)_2\}C(H)C(H)\}$ (**5Q_B(NMeCH)$_2$,H**) the 1,2-cycloaddition products $Cp_2Zr\{N\{B(NMeCH)_2\}C(H)C(R)\}$ (**5Q_B(NMeCH)$_2$,R** (R = Me, Ph or Ar^{CF_3})) and 2,1-cycloaddition product $Cp_2Zr\{N\{B(NMeCH)_2\}C(R)C(H)\}$ (**6Q_B(NMeCH)$_2$,Ph**). QTAIM sums of atomic charges (ΣQ) are given in units of *e*; δ is the delocalisation index for the stated pair of atoms at the bond critical point. Second order perturbation energies $\Delta E_{(L\rightarrow NL)}$ between NBOs are given in kcal mol^{-1}; NBO occupancies (*occ*(NBO)) are in units of *e*. C_α and C_β are the Zr– and N–bonded alkyne C atoms, respectively.

Entry	Geometric, QTAIM or NBO parameter	HCCH	1,2-MeCCH	1,2-PhCCH	1,2-Ar^{CF_3}CCH	2,1-PhCCH
1	$d(N–C_\beta)$	1.405	1.406	1.394	1.385	1.412
2	$d(N_{im}–B)$	1.434	1.433	1.437	1.440	1.438
3	$d(C_\alpha–C_\beta)$	1.368	1.367	1.375	1.378	1.374
4	$d(C_\alpha–C_{ipso})$	*n.a.*	*n.a.*	1.455	1.448	1.494
5	$d(Zr–N_{im})$	2.114	2.108	2.123	2.135	2.114
6	$d(Zr–C_\alpha)$	2.153	2.165	2.172	2.179	2.168
7	$d(Zr–Cp_{cent})$	2.253	2.254	2.246	2.240	2.251
8	$(Cp_{cent}–Zr–Cp_{cent})$	130.3	130.6	131.1	131.4	130.5
9	ΣQ(RCCH)	–0.210	–0.181	–0.230	–0.282	–0.209
10	$\Sigma Q\{N\{B(NMeCH)_2\}C(H)C(R)\}$	–1.113	–1.088	–1.120	–1.160	–1.113
11	$\delta(N_{im}–C_\beta)$	1.142	1.134	1.163	1.182	1.098
12	$\delta(N_{im}–B)$	0.467	0.469	0.464	0.461	0.458
13	$\delta(C_\alpha–C_\beta)$	1.654	1.612	1.545	1.524	1.582
14	$\delta(C_\alpha–C_{ipso})$	*n.a.*	*n.a.*	1.132	1.15	1.010
15	$\delta(Zr–N_{im})$	0.589	0.598	0.574	0.557	0.603
16	$\delta(Zr–C_\alpha)$	0.707	0.696	0.678	0.665	0.699
17	$N_{im}(2p)\rightarrow Zr$	35.3	36.4	31.9	30.3	32.1
18	$N_{im}(2p)\rightarrow B(2p)$	50.5	52.4	51.5	51.5	37.0
19	$N_{im}(2p)\rightarrow\pi^*(C_\alpha–C_\beta)$	35.0	33.4	41.7	45.6	28.2
20	$\pi(C_\alpha–C_\beta)\rightarrow C_{ipso}$	*n.a.*	*n.a.*	44.1	55.0	34.4
21	$\pi(C_\alpha–C_\beta)\rightarrow Zr$	32.7	30.9	28.9	27.1	28.4
22	$occ(N_{im}(2p))$	1.617	1.620	1.595	1.581	1.639
23	$occ(\pi(C_\alpha–C_\beta))$	1.849	1.836	1.790	1.780	1.812
24	$occ(\pi^*(C_\alpha–C_\beta))$	0.176	0.189	0.235	0.251	0.194

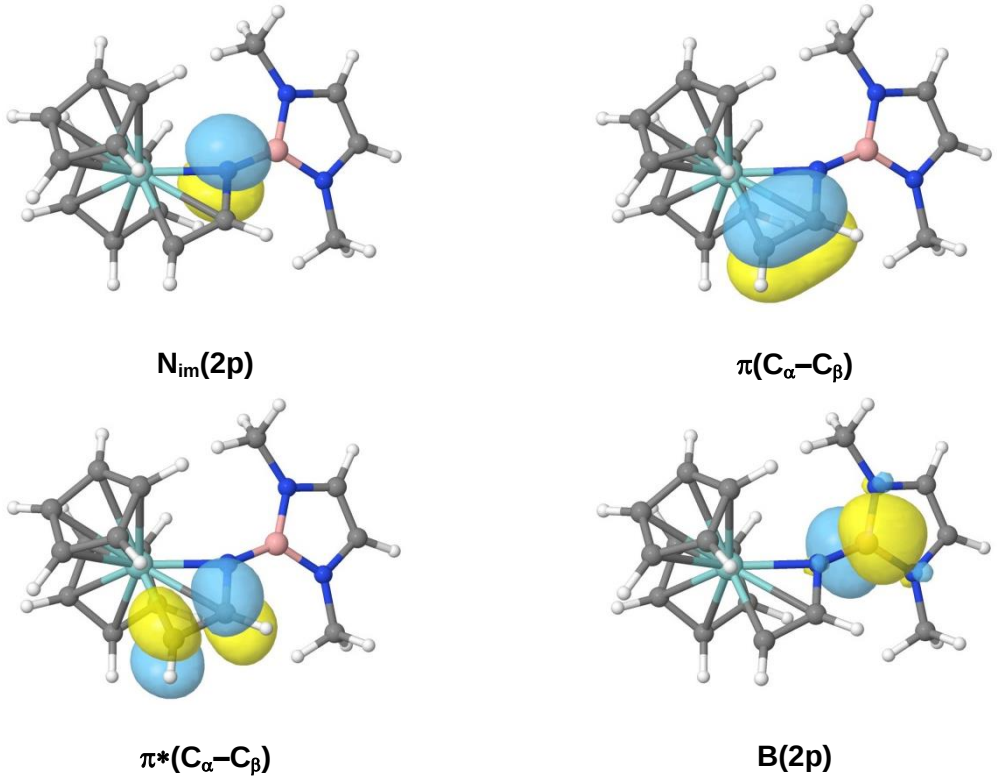

Figure 3.3. Selected natural bond orbitals for $Cp_2Zr\{N\{B(NMeCH)_2\}C(H)C(H)\}$ (**5Q_B(NMeCH)$_2$,H**).

The NBO analysis for **5Q_B(NMeCH)$_2$,H** found a Lewis structure formally described with Zr–N_{im} and Zr–$C_α$ single bonds, lone pairs (2p character) on N_{im} and the two N atoms of $B(NMeCH)_2$, $C_α$–$C_β$ π and π* NBOs for the alkyne moiety, and a vacant NBO (2p) on B. Key NBOs are shown in Figure 3.3. As Table 3.1 shows (entries 17 – 21), N_{im}(2p) interacts with acceptor NBOs on Zr, B(2p) and π*($C_α$–$C_β$). Likewise, π($C_α$–$C_β$) interacts with acceptor NBOs on Zr. Accordingly, the values of *occ*(N_{im}(2p)) and *occ*(π($C_α$–$C_β$)) are less than 2, and that of *occ*(π*($C_α$–$C_β$)) is larger than 0. We also computed the NLMOs for **5Q_B(NMeCH)$_2$,H**, and these closely resemble the NBOs. For example, even the NLMO corresponding to very delocalised N_{im}(2p) had *ca.* 80% of this NBO character, with remaining participation from Zr, B, $C_α$ and $C_β$ in similar % contributions. Thus the N_{im}(2p) and π($C_α$–$C_β$) NBOs in Figure 3.3 can be considered the localised (Lewis equivalent) counterparts of MO68 and MO76 in Figure 3.2.

The advantage of the NBO interpretation is that one can track in an intuitive and quantitative way the effects of varying RCCH in the model compounds **5,6Q_**

B(NMeCH)$_2$,R and the sense of addition (1,2 or 2,1). These were geometrically optimised (R = Me, Ph and Ar^{CF_3}), and the key metric and QTAIM parameters are listed in Table 3.1. Considering first **5Q_B(NMeCH)$_2$,R**, the data show that the bonding to MeCCH is slightly less effective than for HCCH: e.g., less negative Σ*Q*(RCCH) and Σ*Q*{N{B(NMeCH)$_2$}C(H)C(R)} values, smaller δ(N_{im}–C_β) and larger δ(N_{im}–Zr), increased N_{im}(2p)→Zr and reduced N_{im}(2p)→π*(C_α–C_β). Conversely, tracking the sequence R = Me, H, Ph and Ar^{CF_3} shows: increasing charge transfer to alkyne; longer and weaker Zr–N_{im} and C_α–C_β bonds as π*(C_α–C_β) is populated and π(C_α–C_β) is depleted by donation to C_{ipso} of the aryl ring; decrease of *occ*(N_{im}(2p). Interestingly, *d*(Zr–Cp_{cent}) also decreases from R = Me to Ar^{CF_3}, possibly due to the decreased competition between the Cp rings and the slightly less π-donating metallacycle as judged by smaller N_{im}(2p)→Zr and π(C_α–C_β)→Zr energies. Finally, comparing 1,2- and 2,1-addition of PhCCH shows significant differences (**5-** and **6Q_B(NMeCH)$_2$,Ph**) for parameters such as Σ*Q*(PhCCH) (–0.230 *vs* –0.209), N_{im}(2p)→π*(C_α–C_β) (41.7 *vs*. 28.2), *occ*((N_{im}(2p)) (1.595 *vs.* 1.639) and π(C_α–C_β)→C_{ipso} (44.1 *vs.* 34.4), as expected from the earlier discussion.

3.2.2 Thermodynamic preferences: C–H bond activation *vs* 1,2- or 2,1-cycloaddition for Group 4 metallocene imido compounds

As mentioned, Figure 3.1 illustrates the model C–H activation or cycladdition reaction products formed between Cp_2Zr(NR) (**1Q_R′**) and the alkynes RCCH. Table 3.2 gives the gas phase, SCF reaction energies (ΔE, kcal mol^{-1}) for all the systems studied. For the sterically reduced systems under consideration here we may neglect dispersion (van der Waals type) corrections. Since we are interested mainly in electronic preferences, and all reactions of a given alkyne and/or imide have the same magnitude of change in translational entropy, ΔS effects are not included. The results for the metallacyclic cycloaddition compounds can be interpreted using the electronic structure analysis in the previous section.

Table 3.2. DFT (B3PW91/Def2TZVP) gas phase SCF energies ΔE (kcal mol^{-1}) for the reaction of model imides $Cp_2Zr(NR)$ (R = $B(NMeCH)_2$ (**1Q_B(NMeCH)$_2$**), Me (**1Q_Me**), Xyl (**1Q_Xyl**)), $Ind_2Zr\{NB(NMeCH)_2\}$ (**2Q_B(NMeCH)$_2$**) and $Cp_2Ti\{B(NMeCH)_2\}$ (**3Q_B(NMeCH)$_2$**) with terminal alkynes and PhCCMe to form C–H bond activation or 1,2- or 2,1-cycloaddition products of the type **4Q**, **5Q** or **6Q** (*cf.* Figure 3.1).

Entry	Imide	Alkyne	ΔE (kcal mol^{-1}) for the stated reaction type		
			C–H activation	1,2-cycloaddition	2,1-cycloaddition
1	**1Q_B(NMeCH)$_2$**	HCCH	–41.6	–46.6	–46.6
2	**1Q_B(NMeCH)$_2$**	MeCCH	–39.8	–40.6	–40.9
3	**1Q_B(NMeCH)$_2$**	^{t}BuCCH	–39.3	–37.0	–32.8
4	**1Q_B(NMeCH)$_2$**	PhCCH	–41.4	–44.1	–39.3
5	**1Q_B(NMeCH)$_2$**	Ar^{CF_3}CCH	–43.4	–48.3	–43.0
6	**1Q_B(NMeCH)$_2$**	Ar^FCCH	–44.4	–49.6	–40.9
7	**1Q_B(NMeCH)$_2$**	PhCCMe	*n.a.*	–35.9	–32.3
8	**1Q_Me**	MeCCH	–42.0	–42.7	*n.d.*
9	**1Q_Me**	PhCCH	–43.6	–47.0	*n.d.*
10	**1Q_Xyl**	PhCCH	–35.3	–36.8	*n.d.*
11	**2Q_B(NMeCH)$_2$**	PhCCH	–37.4	–36.6	*n.d.*
12	**2Q_B(NMeCH)$_2$**	Ar^FCCH	–40.5	–43.5	*n.d.*
13	**3Q_B(NMeCH)$_2$**	PhCCH	–26.9	–34.5	–30.5
14	**3Q_Xyl**	PhCCH	–20.9	–26.5	–22.2

The reactions of **1Q_B(NMeCH)$_2$** are first considered. Entry 1 (benchmark reaction with HCCH) shows that in the absence of any alkyne R-substituent, cycloaddition is intrinsically favoured on electronic grounds compared to C–H bond activation (ΔΔE = –5.0 kcal mol^{-1} in favour of **5Q_B(NMeCH)$_2$,H** *cf.* **4Q_B(NMeCH)$_2$,H**). Looking further at the C–H bond activation series in entries 2 - 6 shows the expected trend[39–42] as a function of alkyne acidity: the least exothermic reaction is with ^{t}BuCCH and the most favourable is for Ar^FCCH, the difference between the extremes of this range being 5.1 kcal mol^{-1}.

The cycloaddition reactions with MeCCH and ^{t}BuCCH are less favourable for these electron-releasing R-groups as expected from the electronic structure analyses. For MeCCH, there is a small preference for 2,1-addition, probably because the partially positive C_β benefits from the election-releasing nature of methyl group. Significantly, the decrease in ΔE for either cycloaddition reaction is much larger than that for C–H bond addition so that the three processes become electronically competitive. With ^{t}BuCCH (entry 3) the combined effects of the electron-releasing R-group and steric crowding in the metallacycle becomes evident: 2,1-addition is severely disfavoured and 1,2-addition also becomes less competitive. However, 1,2-cycloaddition becomes much more favourable in the series R = Me, Ph, Ar^{CF_3}, Ar^{F}, as expected from the electronic structure considerations. Significantly the increase in magnitude of ΔE increases faster than that for C–H addition, such that cycloaddition becomes increasingly the more thermodynamically favoured process. Changing from PhCCH (entry 4) to PhCCMe (entry 7) results in a decreased magnitude of ΔE, reflecting the increased crowding in the metallacycle and the electron-releasing nature of Me.

The trends in ΔE for the 2,1-cycloaddition reactions with ArCCH are irregular and reflect a combination of electronic and steric effects. Most of the further calculations in this Section focus only on C–H bond activation and 1,2-cycloaddition products.

Entries 8 – 10 summarise the ΔE values for the reactions of MeCCH and/or PhCCH with the zirconocene organomides **1Q_Me** and **1Q_Xyl**. As found for **1Q_B(NMeCH)$_2$**, MeCCH retains a slight preference for cycloaddition, but PhCCH has a much stronger preference both in relative (ΔΔE) and absolute reaction energy terms. Comparison of entries 4, 9 and 10 (reactions of different imides with the same alkyne) reveals the same trend as found in their C–H bond activation reactions with benzene (Chapter Two, Section 2.4): addition reactions of $Cp_2Zr(NMe)$ are the the most exothermic for the small model systems, but those for $Cp_2Zr\{B(NMeCH)_2\}$ are energetically comparable, and significantly more favourable than for $Cp_2Zr(NXyl)$. Finally, entries 11 – 14 give the ΔE values for the bis(indenyl) system $Ind_2Zr\{NB(NMeCH)_2\}$ (**2Q_B(NMeCH)$_2$**) and the titanium congeners, namely $Cp_2Ti\{NB(NMeCH)_2\}$ (**3Q_B(NMeCH)$_2$**) and $Cp_2Ti(NXyl)$ (**3Q_Xyl**). As expected (*cf.* Chapter Two and periodic trends within Group 4), the ΔE values for the reactions of the these systems with PhCCH (either C–H activation or cycloaddition) are less favourable than in the case of **1Q_B(NMeCH)$_2$**.

3.3 Reactions of $Cp_2Zr\{NB(NAr'CH)_2\}(py)$ (11) with the electron rich alkyne ^tBuCCH

On the NMR tube scale in toluene-d_8, the reaction of ^{t}BuCCH with $Cp_2Zr\{NB(NAr'CH)_2\}(py)$ (**11**) was very slow, giving 5% conversion to a single species (**25**) at RT after 16 h, calculated by ^{1}H integration. Upon heating to 55 °C, the colour of the reaction solution changed from red-orange to dark brown over 16 h. The ^{1}H NMR spectrum of the mixture showed that **25** was formed as the major product, and another complex **26** was also generated in 10% NMR yield. The major product is characterised as the azazirconacyclobutene complex $Cp_2Zr\{N\{B(NAr'CH)_2\}C(H)C(^tBu)\}$ (**25**) formed *via* [2+2] 1,2-cycloaddition. On reacting further at 100 °C for another 16 h, complex **25** was quantitatively converted to the initial minor product **26**, identified as $Cp_2Zr\{NHB(NAr'CH)_2\}(CC^tBu)$.

On the preparative scale, complex **25** was isolated in 75% yield as a dark brown solid by carrying out the reaction of **11** with ^{t}BuCCH in benzene at 60 °C. In contrast, performing the reaction of **11** with ^{t}BuCCH in toluene at 100 °C for 16 h, acetylide **26** was exclusively formed and isolated in 47% crystalline yield as bright yellow crystals (Scheme 3.2).

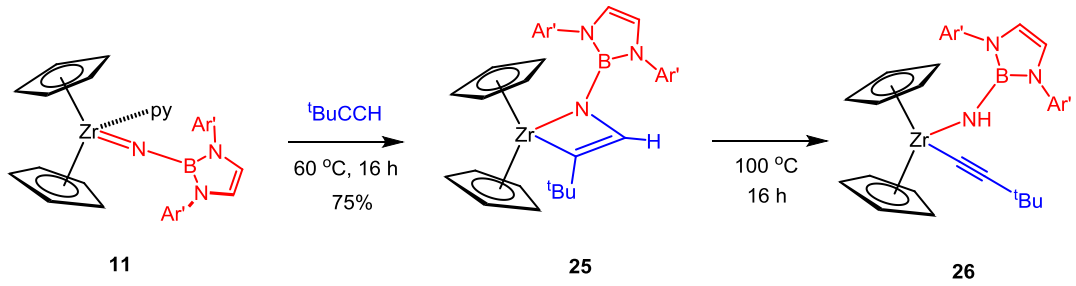

11 **25** **26**

Scheme 3.2. Synthesis of $Cp_2Zr\{N\{B(NAr'CH)_2\}C(H)C(^tBu)\}$ (**25**) and $Cp_2Zr\{NHB(NAr'CH)_2\}(CC^tBu)$ (**26**) from $Cp_2Zr\{NB(NAr'CH)_2\}(py)$ (**11**).

The ^{11}B NMR spectrum of **26** shows a singlet at 24.5 ppm which is characteristic of a zirconocene borylamido moiety. Also, in the ^{1}H NMR spectrum, a broad NH singlet at 5.57 ppm is observed, attributable to the N<u>H</u> of the borylamido ligand. In the ^{13}C NMR spectrum, the two acetylide carbons are assigned at 131.7 and 119.3 ppm, corresponding to the carbon directly bonded to zirconium centre, and the one adjacent to the ^{t}Bu moiety, respectively. In addition, a band at 2081 cm^{-1} in the IR spectrum (Nujol mull) of **26** attributed to ν(C≡C) was observed, consistent with previously reported in titanium and

zirconium acetylide compounds.[23,36,45] In contrast, the ^{11}B NMR spectrum of **25** displays a slightly upfield shifted signal at 22.7 ppm. In the ^{1}H NMR spectrum, a sharp singlet signal, rather than broadened, was observed at 6.66 ppm, this being assigned to the methine proton of ZrC=C<u>H</u> of the azazirconacyclobutene unit. An HSQC correlation of this methine proton to the ^{13}C resonance of C=<u>C</u>H is found at 104.2 ppm, whilst an HMBC correlation is observed to a ^{13}C resonance at 188.6 ppm. This diagnostic highly downfield shifted ^{13}C signal is consistent with the carbon directly bonded to the zirconium centre, which is comparable with the values of other azazirconacyclobutene complexes previously reported by Bergman.[1] Hence this confirms that **25** exists as a single 1,2-cycloaddition (anti-Markovnikov type) regioisomer, as depicted in Scheme 3.2, which minimises the steric clash between the bulky ^{t}Bu and boryl moieties, consistent with the DFT calculations on the model system **5,6Q_B(NMeCH)$_2$,^{t}Bu** (Table 3.2).

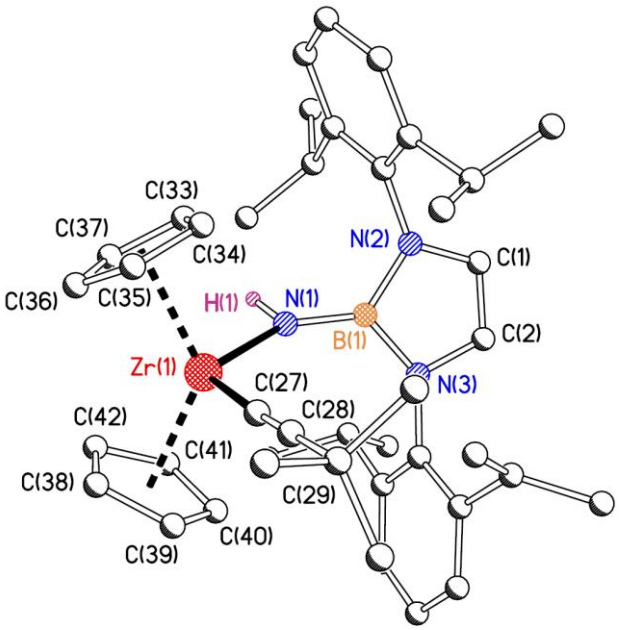

Figure 3.4. Ball and stick plot of $Cp_2Zr\{NHB(NAr'CH)_2\}(CC^{t}Bu)$ (**26**). C–bond H atoms omitted for clarity.

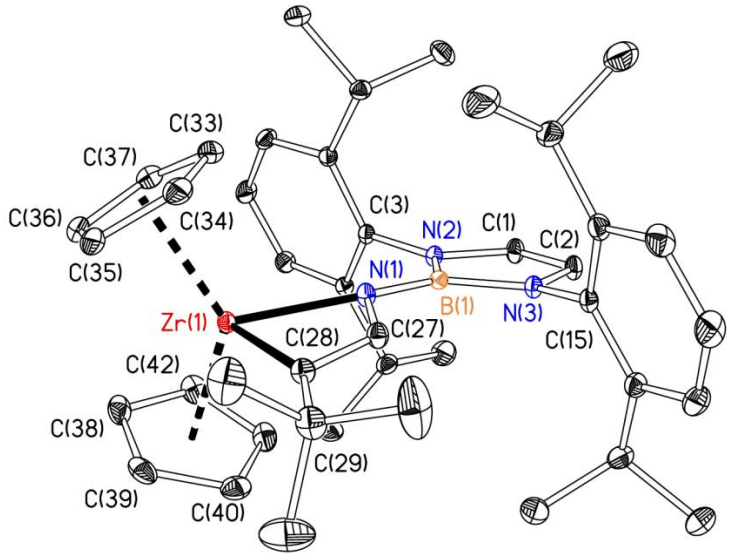

Figure 3.5. Displacement ellipsoid plot (20% probability) of $Cp_2Zr\{N\{B(NAr'CH)_2\}C(H)C(^tBu)\}$ (**25**). H atoms omitted for clarity.

Table 3.3. Selected bond lengths (Å) and angles (°) for $Cp_2Zr\{N\{B(NAr'CH)_2\}C(H)C(^tBu)\}$ (**25**). $Cp_{cent(1)}$ and $Cp_{cent(2)}$ refer to the computed Cp ring centroids for "upper" and "lower" Cp rings, respectively, as depicted in Figure 3.5.

Zr(1)–N(1)	2.1110(10)	$Cp_{cent(1)}$–Zr(1)–$Cp_{cent(2)}$	130.5
Zr(1)–C(28)	2.1631(13)	N(1)–Zr(1)–C(28)	69.94(4)
Zr(1)–$Cp_{cent(1)}$	2.243	Zr(1)–N(1)–B(1)	152.26(8)
Zr(1)–$Cp_{cent(2)}$	2.236	Zr(1)–C(28)–C(27)	83.74(8)
N(1)–B(1)	1.4182(16)	N(1)–C(27)–C(28)	121.4(3)
B(1)–N(2)	1.4564(16)		
B(1)–N(3)	1.4572(16)		
N(1)–C(27)	1.4393(16)		
C(27)–C(28)	1.3553(18)		

Diffraction-quality crystals of **25** and **26** were grown from hexane solutions at 4 °C. The approximate solid state structure of **26** is shown in Figure 3.4 as a ball and stick plot, due to the crystals grown being twinned and highly disordered. Therefore, full refinement could not be carried out. Nonetheless, the ball and stick plot shows the coordination geometry, which contains an acetylide and a borylamide fragment as well as two

cyclopentadienyl ligands. The solid state structure of **25** is shown in Figure 3.5, and selected bond distances and angles are listed in Table 3.3. Molecules of compound **25** possess a pseudo tetrahedral environment, with eclipsed cyclopentadienyl rings, and the κ^2-coordination of the C(28)–C(27)–N(1) unit to form the four-membered azazirconacyclobutene ring with Zr(1) as an anti-Markovnikov (1,2-cycloaddition) regioisomer is confirmed. This moiety appears comparable to those titanium and zirconium analogous which have previously been structurally authenticated,[1,23,27,28] having an N(1)–Zr(1)–C(28) angle of 69.94(4)°, which is slightly wider than that in $Cp_2Zr\{N(Xyl)C(Ph)C(Ph)\}$ (**3.2**) of 66.33(12)° (internal alkyne).[1] However, there is no appropriate anti-Markovnikov azazirconacyclobutene complex incorporating a terminal alkyne for direct structural comparison. The C=C bond length of 1.3553(18) Å is consistent with this being a carbon–carbon double bond, and comparable with those found in other azametallacyclobutene complexes.[1,20,23] The Zr(1)–N(1) and Zr(1)–C(28) bond lengths of 2.1110(10) and 2.1631(13) Å, respectively, are consistent with single bonds, and the sums of angles subtended at N(1) and C(28) of 357.44(15) and 360 (18)°, respectively, imply sp^2-hybridised N(1) and C(28) atoms. The ring B, N and C atoms of the diazaboryl moiety $B(NAr'CH)_2$ are effectively coplanar with the Zr(1)–N(1)–C(27)–C(28) group implying delocalisation of the N(1) $2p_\pi$ lone pair to both the boryl moiety and azametallacyclobutene ring, consistent with the computational studies in Section 3.2.1.

The outcomes from the reaction between **11** and ^{t}BuCCH, where the initial [2+2] cycloaddition yields the kinetic product **25** followed by rearrangement to give the final thermodynamic product **26**, are similar to those of $Cp^*_2Ti(O)(py)$ with PhCCH reported by Bergman.[36] They found that the initial [2+2] cycloaddition product $Cp^*_2Ti\{OC(Ph)C(H)\}$ (**3.3**) can be rearranged to form the hydroxoacetylide product $Cp^*_2Ti(OH)(CCPh)$ (**3.4**), where, however, both the [2+2] cycloaddition and rearrangement were found to be reversible. Bercaw reported similar observations when the tantalum imido compound $[Cp^*_2Ta(N^tBu)(THF)][B(C_6F_5)_4]$ (**2.9**) was reacted with propyne, forming a kinetic mixture of cycloaddition and C–H bond activation products. Quantitative conversion to the C–H bond activation product was achieved by heating the mixture for several hours.[37] More relevantly, the results may follow a similar mechanism to that proposed for the reaction of $Cp^*CpZr(N^tBu)(THF)$ (**1.41**) with ^{t}BuCCH (Scheme 3.1, Section 3.1), in which the inferred 2,1-cycloaddition product

Cp*CpZr{(N^{t}Bu)C(^{t}Bu)C(H)} (**1.42_int**) is proposed to be formed as a transient intermediate based on the small and reverse KIE value.[25] However, for the borylimido compound **11**, the formations of both **25** and **26** are much slower, and the kinetic 1,2-cycloaddition product **25** is thermodynamically stable enough to be isolated. This allows the rearrangement process of azametallacyclobutene complex (**25**) to borylamido-acetylide complex (**26**) to be fully studied.

Consistent with the experimental observations, DFT calculation (B3PW91-D3(bj)/Def2-TZVP with solvent corrections) found **25** and **26** to have very similar energies (ΔG = 1.0 kcal mol^{-1} at 298 K and 0.4 kcal mol^{-1} at 383K), albeit slightly in favour of the [2+2] cycloaddition product. Relative to base-free $Cp_2Zr\{NB(NAr'CH)_2\}$, the DFT reaction free energies to form **25** or **26** are *ca*. 27 kcal mol^{-1} at 298 K, but only *ca*. 22 kcal mol^{-1} at 383 K. *A priori* the rearrangement of **25** to **26** could occur *via* the transient borylimide at 383 K, assuming a negligible kinetic barrier. In addition, $\Delta_r G$ for the overall formation of **25** and pyridine from **11** and ^{t}BuCCH was computed to be –9.9 kcal mol^{-1} at the reaction temperature of 60 °C. DFT calculation were also performed on Bergman's proposed 2,1-cycloaddition intermediate Cp*CpZr{(N^{t}Bu)C(^{t}Bu)C(H)} (**1.42_int**), its 1,2-cycloaddition regioisomer Cp*CpZr{(N^{t}Bu)C(H)C(^{t}Bu)} and the final C–H bond activation product Cp*Cp(NH^{t}Bu)(CC^{t}Bu) (**1.42**). The C–H bond activation product was stable by ΔG = –0.5 kcal mol^{-1} relative to the 1,2-cycloaddition product, comparable to the outcome for **25** and **26**. The proposed (2,1-cycloaddition) intermediate **1.42_int** was computed to be less stable by 15.7 kcal mol^{-1} than its (1,2-cycloaddition) counterpart, consistent with the trend established for the model systems in Section 3.2.2 (Table 3.2).

The [2+2] cycloaddition of zirconocene borylimido complexes with ^{t}BuCCH was further monitored by incorporating different Lewis bases, using $Cp_2Zr\{NB(NAr'CH)_2\}$(L) (L = THF (**13**), py (**11**) or DMAP (**14**)) on the NMR tube scale. Immediate and exclusive formation of **25** was found at RT when **13** was employed. The reaction with **11**, as mentioned above, required elevated temperature (50 °C), and $t_{1/2}$ was measured to be *ca* 0.9 h. The much slower formation of **25** from **11** suggests that this [2+2] cycloaddition proceeds through a transient base free intermediate $Cp_2Zr\{NB(NAr'CH)_2\}$, which is consistent with the first THF dissociation step of the proposed mechanism for the formation of **1.42_int**,[25] and all the other [2+2] cycloadditions of Group 4 metal–nitrogen multiple bonded complexes. This also implies that the RDS of the reaction of **11** with ^{t}BuCCH is pyridine dissociation. This effect was further amplified when **14** was used,

where only 5% conversion to **25** was observed after 5 h (*cf.* $t_{1/2}$ = 0.9 h for **11**) under the same concentration and reaction condition (Table 3.4), as DMAP is a stronger base than pyridine by over two orders of magnitude.[46] The computed $\Delta_r G$ for the reaction of **13**, **11** and **14** with ^{t}BuCCH were –17.1, –10.4 and –8.0 kcal mol^{-1} at 298 K, the $\Delta\Delta G_r$ values reflecting the different Lewis base donor abilities.

In order to obtain a KIE for this process, $Cp_2Zr\{N\{B(NAr'CH)_2\}C(D)C(^tBu)\}$ (**25-*d*$_1$**) was first prepared from **11** using ^{t}BuCCD. Interestingly, on the preparative scale in C_6H_6 at 60 °C, the [2+2] cycloaddition product **25-*d*$_1$** was formed exclusively, hence the absence of $Cp_2Zr\{NDB(NAr'CH)_2\}(CC^tBu)$ (**26-*d*$_1$**) reflects a higher barrier for the conversion of **25-*d*$_1$** to **26-*d*$_1$** (*cf.* **25** to **26**). The thermolysis reactions of **25** and **25-*d*$_1$** forming **26** and **26-*d*$_1$**, respectively, were monitored by ^{1}H NMR spectroscopy at 383 K. The reactions were found to follow first order kinetics as judged by linear semi-logarithmic plots of $-\ln([\mathbf{25}]/[\mathbf{25}]_0)$ and $-\ln([\mathbf{25\text{-}}\boldsymbol{d}_1]/[\mathbf{25\text{-}}\boldsymbol{d}_1])_0$, which suggests the RDS is an intramolecular process. Each monitored reaction was run in duplicate, and the thermolysis of **25-*d*$_1$** was found to be significantly slower than that of **25**, with respective k_{obs} values of 16.70(4) × 10^{-5} s^{-1} and 15.18(4) × 10^{-5} s^{-1} (reaction performed in duplicate), and 4.62(1) × 10^{-5} s^{-1} and 5.25(1) × 10^{-5} s^{-1}. This gives a KIE between 2.89(1) and 3.62(2), indicating that the C–H bond breaking is involved in the RDS.

Table 3.4. Half-lives ($t_{1/2}$) and final product distribution for the reactions of $Cp_2Zr\{NB(NAr'CH)_2\}(L)$ (L = THF (**13**), py (**11**) or DMAP (**14**)) with RCCH (R = ^{t}Bu, Tol, $Ar^{CF_3}CCH$ and Ar^FCCH) in C_6D_6 at RT or 50 °C.

Compounds	Alkyne	Temp (°C)	Product[d]	$t_{1/2}$ (h)
$Cp_2Zr(NB(NAr'CH)_2)(py)$ (**11**)	^{t}BuCCH	50	CA (**25**)	0.9
	TolCCH	50	CA (**27**)	0.9
	TolCCH[a]	50	CA (**27**)	> 5.0
	$Ar^{CF_3}CCH$	RT	40% CH (**30**), 60% CA (**29**)	65.0
	Ar^FCCH	90	20 % CH (**31**), 80% CA (**32**)	*n.d.*
	Ar^FCCH	50	45 % CH (**31**), 55% CA (**32**)	0.6
	Ar^FCCH	RT	91 % CH (**31**), 9% CA (**32**)	11.0
	Ar^FCCH[a]	RT	CH (**31**)	12.0
$Cp_2Zr(NB(NAr'CH)_2)(THF)$ (**13**)	^{t}BuCCH	RT	CA (**25**)	-[b]
	TolCCH	RT	CA (**27**)	-[b]
	$Ar^{CF_3}CCH$	RT	5% CH (**30**), 95% CA (**29**)	-[b]
	Ar^FCCH	RT	9% CH (**31**), 91% CA (**32**)	-[b]
$Cp_2Zr(NB(NAr'CH)_2)(DMAP)$ (**14**)	^{t}BuCCH	50	CA (**25**)	-[c]
	TolCCH	50	CA (**27**)	-[c]
	$Ar^{CF_3}CCH$	RT	CH (**30**)	40.0
	Ar^FCCH	RT	CH (**31**)	6.1
	Ar^FCCH	50	CH (**31**)	0.4

a. reactions with 5 equivalents of pyridine. *b*. immediate reaction. *c*. 5% conversion after 5 h. *d*. CA: [2+2] cycloaddition product. CH: C–H bond activation product.

The KIE values above are comparable with previous values for C–H bond activations of terminal alkynes by $L_nTi{=}X$ compounds (X = O or $NB(NAr'CH)_2$). For example, the rearrangement of **3.3** to **3.4**, mentioned above, has a very similar normal KIE of 2.94(6) at 374 K.[36] Another C–H bond activation of terminal alkyne, Ar^FCCH, by titanium borylimido complex $Ti(N_2N^{py})\{NB(NAr'CH)_2\}(py)$ was reported in our research group, with a similar KIE range of 4.86 – 5.37.[20] The C–H bond activations of sp^3 *n*-pentane and sp^2 benzene, mesitylene and (*E*)-neohexene by Cp*CpZr(N^tBu) (**3.1**) were reported to give slightly large KIEs of 8.9, 7.4, 8.8 and 6.9, respectively.[25] In addition, Wolczanski and co-workers reported a number of reverse processes, C–H bond formation, *via* α-abstraction of Group 4 alkyl-amide complexes, accompanied by elimination of alkane, giving KIEs in the range *ca* 4 – 13.[47–51] The relatively small KIE values for the C–H bond activation of alkynes are suggested to be a result of relatively less linear H transfer in the transition state; i.e. where the transition state has less equal bond-making and –breaking character,[52,53] possibly due to the pre-coordination with corresponding metals.

The rearrangement of **25** to **26** was thus interpreted as initial generation of the base-free borylimide $Cp_2Zr\{NB(NAr'CH)_2\}$ and ^{t}BuCCH *via* a retro-[2+2] process, followed by rate-determining C–H bond activation. Free ^{t}BuCCH was not observed by ^{1}H NMR spectroscopy during the rearrangement reaction of **25** to **26**, which is consistent with the DFT calculation Δ_rG = 22.5 kcal mol^{-1} for the dissociation process from **25** to $Cp_2Zr\{NB(NAr'CH)_2\}$ and ^{t}BuCCH at 383 K. These DFT energies and experimental results thus cannot establish whether the rearrangement (**25** to **26**) occurs *via* "free" ^{t}BuCCH, or whether it remains coordinated during the process as summarised in Scheme 3.3. To test the mechanism further, the rearrangement reaction of **25-*d*$_1$** in the presence of three equivalents of ^{t}BuCCH was performed on the NMR tube scale at 110 °C in toluene-d_8. The ratio of **26**:**26-*d*$_1$** of 3:7, calculated by ^{1}H integration of the NH and NCH resonances, is significantly lower than the statistical ratio of 9:1 (including the KIE of *ca.* 3), indicating that the ^{t}BuCCH regenerated *via* retro-[2+2] strongly coordinates to the zirconium centre. In addition, heating a mixture of **26-*d*$_1$** in the presence of three equivalents of ^{t}BuCCH at 110 °C for 16 h gave no appreciable growth of the NH signal, showing that neither thermolysis of the acetylide compound **26** eliminating ^{t}BuCCH, or direct N<u>H/D</u> atom exchange, are feasible at this temperature. The presence of **26_int** was further confirmed by performing the rearrangement reaction of **25** in the presence of one

equivalent of TolCCH at 100 °C in toluene-d_8, in which the [2+2] cycloaddition product $Cp_2Zr\{N\{B(NAr'CH)_2\}C(H)C(Tol)\}$ (**27**) with TolCCH is more thermodynamically stable giving no further rearrangement (*vide infra*). After 16 h, complexes **27** and **26** were formed in *ca*. 1:9 ratio, again showing that the regenerated ^{t}BuCCH is almost exclusively coordinated on the zirconium centre giving a very slow alkyne exchange reaction, and the formation of **26** is effectively irreversible under these reaction conditions.

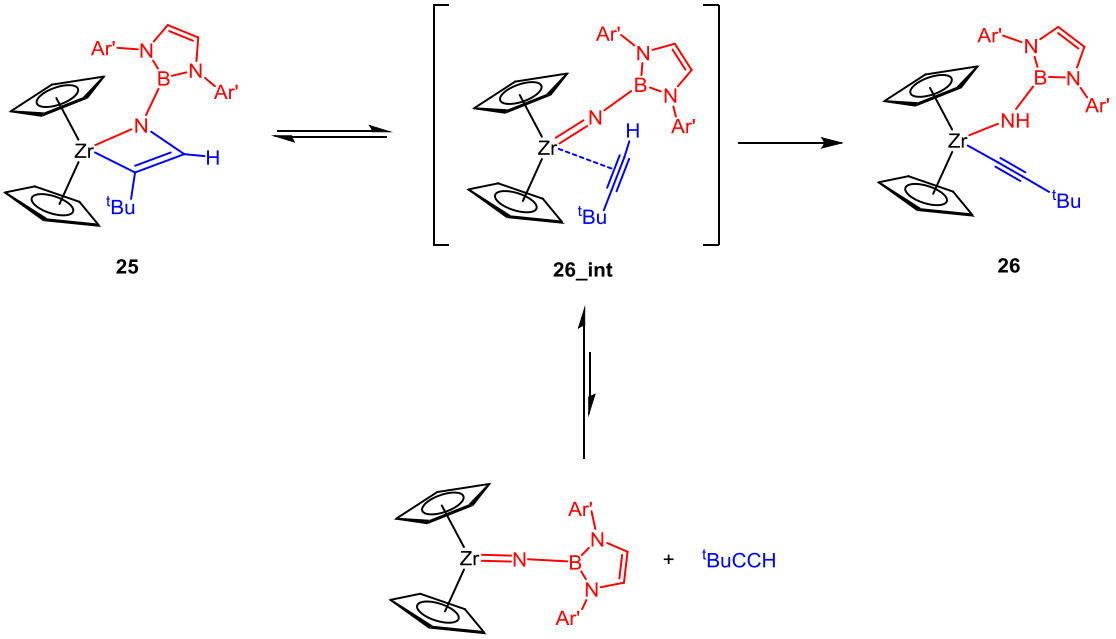

Scheme 3.3. Mechanism of the rearrangement of $Cp_2Zr\{N\{B(NAr'CH)_2\}C(H)C(^tBu)\}$ (**25**) to $Cp_2Zr\{NHB(NAr'CH)_2\}(CC^tBu)$ (**26**) *via* alkyne coordinated intermediate $Cp_2Zr\{NB(NAr'CH)_2\}(^tBuCCH)$ (**26_int**).

The thermolysis of **25-*d*$_1$** to **26-*d*$_1$** with one added equivalent of ^{t}BuCCH was also monitored by ^{1}H NMR spectroscopy at 383 K, in order to demonstrate the extent of alkyne exchange of **26_int** during the rearrangement. The formation of a very small amount of **25** was observed during the reaction, and the maximum **25**:**25-*d*$_1$** ratio was *ca*. 1:9, consistent with the observations above. It should be noted that the intrinsic effects of KIE will also shorten the life time of generated **25** compared to **25-*d*$_1$**, giving faster formation of **26** resulting in a low ratio. However, no appreciable growth of the N<u>H</u> signal was observed in the ^{1}H NMR spectrum of the final product (mostly **26-*d*$_1$**).

In order to test further the mechanism of the rearrangement and the implied intermediacy of **26_int** proposed above, the transformation of **25** to **26** was monitored by ^{1}H NMR spectroscopy in the temperature range 371 – 383 K. The reactions followed first order kinetics over this temperature range as judged by linear semi-logarithmic plots of –

ln([**25**]/[**25**]$_0$) *vs* time. The plots are shown in Figure 3.6, and all reactions are shown to at least 85% conversion (at least approximately three half-lives). An Eyring analysis of the first order rate constants, k_{obs}, was carried out (Figure 3.7). This gave the activation parameters $\Delta H^{\ddagger}$ = 31.4(1.8) kcal mol^{-1} and $\Delta S^{\ddagger}$ = 5.4(4.8) cal mol^{-1} K^{-1} ($\Delta G_{383}{}^{\ddagger}$ = 29.1(2.6) kcal mol^{-1}). The free energy of activation ($\Delta G^{\ddagger}$) value is consistent with a reaction that requires highly elevated temperatures to proceed. Also, the small entropy ($\Delta S^{\ddagger}$) value is close to zero within error. This is consistent with the proposed mechanism, in which the C–H bond breaks while the ^{t}BuCCH coordinates to the zirconium centre, and it would be expected to maintain the vibrational degrees of freedom of the complex.

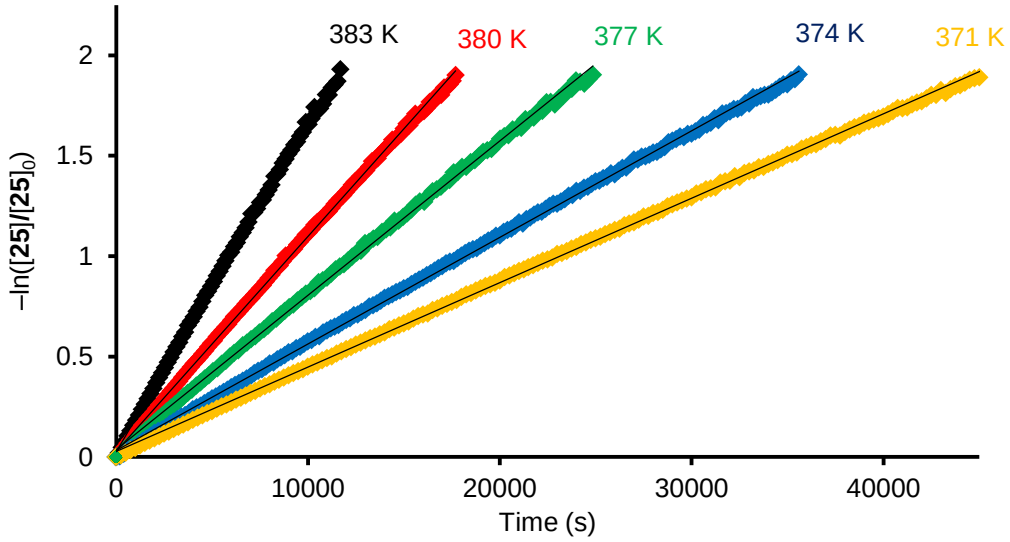

Figure 3.6. First order semi-logarithmic plots for the conversion of $Cp_2Zr\{N\{B(NAr'CH)_2\}C(H)C(^tBu)\}$ (**25**) to $Cp_2Zr\{NHB(NAr'CH)_2\}(CC^tBu)$ (**26**) in toluene-d_8. (avg. r^2 = 0.998, range 0.998 – 0.999).

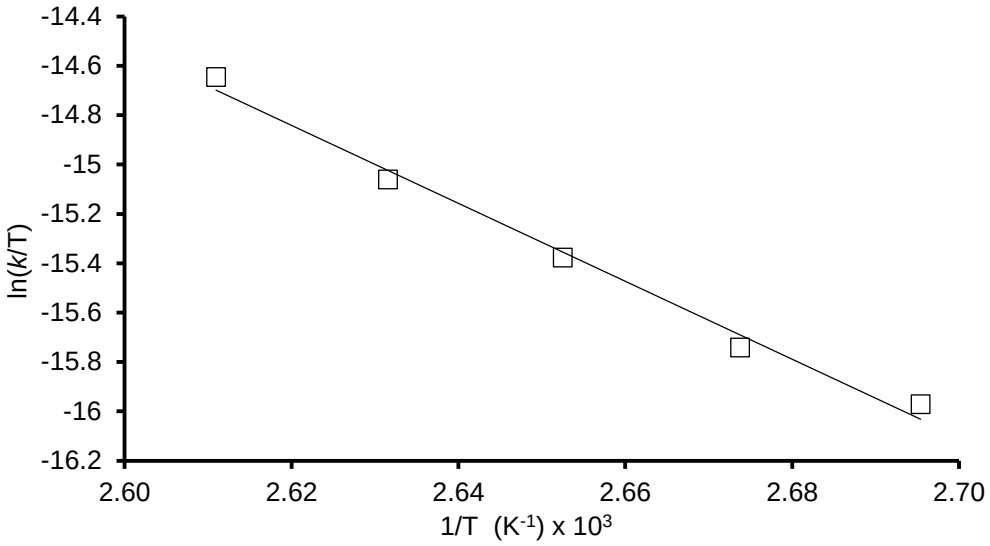

Figure 3.7. Eyring plot for the conversion of $Cp_2Zr\{N\{B(NAr'CH)_2\}C(H)C(^tBu)\}$ (**25**) to $Cp_2Zr\{NHB(NAr'CH)_2\}(CC^tBu)$ (**26**) in toluene-d_8. Activation parameters derived from linear regression analysis (r^2 = 0.990): $\Delta H^{\ddagger}$ = 31.4(1.8) kcal mol^{-1}; $\Delta S^{\ddagger}$ = 5.4(4.8) cal mol^{-1} K^{-1}; $\Delta G_{383}{}^{\ddagger}$ = 29.1(2.6) kcal mol^{-1}.

3.4 Reactions of Group 4 metallocene borylimide complexes with electron deficient terminal aryl alkynes

3.4.1 Reactions of $Cp_2Zr\{NB(NAr'CH)_2\}(py)$ (11) with aryl alkynes

Turning now to the reaction of the aryl alkyne TolCCH with $Cp_2Zr\{NB(NAr'CH)_2\}(py)$ (**11**) in C_6D_6 on the NMR tube scale, only 5% conversion to the azazirconacyclobutene complex $Cp_2Zr\{N\{B(NAr'CH)_2\}C(H)C(Tol)\}$ (**27**) was observed at RT after 16 h, similar to the reaction with ^{t}BuCCH (*vide supra*). Upon heating to 45 – 60 °C, a colour change to deep violet was observed over 16 h, resulting in quantitative conversion to **27** (Scheme 3.4), and further heating at 100 °C for 16 h did not give rearrangement reaction forming the C–H bond activation product. These reaction conditions are reminiscent of those for the reaction with ^{t}BuCCH, suggesting that the RDS in both cases are pyridine dissociation. The half-life ($t_{1/2}$) measured for this reaction at 50 °C of *ca*. 0.9 h is identical to that in the cycloaddition reaction with ^{t}BuCCH (Table 3.4), consistent with this. This was further supported by performing another reaction of **11** with TolCCH in the presence of five equivalents of pyridine at the same reaction conditions. The $t_{1/2}$ was significantly increased to more than 5.0 h (20% conversion). In addition, the reaction of $Cp_2Zr\{NB(NAr'CH)_2\}(THF)$ (**13**) with TolCCH gave immediate formation of **27** at RT,

and in contrast, extremely slow formation of **27** (5% conversion after 5 h) was observed at 50 °C when $Cp_2Zr\{NB(NAr'CH)_2\}(DMAP)$ (**14**) was employed, consistent with the reactions with ^{t}BuCCH.

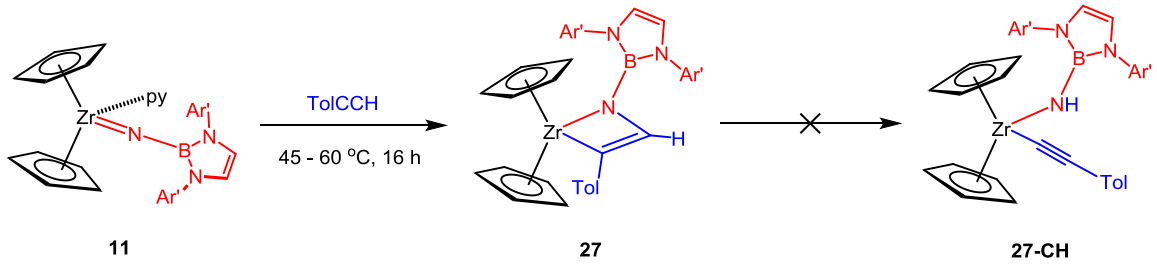

11 **27** **27-CH**

Scheme 3.4. Synthesis of $Cp_2Zr\{N\{B(NAr'CH)_2\}C(H)C(Tol)\}$ (**27**) from $Cp_2Zr\{NB(NAr'CH)_2\}(py)$ (**11**).

The NMR spectra of **27** are analogous to those of **25**, showing an ^{11}B signal at 22.9 ppm. The two ^{1}H doublets *o*- and *m*-C_6H_4Me were observed at 7.10 and 6.80 ppm, as well as a distinctive singlet at 7.33 ppm which is attributed to ZrC=C<u>H</u> of the azazirconacyclobutene unit. An HSQC and an HMBC correlations of this methine proton to the ^{13}C resonance at 108.2 and 173.1 ppm were observed, respectively, which confirm that **27** also exists as a single anti-Markovnikov (1,2-cycloaddition) regioisomer, like **25**.

The lack of any rearrangement of **27** to **27-CH** is in line with the DFT calculation on the small model systems **4Q** and **5Q** discussed in Section 3.2.2. Likewise, the exclusive formation of the 1,2-cycloaddition product is anticipated on both steric and electronic ground. DFT calculation on the full systems **27** and **27-CH** found that the former is favoured by $\Delta G = -6.8$ kcal mol^{-1}, and that $\Delta_r G$ for the formation of **27** from base-free $Cp_2Zr\{NB(NAr'CH)_2\}$ is significantly more exergonic ($\Delta\Delta_r G = -9.1$ kcal mol^{-1}) than for the 1,2-cycloaddition with ^{t}BuCCH (**25**); It is worth mentioning that the corresponding C–H bond activation reaction to form **27-CH** is –3.3 kcal mol^{-1} more favourable than that leading to the C–H bond activation reaction of ^{t}BuCCH (**26**), but this is not thermodynamically competitive with cycloaddition. A test reaction was performed by heating **27** in the presence of one equivalent of PhCCH or Ar^{F}CCH at 90 – 100 °C, no redistribution reaction being observed over 16 h, which indicates the irreversible formation of **27** and its high thermodynamic stability.

Surprisingly, given the favourable $\Delta_r G$ for its formation and thermal stability in solution, **27** was found to be unstable to isolate on the preparative scale, with repeated attempts

resulting in immediate decomposition under vacuum to give borylamine **1.110** and a colour change from deep violet to yellow.

The reaction of **11** with the internal alkyne, PhCCMe, was carried out. On the NMR tube scale, almost no reaction was observed at RT after 16 h. Upon heating to 60 °C, slow formation of $Cp_2Zr\{N\{B(NAr'CH)_2\}C(Me)C(Ph)\}$ (**28**) was observed over 20 h, and the solution colour changed from red-orange to deep turquoise. On the preparative scale, a mixture of **11** and PhCCMe was heated at 60 °C for 20 h in benzene, and **28** was isolated in 44% yield as dark blue crystals (Equation 3.2).

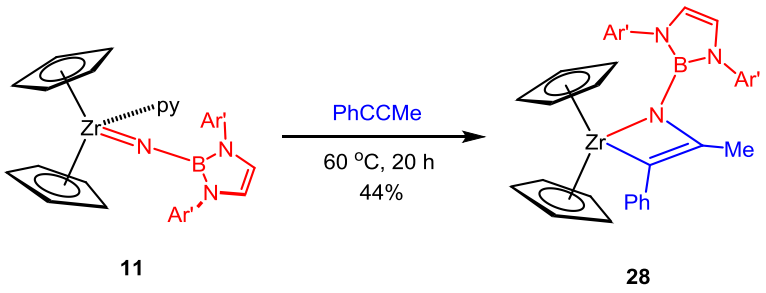

11 **28**

Equation 3.2

The ^{11}B NMR signal of **28** is slightly downfield shifted to 23.4 ppm, compared to those of **27** and **25** which contain terminal alkynes. The ^{1}H resonances corresponding to the alkyne fragment were found at 7.24, 6.97 (Ph) and 1.61 (ZrC=C<u>Me</u>) ppm. These methyl protons display 2- and 3-bond HMBC correlations to the ^{13}C resonances at 119.0 and 172.8 ppm, respectively. In addition, a 3-bond HMBC correlation of the *ortho*-Ph protons to the ^{13}C resonance of Zr–<u>C</u>Ph at 172.8 ppm was also observed. This characteristic downfield shifted signal is comparable to that of the zirconium-bound carbon of **27** at 173.1 ppm, confirming that **28** exists as a single anti-Markovnikov (1,2-cycloaddition) regioisomer, which is expected to be both sterically and electronically (σ- and π-accepting Ph group, and σ-donating Me group) favoured. The DFT computed Δ_rG for the formation of **28** from **11** at 298 K is –7.8 kcal mol^{-1}, less exergonic than for the corresponding cycloaddition with TolCCH (Δ_rG = –19.5 kcal mol^{-1}) or ^{t}BuCCH (Δ_rG = –10.4 kcal mol^{-1}), as expected from the steric and electronic factors outlined in Section 3.2.2 (Table 3.2).

Diffraction-quality crystals of **28** were grown from a hexane solution at 4 °C. The solid state structure is shown in Figure 3.8, and selected bond distances and angles are listed in Table 3.5. Molecules of compound **28** possess a pseudo tetrahedral environment, with

staggered cyclopentadienyl rings, and the four-membered azazirconacyclobutene ring is confirmed to be the anti-Markovnikov (1,2-cycloaddition) regioisomer. The N(1)–Zr(1)–C(29) bite angle of 66.50(9)° is comparable within error to that in $Cp_2Zr\{N(Xyl)C(Ph)C(Ph)\}$ (**3.2**) of 66.33(12)°,[1] and slightly more acute than that in **25** which may reflect a slightly less sterically encumbered azazirconacyclobutene unit. In contrast, the significantly more acute Zr(1)–N(1)–B(1) angle of 142.33(19)° (*cf.* 152.26(8)° (**25**)) may reflect the higher steric repulsion between the Me and boryl moieties. The N(1)–C(28) distance of 1.422(3) Å is shorter within error than that in **25** of 1.4393(16) Å, but comparable to 1.426(5) Å in **3.2**. This arises from the π-accepting nature of the phenyl group as discussed above (Section 3.2.1), which is also reflected by the longer Zr(1)–N(1) bond length (2.142(2) Å) of **28**, compared to that in **25** (2.1110(10) Å). This is the result of the Zr(1)–N(1) bond order decreasing due to less π-donation from N(1) to the Zr–Cp LUMO π* antibonding orbital, thus also resulting in marginally shorter $Zr–Cp_{cent}$ distances. In addition, the sum of angles subtended at C(29), C(28) and N(1) are 357.8(4), 359.6(5) and 359.1(3)°, respectively, indicating they are all formally sp^2-hybridised.

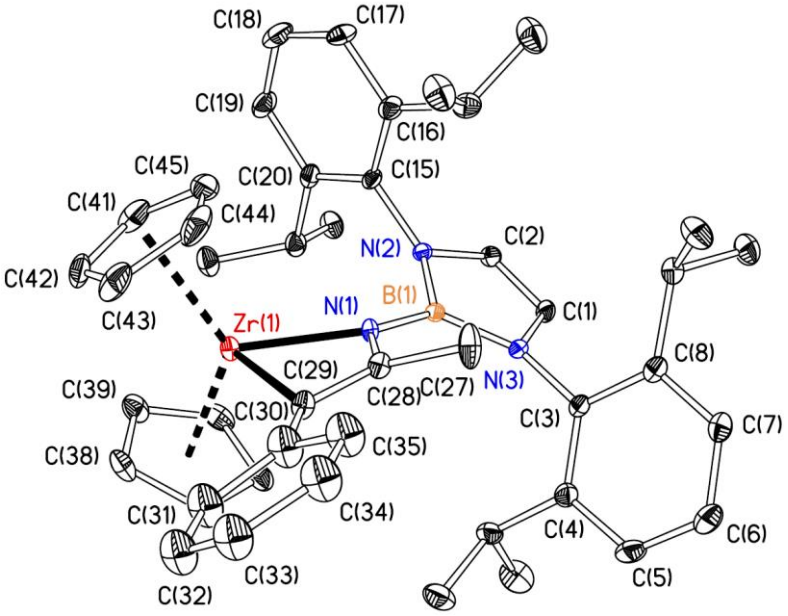

Figure 3.8. Displacement ellipsoid plot (20% probability) of $Cp_2Zr\{N\{B(NAr'CH)_2\}C(Me)C(Ph)\}$ (**28**). H atoms omitted for clarity.

Table 3.5. Selected bond lengths (Å) and angles (°) for $Cp_2Zr\{N\{B(NAr'CH)_2\}C(Me)C(Ph)\}$ (**28**). $Cp_{cent(1)}$ and $Cp_{cent(2)}$ refer to the computed Cp ring centroids for "upper" and "lower" Cp rings, respectively, as depicted in Figure 3.8.

Zr(1)–N(1)	2.142(2)	$Cp_{cent(1)}$–Zr(1)–$Cp_{cent(2)}$	127.9
Zr(1)–C(29)	2.188(3)	N(1)–Zr(1)–C(29)	66.50(9)
Zr(1)–$Cp_{cent(1)}$	2.230	Zr(1)–N(1)–B(1)	142.33(19)
Zr(1)–$Cp_{cent(2)}$	2.234	Zr(1)–C(29)–C(28)	87.50(18)
N(1)–B(1)	1.428(4)	N(1)–C(28)–C(29)	117.0(2)
B(1)–N(2)	1.463(4)		
B(1)–N(3)	1.464(4)		
N(1)–C(28)	1.422(3)		
C(28)–C(29)	1.362(4)		

Next, moving to the reaction of **11** with the more electron deficient terminal alkyne, $Ar^{CF_3}CCH$ (Ar^{CF_3} = 3,5-$C_6H_3(CF_3)_2$), slow formation of two species **29** and **30** was observed on the NMR tube scale at RT. Almost quantitative consumption of **11** was

achieved after 14 days ($t_{1/2}$ = 65 h, Table 3.4), with the colour of the solution changing from red-orange to deep brown. These two species are in a *ca*. 3:2 ratio, and the NMR spectra (*vide infra*) indicate that the major product is $Cp_2Zr\{N\{B(NAr'CH)_2\}C(H)CAr^{CF_3}\}$ (**29**) formed *via* [2+2] 1,2-cycloaddition and the minor one is $Cp_2Zr\{NHB(NAr'CH)_2\}(CCAr^{CF_3})$ (**30**) formed *via* C–H bond activation. It was found that when the reaction of **11** with $Ar^{CF_3}CCH$ was performed at 60 °C in C_6D_6, there was a much greater preference for generating **29** with the **29**:**30** ratio being increased to 9:1.

On the preparative scale, the synthesis of the thermodynamic product **29** was achieved by heating the mixture of **11** and $Ar^{CF_3}CCH$ at 60 °C for 16 h in benzene, with the colour of the solution changing to deep violet from red-orange. Compound **29** was isolated in 59% yield as dark purple crystals (Equation 3.3). Unfortunately, attempts to isolate the acetylide **30** were unsuccessful, due to its relatively high solubility in hydrocarbon solvents and the long reaction time required for its selective formation at low temperature.

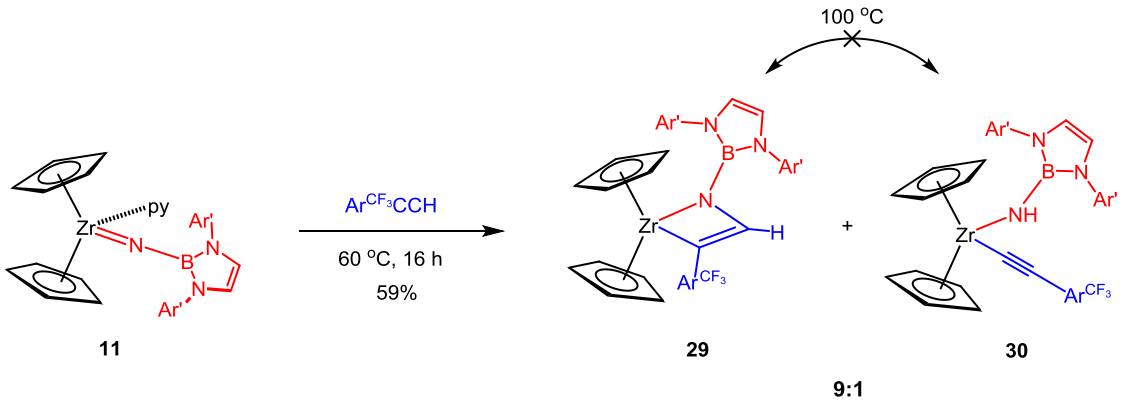

Equation 3.3

The ^1H and ^{13}C NMR spectra of isolated **29** are consistent with this being a single isomer of an azazirconacyclobutene complex with anti-Markovnikov regiochemistry, as described previously for the analogues **25** and **27**. The ^{11}B signal of **29** of 22.7 ppm is comparable with those found in **25** and **27**. The metallacycle methine singlet is observed at 7.39 ppm, with an HSQC correlation to a ^{13}C signal at 115.4 ppm, and an HMBC correlation to a ^{13}C signal at 165.0 ppm which is slightly upfield shifted, compared to that in **25**, **27** and **28**. In the ^{11}B NMR spectrum of the mixture of **29** and **30**, a broad resonance was observed between 24.6 – 22.7 ppm, of which the higher end of this δ range

is attributed to **30**, comparable with that in **26** and other borylamido zirconocene complexes in Chapter Two and Four. The ^{1}H NMR spectrum of **30** displays a diagnostic broad NH signal at 6.03 ppm, and this has no COSY or HMBC correlations. In the ^{13}C NMR spectrum, the two acetylide functional group carbons are assigned at 139.4 and 122.9 ppm which are comparable with those in **25**, corresponding to the carbon directly bonded to Zr, and the one adjacent to the Ar^{CF_3} ring, respectively.

Diffraction-quality crystals of **29** were grown from a hexane solution at 4 °C. The solid state structure is shown in Figure 3.9, and selected bond distances and angles are listed in Table 3.6. Molecules of compound **29** show a comparable structure to the analogues **25** and **28,** possessing a pseudo tetrahedral environment, with eclipsed cyclopentadienyl rings, and the four-membered azazirconacyclobutene ring of Zr(1) is confirmed to be the anti-Markovnikov (1,2-cycloaddition) regioisomer. The short Zr(1)–N(1) and N(1)–C(27) bond lengths of 2.143(2) and 1.407(4) Å, respectively, are comparable with those in **28**, showing the π-donation from the lone pair located at N(1) to the π* antibonding MO of C(27)–C(28), consistent with the computational studies described earlier. The small bite angle of N(1)–Zr(1)–C(28) (67.99(10)°) and wide angle of Zr(1)–N(1)–B(1) (153.4(2)°), are comparable with those in **25** and **28** respectively, reflecting negligible steric contribution of the CF_3 substituents at the two *meta*-positions.

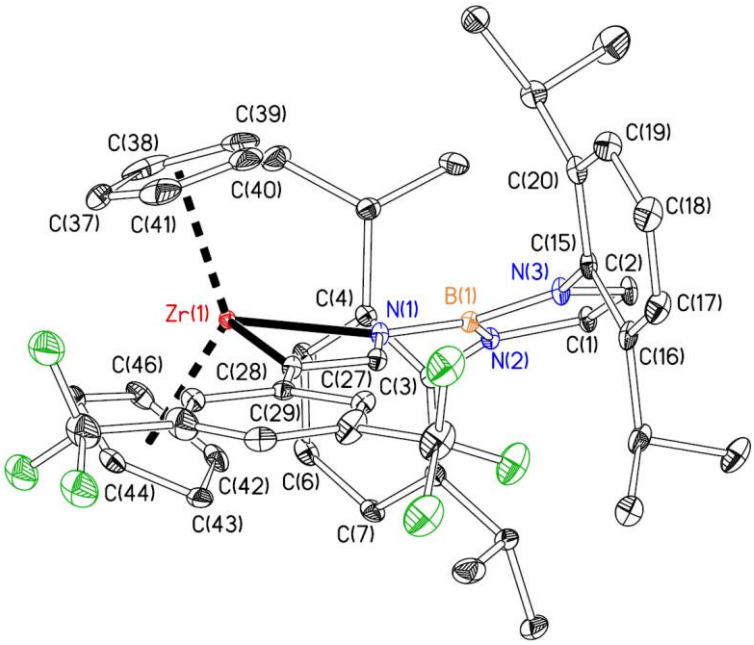

Figure 3.9. Displacement ellipsoid plot (20% probability) of $Cp_2Zr\{N\{B(NAr'CH)_2\}C(H)CAr^{CF_3}\}$ (**29**). H atoms omitted for clarity.

Table 3.6. Selected bond lengths (Å) and angles (°) for $Cp_2Zr\{N\{B(NAr'CH)_2\}C(H)CAr^{CF_3}\}$ (**29**). $Cp_{cent(1)}$ and $Cp_{cent(2)}$ refer to the computed Cp ring centroids for "upper" and "lower" Cp rings, respectively, as depicted in Figure 3.9.

Zr(1)–N(1)	2.143(2)	$Cp_{cent(1)}$–Zr(1)–$Cp_{cent(2)}$	130.1
Zr(1)–C(28)	2.180(3)	N(1)–Zr(1)–C(28)	67.99(10)
Zr(1)–$Cp_{cent(1)}$	2.226	Zr(1)–N(1)–B(1)	153.4(2)
Zr(1)–$Cp_{cent(2)}$	2.231	Zr(1)–C(28)–C(27)	85.00(18)
N(1)–B(1)	1.430(4)	N(1)–C(27)–C(28)	121.4(3)
B(1)–N(2)	1.445(4)		
B(1)–N(3)	1.448(4)		
N(1)–C(27)	1.407(4)		
C(27)–C(28)	1.365(4)		

Unlike the C–H bond activation of ^{t}BuCCH by **11** *via* the rearrangement of the [2+2] cycloaddition intermediate (**25**) requiring high temperature (90 – 110 °C), the C–H bond activation of $Ar^{CF_3}CCH$ by **11** forming **30** is more favoured at lower temperature (i.e. RT), and the [2+2] cycloaddition forming **29** is more favoured at high temperature (60 °C). In addition, both complexes **29** and **30** are found to be thermodynamically stable, tested by heating the mixture of these two complexes at 100 °C in C_6D_6 for 16 h, giving no change in the ratio of these two complexes. This is consistent with the higher stability of the acetylide and metallacycle complexes when the more electron-accepting aryl group is employed. As expected, DFT calculations on the full systems **29** and **30** found a strong thermodynamic preference (ΔG) of –9.2 kcal mol^{-1} in favour of the cycloaddition product. The free energies of formation (ΔG) for **29** and **30** from base-free $Cp_2Zr\{NB(NAr'CH)_2\}$ were –38.8 and –29.6 kcal mol^{-1}, respectively, consistent with their irreversible formation. Therefore, these DFT and experimental results show that complexes **29** or **30** are not intermediates for the formation of each other since both are thermodynamically stable, and their relative extents of formations are completely kinetically controlled.

When the THF adduct $Cp_2Zr\{NB(NAr'CH)_2\}(THF)$ (**13**) was reacted with $Ar^{CF_3}CCH$, immediate consumption of **13** was observed at RT, forming **29** and **30** in a *ca*. 95:5 ratio. The rapid formation of the major product **29** suggests that the [2+2] cycloaddition with

$Ar^{CF_3}CCH$ also proceeds *via* a base-free intermediate $Cp_2Zr\{NB(NAr'CH)_2\}$ and pyridine dissociation is the RDS, this being consistent with the observation in the [2+2] cycloaddition reactions with ^tBuCCH and TolCCH (*vide supra*). In contrast, when $Cp_2Zr\{NB(NAr'CH)_2\}$(DMAP) (**14**) was employed, exclusive formation of the C–H bond activation product **30** was observed with $t_{1/2}$ of 40 h (Table 3.4). These observations reflect that the C–H bond activation of the electron deficient alkyne, $Ar^{CF_3}CCH$, may undergo a different mechanism (with regard to Lewis base dissociation) to the cycloaddition, and Lewis base dissociation may not be involved in this mechanism. This is also in line with the variable reaction outcomes at high or low temperatures; the favourable [2+2] cycloaddition forming **29** at high temperature is facilitated by entropic factors (RDS *via* dissociative pathway), and the favourable C–H bond activation forming **30** at low temperature may reflect that its RDS is potentially associative.

The cycloaddition with acetylene and the C–H bond activation with PhCCH by the titanium imido compound $Cp^*_2Ti(NPh)$ (**2.11**) were previously reported by Bergman *et al*. They reported that the preference for the C–H bond activation is possibly steric in origin as the metallacyclic product with PhCCH would be very sterically congested.[23] However, this is unlikely to be the case for the reactions of **11** with TolCCH and $Ar^{CF_3}CCH$, as no significant steric contribution from the CF_3 substituents at the *meta*-positions would be expected, and no difference should be expected for the reactions of $Ar^{CF_3}CCH$ with **11**, **13** and **14**. In addition, DFT shows a very strong thermodynamic preference for **29**, which would not be the case for a crowded system. In contrast, Bercaw *et al.* found that C–H bond activation by a tantalum imido compound is more favoured when a more acidic alkyne, PhCCH (compared to propyne), was employed, although, no detailed mechanistic study was given. Similar observations have been reported in our research group on the reactions of the titanium borylimido complex $Ti(N_2^{iPr}N^{Me})\{NB(NAr'CH)_2\}$(py) (**1.115**) with TolCCH and Ar^FCCH. It was found that the reaction with TolCCH gave the [2+2] cycloaddition product solely, while the reaction with more acidic Ar^FCCH ($Ar^F = C_6F_5$) gave exclusively C–H bond activation as the first formed (kinetic) product.[20] Thus, the reaction of **11** with the more electron deficient alkyne (more acidic), Ar^FCCH, was performed to see whether more C–H bond activation would kinetically facilitated, even though it is already clear from the DFT calculations that [2+2] cycloaddition is strongly favoured thermodynamically.

When **11** was reacted with Ar^FCCH at RT in C_6D_6 on the NMR tube scale, C–H bond activation was found to be much faster, giving $Cp_2Zr\{NHB(NAr'CH)_2\}(CCAr^F)$ (**31**) as the major product and the minor product $Cp_2Zr\{N\{B(NAr'CH)_2\}C(H)C(Ar^F)\}$ (**32**) *via* [2+2] cycloaddition after 21 h, in a *ca* 9:1 ratio, with the colour of the solution changing from red-orange to pale yellow. Inspired by the favourable formation of **29** at higher temperature, the reaction of **11** with Ar^FCCH in C_6D_6 was also performed at 90 °C. The cycloaddition product **32** was rapidly formed in 1 h and switched to be the major product in a *ca*. 4:1 ratio to **31**, with the colour of the solution changing to deep violet. On the preparative scale, Ar^FCCH was reacted with **11** at RT in benzene solution, and left to stir at RT for 21 h. Product **31** was almost exclusively formed and isolated in 43% yield as pale yellow crystals. In contrast, the reaction of **11** with Ar^FCCH in toluene solution was also heated at 90 °C for 1 h, giving a mixture of **31** and **32** in a *ca*. 2:3 ratio, and **32** was isolated in 39% yield as deep purple crystals (Scheme 3.5). The NMR spectra of **31** and **32** are very similar to those of the homologues **30** and **29**, with ^{11}B signals at 24.7 and 23.0 ppm, respectively. The ^1H NMR spectrum of **31** displays a diagnostic NH resonance at 6.17 ppm as a broad singlet. In contrast, compound **32** shows a sharp singlet for ZrC=C<u>H</u> at 7.69 ppm, with an HSQC and an HMBC correlation to the ^{13}C signals at 120.3 and 146.9 ppm, respectively, in which the latter chemical shift is more upfield shifted than those in other analogues described above. This is again consistent with this metallacycle being a single isomer with anti-Markovnikov (1,2-cycloaddition) regiochemistry, which is both sterically and electronically favoured (*vide supra*). In addition, a band at 2099 cm^{-1} corresponding to ν(C≡C) in the IR spectrum (Nujol mull) of **31** was observed, slightly higher than that in homologous **26** of 2081 cm^{-1}, as found for the respective free alkynes RCCH (R = ^{t}Bu or C_6F_5).

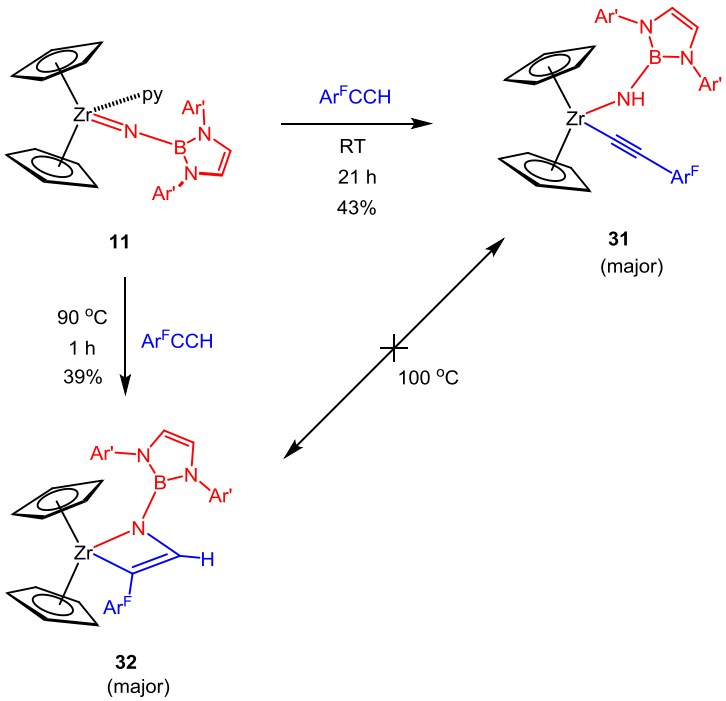

Scheme 3.5. Synthesis of $Cp_2Zr\{NHB(NAr'CH)_2\}(CCAr^F)$ (**31**) and $Cp_2Zr\{N\{B(NAr'CH)_2\}C(H)C(Ar^F)\}$ (**32**) from $Cp_2Zr\{NB(NAr'CH)_2\}(py)$ (**11**).

Diffraction-quality crystals of **31** and **32** were grown from hexane solutions at 4 °C. The solid state structures are shown in Figure 3.10, and selected bond distances and angles are listed in Table 3.7. The metallacylic complex **32** has an analogous structure to those of **25**, **28** and **29**, possessing a pseudo tetrahedral environment, with staggered cyclopentadienyl rings, and the solid state structure confirms that it is the anti-Markovnikov (1,2-cycloaddition) regioisomer. The N(1)–C(27), Zr(1)–N(1) and Zr(1)–C(28) bond distances are all comparable to those in the analogue **29**, and the small N(1)–Zr(1)–C(28) angle of 67.25(4)° and wide Zr(1)–N(1)–B(1) angle of 149.54(8)° may reflect that the substituted F atoms on the aryl ring have very little steric contribution, like that in **29**. In addition, the short N(1)–C(27) bond length of 1.4050(14) Å (*c.f.* **26**) indicates the electron-accepting nature of the aryl ring, consistent with those in **28** and **29**.

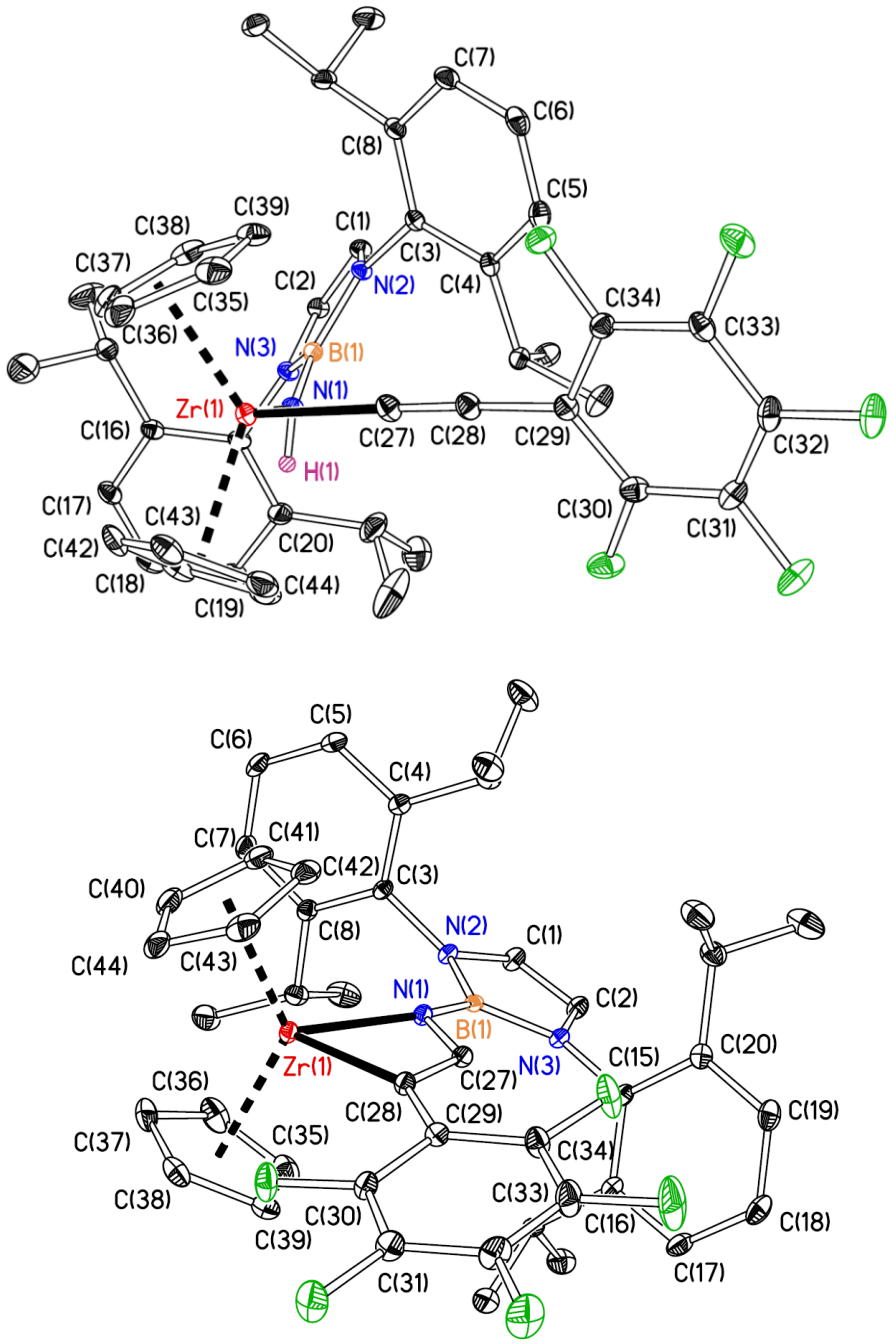

Figure 3.10. Displacement ellipsoid plots (20% probability) of $Cp_2Zr\{NHB(NAr'CH)_2\}(CCAr^F)$ (**31**, top) and $Cp_2Zr\{N\{B(NAr'CH)_2\}C(H)C(Ar^F)\}$ (**32**, bottom). C–bound H atoms omitted for clarity.

Table 3.7. Selected bond lengths (Å) and angles (°) for $Cp_2Zr\{NHB(NAr'CH)_2\}(CCAr^F)$ (**31**) and $Cp_2Zr\{N\{B(NAr'CH)_2\}C(H)C(Ar^F)\}$ (**32**). $Cp_{cent(1)}$ and $Cp_{cent(2)}$ refer to the computed Cp ring centroids for "upper" and "lower" Cp rings, respectively, as depicted in Figure 3.10.

	31	**32**
Zr(1)–N(1)	2.0855(16)	2.1481(9)
$Zr(1)–C_{ac}(1)^a$	2.260(2)	2.1868(12)
$Zr(1)–Cp_{cent(1)}$	2.21	2.22
$Zr(1)–Cp_{cent(2)}$	2.22	2.22
N(1)–B(1)	1.435(3)	1.4336(16)
B(1)–N(2)	1.450(2)	1.4510(15)
B(1)–N(3)	1.448(2)	1.4482(15)
N(1)–C(27)	-	1.4050(14)
C(27)–C(28)	1.213(3)	1.3695(16)
$Cp_{cent(1)}–Zr(1)–Cp_{cent(2)}$	131.3	130.1
$N(1)–Zr(1)–Cp_{cent(1)}$	108.7	114.8
$N(1)–Zr(1)–Cp_{cent(2)}$	106.3	111.0
Zr(1)–N(1)–B(1)	146.43(13)	149.54(8)
$Zr(1)–C_{ac}(1)–C_{ac}(2)^{a,b}$	178.54(17)	86.09(7)
N(1)–C(27)–C(28)	-	119.83(10)
$N(1)–Zr(1)–C_{ac}(1)^a$	102.34(7)	67.25(4)

a. "$C_{ac}(1)$" = C(27) **31**, C(28) **32**. *b*. "$C_{ac}(2)$" = C(28) **31**, C(27) **32**.

The borylamide-acetylide complex **31** also possesses a pseudo tetrahedral environment, with staggered cyclopentadienyl rings. The Zr(1)–N(1)–B(1) linkage of **31** contains the Zr(1)–N(1) bond length of 2.0855(16) Å and the Zr(1)–N(1)–B(1) angle of 149.54(8)°, comparable with those in other borylamido zirconocene complexes in Chapter Two and Four. In addition, the Zr(1)–C(27) bond length of 2.260(2) Å is similar to the values found in previously reported bis(acetylide) zirconocene complexes (2.23 – 2.29 Å).[54–58]

The C≡C bond distance of 1.213(3) Å is comparable to that of the borylamide-acetylide titanium complex, of the type $Ti(N_2N^{py})\{NHB(NAr'CH)_2\}(CCAr^F)$, of 1.2143(15) Å,[20] consistent with a full triple bond.

Upon heating solutions of either **31** or **32** in C_6D_6 at 100 °C for 16 h, no further reaction was observed showing that these compounds are thermodynamically stable as expected because of the strong electron-accepting nature of Ar^F. DFT calculation on the full experimental systems found that **32** was more stable by $\Delta G = -5.2$ kcal mol^{-1} compared to **31**, and $\Delta_r G$ for formation of the latter from base-free $Cp_2Zr\{NB(NAr'CH)_2\}$ was –44.4 kcal mol^{-1}, signalling a highly exergonic and irreversible reaction.

The reaction observations are very similar to those with $Ar^{CF_3}CCH$, and the faster C–H bond activation by this more acidic Ar^FCCH prompted us to move attention to the relative kinetic preferences for C–H bond activation *versus* cycloaddition. The reactions between $Cp_2Zr\{NB(NAr'CH)_2\}(L)$ (L = THF (**13**), py (**11**) or DMAP (**14**)) and Ar^FCCH with 0 or 5 equivalents of pyridine were monitored by ^{1}H NMR spectroscopy at RT (25 °C) or 50 °C. The concentration percentage plots of decay or conversion of **11**, **13**, **14**; **31** and **32** *vs* time are shown in Figure 3.11, and the respective $t_{1/2}$ has been measured, shown in Table 3.4. As was found for the cycloaddition reactions with other alkynes (RCCH, R = ^{t}Bu, Tol and Ar^{CF_3}), the rate of formation of the cycloaddition product **32** follows a trend which is the reverse of the Lewis basicity of the donor ligand: complex **13** (a) gave immediate reaction with Ar^FCCH at RT, yielding cycloaddition product **32** as the major product (*ca.* 9:1 ratio *cf.* **31**); complex **14** (b,f) gave no observable formation of **32** at either RT or 50 °C; the reaction of **11** (c) showed very slow formation of **32** as the minor product (*ca*. ratio 1:9 *cf.* **31**), and the addition of 5 equivalents of pyridine (d) slowed down the cycloaddition further giving negligible formation of **32**. In addition, the reaction of **11** at 50 °C (e) promotes the formation of **32**, giving a *ca*. 1:1 ratio to **31**, in line with the observation for the reaction with $Ar^{CF_3}CCH$ at elevated temperature.

To sum up, the above observations imply that the cycloaddition of **11** with Ar^FCCH proceeds through a rate-determining base dissociation step, which is favoured at elevated temperatures. In contrast, the addition of 5 equivalents of pyridine gave no effect on the rate of C–H bond activation forming **31**, with comparable $t_{1/2}$ (11.0 and 12.0 h with and without added pyridine respectively). In addition, the DMAP coordinated **14** gave even slightly faster C–H bond activation compared to that of **11**, with $t_{1/2}$ of 6.1 h. These

observations indicate that the C–H bond activation follows a completely different mechanistic pathway to the cycloaddition.

Intermolecular competition cycloaddition reactions of **13** with an excess of both TolCCH and RCCH (R = ^{t}Bu, Ar^{CF_3}CCH or Ar^{F}CCH) (1:5:5) were carried out on the NMR tube scale. All the reactions finished immediately at RT, and the relative ratios of the corresponding cycloaddition product (**25**, **29** and **32**) against **27** were calculated to be 1:2, 1:4 and 1:3 where 14% C–H bond activation product **31** was also observed in the reaction with Ar^{F}CCH/TolCCH (1:5:5). Since all the cycloaddition products are thermodynamically stable giving no interconversion (also the case for **25** at RT), these relative ratios indicate the relative rate (Tol > ^{t}Bu > Ar^{F} > Ar^{CF_3}) of [2+2] cycloaddition between the base free intermediate $Cp_2Zr\{NB(NAr'CH)_2\}$ and corresponding alkynes (kinetically controlled), which reflect the relative activation barriers. These results suggest a π-adduct intermediate, which is less favoured for electron-deficient ArCCH (R = Ar^{F} or Ar^{CF_3}). It may also be a combination result with the steric effect, as the cycloaddition with TolCCH is slightly faster than that with ^{t}BuCCH.

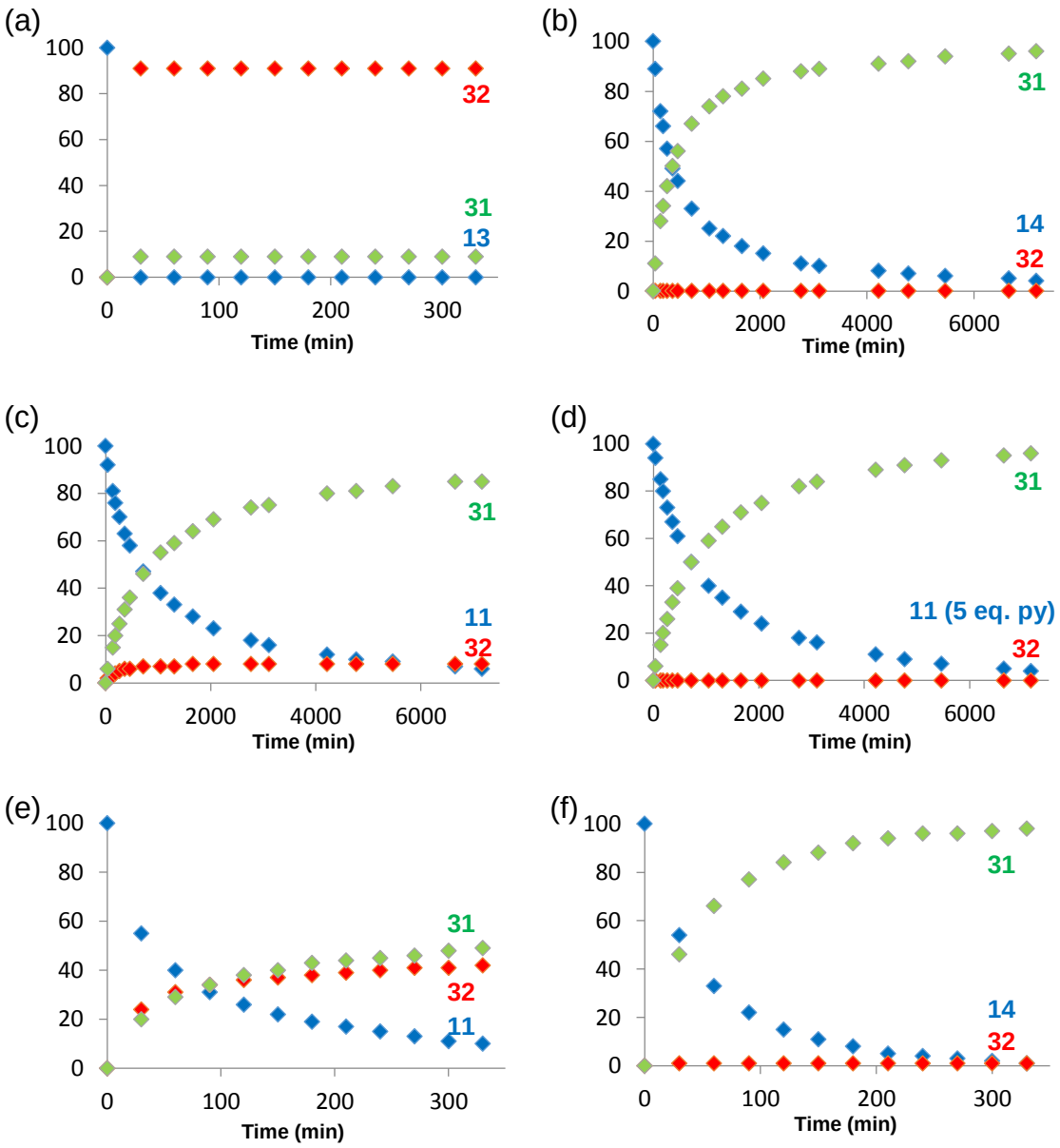

Figure 3.11. (a) – (d): concentration percentage of decay of $Cp_2Zr\{NB(NAr'CH)_2\}(L)$ (L = THF (**13**), py (**11**) or DMAP (**14**), blue), growth of $Cp_2Zr\{NHB(NAr'CH)_2\}(CCAr^F)$ (**31**, green) and $Cp_2Zr\{N\{B(NAr'CH)_2\}C(H)C(Ar^F)\}$ (**32**, red) at RT (25 °C) in C_6D_6 with 0 or 5 equivalent pyridine; (e) – (f): concentration percentage of decay of $Cp_2Zr(NB(NAr'CH)_2\}(L)$ (L = py (**11**) or DMAP (**14**), blue), growth of $Cp_2Zr\{NHB(NAr'CH)_2\}(CCAr^F)$ (**31**, green) and $Cp_2Zr\{N\{B(NAr'CH)_2\}C(H)C(Ar^F)\}$ (**32**, red) at 50 °C in C_6D_6.

Since these π-loaded zirconocene borylimido complexes (**11**, **13**, **14**) are coordinatively saturated and can be considered to have a 20 valence electron count, the direct alkyne pre-coordination (RDS), without dissociating the corresponding Lewis base, is very unlikely to occur. Therefore, it is of interest to see whether the more feasible η^5-η^3 ring slippage (*cf.* Cp ligands), by employing indenyl ligands, can contribute the C–H bond activation reaction without dissociating base. In addition, Mountford *et al.* reported a Cp exchange reaction between the imido complex $Cp^{ipr}Mo(N^tBu)(C_2H_4)Cl$ (Cp^{ipr} = $C_5H_4{}^iPr$) and NaCp, yielding $Cp_2Mo(N^tBu)$.[59] Cp dissociation could be a possible reaction pathway (RDS) for the C–H bond activation reaction of **11** with RCCH (R = Ar^F or Ar^{CF_3}). However, it was found that the isolated and structurally authenticated $Ind_2Zr\{NB(NAr'CH)_2\}(L)$ (L = THF (**22**), py (**23**) or DMAP (**24**)) complexes show η^5-indenyl ligands with only a small degree of distortion (Chapter Two). Hence, these indicate that these strongly coordinated Cp ligands are very unlikely to undergo dissociation pathway at RT.

The reactions of $Ind_2Zr\{NB(NAr'CH)_2\}(L)$ (L = THF (**22**), py (**23**) or DMAP (**24**)) with Ar^FCCH were nonetheless carried out. On the NMR tube scale, both of the cycloaddition and the C–H bond activation reactions were found to be much slower than those of the Cp analogues **11**, **13** and **14**, where the quantitative consumption of **22** required several hours at RT, and the reaction of **23** needed higher temperature (80 °C) for 16 h, possibly due to higher kinetic barriers induced by the more bulky indenyl ligands or the less reactive borylimido ligand as discussed in Chapter Two (Section 2.7). In agreement with the DFT calculations in the model systems, Δ_rG for the formation of the C–H bond activation product $Ind_2Zr\{NH\{B(NAr'CH)_2\}(CCAr^F)$ (**34**) and cycloaddition product $Ind_2Zr\{N\{B(NAr'CH)_2\}C(H)C(Ar^F)\}$ (**33**) from the base-free intermediate $Ind_2Zr\{NB(NAr'CH)_2\}$ was *ca.* 4 kcal mol^{-1} less exergonic than for the bis(cyclopentadienyl) counterparts. Experimentally, both reactions give a mixture of cycloaddition and **33** and **34** in a *ca.* 7:3 ratio after 16 h at corresponding temperatures. The reaction of **24** gave no reaction at RT, and upon heating to 80 °C, very slow formation of **34** (major) and **33** (minor) were observed with a high amount of the decomposition product borylamine **1.110**. On the preparative scale, **22** was reacted with Ar^FCCH at RT for 16 h accompanied by a colour change from yellow to deep violet. Product **33** was isolated in 36% yield as dark purple crystals (Equation 3.4). Unfortunately, the minor product **34** was unable to be isolated due to its low yield in the product mixture and high solubility in hydrocarbon solvents. Therefore, complex **34** was

characterised only by NMR spectroscopy. The ^{11}B signals of **33** and **34** at 22.7 and 24.8 ppm are comparable with those in **32** and **31**, respectively. In the ^{1}H NMR spectrum, the diagnostic sharp singlet of ZrC=C<u>H</u> (**32**) at 7.83 ppm, and a broad NH resonance (**31**) at 3.90 ppm were observed. The ^{1}H signal of ZrC=C<u>H</u> (**33**) showing an HSQC and an HMBC correlation to ^{13}C signals at 127.2 and 142.3 ppm, respectively, indicates that it is the anti-Markovnikov (1,2-cycloaddition) regioisomer.

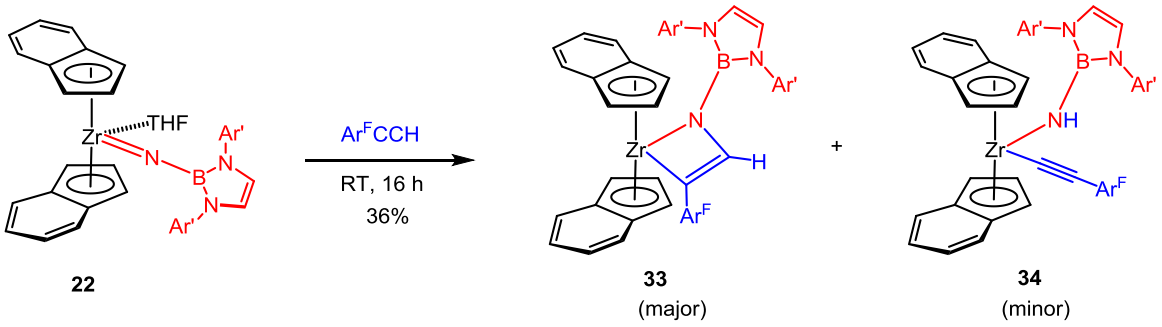

Equation 3.4

Diffraction-quality crystals of **33** were grown from a benzene solution at RT. The solid state structures are shown in Figure 3.12, and selected bond distances and angles are listed in Table 3.8. Compound **33** has a pseudo tetrahedral geometry, in which the indenyl ligands are *gauche* orientated in solid state. The azazirconacyclobutene moiety is comparable with that in **32**. In addition, the comparable N(1)–Zr(1)–C(28) angle of 67.37(6)° and Zr(1)–N(1)–B(1) angle of 147.72(12)° reflect that this azazirconacyclobutene moiety experiences a similar steric environment compared to that in **32**. The values of $\Delta_{Zr-C\text{-}ind}$, HA and FA are all comparable with those of the borylamido analogue $Ind_2Zr\{NHB(NAr'CH)_2\}(Me)$ (**21**), indicating η^5-coordinated indenyl rings.

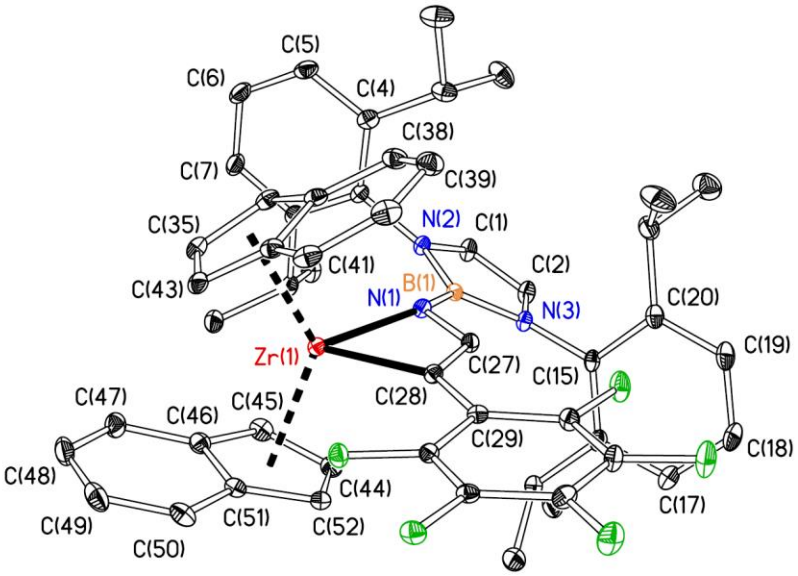

Figure 3.12. Displacement ellipsoid plot (20% probability) of $Ind_2Zr\{N\{B(NAr'CH)_2\}C(H)CAr^F\}$ (**33**). H atoms omitted for clarity.

Table 3.8. Selected bond lengths (Å) and angles (°) for $Ind_2Zr\{N\{B(NAr'CH)_2\}C(H)CAr^F\}$ (**33**). $Ind_{cent(1)}$ and $Ind_{cent(2)}$ refer to the computed centroids for "upper" and "lower" indenyl five-membered rings, respectively, as depicted in Figure 3.12.

Zr(1)–N(1)	2.1441(14)	$Ind_{cent(1)}$–Zr(1)– $Ind_{cent(2)}$	131.4
Zr(1)–C(28)	2.1904(17)	N(1)–Zr(1)–C(28)	67.37(6)
Zr(1)–$Ind_{cent(1)}$	2.24	Zr(1)–N(1)–B(1)	147.72(12)
Zr(1)–$Ind_{cent(2)}$	2.24	Zr(1)–C(28)–C(27)	85.78(11)
N(1)–B(1)	1.429(2)	N(1)–C(27)–C(28)	119.96(15)
B(1)–N(2)	1.451(2)	$HA_{ind(1)}$ [b]	3.92
B(1)–N(3)	1.456(2)	$HA_{ind(2)}$ [b]	3.78
N(1)–C(27)	1.411(2)	$FA_{ind(1)}$ [c]	4.94
C(27)–C(28)	1.365(2)	$FA_{ind(2)}$ [c]	7.10
$\Delta_{Zr-C-ind(1)}$ [a]	0.0702(17)		
$\Delta_{Zr-C-ind(2)}$ [a]	0.1302(18)		

a. slippage parameter, *b*. hinge angle, *c*. fold angle for the "upper" Ind(1) and "lower" Ind(2), respectively, as depicted in Figure 3.12.[60]

3.4.2 Kinetic study of the C–H bond activation reactions of $Cp_2Zr\{NB(NAr'CH)_2\}(L)$ (L = py (11) or DMAP (14)) with Ar^FCCH

A kinetic analysis of the reaction of $Cp_2Zr\{NB(NAr'CH)_2\}(py)$ (**11**) with Ar^FCCH to give $Cp_2Zr\{NHB(NAr'CH)_2\}(CCAr^F)$ (**31**) was carried out in an attempt to gain further in this unusual reaction. The initial rates method was used to extract the rate of the reaction, d[**31**]/d*t* at time = 0, t_0. The reaction of Ar^FCCH with **11** was monitored by ^1H NMR spectroscopy at 298 K, and the formation of the cycloaddition product **32** was negligible under these experimental conditions (< 5%, concentration dependent, *vide infra*). The plot of [**31**] *vs* time gave the non-linear plot in Figure 3.13, and graphical software (*Origin*) was used to fit a curve to all of the data points. Thus, the evolution of product throughout the kinetic study was described (Equation 3.5; 'y_0', 'A_n' and 'B_n' are empirical constants). The curve was then differentiated to obtain an equation for the gradient (Equation 3.6), and the gradient calculated at time = 0 s (Equation 3.7). This gives the calculated initial rate of the reaction, as 9.85(5) × 10^{-6} mol dm^{-3} s^{-1}. The same reaction was carried out with Ar^FCCD and the initial rate of the reaction was measured as 9.83(5) × 10^{-6} mol dm^{-3} s^{-1}, identical to that for the reaction with Ar^FCCH. Thus the KIE of the C–H bond activation is 1.00(1) within error.

Alternatively, the measurement of the competition KIE was carried out by reacting **11** with an excess of both Ar^FCCH and Ar^FCCD (1:5:5) simultaneously on the NMR tube scale. This allowed the KIE to be calculated from the ratio of two isotopologues **31** and **31-*d*$_1$**, by integration of the NH resonance for **31** against the boryl NCH resonances for both **31** and **31-*d*$_1$**. The reaction finished immediately at RT, showing a product mixture of *ca*. 60% **31** and 40% **31-*d*$_1$** (no formation of **32**), which establishes a notable KIE of 1.5.

$$[\text{Products}] = y_0 + \text{A}_1 e^{-t/\text{B}_1} + \text{A}_2 e^{-t/\text{B}_2} \tag{3.5}$$

$$\frac{d[\text{Products}]}{dt} = -\frac{\text{A}_1 e^{-t/\text{B}_1}}{\text{B}_1} - \frac{\text{A}_2 e^{-t/\text{B}_2}}{\text{B}_2} \tag{3.6}$$

$$\left(\frac{d[\text{Products}]}{dt}\right)_{t=0} = -\frac{\text{A}_1}{\text{B}_1} - \frac{\text{A}_2}{\text{B}_2} \tag{3.7}$$

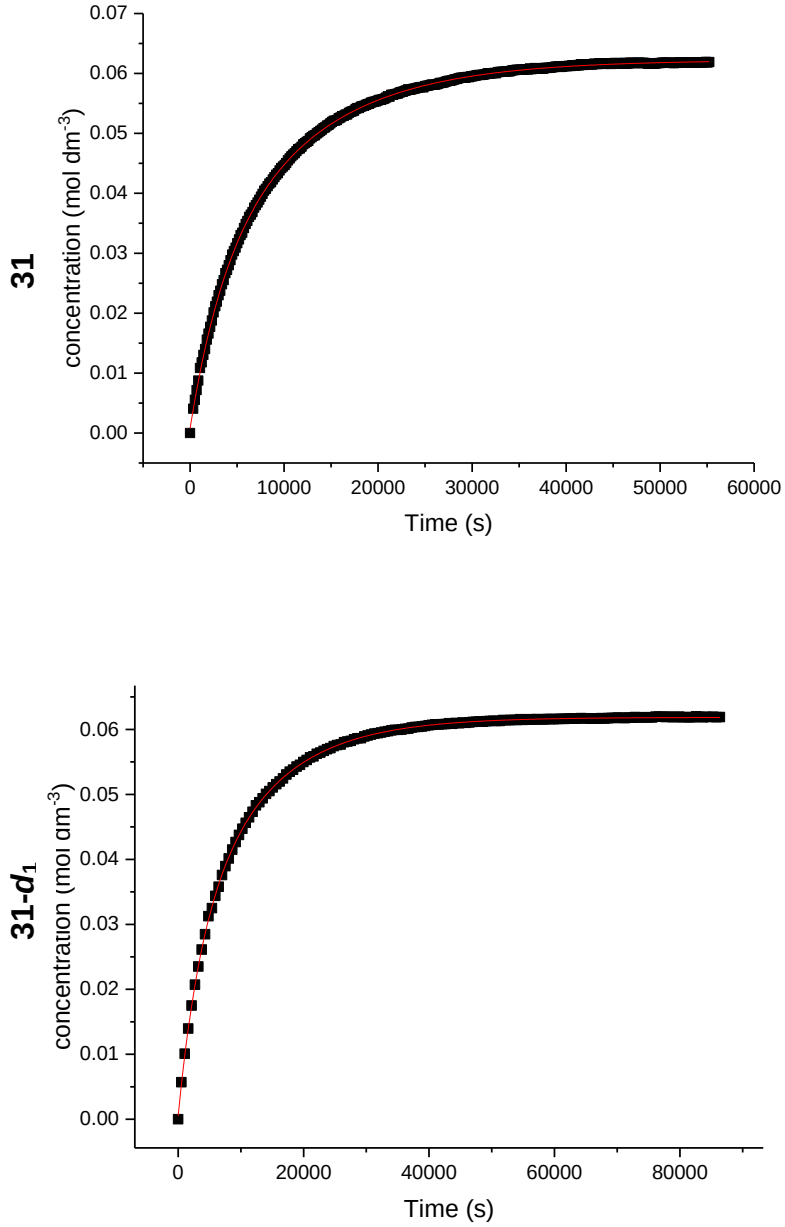

Figure 3.13. Top: plot of $Cp_2Zr\{NHB(NAr'CH)_2\}(CCAr^F)$ (**31**) *vs* time plotted in *Origin*. The best-fit line (r^2 = 0.9999) shown gave A_1 = –0.0210(4), B_1 = 3386(61), A_2 = –0.0405(4), B_2 = 11054(84) giving an initial rate of 9.85(5) × 10^{-6} mol dm^{-3} s^{-1}. Bottom: plot of $Cp_2Zr\{NDB(NAr'CH)_2\}(CCAr^F)$ (**31-d_1**) *vs* time plotted in *Origin*. The best-fit line (r^2 = 0.9999) shown gave A_1 = –0.0225(5), B_1 = 3385(67), A_2 = –0.0388(5), B_2 = 11531(89) giving an initial rate of 9.83(5) × 10^{-6} mol dm^{-3} s^{-1}.

Since the formation of the borylamide-acetylide complex **31** is irreversible (*vide supra*), the KIE of 1.00(1) is believed to show an absence of kinetic isotope effect, rather than an equilibrium isotope effect (EIE) where the multiple equilibria can (in certain circumstances) cancel each other out, or even result in an apparent KIE below 1. Thus, this, as well as the small competition KIE of 1.5, indicates that the C–H bond activation step is not involved in the RDS. Unfortunately, it was found to be potentially problematic for further detailed kinetic studies (e.g. Eyring analysis), as the cycloaddition side reaction appears more significant at low concentration and high temperature. Thus, the DMAP homologue $Cp_2Zr\{NB(NAr'CH)_2\}$(DMAP) (**14**) emerged as an ideal candidate for the later kinetic study with Ar^FCCH, as the cycloaddition side reaction does not occur at all due to the strongly bound DMAP (Table 3.4).

Similar initial rate measurements were performed for the reactions of **14** with Ar^FCCH and Ar^FCCD at 298 K (at lower concentration *cf*. **11**). Identical initial rates of $6.08(7) \times 10^{-6}$ mol dm^{-3} s^{-1} and $6.10(3) \times 10^{-6}$ mol dm^{-3} s^{-1}, respectively, show no kinetic isotope effect (KIE = 1.00(2)). In addition, the competition KIE was found to be 1.5 from the reaction of **14** with an excess of both Ar^FCCH and Ar^FCCD (1:5:5) simultaneously on the NMR tube scale at RT. These values are identical to those from **11**, showing the C–H bond breaking is not involved in the RDS, and there is no effect on KIE by changing the Lewis bases. Bergman described a possible zwitterionic pathway for the C–H bond activation of PhCCH by $Cp^*_2Ti(O)(py)$, in which the titanium-bound oxygen abstracts the weakly acidic alkynyl proton, followed by combination of the resulting ion pair. This zwitterionic pathway was discounted by performing the reaction in THF as a polar solvent, where no rate acceleration was observed, compared to the rate in non-polar benzene or toluene solvent.[36] Therefore, a similar initial rate measurement was also performed for the reaction of **14** with Ar^FCCH in THF-d_8 at 298 K at the same concentration on the NMR tube scale. The calculated initial rate of $5.01(1) \times 10^{-6}$ mol dm^{-3} s^{-1} is effectively identical and slightly smaller than that of the reaction in C_6D_6, hence ruling out the possible zwitterionic pathway.

Next, the reactions between variable equivalents of **14** (1, 2, 2.5, 4 and 5 equivalents) and Ar^FCCH (5 equivalents) were followed at 298 K in C_6D_6, and the corresponding initial rates of **31** formation were calculated by using the method above. The calculated initial rates are found to vary linearly over the range of **14** used, showing the first order dependence on [**14**] (Figure 3.14, bottom). This is consistent with the well-behaved linear

pseudo first order semi-logarithmic plot (at least approximately three half-lives) for the reaction of **14** with Ar^FCCH (10 equivalents) in C_6D_6 at 298 K (Figure 3.15), where the reaction rate constant, k_{obs}, can be extrapolated as 2.81(2) × 10^{-3} dm^3 mol^{-1} s^{-1}.

The reactions between **14** (1 equivalent) and variable amounts of Ar^FCCH (1, 3, 5, 7 and 10 equivalents) were also similarly performed at 298 K in C_6D_6, the calculated corresponding initial rates also show a linear relationship over the range of Ar^FCCH used, also indicating the first order dependence on [Ar^FCCH] (Figure 3.14, top). This is different to the reactions proceeding through a base dissociation pathway, where the onset of saturation kinetics is very evident at high alkyne concentration.[19,61] Therefore, these observations clearly imply that **14** and Ar^FCCH are both involved in the RDS (not *via* base dissociation). According to the absence of KIE, the reaction pathway is likely to be the Ar^FCCH pre-coordination (RDS), followed by non-rate-determining C–H bond breaking. As the experiments above indicate that the rate of the C–H bond activation has zero dependence on the concentration of the Lewis bases (*vide supra*), then the rate equation can be expressed (Equation 3.8). Therefore, the corresponding rate constant (k_{obs}) of the reactions of **11** or **14** with Ar^FCCH was calculated, to be 1.28(1) × 10^{-3} dm^3 mol^{-1} s^{-1} and 3.08(1) × 10^{-3} dm^3 mol^{-1} s^{-1} (the latter being comparable to the k_{obs} measured from the pseudo first order semi-logarithmic plot, *viz*. 2.81(2) × 10^{-3} dm^3 mol^{-1} s^{-1}), respectively, at 298 K, assuming that the reaction of **11** follows the same rate equation. This shows approximately 2.5 times faster C–H bond activation reaction of **14**, consistent with the measured $t_{1/2}$ in Table 3.4.

$$\frac{d[\mathbf{31}]}{dt} = k[\mathbf{14}][\mathrm{Ar^FCCH}] \qquad (3.8)$$

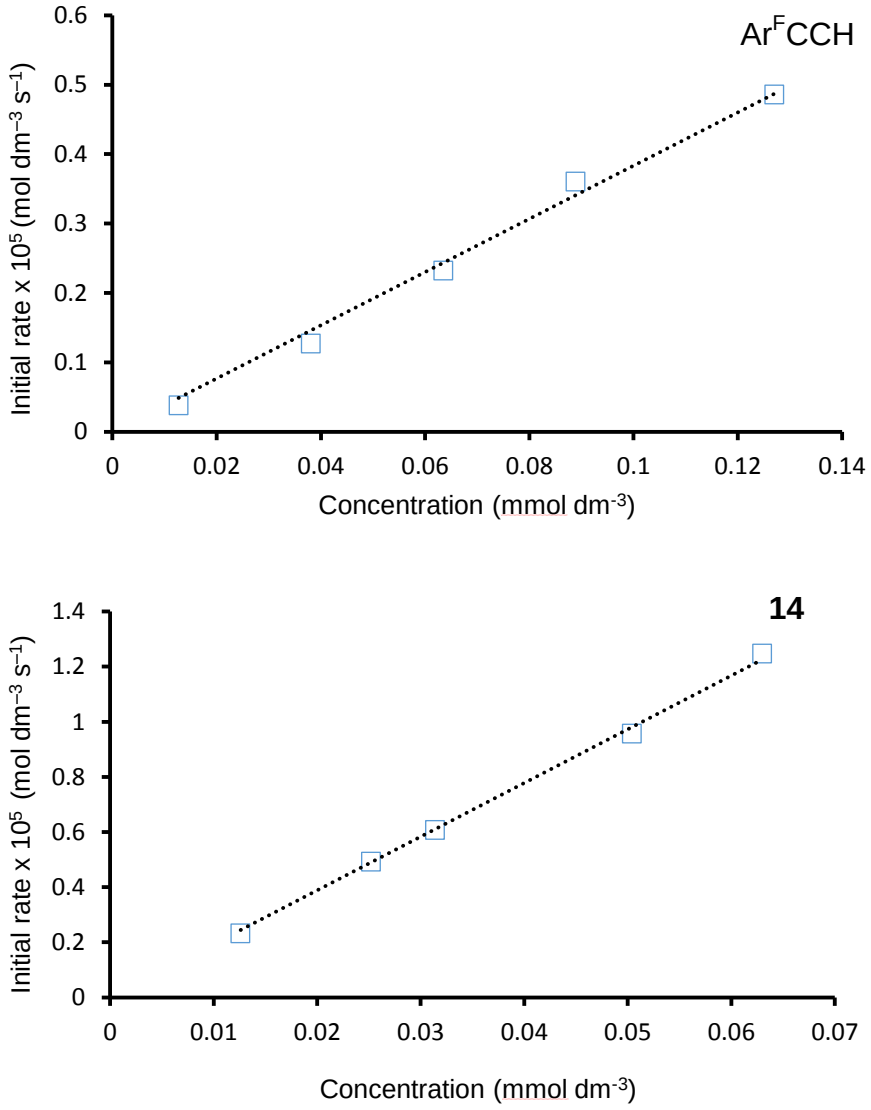

Figure 3.14. Top: plot of initial rate *vs* equivalents of alkynes for the reaction of $Cp_2Zr\{NB(NAr'CH)_2\}(DMAP)$ (**14**) with Ar^FCCH in C_6D_6 at 298 K. (r^2 = 0.996). Bottom: plot of initial rate *vs* equivalents of zirconium complex for the reaction of $Cp_2Zr\{NB(NAr'CH)_2\}(DMAP)$ (**14**) with Ar^FCCH in C_6D_6 at 298 K. (r^2 = 0.998).

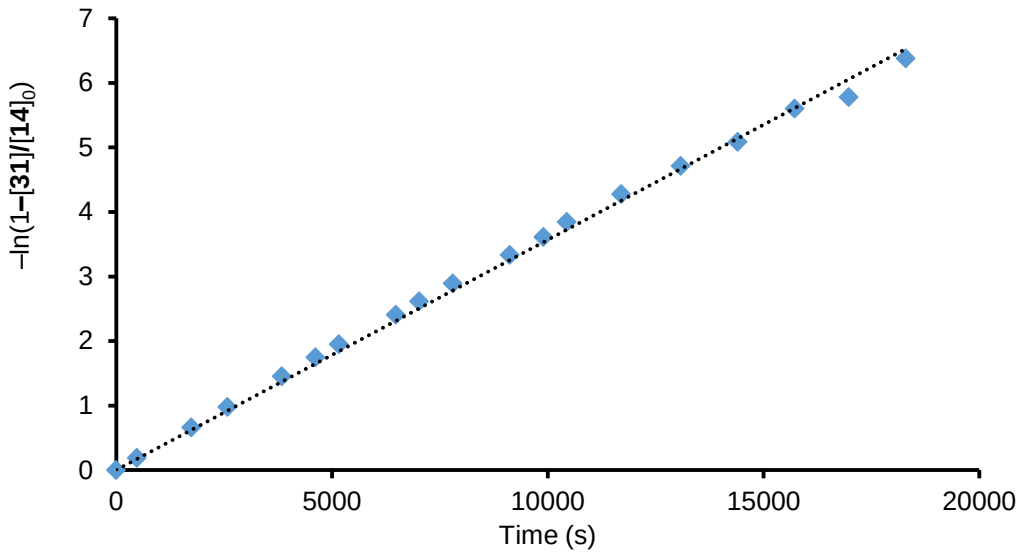

Figure 3.15. Pseudo first order semi-logarithmic plot for the reaction of $Cp_2Zr\{NB(NAr'CH)_2\}(DMAP)$ (**14**) with Ar^FCCH (10 equivalents) in C_6D_6 at 298 K. (r^2 = 0.997).

To gain further insight into the mechanism, the reaction of **14** with Ar^FCCH was monitored by ^1H NMR spectroscopy in the temperature range 298 – 312 K, and the corresponding initial rates were measured. An Eyring analysis of the rate constants, k_{obs} (calculated by Equation 3.8), was carried out (Figure 3.16). This gave the activation parameters $\Delta H^{\ddagger}$ = 11.9(1.0) kcal mol^{-1} and $\Delta S^{\ddagger}$ = –30.2(3.1) cal mol^{-1} K^{-1} ($\Delta G_{298}^{\ddagger}$ = 20.9(1.4) kcal mol^{-1}). The free energy of activation ($\Delta G^{\ddagger}$) value is consistent with a reaction that proceeds at RT. The entropy of activation ($\Delta S^{\ddagger}$) value is strongly negative, which reflects an associative RDS. This is consistent with the proposed reaction pathway, where the alkyne pre-coordinates to the complex before non-rate-determining C–H bond breaking.

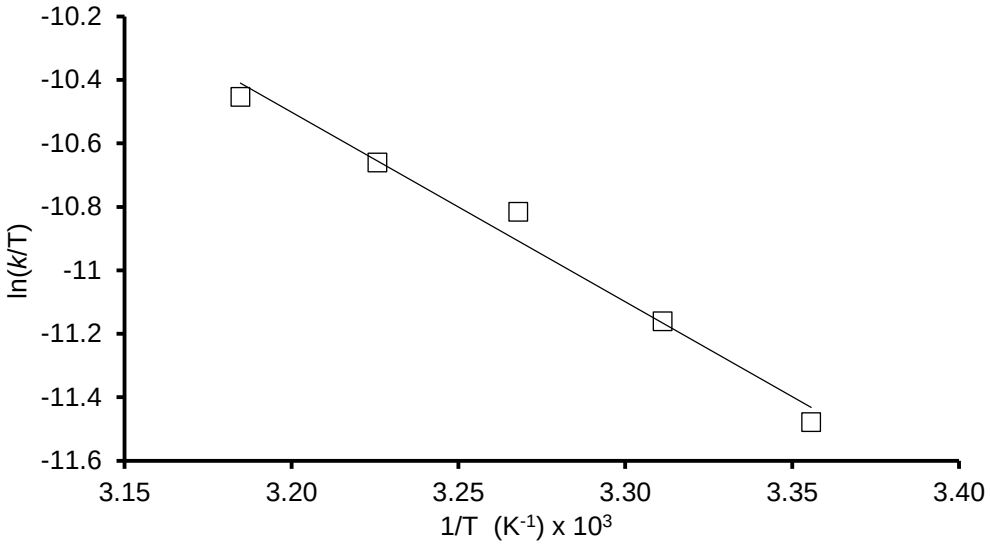

Figure 3.16. Eyring plot for the conversion of $Cp_2Zr\{NB(NAr'CH)_2\}(DMAP)$ (**14**) to $Cp_2Zr\{NHB(NAr'CH)_2\}(CCAr^F)$ (**31**) in C_6D_6. Activation parameters derived from linear regression analysis (r^2 = 0.981): $\Delta H^{\ddagger}$ = 11.9(1.0) kcal mol^{-1}; $\Delta S^{\ddagger}$ = –30.2(3.1) cal mol^{-1} K^{-1}; $\Delta G_{298}^{\ddagger}$ = 20.9(1.4) kcal mol^{-1}.

Determining the energetics of DMAP exchange is important to compare with the free energy of activation ($\Delta G_{298}^{\ddagger}$ = 20.9(1.4) kcal mol^{-1}) above. Measurements of the base exchange of metallocene imido/hydrazido complexes have been successfully achieved by employing prochiral Cp' (C_5H_4Me) ligands or their derivatives. The presence of the methyl substituent reduces the symmetry of the cyclopentadienyl ring, and therefore renders the four ring protons chemically inequivalent in nature when coordinated to the metal fragment without a vertical mirror plane; subsequently, the rate of base exchange can be calculated by measuring the broadening of these four proton resonances at variable temperatures.[61,62] They also confirm that the base exchange of metallocene imide/hydrazide complexes proceeds through a dissociative pathway rather than an associative pathway, as they are 20 VE complexes having no vacant binding site. Thus, the synthesis of Cp' supported zirconium borylimido complexes was next targeted.

In order to prepare the starting material $Cp'_2Zr(Me)Cl$ (**35**), an improved synthesis was developed here, analogous to the preparation of $Cp_2Hf(Me)Cl$ (Section 2.3), by reacting Cp'_2ZrMe_2 with one equivalent of Ph_3CCl at 100 °C for 22 h. Compound **35** was isolated by recrystallisation in 87% yield as colourless crystals. Similar to the preparation of the homologous $Cp_2Zr\{NHB(NAr'CH)_2\}(Me)$ (**9**), the borylamido complex $Cp'_2Zr\{NHB(NAr'CH)_2\}(Me)$ (**36**) was synthesised by reacting **35** with

$LiNHB(NAr'CH)_2$ (**2.5**) at RT in benzene, on the preparative scale. After stirring for 16 h, compound **36** was isolated in 44% yield as pale yellow crystals. Due to the low isolated yield of **36**, synthesis of the corresponding borylimido complex *via* thermolysis was performed by generating **36** *in situ* (Chapter Two). Unfortunately, the thermolysis reaction appeared to be problematic, where the desired borylimido complex formed alongside a high amount of unidentified impurities (especially using weaker Lewis base, e.g. THF and pyridine) at 120 °C after 16 h on the NMR tube scale. These impurities were postulated to result from the C–H bond activation of the methyl substituent on the Cp' ligands forming tuck-in cyclometalated borylamido complexes, which have been widely observed in the reactions of Cp* supported Group 4 imido complexes at high temperature.[25,63–65] Therefore, only the DMAP coordinated $Cp'_2Zr\{NB(NAr'CH)_2\}(DMAP)$ (**37**) was successfully isolated (in 54% yield), by reacting **35** with **2.5** and DMAP in toluene at 120 °C for 16 h (Scheme 3.6).

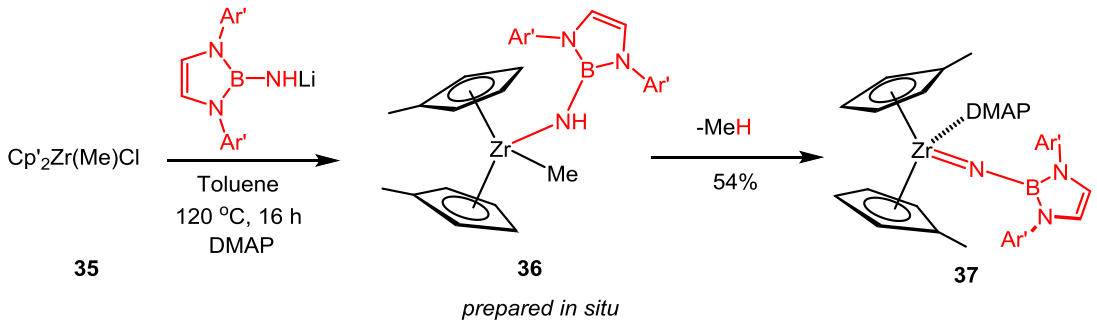

Scheme 3.6. Synthesis of $Cp'_2Zr\{NB(NAr'CH)_2\}(DMAP)$ (**37**) proceeding through *in situ*-generated $Cp'_2Zr\{NHB(NAr'CH)_2\}(Me)$ (**36**).

The ^{11}B signals of **36** and **37** of 25.0 and 19.8 ppm are comparable with those in the Cp homologues $Cp_2Zr\{NHB(NAr'CH)_2\}(Me)$ (**9**) and $Cp_2Zr\{NB(NAr'CH)_2\}(DMAP)$ (**14**), respectively. The ^1H and ^{13}C NMR spectra of the borylamide **36** and borylimide **37** indicate that they have C_s symmetric structures in the solution phase, where only one set of Cp' resonances are observed. Similar to the ^1H signals of the Cp' ligand in **36**, compound **37** also shows four sharp $C_5\underline{H}_4Me$ proton resonances with clear ^1H-^1H coupling and one methyl resonance. This is very different to that observed in the pyridine bound titanocene imide and DMAP bound zirconocene hydrazide complexes (give rapid Lewis base dissociation at RT), where broadening of these signals were observed at RT.[61,62] Other ^1H and ^{13}C signals attributed to the borylamido or borylimido ligands are similar to those in the Cp analogues **9** and **14**.

Diffraction-quality crystals of **36** and **37** were grown from hexane solutions. The molecular structures of **36** and **37** are shown in Figure 3.17 with selected distances and angles in Table 3.9. Both of **36** and **37** have pseudo tetrahedral geometries, in which the Cp' ligands are *syn* and *anti* orientated, respectively, in the solid state. The arrangements of ligands about the zirconium centre are entirely analogous to those in **9** and **11**, respectively. For example, the Zr(1)–N(1)–B(1) linkage of **37** with the Zr(1)–N(1) bond length of 1.898(2) Å and the Zr(1)–N(1)–B(1) angle of 168.45(18)°, as well as the $Cp_{cent(1)}$–Zr(1)–$Cp_{cent(2)}$ angle of 127.5°, are all similar to those in **11**.

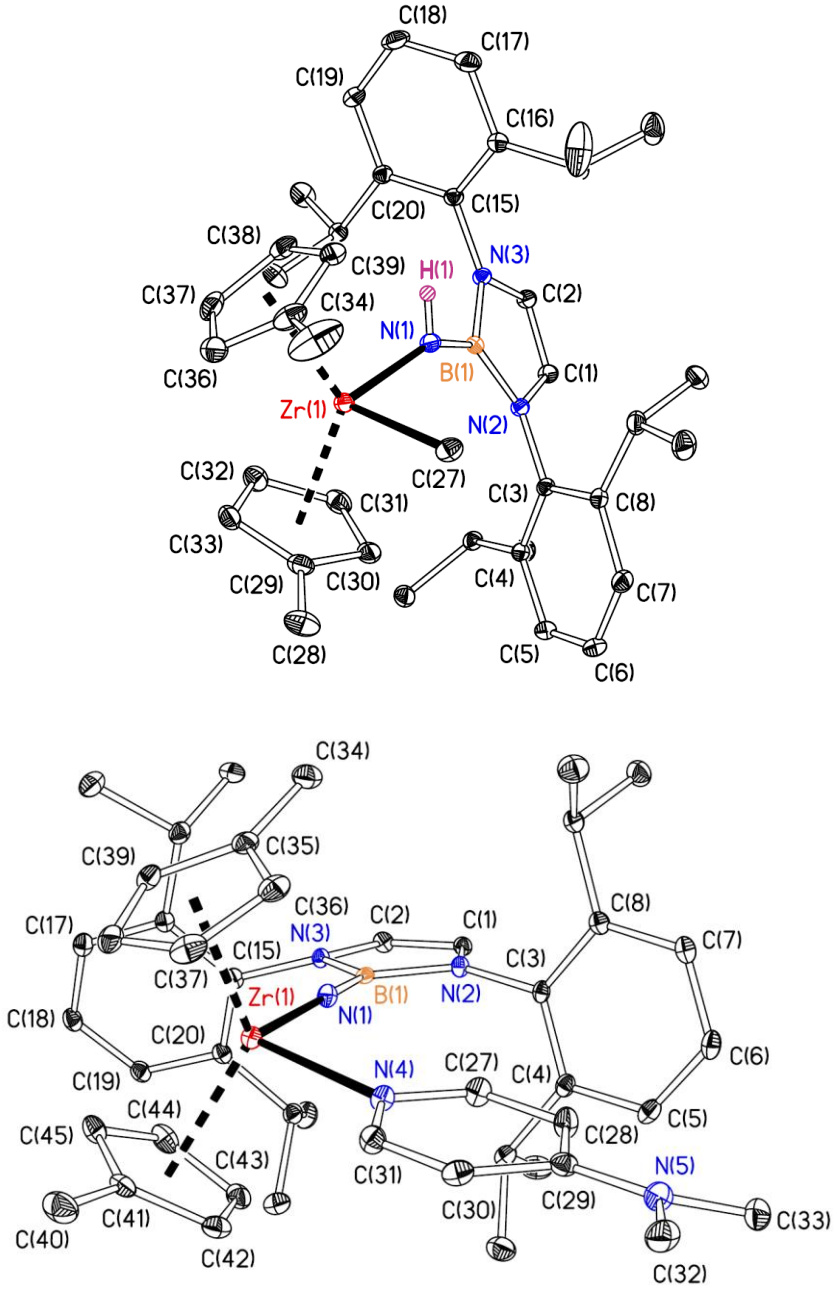

Figure 3.17. Displacement ellipsoid plots (20% probability) of $Cp'_2Zr\{NHB(NAr'CH)_2\}(Me)$ (**36**, top) and $Cp'_2Zr\{NB(NAr'CH)_2\}(DMAP)$ (**37**, bottom). C–bound H atoms omitted for clarity.

Table 3.9. Selected bond lengths (Å) and angles (°) for $Cp'_2Zr\{NHB(NAr'CH)_2\}(Me)$ (**36**) and $Cp'_2Zr\{NB(NAr'CH)_2\}(DMAP)$ (**37**). $Cp_{cent(1)}$ and $Cp_{cent(2)}$ refer to the computed Cp' ring centroids for "upper" and "lower" Cp' rings, respectively, as depicted in Figure 3.17.

	36	**37**
Zr(1)–N(1)	2.085(2)	1.898(2)
$Zr(1)–Cp_{cent(1)}$	2.23	2.31
$Zr(1)–Cp_{cent(2)}$	2.23	2.28
N(1)–B(1)	1.435(3)	1.404(3)
B(1)–N(2)	1.449(3)	1.471(3)
B(1)–N(3)	1.448(3)	1.478(3)
$Cp_{cent(1)}–Zr(1)–Cp_{cent(2)}$	130.2	127.5
$N(1)–Zr(1)–Cp_{cent(1)}$	107.5	109.7
$N(1)–Zr(1)–Cp_{cent(2)}$	109.2	111.6
N(1)–Zr(1)–N(4)/C(27)	96.06(9)	97.60(10)
Zr(1)–N(1)–B(1)	149.42(17)	168.45(18)
N(1)–B(1)–N(2)	132.6(2)	128.0(2)
N(1)–B(1)–N(3)	123.4(2)	130.3(2)

When **37** was reacted with Ar^FCCH at RT, only a C–H bond activation reaction was observed forming $Cp'_2Zr\{NHB(NAr'CH)_2\}(CCAr^F)$ (**38**) quantitatively over 16 h, as expected, and the NMR spectra of the acetylide ligand and the borylamido ligand are very similar to that of **31**. The initial rate was subsequently measured, as above, to be $8.63(2) \times 10^{-6}$ mol dm^{-3} s^{-1} at 298 K, which is very slightly faster than that of analogous **14** ($6.08(7) \times 10^{-6}$ mol dm^{-3} s^{-1} at the same concentration). This reflects that the $\Delta G_{298}^{\ddagger}$ (and presumably $\Delta H^{\ddagger}$, $\Delta S^{\ddagger}$) are very similar for both **14** and **37**. Therefore, if the reaction undergoes a dissociative rate-determining pathway, it should possess an activation free energy ($\Delta G^{\ddagger}$) for DMAP dissociation which is less than 20.9(1.4) kcal mol^{-1}.

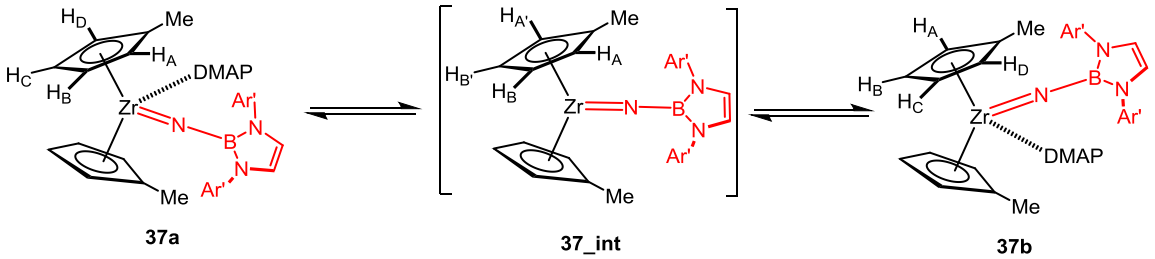

Scheme 3.7. Interchanging of H_A and H_D *via* dissociative DMAP exchange in $Cp'_2Zr\{NB(NAr'CH)_2\}(DMAP)$ (**37**).

During the DMAP dissociation of **37a** forming base free intermediate **37_int**, the eliminated DMAP can either bind in the same position to regenerate **37a**, or on the opposite site yielding **37b**. The latter case leads the pair exchange of the chemically inequivalent ring protons and carbons of Cp', and therefore the rate of DMAP loss (k_{dis}) is equal to twice the rate of DMAP exchange which gives the observed broadening (Scheme 3.7). Since no broadening of H_A/H_D and H_B/H_C was observed at RT, a toluene-d_8 solution of **37** was heated up in the range of 298 – 368 K. However, no appreciable line broadening (< 0.2 Hz) of either the H_A/H_D and H_B/H_C, or the ^{13}C resonances of bound C_A/C_D and C_B/C_C were observed even at 368 K, explicitly reflecting a very slow DMAP dissociation rate. This is consistent with very slow [2+2] cycloaddition of **14** even at 60 °C (*vide supra*), which needs to undergo the rate determining DMAP dissociation pathway. Hence, this very slow DMAP dissociation rate and activation parameters were unable to be measured and calculated at these temperatures. However, the minimum activation free energy can be estimated by assuming a broadening of 0.2 Hz at 368 K occurred (just below the limit for observation). The minimum $\Delta G_{368}^{\ddagger}$ required for DMAP dissociation was calculated by the Eyring equation to be 21.4 kcal mol^{-1}, which would of course be larger in magnitude at RT for a dissociation process, further confirming that the C–H bond activation reaction is not *via* base dissociation pathway.

The suggested associative pathway *via* the rate-determining Ar^FCCH pre-coordination, supported by KIE measurements and reactant order analysis (*vide supra*), is very unlikely to happen at the zirconium centre, since these π-loaded complexes **11** and **14** have 20 VE counts and have no binding site for pre-coordination. One possibility could be that the Lewis acidic boron atom of the borylimido moiety contributes to an outer-sphere pre-coordination, although this atom is electronically saturated by π-donation from the three neighbouring N atoms. To try to gain further insight, we turned to an organoimido

analogue $Cp_2Zr(N^tBu)(THF)$ (**1.4**). Bergman has previously reported the reaction of the imido zirconocene complex **1.4** with PhCCH, and only 1,2-cycloaddition was observed giving $Cp_2Zr\{N(^tBu)C(H)CPh\}$ (**3.4**),[66] same as the reaction of **11** and **13** with TolCCH. In order to see whether the C–H bond activation would occur with more electron-withdrawing terminal alkyne, the reaction of **1.4** with Ar^FCCH was next investigated.

When **1.4** was reacted with Ar^FCCH at RT, an immediate reaction occured to give both the [2+2] cycloaddition product $Cp_2Zr\{N(^tBu)C(H)C(Ar^F)\}$ (**40**) and the C–H bond activation product $Cp_2Zr(NH^tBu)(CCAr^F)$ (**39**) in a *ca*. 7:3 ratio, with a change of the solution colour from yellow to deep green. The mixture was subsequently heated to 100 °C for 16 h, showing no formation of other compounds and the relative ratio of two products remained constant, this implied that both **39** and **40** are thermodynamically stable, like **31** and **32**. Consistent with this, **40** was calculated to be –12.3 kcal mol^{-1} more stable (ΔG) than **39**, and Δ_rG for forming these compounds from base-free $Cp_2Zr(N^tBu)$ (**1.16**) was –41.7 and –29.4 kcal mol^{-1}, respectively. The preference for generating more cycloaddition product by fast THF dissociation is consistent with that of the analogue **13**. However, it cannot rule out that the rapid formation of **39** is also *via* the THF dissociation. Inspired by the exclusive C–H bond activation by **11** and **14**, in which the cycloaddition reaction is supressed by strongly coordinated pyridine and DMAP at RT, reactions of Ar^FCCH with $Cp_2Zr(N^tBu)(L)$ (L = py (**3.5**) and DMAP (**3.6**)) were next performed on the NMR tube scale. The reactions occurred immediately with a change of solution colour from yellow to pale yellow at RT, both giving the C–H bond activation product **39** exclusively (Scheme 3.8).

Due to the rapid C–H bond activation of both **3.5** and **3.6** at RT, the initial rates of the reactions of **3.5** with Ar^FCCH and Ar^FCCD were both measured at 242 K. The corresponding initial rates of $4.89(1) \times 10^{-6}$ mol dm^{-3} s^{-1} and $4.62(3) \times 10^{-6}$ mol dm^{-3} s^{-1}, respectively, give no mechanistically significant kinetic isotope effect (KIE = 1.06(1)). A competition KIE of 1.6 was also measured from the reaction of **3.5** with an excess of both Ar^FCCH and Ar^FCCD (1:5:5) on the NMR tube scale at RT. These observations are entirely analogous to those of **11** and **14**, indicating the C–H bond activation of Ar^FCCH by **3.5** undergoes the same associative alkyne pre-coordination pathway, and because of the less sterically encumbered nature of **3.5**, the kinetic barrier is lower leading to the more rapid reaction. Thus, the reactions of borylimido or *tert*-butylimido zirconocene

complexes with Ar^FCCH show no difference mechanistically, ruling out the possible participation of the boryl moiety in the alkyne pre-coordination.

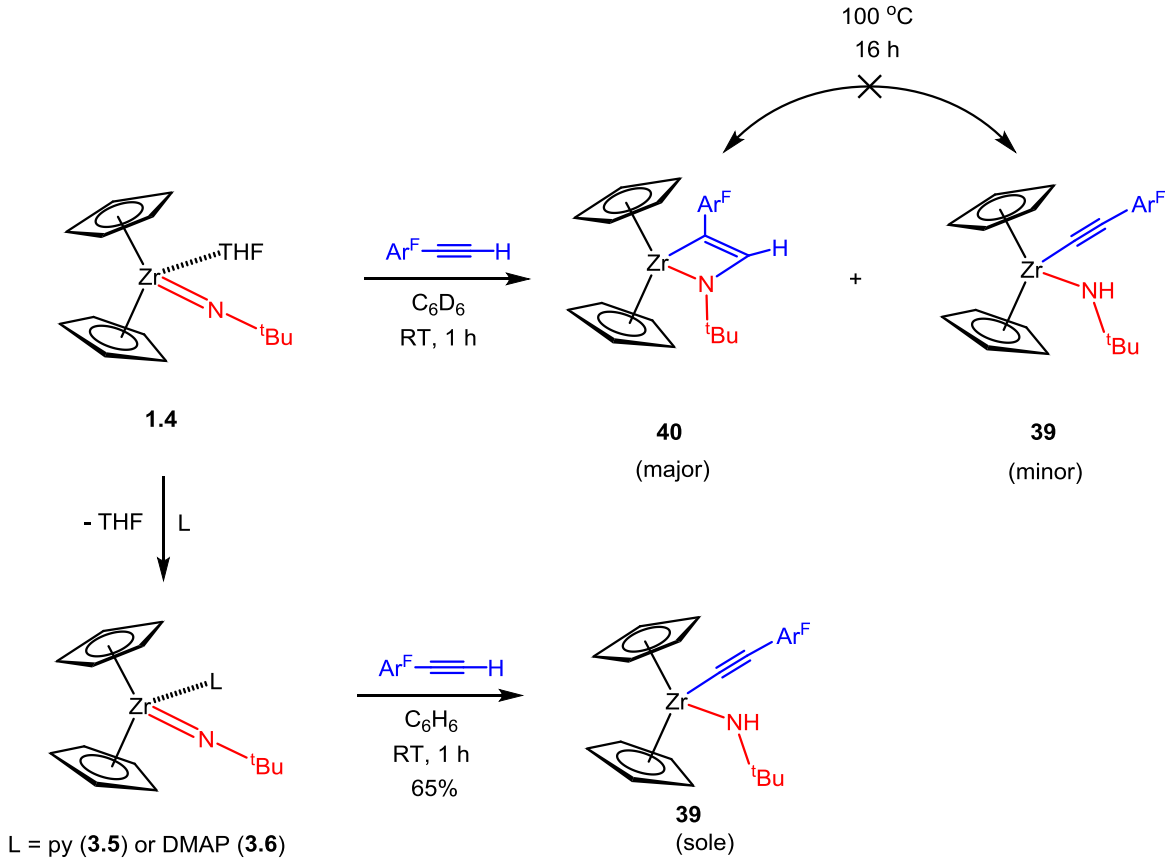

Scheme 3.8. Formation of $Cp_2Zr\{N(^tBu)C(H)C(Ar^F)\}$ (**40**, major) and $Cp_2Zr(NH^tBu)(CCAr^F)$ (**39**, minor) from $Cp_2Zr(N^tBu)(THF)$ (**1.4**), and the exclusive formation of $Cp_2Zr(NH^tBu)(CCAr^F)$ (**39**) from $Cp_2Zr(N^tBu)(L)$ (L = py (**3.5**) and DMAP (**3.6**).

On the preparative scale, compound **39** was exclusively formed from the reaction of **3.5** with Ar^FCCH in benzene at RT for 1 h, and isolated in 65% yield as pale yellow crystals. Unfortunately, attempts to isolate the major cycloaddition product **40** from the reaction of **1.4** with Ar^FCCH at RT was unsuccessful due to the high solubility of all components of the mixture. Therefore, compound **40** was characterised only by NMR spectroscopy. The ^1H NMR spectrum of the isolated **39** shows singlets for the cyclopentadienyl and *tert*-butyl moieties and a NH resonance at 6.33 ppm. The ^{13}C signal of $\underline{C}Me_3$ of 58.4 ppm is comparable with the chemical shift observed in the amido complex $Cp_2Zr(NH^tBu)(Me)$ of 56.5 ppm.[66] In contrast, the metallacyclic complex **40** shows a diagnostic sharp ^1H singlet at 7.88 ppm, attributed to $ZrC=C\underline{H}$, and an HSQC and an HMBC correlation to the ^{13}C

signals at 120.5 and 138.3 ppm were observed respectively.[66] The latter ^{13}C signal is slightly upfield shifted compared to that of **3.2**, but comparable to that of **32**, which indicates its anti-Markovnikov regiochemistry.

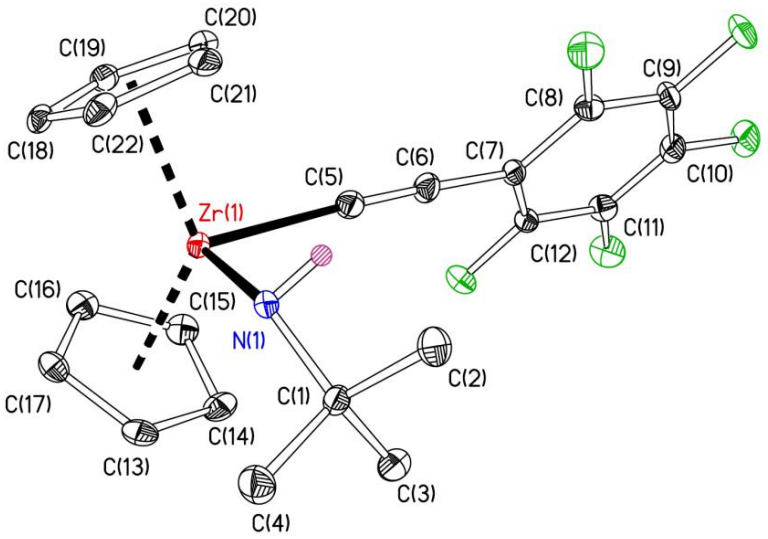

Figure 3.18. Displacement ellipsoid plot (20% probability) of $Cp_2Zr(NH^tBu)(CCAr^F)$ (**39**). C–bound H atoms omitted for clarity.

Table 3.10. Selected bond lengths (Å) and angles (°) for $Cp_2Zr(NH^tBu)(CCAr^F)$ (**39**). Values in brackets are for the second and third crystallographically independent molecules. $Cp_{cent(1)}$ and $Cp_{cent(2)}$ refer to the computed centroids for "upper" and "lower" Cp rings, respectively, as depicted in Figure 3.18.

Zr(1)–N(1)	2.064(4) [2.055(5)] [2.052(4)]
Zr(1)–C(5)	2.274(5) [2.293(5)] [2.278(5)]
Zr(1)–$Cp_{cent(1)}$	2.22 [2.22] [2.24]
Zr(1)–$Cp_{cent(2)}$	2.22 [2.23] [2.24]
C(5)–C(6)	1.202(7) [1.202(7)] [1.192(6)]
N(1)–C(1)	1.488(6) [1.469(7)] [1.493(5)]
$Cp_{cent(1)}$–Zr(1)–$Cp_{cent(2)}$	130.4 [130.4] [131.5]
N(1)–Zr(1)–$Cp_{cent(1)}$	103.9 [115.1] [113.1]
N(1)–Zr(1)–$Cp_{cent(2)}$	114.1 [102.9] [104.8]
Zr(1)–N(1)–C(1)	145.4(3) [150.0(4)] [148.3(3)]
Zr(1)–C(5)–C(6)	177.4(4) [174.9(5)] [174.4(4)]

Diffraction–quality crystals of compound **39** were grown from a hexane solution at 4 °C, and the solid state structures are shown in Figure 3.18 along with selected bond lengths and angles in Table 3.10. The solid state structures of **39** possess pseudo tetrahedral environments, with staggered cyclopentadienyl rings for one of the three crystallographically independent molecules and eclipsed rings for the other two. The Zr(1)–N(1) bond distances of 2.064(4) [2.055(5)] [2.052(4)] Å are similar to that in other zirconocene *tert*-butylamido complexes of 2.06 Å.[67–69] The C(5)–C(6) bond distances of 1.202(7) [1.202(7)] [1.192(6)] Å are comparable within error with that in **31**, consistent with a full triple bond.

3.4.3 Reactions and kinetic study of $Cp_2M\{NB(NAr'CH)_2\}(py)$ (M = Ti (1.117) or Hf (12)) with electron deficient terminal alkynes

Reactions of $Cp_2M(NNPh_2)(DMAP)$ (M = Zr (**1.63**) or Hf) with internal alkynes, such as PhCCPh, have been mechanistically studied in our research group, and the first step of the reaction was confirmed to be *via* initial DMAP dissociation. Therefore, the measured corresponding rate constants show that the reaction of **1.63** is *ca*. 22 times faster than the hafnium congener, due to the much stronger Hf–DMAP bond.[61] In order to gain further insight into the proposed associative C–H bond activation reactions of **11** and **14**, the hafnium congener $Cp_2Hf\{NB(NAr'CH)_2\}(py)$ (**12**) was employed here. If **12** undergoes the same mechanism with Ar^FCCH, the robust Hf–py bond should result in significantly slower pyridine dissociation, and therefore supresses the [2+2] cycloaddition selecting C–H bond activation exclusively, like the DMAP coordinated zirconium analogue.

On the NMR tube scale, when **12** was reacted with TolCCH, no reaction was observed at RT. Even upon heating to 60 °C for 16 h, no appreciable formation of [2+2] cycloaddition product was observed, consistent with the expected much slower pyridine dissociation. In contrast, a reaction of **12** with Ar^FCCH was observed at RT, with a change of the solution colour from pale orange-red to pale yellow. Quantitative conversion of **12** was observed in several hours, giving exclusive C–H bond activation product $Cp_2Hf\{NHB(NAr'CH)_2\}(CCAr^F)$ (**41**), which is faster than the reaction of the zirconium congener **11**. These observation are consistent with that of **14** indicating the C–H bond activation of Ar^FCCH by **12** undergoes a similar mechanistic pathway, and not *via* pyridine dissociation. The initial rate was subsequently measured at 298 K as $1.43(1) \times 10^{-5}$ mol dm^{-3} s^{-1} which is *ca*. 2.4 times faster than that of the reaction of **14** (same

concentration). The rate constant k_{obs} was calculated to be 7.25×10^{-3} dm^3 mol^{-1} s^{-1} by applying Equation 3.8, showing approximately 6 times faster C–H bond activation than the zirconium congener **11** and **14**. The activation free energy was then calculated from the Eyring equation, this being approximately $\Delta G_{298}^{\ddagger}$ = 20.4 kcal mol^{-1}, which is similar and slightly lower to that of the zirconium analogue **14**. The faster C–H bond activation of **12** (*cf.* **11** and **14**) explicitly indicates the RDS is associative, and may involve some degree of binding with the metal centre. The initial rate of the reaction of **12** with Ar^FCCD at 298 K was measured, this being $1.43(1) \times 10^{-5}$ mol dm^{-3} s^{-1}, which gives a KIE of 1.00(1), the same as the KIE obtained in zirconium analogues, showing no kinetic isotope effect. The competition KIE was measured by reacting **12** with an excess of Ar^FCCH and Ar^FCCD (1:5:5) at RT, also giving a KIE of 1.0 in this case. This competition KIE is slightly smaller than that of the zirconium analogues (1.5), which may reflect a less reversible associative process, consistent with stronger Hf–X bonds.

The more selective C–H bond activation by hafnocene borylimido complexes **12** can, therefore, potentially allow the C–H bond activation of less electron deficient terminal alkynes more easily. Therefore, compound **12** was reacted with $Ar^{CF_3}CCH$ in C_6D_6 at RT on the NMR tube scale. Exclusive but slow formation of the C–H bond activation product $Cp_2Hf\{NHB(NAr'CH)_2\}(CCAr^{CF_3})$ (**42**) was observed at RT over 16 h. Upon heating to 50 °C for 2 days, product **42** was almost entirely yielded without appreciable formation of the cycloaddition product.

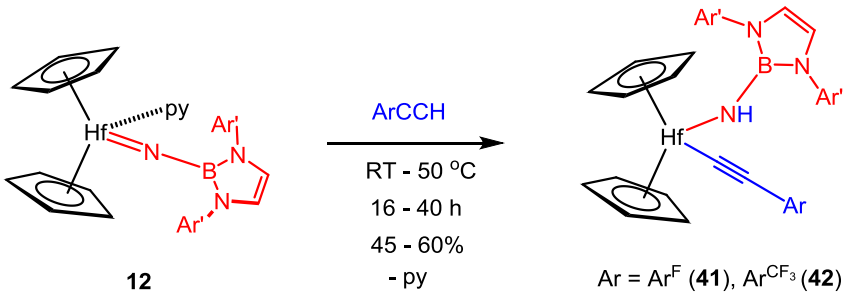

12

Ar = Ar^F (**41**), Ar^{CF_3} (**42**)

Equation 3.9

On the preparative scale, compound **41** was formed by reacting **12** with Ar^FCCH in benzene at RT for 16 h, and isolated in 45% crystalline yield. The reaction of **12** with $Ar^{CF_3}CCH$ was performed in benzene at 50 °C for 40 h, and **42** was isolated in 60% crystalline yield (Equation 3.9). The ^{11}B NMR signals of **41** and **42** are 25.5 and 25.7 ppm, respectively, comparable with that of the borylamido hafnocene complex

$Cp_2Hf\{NHB(NAr'CH)_2\}(Me)$ (**10**) of 25.8 ppm. The ^{1}H and ^{13}C spectra of **41** and **42** are entirely analogous to the zirconium congeners **32** and **30**, respectively.

Diffraction-quality crystals of **41** and **42** were grown from hexane solutions at 4 °C. The solid state structures are shown in Figure 3.19, and selected bond distances and angles are listed in Table 3.11. The solid state structures of **41** and **42** possess pseudo tetrahedral environments, with staggered cyclopentadienyl rings. All the key structural parameters, including Hf–N, Hf–C and C≡C distances, and coordination environments of **41** and **42** are similar, and also comparable with the zirconium congener **31**.

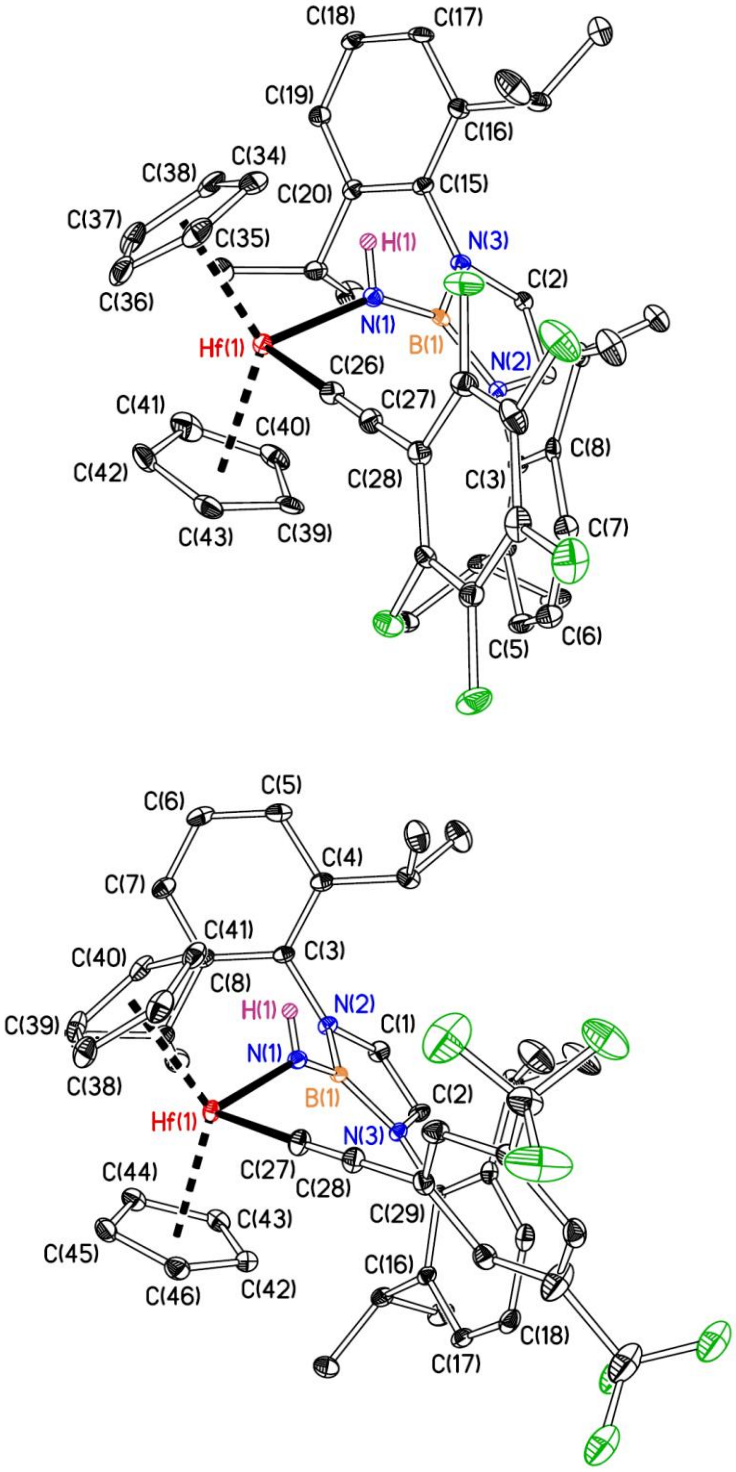

Figure 3.19. Displacement ellipsoid plots (20% probability) of $Cp_2Hf\{NHB(NAr'CH)_2\}(CCAr^F)$ (**41**, top) and $Cp_2Hf\{NHB(NAr'CH)_2\}(CCAr^{CF_3})$ (**42**, bottom). C–bound H atoms omitted for clarity.

Table 3.11. Selected bond lengths (Å) and angles (°) for $Cp_2Hf\{NHB(NAr'CH)_2\}(CCAr^F)$ (**41**) and $Cp_2Hf\{NHB(NAr'CH)_2\}(CCAr^{CF_3})$ (**42**). $Cp_{cent(1)}$ and $Cp_{cent(2)}$ refer to the computed Cp ring centroids for "upper" and "lower" Cp rings, respectively, as depicted in Figure 3.19.

	41	**42**
Hf(1)–N(1)	2.077(3)	2.054(3)
Hf(1)–$C_{ac}(1)^a$	2.241(4)	2.220(4)
Hf(1)–$Cp_{cent(1)}$	2.19	2.19
Hf(1)–$Cp_{cent(2)}$	2.21	2.21
N(1)–B(1)	1.433(5)	1.441(5)
B(1)–N(2)	1.440(5)	1.447(5)
B(1)–N(3)	1.438(5)	1.442(5)
$C_{ac}(1)$–$C_{ac}(2)^{a,b}$	1.191(5)	1.225(6)
$Cp_{cent(1)}$–Hf(1)–$Cp_{cent(2)}$	131.8	131.4
N(1)–Hf(1)–$Cp_{cent(1)}$	106.7	108.3
N(1)–Hf(1)–$Cp_{cent(2)}$	108.6	106.0
Hf(1)–N(1)–B(1)	146.7(3)	143.7(3)
Hf(1)–$C_{ac}(1)$–$C_{ac}(2)^{a,b}$	179.7(4)	177.8(4)
N(1)–Hf(1)–$C_{ac}(1)^a$	100.49(13)	99.98(15)

a. "$C_{ac}(1)$" = C(26) **41**, C(27) **42**. *b*. "$C_{ac}(2)$" = C(27) **41**, C(28) **42**.

As mentioned in Section 3.4.1, the preference for undergoing [2+2] cycloaddition or C–H bond activation of $Cp^*_2Ti(NPh)$ (**2.11**) was stated to be steric in origin, where acetylene gave cycloaddition and PhCCH gave C–H bond activation.[23] Therefore, the marginally smaller hafnium congener **12** may experience a slightly more sterically crowded transition state for the cycloaddition, and thus yield the C–H bond activation more selectively. In order to rule out the possible steric contribution, compound $Cp_2Ti\{NB(NAr'CH)_2\}(py)$ (**1.117**) was employed, which was originally synthesised by another DPhil student in our research group.[70]

On the NMR tube scale, compound **1.117** was reacted with Ar^FCCH or TolCCH in C_6D_6 at RT. Immediate reactions were both observed to give cycloaddition products $Cp_2Ti\{N\{B(NAr'CH)_2\}C(H)C(Ar)\}$ (Ar = Ar^F (**44**) or Tol (**43**)) exclusively. On the preparative scale, the mixture of **1.117** and Ar^FCCH or TolCCH in benzene was stirred for 1 h at RT, and **44** and **43** were isolated in 45% (crystalline) and 78% yield, respectively (Equation 3.10). The NMR spectra of **43** and **44** are comparable with those of the zirconium congeners $Cp_2Zr\{NB(NAr'CH)_2C(H)C(Ar)\}$ (Ar = Ar^F (**32**) and Tol (**27**)), respectively, with identical ^{11}B signals of 22.9 ppm. The diagnostic ^1H signal of TolC=C<u>H</u> sharp singlet was observed at 6.78 and 7.16 ppm, with an HMBC correlation to ^{13}C signals at 195.1 and 165.5 ppm which are slightly downfield shifted compared to those of the zirconium congeners **27** and **32**, respectively. The NMR spectra are consistent with **43** and **44** existing as single anti-Markovnikov (1,2-cycloaddition) regioisomers.

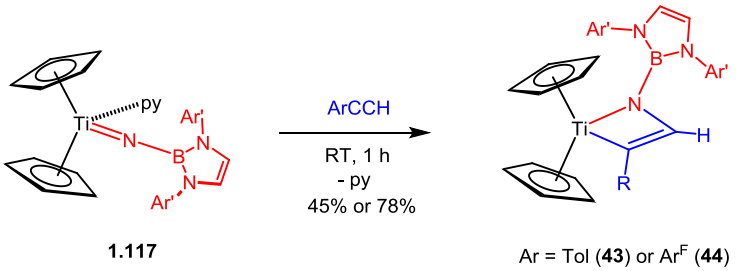

Equation 3.10

Diffraction-quality crystals of **44** were grown from a hexane solution at 4 °C. The solid state structure is shown in Figure 3.20, and selected bond distances and angles are listed in Table 3.12. The metallacyclic complex **44** has an analogous structure to the zirconium congener **32**, possessing a pseudo tetrahedral environment, with staggered cyclopentadienyl rings. The solid state structure confirms its anti-Markovnikov (1,2-cycloaddition) regiochemistry. The Ti(1)–N(1) bond distance of 2.0474(17) Å is comparable with that of $Cp^*_2Ti\{N(Ph)C(H)C(H)\}$ of 2.059(2) Å and $Ti(N_2N^{py})\{NB(NAr'CH)_2C(H)C(Tol)\}$ (**3.7**) of 2.062(2) Å.[20,23] The N(1)–C(27) and C(27)–C(28) bond lengths are similar to those in **32**. Meanwhile, the wider N(1)–Ti(1)–C(28) bite angle of 69.95(7)° and more acute Ti(1)–N(1)–B(1) angle of 146.84(15)° indicate a more sterically congested azametallacyclobutene unit in **44**. These may reflect that the transition state of the [2+2] cycloaddition for titanium borylimide is also more sterically crowded than zirconium and hafnium congeners, and thus less kinetically

favoured. In spite of this, the possibly more sterically favoured C–H bond activation product is still not observed, ruling out that the preference for cycloaddition and C–H bond activation is steric in origin in these cases.

DFT calculations show that in each case the C–H bond activation product was less stable than the observed cycloaddition product (ΔG = 13.2 and 9.1 kcal mol^{-1} for Ar = Tol and Ar^F, respectively). $\Delta_r G$ for formation of the C–H bond activation product was only –15.3 and –20.3 kcal mol^{-1} with respect to the base-free $Cp_2Ti\{NB(NAr'CH)_2\}$ (*cf.* –29.6 and –32.4 kcal mol^{-1} for zirconium congeners $Cp_2Zr\{NHB(NAr'CH)_2\}(CCTol)$ (**27-CH**) and $Cp_2Zr\{NHB(NAr'CH)_2\}(CCAr^F)$ (**31**)). It is interesting to compare the reaction of Bergman's $Cp^*_2Ti(NPh)$ (**2.11**) with PhCCH, leading to the C–H bond activation product $Cp^*_2Ti(NHPh)(CCPh)$, with that of **1.117** and TolCCH forming cycloaddition species **43**. DFT calculations on both systems found cycloaddition to be the thermodynamically preferred outcome: $\Delta_r G$ = –16.5 and –25.8 kcal mol^{-1} for the reaction of **2.11** with PhCCH forming $Cp^*_2Ti(NHPh)(CCPh)$ or its 1,2-cycloaddition counterpart $Cp^*_2Ti\{N(Ph)C(H)C(Ph)\}$; $\Delta_r G$ = –15.3 and –28.5 kcal mol^{-1} for base-free $Cp_2Ti\{NB(NAr'CH)_2\}$ with TolCCH forming the corresponding C–H bond activation product and counterpart **43** (from **1.117** itself the values of $\Delta_r G$ reduce to –10.4 and –23.6 kcal mol^{-1}, respectively, by taking into account pyridine dissociation). Experimentally, **2.11** reacted with HCCH forming the cycloaddition product $Cp^*_2Ti\{N(Ph)C(H)C(H)\}$. The computed $\Delta_r G$ values for C–H bond activation and cycloaddition were –14.8 and –26.7 kcal mol^{-1}, similar to the values for PhCCH. Here the steric limitations are sufficiently reduced to permit formation of the thermodynamic (cycloaddition) product. It was noted by Bergman that $Cp^*_2Ti\{N(Ph)C(H)C(H)\}$ does not undergo exchange with free HCCH,[23] and $\Delta_r G$ for its formation is consistent with that.

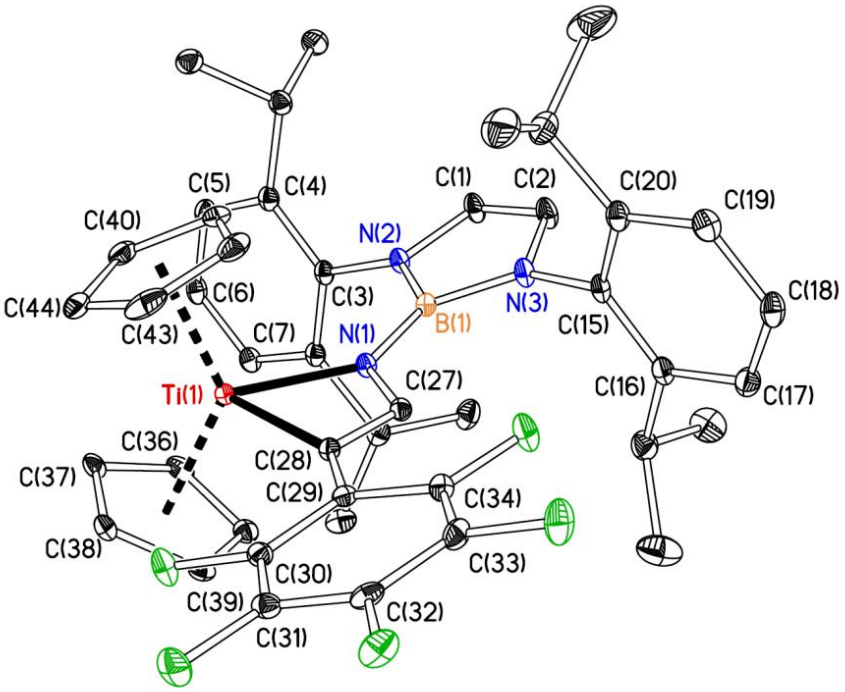

Figure 3.20. Displacement ellipsoid plot (20% probability) of $Cp_2Ti\{N\{B(NAr'CH)_2\}C(H)C(Ar^F)\}$ (**44**). H atoms omitted for clarity.

Table 3.12. Selected bond lengths (Å) and angles (°) for $Cp_2Ti\{N\{B(NAr'CH)_2\}C(H)C(Ar^F)\}$ (**44**). $Cp_{cent(1)}$ and $Cp_{cent(2)}$ refer to the computed Cp ring centroids for "upper" and "lower" Cp rings, respectively, as depicted in Figure 3.20.

Ti(1)–N(1)	2.0474(17)	$Cp_{cent(1)}$–Ti(1)–$Cp_{cent(2)}$	132.2
Ti(1)–C(28)	2.080(2)	N(1)–Ti(1)–C(28)	69.95(7)
Ti(1)–$Cp_{cent(1)}$	2.06	Ti(1)–N(1)–B(1)	146.84(15)
Ti(1)–$Cp_{cent(2)}$	2.07	Ti(1)–C(28)–C(27)	85.99(14)
N(1)–B(1)	1.432(3)	N(1)–C(27)–C(28)	117.71(19)
B(1)–N(2)	1.457(3)		
B(1)–N(3)	1.452(3)		
N(1)–C(27)	1.401(3)		
C(27)–C(28)	1.363(3)		

The metallacycles **43** and **44** were found to be thermodynamically stable giving no further rearrangement at 100 °C over 16 h, and no redistribution reaction can be observed at this

temperature for the mixture of **43** and Ar^FCCH giving in line with the computed endergonic Δ_rG for the formation of base free $Cp_2Ti\{NB(NAr'CH)_2\}$ from the metallacycle (Δ_rG = +29.4 kcal mol^{-1}). The rapid [2+2] cycloadditions are believed to be attributed to the faster pyridine dissociation, as the Ti–py bond is more labile in contrast to the zirconium and hafnium congeners **11** and **12**. Hence, the exclusive formation of **44** could possibly be the kinetic outcome by the fast pyridine dissociation. Therefore, the compound $Cp_2Ti\{NB(NAr'CH)_2\}$(DMAP) (**3.8**) was used to see if the strongly coordinated DMAP would inhibit the cycloaddition, and facilitate the C–H bond activation selectively. When **3.8** reacted with Ar^FCCH at RT, much slower formation of **44** was noticed as expected, with only 45% formation of **44** after 60 h at RT. A C–H bond activation product was still not observed over this period, despite the C–H bond activation product being calculated to be thermodynamically accessible. However, these reaction observations further confirm that the C–H bond activation of this electron deficient Ar^FCCH is not *via* a zwitterionic pathway, as the change of metal should not make a significant difference in the protonation step.

The reactions of $Ti(N_2N^{py})\{NB(NAr'CH)_2\}$(py) (**1.116**) with Ar^FCCH have been previously investigated in our research group.[20] The C–H bond activation product $Ti(N_2N^{py})\{NHB(NAr'CH)_2\}(CCAr^F)$ formed at RT was found to be the kinetic product, which eventually converted to the thermodynamic metallacyclic product $Ti(N_2N^{py})\{N\{B(NAr'CH)_2\}C(H)C(Ar^F)\}$ after 16 h at 60 °C. This is consistent with a relatively small Δ_rG = +8.8 kcal mol^{-1} for forming base-free $Ti(N_2N^{py})\{NHB(NAr'CH)_2\}$ and Ar^FCCH from $Ti(N_2N^{py})\{NHB(NAr'CH)_2\}(CCAr^F)$. Therefore, the non-observed C–H bond activation product from **1.117** is possibly formed initially as a transient intermediate, followed by rearrangement to yield **44**, although the Δ_rG = +15.3 kcal mol^{-1} for forming base-free $Cp_2Ti\{NB(NAr'CH)_2\}$ and Ar^FCCH from $Cp_2Ti\{NHB(NAr'CH)_2\}(CCAr^F)$ is significant larger. To check this, the reaction of **1.117** and Ar^FCCH was monitored in the temperature range of 195 – 273 K by NMR spectroscopy. However, only slow [2+2] cycloaddition could be observed. Speculating that the C–H bond activation of **1.117** would likely follow the same associative mechanism as the zirconium and hafnium congeners **11** and **12**, the absence of the C–H bond activation could be attributed to the highly reversible pre-coordination of Ar^FCCH, or an inaccessible highly sterically congested transition state.

3.4.4 Mechanistic discussion

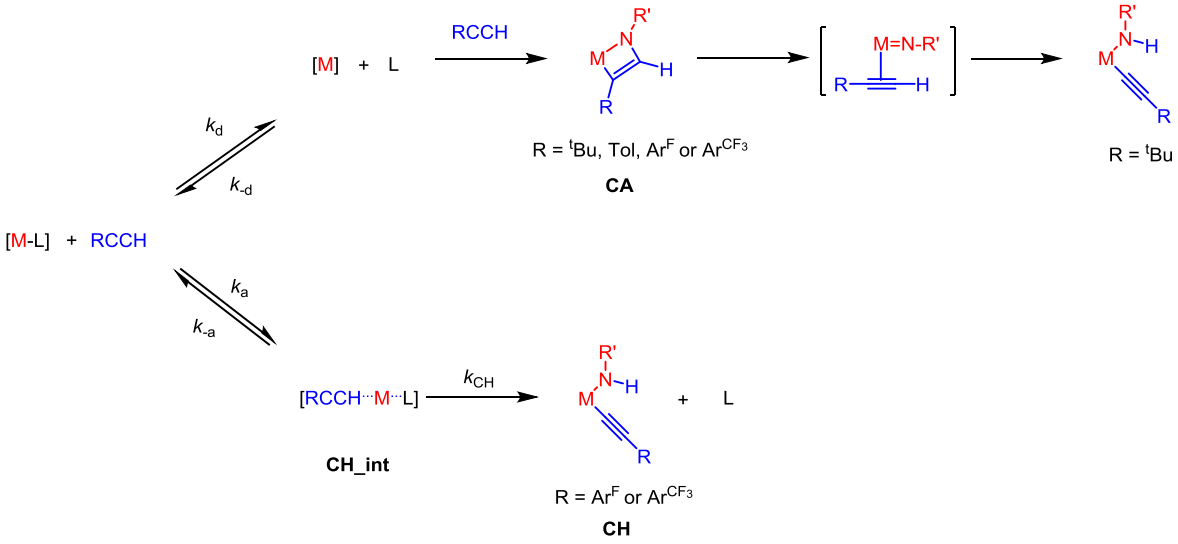

Scheme 3.9. Proposed mechanisms for cycloaddition or C–H bond activation of RCCH (R = ^{t}Bu, Tol, Ar^{CF_3} or Ar^{F}) by (boryl)imido metallocene complexes.

$$\frac{d[\text{CH_int}]}{dt} = k_a[\text{ML}][\text{RCCH}] - k_{-a}[\text{CH_int}] - k_{CH}[\text{CH_int}] = 0 \qquad (3.11)$$

$$[\text{CH_int}] = \frac{k_a[\text{ML}][\text{RCCH}]}{k_{-a} + k_{CH}} \qquad (3.12)$$

$$\frac{d[\text{CH}]}{dt} = k_{CH}[\text{CH_int}]$$

$$= \frac{k_a k_{CH}}{k_{-a} + k_{CH}}[\text{ML}][\text{RCCH}] \qquad (3.13)$$

$$\frac{d[\text{CH}]}{dt} = k_a[\text{ML}][\text{RCCH}] \qquad (3.14)$$

(If $k_{CH} >> k_{-a}$)

The proposed mechanism of C–H bond activation and cycloaddition of terminal alkynes are summarised in Scheme 3.9. As we found for the weak Lewis base (THF) complexes, $Cp_2Zr\{NB(NAr'CH)_2\}(THF)$ (**13**), facile THF dissociation (low $\Delta G^{‡}$) results in rapid

formation of base-free intermediate $Cp_2Zr\{NB(NAr'CH)_2\}$, which facilitates the 1,2-cycloaddition with RCCH (R = ^{t}Bu, Tol, Ar^{CF_3} and Ar^F) forming corresponding metallacycles (denoted **CA**). In the special case of ^{t}BuCCH, the 1,2-cycloaddition product $Cp_2Zr\{N\{B(NAr'CH)_2\}C(H)C(^tBu)\}$ (**25**) is the kinetic product, and further heating results in formation of C–H bond activation product $Cp_2Zr\{NHB(NAr'CH)_2\}(CC^tBu)$ (**26**) *via* a putative ^{t}BuCCH coordinated π-adduct. In all other cases (R = Tol, Ar^{CF_3} and Ar^F), the corresponding metallacycles are significantly more thermodynamically stable than the C–H bond activation counterparts, as shown by DFT calculations (*vide supra*).

When the stronger Lewis base pyridine is employed, less facile (larger $\Delta G^{\ddagger}$) base dissociation is expected, rendering the formation of corresponding metallacycles slower overall, as shown in Table 3.4. This effect is amplified when the even stronger Lewis base DMAP was used. Therefore, the retarded base dissociation pathway (prohibitive $\Delta G^{\ddagger}$) results in C–H bond activation becoming more significant (but not *via* the base dissociation pathway, k_d), especially for more electron-deficient alkynes (e.g. Ar^FCCH). As none of the putative intermediate **CH_int** was observed during the course of C–H bond activation of Ar^FCCH or $Ar^{CF_3}CCH$, a steady-state approximation was applied to **CH_int** in order to obtain the rate law (Equation 3.11 – 3.13).

In the case of $Cp_2Hf\{NB(NAr'CH)_2\}(py)$ (**12**), strong binding with the alkyne could result in a relatively more stable intermediate (**CH_int**). If $k_{CH} >> k_{-a}$, the rate equation can be simplified as Equation 3.14, and $k_{obs} = k_a$. Therefore, overall rate of the C–H bond activation of electron-deficient alkynes is dependent on k_a, as well as concentration of alkynes and borylimido compounds. Since k_a is isotope-insensitive, the deuterium substituted alkyne (Ar^FCCD) should not result in a difference in rate, which shows an absence of KIE, consistent with the experimental observation (KIE = 1.00(1)). In addition, the alkyne-binding step k_a is the product-determining step because this step determines whether a C–H or C–D bond ultimately undergoes functionalisation, and this step is isotope-insensitive.[71] Therefore, an absence of competition KIE is expected, consistent with the experimental values (1.0).

For the zirconium congeners (e.g. **14** and **3.5**), the relatively weak coordination of alkyne in **CH_int** appears to result in alkyne dissociation and exchange (with deuterated alkyne) at this post-RDS stage, thus giving a small competition KIE (1.5 for **14** and 1.6 for **3.5**). Nonetheless, the rate of overall reaction is outweighed by the slowest first step (small k_a), giving an absence of KIE as measured by corresponding initial rates.

3.5 Hydro-borylamination reactions

In Section 1.3.5 (Chapter One), the hydroamination of alkynes by Group 4 imido catalysis was described. It was generally found that the azametallacyclobutene complexes appear as intermediates in the catalytic cycle.[1–5,7,8,12,14,15,21,35,72] Given the formation of several azazirconacyclobutene complexes isolated or formed here, such as **27**, **28** and **29**, the regeneration of borylimido zirconocene complexes giving a hydro-borylamination product by subsequent protonation using borylamine $H_2NB(NAr'CH)_2$ (**1.110**), was targeted for completing the (stoichiometric) cycle. DFT calculations by Prof. Philip Mountford on the hydroamination model of HCCH or PhCCH with $H_2NB(NMeCH)_2$ found that the ΔE (SCF energies) values are comparable to those for the corresponding reactions with $PhNH_2$ or $XylNH_2$. Analogous result were found for full systems based on **1.110**, ^{t}BuCCH or $XylNH_2$ with TolCCH. Further calculation found that although the reaction of **27** with one equivalent of **1.110** to form the enamine product $TolC(H)=C(H)N(H)B(NAr'CH)_2$ (**45**) and base-free $Cp_2Zr\{NB(NAr'CH)_2\}$ was slightly endergonic, the reaction of **27** with two equivalents of the amine **1.110** was fairly exergonic (–5.9 kcal mol^{-1}) and significantly exothermic (–29.0 kcal mol^{-1}), as long as the bis(borylamido) zirconocene complex $Cp_2Zr\{NHB(NAr'CH)_2\}_2$ is kinetically accessible. However, the attempted reaction of **27** with borylamine **1.110** was unsuccessful. On the NMR tube scale, no reaction was observed at RT, whereas heating up to 120 °C for 60 h, only small amount of unidentified species was found. Also, further attempts to use less basic amines, H_2N^tBu and H_2NXyl led to either no reaction or unidentified complex mixtures.

The hydroamination of internal alkynes by the *in situ* generated analogous zirconocene arylimido complex $Cp_2Zr(NXyl)$ (**1.17**) has been fully studied by Bergman and co-workers. They reported that after the initial [2+2] cycloaddition with alkynes, e.g. PhCCPh, the metallacyclic intermediate $Cp_2Zr\{N(Xyl)C(Ph)C(Ph)\}$ is subsequently protonated by H_2NXyl to generate the (enamido)amido zirconocene intermediate $Cp_2Zr(NHXyl)\{N(Xyl)C(Ph)C(Ph)H\}$, which undergoes α-elimination to regenerate **1.17**. This base free transient intermediate **1.17** undergoes a rapid protonation reaction with H_2NXyl to yield the bis(amido) zirconocene complex $Cp_2Zr(NHXyl)_2$ (**1.48**) reversibly. The analogous bis(borylamido) zirconocene complex $Cp_2Zr\{NHB(NAr'CH)_2\}_2$ was, however, found to be synthetically unfeasible (Chapter Two), probably due to the highly sterically congested borylamido ligands. The failure of

forming the boryl-enamine is possibly due to its high kinetic barrier, and highly sterically disfavoured formation of (borylenamido)borylamido zirconocene intermediate. In order to overcome these, the more acidic pinacol was employed.

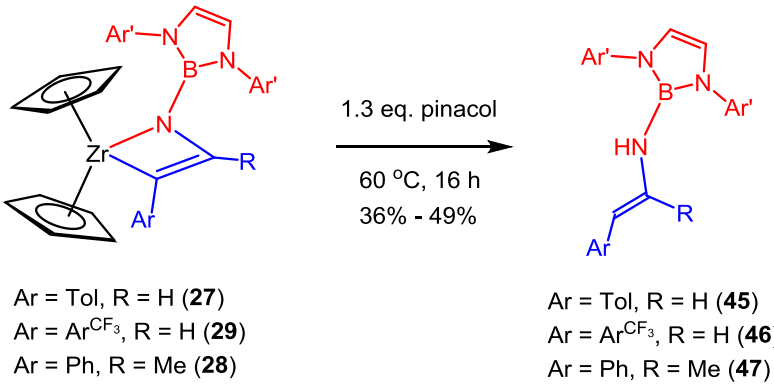

Ar = Tol, R = H (**27**)
Ar = Ar^{CF_3}, R = H (**29**)
Ar = Ph, R = Me (**28**)

Ar = Tol, R = H (**45**)
Ar = Ar^{CF_3}, R = H (**46**)
Ar = Ph, R = Me (**47**)

Equation 3.15

On the NMR tube scale, the *in situ* generated metallacyles **27**, **29** or **28** were reacted with pinacol in C_6D_6. Slow reaction forming corresponding borylenamine product ArC(H)=C(R)N(H)B(NAr'CH)$_2$ (Ar = Tol, R = H (**45**); Ar = Ar^{CF_3}, R = H (**46**); Ar = Ph, R = Me (**47**)) was observed at RT, accompanied by a white precipitate of possible zirconocene pinacolate complexes.[73] Quantitative formation of the corresponding borylenamine was achieved at 60 °C over 16 h, showing only one isomer being formed. On the preparative scale, 1.3 equivalent of pinacol was added into the corresponding *in situ* generated metallacycles (**27**, **29** and **28**) in benzene. After stirring at 60 °C for 16 h, the borylenamines were isolated in 49%, 41% and 36% crystalline yields (Equation 3.15). The ^{11}B NMR spectra of **45**, **46** and **47** show similar signals at 21.0, 20.8 and 21.2 ppm, respectively. The ^{1}H signals display diagnostic NH resonances at 4.16, 4.24 and 3.51 ppm, respectively, as broad doublets (**45** and **46**) having ^{1}H-^{1}H couplings with the adjacent C<u>H</u>, or a singlet (**47**), these confirming that the products are borylenamines, rather than the tautomeric borylimines. The three-bond ^{1}H-^{1}H coupling constants of ArC<u>H</u>=C<u>H</u> of **45** and **46** are 13.7 and 13.6 Hz, respectively, suggesting that they are *trans* isomers.

Diffraction-quality crystals of **45** were grown from a hexane solution at 4 °C. The molecular solid state structure is shown in Figure 3.21, and selected bond distances and angles are listed in Table 3.13. The solid structure confirms that **45** is a borylenamine and exists as a *trans* isomer. The sum of angles subtended for two crystallgraphically independent molecules at N(1) are 358.8(5)° [360.2(5)°] implying sp^2-hybridised N(1).

The torsion angle of B(1)–N(1)···C(27)–C(28) is 169.7° [173.3°] which shows a coplanar geometry of the boryl ring and TolCH=CH moiety, this implying a highly conjugated borylenamine system. Other key structural parameters, including N(1)–C(27) and C(27)–C(28) bond distances, are comparable with the enamine PhC(H)=C(Ph)N(H)Xyl.[1] DFT calculations on the model enamines formed from PhCCH or Ar^{F}CCH and $H_2NB(NMeCH)_2$ found that the enamine tautomer were –7.1 and –8.6 kcal mol^{-1} electronically more stable than the corresponding imides, consistent with the experimental observations.

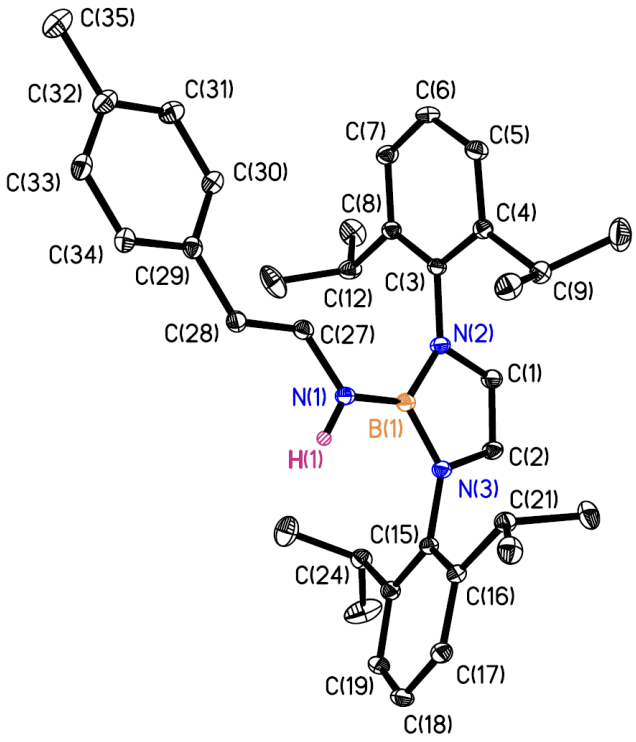

Figure 3.21. Displacement ellipsoid plot (20% probability) of TolC(H)=C(H)N(H)B(NAr'CH)$_2$ (**45**). C–bound H atoms omitted for clarity.

Table 3.13. Selected bond lengths (Å) and angles (°) for TolC(H)=C(H)N(H)B(NAr'CH)$_2$ (**45**). Values in brackets are for the second crystallographically independent molecule.

N(1)–B(1)	1.426(4) [1.432(4)]
B(1)–N(2)	1.441(4) [1.441(4)]
B(1)–N(3)	1.431(4) [1.434(4)]
N(1)–C(27)	1.386(4) [1.386(4)]
C(27)–C(28)	1.331(4) [1.335(4)]
B(1)–N(1)–C(27)	125.8(3) [126.2(3)]
B(1)–N(1)–H(1)	120(3) [116(3)]
C(27)–N(1)–H(1)	113(3) [118(3)]
N(1)–C(27)–C(28)	128.1(3) [127.2(3)]
C(27)–C(28)–C(29)	124.8(3) [124.5(3)]
B(1)–N(1)···C(27)–C(28)	169.7 [173.3]

3.6 Conclusion and Outlook

This Chapter has described the reaction of Group 4 metallocene borylimido complexes with alkynes, giving variable and controllable [2+2] cycloaddition or C–H bond activation reactions. The reaction of Cp$_2$Zr{NB(NAr'CH)$_2$}(py) (**11**) with ^{t}BuCCH showed an initial cycloaddition reaction forming Cp$_2$Zr{N{B(NAr'CH)$_2$}C(H)C(^{t}Bu)} (**25**) as the kinetic product. Further heating of this compound gave a rearrangement reaction *via* C–H bond activation, forming Cp$_2$Zr{NHB(NAr'CH)$_2$}(CC^{t}Bu) (**26**) as the thermodynamic product. The kinetic isotope effect for this rearrangement was measured to be between 2.89(1) and 3.62(2), indicating the RDS is the C–H bond activation. Eyring analyses were carried out, and the extracted small positive activation entropy ($\Delta S^{\ddagger}$ = 5.4(4.8) cal mol^{-1} K^{-1}) suggests that the regenerated ^{t}BuCCH *via* thermolysis remains coordinating on the zirconium centre as a π-adduct, during the C–H bond activation. This was supported by performing crossover reactions by adding TolCCH during the rearrangement of **25**, which shows only a very small amount of the more stable TolCCH incorporated product. This also suggested that the regenerated ^{t}BuCCH strongly coordinated to the zirconium metal giving very slow dissociation even at high temperature.

The reactions of **11** with aryl alkynes, TolCCH and PhCCMe, yielded only the cycloaddition products $Cp_2Zr\{N\{B(NAr'CH)_2\}C(H)C(Tol)\}$ (**27**) and $Cp_2Zr\{N\{B(NAr'CH)_2\}C(Me)C(Ph)\}$ (**28**), respectively. The absence of the C–H bond activation product for the reaction with TolCCH is attributed to the higher thermodynamic stability of the metallacyclic product **27** (also more stable than the C–H bond activation product), which is supported by DFT calculations. Employing the more electron deficient terminal alkynes, $Ar^{CF_3}CCH$ and $Ar^{F}CCH$, the C–H bond activation reactions occurred at RT forming $Cp_2Zr\{NHB(NAr'CH)_2\}(CCAr^{CF_3})$ (**30**) and $Cp_2Zr\{NHB(NAr'CH)_2\}(CCAr^{F})$ (**31**), respectively. The [2+2] cycloaddition with these alkynes can be promoted at elevated temperatures, and proved to undergo the Lewis base dissociation pathway *via* forming the transient complex $Cp_2Zr\{NB(NAr'CH)_2\}$. In all cases, pyridine or DMAP dissociation is found to be the RDS for the [2+2] cycloaddition with alkynes, consistent with earlier studies of organoimido analogues.[72] In contrast, the C–H bond activation of $Cp_2Zr\{NB(NAr'CH)_2\}(L)$ (L = py (**11**), DMAP (**14**)) with $Ar^{F}CCH$ is not *via* base dissociation, showing zero order dependence on [Lewis base] and first order dependence on [Zr] and [$Ar^{F}CCH$]. However, the C–H bond activation shows no KIE, and small intermolecular competition KIE of *ca* 1.5, suggesting the C–H bond activation is not involved in the RDS. These imply that this C–H bond activation undergoes an associative pathway, which is further supported by Eyring analysis showing a large negative activation entropy ($\Delta S^{\ddagger}$ = –30.2(3.1) cal mol^{-1} K^{-1}). This associative pathway is unlikely to involve a zwitterionic intermediate, and is not unique to the borylimido zirconocene complexes (**11** and **14**) since the imido zirconocene $Cp_2Zr(N^{t}Bu)(py)$ (**3.5**) shows similar C–H bond activation and cycloaddition reactions with $Ar^{F}CCH$. Unfortunately, the definitive identity of the associative intermediate for the C–H bond activation of $Ar^{F}CCH$ is still not clear at this stage, but attempts to elucidate *via* DFT are ongoing.

The reactions of $Ar^{F}CCH$ with the hafnium congener $Cp_2Hf\{NB(NAr'CH)_2\}(py)$ (**12**) were faster and show a higher kinetic preference for C–H bond activation. The smaller intermolecular competition KIE of *ca*. 1.0 may reflect a less reversible associative progress, and also suggests that the associative pathway may involve some degree of $Ar^{F}CCH$ pre-coordination with the metal. In contrast, only [2+2] cycloaddition was observed for the titanium congener $Cp_2Ti\{NB(NAr'CH)_2\}(py)$ (**1.117**).

DFT calculations and QTAIM analyses performed on the model complexes: 1,2-cycloaddition (**5Q_R',R**), 2,1-cycloaddition (**6Q_R',R**) and C–H bond activation (**4Q_R',R**) showed the trend that more electron-deficient terminal alkynes result in more stable azametallacycles. The acetylide counterpart (C–H bond activation) is also stabilised in the same trend but by a smaller magnitude. In addition, electron-deficient aryl alkynes favour the 1,2-cycloaddition electronically and sterically compared to 2,1-cycloaddition by stabilising the negative charge on alkyne C_α and facilitating delocalisation of the N_{im} lone pair and C=C π-bond.

In addition, attempts were made to investigate the potential hydro-borylamination. Unfortunately, the protonation of metallacycles by borylamines were unsuccessful. However, the reaction with more acidic pinacol yielded the borylenamine product $ArC(H)=C(R)N(H)B(NAr'CH)_2$ (Ar = Tol, R = H (**45**); Ar = Ar^{CF_3}, R = H (**46**); Ar = Ph, R = Me (**47**) stoichiometrically.

3.7 References

1 P. J. Walsh, A. M. Baranger and R. G. Bergman, *J. Am. Chem. Soc.*, 1992, **114**, 1708–1719.

2 I. Bytschkov and S. Doye, *Eur. J. Org. Chem.*, 2003, **2003**, 935–946.

3 S. Doye, *Synlett*, 2004, **2004**, 1653–1672.

4 A. V Lee and L. L. Schafer, *Eur. J. Inorg. Chem.*, 2007, 2243–2255.

5 T. E. Müller, K. C. Hultzsch, M. Yus, F. Foubelo and M. Tada, *Chem. Rev.*, 2008, **108**, 3795–3892.

6 Y. Li, Y. Shi and A. L. Odom, *J. Am. Chem. Soc.*, 2004, **126**, 1794–1803.

7 S. Banerjee, Y. Shi, C. Cao and A. L. Odom, *J. Organomet. Chem.*, 2005, **690**, 5066–5077.

8 S. Banerjee, E. Barnea and A. L. Odom, *Organometallics*, 2008, **27**, 1005–1014.

9 K. Weitershaus, H. Wadepohl and L. H. Gade, *Organometallics*, 2009, **28**, 3381–3389.

10 A. D. Schwarz, C. S. Onn and P. Mountford, *Angew. Chem. Int. Ed.*, 2012, **51**, 12298–12302.

11 P. D. Schweizer, H. Wadepohl and L. H. Gade, *Organometallics*, 2013, **32**, 3697–3709.

12 A. L. Odom, *Dalton Trans.*, 2005, 225–233.

13 C. Cao, Y. Shi and A. L. Odom, *Org. Lett.*, 2002, **4**, 2853–2856.

14 J. S. Johnson and R. G. Bergman, *J. Am. Chem. Soc.*, 2001, **123**, 2923–2924.

15 A. Tillack, H. Jiao, I. G. Castro, C. G. Hartung and M. Beller, *Chem. - Eur. J.*, 2004, **10**, 2409–2420.

16 L. Ackermann and R. Born, *Tetrahedron Lett.*, 2004, **45**, 9541–9544.

17 V. Khedkar, A. Tillack, M. Michalik and M. Beller, *Tetrahedron Lett.*, 2004, **45**, 3123–3126.

18 J. D. Selby, C. D. Manley, M. Feliz, A. D. Schwarz, E. Clot and P. Mountford, *Chem. Commun.*, 2007, **733**, 4937–4939.

19 A. D. Schofield, A. Nova, J. D. Selby, C. D. Manley, A. D. Schwarz, E. Clot and P. Mountford, *J. Am. Chem. Soc.*, 2010, **132**, 10484–10497.

20 B. Clough, DPhil Thesis, University of Oxford, 2016.

21 K. Weitershaus, B. D. Ward, R. Kubiak, C. Müller, H. Wadepohl, S. Doye and L. H. Gade, *Dalton Trans.*, 2009, 4586–4602.

22 J. L. Polse, A. W. Kaplan, R. A. Andersen and R. G. Bergman, *J. Am. Chem. Soc.*, 1998, **120**, 6316–6328.

23 J. L. Polse, R. A. Andersen and R. G. Bergman, *J. Am. Chem. Soc.*, 1998, **120**, 13405–13414.

24 L. C. Stevenson, DPhil Thesis, University of Oxford, 2015.

25 H. M. Hoyt and R. G. Bergman, *Angew. Chem. Int. Ed. Engl.*, 2007, **46**, 5580–5582.

26 J. D. Selby, C. Schulten, A. D. Schwarz, A. Stasch, E. Clot, C. Jones and P. Mountford, *Chem. Commun.*, 2008, 5101–5103.

27 N. Vujkovic, J. L. Fillol, B. D. Ward, H. Wadepohl, P. Mountford and L. H. Gade, *Organometallics*, 2008, **27**, 2518–2528.

28 B. D. Ward, A. Maisse-Francois, P. Mountford and L. H. Gade, *Chem. Commun.*, 2004, 704–705.

29 D. J. M. Trösch, P. E. Collier, A. Bashall, L. H. Gade, M. McPartlin, P. Mountford and S. Radojevic, *Organometallics*, 2001, **20**, 3308–3313.

30 A. Bashall, P. E. Collier, L. H. Gade, M. McPartlin, P. Mountford and D. J. M. Trösch, *Chem. Commun.*, 1998, 2555–2556.

31 J. D. Selby, C. D. Manley, A. D. Schwarz, E. Clot and P. Mountford, *Organometallics*, 2008, **27**, 6479–6494.

32 N. Vujkovic, B. D. Ward, A. Maisse-François, H. Wadepohl, P. Mountford and L.

H. Gade, *Organometallics*, 2007, **26**, 5522–5534.

33 P. J. Walsh, M. J. Carney and R. G. Bergman, *J. Am. Chem. Soc.*, 1991, **113**, 6343–6345.

34 S. Y. Lee and R. G. Bergman, *Tetrahedron*, 1995, **51**, 4255–4276.

35 A. M. Baranger, P. J. Walsh and R. G. Bergman, *J. Am. Chem. Soc.*, 1993, **115**, 2753–2763.

36 J. L. Polse, R. A. Andersen and R. G. Bergman, *J. Am. Chem. Soc.*, 1995, **117**, 5393–5394.

37 R. E. Blake, D. M. Antonelli, L. M. Henling, W. P. Schaefer, K. I. Hardcastle and J. E. Bercaw, *Organometallics*, 1998, **17**, 718–725.

38 B. A. Clough, S. Mellino, E. Clot and P. Mountford, *J. Am. Chem. Soc.*, 2017, **139**, 11165–11183.

39 H. E. Bryndza, L. K. Fong, R. A. Paciello, W. Tam and J. E. Bercaw, *J. Am. Chem. Soc.*, 1987, **109**, 1444–1456.

40 P. L. Holland, R. A. Andersen, R. G. Bergman, J. Huang and S. P. Nolan, *J. Am. Chem. Soc.*, 1997, **119**, 12800–12814.

41 P. L. Holland, R. A. Andersen and R. G. Bergman, *Comments Inorg. Chem.*, 1999, **21**, 115–129.

42 L. E. Schock and T. J. Marks, *J. Am. Chem. Soc.*, 1988, **110**, 7701–7715.

43 R. F. W. Bader, *Atoms in Molecules: A Quantum Theory*, Oxford University Press, Oxford, 1990.

44 F. Weinhold and C. R. Landis, *Chem. Educ. Res. Pr.*, 2001, **2**, 91–104.

45 L. R. Groom, DPhil Thesis, University of Oxford, 2014.

46 F. Brotzel, B. Kempf, T. Singer, H. Zipse and H. Mayr, *Chem. - Eur. J.*, 2007, **13**, 336–345.

47 J. L. Bennett and P. T. Wolczanski, *J. Am. Chem. Soc.*, 1997, **119**, 10696–10719.

48 C. C. Cummins, S. M. Baxter and P. T. Wolczanski, *J. Am. Chem. Soc.*, 1988, **110**, 8731–8733.

49 C. C. Cummins, C. P. Schaller, G. D. Van Duyne, P. T. Wolczanski, A. W. E. Chan and R. Hoffmann, *J. Am. Chem. Soc.*, 1991, **113**, 2985–2994.

50 C. P. Schaller, C. C. Cummins, P. T. Wolczanski and N. York, *J. Am. Chem. Soc.*, 1996, **118**, 591–611.

51 L. M. Slaughter, P. T. Wolczanski, T. R. Klinckman and T. R. Cundari, *J. Am. Chem. Soc.*, 2000, **122**, 7953–7975.

52 T. H. Lowry and K. S. Richardson, *Mechanism and Theory in Organic Chemistry*, Harper and Row, New York, 1987.

53 B. K. Carpenter, *Determination of Reaction Mechanisms*, Wiley-Interscience, New York, 1984.

54 S. K. Podiyanachari, R. Fröhlich, C. G. Daniliuc, J. L. Petersen, C. Mück-Lichtenfeld, G. Kehr and G. Erker, *Angew. Chem. Int. Ed.*, 2012, **51**, 8830–8833.

55 S. K. Podiyanachari, R. Frohlich, C. G. Daniliuc, J. L. Petersen, G. Kehr, G. Erker, N. Suzuki, S. Yuasa, K. Hagimori, S. Inoue, T. Asada, T. Takemoto and Y. Masuyama, *Dalton. Trans.*, 2012, **41**, 10811–10816.

56 G. Erker, W. Froemberg, R. Benn, R. Mynott, K. Angermund and C. Krueger, *Organometallics*, 1989, **8**, 911–920.

57 R. Choukroun, B. Donnadieu, J.-S. Zhao, P. Cassoux, C. Lepetit and B. Silvi, *Organometallics*, 2000, **19**, 1901–1911.

58 P. J. Walsh, F. J. Hollander and R. G. Bergman, *J. Organomet. Chem.*, 1992, **428**, 13–47.

59 J. C. Green, M. L. H. Green, J. T. James, P. C. Konidaris, G. H. Maunder and P. Mountford, *J. Chem. Soc., Chem. Commun.*, 1992, 1361–1365.

60 S. A. Westcott, A. K. Kakkar, G. Stringer, N. J. Taylor and T. B. Marder, *J. Organomet. Chem.*, 1990, **394**, 777–794.

61 A. D. Schofield, DPhil Thesis, University of Oxford, 2012.

62 S. C. Dunn, P. Mountford and D. A. Robson, *J. Chem. Soc. Dalton. Trans.*, 1997, **2**, 293–304.

63 I. Castillo and T. Don Tilley, *J. Organomet. Chem.*, 2002, **643**–**644**, 431–440.

64 A. D. Schofield and P. Mountford, Unpublished results.

65 B. Clough and P. Mountford, Unpublished results.

66 P. J. Walsh, F. J. Hollander and R. G. Bergman, *Organometallics*, 1993, **12**, 3705–3723.

67 S. Y. Lee and R. G. Bergman, *J. Am. Chem. Soc.*, 1995, **117**, 5877–5878.

68 S. Y. Lee and R. G. Bergman, *J. Am. Chem. Soc.*, 1996, **118**, 6396–6406.

69 C. J. Harlan, J. A. Tunge, B. M. Bridgewater and J. R. Norton, 2000, 2365–2372.

70 B. A. Clough, S. Mellino, A. V Protchenko, M. Slusarczyk, L. C. Stevenson, M. P. Blake, B. Xie, E. Clot and P. Mountford, *Inorg. Chem.*, 2017, **56**, 10794–10814.

71 E. M. Simmons and J. F. Hartwig, *Angew. Chem. Int. Ed.*, 2012, **51**, 3066–3072.

72 A. P. Duncan and R. G. Bergman, *Chem. Rec.*, 2002, **2**, 431–445.

73 J. Scholz, M. Dlikan and K. Thiele, *J. für Prakt. Chemie*, 1988, **330**, 808–810.

Chapter Four

Reactions of zirconium borylimides with polar substrates

4.1 Overview

As mentioned in Chapter One, the Group 4 imido and hydrazido complexes have been utilised in a variety of important organic and inorganic transformations. This commonly offers advantages, such as greater selectivity, mild conditions and increased reaction rates, over traditional approaches to the formation of new carbon–carbon/heteroatom bonds. Reactivity studies of Group 4 imido and hydrazido complexes have displayed fruitful reactivities with small unsaturated molecules. Such reactions usually involve a [2+2] cycloaddition between the polar π-bond to the imido ligand and electrophilic substrates. In particular, the reactions with unsaturated polar substrates, such as heteroallenes and carbonyls have been of considerable interest over the years.

Reactions of the first isolated Group 4 imido complex $Cp_2Zr(N^tBu)(THF)$ (**1.4**) with polar substrates have been extensively explored by Bergman and co-workers.[1–9] In this Chapter, the reactions of a zirconocene borylimido complex with heteroallenes, carbonyls and strained heterocycles will be described and compared to reactions of Bergman's zirconocene imido complex **1.4** with those small molecules. For example, the reactions of **1.4** with ketones resulted in the formation of enolate-amide zirconocene complexes by an α-hydrogen atom abstraction.[7] In contrast, the reaction with aldehydes RC(O)H (R = Ph or ^{i}Pr) yielded corresponding imines $RC(N^tBu)H$ and oligomeric $[Cp_2ZrO]_n$ *via* a [2+2] cycloaddition then cycloreversion.[2,7] Similarly, reaction with CS_2 proceeds through a [2+2] cycloaddition giving the thioazametallacyclobutane intermediate **4.1**, and subsequently generates the sulfido zirconocene complex $[Cp_2Zr(\mu\text{-}S)]_2$ with the concurrent extrusion of ^{t}BuNCS. This is accompanied by a small amount of ^{t}BuNCN^tBu, which is formed in a secondary reaction of **1.4** with generated ^{t}BuNCS.[6] Compound ^{t}BuNCN^tBu can also be independently generated in the reaction of **1.4** with ^{t}BuNCO, accompanied by formation of oligomeric $[Cp_2ZrO]_n$ (Scheme 4.1).[1]

Direct routes to incorporate R_2BN "building blocks" into organic substrates are rather limited, and none go directly from amines or metal-coordinated R_2BN. The only routes reported for the incorporating R_2BN directly are *via* a transient borylnitrene, which is *in situ* generated from corresponding borylazide by UV light irradiation, reported by Bettinger.[10–17] For example, C–H bond activation of CH_4 was observed, forming MeN(H)BCat (Cat = $C_6H_4O_2$), from the reaction of transient borylnitrene [NBCat] with methane under UV irradiation,[10] and the corresponding isocyanate OCNBCat can be

alternatively formed when reacted with CO.[12] Such borylisocyanates were generally formed *via* salt metathesis reactions. For example, the reaction of $ClB(N^tBuCH)_2$ with AgNCO gives $OCNB(N^tBuCH)_2$.[18] Other compounds, such as borylimines, have also been obtained *via* salt metathesis.[19,20]

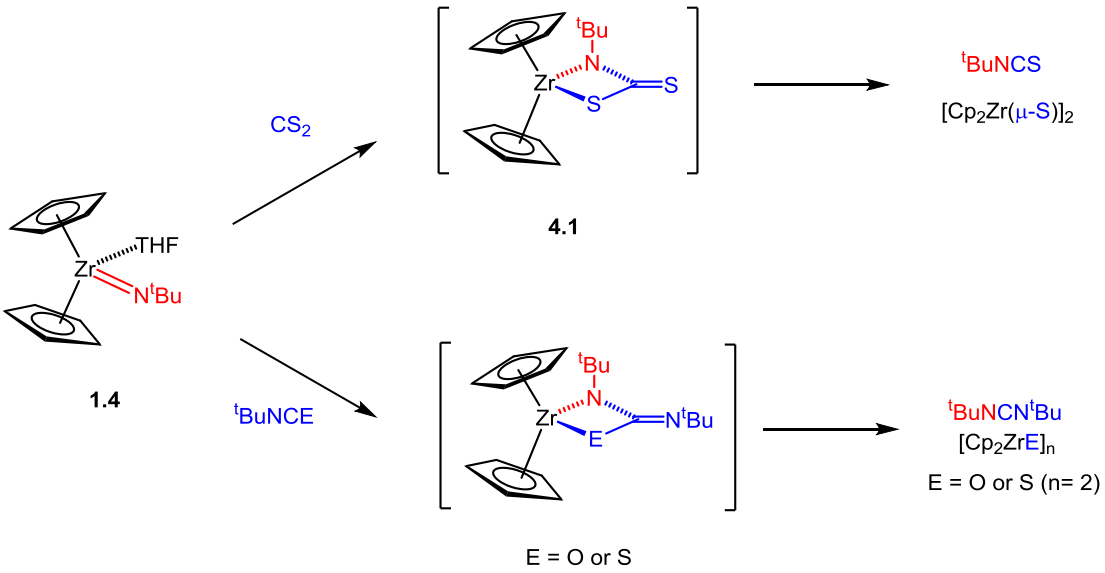

Scheme 4.1. Exemplar reactions of $Cp_2Zr(N^tBu)(THF)$ (**1.4**) with CS_2 and ^{t}BuNCE (E = O or S).[1,6]

This Chapter will describe the reactions of $Cp_2Zr\{NB(NAr'CH)_2\}(py)$ (**11**) with small polar unsaturated molecules. Firstly, functional group exchange reactions with heteroallenes, CE_2 and PhCNE (X = O or S) resulting in the formation of $OCNB(NAr'CH)_2$, $SCNB(NAr'CH)_2$ and $PhNCNB(NAr'CH)_2$ respectively, will be described. Next, its reactions with aldehydes, ketones and esters will be discussed along with DFT studies. Novel reactivity observed between the borylimido zirconocene complex and esters, eliminating ketene and ketene self-trapping, will be described along with the structural characterisation of the reaction products, and compared to reactions with acetyl chloride, acetamide and thioesters. The intramolecular ketene elimination from esters and thioesters will also be further investigated through evidence obtained from the kinetic analysis and the extraction of thermodynamic activation parameters from kinetic measurements. Finally, the reactions with strained heterocycles, epoxides and episulfides will be explored.

4.2 Reactions of $Cp_2Zr\{NB(NAr'CH)_2\}(py)$ (11) with CO_2, CS_2 and PhNCE (E = O or S)

When a degassed C_6D_6 solution of $Cp_2Zr\{NB(NAr'CH)_2\}(py)$ (**11**) in an NMR tube was exposed to an atmosphere of CO_2, and the reaction progress followed by ^1H NMR spectroscopy, colour changing from orange-red to pale yellow accompanied by formation of a white precipitate was observed over 16 h at RT. The appearance of a new single product was observed along with the loss of the signal corresponding to the Cp ligands from the ^1H NMR spectrum of the reaction mixture. Similarly, **11** reacted with CS_2 at RT and a single product was formed quantitatively over 16 h. In this case, no precipitate formed and the resonances corresponding to the Cp ligands could be observed in the ^1H NMR spectrum of the reaction mixture.

The observations above suggest that they undergo analogous reactions to those of **1.4** and titanium imido/hydrazido complexes,[2,7,21–24] in which initial [2+2] cycloaddition of the heteroallenes with the M–N multiple bond is followed by extrusion of an organic compound. Scaling up the reactions of **11** with CO_2 and CS_2, the organic products were separated and confirmed to be a borylisocyanate and a borylisothiocyanate $ECNB(NAr'CH)_2$ (E = O (**48**), S (**49**)), respectively, as a result of overall functional group exchange of the borylimido unit with CE_2. The second E atom of CE_2 goes to form the insoluble oligomeric $[Cp_2ZrO]_n$ or the soluble dimeric $[Cp_2Zr(\mu\text{-}S)]_2$ (Scheme 4.2). The possible side reactions of **11** with generated **48** and **49** were not observed here, unlike the analogous reactions of **1.4** (Section 4.1), possibly due to the bulky boryl moieties in both **11** and **48** or **49**.

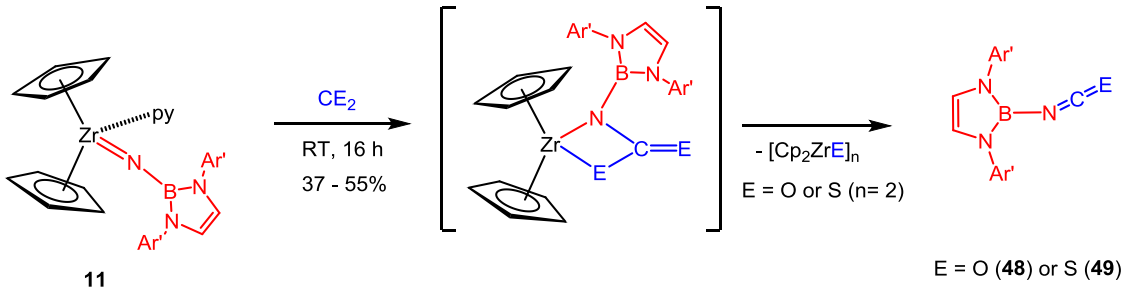

Scheme 4.2. Reactions of $Cp_2Zr\{NB(NAr'CH)_2\}(py)$ (**11**) with CO_2 and CS_2 at RT, forming $ECNB(NAr'CH)_2$ (E = O (**48**), S (**49**)), respectively.

On the preparative scale, **48** and **49** were isolated by extraction using hexane in 55% and 37% crystalline yield, respectively. The ^1H NMR spectra of the borylisocyanate **48** and

the borylisothiocyanate **49** display similar resonances corresponding to the boryl moiety, including a septet (4 H) and two doublets (12 H each) attributed to the four isopropyl groups, and a singlet (2 H) attributed to the backbone protons of the boryl ring. Very low intensity ^{13}C signals at 125.7 and 143.2 ppm of **48** and **49** respectively, were observed corresponding to the central carbon in the iso(thio)cyanate moiety. These values are comparable to those reported in the analogous compounds $ECNB(N^tBuCH)_2$ (E = O (**4.2**), S (**4.3**)) of 123.9 and 140.5 ppm, which were formed from the reaction of $ClB(N^tBuCH)_2$ with AgECN *via* salt metathesis.[18] The IR spectra of **48** and **49** show strong bands at 2305 and 2092 cm^{-1} respectively. These are assigned to the antisymmetric stretches of the NCE units which are comparable to those reported by Weber *et al.* in **4.2** and **4.3** of 2317 and 2122 cm^{-1}, respectively.[18] The mechanism of the reactions of zirconium and titanium imides with CO_2 and CS_2 are well established. As described above, initial cycloaddition to form a (thio)carbamate-type complex takes place. However, this is not observed in the case of the formation of **48** and **49**, which undergoes further extrusion of an iso(thio)cyanate *via* retro-[2+2]. Previous work on titanium imido compounds from our research group has investigated the effect of different imido functionalities on the outcome and rate of reactions with CO_2.[22] It was shown that the transition state on the final step of isocyanate extrusion is stabilised by increased steric bulk, thus explaining the generation of **48** and **49** without observing the short-lived (thio)carbamate-type intermediates.

Compounds **48** and **49** have been also independently synthesised and structurally characterised by another DPhil student in our research group,[25] by either analogous reactions of $Cp^*Ti(hpp)\{NB(NAr'CH)_2\}$ (**4.4**) with CE_2, or the salt metathesis reactions of $BrNB(NAr'CH)_2$ with AgECN. The reactions of **4.4** with CO_2 and CS_2 were much slower and required higher temperature than those of **11**, reflecting a more sterically crowded titanium centre. This resulted in the reaction of **4.4** with other more bulky heteroallenes (e.g. TolNCO) being more kinetically disfavoured.[26]

On the NMR tube scale in C_6D_6, reaction of **11** with PhNCE (E = O or S) was observed, analogous to the reactions with CE_2, but requiring elevated temperature and extended reaction time, which is expected as the compounds PhNCE are more sterically hindered. The reaction of **11** with one equivalent of PhNCO at 65 °C gave a slow colour change to pale yellow from red-orange along with $[Cp_2ZrO]_n$ precipitating over 24 h. In contrast, soluble $[Cp_2Zr(\mu\text{-}S)]_2$ was observed in the reaction with PhNCS under the same reaction

conditions, both similar to the reactions with CO_2 and CS_2. However, the reaction with PhNCE gave the same organic product, borylphenylcarbodiimide $PhNCNB(NAr'CH)_2$ (**50**) in both cases (Scheme 4.3).

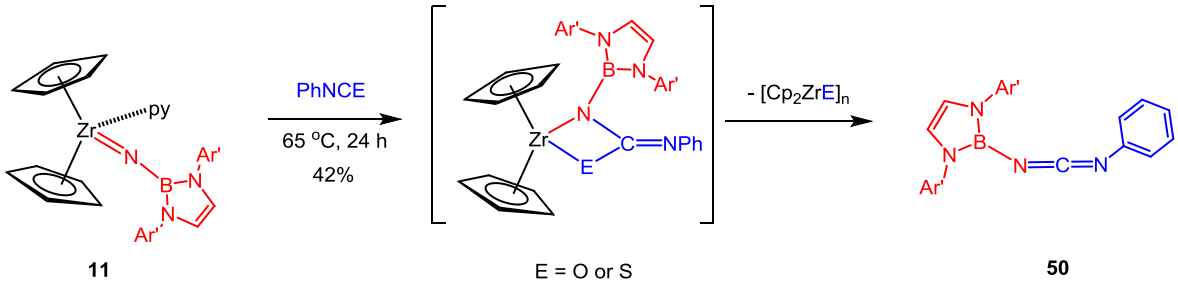

Scheme 4.3. Reactions of $Cp_2Zr\{NB(NAr'CH)_2\}(py)$ (**11**) with PhNCE (E = O or S), forming $PhNCNB(NAr'CH)_2$ (**50**).

On the preparative scale, **50** was formed under the same reaction condition as the NMR tube scale. It was then separated by hexane extraction and isolated in 42% crystalline yield. The ^1H NMR spectrum of **50** shows similar resonances of the borylimine moiety to those in **48** and **49**. In addition, the signals at 6.89, 6.76 and 6.36 ppm are attributed to the protons of *m*-, *p*- and *o*-phenyl, respectively. In the ^{13}C NMR spectrum, a very low intensity and broad signal attributed to the central carbon in the carbodiimide moiety is observed at 128.7 ppm. This value is very similar to that of the analogous mono-borylated carbodiimide $^tBuNCNB(NMeCH_2)_2$ (**4.5**) of 127.8 ppm, and comparable to those of the di-borylated carbodiimides $(RMeN)_2BNCNB(NMeR)_2$ (R = CH_2 (**4.6**) or C_6H_4 (**4.7**)) of 123.0 and 123.2 ppm, respectively, which were all synthesised by Haubold though the reactions of $R'NCNSiMe_3$ with $XB(NMeR)_2$ (R' = $SiMe_3$ or ^tBu, X = Cl or Br).[27] These values are also similar to that of $R'NCNSiMe_3$ (R' = $SiMe_3$ or ^tBu) of 130.7 and 123.9 ppm, respectively.[28] The IR spectrum of **50** shows a very intense band at 2182 cm^{-1}, assigned to the antisymmetric stretches of the NCN units, comparable to the values of **4.5** – **4.7**: 2170, 2220 and 2250 cm^{-1}, respectively.[27]

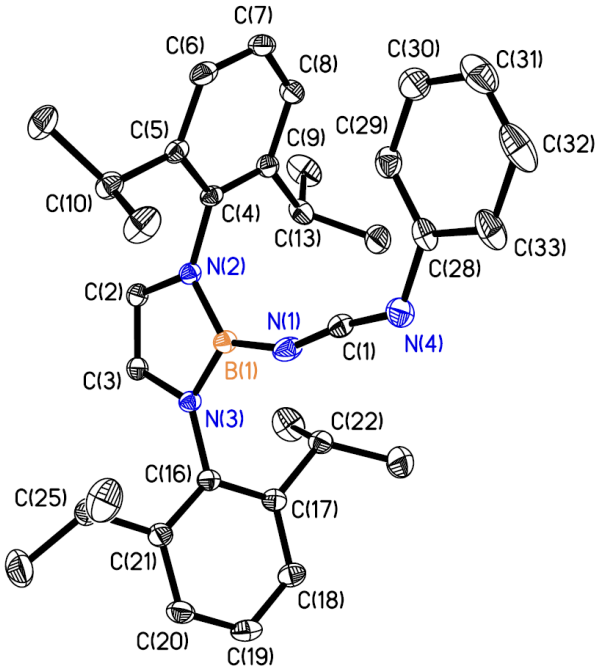

Figure 4.1. Displacement ellipsoid plot (25% probability) of PhNCNB(NAr'CH)$_2$ (**50**). H atoms omitted for clarity.

Table 4.1. Selected bond lengths (Å) and angles (°) for PhNCNB(NAr'CH)$_2$ (**50**).

B(1)–N(1)	1.430(3)	N(1)–B(1)–N(2)	126.7(2)
B(1)–N(2)	1.426(3)	N(1)–B(1)–N(3)	126.48(19)
B(1)–N(3)	1.421(2)	B(1)–N(1)–C(1)	155.8(2)
N(1)–C(1)	1.183(3)	C(28)–N(4)–C(1)	126.5(2)
N(4)–C(1)	1.219(3)	N(1)–C(1)–N(4)	170.9(2)

Diffraction-quality crystals of **50** were grown from hexane at –30 °C. The solid state structure is shown in Figure 4.1, along with selected bond lengths and angles in Table 4.1. The NCN unit is close to linear, with an N(1)–C(1)–N(4) angle of 170.9(2)°. This is comparable to that of the analogous bis(boryl)carbodiimide compound **4.7** of 172°,[27] and those of RNCNR (R = Xyl or 2,6-$C_6H_3{}^iPr$) of 167.82(15)° and 169.3(2)°, respectively. In **50**, the boryl ring is almost coplanar with the carbodiimide moiety, showing the N(2)–B(1)···N(1)–C(1) torsion angle of 11.7°, presumably to maximise conjugation of the N=C=N π bonds with the boryl π-system. In addition, the phenyl ring is also coplanar to them with the C(29)–C(28)···N(4)–C(1) torsion angle of 12.3°, and shows an "Z-configuration" in the solid state. This is probably favoured by the intramolecular C–H···π

interaction between the H(291) atom bonded to C(29) and the π-system of the top Ar' ring of the borylimine fragment (Figure 4.1). The H(291)···Ar' centroid distance is *ca* 2.67 Å, similar to the mean value of the sp^2-C–H···π distance of 2.73 Å in the organic compounds, which provides a stabilisation energy of *ca.* 1.5 – 2.5 kcal mol^{-1}.[29,30] It is also reflected by the R–N–C(1) (R = B(1) or C(28)) angles, where the B(1)–N(1)–C(1) angle of 155.8(2)° is found to be comparable to those of **4.7** of 163.1° and 145.9°,[27] and in the range of the values found in bis(aryl)-carbodiimides of 123 to 180°,[31] while, in contrast, the C(28)–N(4)–C(1) angle of 126.5(2)° is found at the low end of the range, which is in order to make the phenyl and Ar' rings closer in space to provide a short contact between H(291) and the centroid of Ar' ring.

Similar reactions between **1.4** and isocyanates have been previously studied by Bergman (Section 4.1), which initially form a (thio)ureate-type complex followed by extrusion of carbodiimide *via* retro-[2+2]. The formation of **50** was speculated to follow the same pathway, which is analogous to the formation of **48** and **49**. Like the reactions with CE_2, the (thio)ureate-type intermediates were again not observed here before extrusion to give **50**, as the steric bulk of the boryl moiety favours the extrusion reaction.

4.3 Reactions of $Cp_2Zr\{NB(NAr'CH)_2\}(py)$ (11) with organic carbonyl compounds

4.3.1 Reactions of $Cp_2Zr\{NB(NAr'CH)_2\}(py)$ (11) with tolylaldehyde and acetophenone

Reaction of $Cp_2Zr\{NB(NAr'CH)_2\}(py)$ (**11**) with one equivalent of TolC(O)H, as a representative aldehyde, gave the insoluble oxozirconocene oligomer $[Cp_2ZrO]_n$ and the organic metathesis product $TolC(H)NB(NAr'CH)_2$ (**51**, Equation 4.1). The reaction was instantaneous and quantitative at RT on the NMR tube scale, and **51** was isolated in 74% yield on the preparative scale, in which **51** was easily separated from the insoluble $[Cp_2ZrO]_n$ by hexane extraction. Borylimine **51** is postulated to be formed *via* an initial [2+2] cycloaddition, followed by a fast extrusion reaction. Such reactions of the imido zirconocene complex $Cp_2Zr(N^tBu)(THF)$ (**1.4**) with aldehydes producing the corresponding imines have been reported by Bergman, as mentioned in Section 4.1.[7]

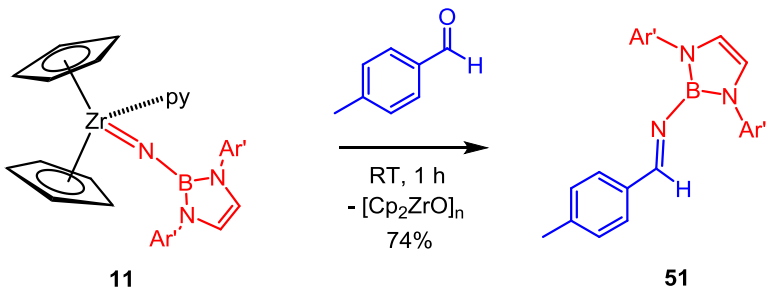

Equation 4.1

The solution ^{1}H, ^{11}B and ^{13}C NMR spectra of **51** are fully consistent with the depicted structure in Equation 4.1. A sharp singlet attributed to the N=C<u>H</u> imine proton at 8.66 ppm, with an HSQC correlation to the ^{13}C signal of N=<u>C</u>H at 167.6 ppm was observed. The borylimine product has been assigned as the thermodynamically more stable *E*-configuration where the steric repulsion between the bulky boryl and tolyl moieties is minimised. DFT calculations performed by Prof. Philip Mountford show that the *E*–isomer is –5.9 and –2.0 kcal mol^{-1}, respectively, more stable than the linear and *Z*–isomers at 298 K. The experimentally observed resonance at 24.3 ppm in the ^{11}B NMR shift is in good agreement with the computed value for the *E*-isomer of 24.2 ppm, as opposed to the values of 25.6 ppm for the *Z*-isomer and 20.7 ppm for the linear isomer. Additionally, a band at 1661 cm^{-1} in the solid state IR spectrum (Nujol mull) attributed to ν(C=N) was observed, again consistent with the computationally determined ν(C=N) frequency of the *E*-isomer (1632 cm^{-1}), rather than that of the *Z*-isomer (1701 cm^{-1}) or the linear isomer (1836 cm^{-1}).

Compound **51** is the first example of an organic borylimine compound containing a bent C=N–B linkage. Several other borylimines, such as dimeric $[Ph_2CNBCat]_2$ (**4.8**) and monomeric Ph_2CNBPh_2 (**4.9**) and $PhC(H)NB(Mes)_2$ (**4.10**), have previously been reported in the literature.[19] Rather than the bent C=N–B linkage of **51**, those monomeric borylimines **4.9** and **4.10** both contain a linear C=N=B linkage which is reflected by the IR spectra, showing an intense ν(C=N=B) band in the region 1765 – 1820 cm^{-1}. This difference is caused by the flanking nitrogen atoms in the boryl ring (**51**), in which the lone pairs compete with the nitrogen in the imine linkage for the boron p-orbital, consequently decreasing the bond order of C=<u>N–B</u>. A similar observation has been found by comparing the compounds Ph_2CNBPh_2 (**4.9**), $(PhCN)_2BPh$[20] and $(Ph_2C=N)_3B$,[32] where the N=B bond order decreases, when more nitrogen atoms are bound to the boron atom, in the sequence of Ph_2CNBPh_2 > $(PhCN)_2BPh$ > $(Ph_2CN)_3B$ with the IR absorption

stretches being of 1790, 1672 and 1667 cm^{-1}, respectively,[19] the lowest value being comparable with that observed in **51** of 1661 cm^{-1}.

An attempted reaction of $Cp_2Zr\{NB(NAr'CH)_2\}(py)$ (**11**) with benzophenone, Ph_2CO, however, showed negligible conversion at 60 °C over 16 h. This is presumably due to the elevated kinetic barrier by the steric bulk of a second phenyl substituent compared to the hydrogen atom in TolC(O)H. In contrast, when **11** reacted with acetophenone (PhC(O)Me), a borylimine product was not generated. Instead, the borylamido zirconocene enolate complex $Cp_2Zr\{NHB(NAr'CH)_2\}\{OC(CH_2)Ph\}$ (**52**) was formed quantitatively by apparent α-hydrogen atom abstraction. On the preparative scale, **11** was mixed with PhC(O)Me in benzene, and stirred at RT for 16 h, resulting in the formation of **52** as a pale yellow oil in 66% yield. The proposed structure of compound **52** is depicted in Equation 4.2 with oxygen binding to the zirconium, where the O–bound form generally exists in the early transition metal enolates while late transition metal enolates are mostly the C–bound form.[33–38] Similar reactions of the imido zirconocene complex **1.4** with a range of ketones have been reported by Bergman and co-workers, forming analogous organoamido zirconocene enolate products.[7]

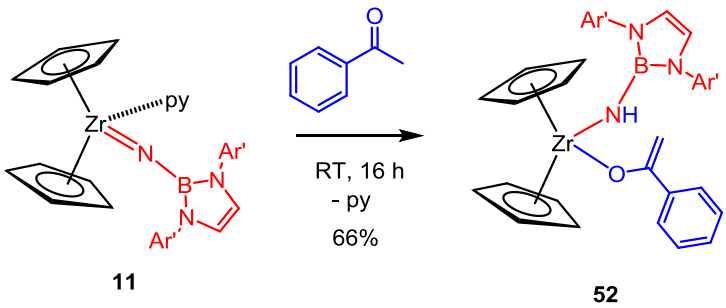

11 **52**

Equation 4.2

In the ^{11}B NMR spectrum of **52**, a resonance at 25.0 ppm was observed which is diagnostic for the formation of a borylamido zirconocene complex supporting the hydrogen atom abstraction from acetophenone. The ^{1}H NMR spectrum of **52** shows a borylamido moiety containing a broad N<u>H</u> singlet, one Cp singlet (10 H) and the resonances for an acetophenone enolate moiety. The terminal vinyl protons at 3.93 and 3.54 ppm with an HSQC correlation to a ^{13}C signal of OC(Ph)<u>C</u>H_2 at 87.0 ppm and an HMBC correlation to a ^{13}C signal of O<u>C</u>(Ph)CH_2 at a high chemical shift of 165.7 ppm were observed, all consistent with reported values in the organoamido zirconocene enolate analogues.[7]

4.3.2 Reactions of $Cp_2Zr\{NB(NAr'CH)_2\}(py)$ (11) with esters

From the reactions of **11** with organic carbonyl compounds, acetophenone and tolylaldehyde, different reaction outcomes were found depending on the accessibility of any α-hydrogen atoms. Since no reactions of metal–nitrogen multiple bonded complexes with MeC(O)X (X is a heteroatom or a heteroatom-containing group) have been reported, it was of interest to expand the chemistry firstly to esters which also contain accessible α-hydrogen atoms, but are considerably less acidic,[39] consistent with the DFT calculated ΔG between the keto and enol forms: +14.7 kcal mol^{-1} for PhC(O)Me; +24.0 kcal mol^{-1} for MeC(O)SMe; +27.8 kcal mol^{-1} for $MeC(O)NMe_2$; and +30.9 kcal mol^{-1} for $MeCO_2Me$ (full B3PW91/Def2TZVP systems with dispersion and solvent correction).

4.3.2.1 Reactions of $Cp_2Zr\{NB(NAr'CH)_2\}(py)$ (11) with $MeCO_2R$ (R = ^{i}Pr, Et, Me)

When compound **11** was reacted with $MeCO_2R$ (R = ^{i}Pr, Et), the borylamido enolate zirconocene complexes, $Cp_2Zr\{NHB(NAr'CH)_2\}\{OC(CH_2)OR\}$ (R = ^{i}Pr (**53**), Et (**54**)), respectively, were formed by α-hydrogen atom abstraction (Equation 4.3). On the NMR tube scale, compound **54** was quantitatively formed over 16 h at RT, whilst the formation of **53** required a slightly elevated temperature (40 °C) and extended reaction time (20 h) due to the increased bulk of the R substituent. On the preparative scale, **53** and **54** were formed in benzene solutions under the same reaction conditions as on the NMR tube scale, and they were isolated in 54% and 76% yields, respectively.

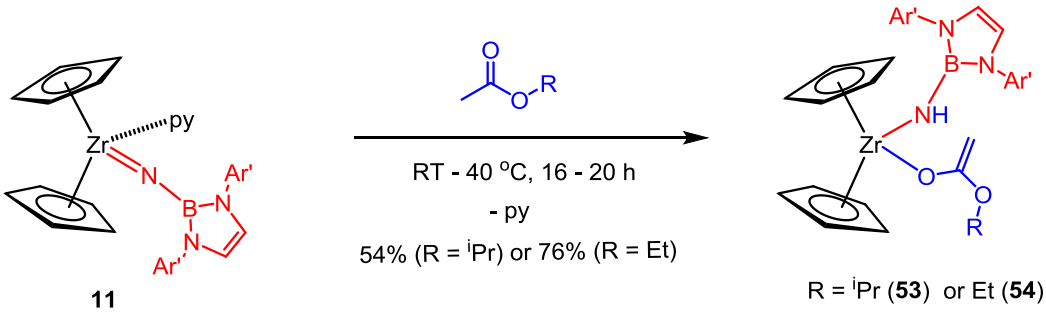

Equation 4.3

The ^{11}B NMR spectra of **53** and **54** both show the same characteristic resonance at 25.0 ppm attributable to a borylamido zirconocene complex. In the ^{1}H NMR spectra (shown for **53**, Figure 4.2), diagnostic NH resonances at 5.19 and 5.23 ppm were observed, respectively, in **53** and **54**. In both cases, the resonances of $OC(OR)=C\underline{H}_2$ were found as an apparent singlet at 3.03 and 2.98 ppm in **53** and **54**, respectively, and are significantly upfield shifted compared to that in **52**. HSQC correlations to the ^{13}C resonances of

OC(OR)=CH_2 were found at 57.4 and 56.1 ppm, respectively, again significantly upfield shifted compared to that in **52** (87.0 ppm). Furthermore, HMBC correlations to a ^{13}C signal of OC(OR)=CH_2 with a high chemical shift at 167.2 and 168.7 ppm respectively were found, comparable with the value for **52** (165.7 ppm). Other ester enolate complexes have been previously reported, in particular for the Group 4 metals, but all of them were synthesised *via* a salt metathesis reaction, and were generally used as a catalyst for methyl methacrylate (MMA) polymerisation.[40–42] Therefore, compounds **53** and **54** were the first examples synthesised *via* an α-hydrogen atom abstraction pathway.

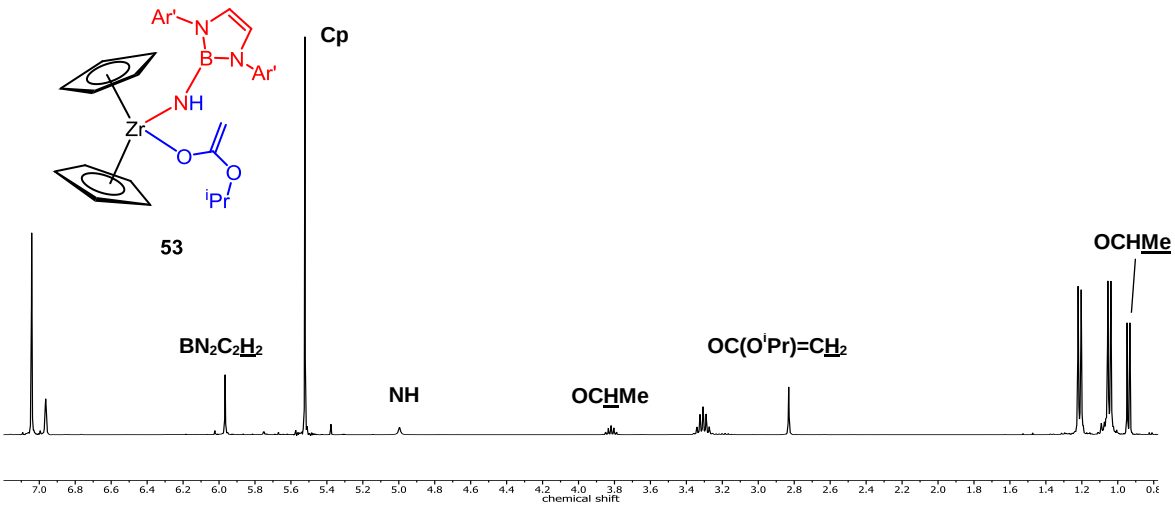

Figure 4.2. ^{1}H NMR spectrum (400.1 MHz) of $Cp_2Zr\{NHB(NAr'CH)_2\}\{OC(CH_2)O^iPr\}$ (**53**) in C_6D_6 at 298 K.

Diffraction-quality crystals of **53** were grown from a hexane solution at –30 °C. The solid-state structure is shown in Figure 4.3, and selected bond lengths and angles are listed in Table 4.2. Molecules of compound **53** possess a pseudo tetrahedral environment at Zr(1), with eclipsed cyclopentadienyl rings. The Zr(1)–N(1)–B(1) linkage of **53** shows Zr(1)–N(1) and N(1)–B(1) single bonds of 2.0907(5) and 1.4389(9) Å, respectively, and a Zr(1)–N(1)–B(1) bond angle of 151.15(13)°, indicating a borylamido moiety, and all parameters are comparable with those described in other borylamido zirconocene analogues in Chapter Two. The sum of angles subtended at C(27) are 360(13)°, confirming the sp^2-hydridised nature of this atom. The Zr(1)–O(1) bond length of 2.0572(5) Å is marginally longer than those found in reported zirconium enolates (*ca.* 1.96 – 2.01 Å),[7,40,43–46] possibly due to the steric demand of the borylamido moiety and π-bonding competition between Zr(1)–O(1) and Zr(1)–N(1) ($2p_\pi$–$4d_\pi$). The C(27)–C(28)

bond distance of 1.3308(12) Å is at the high end of the range of those for the reported zirconium enolates of 1.305 – 1.346 Å.[7,40,43–46] This longer distance is attributed to the conjugated O(2)–C(27) and C(27)–C(28) bonds, which is indicated by a small C(29)–O(2)···C(27)–C(28) dihedral angle of 2.2°, as well as the C(27)–O(2)–C(29) angle of 119.42(7)° showing a formally sp^2-hybridised O(2) atom.

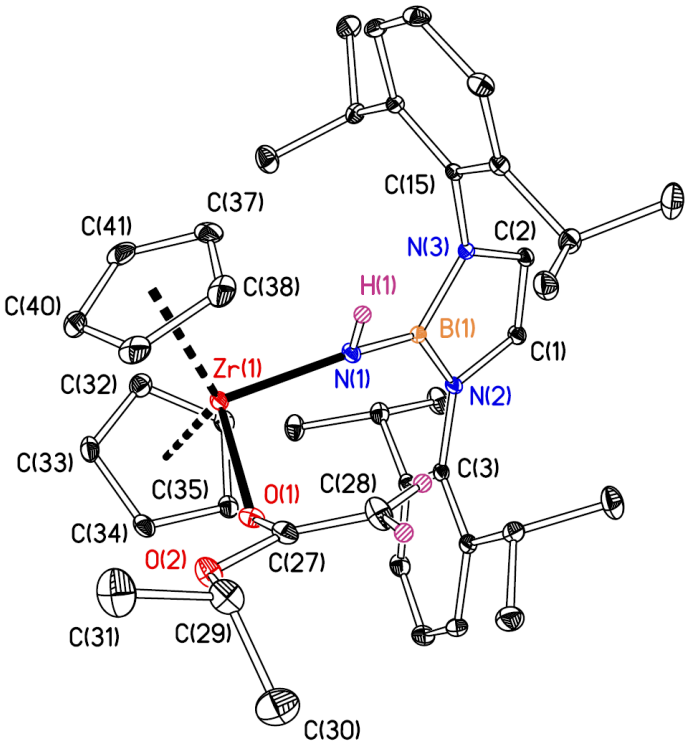

Figure 4.3. Displacement ellipsoid plot (20% probability) of $Cp_2Zr\{NHB(NAr'CH)_2\}\{OC(CH_2)O^iPr\}$ (**53**). Selected H atoms omitted for clarity.

Table 4.2. Selected bond lengths (Å) and angles (°) for $Cp_2Zr\{NHB(NAr'CH)_2\}\{OC(CH_2)O^iPr\}$ (**53**). $Cp_{cent(1)}$ and $Cp_{cent(2)}$ refer to the computed Cp ring centroids for "upper" and "lower" Cp rings, respectively, as depicted in Figure 4.3.

Zr(1)–N(1)	2.0907(5)	$Cp_{cent(1)}$–Zr(1)–$Cp_{cent(2)}$	128.8
Zr(1)–O(1)	2.0572(5)	Zr(1)–N(1)–B(1)	151.15(5)
Zr(1)–$Cp_{cent(1)}$	2.247	N(1)–B(1)–N(2)	133.85(6)
Zr(1)–$Cp_{cent(2)}$	2.211	N(1)–B(1)–N(3)	122.68(6)
N(1)–B(1)	1.4389(9)	Zr(1)–O(1)–C(27)	134.68(5)
B(1)–N(2)	1.4494(9)	C(27)–O(2)–C(29)	119.42(7)
B(1)–N(3)	1.4445(9)		
O(1)–C(27)	1.3206(10)		
C(27)–C(28)	1.3308(12)		
C(27)–O(2)	1.3690(9)		

When **11** was reacted with $R'CO_2Me$ (R' = CH_2SiMe_3, $CHPh_2$, ^iPr and Ph), which contain fewer α–hydrogen atoms and increased steric bulk of R' (*cf.* Me), neither α–hydrogen atom abstraction nor [2+2] cycloaddition was observed at 60 °C. However, when the less sterically hindered $MeCO_2Me$ was employed, α–hydrogen atom abstraction was initially observed to form the ester enolate complex, $Cp_2Zr\{NHB(NAr'CH)_2\}\{OC(CH_2)OMe\}$ (**55**), as the major species at RT over 16 h, accompanied by the formation of another two zirconocene complexes on the NMR tube scale. After another 16 h at 60 °C, **55** was fully consumed, giving quantitative formation of these two final products, namely $Cp_2Zr\{NHB(NAr'CH)_2\}(OMe)$ (**57**) and $Cp_2Zr\{NHB(NAr'CH)_2\}\{OC(CH_2)CH_2CO_2Me\}$ (**56**) in a *ca.* 1:1 ratio (Figure 4.4 and Scheme 4.4). Crystallographic characterisation (shown in Figure 4.11, Section 4.3.2.4) showed that **56** contains a zirconium-bound β-ketoester enolate fragment. On the preparative scale, the reaction was carried out in benzene at 60 °C for 16 h, giving formation of a mixture of **56** and **57** in a *ca.*1:1 ratio, with **56** being isolated (accompanied by 10% remaining **57**), as pale yellow crystals in 23% yield.

The ^{11}B NMR spectra of both **55** and the mixture of **56** and **57** show characteristic broad resonances at *ca*. 25.1 – 25.2 ppm, indicating the formation of borylamido zirconocene complexes. The ^{1}H, ^{11}B and ^{13}C NMR spectra of **55** are analogous to those of **53** and **54**, showing an ester enolate fragment including a terminal vinyl ^{1}H singlet (2 H) of OC(=C$\underline{H}_2$)OMe at 2.98 ppm with an HMBC correlation observed to a ^{13}C resonance of the carbonyl at 169.8 ppm, and an HSQC correlation to a ^{13}C resonance of the vinyl carbon at 54.9 ppm, all comparable with those of **53** and **54**.

^{1}H NMR spectra of both **57** and **56** feature a set of resonances for the borylamido group and a singlet for the Cp ligands. In addition, compound **56** shows terminal vinyl protons at 3.93 and 3.70 ppm, with an HSQC correlation of OC($\underline{C}H_2$)CH_2CO_2Me and an HMBC correlation of O$\underline{C}$(CH_2)CH_2CO_2Me to ^{13}C signals at 88.8 and 161.8 ppm, respectively, all comparable with the values found in the analogous borylamido enolate compound **53**. Furthermore, another low field resonance at 170.8 ppm was found in the ^{13}C NMR spectrum attributed to OC(CH_2)$CH_2\underline{C}O_2$Me in **56**. Both of these low field carbonyl resonances show HMBC correlations with OC(CH_2)C$\underline{H}_2CO_2$Me to a ^{1}H NMR signal at 2.82 ppm, whilst in **57** only a 3 H singlet resonance at 3.45 ppm of ZrO$\underline{Me}$ was observed, without any HMBC correlation.

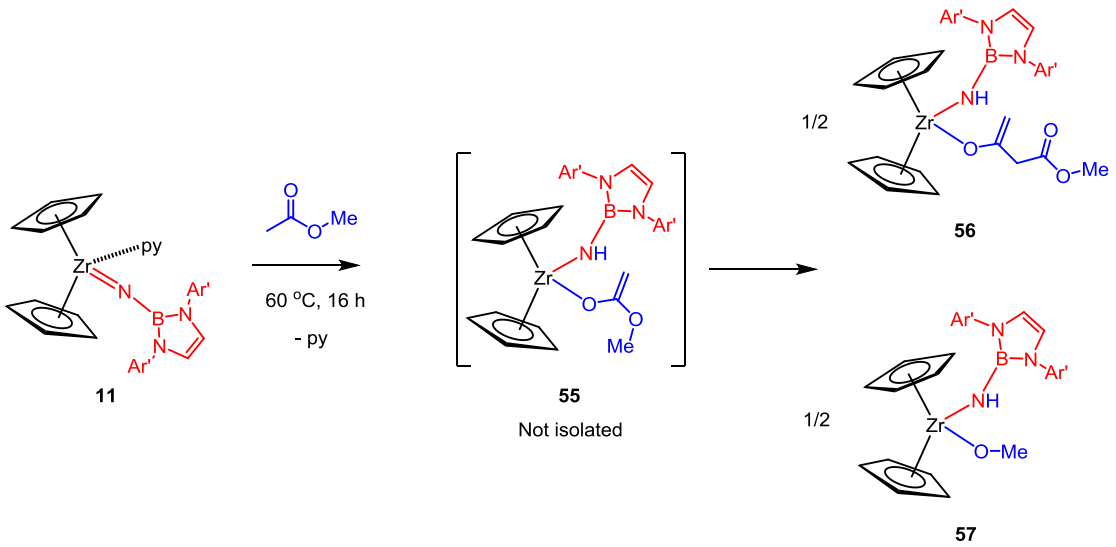

Scheme 4.4. Synthesis of $Cp_2Zr\{NHB(NAr'CH)_2\}\{OC(CH_2)CH_2CO_2Me\}$ (**56**) and $Cp_2Zr\{NHB(NAr'CH)_2\}(OMe)$ (**57**) from the reaction of $Cp_2Zr\{NB(NAr'CH)_2\}(py)$ (**11**) with $MeCO_2Me$, *via* the enolate intermediate $Cp_2Zr\{NHB(NAr'CH)_2\}\{OC(CH_2)OMe\}$ (**55**).

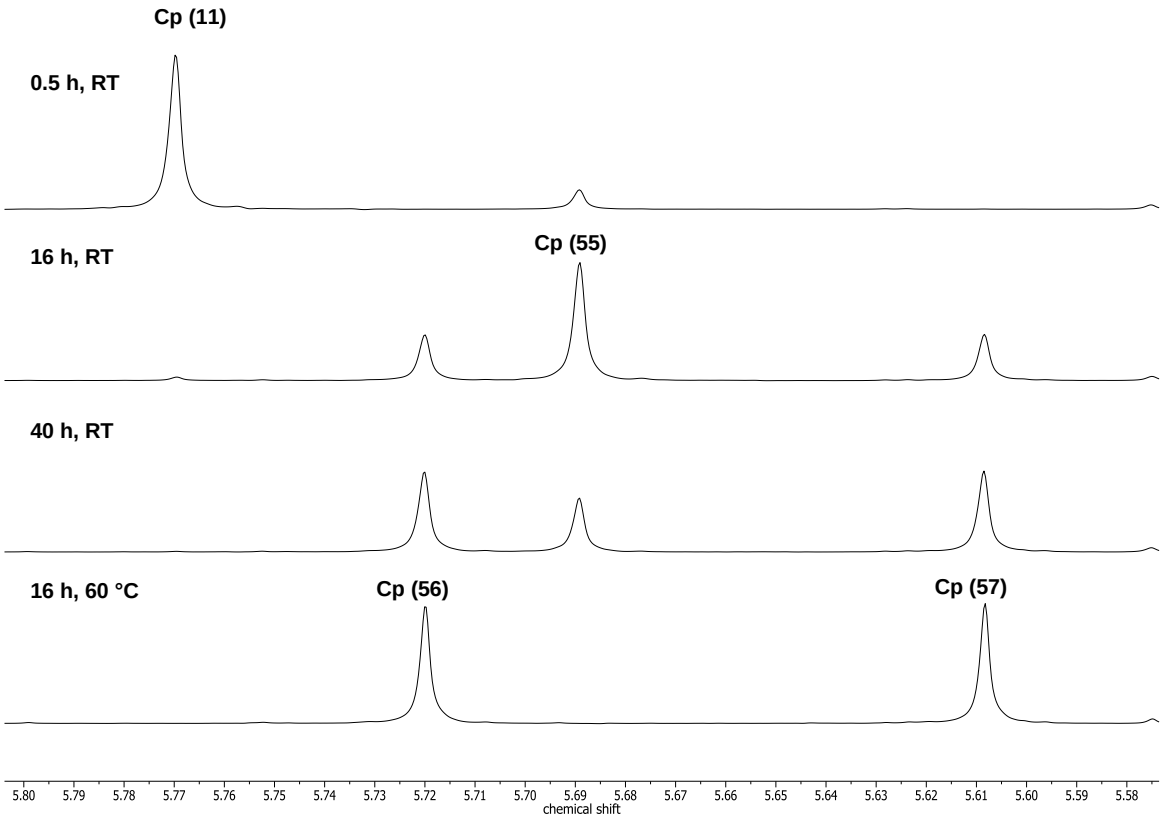

Figure 4.4. Partial ^{1}H NMR spectrum (400.1 MHz) for the reaction of $Cp_2Zr\{NB(NAr'CH)_2\}(py)$ (**11**) with $MeCO_2Me$ forming $Cp_2Zr\{NHB(NAr'CH)_2\}\{OC(CH_2)OMe\}$ (**55**), $Cp_2Zr\{NHB(NAr'CH)_2\}\{OC(CH_2)CH_2CO_2Me\}$ (**56**) and $Cp_2Zr\{NHB(NAr'CH)_2\}(OMe)$ (**57**) in C_6D_6 at 298 K.

Attempts were made to isolate **57** on the preparative scale by reacting **11** with one equivalent of MeOH in toluene at 0 °C. Unfortunately, this protonolysis reaction was not well-controlled, resulting in immediate formation of an oily mixture of the fully protonated borylamine $H_2NB(NAr'CH)_2$ (**1.110**), **57** and unreacted **11** due to the high acidity and low bulk of MeOH. The ^{1}H NMR spectrum of **57** in this mixture is fully consistent with the observed **57** in the ester cleavage reaction. Therefore, the compounds **55** and **57** were characterised by *in situ* NMR experiments only.

Identification of the β-ketoester enolate fragment of **56** was further facilitated by cleavage of the organic fragments from the zirconium centre with one equivalent of H_2O on the NMR tube scale, yielding the insoluble $[Cp_2Zr(O)]_n$, borylamine **1.110** and methyl acetoacetate in which the ^{1}H NMR spectrum is consistent with that of an authentic sample. However, attempts to form **56** independently by reacting **11** with methyl

acetoacetate *via* α-hydrogen atom abstraction only resulted in high amounts of borylamine **1.110** and many unidentified species. This is possibly due to the much more acidic bridging α-methylene protons of methyl acetoacetate, leading to a less controlled reaction. Additionally, the preference for deprotonation at the bridging α-CH_2 rather than the terminal α'-CH_3 may give an O-bound bidentate coordination with the zirconium centre, which is widely known for zirconium, of the type $(L)_nZr(\kappa^2$-O(R)CHC(R')O) (R, R' = Me, CF_3 ^{t}Bu, O^{t}Bu, OMe, and R = Me, R' = O^{t}Bu), [47–51] as well as other metals. Monodentate β-diketone or β-keto ester enolates are generally known for late transition metals, however, in a M–C(H){C(O)R}$_2$ bonding fashion.[52–57] Only a few analogous examples of O–bound monodentate β-keto alkoxy complexes with unsubstituted bridging α-carbon atoms are known, which formed under the aldol condensation reaction between enolates and carbonyls.[58,59]

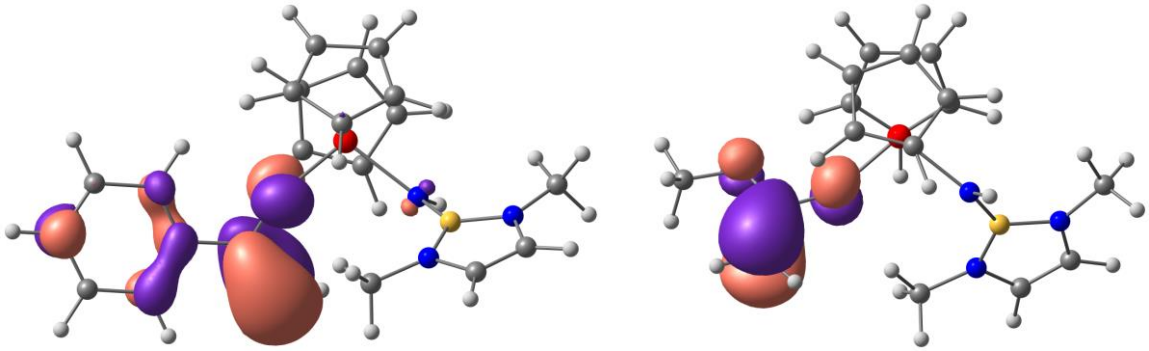

Figure 4.5. DFT computed HOMO-1 of $Cp_2Zr\{NHB(NMeCH)_2\}\{OC(CH_2)Ph\}$ (**52Q**, left, E = –5.78 eV) and $Cp_2Zr\{NHB(NMeCH)_2\}\{OC(CH_2)OMe\}$ (**55Q**, right, E = –5.52 eV). The normalised atomic contributions from C(2p) for the enolate $\underline{C}=CH_2$ and $C=\underline{C}H_2$ carbons are 0.12 and 0.43, respectively for **52Q**, and 0.13 and 0.53 for **55Q**. The HOMO in each case is a ligand-based orbital on $B(NMeCH)_2$.

Figure 4.5 shows the DFT (B3PW91/Def2TZVP) computed HOMO-1 for the model enolate compounds $Cp_2Zr\{NHB(NMeCH)_2\}\{OC(CH_2)Ph\}$ (**52Q**) and $Cp_2Zr\{NHB(NMeCH)_2\}\{OC(CH_2)OMe\}$ (**55Q**). In each case the largest orbital coefficient of these high energy MOs is on the $C=\underline{C}H_2$ carbon, implying high nucleophilicity. However, the HOMO-1 in **52Q** is –0.16 eV more stable, and the coefficient on the terminal carbon lower by 20%, compared to that for **55Q**, suggesting a more nucleophilic $C=\underline{C}H_2$ moiety in the latter case. Analogous results were found for the HOMOs of enols $PhC(OH)CH_2$ and $MeOC(OH)CH_2$ themselves (Appendix, A4).

Attention is now given to the mechanism of formation of the complexes **56** and **57**. After the initial α-hydrogen abstraction giving **55**, it is proposed that the OMe moiety chelates to the zirconium centre, initiating the cleavage of the ester enolate fragment which eliminates ketene (H_2CCO), and accompanied by the formation of **57** *via* the transition state **57_TS**. The liberated ketene then undergoes rapid nucleophilic attack on the α-carbon position by the enolate functional group of unreacted **55**. After further rearrangement, compound **56** was then generated (Scheme 4.5). The reaction of $Cp_2Zr(N^tBu)(THF)$ (**1.4**) with diphenylketene (Ph_2CCO) was previously reported by Bergman, yielding the ketenimine (Ph_2CCN^tBu) and a bimetallic (μ-oxo)(μ-enediolato) zirconocene complex.[2,7] However, no reaction was observed here between transient H_2CCO and the borylimido complex **11** at RT, where compounds **56** and **57** were formed (forming H_2CCO) with unreacted **11** remaining, indicating that **55** is significantly more reactive.

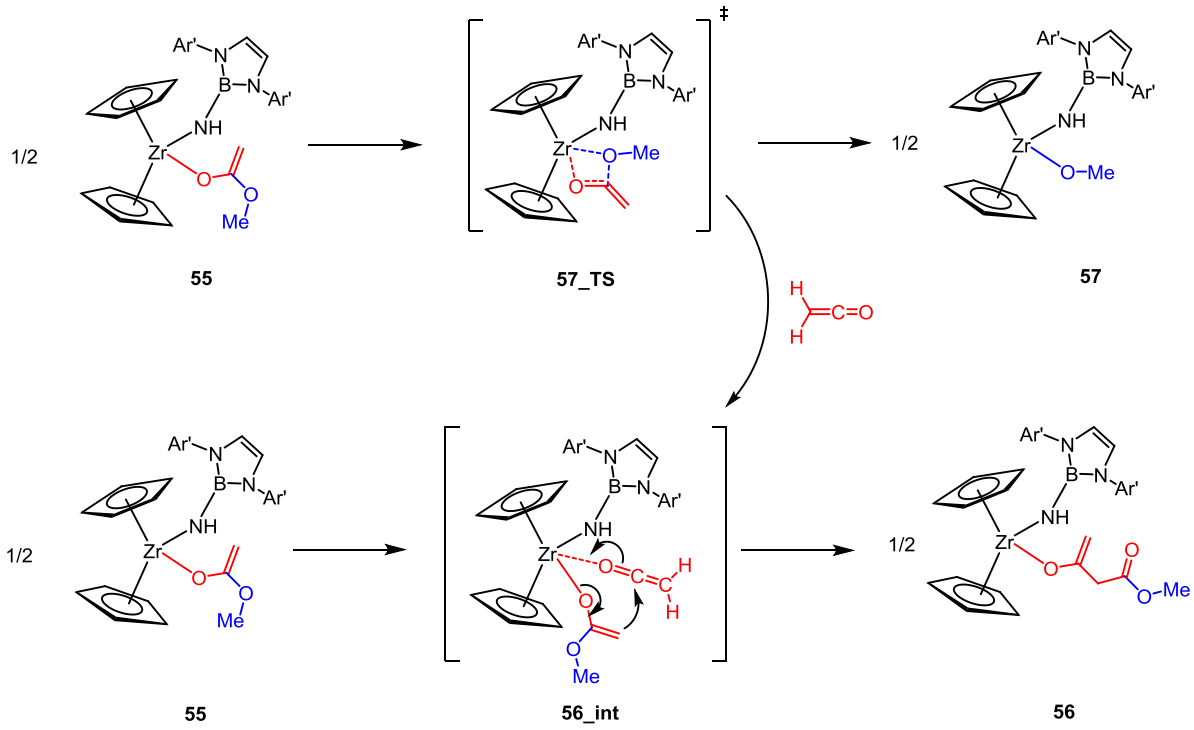

Scheme 4.5. Proposed mechanism for the ketene elimination and self-trapping pathways of $Cp_2Zr\{NHB(NAr'CH)_2\}\{OC(CH_2)OMe\}$ (**55**) to form $Cp_2Zr\{NHB(NAr'CH)_2\}\{OC(CH_2)CH_2CO_2Me\}$ (**56**) and $Cp_2Zr\{NHB(NAr'CH)_2\}(OMe)$ (**57**).

As described above, the enolate cleavage (ketene elimination) reaction of $Cp_2Zr\{NHB(NAr'CH)_2\}\{OC(CH_2)OMe\}$ (**55**) is significantly faster than that of $Cp_2Zr\{NHB(NAr'CH)_2\}\{OC(CH_2)O^iPr\}$ (**53**), demonstrating that the O-chelation of the alkoxy group to the zirconium centre to initiate the ester cleavage is dependent on the steric bulk of the alkoxy group substituent (OMe (**55**) and O^iPr (**53**)), due to the steric repulsion with the bulky borylamido fragment as depicted in Scheme 4.5. In order to elucidate the mechanism, $Cp_2Zr\{NHB(NAr'CH)_2\}\{OC(CH_2)OEt\}$ (**54**) was chosen for kinetic studies (Section 4.3.3), since the ethoxy moiety is marginally more bulky than the methoxy group in **55**, but less sterically crowded than the isopropoxy group in **53**. Consequently, **54** is fairly stable at RT, and gradual enolate cleavage was observed between 50 and 70 °C to give $Cp_2Zr\{NHB(NAr'CH)_2\}\{OC(CH_2)CH_2CO_2Et\}$ (**58**) and $Cp_2Zr\{NHB(NAr'CH)_2\}(OEt)$ (**59**) in a *ca*. 1:1 ratio on the NMR tube scale (Equation 4.4). The NMR spectra are analogous to those of the methyl homologues **56** and **57**.

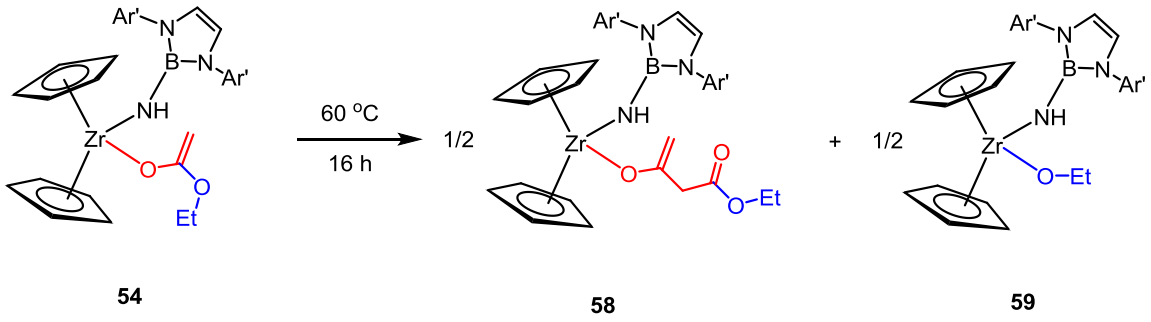

54 **58** **59**

Equation 4.4

Although **58** and **59** could not be separated due to their similarly high solubility in hydrocarbons, **59** was independently synthesised by reacting **11** with EtOH. On the preparative scale, EtOH was slowly added into a toluene solution of **11** at 0 °C. An immediate colour change to pale yellow was observed, and **59** was isolated and purified by crystallisation in 44% yield (Equation 4.5). The diagnostic ^{11}B NMR signal at 25.2 ppm and the broad ^1H signal of NH at 4.03 ppm indicate the formation of a borylamido zirconocene complex, and are accompanied by the ethyl group showing triplet and quartet signals at 0.92 ppm (3 H) and 3.61 (2 H), respectively, in the ^1H NMR spectrum, consistent with the signals observed from the reaction of **54**.

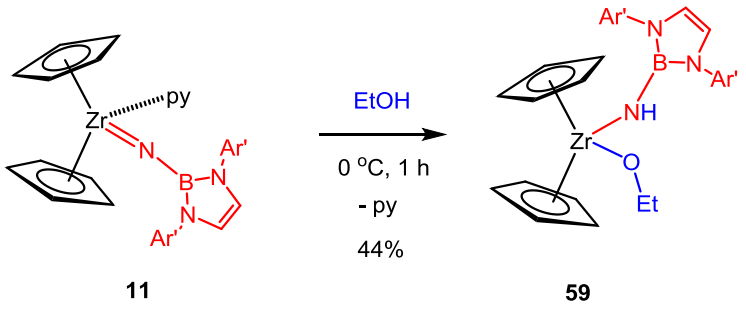

11 **59**

Equation 4.5

Diffraction-quality crystals of **59** were grown from a hexane solution at 0 °C. The solid-state structure is shown in Figure 4.6 with selected bond lengths and angles listed in Table 4.3. Molecules of compound **59** possess a pseudo tetrahedral environment, with eclipsed cyclopentadienyl rings. The Zr(1)–N(1)–B(1) linkage of **59** shows Zr(1)–N(1) and N(1)–B(1) single bonds of 2.1083(16) and 1.425(3) Å, respectively, and a Zr(1)–N(1)–B(1) bond angle of 148.00(13)°, indicating a borylamido moiety, and all parameters are comparable with those of the enolate complex **53**. The Zr(1)–O(1) distance of 1.9676(17) Å is slightly shorter and the Zr(1)–O(1)–C(27) bond angle of 151.9(2)° is somewhat wider than those in **53**. In terms of steric effects, it is possibly because of the less sterically encumbering nature of the ethoxyl ligand. Electronically, the sp^3-hybridised C(27) experiences no π-donation from O(1), and may result in a higher degree of equatorial $2p_\pi$–$4d_\pi$ interaction between O(1) and Zr(1).

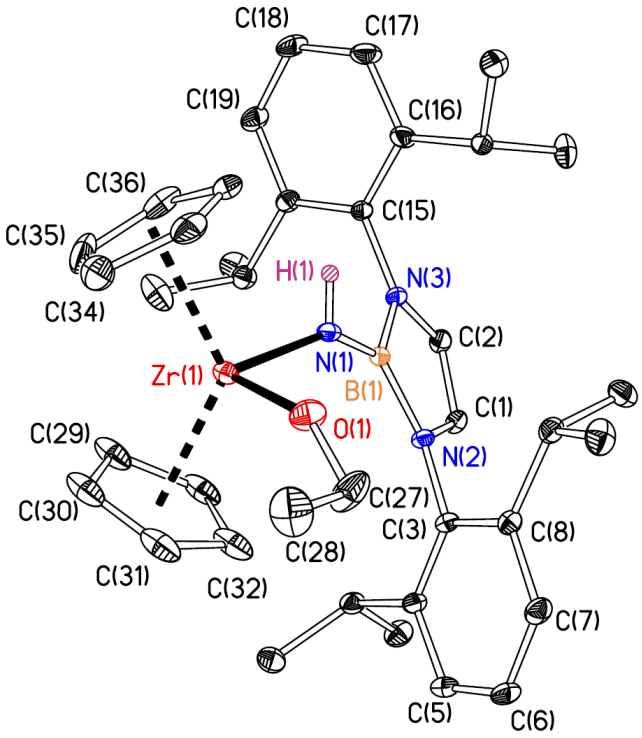

Figure 4.6. Displacement ellipsoid plot (20% probability) of $Cp_2Zr\{NHB(NAr'CH)_2\}(OEt)$ (**59**). C–bound H atoms omitted for clarity.

Table 4.3. Selected bond lengths (Å) and angles (°) for $Cp_2Zr\{NHB(NAr'CH)_2\}(OEt)$ (**59**). $Cp_{cent(1)}$ and $Cp_{cent(2)}$ refer to the computed Cp ring centroids for "upper" and "lower" Cp rings, respectively, as depicted in Figure 4.6.

Zr(1)–N(1)	2.1083(16)	$Cp_{cent(1)}$–Zr(1)–$Cp_{cent(2)}$	128.5
Zr(1)–O(1)	1.9676(17)	Zr(1)–N(1)–B(1)	148.00(13)
Zr(1)–$Cp_{cent(1)}$	2.273	N(1)–B(1)–N(2)	132.40(18)
Zr(1)–$Cp_{cent(2)}$	2.225	N(1)–B(1)–N(3)	124.21(18)
N(1)–B(1)	1.425(3)	Zr(1)–O(1)–C(27)	151.9(2)
B(1)–N(2)	1.456(3)		
B(1)–N(3)	1.448(3)		
O(1)–C(27)	1.383(3)		
C(27)–C(28)	1.470(4)		

Enolate cleavage reactions forming β-ketoesters and alcoholates have been observed since the early 1900s, during the synthesis of ester enolate Grignard and organozinc (Reformatsky) reagents from the reaction of α-haloesters with magnesium or zinc, and usually in low yield.[60–63] Similar to those magnesium and zinc compounds, lithiated ester enolates, for example (2,6-di-*tert*-butyl-4-methylphenyl)-2-methylpropanoate, were also found to be suitable for generating ketenes, the presence of which was proved by trapping with ^{n}BuLi (Scheme 4.6).[64–66] These lithiated ester enolates were later found to be a good entry point for preparing silyloxyvinylstannanes by reacting the *in situ* self-generated ketene with Bu_3SnLi.[67] More recently, Brown and co-workers reported the synthesis of tetrasubstituted alkenes using *in situ* self-generated ketene (R^1R^2CCO) as building blocks from the enolate cleavage reaction of $LiOC(CR^1R^2)OAr$.[68] However, these ketene trapping reactions were found to be problematic and low yielding when the ester enolate is C_2-mono- or unsubstituted, as the monosubstituted ketenes could be deprotonated to give ynolates by the organolithium reagent (^{n}BuLi),[66,69] and in addition, the less bulky ketenes are generally less stable, resulting in fast dimerization.

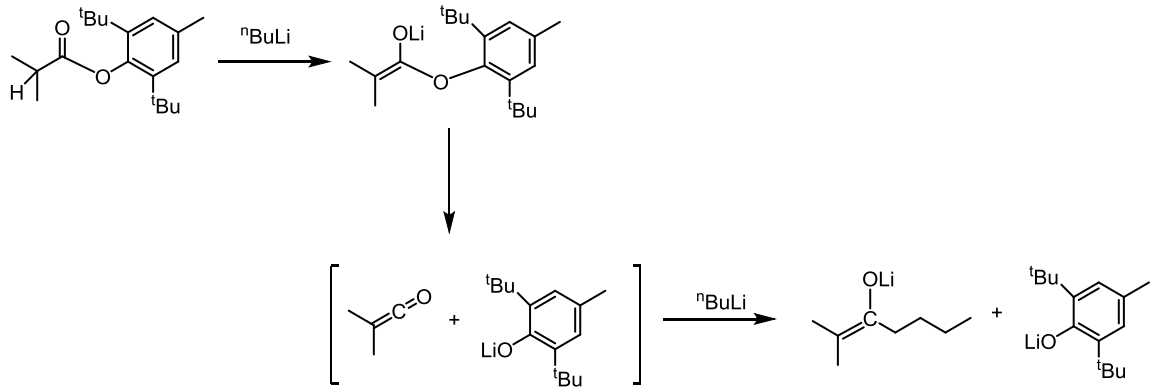

Scheme 4.6. Exemplar cleavage of lithiated (2,6-di-*tert*-butyl-4-methylphenyl)-2-methylpropanoate and ketene trapping by ^{n}BuLi.[64]

These reported ester cleavage reactions are mostly initiated by main group metals (i.e., Li, Mg and Zn). Carpentier and co-workers reported an ester enolate cleavage reaction of a cationic complex $[Cp_2Zr\{\eta^2\text{-}OC(CMe_2)O(^{t}Bu)\}]^{+}$, which is formed by reacting $Cp_2Zr\{OC(CMe_2)O^{t}Bu\}(Me)$ (**4.11**) with $B(C_6F_5)_3$ *via* methyl abstraction. One of the possible pathways for the formation of the final product $[Cp_2Zr\{\mu\text{-}(O_2C^{i}Pr)\}_2]^{2+}$ was postulated to be *via* dimethyl ketene (Me_2CCO) elimination then self-trapping, although it was not possible to verify this by experiment.[70] The requirement for methyl anion abstraction to initiate the ester enolate cleavage is probably in order to provide a vacant

site for O-chelation of the bulky O^{t}Bu group, which is in line with the more stable **53** containing the bulky O^{i}Pr group. For the OEt-substituted compound **54**, the ester cleavage is well controlled (faster than **53**, but slower than main group ester enolates), and the ketene could be *in situ* trapped by unreacted enolate borylamide which allows this reaction to be kinetically and mechanistically studied (*vide infra*). Unfortunately, attempts to perform analogous reactions on *tert*-butylimido zirconocene complex **1.4** with a range of esters, such as $MeCO_2R$ (R = Me, Et, ^{i}Pr or Ph) and $R'CO_2Me$ (R' = Ph, $CSiMe_3$(H)) only resulted in rapid formation of many unidentified species.

4.3.2.2 Reactions of $Cp_2Zr\{NB(NAr'CH)_2\}$(py) (11) with MeC(O)SR (R = Et, Me)

Interestingly, these enolate cleavage (ketene elimination and self-trapping) reactions were also observed for ester analogues, such as thioesters. The reactions of **11** with MeC(O)SR (R = Me or Et) were similarly performed. On the NMR tube scale in C_6D_6, the reactions of **11** with MeC(O)SR (R = Me or Et) were found to give thioester enolate complexes $Cp_2Zr\{NHB(NAr'CH)_2\}\{OC(CH_2)SR\}$ (R = Me (**60**) or Et (**61**)) at RT after 16 h *via* α-hydrogen atom abstraction, which are analogous to the reactions of the respective esters with **11**. Like the reactions of ester enolate complexes, analogous thioester cleavage reactions were observed during the formation of **60** and **61**. However, these were formed in relatively small amounts compared to the formation of **55** and **54**. This allows **61** and the methyl substituted **60** to be isolated and fully characterised. On the preparative scale, **11** reacted with MeC(O)SR (R = Me or Et) in benzene solution at RT for 16 h, giving **60** in 72% crystalline yield and **61** as a yellow solid in 75% yield (Equation 4.6), respectively. The ^{1}H and ^{13}C NMR spectra of isolated **60** and **61** are analogous to those of the ester enolate congeners **55** and **54**, and showing the vinyl signals of OC(SR)=C$\underline{H}_2$ (R = Me (**60**), Et (**61**)) at 3.96, 3.88 ppm and 4.03, 3.97 ppm, respectively, with HMBC correlations to downfield shifted ^{13}C signals of O$\underline{C}$(SR)=CH_2 at 165.3 and 163.4 ppm, respectively.

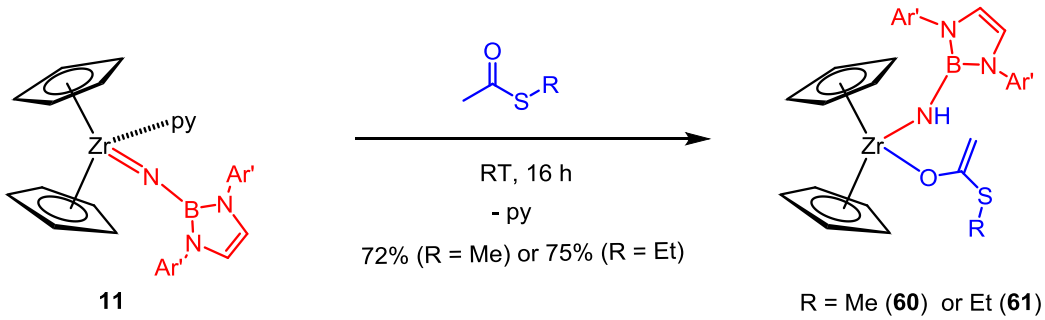

11 R = Me (**60**) or Et (**61**)

Equation 4.6

Diffraction-quality crystals of **60** were grown from a hexane solution at –30 °C. The solid state structure is shown in Figure 4.7, and selected bond distances and angles are listed in Table 4.4. Compound **60** has an analogous structure to that of **53**, possessing a pseudo tetrahedral environment with eclipsed cyclopentadienyl rings. The Zr(1)–N(1)–B(1) linkage of **60** is identical within error to that of **53**, with a Zr(1)–N(1) bond distance of 2.095(4) Å and a Zr(1)–N(1)–B(1) angle of 152.1(3)°. The small C(29)–S(1)···C(27)–C(28) dihedral angle of 4.4° indicates the conjugation between C(29)–S(1) and C(27)–C(28) bonds. This dihedral angle is comparable to that in **53** (2.2°). The shorter C(27)–C(28) bond distance of 1.283(10) Å (*cf.* 1.3308(12) Å in **53**) is probably attributed to the weaker $3p_{\pi}$–$2p_{\pi}$ interaction of S(1)–C(27) in **60**, because of the poorer energetic and overlap match compared to the $2p_{\pi}$–$2p_{\pi}$ interaction of O(2)–C(27) in **53**. A few lanthanide thioester enolate compounds have been reported in the literature, and all contain an additional dative Ln–S bond.[71–73] In contrast, a dative Zr–S interaction was not observed in **60**, possibly due to the steric bulk of the boryl moiety.

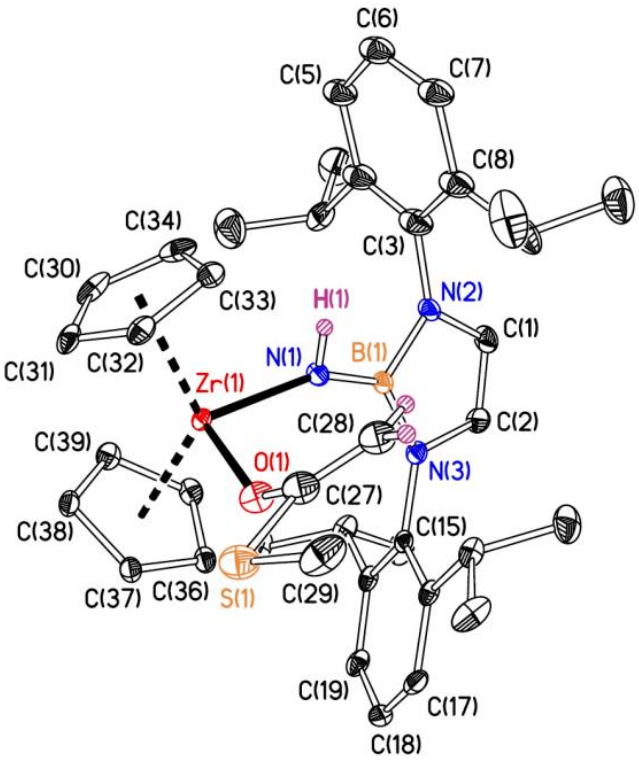

Figure 4.7. Displacement ellipsoid plot (20% probability) of $Cp_2Zr\{NHB(NAr'CH)_2\}\{OC(CH_2)SMe\}$ (**60**). Selected H atoms omitted for clarity.

Table 4.4. Selected bond lengths (Å) and angles (°) for $Cp_2Zr\{NHB(NAr'CH)_2\}\{OC(CH_2)SMe\}$ (**60**). $Cp_{cent(1)}$ and $Cp_{cent(2)}$ refer to the computed Cp ring centroids for "upper" and "lower" Cp rings, respectively, as depicted in Figure 4.7.

Zr(1)–N(1)	2.095(4)	$Cp_{cent(1)}$–Zr(1)–$Cp_{cent(2)}$	129.4
Zr(1)–O(1)	2.031(4)	Zr(1)–N(1)–B(1)	152.1(3)
Zr(1)–$Cp_{cent(1)}$	2.240	N(1)–B(1)–N(2)	121.9(4)
Zr(1)–$Cp_{cent(2)}$	2.219	N(1)–B(1)–N(3)	134.0(4)
N(1)–B(1)	1.432(6)	Zr(1)–O(1)–C(27)	139.8(4)
B(1)–N(2)	1.401(6)	C(27)–S(1)–C(29)	102.0(4)
B(1)–N(3)	1.440(6)		
O(1)–C(27)	1.362(8)		
C(27)–C(28)	1.283(10)		
C(27)–S(1)	1.739(7)		

As found for the ester enolate congeners **55** and **54**, heating **60** and **61** at 60 °C for 23 h in C_6D_6 resulted in quantitative conversion to the β-ketothioester enolate compounds $Cp_2Zr\{NHB(NAr'CH)_2\}\{OC(CH_2)CH_2C(O)SR\}$ (R = Me (**62**) or Et (**64**)), and thiolates $Cp_2Zr\{NHB(NAr'CH)_2\}(SR)$ (R = Me (**63**) or Et (**65**)), in a *ca.* 1:1 ratio on the NMR tube scale (Equation 4.7). The mixtures of **62** and **64**, or **63** and **65** could not be separated and purifed on the preparative scale due to their similarly high solubility in hydrocarbons. To confirm the formation of thiolate products, **65** was independently synthesised in 63% isolated yield by the salt metathesis reaction of $Cp_2Zr\{NHB(NAr'CH)_2\}Cl$ (**16**) with one equivalent of NaSEt (Equation 4.8).

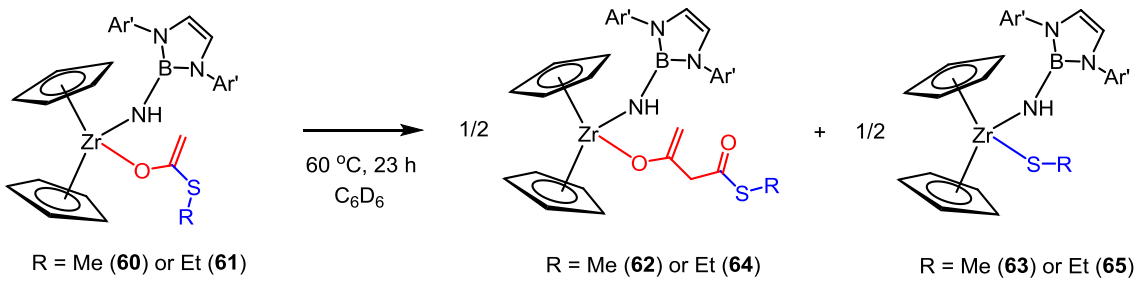

R = Me (**60**) or Et (**61**) R = Me (**62**) or Et (**64**) R = Me (**63**) or Et (**65**)

Equation 4.7

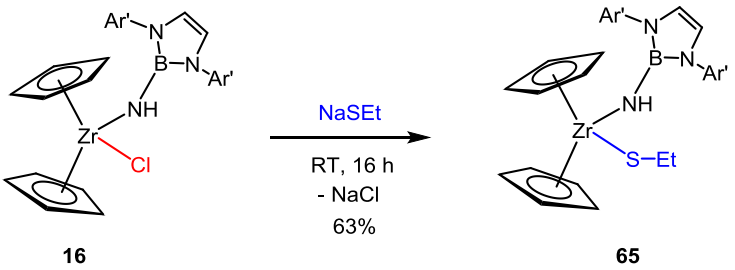

16 **65**

Equation 4.8

^{11}B NMR spectra of these four compounds display resonances between 25.0 and 25.2 ppm showing the formation of zirconocene borylamides. The ^{1}H and ^{13}C NMR spectra of **63** and **65** are analogous to those of the alkoxyl congeners **57** and **59**, along with slightly upfield shifted ^{13}C signals of S$\underline{C}$H$_2$R (R = H (**63**) or Me (**65**)) at 19.1 and 30.1 ppm, respectively. The compounds **62** and **64** have very similar ^{1}H and ^{13}C NMR spectra, including the ^{13}C resonances of O$\underline{C}$(CH$_2$) observed at 161.6 ppm for both, and the HMBC correlations with the vinyl and bridging methylene protons are found to be analogous to those of the β-ketoester enolate congeners **56** and **58**. In contrast, the ^{13}C signals of $\underline{C}$(O)SR (R = Me (**62**) or Et (**64**)) at 195.8 and 195.6 ppm, respectively, are shifted slightly downfield compared to those of $\underline{C}$O$_2$R (R = Me (**56**) or Et (**58**). Thus, the ketene elimination and self-trapping reactions are similar to those which occurred for the ester enolates **55** and **54**; the kinetic studies are discussed in Section 4.3.3. DFT calculations for ketene elimination from the full systems Cp$_2$Zr{NHB(NAr'CH)$_2$}{OC(CH$_2$)EMe} (E = O (**55**), S(**60**)) to form Cp$_2$Zr{NHB(NAr'CH)$_2$}(EMe) (E = O (**57**), S(**63**)) and H$_2$CCO were carried out. The Δ_rG and associated Δ_rH and Δ_rS of these reactions were very similar (Δ_rG = 4.1 and 4.9 kcal mol^{-1}; Δ_rH = 17.9 and 17.0 kcal mol^{-1}, for E = O or S, respectively), but indicated endergonic and very endothermic reaction favoured by the favourable Δ_rS term, 46.1 and 40.4 cal mol^{-1} K^{-1}. The reactions of H$_2$CCO and the enolates, while entropically disfavoured were found to be exergonic (Δ_rG = –21.4 and –16.5 kcal mol^{-1} for E = O or S, respectively), such that the overall reaction represented by Scheme 4.4 and Equation 4.7 for formations of Cp$_2$Zr{NHB(NAr'CH)$_2$}{OC(CH$_2$)CH$_2$C(O)EMe} (E = O (**56**), S (**62**)) and Cp$_2$Zr{NHB(NAr'CH)$_2$}(EMe) (E = O (**57**), S (**63**)) are exergonic with Δ_rG = –17.3 and –11.5 kcal mol^{-1}, respectively. A number of factors clearly influence the differences or similarities between Δ_rG at the various stages of the reaction sequence, and it is not possible to identify a single one in these cases.

4.3.2.3 Reactions of $Cp_2Zr\{NB(NAr'CH)_2\}(py)$ (11) with MeC(O)Cl and $MeC(O)NMe_2$

By changing the atom E of MeC(O)ER from oxygen to sulfur and the R group from Me to Et, similar enolate formation, ketene elimination and self-trapping reactions were found, but with dramatic differences in rates. The rates in each step are potentially tuneable, as the steric demands and nucleophilicity of –ER can affect the overall rates of ketene elimination and self-trapping (Section 4.3.3). Therefore, it is of interest to test the reactions of **11** with the most reactive and unreactive ester analogues, MeC(O)Cl and $MeC(O)NMe_2$.

In an NMR tube scale reaction of **11** with MeC(O)Cl in C_6D_6, none of the putative enolate intermediate $Cp_2Zr\{NHB(NAr'CH)_2\}\{OC(CH_2)Cl\}$ (**16_int**) was observed, and instead, only $Cp_2Zr\{NHB(NAr'CH)_2\}Cl$ (**16**) was slowly formed with a small amount of the decomposition product borylamine $H_2NB(NAr'CH)_2$ (**1.110**) after 40 h at RT, as observed by the ^1H NMR spectrum of the mixture. This is proposed to follow an analogous reaction pathway to the ester and thioester examples, but in this case, relatively slow α-hydrogen atom abstraction generating **16_int** was followed by a rapid enolate cleavage reaction to generate H_2CCO and **16** (Scheme 4.7). This accelerated ketene generation reaction is possibly due to the much less bulky Cl substituent, weaker C–Cl bond and more accessible lone pairs, compared to the –ER (E = O or S, R = Me or Et) substitutents of (thio)esters, which result in the coordination of the chlorine atom to the zirconium centre being more facile. Therefore, as no enolate intermediate was observed during the formation of **16**, the generated ketene was unable to be self-trapped to form the corresponding β-keto ester enolate, thus resulting in the decomposion of **11** to give **1.110** and several unidentified specices, which was also found to be the case in the reaction of **11** with $Me_3Si(H)CCO$ (*vide infra*). Unfortunately, the ketene was again not observed in this case by NMR spectroscopy.

In contrast, the reaction of **11** with $MeC(O)NMe_2$ resulted in the quantitative formation of $Cp_2Zr\{NHB(NAr'CH)_2\}\{OC(CH_2)NMe_2\}$ (**66**) *via* α-hydrogen atom abstraction after 16 h at RT on the NMR tube scale in C_6D_6. On the preparative scale, **11** was treated with $MeC(O)NMe_2$ in benzene solution at RT for 16 h, yielding **66** in 43% crystalline yield (Scheme 4.7). The ^1H, ^{11}B and ^{13}C NMR spectra are analogous to those of the ester and thioester enolate analogues **54** and **61**, and a broad NH singlet and a sharp NMe_2 singlet

were observed at 4.72 and 2.42 ppm respectively. The terminal vinyl protons of the enolate fragement $OC(=C\underline{H}_2)NMe_2$ were found at 2.96 ppm, with an HMBC correlation to a diagnostic ^{13}C signal of the carbonyl unit at 168.1 ppm, and an HSQC correlation to a ^{13}C signal of the vinyl carbon at 62.1 ppm.

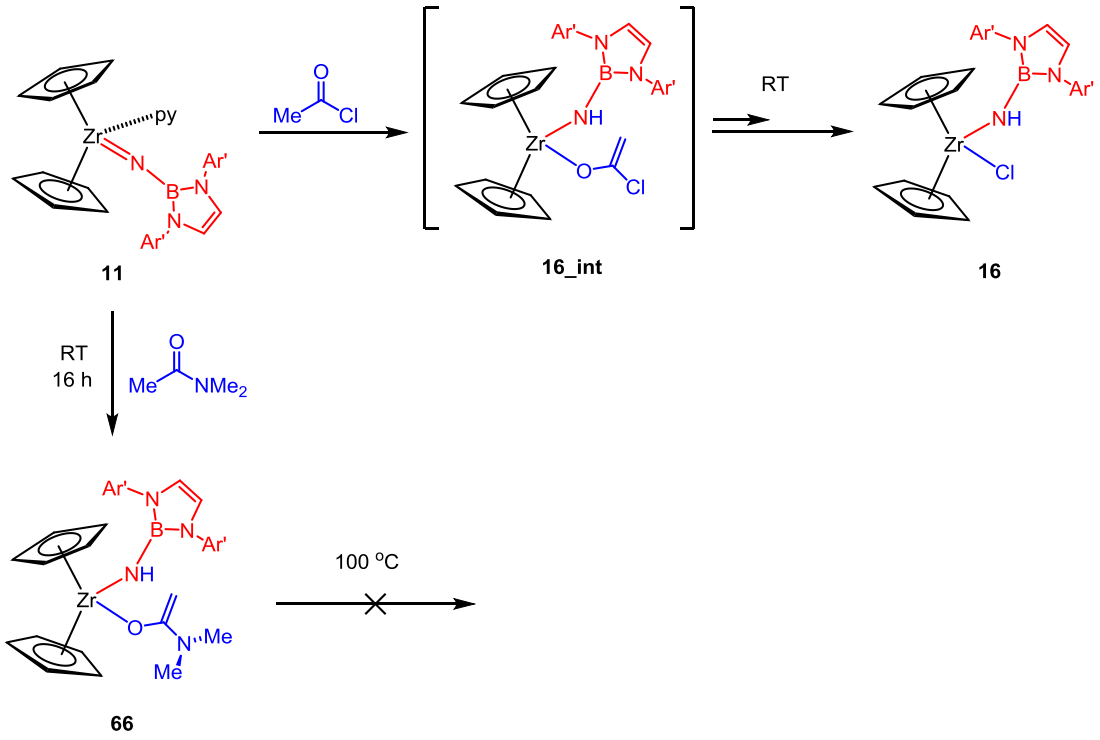

Scheme 4.7. Reactions of $Cp_2Zr\{NB(NAr'CH)_2\}(py)$ (**11**) with $MeC(O)Cl$ and $MeC(O)NMe_2$ to generate $Cp_2Zr\{NHB(NAr'CH)_2\}Cl$ (**16**) and $Cp_2Zr\{NHB(NAr'CH)_2\}\{OC(CH_2)NMe_2\}$ (**66**), respectively.

Diffraction-quality crystals of **66** were grown from a hexane solution at 4 °C. The solid state structure is shown in Figure 4.8, and selected bond distances and angles are listed in Table 4.5. The amide enolate zirconocene borylamide **66** has an analogous structure to those of the (thio)ester enolate analogues **53** and **60**, possessing a pseudo tetrahedral environment with staggered cyclopentadienyl rings. The solid state structure confirms that it contains an O-bound amide enolate and a borylamido ligand, with a Zr(1)–N(1) bond length of 2.091(2) Å and Zr(1)–N(1)–B(1) bond angle of 151.5(2)°, which are comparable with those in the (thio)ester enolate analogues described above. The sum of the angles subtended at N(4) is 353.0(7)°, indicating an sp^2-hybridised N(4) atom, which implies a $2p_\pi$-$2p_\pi$ interaction between the lone pair on N(4) and the C(27)–C(28) π-bond (conjugation). This is also reflected by the longer C(27)–C(28) bond distance of 1.337(6) Å, consistent with those in the ester enolate analogue **53**. However, the sum of the angles

subtended at N(4) is slightly deviated from the expected sum of angles in $MeC(O)NMe_2$ (360°). This may be due to the less energetically favoured $2p_\pi$-$2p_\pi$ interaction with C=C π-bond, compared to the C=O π-bond. Similar formation of the amide enolate complex, $\{\eta^5\text{-}1,2,4\text{-}(Me_3C)_3C_5H_2\}_2Th\{OC(CH_2)NMe_2\}\{C(Ph)C(Ph)(H)\}$ (**4.12**), *via* α-hydrogen atom abstraction was reported by reacting $\{\eta^5\text{-}1,2,4\text{-}(Me_3C)_3C_5H_2\}_2Th(\eta^2\text{-}C_2Ph_2)$ with $MeC(O)NMe_2$.[74] Furthermore, the salt metathesis reaction of Cp_2ZrCl_2 with $LiOC(CH_2)NPh_2$ was reported to generate the zirconocene amide enolate complex $Cp_2Zr\{OC(CH_2)NPh_2\}Cl$ (**4.13**).[75] Both **4.12** and **4.13** also contain a slightly pyramidalised $-NR_2$ fragment, having the angles subtended at nitrogen summing to 349.1 and 355.8°, respectively.

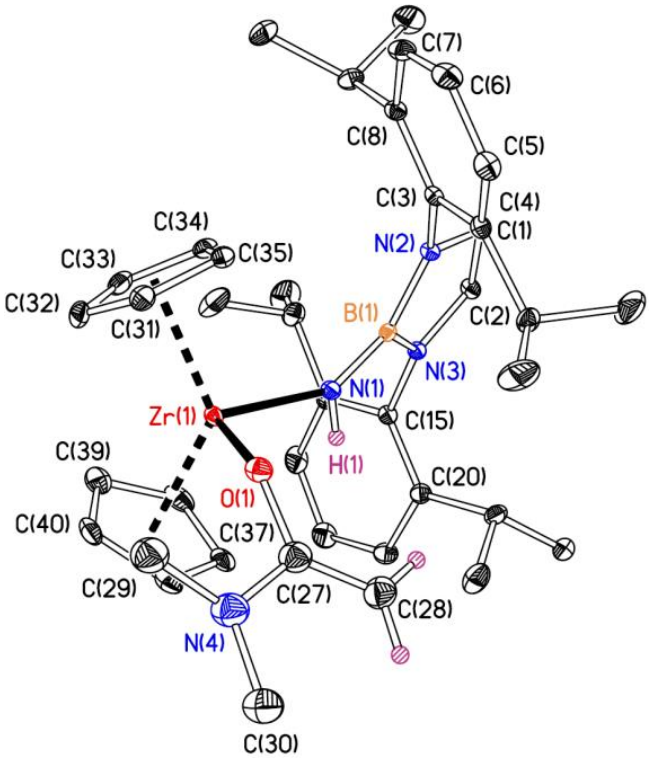

Figure 4.8. Displacement ellipsoid plot (20% probability) of $Cp_2Zr\{NHB(NAr'CH)_2\}\{OC(CH_2)NMe_2\}$ (**66**). Selected H atoms omitted for clarity.

Table 4.5. Selected bond lengths (Å) and angles (°) for $Cp_2Zr\{NHB(NAr'CH)_2\}\{OC(CH_2)NMe_2\}$ (**66**). $Cp_{cent(1)}$ and $Cp_{cent(2)}$ refer to the computed Cp ring centroids for "upper" and "lower" Cp rings, respectively, as depicted in Figure 4.8.

Zr(1)–N(1)	2.091(2)	$Cp_{cent(1)}$–Zr(1)–$Cp_{cent(2)}$	129.2
Zr(1)–O(1)	2.033(2)	Zr(1)–N(1)–B(1)	151.5(2)
Zr(1)–$Cp_{cent(1)}$	2.224	N(1)–B(1)–N(2)	133.9(3)
Zr(1)–$Cp_{cent(2)}$	2.251	N(1)–B(1)–N(3)	122.6(3)
N(1)–B(1)	1.435(4)	Zr(1)–O(1)–C(27)	138.8(2)
B(1)–N(2)	1.446(4)	C(27)–N(4)–C(29)	117.7(4)
B(1)–N(3)	1.452(4)	C(29)–N(4)–C(30)	117.6(4)
O(1)–C(27)	1.397(5)	C(30)–N(4)–C(27)	117.7(4)
C(27)–C(28)	1.337(6)		
C(27)–N(4)	1.349(6)		

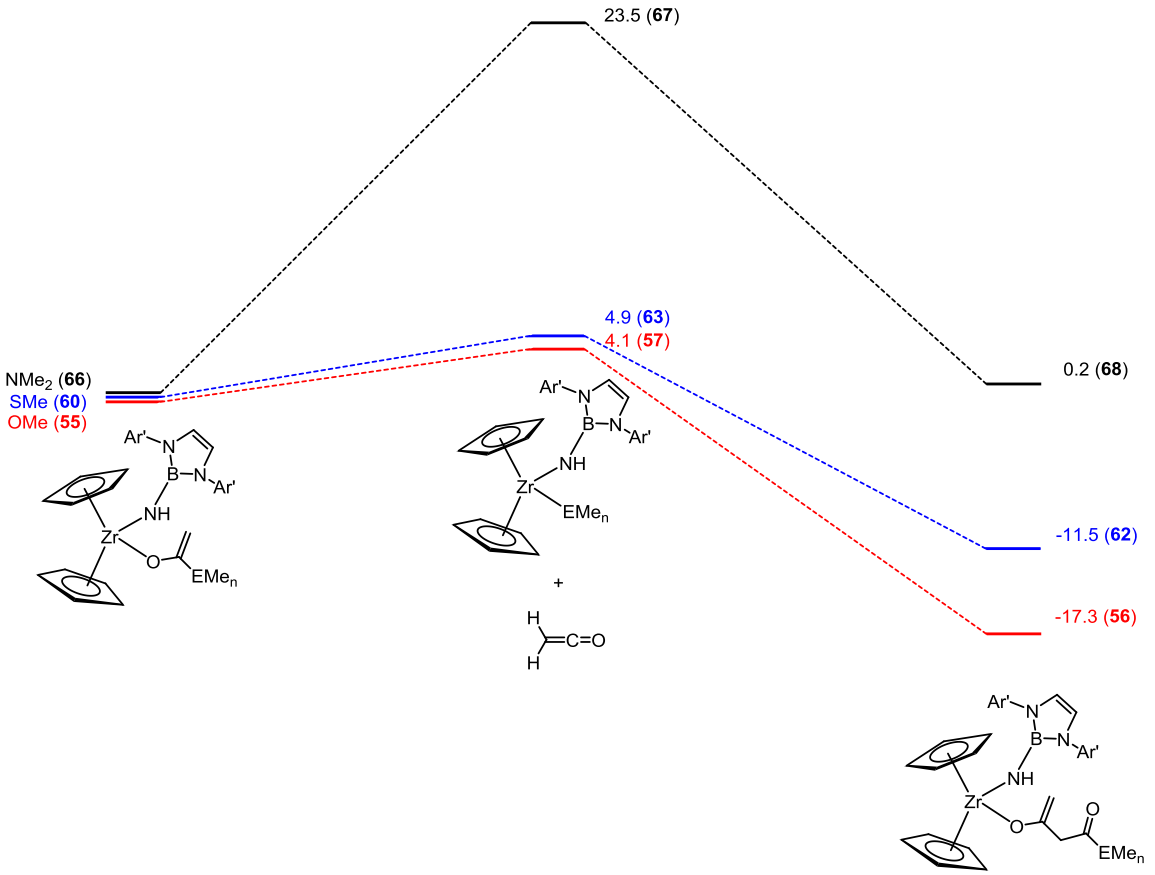

Figure 4.9. Schematic profile of ground state energies ($\Delta_r G$, kcal mol^{-1}, T = 298 K) of enolate cleavage of $Cp_2Zr\{NHB(NAr'CH)_2\}\{OC(CH_2)EMe_n\}$ (E = O, n = 1 (**55**); E = S, n = 1 (**60**); E = N, n = 2 (**66**)) eliminating H_2CCO forming $Cp_2Zr\{NHB(NAr'CH)_2\}(EMe_n)$ (E = O, n = 1 (**57**); E = S, n = 1 (**63**); E = N, n = 2 (**67**)), and self-trapping forming $Cp_2Zr\{NHB(NAr'CH)_2\}\{OC(CH_2)CH_2C(O)EMe_n\}$ (E = O, n = 1 (**56**); E = S, n = 1 (**62**); E = N, n = 2 (**68**)).

No amide enolate cleavage and subsequent ketene self-trapping to form the (hypothetical) product $Cp_2Zr\{NHB(NAr'CH)_2\}(NMe_2)$ (**67**) and $Cp_2Zr\{NHB(NAr'CH)_2\}\{OC(CH_2)CH_2C(O)NMe_2\}$ (**68**) were observed by ^{1}H NMR spectroscopy, even on standing **66** in toluene-d_8 at 100 °C for 16 h. DFT calculations on the ketene elimination reaction of **66** were carried out. Formation of H_2CCO and the bis(amide) $Cp_2Zr\{NHB(NAr'CH)_2\}(NMe_2)$ was again entropically favoured, but was very endothermic with $\Delta_r H$ = +35.9 kcal mol^{-1} (*cf.* +17.9 and +17.0 for the ester **55** and **60** thioester analogues). Although the ketene self-trapping reaction of **66** was calculated to be very favourable ($\Delta_r G$ = –23.3 kcal mol^{-1}), this does not compensate the thermodynamically (and, presumably, kinetically) disfavoured elimination first step ($\Delta_r G$

= +23.5 kcal mol^{-1}), rendering the overall reaction thermodynamically neutral (Figure 4.9).

The formation of enolate esters of $MeC(O)ER_n$ (E = O, S, N) by metal-ligand multiply-bonded complexes has not been seen before, whereas reaction with PhC(O)Me to form keto-enolate is known in the literature.[7] As mentioned above, Δ_rG for formation of the corresponding enol $R_nEC(OH)CH_2$ or $PhC(OH)CH_2$ from the keto form became progressively endergonic and endothermic in the sequence PhC(O)Me < $MeC(O)SMe$ < $MeC(O)NMe_2$ < $MeCO_2Me$. The computed Δ_rG for the reaction of $Cp_2Zr\{NB(NAr'CH)_2\}(py)$ (**11**) with these $MeC(O)EMe_n$ and PhC(O)Me species followed the same sequence (Δ_rG = –12.0 (PhC(O)Me), –7.0 (MeC(O)SMe), –0.7($MeC(O)NMe_2$), 0.3 ($MeCO_2Me$) kcal mol^{-1}). The same factors that disfavour enol formation of the free carbonyl compounds apply also in the metallated versions (loss of conjugation with $\pi_{C=O}$, and repulsion of the E lone pair with $\pi_{C=C}$ in the enol(ate)).

4.3.2.4 Reactions of enolate zirconocene complexes with $Me_3Si(H)CCO$

The transiently formed ketene was not observed by NMR spectroscopy in any of the reactions above, as the ketene self-trapping reaction happens much more rapidly than the ketene generation. To confirm and understand this proposed rapid ketene self-trapping and rearrangement pathway of **55** *via* **56_int** (Scheme 4.5), the reaction was modelled by reacting the isolable ketene $Me_3Si(H)CCO$[76] with the thermally stable enolate compound $Cp_2Zr\{NHB(NAr'CH)_2\}\{OC(CH_2)O^iPr\}$ (**53**). On the NMR tube scale in C_6D_6, the reaction finished immediately at RT without significant colour change (Equation 4.9), and a second ketene trapping reaction of the product with one more equivalent of ketene was not observed. Although both the $Me_3Si(H)CCO$ and **53** are more sterically hindered than H_2CCO and **55**, respectively, immediate product formation was still observed, clearly showing that the ketene trapping step is rapid and unlikely to be the rate-determining step for the formation of **56**, as the full conversion to **56** and **57** from **55** requires several hours at elevated temperatures. The rapid reaction of **53** is consistent with the DFT calculation discussed above, and the high nucleophilicity of $C=\underline{C}H_2$ in the analogous **55** which is suggested by the MO analysis in Figure 4.5.

On the preparative scale, **53** and $Me_3Si(H)CCO$ were mixed in benzene for 10 minutes at RT, yielding the β-ketoester enolate-borylamido zirconocene complex $Cp_2Zr\{NHB(NAr'CH)_2\}\{OC(CHSiMe_3)CH_2CO_2{}^iPr\}$ (**69**) in 79% yield (Equation 4.9),

which was crystallographically characterised (*vide infra*). By way of comparison, an attempted reaction of $Me_3Si(H)CCO$ with **11** was also performed at RT. However, only a small amount of decomposition into borylamine **1.110** and several unidentified species was observed after 16 h. Heating the solution of **11** and $Me_3Si(H)CCO$ only resulted in high amounts of **1.110** and a complicated mixture of products. Therefore, it reflects the relative inertness of **11** towards ketene compared to the enolate zirconocene borylamide **53**.

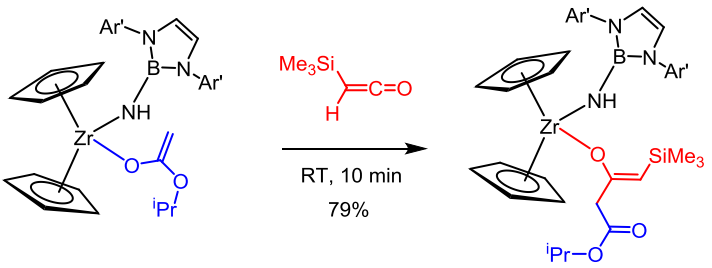

53 **69**

Equation 4.9.

The ^{11}B NMR spectrum of **69** shows a diagnostic resonance at 25.0 ppm which is consistent with the chemical shift for **53**. The ^{1}H and ^{13}C NMR spectra showed that **69** exists as a single isomer, and crystallographic characterisation showed that this isomer has a *Z*-conformation for the new C=C bond (*vide infra*). The spectra of compound **69** are consistent with a C_s symmetric species on the NMR timescale, with one set of resonances for the boryl moiety and one singlet of Cp. Diagnostic ^{13}C signals at 169.0 and 170.0 ppm were observed both with an HMBC correlation to a ^{1}H signal at 2.82 ppm, attributable to the bridging methylene protons of $C(O)C\underline{H_2}CO_2{}^{i}Pr$, hence these confirm the existence of two carbonyl functional groups and are all consistent with those found in the analogous compound **56**. Comparing the ^{1}H NMR spectrum of **69** (Figure 4.10) with that of **53**, all the signals of **69** are slightly downfield shifted, and, two additional signals at 4.37 (1 H) and 0.22 (9 H) ppm were observed which are attributed to the trapped ketene ($Me_3Si(H)CCO$).

This reaction is analogous to the Zr-assisted aldol condensation reaction reported by Floriani and co-workers, in which the amide enolate compound $Cp_2Zr\{OC(CH_2)NPh_2\}Cl$ reacted with PhC(O)H to give $Cp_2Zr\{OC(H)(Ph)CH_2C(O)NPh_2\}Cl$ (**4.14**), which contains an analogous β-keto alkoxy fragment.[58] In the same year, they reported another similar aldol condensation reaction of PhC(O)H with $Cp_2M(Cl)\{OC(CH_2)Fc\}$ (M = Ti or

Zr, Fc = ferrocenyl).[59] In both cases, the reaction proceeds through an initial carbonyl precoordination, followed by C–C bond formation. This suggests that during the self-trapping reaction of ketene with the zirconocene ester enolate **53** or **55**, the ketene may precoordinate to the zirconium centre as depicted in Scheme 4.5.

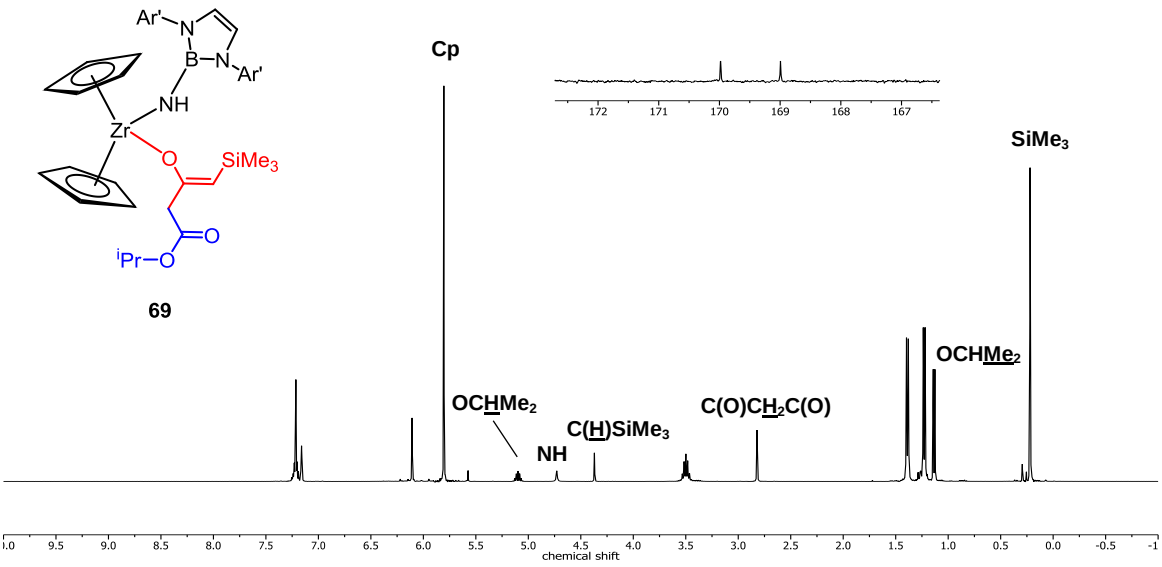

Figure 4.10. ^{1}H NMR spectrum (400.1 MHz) of $Cp_2Zr\{NHB(NAr'CH)_2\}\{OC(CHSiMe_3)CH_2CO_2{}^{i}Pr\}$ (**69**) in C_6D_6 at 298 K, and (insert) carbonyl region of the ^{13}C NMR spectrum of **69**.

Diffraction-quality crystals of **56** and **69** were grown from saturated hexane solutions at 4 °C. The solid-state structures are shown in Figure 4.11 with selected bond lengths and angles listed in Table 4.6. Both complexes possess a pseudo tetrahedral environment of zirconium with staggered cyclopentadienyl rings. The Zr(1)–N(1)–B(1) linkages of **56** and **69** show Zr(1)–N(1) single bonds of 2.093(2) and 2.107(3) Å, and Zr(1)–N(1)–B(1) bond angles of 160.3(2) and 152.2(2)°, respectively, comparable within error with the values found in the enolate borylamide analogue **53**, as well as other zirconocene borylamides described in Chapter Two. The zirconocene moiety was found to be almost identical with the same $Cp_{cent(1)}$–Zr(1)–$Cp_{cent(2)}$ angles of 127.7° and comparable Zr(1)–Cp_{cent} bond distances.

Both **56** and **69** contain an O-bound β-ketoester enolate moiety, including the C(27)–C(28) bond lengths of 1.310(11) and 1.341(4) Å, respectively, comparable with those in analogous **53**. These β-ketoester enolate moieties indicate the C-acylation of enolate by

ketene in both **56** and **69**, analogous to the C-acylation of enolates with carbonyl compounds in the aldol reaction.[58,59,77] The C-acylation of alkyl, alkenyl and aryllithium reagents by ketene has been well exploited for the regio- and stereospecific generation of enolates.[78–80] In contrast, the acylation of an enolate with ketene was found to be either in a C- or O-fashion, depending on the metal cation and the ketene structure.[81] However, O-acylation was not observed in the reaction of zirconocene borylamido compounds **53** and **55** with R(H)CCO (R = H or $SiMe_3$).

There is only one structurally authenticated β-ketoester enolate example reported in literature for all transition metals, namely $Cp_2Zr\{OC(CEt_2)C(Et_2)CO_2Me\}(Me)$ (**4.17**), containing ethyl functional groups and a disubstituted bridging α-carbon, which was synthesised by reacting $Cp_2Zr(Me)Cl$ with $LiOC(CEt_2)C(Et_2)CO_2Me$ *via* salt metathesis.[82] Compound **4.17** shows a Zr(1)–O(1)–C(27) bond angle of 163.6(4)°, deviating significantly from the 120° angle expected for an sp^2-hybridised oxygen, along with a relatively shorter Zr(1)–O(1) bond length of 1.952(4) Å.[82] These indicate a partly sp-hybridised oxygen attributed to a horizontal Zr(1)–O(1) $2p_\pi$–$4d_\pi$ interaction and a vertical π-interaction between the p-orbital (O(1)) and the C=C π-bond. In contrast, the Zr(1)–O(1)–C(27) linkages of **56** and **69** show Zr(1)–O(1) bond lengths of 2.093(2) and 2.107(3) Å, and Zr(1)–O(1)–C(27) bond angle of 140.9(6)° and 146.27(19)°, respectively, which indicates a tendency towards sp-hybridisation of O(1). This is a consequence of the more electron-rich zirconium centres of **56** and **69** (*cf.* **4.17**), where the lone pair located at N(1) of the borylamido ligand can also donate to the equatorial non-bonding d-orbital of zirconium, thus resulting in competition of $2p_\pi$–$4d_\pi$ interactions between the O(1) and N(1) atoms to the zirconium centre. However, these Zr(1)–O(1)–C(27) angles of **56** and **69** are slightly wider than that of **53** (134.68(5)°), which may reflect a stronger π-interaction (vertical) between the p-ortbial (O1) and the C(27)–C(28) π-bond (conjugation), in the absence of O(2) atom adjacent to the C(27) atom. The formation of the *Z*-configuration of **69,** as the kinetic product, is possibly due to the steric repulsion in the transition state between $–SiMe_3$ and the bulky boryl moiety.

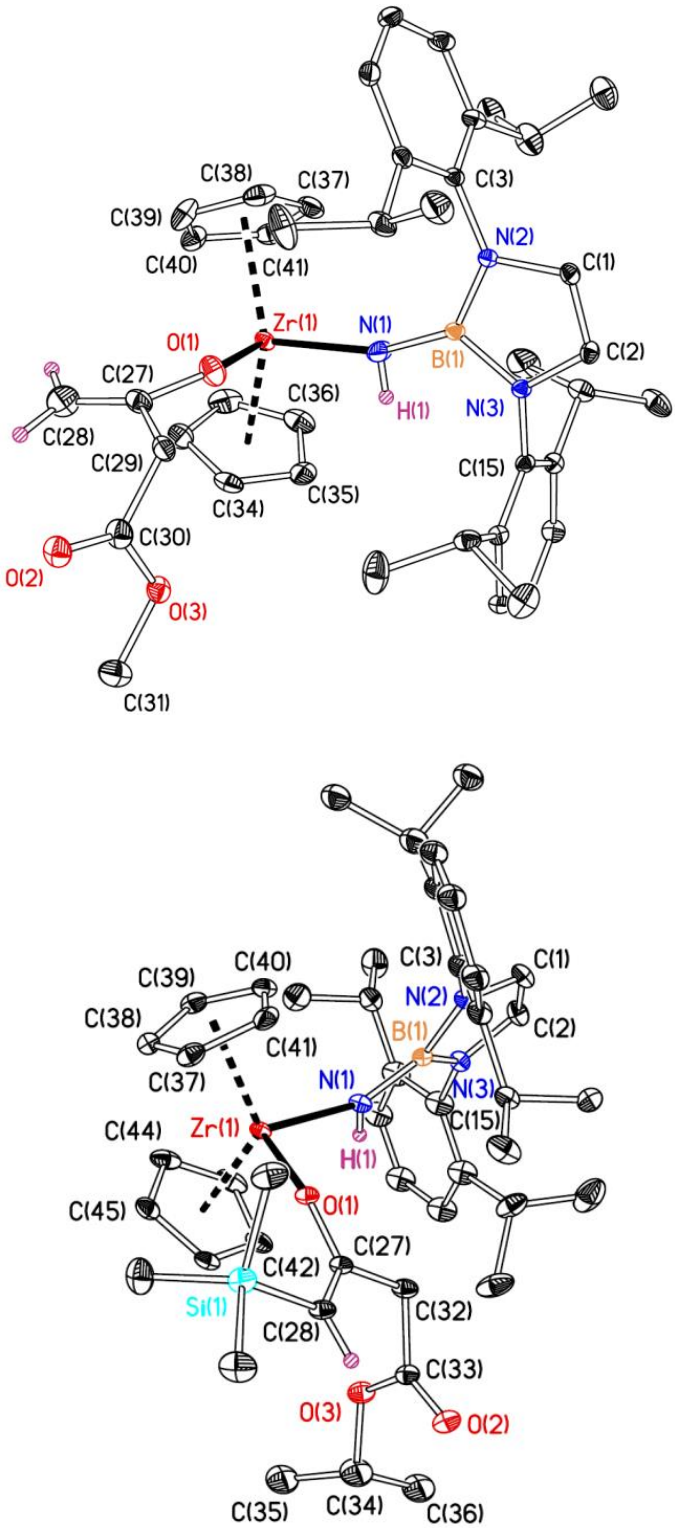

Figure 4.11. Displacement ellipsoid plot (20% probability) of $Cp_2Zr\{NHB(NAr'CH)_2\}\{OC(CH_2)CH_2CO_2Me\}$ (**56**, top) and $Cp_2Zr\{NHB(NAr'CH)_2\}\{OC(CHSiMe_3)CH_2CO_2{}^{i}Pr\}$ (**69**, bottom). Selected H atoms omitted for clarity.

Table 4.6. Selected bond lengths (Å) and angles (°) for $Cp_2Zr\{NHB(NAr'CH)_2\}\{OC(CH_2)CH_2CO_2Me\}$ (**56**) and $Cp_2Zr\{NHB(NAr'CH)_2\}\{OC(CHSiMe_3)CH_2CO_2{}^{i}Pr\}$ (**69**). $Cp_{cent(1)}$ and $Cp_{cent(2)}$ refer to the computed Cp ring centroids for "upper" and "lower" Cp rings, respectively, as depicted in Figure 4.11.

	56	**69**
Zr(1)–N(1)	2.093(2)	2.107(3)
Zr(1)–O(1)	2.106(6)	2.021(2)
Zr(1)– $Cp_{cent(1)}$	2.224	2.227
Zr(1)–$Cp_{cent(2)}$	2.241	2.247
N(1)–B(1)	1.425(3)	1.428(4)
O(1)–C(27)	1.262(11)	1.339(4)
O(2)–$C_e(1)^a$	1.172(7)	1.194(4)
O(3)–$C_e(1)^a$	1.328(7)	1.339(5)
C(27)–C(28)	1.310(11)	1.341(4)
$Cp_{cent(1)}$–Zr(1)–$Cp_{cent(2)}$	127.7	127.7
Zr(1)–N(1)–B(1)	160.3(2)	152.2(2)
Zr(1)–O(1)–C(27)	140.9(6)	146.27(19)
C(27)–$C_e(2)$–$C_e(1)^{a,b}$	112.4(6)	112.3(3)
C(28)–C(27)···$C_e(2)$–$O(1)^{a,c}$	40.07	37.60

a. "$C_e(1)$" = C(30) **56**, C(33) **69**. *b*. "$C_e(2)$" = C(29) **56**, C(32) **69**. *c*. Torsion angle for the linkage

As the ketene self-trapping step is too fast (compared to the previous ketene generation step) to be kinetically studied, it is not clear which oxygen atom (*cf.* O(1) or O(2) for **53** in Figure 4.3) facilitates the nucleophilic attack of the enolate to ketene. Therefore, reactions of $Cp_2Zr\{NHB(NAr'CH)_2\}\{OC(CH_2)OEt\}$ (**54**) and $Cp_2Zr\{NHB(NAr'CH)_2\}\{OC(CH_2)Ph\}$ (**52**) with $Me_3Si(H)CCO$ were performed on the NMR tube scale in C_6D_6 at RT. It was found that **54** reacted with the ketene immediately, like **53**. In contrast, the reaction of **52** was also observed but was significantly slower at

this concentration, requiring more than 2 days to achieve *ca.* 80% conversion and thus reflects the much lower nucleophilicity of the ketone enolate of **52** compared to the ester enolate **54**, consistent with the DFT calculations discussed above (*vide supra*) with the smaller thermodynamic driving force associated with the more stable enolate **52** (Figure 4.5).

Similar NMR tube scale reactions have been performed for thioester enolate complex $Cp_2Zr\{NHB(NAr'CH)_2\}\{OC(CH_2)SEt\}$ (**61**) and amide enolate complex $Cp_2Zr\{NHB(NAr'CH)_2\}\{OC(CH_2)NMe_2\}$ (**66**) with $Me_3Si(H)CCO$ in C_6D_6 at RT. Products $Cp_2Zr\{NHB(NAr'CH)_2\}\{OC(CHSiMe_3)CH_2C(O)SEt\}$ (**71**) or $Cp_2Zr\{NHB(NAr'CH)_2\}\{OC(CHSiMe_3)CH_2C(O)NMe_2\}$ (**72**) were formed quantitatively, respectively, with the NMR spectra being analogous to those of the homologue **69**. The reaction of **61** was found to be significantly slower at this concentration, with the half-life ($t_{1/2}$) measured to be 25 min (*cf.* <1 min for **54**). As suggested by the slow ketene trapping reaction of **52**, the slower reaction of **61** is due to its less nucleophilic enolate moiety, arising from poorer $3p_\pi$–$2p_\pi$ interaction between the C=C π-bond and the 3p lone pair at the S atom. In contrast, instantaneous formation of **72** was observed, attributed to the more nucleophilic amide enolate moiety as indicated by MO and associated orbital energies of the model $Cp_2Zr\{NHB(NMeCH)_2\}\{OC(CH_2)NMe_2\}$ (**66Q**) shown in the Appendix, Figure A3, and favourable thermodynamic driving force (*vide supra*). This confirms that the H_2CCO self-trapping step for **66** should be accessible as predicted by DFT. Therefore, the absence of further reaction from **66** is attributed to the kinetically and thermodynamically unfavourable enolate cleavage pathway to give H_2CCO in the first instance.

4.3.3 Kinetic study of the ketene elimination and trapping reactions of $Cp_2Zr\{NHB(NAr'CH)_2\}\{OC(CH_2)EEt\}$ (E= O (54), S (61))

The overall ketene elimination and self-trapping (overall redistribution) reactions of $Cp_2Zr\{NHB(NAr'CH)_2\}\{OC(CH_2)EEt\}$ (E= O (**54**), S (**61**)) are shown in Scheme 4.8. As none of the putative ketene H_2CCO was observed during the course of either reactions, a steady-state approximation was applied to this ketene in order to obtain the general rate equation (Equation 4.10 - 4.14). The final form of the general rate equation is shown in Equation 4.13.

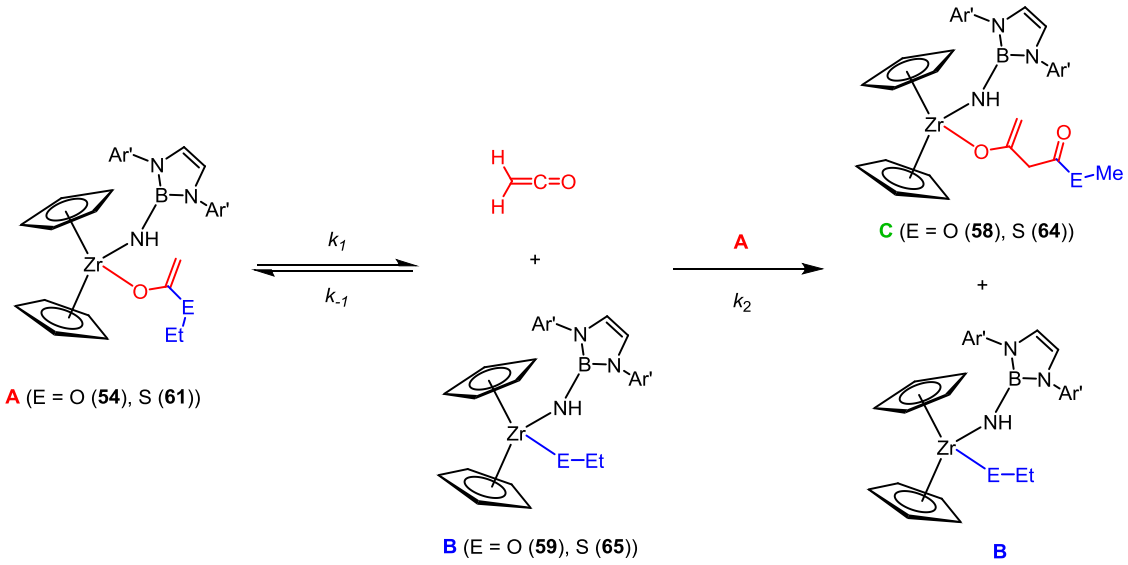

Scheme 4.8. Ketene elimination and self-trapping reactions of $Cp_2Zr\{NHB(NAr'CH)_2\}\{OC(CH_2)SEt\}$ (**61**) and $Cp_2Zr\{NHB(NAr'CH)_2\}\{OC(CH_2)OEt\}$ (**54**).

$$\frac{d[\text{ketene}]}{dt} = k_1[\boldsymbol{A}] - k_{-1}[\mathbf{B}][\text{ketene}] - k_2[\boldsymbol{A}][\text{ketene}] = 0 \qquad (4.10)$$

$$[\text{ketene}] = \frac{k_1[\boldsymbol{A}]}{k_{-1}[\mathbf{B}] + k_2[\boldsymbol{A}]} \qquad (4.11)$$

$$-\frac{d[\boldsymbol{A}]}{dt} = k_1[\boldsymbol{A}] + k_2[\boldsymbol{A}][\text{ketene}] - k_{-1}[\mathbf{B}][\text{ketene}] \qquad (4.12)$$

$$= k_1[\boldsymbol{A}] + \frac{k_1[\boldsymbol{A}](k_2[\boldsymbol{A}] - k_{-1}[\mathbf{B}])}{k_{-1}[\mathbf{B}] + k_2[\boldsymbol{A}]}$$

$$= \frac{2k_1k_2[\boldsymbol{A}]^2}{k_{-1}[\boldsymbol{B}] + k_2[\boldsymbol{A}]} \qquad (4.13)$$

$$and \ -\frac{d[\boldsymbol{A}]}{dt} = 2\frac{d[\boldsymbol{B}]}{dt} = 2\frac{d[\boldsymbol{C}]}{dt} \qquad (4.14)$$

When **A** is **54**, $k_2[\mathbf{A}] + k_{-1}[\mathbf{B}] \approx k_2[\mathbf{A}]$:

$$-\frac{d[\mathbf{54}]}{dt} = 2\frac{d[\mathbf{58}]}{dt} = 2\frac{d[\mathbf{59}]}{dt} = 2k_1[\mathbf{54}] \qquad (4.15)$$

$$\frac{d[\mathbf{59}]}{dt} = k_1[\mathbf{54}]$$

$$\int_{[\mathbf{59}]_0}^{[\mathbf{59}]_t} \frac{1}{[\mathbf{54}]} d[\mathbf{59}] = \int_{t_0}^{t_t} k_1 dt$$

$$and\ [\mathbf{54}] = [\mathbf{54}]_0 - 2[\mathbf{59}] \tag{4.16}$$

$$\int_{[\mathbf{59}]_0}^{[\mathbf{59}]_t} \frac{1}{[\mathbf{54}]_0 - 2[\mathbf{59}]} d[\mathbf{59}] = \int_{t_0}^{t} k_1 dt \tag{4.17}$$

$$\frac{1}{2}\left(\ln[\mathbf{54}]_0 - \ln([\mathbf{54}]_0 - 2[\mathbf{59}])\right) = k_1 t \tag{4.18}$$

$$\ln\left(\frac{[\mathbf{54}]_0}{[\mathbf{54}]_0 - 2[\mathbf{59}]}\right) = 2k_1 t \tag{4.19}$$

$$-\ln\left(1 - \frac{2[\mathbf{59}]}{[\mathbf{54}]_0}\right) = -\ln\left(1 - \frac{2[\mathbf{58}]}{[\mathbf{54}]_0}\right) = -\ln\left(\frac{[\mathbf{54}]}{[\mathbf{54}]_0}\right) = 2k_1 t \tag{4.20}$$

$$and\ k_{\text{obs}} = 2k_1$$

When **A** is **61**, $k_2[\mathbf{A}] + k_{-1}[\mathbf{B}] \approx k_{-1}[\mathbf{B}]$:

$$-\frac{d[\mathbf{61}]}{dt} = 2\frac{d[\mathbf{64}]}{dt} = 2\frac{d[\mathbf{65}]}{dt} = \frac{2k_1k_2[\mathbf{61}]^2}{k_{-1}[\mathbf{65}]} \tag{4.21}$$

Firstly, kinetic studies on the ester enolate complex will be discussed. The enolate cleavage reaction of **54** forming **58** and **59** was monitored by ^{1}H NMR at the temperatures 328 and 340 K. The concentration plots of decay or formation of **54**, **58** and **59** *vs* time at 340 K and 328 K are shown in Figure 4.12. Although a 1:1 ratio of **58** and **59** is expected ideally based on the proposed mechanism, the observed growth of **58** is slightly lower than that of **59** (Figure 4.12, top). This is particularly apparent when the reaction is performed at higher temperature (340 K, Figure 4.12, bottom), and is possibly due to small amounts of other side reactions of these complexes with the highly reactive ketene. Since no induction period was observed in Figure 4.12, the simultaneous formation of **58** and **59**, again, indicate that the ketene self-trapping step is much faster than the rate determining intramolecular enolate cleavage (ketene elimination) step ($k_2 >> k_1$).

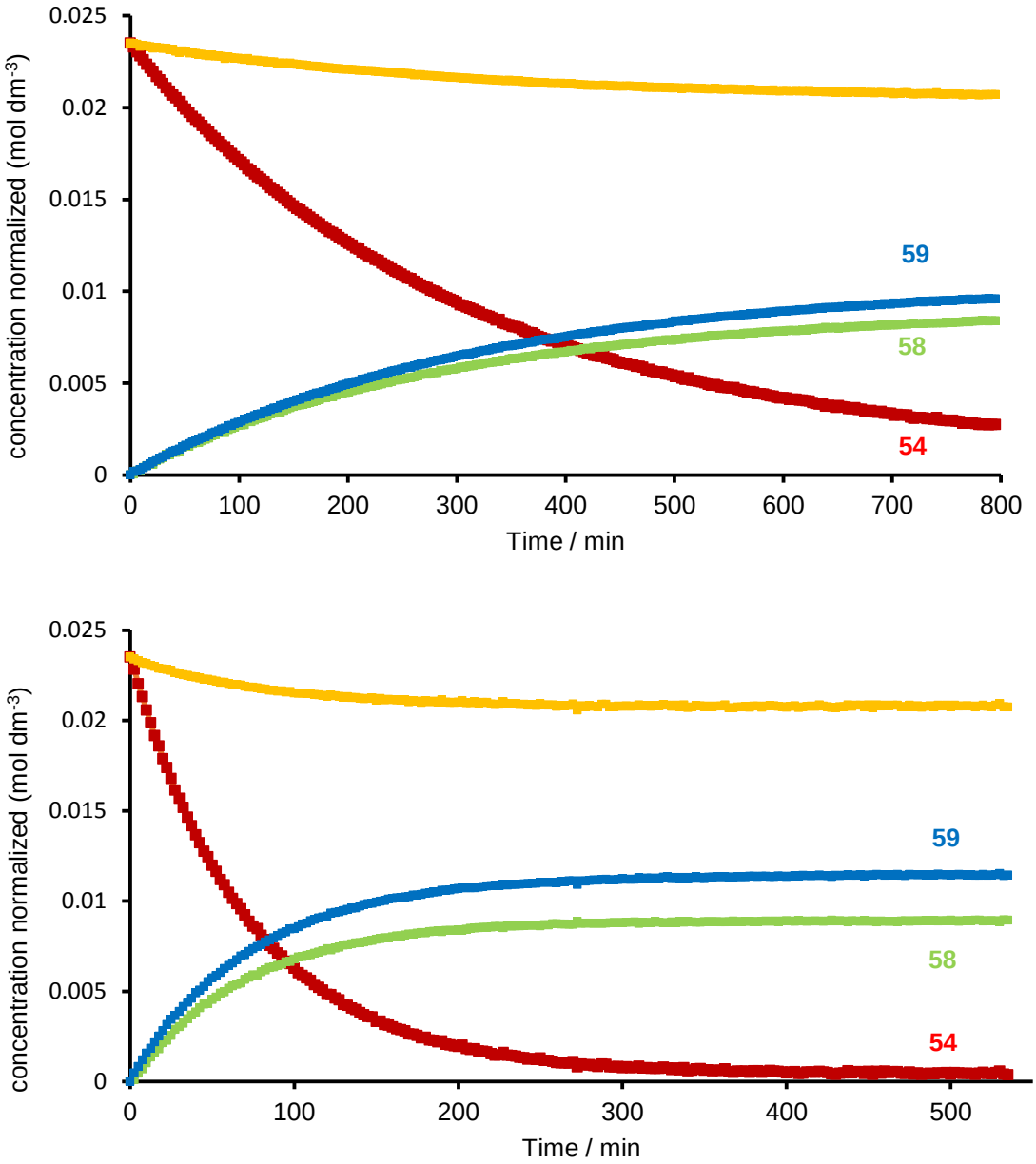

Figure 4.12. Decay of $Cp_2Zr\{NHB(NAr'CH)_2\}\{OC(CH_2)OEt\}$ (**54**, red), growth of $Cp_2Zr\{NHB(NAr'CH)_2\}\{OC(CH_2)CH_2CO_2Et\}$ (**58**, green) and $Cp_2Zr\{NHB(NAr'CH)_2\}(OEt)$ (**59**, blue), and sum of concentrations (yellow) of **54**, **58** and **59** at 328 K (top) and 340 K (bottom) in C_6D_6.

Interestingly, the decay of **54** was found to follow a well-behaved first order kinetics within the first half-life (*ca.* 200 min at 328 K), and to slightly deviate (slower than expected) from the ideal linear behaviour in the late stage, as judged by a semi-logarithmic plot of $\ln([\mathbf{54}]/[\mathbf{54}]_0)$ (Figure 4.13, top). The plots are shown to at least 85%

conversion (approximately three half-lives). Similar plots for products **58** and **59** were displayed using $-\ln(1-2[\mathbf{58}]/[\mathbf{54}]_0)$ and $-\ln(1-2[\mathbf{59}]/[\mathbf{54}]_0)$ *vs* time (Figure 4.13, bottom), and these equations are expressed in Equation 4.16 – 4.20. The ideal first order linear behaviour of **54**, **58** and **59** were also plotted as dashed lines in Figure 4.13, based on the extrapolated k_{obs}(A) and k_{obs}(B), respectively (*vide infra*). The later two plots also follow well-behaved first order linear kinetics in the early stage (*ca.* 200 min), and then the reaction rate appears to slow as the reaction progresses.

The initial linear regions are well-overlapped indicating the rate of formations of **58** and **59** are similar. However, in the late stage of the formation of **58**, the deviation from linearity is more significant compared to **59** and **54**. This is expected, as shown in Figure 4.12, the difference between [**58**] and [**59**] is amplified during the reaction and remaining constant after quantitative conversion, accompanied by the sum of the concentrations being lower than expected (based on $[\mathbf{54}]_0$). This may suggest that the eliminated ketene resulted in deleterious side reactions with the complex mixture, thus such eliminated ketene consumption impeding the self-trapping reaction.

k_{obs} was extrapolated from the linear regions (first half-life, *ca*. 200 min). The k_{obs}(A) of **54** decay ($5.22(1) \times 10^{-5}$ s^{-1}), k_{obs}(B) of **59** ($4.62(7) \times 10^{-5}$ s^{-1}) and k_{obs}(C) of **58** ($4.16(1) \times 10^{-5}$ s^{-1}) formation are very similar to each other, indicating that the rate of **58** formation is dominated by the slowest rate-determining ketene elimination. As the decay of **54** follows well-behaved first order kinetics ($r^2 = 0.998$), k_{obs}(A) was also measured after three half-lives for comparison, as $4.89(1) \times 10^{-5}$ s^{-1}, this being close to the value calculated within one half-life ($5.22(1) \times 10^{-5}$ s^{-1}), but slightly lower because of the decreased rate of consumption noted above.

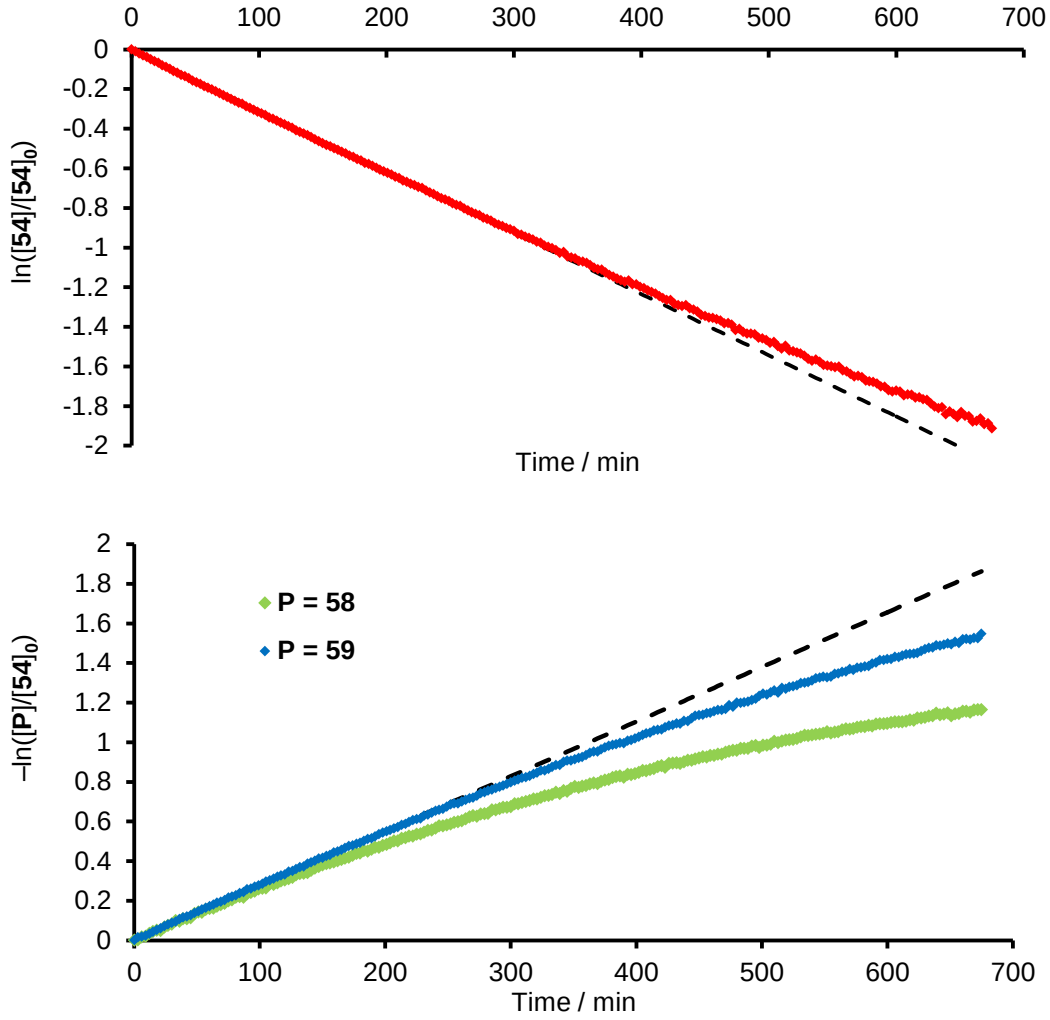

Figure 4.13. Top: first order semi-logarithmic plots for decay of $Cp_2Zr\{NHB(NAr'CH)_2\}\{OC(CH_2)OEt\}$ (**54**, red, r^2 = 0.998) at 328 K in C_6D_6. Dashed lines represent the ideal first order behaviour based on measured k_{obs} from the linear region within the first 200 min of **54**. Bottom: first order semi-logarithmic plots for growth of $Cp_2Zr\{NHB(NAr'CH)_2\}\{OC(CH_2)CH_2CO_2Et\}$ (**58**, green, r^2 = 0.952) and $Cp_2Zr\{NHB(NAr'CH)_2\}(OEt)$ (**59**, blue, r^2 = 0.988). Dashed lines represent the ideal first order behaviour based on measured k_{obs} from the linear region within the first 200 min of **59**.

Guided by the general rate Equation 4.13, the possible backward reaction (from **59** to **54**) was investigated in an attempt to shed light on the relative magnitude of k_{-1} for understanding the first order character in this case. ^{1}H NMR spectra for the conversion of the ester enolate complex $Cp_2Zr\{NHB(NAr'CH)_2\}\{OC(CH_2)OEt\}$ (**54**) to $Cp_2Zr\{NHB(NAr'CH)_2\}\{OC(CH_2)CH_2CO_2Et\}$ (**58)** and $Cp_2Zr\{NHB(NAr'CH)_2\}(OEt)$ (**59**) *with* or *without* adding three equivalents of **59** at 340 K were performed. Both semi-logarithmic plots of ln([**54**]/[**54**]$_0$) *vs* time were found follow well-behaved first order kinetics within the first half life, and become slower than expected as the reaction progresses. It was found that the measured $t_{1/2}$ values are identical as *ca*. 50 min, and the extrapolated k_{obs}(A) within one half-life are 2.18(1) × 10^{-4} s^{-1} and 2.11(1) × 10^{-4} s^{-1}, respectively, being equivalent within error. This indicates that the possible backward reaction (insertion of ketene into the Zr–OMe bond of **59**) is not significant compared to the rapid forward ketene self-trapping (k_2 >> k_{-1}). Thus, the approximation k_2[**54]** >> k_{-1}[**59**] can be applied for the early stage of such reaction. This leads to the rate equation shown in Equation 4.15, and the rate will show a first-order character in **54**, **59** or **58**, with the rate constant k_{obs}(A, B and C) = 2k_1. Therefore, k_1 (328 K) was able to be calculated from k_{obs}(A, B and C) as 2.61(1) × 10^{-5} s^{-1}, 2.41(4) × 10^{-5} s^{-1} and 2.08(1) × 10^{-5} s^{-1}, respectively, being approximately equivalent within error. However, as observed in Figure 4.13, the deviation from linearity in the late stage of such reaction is due to the increased and decreased amount of **59** and **54**, respectively. This results in the approximation k_2[**54]** >> k_{-1}[**59**] being inappropriate, and the reaction appears to have more second order character as the reaction progresses. Therefore, for comparison, the initial rate method (Section 3.3.2, Chapter Three) was alternatively applied to measure the decay rate of **54** as 1.36(1) × 10^{-6} mol dm^{-3} s^{-1} and formation rates of **59** and **58** as 0.56(5) × 10^{-6} mol dm^{-3} s^{-1} and 0.55(1) × 10^{-6} mol dm^{-3} s^{-1}, respectively at this concentration ([**54**]$_0$ = 0.0235 mol dm^{-3}). These give similar k_1 values of 2.89(2) × 10^{-5} s^{-1}, 2.38(10) × 10^{-5} s^{-1} and 2.34(2) × 10^{-5} s^{-1}, respectively, and comparable to the values obtained above from semi-logarithmic plots.

To interrogate the proposed mechanism further, an Eyring analysis of the first order rate constants, k_1, was carried out for the enolate cleavage reaction of **54**. The enolate cleavage reaction of **54** forming **58** and **59** was monitored by ^{1}H NMR spectroscopy in the temperature range 328 – 340 K. The semi-logarithmic plots of –ln([**54**]/[**54**]$_0$) *vs* time are shown in Figure 4.14 (top) to at least 85% conversion (approximately three half-

lives). These linear plots show well-behaved first order kinetics, with only a small degree of deviation in the very end of the reaction. Analysis of the k_1 values gave the activation parameters $\Delta H^{\ddagger}$ = 27.2(0.7) kcal mol^{-1} and $\Delta S^{\ddagger}$ = 2.9(2.0) cal mol^{-1} K^{-1} ($\Delta G_{340}^{\ddagger}$ = 26.2(0.7) kcal mol^{-1}) (Figure 4.14, bottom). For comparison, those activation parameters are alternatively extrapolated from plotting the linear region (one half-life) or calculated using k_1 values found by initial rates (in parentheses), shown in the Appendix A2, being $\Delta H^{\ddagger}$ = 26.8(0.8) (25.8(0.8)) kcal mol^{-1}, $\Delta S^{\ddagger}$ = 1.8(2.0) (–1.1(4.0)) cal mol^{-1} K^{-1} and $\Delta G_{340}^{\ddagger}$ = 26.2(1.0) (26.2(1.9)) kcal mol^{-1}, respectively, which are identical within error to the values obtained above. The Gibbs free energy of activation ($\Delta G^{\ddagger}$) value is consistent with reactions that require elevated temperatures to proceed. The entropy of activation ($\Delta S^{\ddagger}$) value is close to 0 within error. This suggests that the transition state **57_TS** (Scheme 4.5), to cleave enolate forming ketene and alkoxyl complex, is relatively early and occurs without significant departure of H_2CCO from the zirconium coordination sphere.

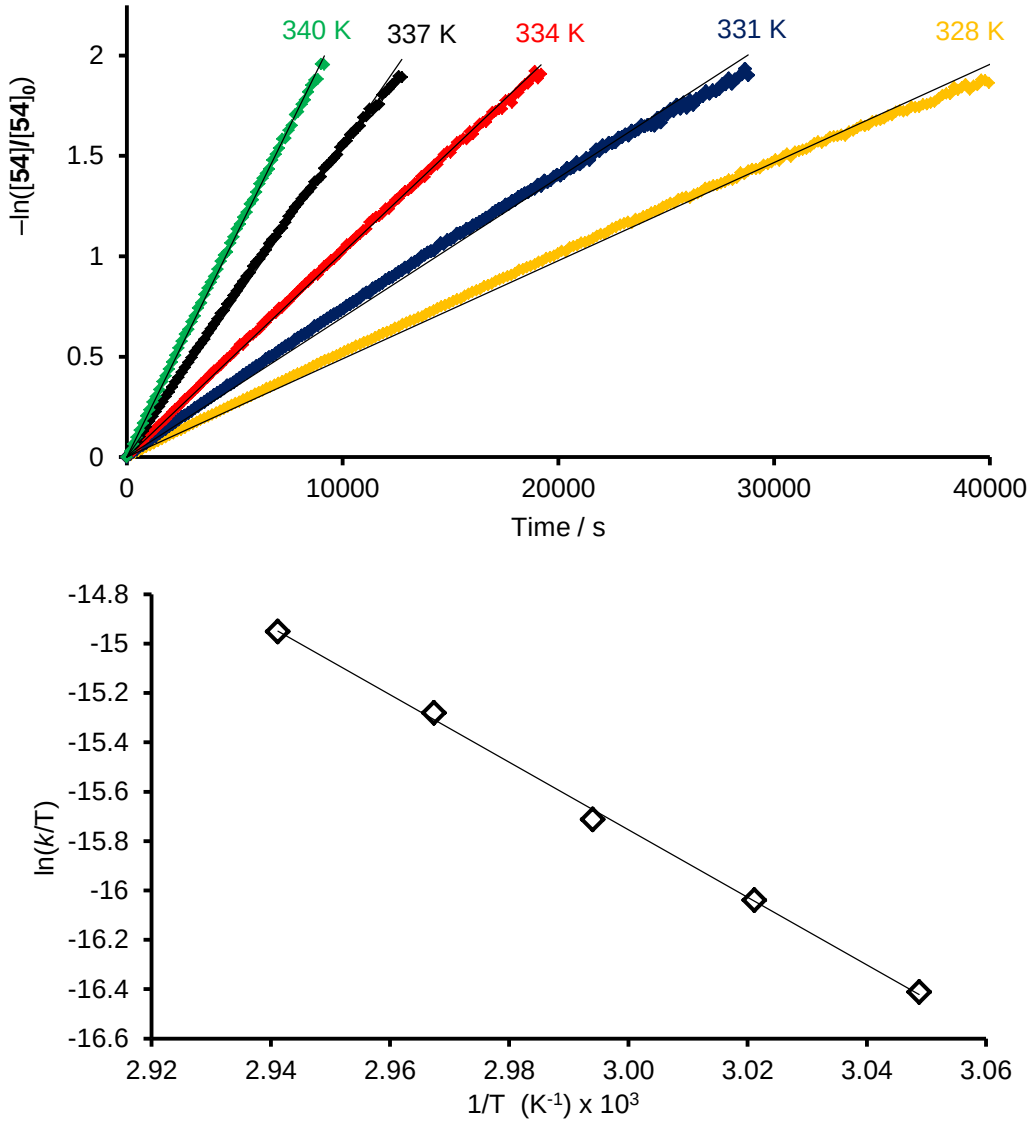

Figure 4.14. Top: first order semi-logarithmic plots for the conversion of $Cp_2Zr\{NHB(NAr'CH)_2\}\{OC(CH_2)OEt\}$ (**54**) to $Cp_2Zr\{NHB(NAr'CH)_2\}\{OC(CH_2)CH_2CO_2Et\}$ (**58**) and $Cp_2Zr\{NHB(NAr'CH)_2\}(OEt)$ (**59**) in C_6D_6. (avg. r^2 = 0.997, range 0.995 – 0.999). Bottom: Eyring plot for the conversion of $Cp_2Zr\{NHB(NAr'CH)_2\}\{OC(CH_2)OEt\}$ (**54**) to $Cp_2Zr\{NHB(NAr'CH)_2\}\{OC(CH_2)CH_2CO_2Et\}$ (**58**) and $Cp_2Zr\{NHB(NAr'CH)_2\}(OEt)$ (**59**) in C_6D_6. Activation parameters derived from linear regression analysis (r^2 = 0.998): $\Delta H^{\ddagger}$ = 27.2(0.7) kcal mol^{-1}; $\Delta S^{\ddagger}$ = 2.9(2.0) cal mol^{-1} K^{-1}; $\Delta G_{340}{}^{\ddagger}$ = 26.1(0.7) kcal mol^{-1}.

Next, the reaction of $Cp_2Zr\{NHB(NAr'CH)_2\}\{OC(CH_2)SEt\}$ (**61**) to from $Cp_2Zr\{NHB(NAr'CH)_2\}(SEt)$ (**65**) and $Cp_2Zr\{NHB(NAr'CH)_2\}\{OC(CH_2)CH_2C(O)SEt\}$ (**64**) was studied and monitored by ^1H NMR spectroscopy at 340 K. This temperature was chosen, in order to make direct comparison with the ethyl-substituted ester enolate congener **54**. It is of interest that the ketene self-trapping appeared to be more controlled, forming **64** almost quantitatively, and the total concentration of **61** and the products remaining constant (Figure 4.15, top), even at 340 K. As found for the reaction of **54**, the simultaneous formation of **65** and **64** indicates that the ketene self-trapping step is also much faster than the rate determining intramolecular enolate cleavage (ketene elimination) step ($k_2 >> k_1$). Surprisingly, this reaction was found to be close to second order kinetic behaviour as judged by linear semi-reciprocal plots of 1/[**61**] *vs* time, with an extrapolated k_{obs} of 4.54(2) × 10^{-4} dm^3 mol^{-1} s^{-1}. The plots are shown to at least 85% conversion (approximately three half-lives) in Figure 4.15 (bottom).

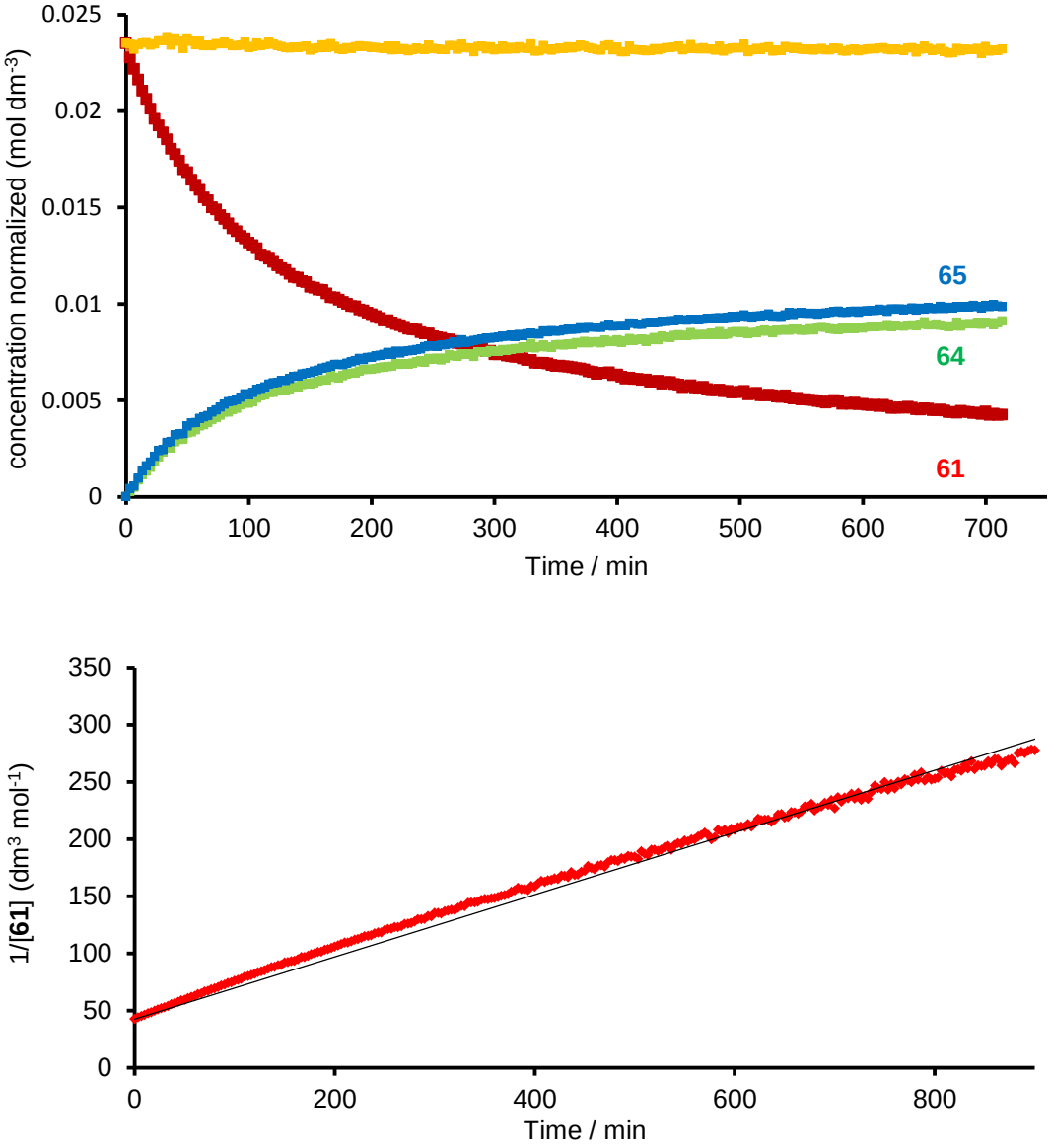

Figure 4.15. Top: decay of $Cp_2Zr\{NHB(NAr'CH)_2\}\{OC(CH_2)SEt\}$ (**61**, red), growth of $Cp_2Zr\{NHB(NAr'CH)_2\}\{OC(CH_2)CH_2C(O)SEt\}$ (**64**, green) and $Cp_2Zr\{NHB(NAr'CH)_2\}(SEt)$ (**65**, blue), and sum of the concentrations (yellow) of **61**, **64** and **65** at 340 K in C_6D_6. Bottom: second order semi-reciprocal plot for the decay of $Cp_2Zr\{NHB(NAr'CH)_2\}\{OC(CH_2)SEt\}$ (**61**, red) at 340 K in C_6D_6. (r^2 = 0.988).

The reaction of **61** was found to be somewhat slower compared to that of **54** with a half-life ($t_{1/2}$) of 127 mins (*cf.* 50 mins for **54**) at the same concentration and temperature (340 K). To account for the second order kinetics, it was suspected that the thioester enolate **61** may be reversibly reformed during the reaction by H_2CCO insertion into the Zr–S bond. The DFT calculations (*vide supra*) on the related $Cp_2Zr\{NHB(NAr'CH)_2\}(EMe)$ (E = O, S) homologues found that Δ_rG for ketene elimination was slightly more endergonic (4.9 kcal mol^{-1} for E = S, *cf.* 4.1 kcal mol^{-1} for E = O), which might lower $\Delta G^{‡}$ for the k_{-1} step and increase k_{-1} relative to k_1 for E = S. In addition, the thiolate ligand (**65**) is more nucleophilic than the alkoxy ligand (**59**). Similar reactions have previously been reported, showing that the ketene Ph(R')CCO (R' = Ph or Et) can be inserted into the bridging thiolate ligands of $[Cp_2Ln(\mu\text{-}SR)]_2$ (R = Et, Bn or Ph, Ln = Yb, Er or Y) to generate the O-bridged thioester enolate compounds $[Cp_2Ln(\mu\text{-}\eta^1\text{:}\eta^2\text{-}OC(SR)C(R)Ph]_2$ (**4.15**).[71–73]

To test for the reversibility of the ketene elimination step for the thioester enolate complex, a crossover reaction was performed by reacting $Cp_2Zr\{NHB(NAr'CH)_2\}\{OC(CH_2)SMe\}$ (**60**) with one equivalent of $Cp_2Zr\{NHB(NAr'CH)_2\}(SEt)$ (**65**, Scheme 4.9). On the NMR tube scale in C_6D_6 at 340 K, the thioester enolate cleavage and ketene self-trapping of **60** to generate $Cp_2Zr\{NHB(NAr'CH)_2\}(SMe)$ (**63**) and $Cp_2Zr\{NHB(NAr'CH)_2\}\{OC(CH_2)CH_2C(O)SMe\}$ (**62**) were observed, as described above. In addition, the eliminated ketene which was generated from **60**, was found to be rapidly trapped by **65** forming the ethyl substituted thioester enolate compound **61** over 3 h at 340 K (Scheme 4.9 and Figure 4.16). After 16 h, the consumption of **61** and the formation of the final product $Cp_2Zr\{NHB(NAr'CH)_2\}\{OC(CH_2)CH_2C(O)SEt\}$ (**64**) were found resulting from the further ketene self-trapping of formed **61**. After 66 h at 340 K, both of the β-ketothioester enolate compounds **64** and **62**, and both of the thiolate compounds **65** and **63** were observed in *ca.* 0.7:1.1:3.3:3.9 ratio, which is comparable to the expected statistical ratio of 1:1:3:3 by assuming no kinetic or thermodynamic preference. Therefore, these clearly illustrate the reversibility of the ketene elimination reaction where the eliminated ketene can undergo rapid nucleophilic attack by simultaneously generated thiolate zirconocene complex to reform the thioester enolate, resulting in a slower reaction overall by such pre-equilibrium.

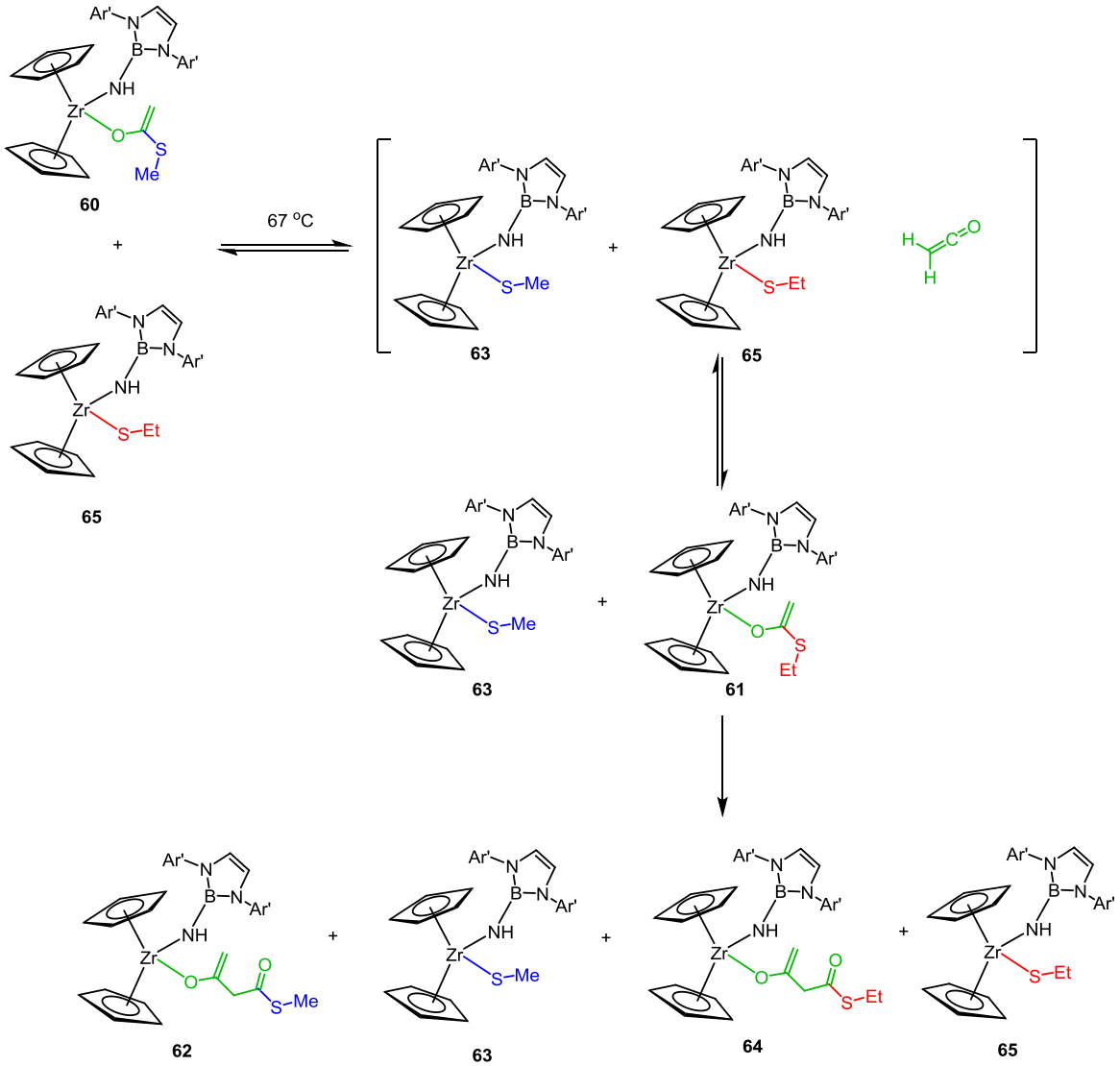

Scheme 4.9. Crossover reaction of $Cp_2Zr\{NHB(NAr'CH)_2\}\{OC(CH_2)SMe\}$ (**60**) with $Cp_2Zr\{NHB(NAr'CH)_2\}(SEt)$ (**65**), generating ethyl substituted $Cp_2Zr\{NHB(NAr'CH)_2\}\{OC(CH_2)SEt\}$ (**61**), $Cp_2Zr\{NHB(NAr'CH)_2\}\{OC(CH_2)CH_2C(O)SEt\}$ (**64**) at 340 K in C_6D_6.

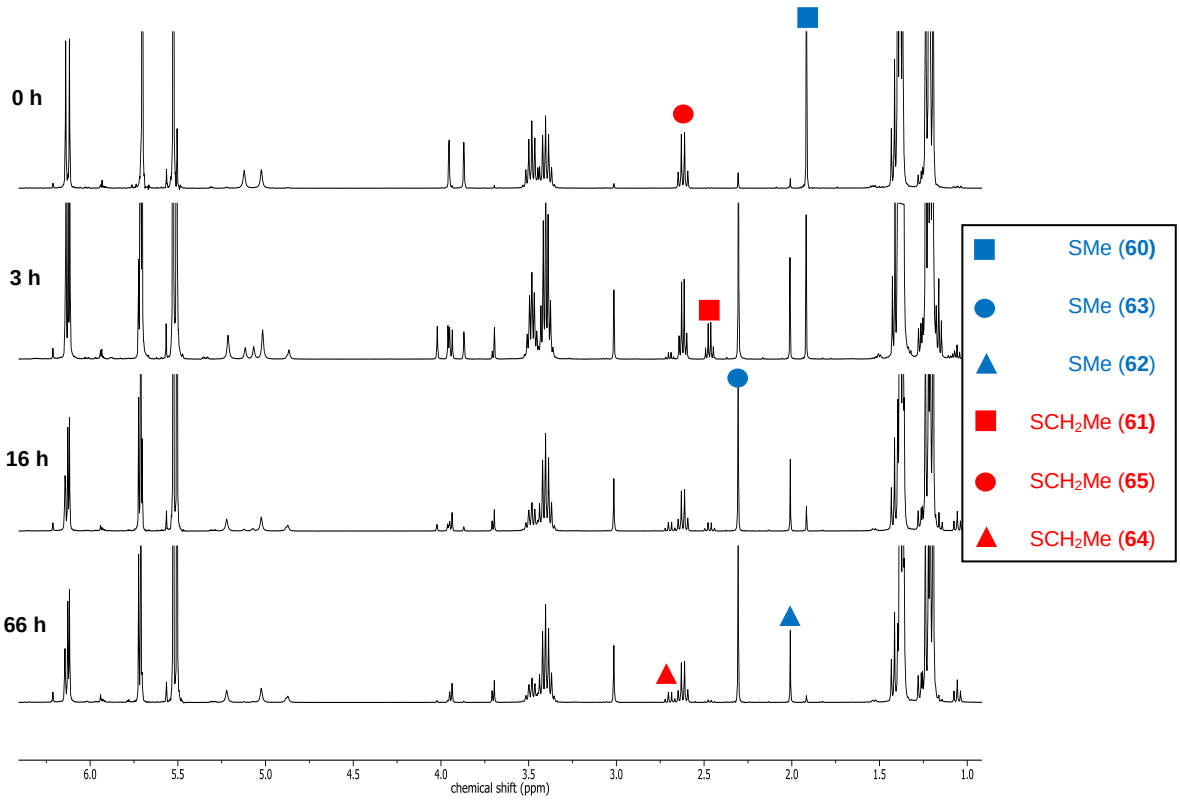

Figure 4.16. Partial ^{1}H NMR spectrum (400.1 MHz) for the crossover reaction of $Cp_2Zr\{NHB(NAr'CH)_2\}\{OC(CH_2)SMe\}$ (**60**) with $Cp_2Zr\{NHB(NAr'CH)_2\}(SEt)$ (**65**) in C_6D_6 at 340 K (*cf.* Scheme 4.9).

To further support the reversibility of the ketene elimination, the reaction of **61** with three equivalents of the corresponding thiolate complex **65** was monitored by ^{1}H NMR spectroscopy at 340 K. The decay plots of **61** *with* or *without* adding **65** are shown in Figure 4.17. By adding three equivalents of **65**, the rate of **61** decay is dramatically decreased, and the $t_{1/2}$ is significantly increased from 127 min to 13.9 h, again determining the reversibility of the ketene elimination step for the thioester enolate (larger k_{-1}). This is in contrast to the reaction of the ester enolate congener **54**, where addition of extra alkoxy complex has no significant effect on rates. Thus for thioester enolate **61**, such pre-equilibrium (enolate cleavage and reformation) may contribute to its more controllable ketene elimination and self-trapping steps, resulting in the sum of the concentrations remaining constant.

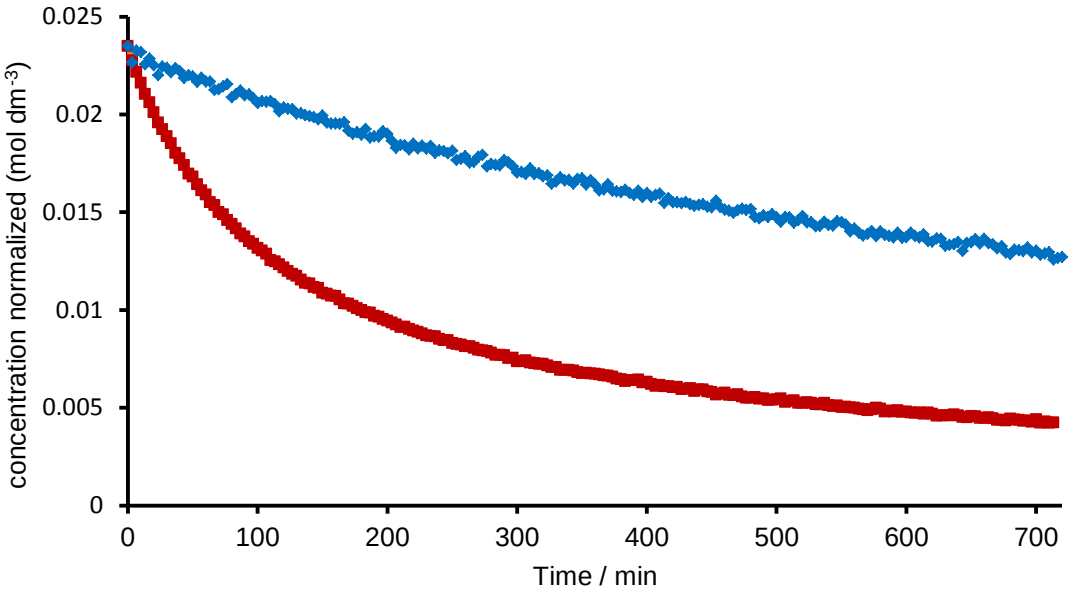

Figure 4.17. Decay of $Cp_2Zr\{NHB(NAr'CH)_2\}\{OC(CH_2)SEt\}$ (**61**, red), and $Cp_2Zr\{NHB(NAr'CH)_2\}\{OC(CH_2)SEt\}$ (**61**, blue) with three equivalents of $Cp_2Zr\{NHB(NAr'CH)_2\}(SEt)$ (**65**) at 340 K in C_6D_6.

For the thioester enolate compound **61**, the backward reaction is more significant indicating a large k_{-1}. In addition, based on the relative rate comparison of the $Me_3Si(H)CCO$ trapping reactions with ester enolate **54** and thioester congener **61**, the ketene self-trapping for thioester enolate **61** is expected to be significantly slower, with a comparably smaller k_2. The smaller k_2 implied by the model reaction with $Me_3Si(H)CCO$ is consistent with additional DFT calculations on the model thioester enolate $Cp_2Zr\{NHB(NMeCH)_2\}\{OC(CH_2)SMe\}$ (**60Q**). The HOMO-1 of **60Q** resembled that of the OMe congener **55Q** (Figure 4.5), but had only a 44% weighting on the 2p C atom of $C=\underline{C}H_2$ (Appendix, Figure A3) compared to 53% found for **55Q** (suggesting lower nucleophilicity), where the same trend was observed in enols (Appendix, Figure A4). Finally, recall that DFT calculations (*vide supra*) showed that H_2CCO trapping by thioester enolate **60** was 5.0 kcal mol^{-1} less exergonic than that for enolate congener **55**, which again would imply a reduced k_2 for the thioester enolate system. Such a difference may result in $k_{-1} >> k_2$ overall, and the approximation k_{-1}[**65**] >> k_2[**61**], even in the early stage at high [**61**], can be applied. This leads to the rate equation shown in Equation 4.21 for the reaction of thioester enolates, and the rate will show a dependence on **61** with second-order character, with the k_{obs} being a combination of k_1, k_{-1}, k_2 and [**65**]. Having

[**65**] as a factor in the rate equation explains the slightly non-linear nature of the semi-reciprocal *vs* time plot for **61** decay in Figure 4.15 (bottom), in which [**65**] is increasing as the reaction progresses.

4.4 Reactions of $Cp_2Zr\{NB(NAr'CH)_2\}(py)$ (11) with strained heterocycles

4.4.1 Reactions of $Cp_2Zr\{NB(NAr'CH)_2\}(py)$ (11) with epoxides

When **11** was treated with one equivalent of the epoxides, 1,2-epoxy-2-methylpropane or propylene oxide, which contain accessible β-hydrogens, on the NMR tube scale in C_6D_6, quantitative formation of a single product was observed at 50 °C in each case. Crystallographic and NMR characterisation (*vide infra*) showed that the alkoxyl allylic zirconocene borylamide $Cp_2Zr\{NHB(NAr'CH)_2\}\{OCH_2C(CH_2)R\}$ (R = Me (**74**) or H (**75**)) was formed respectively *via* β-hydrogen atom abstraction. On the preparative scale, **11** was mixed with 1,2-epoxy-2-methylpropane in benzene at 50 °C, and the orange-red solution slowly changed to pale yellow over 16 h, yielding **74** in 55% crystalline yield. The reaction between **11** and propylene oxide required the same reaction condition, yielding **75** as a red solid in 71% yield (Scheme 4.10).

The ^{1}H and ^{11}B NMR spectra of both **74** and **75** show the same diagnostic features of zirconocene borylamido compounds, including ^{11}B signals both at 25.3 ppm and broad ^{1}H singlet NH resonances at 4.22 ppm attributable to the borylamido fragment, like other zirconocene borylamides isolated in Section 4.3. In the ^{1}H NMR spectrum of **74**, new singlet vinyl protons at 4.89 and 4.81 ppm were observed, with an HSQC correlation observed to a ^{13}C signal of $OCH_2C(=\underline{C}H_2)CH_3$ at 108.5 ppm, and an HMBC correlation to a quaternary ^{13}C signal of $OCH_2\underline{C}(=CH_2)CH_3$ at 146.8 ppm. This quaternary ^{13}C signal also shows HMBC correlations to a ^{1}H signal (3 H) at 1.57 ppm attibuted to one methyl group, and a ^{1}H signal (2 H) at 4.00 ppm attributed to methylene protons of $ZrOC\underline{H}_2$. In contrast, the ^{1}H NMR spectrum of **75** shows two doublet of doublet terminal vinyl signals at 5.09 and 5.00 ppm, with HSQC correlations to a ^{13}C signal of $OCH_2CH=\underline{C}H_2$ at 112.7 ppm, and HMBC correlations to a ^{13}C signal of $OCH_2\underline{C}H=CH_2$ at 140.3 ppm. In this case, the ^{13}C signal at 140.3 ppm shows an HSQC correlation with a high multiplicity (tdd) ^{1}H signal at 5.77 ppm, due to the coupling with the methylene and terminal vinyl protons.

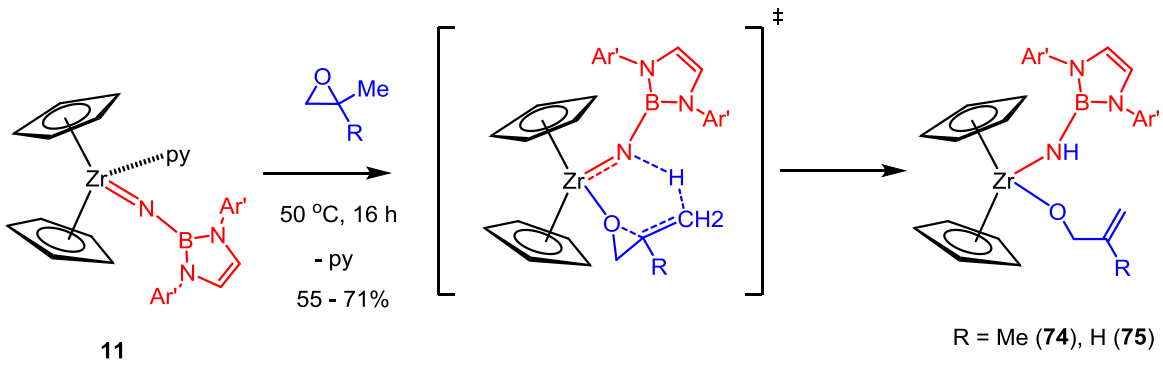

Scheme 4.10. Synthesis of $Cp_2Zr\{NHB(NAr'CH)_2\}\{OCH_2C(CH_2)R\}$ (R = Me (**74**) or H (**75**)) from $Cp_2Zr\{NB(NAr'CH)_2\}(py)$ (**11**).

Diffraction-quality crystals of **74** were grown from a hexane solution at –30 °C. The solid state structure is shown in Figure 4.18, and selected bond distances and angles are listed in Table 4.7. This allylic alkoxyl borylamido zirconocene compound **74** has an analogous structure to that of other isolated borylamido zirconocene compounds (*vide supra*), having a pseudo tetrahedral environment with staggered cyclopentadienyl rings. The Zr(1)–N(1)–B(1) linkage of **74** shows a Zr(1)–N(1) bond length of 2.092(3) Å, and a Zr(1)–N(1)–B(1) bond angle of 150.7(2)°, indicating a borylamido moiety and similar to those found in **59** and **53** (Section 4.3.2). The Zr(1)–O(1) bond length is 1.968(3) Å, comparable to that of the ethoxyl analogue **59** and marginally shorter than that of **53** and **60**. Like **59**, this indicates some degree of $2p_\pi$–$4d_\pi$ interaction between Zr(1) and O(1), and π-interaction between O(1) and C(27) is not possible due to the sp^3-hybridised C(27). The sum of the angles subtended at C(28) of 360(10)° indicates an sp^2-hybridised C(28), and the C(28)–C(29) bond length of 1.303(10) Å implies a C=C double bond.[83]

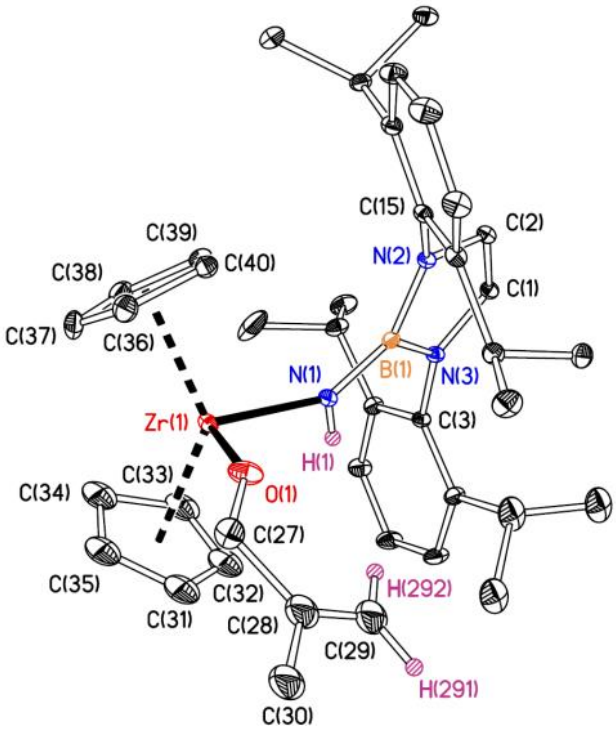

Figure 4.18. Displacement ellipsoid plot (20% probability) of $Cp_2Zr\{NHB(NAr'CH)_2\}\{OCH_2C(CH_2)CH_3\}$ (**74**). Selected H atoms omitted for clarity.

Table 4.7. Selected bond lengths (Å) and angles (°) for $Cp_2Zr\{NHB(NAr'CH)_2\}\{OCH_2C(CH_2)CH_3\}$ (**74**). $Cp_{cent(1)}$ and $Cp_{cent(2)}$ refer to the computed Cp ring centroids for "upper" and "lower" Cp rings, respectively, as depicted in Figure 4.18.

Zr(1)–N(1)	2.092(3)	$Cp_{cent(1)}$–Zr(1)–$Cp_{cent(2)}$	131.0
Zr(1)–O(1)	1.968(3)	Zr(1)–N(1)–B(1)	150.7(2)
Zr(1)–$Cp_{cent(1)}$	2.239	N(1)–B(1)–N(2)	133.4(3)
Zr(1)–$Cp_{cent(2)}$	2.269	N(1)–B(1)–N(3)	123.0(3)
N(1)–B(1)	1.427(4)	Zr(1)–O(1)–C(27)	149.8(3)
B(1)–N(2)	1.452(4)	C(27)–C(28)–C(29)	121.6(6)
B(1)–N(3)	1.447(4)	C(29)–C(28)–C(30)	124.2(6)
O(1)–C(27)	1.369(4)	C(30)–C(28)–C(27)	114.2(6)
C(28)–C(29)	1.303(10)		
C(28)–C(30)	1.486(9)		

Next, cyclohexene oxide, in which the β-hydrogen atoms are less accessible, was reacted with **11**. A much slower reaction was noticed on the NMR tube scale in C_6D_6 at 60 °C over 16 h. The colour of the solution slowly changed to dark red from orange-red, and the ^{1}H NMR spectrum of the reaction mixture indicated quantitative conversion to an allylic alkoxyl borylamido zirconocene complex. On the preparative scale, **11** was reacted with cyclohexene oxide in toluene solution at 90 °C for 16 h. The product $Cp_2Zr\{NHB(NAr'CH)_2\}$(O-cyclohex-2,3-ene) (**76**) was formed *via* β-hydrogen atom abstraction and isolated in 66% yield (Equation 4.22).

The ^{1}H and ^{11}B NMR spectra of **76** are consistent with a zirconocene borylamido compound, showing a diagnostic ^{11}B signal at 25.5 ppm and a broad NH ^{1}H singlet at 3.72 ppm. The ^{1}H and ^{13}C features of the zirconocene borylamido fragments are analogous to those of **74** and **75** showing a C_s symmetric species. In addition, three multiplets (1 H each) at 5.58, 5.45 and 4.19 ppm were observed in the ^{1}H NMR spectrum, which are attributed to the methine protons of vinyl and ZrOC<u>H</u> moieties, while the rest of the methylene protons (2 H each) of the cyclohexene fragment were found at 1.83, 1.56 and 1.20 ppm as complex multiplets.

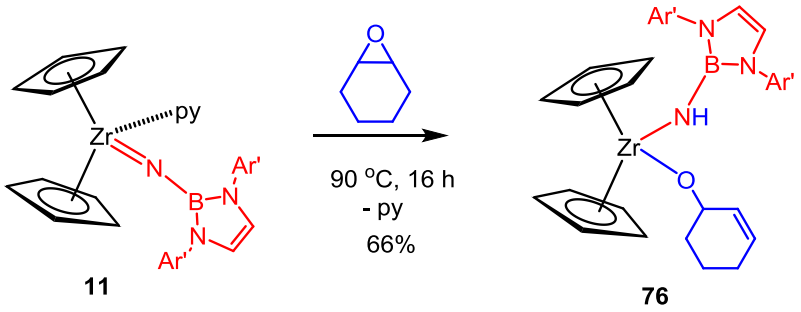

Equation 4.22.

As mentioned above, the characterisations of the products **74**, **75** and **76** clearly imply that the allylic alkoxyl borylamido zirconocene products were formed *via* β-hydrogen atom abstraction of epoxides, and the proposed six-membered-ring transition state has been depicted in Scheme 4.10. Analogous elimination reactions have been reported for the imido zirconocene compound **1.4** by Bergman *et al*. They found that when **1.4** was reacted with epoxides (1,2-epoxy-2-methylpropane, propylene oxide or cyclohexene oxide) which contain accessible β-hydrogens, β-hydrogen atom abstraction forming the corresponding allylic alkoxyl amido zirconocene compounds was observed;[5] the same outcome as the reactions of **11**. Detailed DFT calculations have been performed and

discussed by Venuvanalingam *et al*.[84] Both the experimental and computational results indicate that the pre-coordination of epoxide to the zirconium center is the first step, in which the lone pair on the oxygen atom is donated to the non-bonding molecular orbital of the zirconium atom. Then the epoxide imido zirconocene complex undergoes an elimination reaction proceeding through a six-membered-ring transition state, where all bonds are made and broken concertedly, and a C_α–C_β π-bond was simultaneous formed when the β-hydrogen transfers to the anionic imido nitrogen atom. The observed reactions of **11** with epoxides with accessible β-hydrogen atoms are consistent with those of **1.4**, and in both cases, [2+3] cycloaddition was not observed. The previously reported calculations indicate that the β-hydrogen abstraction pathway is both kinetically and thermodynamically favoured over the [2+3] cycloaddition.[84] In contrast, the reactions of **1.4** with other heterocycles (e.g. styrene oxide, butadiene monoepoxide and N-tosyl-2-phenylaziridine) without accessible β-hydrogens gave only [2+3] cycloaddition.[5] The mechanism was also studied by DFT calculation, revealing that [2+3] cycloaddition undergoes a zwitterionic path rather than a diradical path.[84] However, this [2+3] cycloaddition reaction was found not to be the case for the reaction of **11** with styrene oxide.

When **11** was treated with styrene oxide on the NMR tube scale in C_6D_6, slow conversion to a single product was observed over 16 h at 60 °C by the ^{1}H NMR spectrum of the reaction mixture, and the colour of the solution slowly changed from red-orange to red. The ^{1}H NMR spectrum indicated quantitative conversion to a zirconocene borylamido product, and the expected [2+3] cycloaddition did not occur.

On the preparative scale, styrene oxide was reacted with **11** in toluene solution at 90 °C for 2.5 h. The product $Cp_2Zr\{NHB(NAr'CH)_2\}\{OC(H)=C(H)Ph\}$ (**77**) was isolated in 72% yield. The ^{11}B and ^{1}H NMR spectra of isolated **77** are consistent with this being a single geometric isomer form of an enolate borylamido zirconocene complex, with a diagnostic ^{11}B signal at 25.0 ppm and ^{1}H NH singlet at 5.32 ppm. Two methine (1H) doublets are observed at 6.46 and 5.15 ppm respectively, which share a COSY correlation, and the three bond C···H coupling constants were calculated to be 6.9 Hz, suggesting that they are attributable to an alkenyl fragment which holds an *Z*-configuration. Two HMBC correlations to the ^{1}H signal at 5.15 ppm of ZrCH=C<u>H</u>Ph were observed for the ^{13}C signals at 153.4 and 138.7 ppm, in which the signal at 153.4

ppm shows an HSQC correlation to another methine doublet of ZrC<u>H</u>=CHPh at 6.46 ppm, and the signal at 138.7 ppm is attrbutable to the quaternary carbon of *i*-Ph. In addition, ^{1}H–^{1}H ROESY NMR experiment showed the presence of an nOe between these two methine protons, further confirming that the product is an *Z*-isomer.

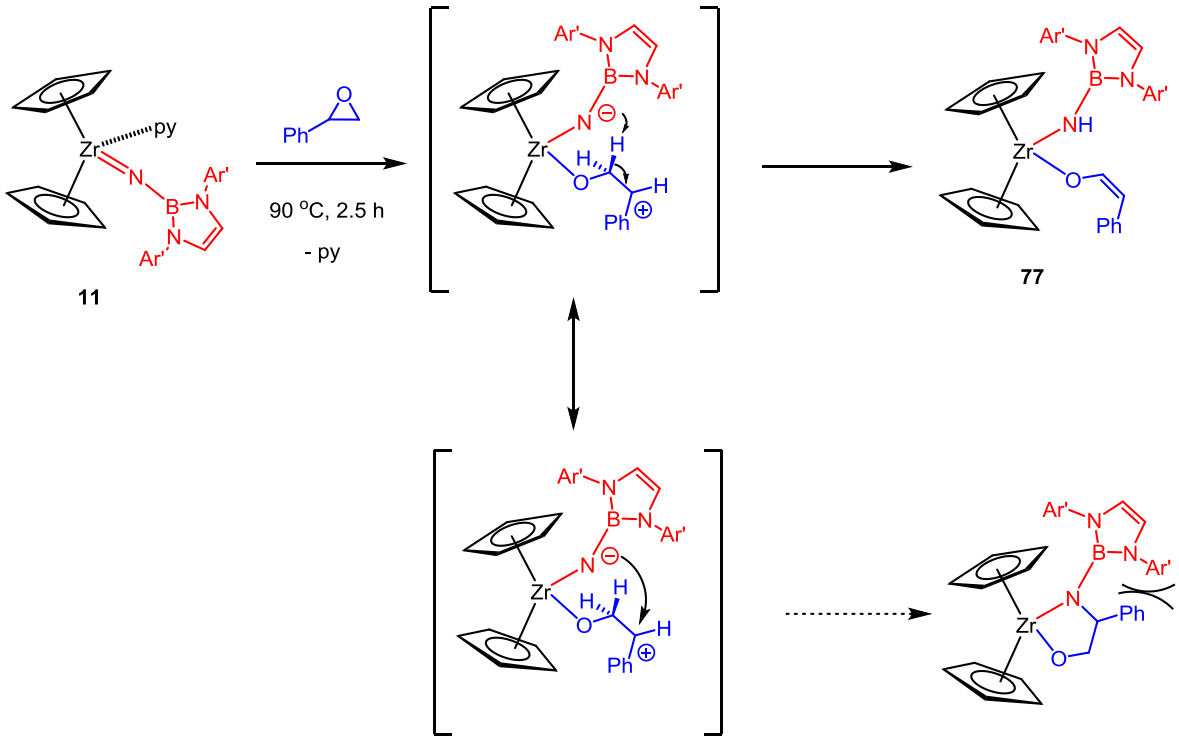

Scheme 4.11. Proposed mechanism for the formation of $Cp_2Zr\{NHB(NAr'CH)_2\}\{OC(H)=C(H)Ph\}$ (**77**) from $Cp_2Zr\{NB(NAr'CH)_2\}(py)$ (**11**) and styrene oxide, and the unobserved representative [2+3] cycloaddition.

The formation of enolate borylamido zirconocene **77** is unexpected, since the reported reactions of **1.4** with styrene oxide and other epoxides, which have no accessible β-hydrogens, only resulted in [2+3] cycloaddition (*vide supra*). If the formation of **77** follows the same zwitterionic mechanism described for the [2+3] cycloaddition of **1.4**, the Zr–O dative bond is firstly converted into a full covalent bond, and the C_α–O bond is cleaved simultaneously forming a carbocation by migrating the bond pair onto the oxygen atom as a lone pair. This induces a reorganisation of the Zr=N bond into a Zr–N bond along with the π bond pair being converted to an additional lone pair on the nitrogen atom making a nitrogen-anion. For **1.4**, the zwitterionic intermediate leads to the formation of a metallacycle *via* formal [2+3] cycloaddition by attack of the nitrogen-anion on the carbocation. However, since the generated carbocation is more stable at the position

adjacent to the phenyl substituent, the [2+3] cycloaddition product of **11** suffers much higher steric repulsion between the bulky boryl moiety (compared to the *tert*-butyl substituent of **1.4**) and the phenyl substituent, resulting in [2+3] cycloaddition being unfavourable both kinetically and thermodynamically (Scheme 4.11).

In the case of the formation of **77**, this zwitterionic intermediate is proposed to instead undergo α-hydrogen atom abstraction, where the formally anionic nitrogen abstracts a methylene proton which is adjacent to the oxygen generating a C=C double bond (Scheme 4.11), analogous to an E_1 elimination reaction. This proposed mechanism also explains the formation of *Z*-isomer where the phenyl substituent adjacent to the carbocation in the zwitterionic intermediate prefers to orientate *trans* to the bulky boryl moiety, in order to minimise the steric clash, as depicted in Scheme 4.11. The mechanism can also be analogous to the one-step β-hydrogen abstraction discussed above, involving a similar five-membered-ring transition state. However, the product having an *E*-configuration would be expected *via* this one-step pathway.

Unfortunately, further studies on reactions of **11** with 3,3-dimethyl-1,2-epoxybutane and *N*-tosyl-aziridine gave no reaction, possibly due to the bulky substituents in these two cases.

4.4.2 Reactions of $Cp_2Zr\{NB(NAr'CH)_2\}(py)$ (11) with episulfides

When **11** was reacted with propylene sulfide on the NMR tube scale at 60 °C over 16 h, two products were formed in a *ca* 8:1 ratio. Quantitative conversion of **11** required slightly more than one equivalent of propylene sulfide, and the generation of propene was observed, by ^{1}H NMR spectroscopy. The ^{11}B NMR spectrum of this mixture shows a broad signal at around 25.0 ppm. The ^{1}H NMR characterisation of the mixture indicates that the minor product is the allylic sulfide complex $Cp_2Zr\{NHB(NAr'CH)_2\}(SCH_2CHCH_2)$ (**78**), having an analogous ^{1}H NMR spectrum to that of the oxygen congener **75**. The ^{1}H NMR spectrum shows an NH resonance at 5.15 ppm and a complex set of multiplets for the SCH_2CHCH_2 environment, in which the terminal alkenyl resonances was observed at 5.31 and 5.06 ppm. The minor formation of **78** is proposed to proceed *via* β-hydrogen atom abstraction, which is similarly observed by Bergman in the reaction of **1.4** with propylene sulfide,[5] where the generation of propene was also observed. However, this was also accompanied by the formation of insoluble and soluble $(C_3S)_n$ poly/oligomer *via* desulfurisation of the episulfide, when an

excess of propylene sulfide was employed. In the case of the reaction of **11** with propylene sulfide, no precipitation was observed and the major product containing new ^{1}H and ^{13}C resonances corresponding to Cp and boryl fragments were observed, which implies that desulfurised propylene sulfide resulted in the formation of a new complex in this case, rather than polymerisation. Since the major product was generated *via* elimination of alkene, in order to avoid the side reaction of β-hydrogen atom abstraction, the reaction of **11** with ethylene sulfide, which has no β-hydrogen atoms, was alternatively performed.

The reaction of **11** with one equivalent of ethylene sulfide generated a single product at 60 °C over 16 h, which is the major product observed above in the reaction with propylene sulfide on the NMR tube scale in C_6D_6, however, only half of **11** was consumed. Another equivalent of ethylene sulfide was then added to the reaction solution, and quantitative formation of the product was then achieved. Ethylene was observed in the reaction ^{1}H NMR spectrum of the mixture showing an intense singlet at 5.25 ppm, and the solution colour slowly changed to yellow from orange-red.

On the preparative scale, **11** and two equivalents of ethylene sulfide were mixed in toluene at 90 °C over 2 h, yielding quantitative formation of the product in 75% yield. Crystallographic characterisation (*vide infra*) showed that this compound was a disulfide bridged zirconocene borylamide dimer, $[Cp_2Zr\{\mu\text{-}N\{B(NAr'CH)_2\}S_2\}]_2$ (**79**), in which two borylamido zirconocene moieties are linked by two disulfide bridges resulting in a $(Zr–N–S–S)_2$ eight-membered metallacycle (Equation 4.23). Similar sulfide and selenide abstraction reactions have been previously observed by Gade *et* al, in the reaction of the hydrazido zirconium complex $Zr(N_2^{TBS}N^{py})(NNPh_2)(py)$ (**1.64**, Chapter One) with 0.5 equivalent propylene sulfide or Ph_3PSe to give $Zr(N_2^{TBS}N^{py})(NPh_2)\}_2(\mu\text{-}N_2E)$ (E = S (**1.79**) or Se (**1.80**)) in which the zirconium complex fragments are linked by a central bridging $[EN_2]$ (E = S or Se) moiety.[85] In addition, the desulfurisation of propylene sulfide to form the disulfide-bridged complex $[CpMoS_2]_2$ was also previously observed when reacted with $CpMo(H)(CO)_2\{P(OPh)_3\}$.[86]

A number of the analogous sulfide bridged complexes $[LMS_2]_n$ (M = Cu, Co, Fe, Ru) were reported from reactions with S_8.[87–89] Therefore, reaction of **11** with S_8 was also performed on the NMR tube scale in C_6D_6, in which formation of **79**, as the major product, was again observed at 60 °C over 5 h, but upon continued heating at 60 °C leads

to formation of many unidentified species. Unfortunately, attempts to react elemental Se with **11** gave no reaction even at 90 °C.

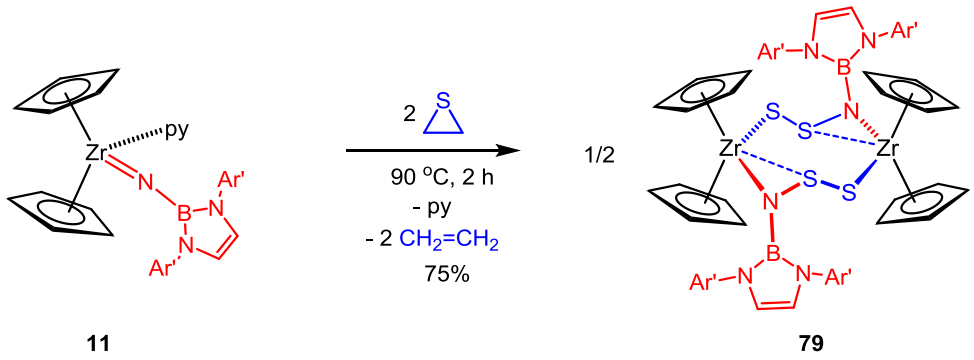

11 **79**

Equation 4.23

The ^{11}B NMR spectrum of **79** shows a resonance at 24.8 ppm, slightly upfield shifted compared to that of zirconocene borylamides (*vide supra*). The ^{1}H NMR spectrum is indicative of a C_2 symmetric species, with the two singlet resonances attributed to Cp ligands orientated "up" or "down". The four isopropyl groups of each borylamido moiety are also not chemically equivalent, with two septets (4 H each) and four doublets (12 H) each being observed.

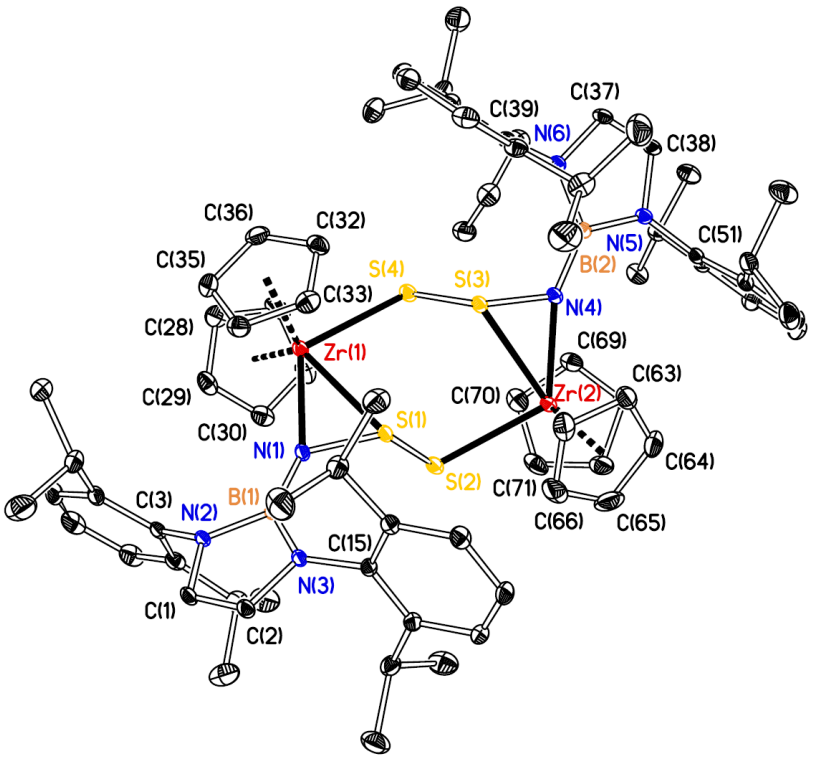

Figure 4.19. Displacement ellipsoid plot (20% probability) of $[Cp_2Zr\{\mu\text{-}N\{B(NAr'CH)_2\}S_2\}]_2$ (**79**). H atoms omitted for clarity.

Table 4.8. Selected bond lengths (Å) and angles (°) for $[Cp_2Zr\{\mu\text{-}N\{B(NAr'CH)_2\}S_2\}]_2$ (**79**). $Cp_{cent(1)}$ and $Cp_{cent(2)}$ refer to the computed Cp ring centroids for "upper" and "lower" Cp rings bound to Zr(1), and $Cp_{cent(3)}$ and $Cp_{cent(4)}$ refer to the computed Cp ring centroids for "upper" and "lower" Cp rings bound to Zr(2), respectively, as depicted in Figure 4.19.

Zr(1)–N(1)	2.1972(15)	$Cp_{cent(1)}$–Zr(1)–$Cp_{cent(2)}$	126.9
Zr(2)–N(4)	2.1908(16)	$Cp_{cent(3)}$–Zr(1)–$Cp_{cent(4)}$	127.9
Zr(1)–$Cp_{cent(1)}$	2.239	S(1)–Zr(1)–S(4)	83.953(15)
Zr(1)–$Cp_{cent(2)}$	2.241	S(3)–Zr(2)–S(2)	85.189(16)
Zr(2)–$Cp_{cent(3)}$	2.237	N(1)–Zr(1)–S(4)	121.12(4)
Zr(2)–$Cp_{cent(4)}$	2.236	N(4)–Zr(2)–S(2)	121.56(4)
Zr(1)–S(1)	2.5954(5)	Zr(1)–N(1)–B(1)	153.49(13)
Zr(1)–S(4)	2.6165(5)	Zr(2)–N(4)–B(2)	155.21(13)
Zr(2)–S(3)	2.6134(5)	Zr(1)–S(1)–S(2)	100.83(2)
Zr(2)–S(2)	2.6021(5)	Zr(2)–S(3)–S(4)	101.19(2)
N(1)–B(1)	1.436(2)	Zr(1)–S(4)–S(3)	102.98(2)
N(4)–B(2)	1.442(2)	Zr(2)–S(2)–S(1)	101.02(2)
B(1)–N(2)	1.453(2)	N(1)–B(1)–N(2)	126.18(16)
B(1)–N(3)	1.450(2)	N(4)–B(2)–N(5)	126.55(18)
B(2)–N(5)	1.458(3)	N(1)–B(1)–N(3)	130.05(16)
B(2)–N(6)	1.460(3)	N(4)–B(2)–N(6)	129.05(17)
S(1)–S(2)	2.0824(7)	B(1)–N(1)–S(1)	119.02(13)
S(3)–S(4)	2.0862(7)	B(2)–N(4)–S(3)	120.59(13)
N(1)–S(1)	1.6737(15)		
N(4)–S(3)	1.6714(16)		

Diffraction-quality crystals of **79** were successfully grown from a benzene solution at RT. The solid state structure is shown in Figure 4.19, and selected bond distances and angles are listed in Table 4.8. Compound **79** has a pseudo trigonal bipyramidal zirconium centre, with staggered cyclopentadienyl rings on Zr(1) and eclipsed cyclopentadienyl rings on Zr(2). Each $SSNB(NAr'CH)_2$ ligand has η^2-N,S coordination to one zirconium centre *via*

adjacent sulfur and nitrogen atoms, and shows coordination to another zirconium centre *via* the terminal sulfur atom. The Zr(1)–N(1) and Zr(2)–N(4) bond distances are 2.1972(15) and 2.1908(16) Å, respectively, significantly longer than those found in the zirconocene borylamide complexes. The long Zr–N bond distance is comparable to that previously observed in a similar η^2-N,S coordination zirconocene complex $Cp_2ZrCl(Ph_4P_2N_4S_2{}^tBu)$ (2.206(5) Å),[90] as well as in other η^2-coordinated zirconocene complexes with the Zr–N bond distances in the range 2.105(4) – 2.267(3) Å.[91–93] This indicates that the borylamido moiety is acting as a one-electron (σ-only) donor. The N(1)–S(1) and N(4)–S(3) bond lengths of 1.6737(15) and 1.6714(16) Å, respectively, fall at the low end of the range of 1.672(4) – 1.720(3) Å found in other three-membered η^2-N,S coordinated metallocycles,[94–97] possibly due to the N(1) and N(4), in this case, being sp^2-hybridised with sums of the angles subtended of 355.54(19)° and 359.83(19)°, respectively.

There are no appropriate complexes for direct structural comparison. However, disulfide-bridged complex dimers have been widely reported, and they in general have a chair conformation.[87,98–105] In contrast, the core six-membered–Zr_2S_4 ring within **79** shows a twist boat confirmation, in which all four Zr–S bond lengths are comparable, and marginally longer than Zr–S single bonds found in complexes $(\eta^5\text{-}C_5R_5)_2Zr(\eta^2\text{-}S_n)$ (R = H or Me, n = 2, 3, or 5, **4.16**) which are within the range 2.521(1) – 2.561(2) Å.[106–108] In addition, the S(1)–S(2) and S(3)–S(4) bond lengths of **79** are 2.0824(7) and 2.0862(7) Å, respectively, also slightly longer than the S–S single bond in **4.16** and S_8 which are within the range of 2.047(3) – 2.066(8) Å.[106–109] These slightly elongated Zr–S and S–S bonds are probably a result of the steric repulsion between the two zirconocene borylamido moieties in the ring. However, the mechanism of this reaction is not apparent, and the investigation is ongoing.

4.5 Conclusion and Outlook

This Chapter has described the reactions of the borylimido zirconocene complex $Cp_2Zr\{NB(NAr'CH)_2\}(py)$ (**11**) with oxygen- and sulfur- containing polar molecules. Firstly, the reactions of **11** with heteroallenes, CE_2 and PhNCE (E = O or S), were investigated, giving products $ECNB(NAr'CH)_2$ (E = O (**48**), S (**49**)) and $PhNCNB(NAr'CH)_2$ (**50**), respectively, as a result of functional group exchange of the

borylimido unit, with concomitant formation of the polymeric/oligomeric $[Cp_2ZrO]_n$ or dimeric $[Cp_2Zr(\mu\text{-}S)]_2$.

Next, the reaction with tolylaldehyde, which proceeds through an initial [2+2] cycloaddition followed by rapid extrusion to give borylimine $TolC(H)NB(NAr'CH)_2$ (**51**) was described. Meanwhile, the reactions with ketones and esters, $MeCO_2R$, showed α–hydrogen atom abstraction reactions forming corresponding enolate borylamido zirconocene complexes, and the ester enolate complexes $Cp_2Zr\{NHB(NAr'CH)_2\}\{OC(CH_2)OR\}$ (R = ^{i}Pr (**53**), Et (**54**)) were successfully isolated.

These ester enolate borylamido zirconocene complexes were found to be an intermediate prior to further rearrangement, where the ketene H_2CCO was eliminated *via* an ester enolate cleavage pathway to generate the corresponding alkoxy borylamido zirconocene compounds. The eliminated ketene was subsequently self-trapped by the unreacted nucleophilic enolate intermediate, forming the β-ketoester enolate-borylamido zirconocene products. The exemplar product $Cp_2Zr\{NHB(NAr'CH)_2\}\{OC(CH_2)CH_2CO_2Me\}$ (**56**) was isolated, supported by crystallographic characterisation, in the case when $MeCO_2Me$ was employed. A similar ketene trapping reaction was modelled by reacting **53** with thermally stable $Me_3Si(H)CCO$, which also gave a β-ketoester enolate-borylamido compound $Cp_2Zr\{NHB(NAr'CH)_2\}\{OC(CHSiMe_3)CH_2CO_2{}^iPr\}$ (**69**) having a comparable solid state structure to that of **56**. The kinetic analysis by ^{1}H NMR spectroscopy showed that the first order rate constant of the decay of the ester enolate complex is *ca*. twice as fast as those of the formation of alkoxy and β-ketoester enolate products without any induction period, indicating that the ester enolate cleavage is the rate-determining step, and the ketene self-trapping is rapid, resulting in these two products forming concurrently. The activation parameters extracted from the Eyring analyses reflect that the ester enolate cleavage step is an intramolecular process and the generated ketene may remain coordinated to the zirconium centre throughout the rate-determining step.

This novel reaction in the borylamido zirconocene complex was also applicable for other ester derivatives $MeC(O)ER_n$ (E= S, R = Me or Et, n = 1; E = N, R= Me, n = 2; E = Cl, n = 0), and the rate of the ester enolate cleavage step is highly dependent on the steric bulk of R and nucleophilicity of E. The kinetic analysis of the thioester enolate complex, $Cp_2Zr\{NHB(NAr'CH)_2\}\{OC(CH_2)SEt\}$ (**61**) proves that it also undergoes a similar

enolate cleavage (ketene elimination) and ketene self-trapping reactions, but the thiolate ligand of the product $Cp_2Zr\{NHB(NAr'CH)_2\}(SEt)$ (**65**) shows high affinity to nuelcophilic attack on the eliminated ketene to reform **61**. However, the ketene self-trapping is always much faster than the ketene generation in all cases, and thus ketene was never observed by NMR spectroscopy.

Finally, compound **11** shows high elimination reactivity when reacted with strained heterocycles; the reaction with epoxides with accessible β-hydrogen atoms gives elimination of a β-hydrogen atom and protonation of the borylimido ligand, whereas in the reaction with an epoxide without accessible β-hydrogens, namely styrene oxide, elimination of an α-hydrogen atom was observed instead. Furthermore, the disulfide-bridged zirconocene borylamido dimer $[Cp_2Zr\{\mu\text{-}N\{B(NAr'CH)_2\}S_2\}]_2$ (**79**) was isolated and structrally characterised, when **11** was reacted with two equivalents of the episulfides, propylene sulfide or ethylene sulfide, *via* desulfurisation, eliminating the respective alkene. A small amount of β-hydrogen atom abstraction (*ca* 11%) was also observed while using propylene sulfide (which has accessible β-hydrogen atoms) giving borylamido zirconocene allylic thiolate complex $Cp_2Zr\{NHB(NAr'CH)_2\}(SCH_2CHCH_2)$ (**78**).

4.6 References

1 P. J. Walsh, F. J. Hollander and R. G. Bergman, *Organometallics*, 1993, **12**, 3705–3723.

2 A. P. Duncan and R. G. Bergman, *Chem. Rec.*, 2002, **2**, 431–445.

3 H. M. Hoyt and R. G. Bergman, *Angew. Chem. Int. Ed. Engl.*, 2007, **46**, 5580–5582.

4 S. Y. Lee and R. G. Bergman, *J. Am. Chem. Soc.*, 1995, **117**, 5877–5878.

5 S. A. Blum, V. A. Rivera, R. T. Ruck, F. E. Michael and R. G. Bergman, *Organometallics*, 2005, **24**, 1647–1659.

6 R. L. Zuckerman and R. G. Bergman, *Organometallics*, 2000, **19**, 4795–4809.

7 S. Y. Lee and R. G. Bergman, *J. Am. Chem. Soc.*, 1996, **118**, 6396–6406.

8 S. Y. Lee and R. G. Bergman, *Tetrahedron*, 1995, **51**, 4255–4276.

9 K. E. Meyer, P. J. Walsh and R. G. Bergman, *J. Am. Chem. Soc.*, 1995, **117**, 974–985.

10 H. F. Bettinger and H. Bornemann, *J. Am. Chem. Soc.*, 2006, **128**, 11128–11134.

11 H. F. Bettinger, *Inorg. Chem.*, 2007, **46**, 5188–5195.

12 H. F. Bettinger, M. Filthaus, H. Bornemann and I. M. Oppel, *Angew. Chem. Int. Ed.*, 2008, **47**, 4744–4747.

13 H. F. Bettinger, M. Filthaus and P. Neuhaus, *Chem. Commun. (Camb).*, 2009, 2186–2188.

14 S. Biswas, I. M. Oppel and H. F. Bettinger, *Inorg. Chem.*, 2010, **49**, 4499–4506.

15 H. F. Bettinger and H. Bornemann, *Zeitschrift fur Anorg. und Allg. Chemie*, 2011, **637**, 2169–2174.

16 M. Filthaus, L. Schwertmann, P. Neuhaus, R. W. Seidel, I. M. Oppel and H. F. Bettinger, *Organometallics*, 2012, **31**, 3894–3903.

17 M. Müller, C. Maichle-Mössmer and H. F. Bettinger, *Chem. Commun.*, 2013, **49**, 11773.

18 L. Weber, E. Dobbert, R. Boese, M. T. Kirchner and D. Bläser, *Eur. J. Inorg. Chem.*, 1998, 1145–1152.

19 C. Summerford and K. Wade, *J. Chem. Soc. A*, 1970, 2010–2016.

20 C. Summerford and K. Wade, *J. Chem. Soc. A*, 1969, 1487–1491.

21 A. E. Guiducci, A. R. Cowley, M. E. G. Skinner and P. Mountford, *J. Chem. Soc. Dalton. Trans.*, 2001, 1392–1394.

22 A. E. Guiducci, C. L. Boyd, E. Clot and P. Mountford, *Dalton Trans.*, 2009, 5960–5979.

23 A. E. Guiducci, C. L. Boyd and P. Mountford, *Organometallics*, 2006, **25**, 1167–1187.

24 P. J. Tiong, A. Nova, L. R. Groom, A. D. Schwarz, J. D. Selby, A. D. Schofield, E. Clot and P. Mountford, *Organometallics*, 2011, **30**, 1182–1201.

25 B. Clough, DPhil Thesis, University of Oxford, 2016.

26 M. Slusarczyk and P. Mountford, Unpublished results.

27 W. Einholz and W. Haubold, *Zeitschrift fuer Naturforschung, Tl. B Anorg. Chemie, Org. Chem*, 1986, **41B**, 1367–1372.

28 I. Ruppert, *Angew. Chemi*, 1977, **89**, 336–338.

29 O. Takahashi, Y. Kolno, S. Iwasaki, K. Saito, M. Iwaoka, S. Tomoda, Y. Umezawa, S. Tsuboyama and M. Nishio, *Bull. Chem. Soc. Jpn.*, 2001, **74**, 2421–2430.

30 M. Nishio, *Phys. Chem. Chem. Phys.*, 2011, **13**, 13873.

31 A. Williams and I. T. Ibrahim, *Chem. Rev.*, 1981, **81**, 589–636.

32 I. Pattison, K. Wade and B. K. Wyatt, *J. Chem. Soc. A*, 1968, 837–842.

33 W. A. Howard and G. Parkin, *J. Am. Chem. Soc.*, 1994, **116**, 606–615.

34 P. Veya, C. Floriani, A. Chiesi-Villa and C. Guastini, *Organometallics*, 1991, **10**, 2991–2993.

35 M. D. Curtis, S. Thanedar and M. Butler, *Organometallics*, 1984, 1855–1859.

36 J. M. Manriquez, D. R. McAlister, R. D. Sanner and J. E. Bercaw, *J. Am. Chem. Soc.*, 1978, **100**, 2716–2724.

37 D. C. Sonnenberger, E. A. Mintz and T. J. Marks, *J. Am. Chem. Soc.*, 1984, **106**, 3484–3491.

38 S. R. John and R. H. Grubbs, *J. Am. Chem. Soc.*, 1983, **105**, 1664–1665.

39 J. March, *Advanced Organic Chemistry*, Wiley-Interscience, New York, 4th edn., 1992.

40 A. D. Bolig and E. Y. X. Chen, *J. Am. Chem. Soc.*, 2004, **126**, 4897–4906.

41 A. Rodriguez-Delgado, W. R. Mariott and E. Y.-X. Chen, *Macromolecules*, 2004, **37**, 3092–3100.

42 K. Hortmann and J. Diebold, *J. Organomet. Chem.*, 1993, **445**, 107–109.

43 S. Gambarotta, S. Strologo, C. Floriani, A. Chiesi-Villa and C. Guastini, *Inorg. Chem.*, 1985, **24**, 654–660.

44 E. Lu, Y. Li and Y. Chen, *Chem. Commun.*, 2010, **46**, 4469–4471.

45 W. A. Howard, T. M. Trnka, M. Waters and G. Parkin, *J. Organomet. Chem.*, 1997, **528**, 95–121.

46 G. Stojcevic, H. Kim, N. J. Taylor, T. B. Marder and S. Collins, *Angew. Chem. Int. Ed.*, 2004, **43**, 5523–5526.

47 F. Hentschel, V. V Vinogradov, A. V Vinogradov, A. V Agafonov, V. V Guliants, I. Persson, G. A. Seisenbaeva and V. G. Kessler, *Polyhedron*, 2015, **89**, 297–303.

48 M. Elder, *Inorg. Chem.*, 1969, **8**, 2103–2109.

49 G. A. Seisenbaeva, S. Gohil and V. G. Kessler, *J. Mater. Chem.*, 2004, **14**, 3177–3190.

50 R. Pothiraja, A. Milanov, H. Parala, M. Winter, R. A. Fischer and A. Devi, *Dalton. Trans.*, 2009, 663.

51 U. Patil, M. Winter, H.-W. Becker and A. Devi, *J. Mater. Chem.*, 2003, **13**, 2177–2184.

52 D. Matković-Čalogović, *Acta Crystallogr. Sect. C*, 1987, **43**, 1473–1475.

53 Q. Chang, C. Hu, J. Chen, M. Xie, W. Liu, Q. Ye, Y. Yu, X. Chen and L. Chen,

Transit. Met. Chem., 2011, **36**, 337–340.

54 G. R. Newkome, V. K. Gupta, H. C. R. Taylor and F. R. Fronczek, *Organometallics*, 1984, **3**, 1549–1554.

55 B. J. Truscott, D. J. Nelson, C. Lujan, A. M. Z. Slawin and S. P. Nolan, *Chem. Eur. J.*, 2013, **19**, 7904–7916.

56 J. Vicente, M.-T. Chicote, M. D. Abrisqueta, M. M. Alvarez-Falcón, M. C. Ramírez de Arellano and P. G. Jones, *Organometallics*, 2003, **22**, 4327–4333.

57 M. Horike, Y. Kai, N. Yasuoka and N. Kasa, *J. Organomet. Chem.*, 1974, **72**, 441–451.

58 P. G. Cozzi, P. Veya and C. Floriani, *Organometallics*, 1995, **14**, 4092–4100.

59 P. Veya, P. G. Cozzi, C. Floriani and F. P. Rotzinger, *Organometallics*, 1995, 4101–4108.

60 A. C. O. Hann and A. Lapworth, *Proc. Chem. Soc.*, 1903, **19**, 189–90.

61 E. E. Blaise and L. Marcilly, *Bull. Soc. Chim*, 1904, **19**, 110.

62 A. S. Hussey and M. S. Newman, *J. Am. Chem. Soc.*, 1948, **70**, 3024–3026.

63 W. R. Vaughan, S. C. Bernstein and M. E. Lorber, *J. Organomet. Chem.*, 1967, **30**, 1790–1795.

64 D. Seebach, R. Amstutz, T. Laube, W. B. Schweizer and J. D. Dunitz, *J. Am. Chem. Soc.*, 1985, **107**, 5403–5409.

65 R. Haener, T. Laube and D. Seebach, *J. Am. Chem. Soc.*, 1985, **107**, 5396–5403.

66 D. F. Sullivan, R. P. Woodbury and M. W. Rathke, *J. Org. Chem.*, 1977, **42**, 2038–2039.

67 A. Barbero and F. J. Pulido, *Synlett*, 2001, 827–829.

68 W. You, Y. Li and M. K. Brown, *Org. Lett.*, 2013, **15**, 1610–1613.

69 U. Schöllkopf and J. Hoppe, *Angew. Chem. Int. Ed.*, 1975, **87**, 814–815.

70 B. Lian, L. Toupet and J. Carpentier, *Chem. Eur. J.*, 2004, **10**, 4301–4307.

71 C.-M. Zhang, R.-T. Liu, Z.-X. Chen and X.-G. Zhou, *Chinese J. Chem.*, 2006, **24**, 231–234.

72 C. Zhang, Y. Lin, Z. Chen and X. Zhou, *J. Rare Earths*, 2006, **24**, 9–14.

73 C. Zhang, R. Liu, X. Zhou, Z. Chen, L. Weng and Y. Lin, *Organometallics*, 2004, **23**, 3246–3251.

74 B. Fang, L. Zhang, G. Hou, G. Zi, D.-C. Fang and M. D. Walter, *Chem. Sci.*, 2015, **6**, 4897–4906.

75 P. Veya, C. Floriani, A. Chiesi-Villa and C. Guastini, *Chem. Commun.*, 1991, **1**,

1166–1167.

76 Y. Kita, N. Fu and T. T. Tidwell, in *Encyclopedia of Reagents for Organic Synthesis*, John Wiley & Sons, Ltd, 2001.

77 A. T. Nielsen and W. J. Houlihan, *Org. React.*, 1968, **16**, 1–438.

78 L. M. Baigrie, H. R. Seiklay and T. T. Tidwell, *J. Am. Chem. Soc.*, 1985, **107**, 5391–5396.

79 L. M. Bairgrie, D. Lenoir, H. R. Seikaly and T. T. Tidwell, *J. Org. Chem.*, 1985, **51**, 1059–1060.

80 H. R. Seikaly and T. T. Tidwell, *Tetrahedron*, 1986, **42**, 2587–2613.

81 L. M. Bairgrie, R. Leung-Toung and T. T. Tidwell, *Tetrahedron Lett.*, 1988, **29**, 1673–1676.

82 T. Stuhldreier, K. Helmut and H. Hartwig, *Organometallics*, 2000, **19**, 5231–5234.

83 F. H. Allen, O. Kennard, D. G. Watson, L. Brammer, A. G. Orpen and R. Taylor, *J. Chem. Soc. Perkin Trans. 2*, 1987, S1.

84 D. Senthilnathan and P. Venuvanalingam, *Eur. J. Inorg. Chem.*, 2011, 2842–2855.

85 H. Herrmann, J. L. Fillol, H. Wadepohl and L. H. Gade, *Angew. Chem. Int. Ed.*, 2007, **46**, 8426–8430.

86 V. W. Beck, W. Danzer and G. Thiel, *Angew. Chem. Int. Ed. Engl*, 1973, **10**, 625–626.

87 J. T. York, E. C. Brown and W. B. Tolman, *Angew. Chem. Int. Ed.*, 2005, **44**, 7745–7748.

88 B. H. Brunner, N. Janietz, W. Meier, G. Sergeson, J. Wachter, T. Zahn and M. L. Ziegler, *Angew. Chem. Int. Ed. Engl*, 1985, **57**, 1060–1061.

89 J. Amarasekera, T. B. Rauchfuss and A. L. Rheingold, *Inorg. Chem.*, 1987, **26**, 2017–2018.

90 T. Chivers, R. W. Hilts, M. Parvez and R. Vollmerhaus, *Inorg. Chem.*, 1994, 3459–3466.

91 N. Dufour, J. Majoral, A. Caminade and R. Choukroun, *Organometallics*, 1991, **10**, 45–48.

92 M. J. Carney, P. J. Walsh and R. G. Bergman, *J. Am. Chem. Soc.*, 1990, **112**, 6426–6428.

93 A. D. Schofield and P. Mountford, Unpublished results.

94 T. Komuro, T. Matsuo, H. Kawaguchi and K. Tatsumi, *Inorg. Chem.*, 2005, **44**, 1381–1382.

95 Z. W, Y. H, Y. Li and B. I, *Russ. Chem. Bull*, 2014, **63**, 953–962.

96 W. Zhong, Q. Yang, Y. Shang, G. Liu, H. Zhao, Y. Li and H. Yan, *Organometallics*, 2012, **31**, 6658–6668.

97 D. M. Hankin, A. A. Danopoulos, G. Wilkinson, T. K. N. Sweet, M. B. Hursthouse, W. Cardijj, P. O. Box and C. Cfi, *Dalton. Trans.*, 1996, 4063–4069.

98 R. D. Adams, B. Captain, O.-S. Kwon, P. J. Pellechia and S. Sanyal, *J. Organomet. Chem.*, 2004, **689**, 1370–1376.

99 H. W. Roesky, T. Gries, P. G. Jones, K.-L. Weber and G. M. Sheldrick, *J. Chem. Soc., Dalt. Trans. Dalt. Trans.*, 1984, 1781–1784.

100 H. Brunner, N. Janietz, W. Meier, G. Sergeson, J. Wachter, T. Zahn and M. L. Ziegler, *Angew. Chem. Int. Ed. Engl*, 1985, **24**, 1060–1061.

101 D. M. Giolando, T. B. Rauchfuss, A. L. Rheingold and S. R. Wilson, *Organometallics*, 1987, **6**, 667–675.

102 R. J. Pleus, W. Saak and S. Pohl, *Z. Anorg. Allg. Chem.*, 2001, **627**, 250–253.

103 T. Koyama, Y. Koide and K. Matsumoto, *Inorg. Chem.*, 1999, **38**, 3241–3243.

104 S. Yao, C. Milsmann, E. Bill, K. Wieghardt and M. Driess, *J. Am. Chem. Soc.*, 2008, **130**, 13536–13537.

105 R. D. Adams, O.-S. Kwon and M. D. Smith, *Inorg. Chem.*, 2002, **41**, 6281–6290.

106 A. Shaver and M. Mccall, *Can. J. Chem.*, 1987, **65**, 1676–1680.

107 W. A. Howard and G. Parkin, *Polyhedron*, 1995, **14**, 25–44.

108 W. A. Howard, T. M. Trnka and G. Parkin, *Organometallics*, 1995, **3**, 4037–4039.

109 A. C. Gallacher and A. A. Pinkerton, *Acta Crystallogr. Sect. C*, 1993, **49**, 125–126.

Chapter Five

Experimental details and characterising data

5.1 General methods and implementation

All manipulations were carried out using standard Schlenk line or dry-box techniques under an atmosphere of argon or dinitrogen. Solvents were either degassed by sparging with dinitrogen and dried by passing through a column of the appropriate drying agent[1] or refluxed over sodium (toluene), potassium (THF), Na/K alloy (Et_2O) or CaH_2 (pyridine) and distilled. Deuterated solvents were dried over sodium (toluene-d_8), potassium (C_6D_6), CaH_2 (pyridine-d_5) or P_2O_5 (CD_2Cl_2), distilled under reduced pressure and stored under argon in Teflon valve ampoules. Unless otherwise stated NMR samples were prepared under dinitrogen in 5 mm Wilmad 507-PP tubes fitted with J. Young Teflon valves. ^{1}H, $^{13}C\{^{1}H\}$, $^{11}B\{^{1}H\}$, $^{19}F\{^{1}H\}$ and ^{2}H spectra were recorded on a Bruker Ascend 400 NMR spectrometer, a Bruker Avance III 500 NMR spectrometer or on a Bruker AVC 500 spectrometer fitted with a ^{13}C cryoprobe. Unless otherwise stated, all NMR spectra were recorded at 298 K. ^{1}H and $^{13}C\{^{1}H\}$ and spectra were referenced internally to residual protio-solvent (^{1}H) or solvent (^{13}C) resonances, and are reported relative to tetramethylsilane ($\delta = 0$ ppm). ^{2}H NMR spectra were referenced to the natural abundance deuterium resonance of the protio solvent. ^{19}F and ^{11}B NMR specra were referenced externally to $CFCl_3$ and $Et_2O{\cdot}BF_3$ respectively. Assignments were confirmed as necessary with the use of two dimensional $^{1}H–^{1}H$, $^{13}C–^{1}H$ and $^{19}F–^{19}F$ correlation experiments. Chemical shifts are quoted in δ (ppm) and coupling constants in Hz. Unless otherwise stated, IR spectra were recorded on a Thermo Scientific Nicolet iS5 FTIR spectrometer and samples prepared in a dry-box using NaCl plates as a Nujol mull or as a thin film. The data are quoted in wavenumbers (cm^{-1}). Mass spectra were recorded by the mass spectrometry service of Oxford University's Department of Chemistry. Elemental analyses were carried out by the Elemental Analysis Service at the London Metropolitan University.

5.2 Literature preparations

$BrB(N^{i}PrCH_2)_2$,[2] $H_2NB(N^{t}BuCH_2)_2$,[3] $BrB(N^{i}Pr)_2C_6H_4$,[4] $H_2NB(NAr'CH)_2$[5], $Cp_2Zr(Me)Cl$,[6,7] Cp_2HfMe_2,[8] $Ind_2Zr(Me)Cl$,[9] Cp'_2ZrMe_2,[10] $Cp_2Zr(N^{t}Bu)(py)$ (**3.5**),[11] $HCCAr^{F}$,[12,13] $DCCAr^{F}$,[14] $DCC^{t}Bu$,[15] $Me_3SiC(H)CO$[16] and $LiNHB(NAr'CH)_2$ (**2.5**)[5] were synthesised according to literature procedures.

All other reagents were purchased from commercial suppliers, and (for liquid reagents) degassed before use, unless specified otherwise. ^{t}BuCCH, Ar^{CF_3}CCH, TolCCH, MeCCPh, PhC(O)Me, TolC(O)H, $MeCO_2Me$, $MeCO_2Et$, $MeCO_2{}^{i}Pr$, MeC(O)SMe, MeC(O)SEt, epoxy-2-methylpropane, propylene oxide, styrene oxide, cyclohexene oxide, PhNCO and PhNCS were dried over CaH_2 and distilled before use. DMAP was sublimed under dynamic vacuum at 100 °C and transferred to the dry-box.

5.3 X-ray data collection and processing parameters

Crystals were mounted on glass fibers using perfluoropolyether oil and cooled rapidly in a stream of cold N_2 using an Oxford Cryosystems Cryostream unit. Diffraction data were measured using either an Enraf-Nonius KappaCCD or Agilent Technologies Supernova diffractometer using Mo-K_α or Cu-K_α radiation, respectively. As appropriate, absorption and decay corrections were applied to the data and equivalent reflections merged.[17] The structures were solved with SIR92[18] or Superflip,[19] and further refinements and all other crystallographic calculations were performed using the CRYSTALS program suite.[20] Other details of the structure solutions and refinements are given in the individual CIFs contained in the CD Appendix.

5.4 Computational details

DFT calculations described in this Thesis were performed by Philip Mountford. Geometry optimisations were performed with the Gaussian09 package[21] at the B3PW91 level of hybrid density functional theory,[22,23] with inclusion of Grimme's D3(bj) correction[24,25] in the optimisation process except for sterically-pruned model systems. For geometry optimisations in the gas phase all atoms were represented by the Def2-SVP basis set.[26] For sterically-pruned model systems additional single-point calculations were carried out on the optimised geometry using the Def2-TZVP basis set.[27] For systems with realistic steric bulk, single-point calculations took into account both solvent and dispersion effects. The solvent (benzene) influence was taken into consideration through single point calculations on the gas-phase optimized geometry with SCRF calculations within the SMD model.[28] For the SCRF calculations all the atoms were treated with a Def2-TZVP basis set.[27] Influence of the dispersion forces was also considered by computing the D3(bj) corrections.[24,25] SCF energies reported in this work are for gas-phase model systems using the Def2-TZVP basis set. For larger systems (Def2-TZVP

basis sets) the Gibbs free energies and enthalpies were obtained by summing the SMD energy, the gas-phase Gibbs or enthalpy contribution at 298 K (or another temperature where specified) obtained from the geometry optimisations, and the D3(bj) correction. The NBO analyses were carried out using NBO 6.0,[29] on wavefunctions computed with B3PW91 in the gas phase with the Def2 family of basis sets for all atoms. Atoms-in-molecules analyses were performed using the AIMALL programme,[30] using Gaussian09 wavefunction files as input.

5.5 Experimental details and characterising data for Chapter two

$H_2NB(N^iPrCH_2)_2$ (1) and $HN\{B(N^iPrCH_2)_2\}_2$ (2). A solution of $BrB(N^iPrCH_2)_2$ (1.00 g, 4.30 mmol) in hexane (50 mL) at RT was rapidly stirred under a flow of dry NH_3, which immediately led to the formation of a white precipitate of NH_4Br. After 20 min the reaction vessel was sealed, and the mixture stirred for a further 30 min. The suspension was then filtered. Removal of all volatiles from the filtrate *in vacuo* led to 1:1 **1** and **2**. Products were then separated and purified by distillation under 10^{-1} bar at 60 – 70 °C yielding colourless oil (**1**) Yield: 0.223 g (29%) and white crystals (**2**) Yield: 0.297 g (43%).

*Data for $H_2NB(N^iPrCH_2)_2$ (**1**).* ^{1}H NMR (C_6D_6, 400.1 MHz): δ 3.12 (2 H, sept, ^3J = 6.9 Hz, C<u>H</u>MeMe), 3.00 (4 H, s, NCH_2), 1.43 (2 H, s, NH_2), 1.06 (12 H, d, ^3J = 6.6 Hz, CHMe<u>Me</u>) ppm. $^{13}C\{^1H\}$ NMR (C_6D_6, 100.6 MHz): δ 45.0 (<u>C</u>HMeMe), 42.0 (NCH_2), 21.6 (CHMe<u>Me</u>) ppm. $^{11}B\{^1H\}$ NMR (C_6D_6, 128.4 MHz): δ 24.8 ppm. IR (NaCl plates, Nujol mull, cm^{-1}): 3510, 3420 (m, N–H), 2351(w), 1596 (w), 1379 (m), 1330 (s), 1204 (m), 1187 (m), 1024 (w), 966 (w), 804 (w), 764 (w), 620 (m). EI-MS: *m/z* =169 $[M]^+$ (10%). Satisfactory elemental analysis could not be obtained.

*Data for $HN\{B(N^iPrCH_2)_2\}_2$ (**2**).* ^{1}H NMR (C_6D_6, 400.1 MHz): δ 3.65 (4 H, sept, ^3J = 6.9 Hz, C<u>H</u>MeMe), 3.03 (8 H, s, NCH_2), 1.89 (1 H, s, NH), 1.12 (24 H, d, ^3J = 6.6 Hz, CHMe<u>Me</u>) ppm. $^{13}C\{^1H\}$ NMR (C_6D_6, 100.6 MHz): δ 44.5 (<u>C</u>HMeMe), 40.7 (NCH_2), 21.4 (CHMe<u>Me</u>) ppm. $^{11}B\{^1H\}$ NMR (C_6D_6, 128.4 MHz): δ 26.6 ppm. IR (NaCl plates, Nujol mull, cm^{-1}): 3398 (w, N–H), 2351(w), 1596 (w), 1379 (m), 1330 (s), 1204 (m), 1187 (m), 1024 (w), 966 (w), 804 (w), 764 (w), 620 (m). EI-HRMS: *m/z* found (calcd. for $C_{16}H_{37}B_2N_5$, $[M]^+$) 321.3248 (321.3235). Anal. found (calcd. for $C_{16}H_{37}B_2N_5$): C, 59.93 (59.84); H, 11.58 (11.61); N, 21.73 (21.81)%.

Alternative independent synthesis of $H_2NB(N^iPrCH_2)_2$ (1). A hexane solution (20 mL) of $BrB(N^iPrCH_2)_2$ (1.00 g, 4.30 mmol) was added in 1 mL portions to liquid NH_3 (20 mL) at –78 °C, then the mixture allowed to warm to RT over 3 h, during which time the excess NH_3 boil-off was released through an oil bubbler with N_2 flow. The mixture was then filtered, and the volatiles removed from the filtrate under reduced pressure. This crude product was purified by extraction into hexane (2 × 10 mL), and removal of the hexane under reduced pressure, yielding **1** as a colourless oil, which was then dried *in vacuo*. Yield: 0.538 g (74%).

Alternative independent synthesis of $HN\{B(N^iPrCH_2)_2\}_2$ (2). To the hexane (20 mL) solution of $BrB(N^iPrCH_2)_2$ (0.250 g, 1.10 mmol) and Et_3N (0.138 g, 1.36 mmol), was added $H_2NB(N^iPrCH_2)_2$ (0.180 g, 1.10 mmol). After stirring for 2 h at RT, the filtrate was collected and all the volatiles were removed under reduced pressure, while a white solid was further purified by recrystallisation at 4 °C. Yield: 0.143 g (81%). Diffraction-quality crystals were grown from a saturated hexane solution at 4 °C.

$Cp_2Zr\{NHB(N^iPrCH_2)_2\}(Me)$ (3). To the solution of $H_2NB(N^iPrCH_2)_2$ (**1**, 0.102 g, 0.604 mmol) in hexane (10 mL) was added ^{n}BuLi (1.6 M, 0.97 mL) dropwisely at –78 °C. The resulting solution was left stirring at RT for 1 h. Volatiles were then removed under reduced pressure, and the benzene (10 mL) solution of $Cp_2ZrMeCl$ (0.165 g, 0.604 mmol) was added into the resulting white solid. After 16 h stirring at RT, the volatiles were removed under reduced pressure and the resulting solid extracted into hexane (2 × 10 mL) and dried *in vacuo*, yielding **3** as a red oil. Yield: 0.149 g (61%).

^{1}H NMR (C_6D_6, 400.1 MHz): δ 5.77 (10 H, s, C_5H_5), 4.81 (1 H, s, NH), 3.55 (2 H, sept, ^3J = 6.9 Hz, C<u>H</u>MeMe), 3.02 (4 H, s, NCH_2), 1.13 (12 H, d, ^3J = 6.9 Hz, CHMe<u>Me</u>), 0.17 (3 H, s, ZrMe) ppm. $^{13}C\{^1H\}$ NMR (C_6D_6, 100.6 MHz): δ 109.8 (C_5H_5), 44.4 (<u>C</u>HMeMe), 40.5 (NCH_2), 21.6 (CHMe<u>Me</u>), 17.8 (ZrMe) ppm. $^{11}B\{^1H\}$ NMR (C_6D_6, 128.4 MHz): δ 28.9 ppm. IR (NaCl plates, Nujol mull, cm^{-1}): 3339 (w, N–H), 1670 (w), 1613 (m), 1474 (s), 1317 (s), 1209 (m), 1110 (m), 1065 (w), 1020 (s), 791 (s), 733 (s), 643 (w). Anal. found (calcd. for $C_{19}H_{32}BN_3Zr$): C, 56.23 (56.41); H, 7.84 (7.97); N, 10.17 (10.39)%.

$Cp_2Zr\{NHB(N^tBuCH_2)_2\}(Me)$ (4). To the solution of $H_2NB(N^tBuCH_2)_2$ (0.139 g, 0.733 mmol) in hexane (10 mL) was added ^{n}BuLi (1.6 M, 1.17 mL) dropwisely at –78 °C. The resulting solution was left stirring at RT for 1 h. Volatiles were then removed under

reduced pressure, and the benzene (10 mL) solution of $Cp_2ZrMeCl$ (0.200 g, 0.733 mml) was added into the resulting white solid. After 16 h stirring at RT, The volatiles removed again under reduced pressure, and the resulting solid was then washed with cold (0 °C) hexane (2 × 5 mL), yielding **4** as a pale yellow powder. Yield: 0.110 g (42%).

^{1}H NMR (C_6D_6, 400.1 MHz): δ 5.83 (10 H, s, C_5H_5), 4.63 (1 H, s, NH), 3.01 (4 H, s, NCH_2), 1.25 (18 H, s, CMe_3), 0.13 (3 H, s, ZrMe) ppm. ^{13}C{^{1}H} NMR (C_6D_6, 100.6 MHz): δ 110.2 (C_5H_5), 51.6 ($\underline{C}Me_3$), 44.0 (NCH_2), 30.6 ($C\underline{Me}_3$), 22.0 (ZrMe) ppm. ^{11}B{^{1}H} NMR (C_6D_6, 128.4 MHz): δ 29.9 ppm. IR (NaCl plates, Nujol mull, cm^{-1}): 3321 (w, N–H), 1703(w), 1622 (w), 1379 (s), 1298 (m), 1262 (m), 1218 (m), 1088 (m), 1011 (s), 908 (s), 805 (s), 715 (w), 616 (w). Satisfactory elemental analysis could not be obtained.

$H_2NB(N^iPr)_2C_6H_4$ (5). A hexane solution (20 mL) of $BrB(N^iPr)_2C_6H_4$ (1.00 g, 3.60 mmol) was added in 1 mL portions to liquid NH_3 (20 mL) at –78 °C, then the mixture allowed to warm to RT over 3 h, during which time the excess NH_3 boil-off was released through an oil bubbler with N_2 flow. The mixture was then filtered, and the volatiles removed from the filtrate under reduced pressure. This crude product was purified by extraction into hexane (2 × 10 mL), and removal of the hexane under reduced pressure, yielding **5** as a colourless oil, which was then dried *in vacuo*. Yield: 0.562 g (72%).

^{1}H NMR (C_6D_6, 400.1 MHz): δ 7.05 (2 H, dd, ^3J = 5.7 Hz, ^4J = 3.3 Hz, 2,5-C_6H_4), 6.89 (2 H, dd, ^3J = 5.7 Hz, ^4J = 3.3 Hz, 3,4-C_6H_4), 3.75 (2 H, sept, ^3J = 6.6 Hz, C$\underline{H}$MeMe), 1.78 (2 H, s, NH_2), 1.16 (12 H, d, ^3J = 6.6 Hz, CHMe$\underline{Me}$) ppm. ^{13}C{^{1}H} NMR (C_6D_6, 100.6 MHz): δ 137.5 (1,6-C_6H_4), 117.8 (2,5-C_6H_4), 108.1 (3,4-C_6H_4), 44.4 ($\underline{C}$HMeMe), 22.2 (CHMe$\underline{Me}$) ppm. ^{11}B{^{1}H} NMR (C_6D_6, 128.4 MHz): δ 24.1 ppm. IR (NaCl plates, Nujol mull, cm^{-1}): 3533, 3452 (m, N–H), 3034 (w), 2351 (w), 1879 (w), 1820 (w), 1775 (w), 1721 (w), 1591 (m), 1366 (m), 1379 (m), 1379 (m), 1191 (w), 1169 (w), 1034 (m), 881 (w), 800 (s), 715 (s), 638 (s). EI-MS: *m/z* =217 $[M]^+$ (1%) Anal. found (calcd. for $C_{12}H_{20}B_1N_3$): C, 66.29 (66.38); H, 9.46 (9.29); N, 19.26 (19.35)%.

$HN\{B(N^iPr)_2C_6H_4\}_2$ (6). A solution of $BrB(N^iPr)_2C_6H_4$ (1.00 g, 3.60 mmol) in hexane (50 mL) at RT was rapidly stirred under a flow of dry NH_3, which immediately led to the formation of a white precipitate of NH_4Br. After 20 min the reaction vessel was sealed, and the mixture stirred for a further 30 min. The suspension was filtered. Removal of all

volatiles from the filtrate and recrystallisation at 4 °C yields **6** as colourless crystals. Yield: 0.27 g (36%).

^{1}H NMR (C_6D_6, 400.1 MHz): δ 7.10 – 7.04 (8 H, overlapping 2 × m, 2,3,4,5-C_6H_4), 4.03 (4 H, sept, ^{3}J = 6.6 Hz, C<u>H</u>MeMe), 2.30 (1 H, s, NH), 1.30 (24 H, d, ^{3}J = 6.6 Hz, CHMe<u>Me</u>) ppm. ^{13}C{^{1}H} NMR (C_6D_6, 100.6 MHz): δ 136.8 (1,6-C_6H_4), 118.3 (2,5-C_6H_4), 110.3 (3,4-C_6H_4), 45.2 (<u>C</u>HMeMe), 22.3 (CH<u>MeMe</u>) ppm. ^{11}B{^{1}H} NMR (C_6D_6, 128.4 MHz): δ 24.5 ppm. IR (NaCl plates, Nujol mull, cm^{-1}): 3416 (w, N–H), 2719 (w), 1892 (w), 1852 (w), 1739 (w), 1596 (s), 1285 (m), 1200 (m), 1159 (m), 1137 (w), 1083(w), 1016 (w), 899 (w), 800 (m), 724 (s), 656 (m), 639 (m). EI-HRMS: *m/z* found (calcd. for $C_{24}H_{37}B_2N_5$, $[M]^+$) 415.3294 (415.3308). Anal. found (calcd. for $C_{24}H_{37}B_2N_5$): C, 69.15 (69.09); H, 9.09 (8.94); N, 16.68 (16.79)%.

$Cp_2Zr\{NHB(N^iPr)_2C_6H_4\}(Me)$ (7). To the solution of $H_2NB(N^iPr)_2C_6H_4$ (**5**, 0.159 g, 0.733 mmol) in hexane (10 mL) was added ^{n}BuLi (1.6 M, 1.17 mL) dropwisely at –78 °C. The resulting solution was left stirring at RT for 1 h. Volatiles were then removed under reduced pressure, and the benzene (10 mL) solution of $Cp_2ZrMeCl$ (0.200 g, 0.733 mml) was added into the resulting white solid. After 16 h stirring at RT, The volatiles removed again under reduced pressure, and the resulting solid was then washed with cold (0 °C) hexane (2 × 12 mL), yielding **7** as a pale yellow powder. Yield: 0.301 g (85%).

^{1}H NMR (C_6D_6, 400.1 MHz): δ 7.17(2 H, m, 2,5-C_6H_4), 7.10 (2 H, m, 3,4-C_6H_4), 5.71 (10 H, s, C_5H_5), 4.93 (1 H, s, NH), 4.17 (2 H, sept, ^{3}J = 6.9 Hz, C<u>H</u>MeMe), 1.43 (12 H, d, ^{3}J = 6.9 Hz, CHMe<u>Me</u>), 0.22 (3 H, s, ZrMe) ppm. ^{13}C{^{1}H} NMR (C_6D_6, 100.6 MHz): δ 136.5 (1,6-C_6H_4), 118.0 (2,5-C_6H_4), 110.5 (3,4-C_6H_4), 110.0 (C_5H_5), 44.7 (<u>C</u>HMeMe), 22.2 (CHMe<u>Me</u>), 19.0 (ZrMe) ppm. ^{11}B{^{1}H} NMR (C_6D_6, 128.4 MHz): δ 27.5 ppm. IR (NaCl plates, Nujol mull, cm^{-1}): 3308 (w, N–H), 1703 (w), 1596 (s), 1483 (s), 1406 (m), 1285 (s), 1142 (m), 1119 (w), 1105 (w), 1087(w), 1016 (s), 894 (w), 809 (s), 728 (s), 692 (w), 660 (w), 611 (w). Anal. found (calcd. for $C_{23}H_{32}BN_3Zr$): C, 60.84 (61.04); H, 7.28 (7.13); N, 9.17 (9.29)%.

$Cp_2Zr\{NB(N^iPr)_2C_6H_4\}(DMAP)$ (8). $Cp_2Zr\{NHB(N^iPr)_2C_6H_4\}(Me)$ (**7**, 0.300 g, 0.663 mmol), DMAP (0.089 g, 0.730 mmol) and toluene (15 mL) were added to a Rotaflo ampoule with a Teflon valve, which was partially evacuated and sealed before being heated to 120 ℃ for 23 h. Upon cooling to RT, the pale yellow solution filtered into the schlenk and all the volatiles removed under reduced pressure. The resulting solid was

dissolved in 3 mL of toluene, and the solution was layered with 6 mL of hexane at 4 °C. Translucent yellow crystals formed over several days and were recovered by decanting the solvent. Yield: 0.137 g (37%).

^{1}H NMR (C_6D_6, 400.1 MHz): δ 8.29 (2 H, d, ^{3}J = 7.4 Hz, 2,6-$C_5\underline{H}_4NMe_2$), 7.17 (2 H, m 2,5-C_6H_4), 7.12 (2 H, m, 3,4-C_6H_4), 6.21 (10 H, s, C_5H_5), 5.75 (2 H, d, ^{3}J = 7.4 Hz, 3,5-$C_5\underline{H}_4NMe_2$), 4.51 (2 H, sept, ^{3}J = 6.9 Hz, C<u>H</u>MeMe), 2.03 (6 H, s, $C_5H_4N\underline{Me}_2$), 1.62 (12 H, d, ^{3}J = 6.9 Hz, CH<u>Me</u>Me) ppm. ^{13}C{^{1}H} NMR (C_6D_6, 100.6 MHz): δ 154.2 (4-$\underline{C}_5H_4NMe_2$), 153.2 (2,6-$\underline{C}_5H_4NMe_2$), 137.7 (1,6-C_6H_4), 127.9 (2,5-C_6H_4), 116.4 (3,4-C_6H_4), 110.5 (C_5H_5), 105.5 (3,5-$\underline{C}_5H_4NMe_2$), 44.0 (<u>C</u>HMeMe), 37.8 ($C_5H_4N\underline{Me}_2$), 21.8 (CHMe<u>Me</u>) ppm. ^{11}B{^{1}H} NMR (C_6D_6, 128.4 MHz): δ 20.7 ppm. IR (NaCl plates, Nujol mull, cm^{-1}): 1761 (w), 1618 (s), 1587 (m), 1513 (s), 1294 (m), 1227 (m), 1191 (w), 1164 (w), 1128 (m), 1076 (m), 998 (s), 957 (m), 890 (m), 791 (s), 755 (s), 674 (m), 655 (m). Anal. found (calcd. for $C_{43}H_{56}BN_5Zr$): C, 62.47 (62.35); H, 7.02 (6.86); N, 12.23 (12.54)%.

$Cp_2Zr\{NHB(NAr'CH)_2\}(Me)$ (9). To a mixture of $Cp_2Zr(Me)Cl$ (0.133 g, 0.490 mmol) and $LiNHB(NAr'CH)_2$ (0.200 g, 0.490 mmol) in a Schlenk tube, was added benzene (10 mL) and the resulting solution was left stirring at RT for 16 h. The volatiles were removed under reduced pressure and the resulting solid extracted into hexane (3 × 10 mL), then the hexane removed under reduced pressure. The product was then washed with cold (0 °C) hexane (2 × 5 mL) and dried *in vacuo*, yielding **9** as a pale yellow powder. Yield: 0.150 g (49%). Diffraction-quality crystals were grown from a saturated hexane solution at 4 °C.

^{1}H NMR (C_6D_6, 400.1 MHz): δ 7.24 (6 H, overlapping 2 × m, *m*- and *p*-$C_6\underline{H}_3{}^{i}Pr_2$), 6.13 (2 H, s, NCH), 5.41 (10 H, s, C_5H_5), 5.16 (1 H, s, NH), 3.42 (4 H, sept., ^{3}J = 6.9 Hz, C<u>H</u>MeMe), 1.37 (12 H, d, ^{3}J = 6.9 Hz, CH<u>Me</u>Me), 1.20 (12 H, d, ^{3}J = 6.9 Hz, CHMe<u>Me</u>), –0.06 (3 H, s, ZrMe) ppm. ^{13}C{^{1}H} NMR (C_6D_6, 100.6 MHz): δ 147.7 (*o*-$\underline{C}_6H_3{}^{i}Pr_2$), 140.8 (*i*-$\underline{C}_6H_3{}^{i}Pr_2$), 128.3 (*p*-$\underline{C}_6H_3{}^{i}Pr_2$), 124.8 (*m*-$\underline{C}_6H_3{}^{i}Pr_2$), 118.1 (NCH), 110.8 ($C_5H_5$), 29.6 (<u>C</u>HMeMe), 26.3 (CHMe<u>Me</u>), 24.3 (CH<u>Me</u>Me), 21.9 (ZrMe) ppm. ^{11}B{^{1}H} NMR (C_6D_6, 128.4 MHz): δ 24.8 ppm. IR (NaCl plates, Nujol mull, cm^{-1}): 3281 (w, N–H), 1578 (m), 1402 (m), 1366 (m), 1249 (s), 1096 (w), 1006 (m), 796 (s), 742 (m), 657 (m). EI-MS: *m/z* = 637 $[M]^+$ (<1%), 623 $[M - CH_3]^+$ (15%). Satisfactory elemental analysis could not be obtained.

Improved synthesis of $Cp_2Hf(Me)Cl$. To a mixture of Cp_2HfMe_2 (1.00 g, 2.95 mmol) and Ph_3CCl (0.820 g, 2.95 mmol) in a Schlenk tube, was added toluene (80 mL). Then the colourless solution was heated up to 95 °C for 22 h. Upon cooling to RT, the volatiles were removed under reduced pressure and recrystallised in hexane at –30 °C to yield white needles which were then washed with cold (–30 °C) hexane (5 mL). Yield: 0.850 g (80%). The NMR data was in good agreement with the literature.[31]

^{1}H NMR (C_6D_6, 400.1 MHz): δ 5.68 (10 H, s, C_5H_5), 0.26 (3 H, s, HfMe) ppm.

$Cp_2Hf\{NHB(NAr'CH)_2\}(Me)$ (10). To a mixture of $Cp_2Hf(Me)Cl$ (0.263 g, 0.730 mmol) and $LiNHB(NAr'CH)_2$ (0.300 g, 0.730 mmol) in a Schlenk tube, was added benzene (10 mL) and the resulting solution was left stirring at RT for 16 h. The volatiles were removed under reduced pressure and the resulting solid extracted into hexanes (3 × 10 mL), and then the hexane removed under reduced pressure again. The remaining solid was then washed with cold (0 °C) hexane (2 × 4 mL) and dried *in vacuo*, yielding **10** as a white powder. Yield: 0.220 g (41%). Diffraction-quality crystals were grown from a saturated hexane solution at 4 °C.

^{1}H NMR (C_6D_6, 400.1 MHz): δ 7.24 (6 H, overlapping 2 × m, *m*- and *p*-$C_6\underline{H}_3{}^iPr_2$), 6.14 (2 H, s, NCH), 5.36 (10 H, s, C_5H_5), 4.46 (1 H, s, NH), 3.42 (4 H, sept., ^3J = 6.9 Hz, C<u>H</u>MeMe), 1.38 (12 H, d, ^3J = 6.9 Hz, CH<u>Me</u>Me), 1.20 (12 H, d, ^3J = 6.9 Hz, CHMe<u>Me</u>), –0.20 (3 H, s, HfMe) ppm. $^{13}C\{^1H\}$ NMR (C_6D_6, 100.6 MHz): δ 147.0 (*o*-$\underline{C}_6H_3{}^iPr_2$), 140.0 (*i*-$\underline{C}_6H_3{}^iPr_2$), 127.5 (*p*-$\underline{C}_6H_3{}^iPr_2$), 124.0 (*m*-$\underline{C}_6H_3{}^iPr_2$), 117.4 (NCH), 109.3 ($C_5H_5$), 28.8 (<u>C</u>HMeMe), 25.6 (CHMe<u>Me</u>), 24.4 (HfMe), 23.5 (CH<u>Me</u>Me) ppm. $^{11}B\{^1H\}$ NMR (C_6D_6, 128.4 MHz): δ 25.8 ppm. IR (NaCl plates, Nujol mull, cm^{-1}): 3294 (w, N–H), 1582 (m), 1555 (m), 1357 (s), 1254 (m), 1173 (m), 1142 (m), 1052 (m), 1007 (s), 957 (m), 926 (m), 805 (s), 746 (s), 715(w), 647 (s). EI-MS: *m/z* = 727 $[M]^+$ (10%). Satisfactory elemental analysis could not be obtained.

$Cp_2Zr\{NB(NAr'CH)_2\}(py)$ (11). $Cp_2Zr(Me)Cl$ (1.66 g, 6.11 mmol), $LiNHB(NAr'CH)_2$ (2.50 g, 6.11 mmol), pyridine (833 µL, 9.17 mmol) and toluene (40 mL) were added to a Rotaflo ampoule with a Teflon valve, which was heated to 120 °C for 30 mins and sealed before being heated for another 16 h. Upon cooling to RT, the red solution was filtered into a Schlenk flask and the volatiles removed under reduced pressure. The resulting orange solid was then washed with hexane (3 × 10 mL) and dried *in vacuo*, yielding a pale orange powder (2.50 g). The filtrate was also concentrated and cooled to 4 °C, upon

which crystals grew. The combined yield was 2.80 g (85%). Diffraction-quality crystals were grown from a saturated hexane solution at 4 °C.

^{1}H NMR (C_6D_6, 400.1 MHz): δ 7.85 (2 H, d, ^{3}J = 4.9 Hz, 2,6-py), 7.29 (6 H, s, *m*- and *p*-$C_6\underline{H}_3{}^{i}Pr_2$), 6.71 (1 H, t, ^{3}J = 7.7 Hz, 4-py), 6.31 (2 H, m, 3,5-py), 6.06 (2 H, s, NCH), 5.77 (10 H, s, C_5H_5), 3.85 (4 H, sept., ^{3}J = 6.9 Hz, C<u>H</u>MeMe), 1.51 (12 H, d, ^{3}J = 6.9 Hz, CH<u>Me</u>Me), 1.35 (12 H, d, ^{3}J = 6.9 Hz, CHMe<u>Me</u>) ppm. ^{13}C{^{1}H} NMR (C_6D_6, 100.6 MHz): δ 154.9 (2,6-py), 148.3 (*o*-$\underline{C}_6H_3{}^{i}Pr_2$), 143.8 (*i*-$\underline{C}_6H_3{}^{i}Pr_2$), 137.9 (4-py), 126.9 (*m*-$\underline{C}_6H_3{}^{i}Pr_2$), 124.6 (3,5-py), 123.9 (*p*-$\underline{C}_6H_3{}^{i}Pr_2$), 117.7 (NCH), 111.0 ($C_5H_5$), 29.3 (<u>C</u>HMeMe), 25.9 (CHMe<u>Me</u>), 24.3 (CH<u>Me</u>Me) ppm. ^{11}B{^{1}H} NMR (C_6D_6, 128.4 MHz): δ 20.2 ppm. IR (NaCl plates, Nujol mull, cm^{-1}): 1600 (m), 1578 (w), 1560 (w), 1435 (s), 1420 (m), 1270 (m), 1249 (m), 1141 (m), 1055 (m), 1005 (m), 933 (m), 884 (m), 846 (s), 770 (s), 701 (m), 641 (s), 625 (w). Anal. found (calcd. for $C_{41}H_{51}BN_4Zr$): C, 69.95 (70.16); H, 7.36 (7.32); N, 7.93 (7.98)%.

$Cp_2Hf\{NB(NAr'CH)_2\}(py)$ (12). $Cp_2Hf(Me)Cl$ (0.292 g, 0.811 mmol), $LiNHB(NAr'CH)_2$ (0.331 g, 0.811 mmol), pyridine (196 µL, 2.43 mmol) and toluene (15 mL) were added to a Rotaflo ampoule with a Teflon valve, which was heated to 120 °C for 30 min and sealed before being heated for another 60 h. Upon cooling to RT, the red solution was filtered into a Schlenk flask and the volatiles removed under reduced pressure. The resulting orange solid was then washed with cold (0 °C) hexane (3 × 5 mL) and dried *in vacuo*, yielding a pale orange powder. Yield: 0.268 g (42%). Diffraction-quality crystals were grown from a saturated hexane solution at 4 °C.

^{1}H NMR (C_6D_6, 400.1 MHz): δ 7.96 (2 H, d, ^{3}J = 4.9 Hz, 2,6-py), 7.30 (6 H, s, *m*- and *p*-$C_6\underline{H}_3{}^{i}Pr_2$), 6.67 (1 H, t, ^{3}J = 7.7 Hz, 4-py), 6.27 (2 H, m, 3,5-py), 6.13 (2 H, s, NCH), 5.70 (10 H, s, C_5H_5), 3.93 (4 H, sept., ^{3}J = 6.9 Hz, C<u>H</u>MeMe), 1.51 (12 H, d, ^{3}J = 6.9 Hz, CH<u>Me</u>Me), 1.38 (12 H, d, ^{3}J = 6.9 Hz, CHMe<u>Me</u>) ppm. ^{13}C{^{1}H} NMR (C_6D_6, 100.6 MHz): δ 155.1 (2,6-py), 147.9 (*o*-$\underline{C}_6H_3{}^{i}Pr_2$), 143.7 (*i*-$\underline{C}_6H_3{}^{i}Pr_2$), 137.4 (4-py), 126.1 (*m*-$\underline{C}_6H_3{}^{i}Pr_2$), 124.1 (3,5-py), 123.3 (*p*-$\underline{C}_6H_3{}^{i}Pr_2$), 117.2 (NCH), 109.8 ($C_5H_5$), 28.7 (<u>C</u>HMeMe), 25.4 (CHMe<u>Me</u>), 23.8 (CH<u>Me</u>Me) ppm. ^{11}B{^{1}H} NMR (C_6D_6, 128.4 MHz): δ 23.8 ppm. IR (NaCl plates, Nujol mull, cm^{-1}): 1691 (w), 1651 (w), 1596 (s), 1560 (m), 1249 (m), 1209 (m), 1110 (m), 1065 (m), 1007 (w), 945 (w), 867 (m), 845 (m), 800 (s), 688 (s), 688 (s), 661 (m), 634 (m). EI-MS: *m/z* = 790 $[M]^+$ (15%). Anal. found (calcd. for $C_{41}H_{51}BN_4Hf$): C, 62.27 (62.40); H, 6.42 (6.51); N, 6.95 (7.10)%.

$Cp_2Zr\{NB(NAr'CH)_2\}(THF)$ (13). $Cp_2Zr(Me)Cl$ (0.200 g, 0.737 mmol), $LiNHB(NAr'CH)_2$ (0.300 g, 0.737 mmol), THF (1.20 mL, 14.7 mmol) and toluene (15 mL) were added to a Rotaflo ampoule with a Teflon valve, which was partially evacuated and sealed before being heated to 120 °C for 20 h. Upon cooling to RT, the yellow solution was filtered into a Schlenk flask and the volatiles removed under reduced pressure. The resulting yellow solid was then recrystallised in hexane at –30 °C. Yield: 0.217 g (42%). Diffraction-quality crystals were grown from a saturated hexane solution at 4 °C.

^{1}H NMR (C_6D_6, 400.1 MHz): δ 7.21 (6 H, s, *m*- and *p*-$C_6\underline{H}_3{}^i Pr_2$), 6.06 (2 H, s, NCH), 5.80 (10 H, s, C_5H_5), 3.78 (4 H, sept., ^3J = 6.9 Hz, C<u>H</u>MeMe), 2.71 (4 H, m, OCH_2), 1.56 (12 H, d, ^3J = 6.9 Hz, CH<u>Me</u>Me), 1.34 (12 H, d, ^3J = 6.9 Hz, CHMe<u>Me</u>), 0.95 (4 H, m, $OCH_2C\underline{H}_2$), ppm. $^{13}C\{^1H\}$ NMR (C_6D_6, 100.6 MHz): δ 147.5 (*o*-$\underline{C}_6H_3{}^i Pr_2$), 143.0 (*i*-$\underline{C}_6H_3{}^i Pr_2$), 126.2 (*m*-$\underline{C}_6H_3{}^i Pr_2$), 123.1 (*p*-$\underline{C}_6H_3{}^i Pr_2$), 116.9 (NCH), 110.0 ($C_5H_5$), 77.2 ($OCH_2$), 28.7 (<u>C</u>HMeMe), 25.9 ($OCH_2\underline{C}H_2$), 25.5 (CHMe<u>Me</u>), 23.8 (CH<u>Me</u>Me) ppm. $^{11}B\{^1H\}$ NMR (C_6D_6, 128.4 MHz): δ 19.9 ppm. IR (NaCl plates, Nujol mull, cm^{-1}): 1587 (m), 1565 (m), 1520 (m), 1428 (w), 1276 (m), 1245 (m), 1137 (m), 1115 (w), 1092 (m), 1007 (s), 934 (m), 881 (m), 787 (s), 760 (m), 714 (m), 660 (m), 651 (w). EI-MS: *m/z* = 621 $[M - THF]^+$ (4%). Anal. found (calcd. for $C_{40}H_{54}BN_3OZr$): C, 69.05 (69.14); H, 7.90 (7.83); N, 6.14 (6.05)%.

$Cp_2Zr\{NB(NAr'CH)_2\}(DMAP)$ (14). $Cp_2Zr(Me)Cl$ (0.215 g, 0.737 mmol), $LiNHB(NAr'CH)_2$ (0.300 g, 0.737 mmol), DMAP (0.099 g, 0.811 mmol) and toluene (15 mL) were added to a Rotaflo ampoule with a Teflon valve, which was heated to 120 °C for 30 mins and sealed before being heated for another 16 h. Upon cooling to RT, the green solution was filtered into a Schlenk flask and the volatiles removed under reduced pressure. The resulting pale green solid was then washed with hexane (3 × 10 mL) and dried *in vacuo*, yielding a pale green powder. Yield: 0.400 g (73%).

^{1}H NMR (C_6D_6, 400.1 MHz): δ 7.57 (2 H, d, ^3J = 7.4 Hz, 2,6-$C_5\underline{H}_4NMe_2$), 7.26 (6 H, overlapping 2 × m,, *m*- and *p*-$C_6\underline{H}_3{}^i Pr_2$), 6.09 (2 H, s, NCH), 5.89 (10 H, s, C_5H_5), 5.57 (2 H, d, ^3J = 7.4 Hz, 3,5- $C_5\underline{H}_4NMe_2$), 3.93 (4 H, sept., ^3J = 6.9 Hz, C<u>H</u>MeMe), 2.13 (6 H, s, $C_5\underline{H}_4N\underline{Me}_2$), 1.51 (12 H, d, ^3J = 6.9 Hz, CH<u>Me</u>Me), 1.35 (12 H, d, ^3J = 6.9 Hz, CHMe<u>Me</u>) ppm. $^{13}C\{^1H\}$ NMR (C_6D_6, 100.6 MHz): δ 153.7 (2,6- $\underline{C}_5H_4NMe_2$), 147.8 (*o*-$\underline{C}_6H_3{}^i Pr_2$), 143.6 (*i*-$\underline{C}_6H_3{}^i Pr_2$), 126.0 (*m*-$\underline{C}_6H_3{}^i Pr_2$), 123.3 (*p*-$\underline{C}_6H_3{}^i Pr_2$), 117.1 (NCH),

111.1 (C_5H_5), 106.0 (3,5- $\underline{C}_5H_4NMe_2$), 38.0 ($C_5H_4N\underline{Me}_2$), 28.8 ($\underline{C}$HMeMe), 25.4 (CHMe$\underline{Me}$), 23.9 (CH$\underline{Me}$Me) ppm. $^{11}B\{^1H\}$ NMR (C_6D_6, 128.4 MHz): δ 19.7 ppm. IR (NaCl plates, Nujol mull, cm^{-1}): 1622 (s), 1542 (m), 1366 (s), 1272 (m), 1106 (m), 1016 (m), 944 (w), 876 (w), 830 (w), 801 (m), 796 (m), 776 (s), 760 (m), 638 (m). EI-MS: *m/z* = 743 $[M]^+$ (<1%), 621 $[M - DMAP]^+$ (6%). Anal. found (calcd. for $C_{43}H_{56}BN_5Zr$): C, 69.27 (69.33); H, 7.73 (7.58); N, 9.27 (9.40)%.

Alternative synthesis of $Cp_2Zr\{NB(NAr'CH)_2\}(DMAP)$ (14). Cp_2ZrCl_2 (0.215 g, 0.737 mmol), $LiNHB(NAr'CH)_2$ (0.300 g, 0.737 mmol), DMAP (0.0990 g, 0.811 mmol) and toluene (15 mL) were added into a Rotaflo ampoule with a Teflon valve. Then $LiN(SiMe_3)_2$ (123 mg, 0.737 mmol) was added after 2 hours stirring at RT. The ampoule was heated to 120 °C for 30 mins and sealed before being heated for another 16 h. Upon cooling to RT, the green solution was filtered into a Schlenk flask and the volatiles removed under reduced pressure. The resulting pale green solid was then washed with hexane (3 × 10 mL) and dried *in vacuo*, yielding a pale green powder. Yield: 0.430 g (78%). The ^1H NMR spectrum was identical to that of a sample prepared *via* previously described method.

$Cp_2Hf\{NB(NAr'CH)_2\}(DMAP)$ (15). $Cp_2Hf(Me)Cl$ (0.264 g, 0.737 mmol), $LiNHB(NAr'CH)_2$ (0.300 g, 0.737 mmol), DMAP (0.122 g, 0.811 mmol) and toluene (15 mL) were added to a Rotaflo ampoule with a Teflon valve, which was heated to 120 °C for 30 min and sealed before being heated for another 60 h. Upon cooling to RT, the green solution was filtered into a Schlenk flask and the toluene removed under reduced pressure. The resulting pale green solid was then washed with hexane (3 × 10 mL) and dried *in vacuo*, yielding a pale green powder. Yield: 0.330 g (55%).

^1H NMR (C_6D_6, 400.1 MHz): δ 7.67 (2 H, d, ^3J = 7.4 Hz, 2,6-$C_5\underline{H}_4NMe_2$), 7.27 (6 H, overlapping 2 × m, *m*- and *p*-$C_6\underline{H}_3{}^iPr_2$), 6.15 (2 H, s, NCH), 5.83 (10 H, s, C_5H_5), 5.51 (2 H, d, ^3J = 7.4 Hz, 3,5-$C_5\underline{H}_4NMe_2$), 4.00 (4 H, sept., ^3J = 6.9 Hz, C$\underline{H}$MeMe), 2.13 (6 H, s, $C_5H_4N\underline{Me}_2$), 1.58 (12 H, d, ^3J = 6.9 Hz, CH$\underline{Me}$Me), 1.41 (12 H, d, ^3J = 6.9 Hz, CHMe$\underline{Me}$) ppm. $^{13}C\{^1H\}$ NMR (C_6D_6, 100.6 MHz): δ 153.7 (2,6- $\underline{C}_5H_4NMe_2$), 147.8 (*o*-$\underline{C}_6H_3{}^iPr_2$), 143.6 (*i*-$\underline{C}_6H_3{}^iPr_2$), 126.0 (*m*-$\underline{C}_6H_3{}^iPr_2$), 123.3 (*p*-$\underline{C}_6H_3{}^iPr_2$), 117.1 (NCH), 111.1 ($C_5H_5$), 106.0 (3,5- $\underline{C}_5H_4NMe_2$), 38.0 ($C_5H_4N\underline{Me}_2$), 28.8 ($\underline{C}$HMeMe), 25.4 (CHMe$\underline{Me}$), 23.9 (CH$\underline{Me}$Me) ppm. $^{11}B\{^1H\}$ NMR (C_6D_6, 128.4 MHz): δ 22.9 ppm. IR (NaCl plates, Nujol mull, cm^{-1}): 1780 (w), 1631 (s), 1533 (s), 1258 (m), 1222 (m), 1178

(w), 1106 (m), 1070 (s), 1016 (s), 957 (w), 930 (w), 872 (m), 845 (m), 791 (s), 760 (m), 665 (m), 634 (m). EI-MS: *m/z* = 743 $[M]^+$ (<1%), 621 $[M - \text{DMAP}]^+$ (90%). Anal. found (calcd. for $C_{43}H_{56}BN_5Hf$): C, 61.82 (62.06); H, 6.87 (6.78); N, 8.32 (8.42)%.

$Cp_2Zr\{NHB(NAr'CH)_2\}Cl$ (16). To a mixture of Cp_2ZrCl_2 (0.143 g, 0.490 mmol) and $LiNHB(NAr'CH)_2$ (0.200 g, 0.490 mmol) in a Schlenk tube, was added benzene (10 mL) and the resulting solution was left stirring at RT for 16 h. The volatiles were removed under reduced pressure and the resulting solid extracted into hexanes (3 × 15 mL), then the hexane removed under reduced pressure. The remaining solid was then washed with hexane (3 × 5 mL) and dried *in vacuo*, yielding **16** as a yellow powder. Yield: 0.240 g (75%).

^{1}H NMR (C_6D_6, 400.1 MHz): δ 7.24 (6 H, overlapping 2 × m, *m*- and *p*-$C_6\underline{H}_3{}^i\text{Pr}_2$), 6.18 (1 H, s, NH), 6.15 (2 H, s, NCH), 5.57 (10 H, s, C_5H_5), 3.43 (4 H, sept., ^3J = 6.9 Hz, C<u>H</u>MeMe), 1.39 (12 H, d, ^3J = 6.9 Hz, CH<u>Me</u>Me), 1.20 (12 H, d, ^3J = 6.9 Hz, CHMe<u>Me</u>) ppm. $^{13}C\{^1H\}$ NMR (C_6D_6, 100.6 MHz): δ 146.9 (*o*-$\underline{C}_6H_3{}^i\text{Pr}_2$), 139.7 (*i*-$\underline{C}_6H_3{}^i\text{Pr}_2$), 127.8 (*p*-$\underline{C}_6H_3{}^i\text{Pr}_2$), 124.2 (*m*-$\underline{C}_6H_3{}^i\text{Pr}_2$), 117.5 (NCH), 112.8 ($C_5H_5$), 28.9 (<u>C</u>HMeMe), 25.5 (CHMe<u>Me</u>), 23.6 (CH<u>Me</u>Me) ppm. $^{11}B\{^1H\}$ NMR (C_6D_6, 128.4 MHz): δ 24.9 ppm. IR (NaCl plates, Nujol mull, cm^{-1}): 3290 (w, N–H), 1581 (w), 1397 (m), 1382 (m), 1296 (w), 1270 (m), 1147 (w), 1115 (w), 1096 (w), 1042 (m), 1024 (m), 1002 (m), 970 (w), 890 (m), 817 (s), 805 (s), 776 (m), 751 (s), 656 (m). EI-MS: *m/z* = 657 $[M]^+$ (8%). Anal. found (calcd. for $C_{36}H_{47}BClN_3Zr$): C, 65.37 (65.59); H, 7.08 (7.19); N, 6.20 (6.37)%.

$Cp_2Hf\{NHB(NAr'CH)_2\}Cl$ (17). To a mixture of Cp_2HfCl_2 (0.289 g, 0.760 mmol) and $LiNHB(NAr'CH)_2$ (0.311 g, 0.760 mmol) in a Schlenk tube, was added benzene (10 mL) and the resulting solution was left stirring at RT for 16 h. The volatiles were removed under reduced pressure and the resulting solid extracted into hexanes (3 × 10 mL), and then volatiles removed under reduced pressure again. The remaining solid was then washed with hexane (3 × 5 mL) and dried *in vacuo*, yielding **17** as a white powder. Yield: 0.410 g (72%). Diffraction-quality crystals were grown from a saturated hexane solution at 4 °C.

^{1}H NMR (C_6D_6, 400.1 MHz): δ 7.24 (6 H, s, *m*- and *p*-$C_6\underline{H}_3{}^i\text{Pr}_2$), 6.16 (2 H, s, NCH), 5.51 (10 H, s, C_5H_5), 5.1 (1 H, s, NH), 3.45 (4 H, sept., ^3J = 6.9 Hz, C<u>H</u>MeMe), 1.39 (12 H, d, ^3J = 6.9 Hz, CH<u>Me</u>Me), 1.22 (12 H, d, ^3J = 6.9 Hz, CHMe<u>Me</u>) ppm. $^{13}C\{^1H\}$ NMR (C_6D_6, 100.6 MHz): δ 146.9 (*o*-$\underline{C}_6H_3{}^i\text{Pr}_2$), 139.7 (*i*-$\underline{C}_6H_3{}^i\text{Pr}_2$), 127.8 (*p*-$\underline{C}_6H_3{}^i\text{Pr}_2$), 124.2

(*m*-C$_6$H$_3$^{i}Pr$_2$), 117.5 (NCH), 112.8 (C$_5$H$_5$), 28.9 (CHMeMe), 25.5 (CHMeMe), 23.6 (CHMeMe) ppm. ^{11}B{^{1}H} NMR (C$_6$D$_6$, 128.4 MHz): δ 24.9 ppm. IR (NaCl plates, Nujol mull, cm^{-1}): 3290 (w, N–H), 1581 (w), 1397 (m), 1382 (m), 1296 (w), 1270 (m), 1147 (w), 1115 (w), 1096 (w), 1042 (m), 1024 (m), 1002 (m), 970 (w), 890 (m), 817 (s), 805 (s), 776 (m), 751 (s), 656 (m). EI-MS: *m/z* = 747 [*M*]$^+$ (4%). Anal. found (calcd. for C$_{36}$H$_{47}$BClN$_3$Hf): C, 58.02 (57.92); H, 6.28 (6.35); N, 5.46(5.63)%.

Cp$_2$Zr{NHB(NAr'CH)$_2$}(Ph) (18). Cp$_2$Zr(Me)Cl (0.133 g, 0.489 mmol), LiNHB(NAr'CH)$_2$ (0.200 g, 0.489 mmol) and benzene (10 mL) were added to a Rotaflo ampoule with a Teflon valve, which was then heated to 90 °C for 7 days. Upon cooling to RT, the yellow solution was filtered into a Schlenk flask and the benzene removed under reduced pressure. The resulting yellow solid was then recrystallised in hexane at –30 °C. Yield: 0.140 g (40%). Diffraction-quality crystals were grown from a saturated hexane solution at 4 °C.

^{1}H NMR (C$_6$D$_6$, 400.1 MHz): δ 7.24 (6 H, overlapping 2 × m, *m*- and *p*-C$_6$H$_3$^{i}Pr$_2$), 7.12 (5 H, overlapping 3 × m, Ph), 6.11 (2 H, s, NCH), 5.52 (10 H, s, C$_5$H$_5$), 5.45 (1 H, s, NH), 3.47 (4 H, sept., ^3J = 6.9 Hz, CHMeMe), 1.33 (12 H, d, ^3J = 6.9 Hz, CHMeMe), 1.22 (12 H, d, ^3J = 6.9 Hz, CHMeMe) ppm. ^{13}C{^{1}H} NMR (C$_6$D$_6$, 100.6 MHz): δ 178.9 (*i*-C$_6$H$_5$), 146.9 (*o*-C$_6$H$_3$^{i}Pr$_2$), 140.2 (*i*-C$_6$H$_3$^{i}Pr$_2$), 140.0 (*m*-C$_6$H$_5$), 127.7 (*m*-C$_6$H$_3$^{i}Pr$_2$), 126.9 (*o*-C$_6$H$_5$), 124.2 (*p*-C$_6$H$_3$^{i}Pr$_2$), 124.1 (*p*-C$_6$H$_5$), 117.7 (NCH), 111.1 (C$_5$H$_5$), 28.8 (CHMeMe), 25.7 (CHMeMe), 23.4 (CHMeMe) ppm. ^{11}B{^{1}H} NMR (C$_6$D$_6$, 128.4 MHz): δ 24.8 ppm. IR (NaCl plates, Nujol mull, cm^{-1}): 3291 (w, N–H), 1584 (m), 1565 (m), 1527 (m), 1391 (s), 1372 (m), 1340 (s), 1121 (m), 1099 (m), 1052 (m), 1099 (m), 872 (w), 793 (s), 755 (m), 672 (m), 622 (m). EI-MS: *m/z* = 699 [*M*]$^+$ (<1%). Satisfactory elemental analysis could not be obtained.

Cp$_2$Zr{NHB(NAr'CH)$_2$}(H) (19). To a mixture of Cp$_2$Zr(H)Cl (0.253 g, 0.978 mmol) and LiNHB(NAr'CH)$_2$ (0.400 g, 0.978 mol) in a Schlenk tube, was added benzene (10 mL) and the resulting solution was left stirring at RT for 16 h. The volatiles were removed under reduced pressure and the resulting solid extracted into hexanes (3 × 10 mL) and cooled to 4 °C, upon which crystals grew, yielding **19** as pale yellow crystals. Yield: 0.230 g (38%). Diffraction-quality crystals were grown from a saturated hexane solution at 4 °C.

^{1}H NMR (C_6D_6, 400.1 MHz): δ 7.23 (6 H, overlapping 2 × m, *m*- and *p*-$C_6\underline{H}_3{}^{i}Pr_2$), 6.08 (2 H, s, NCH), 5.47 (10 H, s, C_5H_5), 5.22 (1 H, s, NH), 4.71 (1 H, s, ZrH), 3.37 (4 H, sept., ^{3}J = 6.9 Hz, C<u>H</u>MeMe), 1.40 (12 H, d, ^{3}J = 6.9 Hz, CH<u>Me</u>Me), 1.22 (12 H, d, ^{3}J = 6.9 Hz, CHMe<u>Me</u>) ppm. ^{13}C{^{1}H} NMR (C_6D_6, 100.6 MHz): δ 147.0 (*o*-$\underline{C}_6H_3{}^{i}Pr_2$), 139.8 (*i*-$\underline{C}_6H_3{}^{i}Pr_2$), 127.6 (*p*-$\underline{C}_6H_3{}^{i}Pr_2$), 124.2 (*m*-$\underline{C}_6H_3{}^{i}Pr_2$), 117.1 (NCH), 106.6 ($C_5H_5$), 28.6 (<u>C</u>HMeMe), 25.3 (CHMe<u>Me</u>), 23.7 (CH<u>Me</u>Me) ppm. ^{11}B{^{1}H} NMR (C_6D_6, 128.4 MHz): δ 24.5 ppm. IR (NaCl plates, Nujol mull, cm^{-1}): 3289 (w, N–H), 1870 (w), 1798 (w), 1708 (m), 1582 (m, Zr–H), 1560 (s), 1353 (s), 1209 (m), 1249 (s), 1200 (m), 1119 (m), 1061 (s), 975 (m), 921 (w), 903 (m), 809 (s), 764 (m), 701 (w), 647 (m). EI-MS: *m/z* = 621 $[M - H_2]^+$ (10%). Anal. found (calcd. for $C_{36}H_{48}BN_3Zr$): C, 69.06 (69.20); H, 7.86 (7.74); N, 6.60 (6.73)%.

Alternative NMR tube scale synthesis of $Cp_2Zr\{NHB(NAr'CH)_2\}(H)$ (19). To a freeze-pump-thawed solution of $Cp_2Zr\{NB(NAr'CH)_2\}(py)$ (**11**, 10.0 mg, 14.2 μmol) in C_6D_6 (0.6 mL) in an NMR tube equipped with a J. Young Teflon valve was heated up to 60 °C under H_2 (1.2 atm) for 16 h. The reaction was monitored by ^{1}H NMR spectroscopy. ^{1}H NMR spectroscopy indicated that a reaction had occurred cleanly to give the known product $Cp_2Zr\{NHB(NAr'CH)_2\}H$ (**19**).

Alternative NMR tube scale synthesis of $Cp_2Zr\{NB(NAr'CH)_2\}(py)$ (11). To a solution of $Cp_2Zr\{NHB(NAr'CH)_2\}(H)$ **(19**, 10.0 mg, 16.0 μmol) in C_6D_6 (0.6 mL) in an NMR tube equipped with a J. Young Teflon valve was added pyridine (1.50 μL, 18.6 μmol). The reaction was heated up to 120 °C for 16 h and monitored by ^{1}H NMR spectroscopy. ^{1}H NMR spectroscopy showed that the reaction reached an equilibrium mixture containing 71% **11** and 29% **19**.

NMR tube scale synthesis of $Cp_2Zr(NH^tBu)(H)$ (20). Exposure of a freeze-pump-thawed solution of $Cp_2Zr(N^tBu)(THF)$ (**1.4**, 10.0 mg, 27.4 μmol) in C_6D_6 (0.6 mL) in an NMR tube equipped with a J. Young Teflon valve to H_2 (1.2 atm) at RT. The product **20** was quantitively formed immediately and subsquently characterised by ^{1}H and ^{13}C spectroscopy at RT.

^{1}H NMR (C_6D_6, 400.1 MHz): δ 5.77 (10 H, s, C_5H_5), 5.72 (1 H, s, NH), 4.29 (1 H, s, ZrH), 1.08 (9 H, s, CMe_3) ppm. ^{13}C{^{1}H} NMR (C_6D_6, 100.6 MHz): δ 105.3 (C_5H_5), 57.1 ($\underline{C}Me_3$), 35.3 ($C\underline{Me}_3$) ppm.

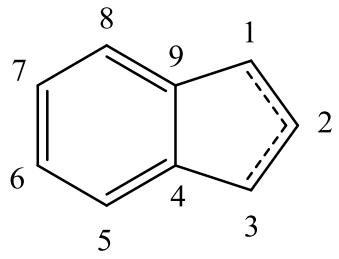

$Ind_2Zr\{NHB(NAr'CH)_2\}(Me)$ (21). To a mixture of $Ind_2Zr(Me)Cl$ (0.227 g, 0.614 mmol) and $LiNHB(NAr'CH)_2$ (0.250 g, 0.614 mmol) in a Schlenk tube, was added benzene (10 mL) and the resulting solution was left stirring at RT for 16 h. The volatiles were removed under reduced pressure and the resulting solid extracted into hexane (3 × 10 mL) and then the hexane removed under reduced pressure. The resulting yellow solid was then recrystallised in hexane at –30 °C. Yield: 0.300 g (66%). Diffraction-quality crystals were grown from a saturated hexane solution at 4 °C.

^{1}H NMR (C_6D_6, 400.1 MHz): δ 7.27 (6 H, overlapping 2 × m, *m*- and *p*-$C_6\underline{H}_3{}^i Pr_2$), 7.18 (2 H, d, ^3J = 8.4 Hz, 6- or 7-Ind), 6.95 (2 H, d, ^3J = 8.4 Hz, 6- or 7-Ind), 6.75 (2 H, t, ^3J = 8.0 Hz, 5- or 8-Ind), 6.55 (2 H, t, ^3J = 8.0 Hz, 5- or 8-Ind), 6.09 (2 H, s, NCH), 5.81 (2 H, m, 1- or 3-Ind), 5.46 (2 H, m, 1- or 3-Ind), 5.42 (2 H, t, ^3J = 3.2 Hz,, 2-Ind), 3.50 (1 H, s, NH), 3.30 (4 H, sept., ^3J = 6.9 Hz, C<u>H</u>MeMe), 1.36 (12 H, d, ^3J = 6.9 Hz, CH<u>Me</u>Me), 1.17 (12 H, d, ^3J = 6.9 Hz, CHMe<u>Me</u>), –0.29 (3 H, s, ZrMe) ppm. $^{13}C\{^1H\}$ NMR (C_6D_6, 100.6 MHz): δ 147.4 (*o*-$\underline{C}_6H_3{}^i Pr_2$), 140.8 (*i*-$\underline{C}_6H_3{}^i Pr_2$), 127.9 (*p*-$\underline{C}_6H_3{}^i Pr_2$), 125.2 (*m*-$\underline{C}_6H_3{}^i Pr_2$), 124.8 – 124.4 (4 – 9-Ind), 118.4 (NCH), 118.3 (2-Ind), 100.8 (1- or 3-Ind), 100.2 (1- or 3-Ind), 29.3 (<u>C</u>HMeMe), 27.2 (ZrMe), 26.5 (CHMe<u>Me</u>), 23.9 (CH<u>Me</u>Me) ppm. $^{11}B\{^1H\}$ NMR (C_6D_6, 128.4 MHz): δ 24.7 ppm. IR (NaCl plates, Nujol mull, cm^{-1}): 3249 (m, N–H), 2360 (w), 2328 (w), 1582 (w), 1555 (w), 1375 (s), 1276 (w), 1253 (w), 1191 (w), 1142 (w), 1110 (w), 1061 (m), 971 (w), 930 (w), 890 (w), 827 (s), 800 (s), 773 (s), 746 (s), 652 (s). Anal. found (calcd. for $C_{45}H_{54}BN_3Zr$): C, 72.94 (73.14); H, 7.53 (7.37); N, 5.52 (5.69)%.

$Ind_2Zr\{NB(NAr'CH)_2\}(THF)$ (22). $Ind_2Zr(Me)Cl$ (0.227 g, 0.614 mmol), $LiNHB(NAr'CH)_2$ (0.250 g, 0.614 mmol), THF (0.990 mL, 12.3 mmol) and toluene (15 mL) were added to a Rotaflo ampoule with a Teflon valve, which was partially evacuated and sealed before being heated to 120 °C for 3 h. Upon cooling to RT, the yellow solution was filtered into a Schlenk flask and volatiles removed under reduced pressure. The resulting yellow solid was then recrystalised in hexane at –30 °C. Yield: 0.320 g (65%).

^{1}H NMR (C_6D_6, 400.1 MHz): δ 7.25 (6 H, overlapping 2 × m, *m*- and *p*-$C_6\underline{H}_3{}^{i}Pr_2$), 7.07 (2 H, d, ^{3}J = 8.0 Hz, 6- or 7-Ind), 6.99 (2 H, t, ^{3}J = 8.0 Hz, 6- or 7-Ind), 6.98 (2 H, m, 2-Ind), 6.71 (4 H, overlapping 2 × m, 5,8-Ind), 6.05 (2 H, s, NCH), 6.00 (2 H, m, 1- or 3-Ind), 5.54 (2 H, m, 1- or 3-Ind), 3.78 (4 H, sept., ^{3}J = 6.9 Hz, C<u>H</u>MeMe), 2.56 (4 H, m, OCH_2), 1.58 (12 H, d, ^{3}J = 6.9 Hz, CH<u>Me</u>Me), 1.34 (12 H, d, ^{3}J = 6.9 Hz, CHMe<u>Me</u>), 0.94 (4 H, m, $OCH_2C\underline{H}_2$) ppm. $^{13}C\{^{1}H\}$ NMR (C_6D_6, 100.6 MHz): δ 147.3 (*o*-$\underline{C}_6H_3{}^{i}Pr_2$), 142.5(*i*-$\underline{C}_6H_3{}^{i}Pr_2$), 130.2 (4- or 9-Ind), 127.9 (4- or 9-Ind), 126.7 (*p*-$\underline{C}_6H_3{}^{i}Pr_2$), 123.3 (*m*-$\underline{C}_6H_3{}^{i}Pr_2$), 122.4 – 121.4 (2, 5, 6, 7, 8-Ind), 117.0 (NCH), 97.1 (1- or 3-Ind), 94.0 (1- or 3-Ind), 76.6 (OCH_2), 28.9 (<u>C</u>HMeMe), 26.3 ($OCH_2\underline{C}H_2$), 25.8 (CHMe<u>Me</u>), 23.7 (CH<u>Me</u>Me) ppm. $^{11}B\{^{1}H\}$ NMR (C_6D_6, 128.4 MHz): δ 18.0 ppm. IR (NaCl plates, Nujol mull, cm^{-1}): 2369 (m), 2337 (w), 1582 (w), 1411 (s), 1375 (s), 1276 (w), 1249 (w), 1142 (w), 1115 (w), 1061 (m), 1006 (w), 930 (w), 894 (m), 862 (m), 800 (s), 787 (s), 737 (m), 643 (s). Satisfactory elemental analysis could not be obtained.

$Ind_2Zr\{NB(NAr'CH)_2\}(py)$ (23). $Ind_2Zr(Me)Cl$ (0.227 g, 0.614 mmol), $LiNHB(NAr'CH)_2$ (0.250 g, 0.614 mmol), pyridine (74.0 µL, 0.921 mmol) and toluene (15 mL) were added to a Rotaflo ampoule with a Teflon valve, which was heated to 120 °C for 30 mins and sealed before being heated for another 3 h. Upon cooling to RT, the red solution was filtered into a Schlenk flask and the volatiles removed under reduced pressure. The resulting solid was then washed with hexane (3 × 10 mL) and dried *in vacuo*, yielding a pale orange powder. Yield: 0.360 g (74%). Diffraction-quality crystals were grown from a saturated toluene solution at 4 °C.

^{1}H NMR (C_6D_6, 400.1 MHz): δ 7.32 (6 H, s, *m*- and *p*-$C_6\underline{H}_3{}^{i}Pr_2$), 6.97 (4 H, overlapping 2 × m, 6,7-Ind), 6.96 (2 H, m, 2,6-py), 6.71 (2 H, m, 2-Ind), 6.70 (1 H, t, ^{3}J = 7.7 Hz, 4-py), 6.60 (4 H, overlapping 2 × m, 5,8-Ind), 6.26 (2 H, m, 3,5-py), 6.06 (2 H, s, NCH), 5.86 (2 H, m, 1- or 3-Ind), 5.80 (2 H, m, 1- or 3-Ind), 3.85 (4 H, sept., ^{3}J = 6.9 Hz, C<u>H</u>MeMe), 1.55 (12 H, d, ^{3}J = 6.9 Hz, CH<u>Me</u>Me), 1.37 (12 H, d, ^{3}J = 6.9 Hz, CHMe<u>Me</u>) ppm. $^{13}C\{^{1}H\}$ NMR (C_6D_6, 100.6 MHz): δ 153.4 (2,6-py), 148.0 (*o*-$\underline{C}_6H_3{}^{i}Pr_2$), 143.1 (*i*-$\underline{C}_6H_3{}^{i}Pr_2$), 138.2 (4-py), 128.7 (4- or 9-Ind), 128.5 (4- or 9-Ind), 127.3 (*m*-$\underline{C}_6H_3{}^{i}Pr_2$), 124.1 (*p*-$\underline{C}_6H_3{}^{i}Pr_2$), 124.0 (3,5-py), 124.0 – 121.1 (2, 5, 6, 7, 8-Ind), 117.7 (NCH), 98.9 (1- or 3-Ind), 95.0 (1- or 3-Ind), 29.5 (<u>C</u>HMeMe), 26.2 (CHMe<u>Me</u>), 24.4 (CH<u>Me</u>Me) ppm. $^{11}B\{^{1}H\}$ NMR (C_6D_6, 128.4 MHz): δ 17.7 ppm. IR (NaCl plates, Nujol mull, cm^{-1}): 2360 (w), 2333 (w), 1604 (s), 1411 (s), 1366 (s), 1263 (w), 1209 (w), 1151 (w), 1119 (w), 1056 (w), 1038 (w), 993 (w), 944 (m), 880 (m), 849 (m), 800 (m), 768 (m), 737 (m), 696

(m), 651 (s). Anal. found (calcd. for $C_{49}H_{55}BN_4Zr$): C, 73.33 (73.38); H, 6.87 (6.91); N, 6.77 (6.99)%.

$Ind_2Zr\{NB(NAr'CH)_2\}(DMAP)$ (24). $Ind_2Zr(Me)Cl$ (0.227 g, 0.614 mmol), $LiNHB(NAr'CH)_2$ (0.250 g, 0.614 mmol), DMAP (0.0750 g, 0.811 mmol) and toluene (15 mL) were added to a Rotaflo ampoule with a Teflon valve, which was heated to 120 °C for 30 mins and sealed before being heated for another 3 h. Upon cooling to RT, the pale green solution was filtered into a Schlenk flask and the toluene removed under reduced pressure. The resulting solid was then washed with hexane (3 × 15 mL) and dried *in vacuo*, yielding a pale green powder. Yield: 0.390 g (76%). Diffraction-quality crystals were grown from a saturated benzene solution at RT.

^{1}H NMR (C_6D_6, 400.1 MHz): δ 7.36 (6 H, overlapping 2 × m, *m*- and *p*-$C_6\underline{H}_3{}^i Pr_2$), 6.97 (4 H, overlapping 2 × m, 6,7-Ind), 7.11 (2 H, d, ^3J = 8.0 Hz, 6- or 7-Ind), 7.02 (2 H, t, ^3J = 3.2 Hz, 2-Ind), 6.99 (2 H, t, ^3J = 8.0 Hz, 6- or 7-Ind), 6.76 (2 H, d, ^3J = 7.4 Hz, 2,6-$C_5\underline{H}_4NMe_2$), 6.73 (4 H, overlapping 2 × m, 5,8-Ind), 6.09 (2 H, s, NCH), 5.96 (2 H, m, 1- or 3-Ind), 5.86 (2 H, m, 1- or 3-Ind), 5.56 (2 H, d, ^3J = 7.4 Hz, 3,5-$C_5\underline{H}_4NMe_2$), 3.93 (4 H, sept., ^3J = 6.9 Hz, C<u>H</u>MeMe), 2.07 (6 H, s, $C_5H_4N\underline{Me}_2$), 1.62 (12 H, d, ^3J = 6.9 Hz, CH<u>Me</u>Me), 1.40 (12 H, d, ^3J = 6.9 Hz, CHMe<u>Me</u>) ppm. $^{13}C\{^1H\}$ NMR (C_6D_6, 100.6 MHz): δ 154.1 (4-$\underline{C}_5H_4NMe_2$), 152.4 (2,6-$\underline{C}_5H_4NMe_2$), 147.7 (*o*-$\underline{C}_6H_3{}^i Pr_2$), 142.9 (*i*-$\underline{C}_6H_3{}^i Pr_2$), 128.6 (4- or 9-Ind), 127.9 (4- or 9-Ind), 126.5 (*m*-$\underline{C}_6H_3{}^i Pr_2$), 123.6 (*p*-$\underline{C}_6H_3{}^i Pr_2$), 122.9 – 120.3 (2, 5, 6, 7, 8-Ind), 117.2 (NCH), 105.5 (3,5-$\underline{C}_5H_4NMe_2$), 98.2 (1- or 3-Ind), 94.2 (1- or 3-Ind), 38.0 ($C_5H_4N\underline{Me}_2$), 28.9 (<u>C</u>HMeMe), 25.7 (CHMe<u>Me</u>), 23.9 (CH<u>Me</u>Me) ppm. $^{11}B\{^1H\}$ NMR (C_6D_6, 128.4 MHz): δ 18.3 ppm. IR (NaCl plates, Nujol mull, cm^{-1}): 2364 (w), 2332 (w), 1613 (s), 1528 (s), 1416 (m), 1267 (m), 1225 (m), 1106 (m), 1056 (m), 1007 (s), 930 (w), 876 (w), 836 (m), 813 (m), 791 (m), 773 (s), 723 (m), 643 (s). Anal. found (calcd. for $C_{51}H_{60}BN_5Zr$): C, 72.41 (72.48); H, 7.23 (7.16); N, 8.20 (8.29)%.

5.6 Experimental details and characterising data for Chapter Three

$Cp_2Zr\{N\{B(NAr'CH)_2\}C(H)C(^tBu)\}$ (25). To a solution of $Cp_2Zr\{NB(NAr'CH)_2\}(py)$ (**11**, 0.260 g, 0.370 mmol) in toluene (10 mL) was added ^{t}BuCCH (55 µL, 0.447 mmol) at RT. The reaction mixture was heated to 60 °C and stirred for 16 h, after which the volatiles were removed under reduced pressure to yield **25** as a deep red solid, which was

then dried *in vacuo*. Yield : 0.195 g (75%). Diffraction-quality crystals were grown from a saturated hexane solution at RT.

^{1}H NMR (C_6D_6, 500.3 MHz): δ 7.23 (6 H, overlapping 2 × m, *m*- and *p*-$C_6\underline{H}_3{}^{i}Pr_2$), 6.66 (1 H, s, ZrC=CH), 6.02 (2 H, s, NCH), 5.66 (10 H, s, C_5H_5), 3.47 (4 H, sept., ^{3}J = 6.9 Hz, C<u>H</u>MeMe), 1.37 (12 H, d, ^{3}J = 6.9 Hz, CH<u>Me</u>Me), 1.26 (12 H, d, ^{3}J = 6.9 Hz, CHMe<u>Me</u>), 0.99 (9 H, s, C<u>Me</u>$_3$) ppm. ^{13}C{^{1}H} NMR (C_6D_6, 125.7 MHz): δ 188.6 (Zr<u>C</u>=CH), 147.2 (-*o*-<u>C</u>$_6$H$_3{}^{i}$Pr$_2$), 141.3 (*i*-<u>C</u>$_6$H$_3{}^{i}$Pr$_2$), 127.5 (*p*-<u>C</u>$_6$H$_3{}^{i}$Pr$_2$), 123.8 (*m*-<u>C</u>$_6$H$_3{}^{i}$Pr$_2$), 118.8 (NCH), 110.2 (C_5H_5), 104.2 (ZrC=<u>C</u>H), 38.5 (<u>C</u>Me$_3$), 33.2 (C<u>Me</u>$_3$), 28.8 (<u>C</u>HMeMe), 25.7 (CHMe<u>Me</u>), 23.4 (CH<u>Me</u>Me) ppm. ^{11}B{^{1}H} NMR (C_6D_6, 128.4 MHz): δ 22.7 ppm. IR (NaCl plates, Nujol mull, cm^{-1}): 2281 (w), 1928 (w), 1861 (w), 1793 (w), 1667 (w), 1582 (m), 1258 (s), 1191 (w), 1110 (m), 1083 (m), 1056 (m), 1011 (s), 930 (m), 894 (m), 796 (s), 750 (s), 723 (m), 638 (s). Anal. found (calcd. for $C_{42}H_{56}BN_3Zr$): C, 71.40 (71.56); H, 8.18 (8.01); N, 6.04 (5.96)%.

Cp$_2$Zr{NB(NAr'CH)$_2$C(D)C(^{t}Bu)} (**25-*d*$_1$**) was prepared analogously to **25**, using Cp$_2$Zr{NB(NAr'CH)$_2$}(py) (**11**, 0.260 g, 0.370 mmol) and ^{t}BuCCD (55 µL, 0.447 mmol). Yield: 0.205 g (79%). The ^{1}H NMR spectrum was identical to that of **25**, other than the absence of the NH resonance.

Cp$_2$Zr{NHB(NAr'CH)$_2$}(CC^{t}Bu) (**26**). To a solution of Cp$_2$Zr{NB(NAr'CH)$_2$}(py) (**11**, 0.260 g, 0.370 mmol) in toluene (10 mL) was added ^{t}BuCCH (55 µL, 0.447 mmol) at RT. The reaction mixture was heated to 100 °C and stirred for 21 h, resulting in a yellow solution. The volatiles were then removed under reduced pressure, and the crude product dissolved in hexane (15 mL) and cooled to 4 °C, resulting in yellow, diffraction-quality crystals of **26**. Yield : 0.123 g (47%).

^{1}H NMR (C_6D_6, 500.3 MHz): δ 7.23 (6 H, s, *m*- and *p*-$C_6\underline{H}_3{}^{i}Pr_2$), 6.11 (2 H, s, NCH), 5.60 (10 H, s, C_5H_5), 5.57 (1 H, s, NH), 3.41 (4 H, sept., ^{3}J = 6.9 Hz, C<u>H</u>MeMe), 1.44 (12 H, d, ^{3}J = 6.9 Hz, CH<u>Me</u>Me), 1.32 (9 H, s, C<u>Me</u>$_3$), 1.23 (12 H, d, ^{3}J = 6.9 Hz, CHMe<u>Me</u>) ppm. ^{13}C{^{1}H} NMR (C_6D_6, 125.7 MHz): δ 147.1 (*o*-<u>C</u>$_6$H$_3{}^{i}$Pr$_2$), 139.9 (*i*-<u>C</u>$_6$H$_3{}^{i}$Pr$_2$), 131.7 (Zr<u>C</u>C^{t}Bu), 127.6 (*p*-<u>C</u>$_6$H$_3{}^{i}$Pr$_2$), 124.1 (*m*-<u>C</u>$_6$H$_3{}^{i}$Pr$_2$), 119.3 (ZrC<u>C</u>^{t}Bu), 117.2 (NCH), 110.3 (C_5H_5), 31.1 (C<u>Me</u>$_3$), 28.9 (<u>C</u>Me$_3$), 28.8 (<u>C</u>HMeMe), 25.6 (CHMe<u>Me</u>), 23.9 (CH<u>Me</u>Me) ppm. ^{11}B{^{1}H} NMR (C_6D_6, 128.4 MHz): δ 24.5 ppm. IR (NaCl plates, Nujol mull, cm^{-1}): 3245 (w, N–H), 2081 (s, ν(C≡C)), 1703 (w), 1565 (w), 1236 (m), 1195 (m), 1142 (m), 1065 (m), 1007 (s), 962 (m), 938 (m), 881 (s), 800 (s), 755 (s), 719 (m), 643

(s). EI-MS: *m/z* = 702 $[M]^+$ (< 1%). Anal. found (calcd. for $C_{42}H_{56}BN_3Zr$): C, 71.55 (71.56); H, 8.18 (8.20); N, 6.04 (6.16)%.

Kinetic isotope effect measurements for the conversion of $Cp_2Zr\{N\{B(NAr'CH)_2\}C(H)C(^tBu)\}$ (25) to $Cp_2Zr\{NHB(NAr'CH)_2\}(CC^tBu)$ (26). A toluene-d_8 (0.6 mL) of $Cp_2Zr\{N\{B(NAr'CH)_2\}C(H)C(^tBu)\}$ (**25**, 0.0100 g, 0.0142 mmol) was transferred to an NMR tube equipped with a J. Youngs Valve. A blank toluene-d_8 was added to the NMR probe, locked and shimmed, and the probe heated to 383 K. After thermal equilibration, the experimental sample replaced the blank sample and an array was set up to record a ^{1}H NMR spectrum (4 scans) every 150 s (or every 260 s for **25-*d*$_1$**). The decay of 25 was calculated by measuring the integral of C_5H_5. First order rate constants were obtained from linear plots of $-\ln([\mathbf{25}]/[\mathbf{25}]_0)$ *vs* time.

Kinetic measurements for the conversion of $Cp_2Zr\{N\{B(NAr'CH)_2\}C(H)C(^tBu)\}$ (25) to $Cp_2Zr\{NHB(NAr'CH)_2\}(CC^tBu)$ (26). The general procedure is as follows. In a dry-box, a toluene-d_8 solution (0.6 mL) of $Cp_2Zr\{NB(NAr'CH)_2C(H)C(^tBu)\}$ (**25**, 0.0100 g, 0.0142 mmol) was transferred to an NMR tube fitted with a J. Youngs valve. A blank toluene-d_8 sample was added to the NMR probe at RT, locked and shimmed, and the probe heated to the relevant temperature (371, 374, 377, 380, 383 K). After thermal equilibration, the experimental sample replaced the blank sample and an array was set up to record a ^{1}H NMR spectrum (4 scans) every 150 s – 250 s. The formation of **26** was calculated by measuring the integral of C_5H_5. First order rate constants were obtained from linear plots of $-\ln([\mathbf{25}]/[\mathbf{25}]_0)$ *vs* time.

NMR tube scale reaction of $Cp_2Zr\{N\{B(NAr'CH)_2\}C(D)C(^tBu)\}$ (25-*d*$_1$) with ^{t}BuCCH. To a toluene-d_8 solution of $Cp_2Zr\{N\{B(NAr'CH)_2\}C(D)C(^tBu)\}$ (**25-*d*$_1$,** 0.0100 g, 0.0142 mmol) in an NMR tube equipped with a J. Youngs valve was added ^{t}BuCCH (1.75 µL, 0.0142 mmol). A blank toluene-d_8 was added to the NMR probe, locked and shimmed, and the probe heated to 383 K. After thermal equilibration, the experimental sample replaced the blank sample and an array was set up to record a ^{1}H NMR spectrum (4 scans) every 310 s. The decay of **25-*d*$_1$** and the formation of **25** was calculated by measuring the integral of C_5H_5 and ZrC=CH respectively.

NMR tube scale reaction of $Cp_2Zr\{N\{B(NAr'CH)_2\}C(H)C(^tBu)\}$ (25) with TolCCH. To a toluene-d_8 solution of $Cp_2Zr\{N\{B(NAr'CH)_2\}C(H)C(^tBu)\}$ (**25,** 0.0100 g, 0.0142 mmol) in an NMR tube equipped with a J. Youngs valve was added TolCCH (1.8 µL,

0.0142 mmol). After heating at 383 K for 6 h, a mixture containing $Cp_2Zr\{NB(NAr'CH)_2\}C(H)C(Tol)\}$ (**27**) (12%) and $Cp_2Zr\{NHB(NAr'CH)_2\}(CC^tBu)$ (**26**) (88%) was indicated by ^1H NMR spectroscopy.

NMR tube scale synthesis of $Cp_2Zr\{N\{B(NAr'CH)_2\}C(H)C(Tol)\}$ (27). To a solution of $Cp_2Zr\{NB(NAr'CH)_2\}(py)$ (**11**, 0.0165g, 0.0236 mmol) in C_6D_6 (0.6 mL) in an NMR tube equipped with a J. Young Teflon valve was added TolCCH (3.1 µL, 0.0236 mmol) *via* microsyringe. The solution was heated at 60 °C for 16 hours. ^1H NMR spectroscopy indicated that $Cp_2Zr\{N\{B(NAr'CH)_2\}C(H)C(Tol)\}$ (**27**) had formed quantitatively and was subsequently characterised by ^1H, ^{13}C and ^{11}B NMR spectroscopy.

^1H NMR (C_6D_6, 400.1 MHz): δ 7.33 (1 H, s, ZrC=CH), 7.32 – 7.23 (6 H, overlapping 2 × m, *m*- and *p*-$C_6\underline{H}_3{}^i Pr_2$), 7.10 (2 H, d, ^3J = 8.0 Hz, *m*-$C_6\underline{H}_4Me$), 6.80 (2 H, d, ^3J = 8.0 Hz, *o*-$C_6\underline{H}_4Me$), 6.04 (2 H, s, NCH), 5.67 (10 H, s, C_5H_5), 3.46 (4 H, sept., ^3J = 6.9 Hz, C<u>H</u>MeMe), 2.24 (3 H, s, $C_6H_4\underline{Me}$), 1.34 (12 H, d, ^3J = 6.9 Hz, CH<u>Me</u>Me), 1.27 (12 H, d, ^3J = 6.9 Hz, CHMe<u>Me</u>) ppm. $^{13}C\{^1H\}$ NMR (C_6D_6, 100.6 MHz): δ 173.1 (Zr<u>C</u>=CH), 147.1 (*o*-$\underline{C}_6H_3{}^i Pr_2$), 142.3 (*p*-$\underline{C}_6H_4Me$), 141.1 (*i*-$\underline{C}_6H_3{}^i Pr_2$), 133.1 (*i*-$\underline{C}_6H_4Me$), 129.3 (*o*-$\underline{C}_6H_4Me$), 127.2 (*p*-$\underline{C}_6H_3{}^i Pr_2$), 125.2 (*m*-$\underline{C}_6H_4Me$), 123.9 (*m*-$\underline{C}_6H_3{}^i Pr_2$), 118.8 (NCH), 110.9 ($C_5H_5$), 108.2 (ZrC=<u>C</u>H), 28.9 (<u>C</u>HMeMe), 25.7 (CHMe<u>Me</u>), 23.4 ($C_6H_4\underline{Me}$) ppm. $^{11}B\{^1H\}$ NMR (C_6D_6, 128.4 MHz): δ 22.9 ppm.

$Cp_2Zr\{N\{B(NAr'CH)_2\}C(Me)C(Ph)\}$ (28). To a solution of $Cp_2Zr\{NB(NAr'CH)_2\}(py)$ (**11**, 0.260 g, 0.370 mmol) in benzene (10 mL) was added MeCCPh (51 µL, 0.407 mmol) at RT. The reaction mixture was heated to 60 °C and stirred for 20 h, after which the volatiles were removed under reduced pressure, and the crude producct dissolved in hexane (20 mL) and cooled to 4 °C, resulting in deep violet, diffraction-quality crystals of **28**. Yield: 0.120 g (44%).

^1H NMR (C_6D_6, 400.1 MHz): δ 7.24 (2 H, m, *m*-$C_6\underline{H}_5$), 7.18 (6 H, overlapping 2 × m, *m*- and *p*-$C_6\underline{H}_3{}^i Pr_2$), 6.97 (3 H, overlapping 2 × m, *o*- and *p*-$C_6\underline{H}_5$), 6.10 (2 H, s, NCH), 5.76 (10 H, s, C_5H_5), 3.50 (4 H, sept., ^3J = 6.9 Hz, C<u>H</u>MeMe), 1.61 (3 H, s, ZrC=CMe), 1.35 (12 H, d, ^3J = 6.9 Hz, CH<u>Me</u>Me), 1.23 (12 H, d, ^3J = 6.9 Hz, CHMe<u>Me</u>) ppm. $^{13}C\{^1H\}$ NMR (C_6D_6, 100.6 MHz): δ 172.8 (Zr<u>C</u>=CMe), 147.1 (*i*-$\underline{C}_6H_5$), 146.7 (*o*-$\underline{C}_6H_3{}^i Pr_2$), 141.1 (*i*-$\underline{C}_6H_3{}^i Pr_2$), 128.2 (*m*-$\underline{C}_6H_5$), 127.7 (*p*-$\underline{C}_6H_3{}^i Pr_2$), 127.4 (*o*-$\underline{C}_6H_5$), 124.1 (*m*-$\underline{C}_6H_3{}^i Pr_2$), 123.3 (*p*-$\underline{C}_6H_5$), 119.7 (NCH), 119.0 (ZrC=<u>C</u>Me), 111.5 (C_5H_5), 28.8 (<u>C</u>HMeMe), 26.3 (CHMe<u>Me</u>), 23.4 (CH<u>Me</u>Me), 20.2 (ZrC=C<u>Me</u>) ppm. $^{11}B\{^1H\}$ NMR

(C_6D_6, 128.4 MHz): δ 23.4 ppm. IR (NaCl plates, Nujol mull, cm^{-1}): 2364 (w), 2324 (w), 1649 (m), 1582 (w), 1560 (w), 1258 (m), 1116 (w), 1106 (w), 1102 (w), 935 (w), 804 (s), 724 (w). EI-MS: *m/z* = 519 $[PhC(H)=C(Me)N(H)B(NAr'CH)_2]^+$ (45%). Anal. found (calcd. for $C_{45}H_{54}BN_3Zr$): C, 72.99 (73.14); H, 7.23 (7.37); N, 5.75 (5.69)%.

$Cp_2Zr\{N\{B(NAr'CH)_2\}C(H)C(Ar^{CF_3})\}$ (29). To a solution of $Cp_2Zr\{NB(NAr'CH)_2\}(py)$ (**11**, 0.260 g, 0.370 mmol) in benzene (10 mL) was added $Ar^{CF_3}CCH$ (72 µL, 0.407 mmol) at RT. The reaction mixture was heated to 60 °C and stirred for 16 h, after which the volatiles were removed under reduced pressure, and the crude producct dissolved in hexane (20 mL) and cooled to 4 °C, resulting in deep violet, diffraction-quality crystals of **29**. Yield: 0.188 g (59%).

^1H NMR (C_6D_6, 400.1 MHz): δ 7.54 (2 H, s, *o*-Ar^{CF_3}), 7.39 (1 H, s, ZrC=CH), 7.23 (6 H, overlapping 2 × m, *m*- and *p*-$C_6\underline{H}_3{}^iPr_2$), 7.13 (1 H, s, Ar^{CF_3}), 6.01 (2 H, s, NCH), 5.54 (10 H, s, C_5H_5), 3.34 (4 H, sept., ^3J = 6.9 Hz, C<u>H</u>MeMe), 1.28 (12 H, d, ^3J = 6.9 Hz, CH<u>Me</u>Me), 1.21 (12 H, d, ^3J = 6.9 Hz, CHMe<u>Me</u>) ppm. $^{13}C\{^1H\}$ NMR (C_6D_6, 100.6 MHz): δ 165.0 (Zr<u>C</u>=CH), 146.9 (*o*-$\underline{C}_6H_3{}^iPr_2$), 140.4 (*i*-$\underline{C}_6H_3{}^iPr_2$), 131.1 (*m*-$Ar^{CF_3}$), 127.9 (*p*-$\underline{C}_6H_3{}^iPr_2$), 126.1 (*i*-$Ar^{CF_3}$), 124.9 (*o*-$Ar^{CF_3}$), 124.0 (*m*-$\underline{C}_6H_3{}^iPr_2$), 118.9 (NCH), 115.6 (*p*-Ar^{CF_3}), 115.4 (ZrC=<u>C</u>H), 111.4 (C_5H_5), 28.9 (<u>C</u>HMeMe), 25.7 (CHMe<u>Me</u>), 23.3 (CH<u>Me</u>Me) ppm. Resonances attributable to carbons directly bound to ^{19}F atoms were not observed. $^{19}F\{H\}$ NMR (C_6D_6, 376.5 MHz): –62.4 (6 F, s, Ar^{CF_3}) ppm. $^{11}B\{^1H\}$ NMR (C_6D_6, 128.4 MHz): δ 22.7 ppm. IR (NaCl plates, Nujol mull, cm^{-1}): 1937 (w), 1865 (w), 1798 (w), 1699 (w), 1604 (s), 1492 (w), 1267 (s), 1209 (m), 1178 (m), 1124 (m), 1007 (m), 863 (w), 796 (s), 760 (m), 696 (w), 679 (m), 661(s). EI-MS: *m/z* = 858 $[M]^+$ (8%). Anal. found (calcd. for $C_{46}H_{50}BF_6N_3Zr$): C, 64.04 (64.17); H, 6.00 (5.85); N, 4.88 (4.88)%.

NMR tube scale synthesis of $Cp_2Zr\{NHB(NAr'CH)_2\}(CCAr^{CF_3})$ (30) and $Cp_2Zr\{N\{B(NAr'CH)_2\}C(H)C(Ar^{CF_3})\}$ (29). To a C_6D_6 solution of $Cp_2Zr\{NB(NAr'CH)_2\}(py)$ (11, 0.0200 g, 0.0285mmol) in an NMR tube equipped with a J. Youngs valve was added $Ar^{CF_3}CCH$ (5 µL, 0.0285 mmol). The reaction was monitored by ^1H NMR. After 7 days at RT, ^1H NMR showed $Cp_2Zr\{N\{B(NAr'CH)_2\}C(H)C(Ar^{CF_3})\}$ (**29**) and $Cp_2Zr\{NHB(NAr'CH)_2\}(CCAr^{CF_3})$ **(30)** in 60:40% ratio. Compound **30** was subsequently characterised by ^1H, ^{13}C, ^{11}B and ^{19}F spectroscopy at RT.

^{1}H NMR (C_6D_6, 500.3 MHz): δ 7.87 (2 H, s, *o*-Ar^{CF_3}), 7.60 (1 H, s, *p*-Ar^{CF_3}), 7.25 (6 H, s, *m*- and *p*-$C_6\underline{H}_3{}^{i}Pr_2$), 6.09 (2 H, s, NCH), 6.03 (1 H, s, NH), 5.59 (10 H, s, C_5H_5), 3.35 (4 H, sept., ^{3}J = 6.9 Hz, C<u>H</u>MeMe), 1.38 (12 H, d, ^{3}J = 6.9 Hz, CH<u>Me</u>Me), 1.18 (12 H, d, ^{3}J = 6.9 Hz, CHMe<u>Me</u>) ppm. ^{13}C{^{1}H} NMR (C_6D_6, 125.7 MHz): δ 150.4 (*o*-$\underline{C}_6H_3{}^{i}Pr_2$), 139.5 (*i*-$\underline{C}_6H_3{}^{i}Pr_2$), 139.4 (Zr<u>C</u>CAr^{CF_3}), 131.9 (*m*-Ar^{CF_3}), 131.1 (*o*-Ar^{CF_3}), 128.0 (*p*-$\underline{C}_6H_3{}^{i}Pr_2$), 125.1 (*i*-$Ar^{CF_3}$), 124.2 (*m*-$\underline{C}_6H_3{}^{i}Pr_2$), 122.9 (ZrC<u>C</u>Ar^{CF_3}), 119.4 (*p*-Ar^{CF_3}), 117.4 (NCH), 110.4 (C_5H_5), 28.8 (<u>C</u>HMeMe), 25.5 (CHMe<u>Me</u>), 23.5 (CH<u>Me</u>Me) ppm. Resonances attributable to carbons directly bound to ^{19}F atoms were not observed. ^{19}F{H} NMR (C_6D_6, 376.5 MHz): –62.8 (6 F, s, Ar^{CF_3}) ppm. ^{11}B{^{1}H} NMR (C_6D_6, 128.4 MHz): δ 24.6 ppm.

$Cp_2Zr\{NHB(NAr'CH)_2\}(CCAr^F)$ (31). To a solution of $Cp_2Zr\{NB(NAr'CH)_2\}$(py) (**11**, 0.260 g, 0.370 mmol) in benzene (10 mL) was added Ar^FCCH (54 μL, 0.407 mmol) at RT. The reaction mixture was left at RT and stirred for 21 h, resulting in a yellow solution. The volatiles were then removed under reduced pressure, and the crude producct dissolved in hexane (10 mL) and cooled to 4 °C, resulting in yellow, diffraction-quality crystals of **31**. Yield: 0.130 g (43%).

^{1}H NMR (C_6D_6, 400.1 MHz): δ 7.22 (6 H, overlapping 2 × m, *m*- and *p*-$C_6\underline{H}_3{}^{i}Pr_2$), 6.17 (1 H, s, NH), 6.09 (2 H, s, NCH), 5.61 (10 H, s, C_5H_5), 3.37 (4 H, sept., ^{3}J = 6.9 Hz, C<u>H</u>MeMe), 1.41 (12 H, d, ^{3}J = 6.9 Hz, CH<u>Me</u>Me), 1.20 (12 H, d, ^{3}J = 6.9 Hz, CHMe<u>Me</u>) ppm. ^{13}C{^{1}H} NMR (C_6D_6, 100.6 MHz): δ 146.6 (*o*-$\underline{C}_6H_3{}^{i}Pr_2$), 139.2 (*i*-$\underline{C}_6H_3{}^{i}Pr_2$), 128.4 (*p*-$\underline{C}_6H_3{}^{i}Pr_2$), 124.2 (*m*-$\underline{C}_6H_3{}^{i}Pr_2$), 117.4 (NCH), 110.5 ($C_5H_5$), 28.8 (<u>C</u>HMeMe), 25.4 (CHMe<u>Me</u>), 23.6 (CH<u>Me</u>Me) ppm. Those resonances belonging to the acetylide ligand could not be satisfactorily assigned. ^{19}F{H} NMR (C_6D_6, 376.5 MHz): –138.8 (2 F, m, *o*-Ar^F), –157.6 (1 F, t, ^{3}J = 21.4 Hz, *p*-Ar^F), –163.8 (2 F, m, *m*-Ar^F) ppm. ^{11}B{^{1}H} NMR (C_6D_6, 128.4 MHz): δ 24.7 ppm. IR (NaCl plates, Nujol mull, cm^{-1}): 3308 (w, N–H), 2099 (m, ν(C≡C)), 1582 (m), 1515 (w), 1271 (w), 1234 (w), 1196 (w), 1106 (m), 1061 (w), 1011 (s), 984 (s), 966 (s), 885 (m), 809 (s), 746 (m), 656 (m). EI-MS: *m/z* = 702 $[M]^+$ (10%). Anal. found (calcd. for $C_{44}H_{47}BF_5N_3Zr$): C, 64.73 (64.85); H, 5.84 (5.81); N, 5.10 (5.16)%.

$Cp_2Zr\{N\{B(NAr'CH)_2\}C(H)C(Ar^F)\}$ (32). To a solution of $Cp_2Zr\{NB(NAr'CH)_2\}$(py) (**11**, 0.260 g, 0.370 mmol) in toluene (10 mL) was added Ar^FCCH (54 μL, 0.407 mmol) at 90 °C. The reaction mixture was stirred for 1 h at this temperature, after which the

volatiles were then removed under reduced pressure, and the crude products mixture of **32** (60%) and **31** (40%) dissolved in hexane (20 mL) and cooled to 4 °C, resulting in deep violet, diffraction-quality crystals of **32**. Yield: 0.118 g (39%).

^{1}H NMR (C_6D_6, 400.1 MHz): δ 7.69 (1 H, s, ZrC=CH), 7.21 (6 H, overlapping 2 × m, *m*- and *p*-$C_6\underline{H}_3{}^{i}Pr_2$), 6.00 (2 H, s, NCH), 5.70 (10 H, s, C_5H_5), 3.40 (4 H, sept., ^{3}J = 6.9 Hz, C<u>H</u>MeMe), 1.36 (12 H, d, ^{3}J = 6.9 Hz, CH<u>Me</u>Me), 1.24 (12 H, d, ^{3}J = 6.9 Hz, CHMe<u>Me</u>) ppm. ^{13}C{^{1}H} NMR (C_6D_6, 100.6 MHz): δ 146.9 (Zr<u>C</u>=CH), 146.8 (*o*-$\underline{C}_6H_3{}^{i}Pr_2$), 140.4 (*i*-$\underline{C}_6H_3{}^{i}Pr_2$), 128.4 (*p*-$\underline{C}_6H_3{}^{i}Pr_2$), 124.0 (*m*-$\underline{C}_6H_3{}^{i}Pr_2$), 120.3 (ZrC=<u>C</u>H), 119.2 (NCH), 112.5 (C_5H_5), 28.9 (<u>C</u>HMeMe), 25.9 (CHMe<u>Me</u>), 23.3 (CH<u>Me</u>Me) ppm. Those resonances belonging to the Ar^F ring could not be satisfactorily assigned. ^{19}F{H} NMR (C_6D_6, 376.5 MHz): –144.6 (2 F, m, *o*-Ar^F), –166.1 (1 F, t, ^{3}J = 21.4 Hz, *p*-Ar^F), –166.6 (2 F, m, *m*-Ar^F) ppm. ^{11}B{^{1}H} NMR (C_6D_6, 128.4 MHz): δ 23.0 ppm. IR (NaCl plates, Nujol mull, cm^{-1}): 2364 (w), 2333 (w), 1942 (w), 1861 (w), 1798 (w), 1699 (w), 1591 (s), 1506 (s), 1303 (m), 1258 (s), 1196 (w), 1110 (m), 1074 (w), 1016 (s), 962 (s), 894 (w), 880(m), 804 (s), 755 (m), 706 (w), 643 (m). EI-MS: *m/z* = 595 $[Ar^FC(H)=C(H)N(H)B(NAr'CH)_2]^+$ (90%). Anal. found (calcd. for $C_{44}H_{47}BF_5N_3Zr$): C, 64.76 (64.85); H, 5.90 (5.81); N, 5.07 (5.16)%.

Kinetic isotope effect measurements for the reaction of $Cp_2Zr\{NB(NAr'CH)_2\}(py)$ (11) with $HCCAr^F$ to form $Cp_2Zr\{NHB(NAr'CH)_2\}(CCAr^F)$ (31). To a C_6D_6 solution (0.6 mL) of $Cp_2Zr\{NB(NAr'CH)_2\}(py)$ (**11**, 0.0260 g, 0.0370 mmol) in an NMR tube equipped with a J. Youngs valve was added Ar^FCCH or Ar^FCCD (10 µL, 0.0370 mmol) *via* microsyringe. The NMR tube was transferred to a termperature-regulated (298 K) probe and the reaction monitored by ^{1}H NMR spectroscopy using an array which recorded spectra (4 scans) every 180 s. The formation of **31** (or **31-*d*$_1$**) was calculated by measuing the integral of an NCH resonance. Initial rate constants were obtained from plots of [**31**] *vs* time using *Origin*.

Competition reaction of $Cp_2Zr\{NB(NAr'CH)_2\}(py)$ (11) with $HCCAr^F$ and $DCCAr^F$. To a vial containing $Cp_2Zr\{NB(NAr'CH)_2\}(py)$ (**11**, 0.008 g, 0.0114 mmol) was added a C_6D_6 solution (0.6 mL) of $HCCAr^F$ (7.5 µL, 0.057 mmol) and $DCCAr^F$ (7.5 µL, 0.057 mmol). The mixture was then left at RT for 1 h, with ^{1}H NMR integration showing the products to be 60% **31** and 40% **31-*d*$_1$**.

Kinetic isotope effect measurements for the reaction of $Cp_2Zr\{NB(NAr'CH)_2\}(DMAP)$ (14) with $HCCAr^F$ to form $Cp_2Zr\{NHB(NAr'CH)_2\}(CCAr^F)$ (31). To a C_6D_6 solution (0.6 mL) of $Cp_2Zr\{NB(NAr'CH)_2\}(DMAP)$ (**14**, 0.0140 g, 0.0185 mmol) in an NMR tube equipped with a J. Youngs valve was added $HCCAr^F$ or $DCCAr^F$ (5 µL, 0.0370 mmol) *via* microsyringe. The NMR tube was transferred to a termperature-regulated (298 K) probe and the reaction monitored by ^1H NMR spectroscopy using an array which recorded spectra (4 scans) every 168 s. The formation of **31** (or **31-*d*$_1$**) was calculated by measuing the integral of an NCH resonance. Initial rate constants were obtained from plots of [**31**] *vs* time using *Origin*. Same measurement was also followed for the reaction of $Cp_2Zr\{NB(NAr'CH)_2\}(DMAP)$ (**14**, 0.0140 g, 0.0185 mmol) with $HCCAr^F$ (5 µL, 0.0185 mmol) in THF-d_8.

Competition reaction of $Cp_2Zr\{NB(NAr'CH)_2\}(DMAP)$ (14) with $HCCAr^F$ and $DCCAr^F$. To a vial containing $Cp_2Zr\{NB(NAr'CH)_2\}(DMAP)$ (**14**, 0.0085 g, 0.0114 mmol) was added a C_6D_6 solution (0.6 mL) of $HCCAr^F$ (7.5 µL, 0.057 mmol) and $DCCAr^F$ (7.5 µL, 0.057 mmol). The mixture was then left at RT for 1 h, with ^1H NMR integration showing the products to be 59% **31** and 41% **31-*d*$_1$**.

Measurement of reaction order with respect to $HCCAr^F$ for the reaction of $Cp_2Zr\{NB(NAr'CH)_2\}(DMAP)$ (14) with $HCCAr^F$ to form $Cp_2Zr\{NHB(NAr'CH)_2\}(CCAr^F)$ (31). The general procedure is as follows. To a C_6D_6 solution (0.6 mL) of $Cp_2Zr\{NB(NAr'CH)_2\}(DMAP)$ (**14**, 0.0057 g, 0.0075 mmol) in an NMR tube equipped with a J. Youngs valve was added $HCCAr^F$ (1 µL, 0.0075 mmol) *via* microsyringe. The NMR tube was transferred to a termperature-regulated (298 K) probe and the reaction monitored by ^1H NMR spectroscopy. The formation of **31** was calculated by measuing the integral of an NCH resonance. Initial rate constants were obtained from plots of [**31**] *vs* time using *Origin*. Same reactions were followed with different amount of $HCCAr^F$ (0.0225, 0.0375, 0.0525, 0.075 mmol). The order of reaction with respect to $HCCAr^F$ was obtained from plots of initial rate constants *vs* $[HCCAr^F]$.

Measurement of reaction order with respect to $Cp_2Zr\{NB(NAr'CH)_2\}(DMAP)$ (14) for the reaction of $Cp_2Zr\{NB(NAr'CH)_2\}(DMAP)$ (14) with $HCCAr^F$ to form $Cp_2Zr\{NHB(NAr'CH)_2\}(CCAr^F)$ (31). The general procedure is as follows. To a C_6D_6 solution (0.6 mL) of $Cp_2Zr\{NB(NAr'CH)_2\}(DMAP)$ (**14**, 0.0057 g, 0.0075 mmol) in an

NMR tube equipped with a J. Youngs valve was added $HCCAr^F$ (5 µL, 0.0375 mmol) *via* microsyringe. The NMR tube was transferred to a termperature-regulated (298 K) probe and the reaction monitored by ^1H NMR spectroscopy. The formation of **31** was calculated by measuing the integral of an NCH resonance. Initial rate constants were obtained from plots of [**31**] *vs* time using *Origin*. Same reactions were also followed with different amount of $Cp_2Zr\{NB(NAr'CH)_2\}(DMAP)$ (**14**) (0.015, 0.0188, 0.030, 0.0375 mmol). The order of reaction with respect to (**14**) was obtained from plots of initial rate constants *vs* [**14**].

Kinetic measurements for the conversion of $Cp_2Zr\{NB(NAr'CH)_2\}(DMAP)$ (14) to $Cp_2Zr\{NHB(NAr'CH)_2\}(CCAr^F)$ (31). The general procedure is as follows. In a dry-box, to a C_6D_6 solution (0.6 mL) of $Cp_2Zr\{NB(NAr'CH)_2\}(DMAP)$ (**14**, 0.0140 g, 0.0185 mmol) in an NMR tube fitted with a J. Youngs valve was added $HCCAr^F$ (5 µL, 0.037 mmol). A blank C_6D_6 sample was added to the NMR probe at RT, locked and shimmed, and the probe heated to the relevant temperature (298, 302, 306, 310, 314 K). After thermal equilibration, the experimental sample replaced the blank sample and an array was set up to record a ^1H NMR spectrum (4 scans) every 150s. The formation of **31** was calculated by measuing the integral of an NCH resonance. Initial rate constants were obtained from plots of [**31**] *vs* time using *Origin*.

NMR tube scale reaction of $Cp_2Zr\{NB(NAr'CH)_2\}(L)$ with HCCR. The general procedure is as follows. To a C_6D_6 solution (0.6 mL) of relevant compound: $Cp_2Zr\{NB(NAr'CH)_2\}(L)$ (L = py (**11**), THF (**13**) or DMAP (**14**), 0.0114 mmol) in an NMR tube equipped with a J. Youngs valve was added HCCR (R = ^{t}Bu, Tol, Ar^{CF_3} or Ar^F, 0.0114 mmol) *via* microsyringe and the reaction monitored by ^1H NMR spectroscopy at RT. The formations of corresponding metallacycle or acetylide products were calculated by measuing the integral of C_5H_5 resonances. Similar reactions were performed with 5 equivalents of pyridine, or at 50 °C.

$Ind_2Zr\{N\{B(NAr'CH)_2\}C(H)C(Ar^F)\}$ (33). To a solution of $Ind_2Zr\{NB(NAr'CH)_2\}(THF)$ (**22**, 0.250 g, 0.314 mmol) in benzene (15 mL) was added Ar^FCCH (46 µL, 0.346 mmol) at RT. The reaction mixture was left at RT and stirred for 16 h, resulting in a deep violet solution. The volatiles were then removed under reduced pressure, and the crude producct dissolved in hexane (20 mL) and cooled to 4 °C, resulting in deep violet, diffraction-quality crystals of **33**. Yield: 0.114 g (36%).

^{1}H NMR (C_6D_6, 400.1 MHz): δ 7.83 (1 H, s, ZrC=CH), 7.34 (2 H, d, ^{3}J = 8.0 Hz, 6- or 7-Ind), 7.26 (6 H, overlapping 2 × m, *m*- and *p*-$C_6\underline{H}_3{}^{i}Pr_2$), 7.06 (2 H, d, ^{3}J = 8.0 Hz, 6- or 7-Ind), 6.68 (2 H, m, 5- or 8-Ind), 6.53 (2 H, m, 5- or 8-Ind), 6.16 (2 H, m, 1- or 3-Ind), 6.06 (2 H, s, NCH), 5.90 (2 H, m, 2-Ind), 4.73 (2 H, m, 1- or 3-Ind), 3.49 (4 H, sept., ^{3}J = 6.9 Hz, C<u>H</u>MeMe), 1.43 (12 H, d, ^{3}J = 6.9 Hz, CH<u>Me</u>Me), 1.27 (12 H, d, ^{3}J = 6.9 Hz, CHMe<u>Me</u>) ppm. ^{13}C{^{1}H} NMR (C_6D_6, 100.6 MHz): δ 146.8 (*o*-$\underline{C}_6H_3{}^{i}Pr_2$), 142.3 (Zr<u>C</u>=CH), 140.6 (*i*-$\underline{C}_6H_3{}^{i}Pr_2$), 128.2 (*p*-$\underline{C}_6H_3{}^{i}Pr_2$), 128.0 (4- or 9-Ind), 127.2 (ZrC=<u>C</u>H), 126.3 (4- or 9-Ind), 125.0 – 125.1 (5, 6, 7, 8-Ind), 124.2 (*m*-$\underline{C}_6H_3{}^{i}Pr_2$), 119.4 (NCH), 117.1 (2-Ind), 104.4 (1- or 3-Ind), 100.1 (1- or 3-Ind), 29.1 (<u>C</u>HMeMe), 26.4 (CHMe<u>Me</u>), 23.2 (CH<u>Me</u>Me) ppm. Those resonances belonging to the Ar^F ring could not be satisfactorily assigned. ^{19}F{H} NMR (C_6D_6, 376.5 MHz): –142.3 (2 F, m, *o*-Ar^F), –166.8 (3 F, overlapping 2 × m, *o*- and *p*-Ar^F) ppm. ^{11}B{^{1}H} NMR (C_6D_6, 128.4 MHz): δ 22.7 ppm. IR (NaCl plates, Nujol mull, cm^{-1}): 1951 (w), 1915 (w), 1860 (w), 1811 (w), 1685 (w), 1596 (w), 1578 (w), 1334 (m), 1263 (s), 1231 (m), 1196 (w), 1115 (m), 1088 (m), 1016 (m), 966 (s), 930 (m), 890 (s), 858 (s), 822 (s), 769 (s), 742 (s), 724 (s), 670 (s). EI-MS: *m/z* = 595 $[Ar^FC(H)=C(H)N(H)B(NAr'CH)_2]^+$ (45%). Anal. found (calcd. for $C_{52}H_{51}BF_5N_3Zr$): C, 68.30 (68.26); H, 5.70 (5.62); N, 4.56 (4.59)%.

NMR tube scale synthesis of $Ind_2Zr\{N\{B(NAr'CH)_2\}C(H)C(Ar^F)\}$ (33) and $Ind_2Zr\{NH\{B(NAr'CH)_2\}(CCAr^F)$ (34). To a C_6D_6 solution of $Ind_2Zr\{NB(NAr'CH)_2\}(py)$ (23, 0.0180 g, 0.0225mmol) in an NMR tube equipped with a J. Youngs valve was added $HCCAr^F$ (3 μL, 0.0225 mmol). The reaction was monitored by ^{1}H NMR. After 2 days at 80 °C, ^{1}H NMR showed the formation of $Ind_2Zr\{N\{B(NAr'CH)_2\}C(H)C(Ar^F)\}$ (**33**) and $Ind_2Zr\{NH\{B(NAr'CH)_2\}(CCAr^F)$ (**34**) in 62:38% ratio. Similar NMR tube scale synthesis was also followed by the reaction between $Ind_2Zr\{NB(NAr'CH)_2\}(THF)$ (22, 0.0157 g, 0.0197mmol) and $HCCAr^F$ (2.6 μL, 0.0197 mmol) at RT for 16 h, with ^{1}H NMR integration showing **33** and **34** in 72:28% ratio. Compound **34** was subsequently characterised by ^{1}H, ^{13}C, ^{11}B and ^{19}F spectroscopy at RT.

^{1}H NMR (C_6D_6, 400.1 MHz): δ 7.24 (10 H, overlapping 4 × m, 6, 7-Ind and *m*, *p*-$C_6\underline{H}_3{}^{i}Pr_2$), 6.76 (2 H, m, 5- or 8-Ind), 6.52 (2 H, m, 5- or 8-Ind), 6.36 (2 H, m, 1- or 3-Ind), 6.09 (2 H, s, NCH), 5.81 (2 H, m, 1- or 3-Ind), 5.32 (2 H, m, 2-Ind), 3.90 (1 H, s, NH), 3.20 (4 H, sept., ^{3}J = 6.9 Hz, C<u>H</u>MeMe), 1.36 (12 H, d, ^{3}J = 6.9 Hz, CH<u>Me</u>Me), 1.16 (12 H, d, ^{3}J = 6.9 Hz, CHMe<u>Me</u>) ppm. ^{13}C{^{1}H} NMR (C_6D_6, 100.6 MHz): δ 146.8 (-

o-$\underline{C}_6H_3{}^iPr_2$), 139.6 (*i*-$\underline{C}_6H_3{}^iPr_2$), 128.3 (*p*-$\underline{C}_6H_3{}^iPr_2$), 127.4 – 123.5 (4 – 9-Ind), 125.0 (*m*-$\underline{C}_6H_3{}^iPr_2$), 118.4 (1- or 3-Ind), 117.9 (NCH), 101.1 (1- or 3-Ind), 100.1 (2-Ind), 28.8 (<u>C</u>HMeMe), 26.2 (CHMe<u>Me</u>), 23.2 (CH<u>Me</u>Me) ppm. Those resonances belonging to the acetylide ligand could not be satisfactorily assigned. $^{19}F\{H\}$ NMR (C_6D_6, 376.5 MHz): –138.2 (2 F, m, *o*-Ar^F), –157.7 (1 F, t, ^3J = 21.4 Hz, *p*-Ar^F), –163.9 (2 F, m, *m*-Ar^F) ppm. $^{11}B\{^1H\}$ NMR (C_6D_6, 128.4 MHz): δ 24.8 ppm.

Improved synthesis of Cp'$_2$Zr(Me)Cl (35). To a mixture of Cp'$_2$Zr(Me)$_2$ (1.70 g, 6.08 mmol) and Ph_3CCl (1.70 g, 6.08 mmol) in a Schlenk tube, was added toluene (80 mL). Then the colourless solution was heated up to 100 °C for 22 h. Upon cooling to RT, the volatiles removed under reduced pressure and the crude product recrystallised in hexane at –30 °C to yield white needles which were washed with cold (–30 °C) hexane (5 mL) and dried *in vacuo*. Yield: 1.59 g (87%). The NMR data was in good agreement with the literature.[32]

^1H NMR (toluene-d_8, 400.1 MHz): δ 5.76, 5.62 (2 H, m, 3,4-$C_5\underline{H}_4Me$), 5.49, 5.45 (2 H, m, 2,5-$C_5\underline{H}_4Me$), 2.07 (6 H, s, $C_5H_4\underline{Me}$), 0.32 (3 H, s, ZrMe) ppm.

Cp'$_2$Zr{NHB(NAr'CH)$_2$}(Me) (36). To a mixture of Cp'$_2$Zr(Me)Cl (**35**, 0.161 g, 0.540 mmol) and LiNHB(NAr'CH)$_2$ (0.220 g, 0.540 mmol) in a Schlenk tube, was added benzene (10 mL) and the resulting solution was left stirring at RT for 16 h. The volatiles removed under reduced pressure and the resulting solid extracted into hexanes (3 × 10 mL), then hexane removed again under reduced pressure. The resulting yellow solid was then recrystallised in hexane at –30 °C. Yield: 0.160 g (44%). Diffraction-quality crystals were grown from a saturated hexane solution at 4 °C.

^1H NMR (C_6D_6, 400.1 MHz): δ 7.24 (6 H, overlapping 2 × m, *m*- and *p*-$C_6\underline{H}_3{}^iPr_2$), 5.50, 5.36 (2 H, m, 3,4-$C_5\underline{H}_4Me$), 5.23, 5.10 (2 H, m, 2,5-$C_5\underline{H}_4Me$), 4.89 (2 H, s, NCH), 3.44 (4 H, sept., ^3J = 6.9 Hz, C<u>H</u>MeMe), 1.69 (6 H, s, $C_5H_4\underline{Me}$), 1.39 (12 H, d, ^3J = 6.9 Hz, CH<u>Me</u>Me), 1.20 (12 H, d, ^3J = 6.9 Hz, CHMe<u>Me</u>), –0.13 (3 H, s, ZrMe) ppm. $^{13}C\{^1H\}$ NMR (C_6D_6, 100.6 MHz): δ 147.0 (*o*-$\underline{C}_6H_3{}^iPr_2$), 140.3 (*i*-$\underline{C}_6H_3{}^iPr_2$), 127.4 (*p*-$\underline{C}_6H_3{}^iPr_2$), 124.0 (*m*-$\underline{C}_6H_3{}^iPr_2$), 121.6 (1-$\underline{C}_5H_4Me$), 117.5 (NCH), 112.3, 110.5 (2,5-$\underline{C}_5H_4Me$), 110.1, 106.9 (3,4-$\underline{C}_5H_4Me$), 28.8 (<u>C</u>HMeMe), 25.7 (CHMe<u>Me</u>), 24.0 (ZrMe), 23.5 (CH<u>Me</u>Me), 14.4 ($C_5H_4\underline{Me}$) ppm. $^{11}B\{^1H\}$ NMR (C_6D_6, 128.4 MHz): δ 25.0 ppm. IR (NaCl plates, Nujol mull, cm^{-1}): 3294 (w, N–H), 1937 (w), 1861 (w), 1789 (w), 1699 (w), 1582 (m), 1555 (w), 1271 (w), 1244 (w), 1187 (w), 1146 (w), 1100 (m), 1156 (m), 1029 (m), 966

(s), 885 (m), 862(s), 795 (m), 773 (s), 710 (m), 656 (s), 611 (w). Anal. found (calcd. for $C_{39}H_{54}BN_3Zr$): C, 70.05 (70.24); H, 8.28 (8.16); N, 6.21 (6.30)%.

Cp'$_2$Zr{NB(NAr'CH)$_2$}(DMAP) (37). Cp'$_2$Zr(Me)Cl (**35**, 0.233 g, 0.737 mmol), LiNHB(NAr'CH)$_2$ (0.300 g, 0.737 mmol), DMAP (0.0990 g, 0.811 mmol) and toluene (15 mL) were added to a Rotaflo ampoule with a Teflon valve, which was heated to 120 °C for 30 min and sealed before being heated for another 16 h. Upon cooling to RT, the green solution was filtered into a Schlenk flask and the toluene removed under reduced pressure. The resulting pale green solid was then washed with hexane (3 × 12 mL), yielding a pale green powder. Yield: 0.290 g (52%). Diffraction-quality crystals were grown from a saturated benzene solution at RT.

^{1}H NMR (C_6D_6, 400.1 MHz): δ 7.66 (2 H, d, ^3J = 7.4 Hz, 2,6-$C_5\underline{H}_4NMe_2$), 7.32 (6 H, overlapping 2 × m, *m*- and *p*-$C_6\underline{H}_3{}^i Pr_2$), 6.11 (2 H, s, NCH),), 5.91 (6 H, overlapping 3 × m, 2,3,4-$C_5\underline{H}_4Me$), 5.57 (2 H, d, ^3J = 7.4 Hz, 3,5-$C_5\underline{H}_4NMe_2$), 5.49 (2 H, m, 5-$C_5\underline{H}_4Me$), 3.98 (4 H, sept., ^3J = 6.9 Hz, C$\underline{H}$MeMe), 2.11 (6 H, s, $C_5H_4N\underline{Me}_2$), 1.83 (6 H, s, $C_5H_4\underline{Me}$), 1.58 (12 H, d, ^3J = 6.9 Hz, CH$\underline{Me}$Me), 1.40 (12 H, d, ^3J = 6.9 Hz, CHMe$\underline{Me}$) ppm. ^{13}C{^{1}H} NMR (C_6D_6, 100.6 MHz): δ 153.7 (2,6-$\underline{C}_5H_4NMe_2$), 153.2 (4-$\underline{C}_5H_4NMe_2$), 147.4 (*o*-$\underline{C}_6H_3{}^i Pr_2$), 143.5 (*i*-$\underline{C}_6H_3{}^i Pr_2$), 125.5 (*m*-$\underline{C}_6H_3{}^i Pr_2$), 123.0 (*p*-$\underline{C}_6H_3{}^i Pr_2$), 120.2 (1-$\underline{C}_5H_4Me$), 116.9 (NCH), 112.8, 109.5(2,5-$\underline{C}_5H_4Me$), 108.8, 107.3 (3,4-$\underline{C}_5H_4Me$), 105.6 (3,5-$\underline{C}_5H_4NMe_2$), 37.6 ($C_5H_4N\underline{Me}_2$), 28.4 ($\underline{C}$HMeMe), 25.4 (CHMe$\underline{Me}$), 23.5 (CH$\underline{Me}$Me), 18.3 ($C_5H_4\underline{Me}$) ppm. ^{11}B{^{1}H} NMR (C_6D_6, 128.4 MHz): δ 19.8 ppm. IR (NaCl plates, Nujol mull, cm^{-1}): 1771 (w), 1613 (s), 1533 (m), 1376 (s), 1258 (m), 1182 (m), 1123 (s), 1011 (s), 984 (w), 949 (w), 930 (w), 872 (w), 844 (w), 786 (m), 755 (m), 715 (w), 647 (s). Anal. found (calcd. for $C_{45}H_{61}BN_5Zr$): C, 69.82 (69.92); H, 7.83 (7.82); N, 9.09 (9.06)%.

NMR tube scale synthesis and kinetic measurements of Cp'$_2$Zr{NHB(NAr'CH)$_2$}(CCAr^F) (38). To a solution of Cp'$_2$Zr{NB(NAr'CH)$_2$}(DMAP) (**37**, 0.0146g, 0.0186 mmol) in C_6D_6 (0.6 mL) in an NMR tube equipped with a J. Young Teflon valve was added HCCAr^F (5 μL, 0.0370 mmol) *via* microsyringe. The NMR tube was transferred to a termperature-regulated (298 K) probe and the reaction monitored by ^{1}H NMR spectroscopy using an array which recorded spectra (4 scans) every 120 s. The formation of **38** was calculated by measuing the integral of an NCH resonance. Initial rate constants were obtained from plots of [**38**]

vs time using *Origin*. Compound **38** was subsequently characterised by ^{1}H, ^{13}C, ^{11}B and ^{19}F spectroscopy at RT.

^{1}H NMR (C_6D_6, 400.1 MHz): δ 7.22 (6 H, overlapping 2 × m, *m*- and *p*-$C_6\underline{H}_3{}^{i}Pr_2$), 6.09 (2 H, s, NCH), 5.88 (1 H, s, NH), 5.62 (2 H, m, 3-$C_5\underline{H}_4Me$), 5.43 (6 H, overlapping 3 × m, 2,4,5-$C_5\underline{H}_4Me$), 3.39 (4 H, sept., ^{3}J = 6.9 Hz, C<u>H</u>MeMe), 1.97 (6 H, s, $C_5H_4\underline{Me}$), 1.41 (12 H, d, ^{3}J = 6.9 Hz, CH<u>Me</u>Me), 1.20 (12 H, d, ^{3}J = 6.9 Hz, CHMe<u>Me</u>) ppm. ^{13}C{^{1}H} NMR (C_6D_6, 100.6 MHz): δ 147.0 (*o*-$\underline{C}_6H_3{}^{i}Pr_2$), 139.9 (*i*-$\underline{C}_6H_3{}^{i}Pr_2$), 127.7 (*p*-$\underline{C}_6H_3{}^{i}Pr_2$), 124.2 (*m*-$\underline{C}_6H_3{}^{i}Pr_2$), 123.9 (1-$\underline{C}_5H_4Me$), 117.6 (NCH), 114.2, 111.4 (2,5-$\underline{C}_5H_4Me$), 110.3, 106.9 (3,4-$\underline{C}_5H_4Me$), 28.8 (<u>C</u>HMeMe), 25.6 (CHMe<u>Me</u>), 23.5 (CH<u>Me</u>Me), 15.5 ($C_5H_4\underline{Me}$) ppm. Those resonances belonging to the acetylide ligand could not be satisfactorily assigned. ^{19}F{H} NMR (C_6D_6, 376.5 MHz): –138.6 (2 F, m, *o*-Ar^F), –157.8 (1 F, t, ^{3}J = 21.4 Hz, *p*-Ar^F), –163.9 (2 F, m, *m*-Ar^F) ppm. ^{11}B{^{1}H} NMR (C_6D_6, 128.4 MHz): δ 24.8 ppm.

$Cp_2Zr(NH^tBu)(CCAr^F)$ (39). To a solution of $Cp_2Zr(N^tBu)(py)$ (**3.5**, 0.200 g, 0.549 mmol) in benzene (10 mL) was added Ar^FCCH (80 µL, 0.604 mmol) at RT. The reaction mixture was left at RT and stirred for 1 h, resulting in a yellow solution. The volatiles were then removed under reduced pressure, and the crude product dissolved in hexane (10 mL) and cooled to 4 °C, resulting in yellow, diffraction-quality crystals of **39**. Yield: 0.173 g (65%).

^{1}H NMR (C_6D_6, 400.1 MHz): δ 6.33 (1 H, s, NH), 5.86 (10 H, s, C_5H_5), 1.17 (9 H, s, CMe_3) ppm. ^{13}C{^{1}H} NMR (C_6D_6, 100.6 MHz): δ 109.5 (C_5H_5), 58.4 ($\underline{C}Me_3$), 24.2 ($C\underline{Me}_3$) ppm. Those resonances belonging to the acetylide ligand could not be satisfactorily assigned. ^{19}F{H} NMR (C_6D_6, 376.5 MHz): –139.5 (2 F, m, *o*-Ar^F), –158.7 (1 F, t, ^{3}J = 22.2 Hz, *p*- Ar^F), –164.1 (2 F, m, *m*-Ar^F) ppm. IR (NaCl plates, Nujol mull, cm^{-1}): 3308 (w, N–H), 2638 (w), 2436 (w), 2090 (s, ν(C≡C)), 1906 (w), 1802 (w), 1699 (m), 1627 (w), 1254 (w), 1200 (s), 1128 (m), 1074 (m), 1025 (s), 966 (s), 849 (m), 804 (s), 760 (m), 602 (s). Anal. found (calcd. for $C_{22}H_{20}F_5NZr$): C, 54.45 (54.53); H, 4.19 (4.16); N, 3.00 (2.89)%.

NMR tube scale reaction of $Cp_2Zr(N^tBu)(THF)$ (1.4) with $HCCAr^F$ to form $Cp_2Zr(NH^tBu)(CCAr^F)$ (39) and $Cp_2Zr\{N(^tBu)C(H)C(Ar^F)\}$ (40). To a C_6D_6 solution (0.6 mL) of $Cp_2Zr(N^tBu)(THF)$ (**1.4**, 0.0160 g, 0.0440 mmol) in an NMR tube equipped with a J. Youngs valve was added $HCCAr^F$ (6 µL, 0.0440 mmol) *via* microsyringe at RT.

After 1 h the volatiles were removed under reduced pressure and the resultant mixture dried *in vacuo* before being redissolved in C_6D_6 (0.6 mL). ^{1}H NMR spectroscopy indicated that $Cp_2Zr(NH^tBu)(CCAr^F)$ **39** and $Cp_2Zr\{N(^tBu)C(H)C(Ar^F)\}$ **40** formed in 31:69% ratio. Compound **40** was subsequently characterised by ^{1}H, ^{13}C and ^{19}F spectroscopy at RT.

^{1}H NMR (C_6D_6, 400.1 MHz): δ 7.88 (ZrC=CH), 5.81 (10 H, s, C_5H_5), 0.95 (9 H, s, CMe_3) ppm. $^{13}C\{^1H\}$ NMR (C_6D_6, 100.6 MHz): δ 138.3 (Zr<u>C</u>=CH), 120.5 (ZrC=<u>C</u>H), 111.9 (C_5H_5), 55.7 (<u>C</u>Me$_3$), 31.6 (C<u>Me</u>$_3$) ppm. Those resonances belonging to the Ar^F ring could not be satisfactorily assigned. $^{19}F\{H\}$ NMR (C_6D_6, 376.5 MHz): –146.9 (2 F, m, *o*-Ar^F), –166.7 (2 F, m, *m*-Ar^F), –170.2 (1 F, m, *p*-Ar^F) ppm.

Kinetic isotope effect measurements for the reaction of $Cp_2Zr(N^tBu)(py)$ (3.5) with $HCCAr^F$ to form $Cp_2Zr(NH^tBu)(CCAr^F)$ (39). In the dry-box, a toluene-d_8 solution (0.3 mL) of $Cp_2Zr(N^tBu)(py)$ (**3.5**, 0.0098 g, 0.0264 mmol) was transferred in an NMR tube equipped with a J. Youngs valve. Another toluene-d_8 solution (0.4 mL) of $HCCAr^F$ or $DCCAr^F$ (3.5 µL, 0.0264 mmol) was also transferred in an other NMR tube equipped with a J. Youngs valve. These two NMR tubes were subsquently equipped by adaptors which connected to the Schlenk line, and both NMR tubes were precooled to –78 °C. The $HCCAr^F$ or $DCCAr^F$ solution was then cannula transferred into the NMR tube containing $Cp_2Zr(N^tBu)(py)$ (**3.5**). The NMR probe was precooled to 242 K and the a blank toluene-d_8 sample added, locked and shimmed. The experimental sample then replaced the blank samplle and allowed to thermally equilibrate. The reaction monitored by ^{1}H NMR spectroscopy using an array which recorded spectra (4 scans) every 150 s. The formation of **39** (or **39-*d*$_1$**) was calculated by measuing the integral of an C_5H_5 resonance. Initial rate constants were obtained from plots of [**39**] *vs* time using *Origin*.

Competition reaction of $Cp_2Zr(N^tBu)(py)$ (3.5) with $HCCAr^F$ and $DCCAr^F$. To a vial containing $Cp_2Zr(N^tBu)(py)$ (**3.5**, 0.0070 g, 0.0188 mmol) was added a C_6D_6 solution (0.6 mL) of $HCCAr^F$ (12.5 µL, 0.0942 mmol) and $DCCAr^F$ (12.5 µL, 0.0942 mmol). The mixture was then left at RT for 1 h, with ^{1}H NMR integration showing the products to be 62% **39** and 38% **39-*d*$_1$**.

$Cp_2Hf\{NHB(NAr'CH)_2\}(CCAr^F)$ (41). To a solution of $Cp_2Hf\{NB(NAr'CH)_2\}(py)$ (**12**, 0.300 g, 0.380 mmol) in benzene (10 mL) was added $HCCAr^F$ (60 µL, 0.456 mmol) at RT. The reaction mixture was stirred for 12 h at RT. The volatiles were then removed

under reduced pressure, and the crude producct dissolved in hexane (15 mL) and cooled to 4 °C, resulting in yellow, diffraction-quality crystals of **41**. Yield: 0.154 g (45%).

^{1}H NMR (C_6D_6, 400.1 MHz): δ 7.22 (6 H, overlapping 2 × m, *m*- and *p*-$C_6\underline{H}_3{}^{i}Pr_2$), 6.10 (2 H, s, NCH), 5.55 (10 H, s, C_5H_5), 5.22 (1 H, s, NH), 3.38 (4 H, sept., ^{3}J = 6.9 Hz, C<u>H</u>MeMe), 1.40 (12 H, d, ^{3}J = 6.9 Hz, CH<u>Me</u>Me), 1.22 (12 H, d, ^{3}J = 6.9 Hz, CHMe<u>Me</u>) ppm. ^{13}C{^{1}H} NMR (C_6D_6, 100.6 MHz): δ 147.0 (*o*-$\underline{C}_6H_3{}^{i}Pr_2$), 139.6 (*i*-$\underline{C}_6H_3{}^{i}Pr_2$), 127.9 (*p*-$\underline{C}_6H_3{}^{i}Pr_2$), 124.2 (*m*-$\underline{C}_6H_3{}^{i}Pr_2$), 117.5 (NCH), 109.5 ($C_5H_5$), 28.8 (<u>C</u>HMeMe), 25.5 (CHMe<u>Me</u>), 23.5 (CH<u>Me</u>Me) ppm. Those resonances belonging to the acetylide ligand could not be satisfactorily assigned. ^{19}F{H} NMR (C_6D_6, 376.5 MHz): –138.7 (2 F, m, *o*-Ar^F), –157.4 (1 F, t, ^{3}J = 21.4 Hz, *p*-Ar^F), –163.4 (2 F, m, *m*-Ar^F) ppm. ^{11}B{^{1}H} NMR (C_6D_6, 128.4 MHz): δ 25.5 ppm. IR (NaCl plates, Nujol mull, cm^{-1}): 3321 (w, N–H), 2099 (m, ν(C≡C)), 1726 (w), 1627 (w), 1582 (m), 1510 (m), 1281 (w), 1254 (w), 1164 (w), 1141 (m), 1110 (w), 1056 (s), 1020 (m), 957 (s), 899 (m), 804 (s), 760 (s), 656 (s). Anal. found (calcd. for $C_{44}H_{47}BF_5N_3Hf$): C, 58.60 (58.58); H, 5.12 (5.25); N, 4.57 (4.66)%.

Kinetic isotope effect measurements for the reaction of $Cp_2Hf\{NB(NAr'CH)_2\}(py)$ (12) with $HCCAr^F$ to form $Cp_2Hf\{NHB(NAr'CH)_2\}(CCAr^F)$ (41). To a C_6D_6 solution (0.6 mL) of $Cp_2Hf\{NB(NAr'CH)_2\}(py)$ (**12**, 0.0149 g, 0.0185 mmol) in an NMR tube equipped with a J. Youngs valve was added $HCCAr^F$ or $DCCAr^F$ (5 µL, 0.0370 mmol) *via* microsyringe. The NMR tube was transferred to a termperature-regulated (298 K) probe and the reaction monitored by ^{1}H NMR spectroscopy using an array which recorded spectra (4 scans) every 150 s. The formation of **41** (or **41-*d*$_1$**) was calculated by measuing the integral of an NCH resonance. Initial rate constants were obtained from plots of [**41**] *vs* time using *Origin*.

Competition reaction of $Cp_2Hf\{NB(NAr'CH)_2\}(py)$ (12) with $HCCAr^F$ and $DCCAr^F$. To a vial containing $Cp_2Hf\{NB(NAr'CH)_2\}(py)$ (**12**, 0.009 g, 0.0114 mmol) was added a C_6D_6 solution (0.6 mL) of $HCCAr^F$ (7.5 µL, 0.057 mmol) and $DCCAr^F$ (7.5 µL, 0.057 mmol). The mixture was then left at RT for 1 h, with ^{1}H NMR integration showing the products to be 50% **41** and 50% **41-*d*$_1$**.

$Cp_2Hf\{NHB(NAr'CH)_2\}(CCAr^{CF_3})$ (42). To a solution of $Cp_2Hf\{NB(NAr'CH)_2\}(py)$ (**12**, 0.269 g, 0.341 mmol) in benzene (10 mL) was added $HCCAr^{CF_3}$ (72 µL, 0.408 mmol) at RT. The reaction mixture was heated to 50 °C and stirred for 40 h, after which

the volatiles were removed under reduced pressure, and the crude product dissolved in hexane (15 mL) and cooled to 4 °C, resulting in pale yellow, diffraction-quality crystals of **42**. Yield: 0.194 g (60%).

^{1}H NMR (C_6D_6, 400.1 MHz): δ 7.87 (2 H, s, *o*-Ar^{CF_3}), 7.60 (1 H, s, *p*-Ar^{CF_3}), 7.22 (6 H, s, *m*- and *p*-$C_6\underline{H}_3{}^{i}Pr_2$), 6.11 (2 H, s, NCH), 5.53 (10 H, s, C_5H_5), 5.08 (1 H, s, NH), 3.37 (4 H, sept., ^{3}J = 6.9 Hz, C<u>H</u>MeMe), 1.38 (12 H, d, ^{3}J = 6.9 Hz, CH<u>Me</u>Me), 1.20 (12 H, d, ^{3}J = 6.9 Hz, CHMe<u>Me</u>) ppm. ^{13}C{^{1}H} NMR (C_6D_6, 100.6 MHz): δ 150.0 (*o*-$\underline{C}_6H_3{}^{i}Pr_2$), 139.6 (*i*-$\underline{C}_6H_3{}^{i}Pr_2$), 132.0 (*m*-$Ar^{CF_3}$), 131.1 (*o*-$Ar^{CF_3}$), 129.1 (Hf<u>C</u>C$Ar^{CF_3}$), 127.9 (*p*-$\underline{C}_6H_3{}^{i}Pr_2$), 124.2 (*m*-$\underline{C}_6H_3{}^{i}Pr_2$), 123.9 (HfC<u>C</u>$Ar^{CF_3}$), 120.9 (*i*-$Ar^{CF_3}$), 119.5 (*p*-$Ar^{CF_3}$), 117.5 (NCH), 109.4 ($C_5H_5$), 28.8(<u>C</u>HMeMe), 25.6 (CHMe<u>Me</u>), 23.5 (CH<u>Me</u>Me) ppm. Resonances attributable to carbons directly bound to ^{19}F atoms were not observed. ^{19}F{H} NMR (C_6D_6, 376.5 MHz): –62.8 (6 F, s, Ar^{CF_3}) ppm. ^{11}B{^{1}H} NMR (C_6D_6, 128.4 MHz): δ 25.7 ppm. IR (NaCl plates, Nujol mull, cm^{-1}): 3306 (w, N–H), 2085 (w, ν(C≡C)), 1937 (w), 1865 (w), 1798 (w), 1699 (w), 1604 (s), 1492 (w), 1267 (s), 1209 (m), 1178 (m), 1124 (m), 1007 (m), 863 (w), 796 (s), 760 (m), 696 (w), 679 (m), 661 (s). Anal. found (calcd. for $C_{46}H_{50}BF_6N_3Hf$): C, 58.19 (58.27); H, 5.47 (5.32); N, 4.40 (4.43)%.

$Cp_2Ti\{N\{B(NAr'CH)_2\}C(H)C(Tol)\}$ (43). To a solution of $Cp_2Ti\{NB(NAr'CH)_2\}(py)$ (**1.117**, 0.200 g, 0.304 mmol) in benzene (10 mL) was added HCCTol (42 µL, 0.334 mmol) at RT. The reaclltion mixture was stirred for 2 h at RT, after which the volatiles were removed under reduced pressure to yield **43** as a deep red solid, which was then dried *in vacuo*. Yield : 0.165 g (78%).

^{1}H NMR (C_6D_6, 400.1 MHz): δ 7.26 (6 H, overlapping 2 × m, *m*- and *p*-$C_6\underline{H}_3{}^{i}Pr_2$), 7.03 (2 H, d, ^{3}J = 8.0 Hz, *m*-$C_6\underline{H}_4Me$), 6.78 (1 H, s, TiC=CH), 6.65 (2 H, d, ^{3}J = 8.0 Hz, *o*-$C_6\underline{H}_4Me$), 6.07 (2 H, s, NCH), 5.56 (10 H, s, C_5H_5), 3.54 (4 H, sept., ^{3}J = 6.9 Hz, C<u>H</u>MeMe), 2.22 (3 H, s, $C_6H_4\underline{Me}$), 1.35 (12 H, d, ^{3}J = 6.9 Hz, CH<u>Me</u>Me), 1.27 (12 H, d, ^{3}J = 6.9 Hz, CHMe<u>Me</u>) ppm. ^{13}C{^{1}H} NMR (C_6D_6, 100.6 MHz): δ 195.1 (Ti<u>C</u>=CH), 147.2 (*o*-$\underline{C}_6H_3{}^{i}Pr_2$), 142.5 (*i*-$\underline{C}_6H_4Me$), 141.3 (*i*-$\underline{C}_6H_3{}^{i}Pr_2$), 133.0 (*p*-$\underline{C}_6H_4Me$), 129.3 (*m*-$\underline{C}_6H_4Me$), 127.6 (*p*-$\underline{C}_6H_3{}^{i}Pr_2$), 123.9 (*o*-$\underline{C}_6H_4Me$), 123.8 (*m*-$\underline{C}_6H_3{}^{i}Pr_2$), 118.8 (NCH), 112.6 ($C_5H_5$), 92.2 (TiC=<u>C</u>H), 28.9 (<u>C</u>HMeMe), 26.1 (CHMe<u>Me</u>), 23.1 (CH<u>Me</u>Me), 21.2 ($C_6H_4\underline{Me}$) ppm. ^{11}B{^{1}H} NMR (C_6D_6, 128.4 MHz): δ 22.9 ppm. IR (NaCl plates, Nujol mull, cm^{-1}): 2360 (w), 2324 (w), 1942 (w), 1861 (w), 1726 (w), 1564 (w), 1519 (s), 1209 (w), 1110 (w), 1052 (w), 998 (w), 885 (w), 809 (s), 746 (m), 728 (m), 706 (w), 679 (w),

634 (s). EI-MS: *m/z* = 692 $[M]^+$ (1%). Satisfactory elemental analysis could not be obtained.

$Cp_2Ti\{N\{B(NAr'CH)_2\}C(H)C(Ar^F)\}$ (44). To a solution of $Cp_2Ti\{NB(NAr'CH)_2\}(py)$ (**1.117**, 0.200 g, 0.304 mmol) in benzene (10 mL) was added $HCCAr^F$ (44 µL, 0.334 mmol) at RT and stirred for 2 h. The volatiles were then removed under reduced pressure, and the crude product dissolved in hexane (15 mL) and cooled to 4 °C, resulting in deep red, diffraction-quality crystals of **44**. Yield: 0.116 g (45%).

^{1}H NMR (C_6D_6, 400.1 MHz): δ 7.20 (6 H, overlapping 2 × m, *m*- and *p*-$C_6\underline{H}_3{}^iPr_2$), 7.16 (1 H, s, TiC=CH), 6.03 (2 H, s, NCH), 5.57 (10 H, s, C_5H_5), 3.46 (4 H, sept., ^3J = 6.9 Hz, C<u>H</u>MeMe), 1.36 (12 H, d, ^3J = 6.9 Hz, CH<u>Me</u>Me), 1.21 (12 H, d, ^3J = 6.9 Hz, CHMe<u>Me</u>) ppm. $^{13}C\{^1H\}$ NMR (C_6D_6, 100.6 MHz): δ 165.5 (Ti<u>C</u>=CH), 146.9 (*o*-$\underline{C}_6H_3{}^iPr_2$), 140.5 (*i*-$\underline{C}_6H_3{}^iPr_2$), 128.6 (*p*-$\underline{C}_6H_3{}^iPr_2$), 124.0 (*m*-$\underline{C}_6H_3{}^iPr_2$), 119.2 (NCH), 114.6 ($C_5H_5$), 105.8 (TiC=<u>C</u>H), 29.0 (<u>C</u>HMeMe), 26.4 (CHMe<u>Me</u>), 23.1 (CH<u>Me</u>Me) ppm. Those resonances belonging to the Ar^F ring could not be satisfactorily assigned. $^{19}F\{H\}$ NMR (C_6D_6, 376.5 MHz): –145.2 (2 F, m, *o*-Ar^F), –166.0 (2 F, m, *m*-Ar^F), –167.3 (1 F, t, ^3J = 21.4 Hz, *p*-Ar^F) ppm. $^{11}B\{^1H\}$ NMR (C_6D_6, 128.4 MHz): δ 22.9 ppm. IR (NaCl plates, Nujol mull, cm^{-1}): 1510 (s), 1294 (m), 1263 (m), 1191 (m), 1119 (s), 1083 (w), 1029 (s), 971 (s), 926 (w), 890 (w), 809 (s), 746 (s), 724 (w), 638 (s). EI-MS: *m/z* = 771 $[M]^+$ (1%). Anal. found (calcd. for $C_{44}H_{47}BF_5N_3Ti$): C, 68.38 (68.50); H, 6.00 (6.14); N, 5.51 (5.45)%.

$TolC(H)=C(H)N(H)B(NAr'CH)_2$ (45). To a solution of $Cp_2Zr\{NB(NAr'CH)_2\}(py)$ (**11**, 0.250 g, 0.356 mmol) in toluene (10 mL) was added HCCTol (50 µL, 0.393 mmol) at RT. The reaction mixture was heated to 90 °C and stirred for 1 h, after which the solution was transfered into a Schlenk flask containing pinacol (0.0550 g, 0.463 mmol), and the solution was heated to 60 °C. After 16 h, the volatiles were removed under reduced pressure, and the crude product extracted in hexane (10 mL) and cooled to –30 °C, resulting in colourless, diffraction-quality crystals of **45**. Yield: 0.091 g (49%).

^{1}H NMR (C_6D_6, 400.1 MHz): δ 7.31 (6 H, overlapping 2 × m, *m*- and *p*-$C_6\underline{H}_3{}^iPr_2$), 6.89 (2 H, d, ^3J = 8.0 Hz, *m*-$C_6\underline{H}_4Me$), 6.69 (2 H, d, ^3J = 8.0 Hz, *o*-$C_6\underline{H}_4Me$), 6.19 (1 H, t, ^3J = 13.7 Hz, TolC(H)=C<u>H</u>), 5.97 (2 H, s, NCH), 4.74 (1 H, d, ^3J = 13.7 Hz, TolC(<u>H</u>)=CH), 4.16 (1 H, d, ^3J = 13.7 Hz, N<u>H</u>), 3.36 (4 H, sept., ^3J = 6.9 Hz, C<u>H</u>MeMe), 2.07 (3 H, s, $C_6H_4\underline{Me}$), 1.28 (24 H, overlapping 2 × m, CH<u>MeMe</u>) ppm. $^{13}C\{^1H\}$ NMR (C_6D_6, 100.6 MHz): δ 147.3 (*o*-$\underline{C}_6H_3{}^iPr_2$), 138.4 (*i*-$\underline{C}_6H_3{}^iPr_2$), 136.3 (*i*-$\underline{C}_6H_4Me$), 133.5 (*p*-$\underline{C}_6H_4Me$),

129.6 (TolC(H)=CH), 129.4 (*m*-C_6H_4Me), 127.8 (*p*-$C_6H_3{}^iPr_2$), 124.2 (*m*-$C_6H_3{}^iPr_2$), 122.9 (*o*-C_6H_4Me), 117.8 (NCH), 105.9 (TolC(H)=CH), 28.8 (CHMeMe), 24.4 (CHMeMe), 24.1 (CHMeMe), 21.0 (C_6H_4Me) ppm. $^{11}B\{^1H\}$ NMR (C_6D_6, 128.4 MHz): δ 21.0 ppm. IR (NaCl plates, Nujol mull, cm^{-1}): 3308 (w, N–H), 2391 (w), 2346 (w), 1600 (s), 1573 (m), 1551 (m), 1281 (w), 1187 (s), 1173 (m), 1052 (w), 1016 (w), 939 (m), 899 (s), 800 (s), 755 (s), 692 (s), 647 (s). EI-HRMS: *m/z* found (calcd. For $C_{35}H_{46}BN_3$, $[M]^+$) 518.3802 (518.3821). Anal. found (calcd. for $C_{35}H_{46}BN_3$): C, 80.77 (80.91); H, 9.08 (8.92); N, 7.94 (8.09)%.

$Ar^{CF_3}C(H)=C(H)N(H)B(NAr'CH)_2$ (46). To a solution of $Cp_2Zr\{NB(NAr'CH)_2\}(py)$ (**11**, 0.280 g, 0.399 mmol) in toluene (10 mL) was added $HCCAr^{CF_3}$ (78 µL, 0.439 mmol) at RT. The reaction mixture was heated to 90 °C and stirred for 1 h, after which the solution was transfered into a Schlenk flask containing pinacol (0.0615 g, 0.519 mmol), and the solution was heated back to 60 °C. After 16 h, the volatiles were removed under reduced pressure, and the crude product extracted in hexane (10 mL) and cooled to –30 °C, resulting in colourless crystals of **46**. Yield: 0.101 g (41%).

^1H NMR (C_6D_6, 400.1 MHz): δ 7.37 (1 H, s, *o*-Ar^{CF_3}), 7.33 (6 H, overlapping 2 × m, *m*- and *p*-$C_6H_3{}^iPr_2$), 6.91 (2 H, s, *p*-Ar^{CF_3}), 6.38 (1 H, t, ^3J = 13.6 Hz, $Ar^{CF_3}C(H)=CH$), 5.95 (2 H, s, NCH), 4.24 (1 H, d, ^3J = 13.6 Hz, NH), 4.15 (1 H, d, ^3J = 13.6 Hz, $Ar^{CF_3}C(H)=CH$), 3.26 (4 H, sept., ^3J = 6.9 Hz, CHMeMe), 1.21 (24 H, overlapping 2 × m, CHMeMe) ppm. $^{13}C\{^1H\}$ NMR (C_6D_6, 100.6 MHz): δ 147.1 (*o*-$C_6H_3{}^iPr_2$), 141.6 (*i*-Ar^{CF_3}), 137.7 (*i*-$C_6H_3{}^iPr_2$), 133.8 ($Ar^{CF_3}C(H)=CH$), 131.9 (*m*-Ar^{CF_3}), 128.7 (*p*-$C_6H_3{}^iPr_2$), 124.3 (*m*-$C_6H_3{}^iPr_2$), 123.2 (*o*-Ar^{CF_3}), 117.8 (NCH), 116.9 (*p*-Ar^{CF_3}), 113.3 ($Ar^{CF_3}C(H)=CH$), 28.8 (CHMeMe), 24.3 (CHMeMe), 24.0 (CHMeMe) ppm. Resonances attributable to carbons directly bound to ^{19}F atoms were not observed. $^{19}F\{H\}$ NMR (C_6D_6, 376.5 MHz): –62.8 (6 F, s, Ar^{CF_3}) ppm. $^{11}B\{^1H\}$ NMR (C_6D_6, 128.4 MHz): δ 20.8 ppm. IR (NaCl plates, Nujol mull, cm^{-1}): 3389 (w, NH), 2355 (w), 2324 (w), 1950 (w), 1901 (w), 1771 (w), 1649 (s), 1604 (s), 1276 (s), 1173 (m), 1128 (m), 962 (s), 935 (s), 886 (s), 804 (s), 840 (m), 728 (m), 683 (s), 647 (m). EI-HRMS: *m/z* found (calcd. For $C_{36}H_{42}BF_6N_3$, $[M]^+$) 641.3431 (641.3407).

$PhC(H)=C(Me)N(H)B(NAr'CH)_2$ (47). To a solution of $Cp_2Zr\{NB(NAr'CH)_2\}(py)$ (**11**, 0.270 g, 0.385 mmol) in toluene (10 mL) was added MeCCPh (49 µL, 0.385 mmol) at RT. The reaction mixture was heated to 90 °C and stirred for 1 h, after which the solution

was transfered into a Schlenk flask containing pinacol (0.0590 g, 0.501 mmol), and the solution was heated back to 60 °C. After 16 h, the volatiles were removed under reduced pressure, and the crude product was extracted into hexane, and the volatiles were removed again under reduced pressure. The crude pale yellow oil was dried *in vacuo*. Yield: 0.71 g (36%).

^{1}H NMR (C_6D_6, 400.1 MHz): δ 7.19 (6 H, overlapping 2 × m, *m*- and *p*-$C_6\underline{H}_3{}^{i}Pr_2$), 7.07 (2 H, t, ^{3}J = 7.9 Hz, *m*-$C_6\underline{H}_5$), 6.91 (1 H, t, ^{3}J = 7.9 Hz, *p*-$C_6\underline{H}_5$), 6.74 (2 H, d, ^{3}J = 7.9 Hz, *o*-$C_6\underline{H}_5$), 6.05 (2 H, s, NCH), 5.45 (1 H, s, PhC(H)=CMe), 3.51 (1 H, s, NH), 3.44 (4 H, sept., ^{3}J = 6.9 Hz, C<u>H</u>MeMe), 1.42 (3 H, s, PhC(H)=C<u>Me</u>), 1.32 (12 H, d, ^{3}J = 6.9 Hz, CH<u>Me</u>Me), 1.25 (12 H, d, ^{3}J = 6.9 Hz, CHMe<u>Me</u>) ppm. ^{13}C{^{1}H} NMR (C_6D_6, 100.6 MHz): δ 146.8 (*o*-$\underline{C}_6H_3{}^{i}Pr_2$), 139.4 (*i*-$\underline{C}_6H_3{}^{i}Pr_2$), 136.9 (PhC(H)=<u>C</u>Me), 128.3 (*p*-$\underline{C}_6H_5$), 127.7 (*m*-$\underline{C}_6H_5$), 127.6 (*p*-$\underline{C}_6H_3{}^{i}Pr_2$), 124.6 (*i*-$\underline{C}_6H_5$), 124.1 (*p*-$\underline{C}_6H_5$), 124.0 (*m*-$\underline{C}_6H_3{}^{i}Pr_2$), 118.2 (NCH), 108.7 (Ph<u>C</u>(H)=CMe), 28.7 (<u>C</u>HMeMe), 24.9 (CHMe<u>Me</u>), 23.8 (CH<u>Me</u>Me) 19.7 (PhC(H)=C<u>Me</u>) ppm. ^{11}B{^{1}H} NMR (C_6D_6, 128.4 MHz): δ 21.2 ppm. IR (NaCl plates, Nujol mull, cm^{-1}): 3388 (s, N–H), 2351 (w), 2324 (w), 1946 (m), 1861 (m), 1738 (m), 1263 (s), 1101 (s), 1022 (s), 939 (m), 791 (s), 706 (m), 647 (w). EI-HRMS: *m/z* found (calcd. For $C_{35}H_{46}BN_3$, $[M]^+$) 518.3807 (519.3785).

5.7 Experimental details and characterising data for Chapter Four

Reaction of $Cp_2Zr\{NB(NAr'CH)_2\}(py)$ (11) with CO_2: synthesis of $OCNB(NAr'CH)_2$ (48). A solution of $Cp_2Zr\{NB(NAr'CH)_2\}(py)$ (**11**, 0.200 g, 0.285 mmol) in benzene (10 mL) was freeze-pump-thaw-degassed three times. The solution was then exposed to CO_2 at a pressure of *ca.* 1.2 atm. The mixture was left to stir at RT for 16 h. The volatiles were then removed under reduced pressure, and the crude product extracted in hexane (20 mL). The filtrate was concentrated to 5 mL and cooled to –30 °C overnight, resulting in pale yellow crystals of **48**. Yield: 0.067 g (55%).

^{1}H NMR (C_6D_6, 400.1 MHz): δ 7.23 – 7.12 (6 H, overlapping 2 × m, *m*- and *p*-$C_6\underline{H}_3{}^{i}Pr_2$), 5.95 (2 H, s, NCH), 3.14 (4 H, sept., ^{3}J = 6.9 Hz, C<u>H</u>MeMe), 1.26 (12 H, d, ^{3}J = 6.9 Hz, CH<u>Me</u>Me), 1.19 (12 H, d, ^{3}J = 6.9 Hz, CHMe<u>Me</u>) ppm. ^{13}C{^{1}H} NMR (C_6D_6, 125.7 MHz): δ 146.5 (*o*-$\underline{C}_6H_3{}^{i}Pr_2$), 136.8 (*i*-$\underline{C}_6H_3{}^{i}Pr_2$), 128.5 (*p*-$\underline{C}_6H_3{}^{i}Pr_2$), 125.7 (NCO), 123.9 (*m*-$\underline{C}_6H_3{}^{i}Pr_2$), 118.2 (NCH), 28.9 (<u>C</u>HMeMe), 24.4 (CH<u>Me</u>Me), 24.1 (CHMe<u>Me</u>) ppm. ^{11}B{^{1}H} NMR (C_6D_6, 128.4 MHz): δ 17.8 ppm. IR (NaCl plates, Nujol mull, cm^{-1}): 3117

(w), 3070 (w), 3028 (w), 2388 (w), 2305 (s, NCO as stretch), 1940 (m), 1868 (m), 1715 (w), 1682 (w), 1587 (w), 1573 (w), 1537 (s), 1502 (s), 1407 (m), 1360 (m), 1231 (m), 1192 (m), 1179 (w), 1116 (w), 1102 (w), 1059 (m), 1041 (w), 937 (m), 910 (m), 760 (m), 692 (m), 668 (w), 649 (m), 597 (w). EI-HRMS: *m/z* found (calcd. for $C_{27}H_{36}BN_3O$, $[M]^+$) 429.2957 (429.2951). Anal. found (calcd. for $C_{27}H_{36}BN_3O$): C, 75.44 (75.52); H, 8.54 (8.45); N, 9.63 (9.79)%.

Reaction of $Cp_2Zr\{NB(NAr'CH)_2\}(py)$ (11) with CS_2: synthesis of $SCNB(NAr'CH)_2$ (49). A solution of $Cp_2Zr\{NB(NAr'CH)_2\}(py)$ (**11**, 0.200 g, 0.285 mmol) in benzene (10 mL) was added CS_2 (34.6 μL, 0.570 mmol). The mixture was left to stir at RT for 16 h. The volatiles were then removed under reduced pressure, and the crude mixture separated with hexane (2 × 5 mL). The filtrate was concentrated to 5 mL and cooled to 4 °C, resulting in pale yellow crystals of **49**. Yield: 0.039 g (37%).

^{1}H NMR (C_6D_6, 400.1 MHz): δ 7.22 – 7.11 (6 H, overlapping 2 × m, *m*- and *p*-$C_6\underline{H}_3{}^i Pr_2$), 5.91 (2 H, s, NCH), 3.10 (4 H, sept., ^3J = 6.9 Hz, C<u>H</u>MeMe), 1.30 (12 H, d, ^3J = 6.9 Hz, CH<u>Me</u>Me), 1.18 (12 H, d, ^3J = 6.9 Hz, CHMe<u>Me</u>) ppm. $^{13}C\{^1H\}$ NMR (C_6D_6, 125.7 MHz): δ 146.3 (*o*-$\underline{C}_6H_3{}^i Pr_2$), 143.2 (NCS), 136.4 (*i*-$\underline{C}_6H_3{}^i Pr_2$), 128.6 (*p*-$\underline{C}_6H_3{}^i Pr_2$), 123.9 (*m*-$\underline{C}_6H_3{}^i Pr_2$), 118.6 (NCH), 28.9 (<u>C</u>HMeMe), 24.5 (CH<u>Me</u>Me), 24.0 (CHMe<u>Me</u>) ppm. $^{11}B\{^1H\}$ NMR (C_6D_6, 128.4 MHz): δ 16.0 ppm. IR (NaCl plates, Nujol mull, cm^{-1}): 3111 (w), 3071 (w), 2176 (m), 2092 (s, NCS as stretch), 1943 (w), 1707 (w), 1614 (w), 1590 (m), 1549 (m), 1505 (m), 1413 (m), 1394 (m), 1343 (w), 1328 (m), 1280 (w), 1230 (w), 1197 (w), 1182 (m), 1116 (m), 1101 (w), 1058 (m), 992 (w), 935 (w), 913 (m), 855 (m), 759 (s), 696 (m), 668 (m), 659 (m), 649 (m). FI-HRMS: *m/z* found (calcd. for $C_{27}H_{36}BN_3S$, $[M]^+$) 445.2722 (445.2723). Anal. found (calcd. for $C_{27}H_{36}BN_3S$): C, 72.94 (72.80); H, 8.25 (8.15); N, 9.51 (9.43)%.

Reaction of $Cp_2Zr\{NB(NAr'CH)_2\}(py)$ (11) with PhNCO: synthesis of $PhN{=}C{=}NB(NAr'CH)_2$ (50). To a solution of $Cp_2Zr\{NB(NAr'CH)_2\}(py)$ (**11**, 0.300 g, 0.428 mmol) in benzene (15 mL) was added PhNCO (51.2 μL, 0.471 mmol) at RT. The reaction mixture was heated to 65 °C and stirred for 24 h, after which the volatiles were removed under reduced pressure, and the crude product extracted into hexane (20 mL). The filtrate was concentrated to 6 mL and cooled to –30 °C, resulting in colourless, diffraction-quality crystals of **50**. Yield: 0.089 g (42%).

^{1}H NMR (C_6D_6, 400.1 MHz): δ 7.17 (6 H, overlapping 2 × m, *m*- and *p*-$C_6\underline{H}_3{}^{i}Pr_2$), 6.89 (2 H, m, *m*-$C_6\underline{H}_5$), 6.76 (1 H, m, *p*-$C_6\underline{H}_5$), 6.36 (2 H, m, *o*-$C_6\underline{H}_5$), 6.02 (2 H, s, NCH), 3.25 (4 H, sept., ^{3}J = 6.9 Hz, C<u>H</u>MeMe), 1.30 (12 H, d, ^{3}J = 6.9 Hz, CH<u>Me</u>Me), 1.21 (12 H, d, ^{3}J = 6.9 Hz, CHMe<u>Me</u>) ppm. ^{13}C{^{1}H} NMR (C_6D_6, 100.6 MHz): δ 146.7 (*o*-$\underline{C}_6H_3{}^{i}Pr_2$), 139.9 (*i*-$\underline{C}_6H_5$), 137.5 (*i*-$\underline{C}_6H_3{}^{i}Pr_2$), 129.4 (*m*-$\underline{C}_6H_5$), 128.7 (N=C=N), 127.9 (*p*-$\underline{C}_6H_3{}^{i}Pr_2$), 124.0 (*m*-$\underline{C}_6H_3{}^{i}Pr_2$), 123.8 (overlapping, *m*- and *p*-$\underline{C}_6H_5$), 118.3 (NCH), 28.9 (<u>C</u>HMeMe), 24.4 (CHMe<u>Me</u>), 24.1 (CH<u>Me</u>Me) ppm. ^{11}B{^{1}H} NMR (C_6D_6, 128.4 MHz): δ 18.7 ppm. IR (NaCl plates, Nujol mull, cm^{-1}): 3106 (w), 2721 (w), 2182 (s, NCN as stretch), 1597 (m), 1572 (w), 1552 (w), 1485 (s), 1400 (m), 1372 (w), 1316 (w), 1288 (w), 1193 (w), 1167 (w), 1110 (w), 1077 (w), 1021 (w), 934 (w), 912 (m), 805 (s), 754 (s), 774 (w), 723 (m), 692 (m), 647 (s). EI-HRMS: *m/z* found (calcd. For $C_{33}H_{41}BN_4$, $[M]^+$) 503.3455 (503.3461). Anal. found (calcd. for $C_{33}H_{41}BN_4$): C, 78.70 (78.56); H, 8.25 (8.19); N, 10.94 (11.11)%.

TolC(H)=NB(NAr'CH)$_2$ (51). To a solution of $Cp_2Zr\{NB(NAr'CH)_2\}(py)$ (**11**, 0.275 g, 0.392 mmol) in benzene (15 mL) was added TolC(O)H (51.0 µL, 0.431 mmol) at RT. The reaction mixture was stirred at RT for 1 h, after which the volatiles were removed under reduced pressure. The crude product extracted into hexane (20 mL), and dried *in vacuo*, yielding **51** as a pale yellow solid. Yield: 0.147 g (74%).

^{1}H NMR (C_6D_6, 400.1 MHz): δ 8.66 (1 H, s, TolC(<u>H</u>)), 7.43 (2 H, d, ^{3}J = 7.8 Hz, *o*-$C_6\underline{H}_4CH_3$), 7.23-7.14 (6 H, overlapping 2 × m, *m*- and *p*-$C_6\underline{H}_3{}^{i}Pr_2$), 6.68 (2 H, d, ^{3}J = 7.8 Hz, *m*-$C_6\underline{H}_4CH_3$), 6.20 (2 H, s, NCH), 3.45 (4 H, sept, ^{3}J = 6.9 Hz, C<u>H</u>Me$_2$), 1.86 (3 H, s, $C_6H_4C\underline{H}_3$), 1.31 (12 H, d, ^{3}J = 6.8 Hz, CH<u>Me</u>Me), 1.28 (12 H, d, ^{3}J = 6.8 Hz, CHMe<u>Me</u>) ppm. ^{13}C{^{1}H} NMR (C_6D_6, 100.6 MHz): δ 167.6 (Tol<u>C</u>(H)), 147.6 (*p*-$\underline{C}_6H_3{}^{i}Pr_2$), 146.6 (*o*-$\underline{C}_6H_3{}^{i}Pr_2$), 141.4 (*p*-$\underline{C}_6H_4CH_3$), 138.9 (*i*-$\underline{C}_6H_3{}^{i}Pr_2$), 136.8 (*i*-$\underline{C}_6H_4CH_3$), 129.3 (*m*-$\underline{C}_6H_4CH_3$), 128.8 (*o*-$\underline{C}_6H_4CH_3$), 123.7 (*m*-$\underline{C}_6H_3{}^{i}Pr_2$), 118.9 (NCH), 28.9 (<u>C</u>HMeMe), 24.5 (CH<u>Me</u>Me), 24.2 (CHMe<u>Me</u>), 21.2 ($C_6H_4\underline{C}H_3$) ppm. ^{11}B{^{1}H} NMR (C_6D_6, 128.4 MHz): δ 24.3 ppm. IR (NaCl plates, Nujol mull, cm^{-1}): 2723 (w), 1706 (w), 1661 (m), 1607 (m), 1576 (m), 1460 (s), 1378 (s), 1329 (s), 1301 (s), 1260 (s), 1217 (m), 1103 (m), 1057 (m), 1018 (m), 935 (w), 908 (w), 853 (w), 805 (s), 761 (m), 722 (m), 660 (m). ESI-HRMS: *m/z* found (calcd for $C_{34}H_{45}BN_3$, $[M]^+$): 506.3707 (506.37065).

Cp$_2$Zr{NHB(NAr'CH)$_2$}{OC(CH$_2$)Ph} (52). To a solution of $Cp_2Zr\{NB(NAr'CH)_2\}(py)$ (**11**, 0.275 g, 0.392 mmol) in benzene (15 mL) was added

PhC(O)Me (50.4 μL, 0.431 mmol) at RT. The reaction mixture was stirred at RT for 16 h, after which the volatiles were removed under reduced pressure. The crude product extracted into hexane (20 mL), and dried *in vacuo*, yielding **52** as a pale yellow oil. Yield: 0.192 g (66%).

^{1}H NMR (C_6D_6, 400.1 MHz): δ 7.57 (2 H, m, *o*-C_6H_5), 7.23 (2 H, m, *m*-C_6H_5), 7.22 (6 H, overlapping 2 × m, *m*- and *p*-$C_6\underline{H}_3{}^{i}Pr_2$), 7.21 (1 H, m, *p*-$C_6H_5$), 6.14 (2 H, s, NCH), 5.66 (10 H, s, C_5H_5), 4.96 (1 H, s, NH), 4.68 (1 H, s, C(O)=C$\underline{H}$H), 3.93 (1 H, s, C(O)=CH$\underline{H}$), 3.58 (4 H, sept., ^{3}J = 6.9 Hz, C$\underline{H}$MeMe), 1.36 (12 H, d, ^{3}J = 6.9 Hz, CH$\underline{Me}$Me), 1.24 (12 H, d, ^{3}J = 6.9 Hz, CHMe$\underline{Me}$) ppm. ^{13}C{^{1}H} NMR (C_6D_6, 100.6 MHz): δ 165.6 ($\underline{C}$(O)=CH_2), 147.1 (*o*-$\underline{C}_6H_3{}^{i}Pr_2$), 140.4 (*i*-$\underline{C}_6H_3{}^{i}Pr_2$), 140.2 (*i*-$C_6H_5$), 128.2 (*p*-$C_6H_5$), 127.9 (*m*-$\underline{C}_6H_3{}^{i}Pr_2$), 127.6 (*m*-$C_6H_5$), 125.8 (*o*-$C_6H_5$), 124.2 (*p*-$\underline{C}_6H_3{}^{i}Pr_2$), 117.6 (NCH), 112.1 ($C_5H_5$), 87.0 (C(O)=$\underline{C}H_2$) 28.8 ($\underline{C}$HMeMe), 25.5 (CHMe$\underline{Me}$), 23.6 (CH$\underline{Me}$Me) ppm. ^{11}B{^{1}H} NMR (C_6D_6, 128.4 MHz): δ 25.0 ppm. IR (NaCl plates, Nujol mull, cm^{-1}): 3295 (w, N–H), 2724 (m), 2603 (w), 2367 (w), 2269 (w), 2072 (w), 1934 (m), 1670 (m), 1800 (m), 1682 (s), 1254 (w), 1173 (w), 1024 (w), 971 (m), 940 (m), 889 (m), 813 (w), 661 (w), 566 (w). Anal. found (calcd. for $C_{44}H_{54}BN_3OZr$): C, 71.12 (71.13); H, 7.45 (7.33); N, 5.49 (5.66)%.

$Cp_2Zr\{NHB(NAr'CH)_2\}\{OC(CH_2)O^{i}Pr\}$ (53). To a solution of $Cp_2Zr\{NB(NAr'CH)_2\}$(py) (**11**, 0.260 g, 0.370 mmol) in benzene (15 mL) was added $MeCO_2{}^{i}Pr$ (47.9 μL, 0.407 mmol) at RT. The reaction mixture was stirred at 40 °C for 20 h, after which the volatiles were removed under reduced pressure, and the crude product dissolved in hexane (10 mL) and cooled to 4 °C, resulting in pale yellow, diffraction-quality crystals of **53**. Yield: 0.145 g (54%).

^{1}H NMR (C_6D_6, 400.1 MHz): δ 7.24 (6 H, s, *m*- and *p*-$C_6\underline{H}_3{}^{i}Pr_2$), 6.16 (2 H, s, NCH), 5.72 (10 H, s, C_5H_5), 5.19 (1 H, s, NH), 4.01 (1 H, sept., ^{3}J = 6.0 Hz, OC$\underline{H}$Me$_2$), 3.50 (4 H, sept., ^{3}J = 6.9 Hz, C$\underline{H}$MeMe), 3.03 (2 H, s, C(O)=C$\underline{H}_2$), 1.42 (12 H, d, ^{3}J = 6.9 Hz, CH$\underline{Me}$Me), 1.25 (12 H, d, ^{3}J = 6.9 Hz, CHMe$\underline{Me}$), 1.14 (6 H, d, ^{3}J = 6.0 Hz, OCH$\underline{Me}_2$) ppm. ^{13}C{^{1}H} NMR (C_6D_6, 100.6 MHz): δ 167.2 ($\underline{C}$(O)=CH_2), 147.1 (*o*-$\underline{C}_6H_3{}^{i}Pr_2$), 140.1 (*i*-$\underline{C}_6H_3{}^{i}Pr_2$), 127.5 (*m*-$\underline{C}_6H_3{}^{i}Pr_2$), 124.2 (*p*-$\underline{C}_6H_3{}^{i}Pr_2$), 117.4 (NCH), 112.3 ($C_5H_5$), 68.4 (O$\underline{C}HMe_2$), 57.4 (C(O)=$\underline{C}H_2$), 28.8 ($\underline{C}$HMeMe), 25.6 (CHMe$\underline{Me}$), 23.6 (CH$\underline{Me}$Me), 22.2 (OCH$\underline{Me}_2$) ppm. ^{11}B{^{1}H} NMR (C_6D_6, 128.4 MHz): δ 25.0 ppm. IR (NaCl plates, Nujol mull, cm^{-1}): 3289 (w, N–H), 3112 (w), 2719 (w), 2289 (w), 1873 (w), 1800 (w), 1718

(w), 1614 (s), 1257 (m), 1176 (m), 1119 (m), 1060 (w), 1041 (w), 1015 (m), 982 (s), 892 (s), 807 (s), 749 (s), 712 (s), 659 (s), 594 (m), 538 (w). Anal. found (calcd. for $C_{41}H_{56}BN_3O_2Zr$): C, 67.79 (67.93); H, 7.82 (7.79); N, 5.73 (5.80)%.

$Cp_2Zr\{NHB(NAr'CH)_2\}\{OC(CH_2)OEt\}$ (54). To a solution of $Cp_2Zr\{NB(NAr'CH)_2\}(py)$ (**11**, 0.260 g, 0.370 mmol) in benzene (15 mL) was added $MeCO_2Et$ (38.0 µL, 0.389 mmol) at RT. The reaction mixture was stirred at RT for 16 h, after which the volatiles were removed under reduced pressure, and the crude product dissolved in hexane (8 mL) and cooled to –30 °C, resulting in pale yellow crystals of **54**. Yield: 0.200 g (76%).

^{1}H NMR (C_6D_6, 400.1 MHz): δ 7.24 (6 H, s, *m*- and *p*-$C_6\underline{H}_3{}^i Pr_2$), 6.16 (2 H, s, NCH), 5.71 (10 H, s, C_5H_5), 5.23 (1 H, s, NH), 3.53 (2 H, q, ^3J = 7.2 Hz, $OC\underline{H}_2CH_3$), 3.50 (4 H, sept., ^3J = 6.9 Hz, C<u>H</u>MeMe), 2.98 (2 H, s, C(O)=C$\underline{H}_2$), 1.41 (12 H, d, ^3J = 6.9 Hz, CH<u>Me</u>Me), 1.23 (12 H, d, ^3J = 6.9 Hz, CHMe<u>Me</u>), 1.08 (3 H, t, ^3J = 7.2 Hz, $OCH_2C\underline{H}_3$) ppm. $^{13}C\{^1H\}$ NMR (C_6D_6, 100.6 MHz): δ 168.7 (<u>C</u>(O)=CH_2), 147.1 (*o*-$\underline{C}_6H_3{}^i Pr_2$), 140.1 (*i*-$\underline{C}_6H_3{}^i Pr_2$), 128.1 (*m*-$\underline{C}_6H_3{}^i Pr_2$), 127.5 (*p*-$\underline{C}_6H_3{}^i Pr_2$), 117.4 (NCH), 112.4 ($C_5H_5$), 62.3 ($O\underline{C}H_2CH_3$), 56.1 (C(O)=<u>C</u>$H_2$), 28.8 (<u>C</u>HMeMe), 25.6 (CHMe<u>Me</u>), 23.6 (CH<u>Me</u>Me), 14.9 ($OCH_2\underline{C}H_3$) ppm. $^{11}B\{^1H\}$ NMR (C_6D_6, 128.4 MHz): δ 25.0 ppm. IR (NaCl plates, Nujol mull, cm^{-1}): 3272 (w, N–H), 3126 (w), 2707 (w), 2359 (w), 2331 (w), 1940 (w), 1873 (w), 1816 (w), 1723 (s), 1620 (s), 1462 (m), 1263 (m), 1201 (w), 1139 (w), 1060 (w), 1004 (s), 970 (s), 934 (w), 895 (m), 802 (s), 765 (w), 751 (s), 698 (m), 656 (s). Anal. found (calcd. for $C_{40}H_{54}BN_3O_2Zr$): C, 67.48 (67.58); H, 7.80 (7.66); N, 5.85 (5.91)%.

NMR tube scale synthesis of $Cp_2Zr\{NB(NAr'CH)_2\}\{OC(CH_2)OMe\}$ (55). To a C_6D_6 solution (0.6 mL) of $Cp_2Zr\{NB(NAr'CH)_2\}(py)$ (**11**, 0.0160 g, 0.0228 mmol) in an NMR tube equipped with a J. Youngs valve was added $MeCO_2Me$ (2.0 µL, 0.0251 mmol) *via* microsyringe. On standing for 10 h at RT, the ^{1}H NMR spectroscopy indicated the formation of major product $Cp_2Zr\{NB(NAr'CH)_2\}\{OC(CH_2)OMe\}$ (**55**) which was subsquently characterised by ^{1}H, ^{13}C and ^{11}B spectroscopy at RT.

^{1}H NMR (C_6D_6, 400.1 MHz): δ 7.23 (6 H, s, *m*- and *p*-$C_6\underline{H}_3{}^i Pr_2$), 6.16 (2 H, s, NCH), 5.69 (10 H, s, C_5H_5), 5.22 (1 H, s, NH), 3.50 (4 H, sept., ^3J = 6.9 Hz, C<u>H</u>MeMe), 3.23 (3 H, s, OCH_3), 2,98 (2 H, s, C(O)=C$\underline{H}_2$), 1.40 (12 H, d, ^3J = 6.9 Hz, CH<u>Me</u>Me), 1.23 (12 H, d, ^3J = 6.9 Hz, CHMe<u>Me</u>) ppm. $^{13}C\{^1H\}$ NMR (C_6D_6, 100.6 MHz): δ 169.8 (<u>C</u>(O)=CH_2), 147.1 (*o*-$\underline{C}_6H_3{}^i Pr_2$), 140.1 (*i*-$\underline{C}_6H_3{}^i Pr_2$), 127.6 (*m*-$\underline{C}_6H_3{}^i Pr_2$), 124.2 (*p*-$\underline{C}_6H_3{}^i Pr_2$), 117.4

(NCH), 112.4 (C_5H_5), 54.9 (C(O)=$\underline{C}H_2$), 53.1 (O$\underline{Me}$), 28.8 ($\underline{C}$HMeMe), 25.6 (CHMe$\underline{Me}$), 23.5 (CH$\underline{Me}$Me) ppm. $^{11}B\{^1H\}$ NMR (C_6D_6, 128.4 MHz): δ 25.1 ppm.

$Cp_2Zr\{NHB(NAr'CH)_2\}\{OC(CH_2)CH_2CO_2Me\}$ (56) and $Cp_2Zr\{NHB(NAr'CH)_2\}(OMe)$ (57). To a solution of $Cp_2Zr\{NB(NAr'CH)_2\}(py)$ (**11**, 0.300 g, 0.427 mmol) in benzene (15 mL) was added $MeCO_2Me$ (35.6 μL, 0.449 mmol) at RT. The reaction mixture was stirred at 60 °C for 16 h, after which the volatiles were removed under reduced pressure yielding **56** and **57** in *ca.* 1:1 ratio. The crude products redissolved in hexane (15 mL) and cooled to 4 °C, resulting in pale yellow, diffraction-quality crystals of **56**. Yield: 0.073 g (23%). Compound **57** was subsequently characterised by ^1H, ^{11}B and ^{13}C NMR spectroscopy.

*Data for $Cp_2Zr\{NHB(NAr'CH)_2\}\{OC(CH_2)CH_2CO_2Me\}$ (**56**).* ^1H NMR (C_6D_6, 400.1 MHz): δ 7.22 (6 H, s, *m*- and *p*-$C_6\underline{H}_3{}^iPr_2$), 6.15 (2 H, s, NCH), 5.72 (10 H, s, C_5H_5), 4.88 (1 H, s, NH), 3.93 (1 H, s, C(O)=C$\underline{H}$H), 3.70 (1 H, s, C(O)=CH$\underline{H}$), 3.49 (4 H, sept., ^3J = 6.9 Hz, C$\underline{H}$MeMe), 3.38 (3 H, s, OCH_3), 2.82 (2 H, s, C(O)C$\underline{H}_2$C(O)), 1.38 (12 H, d, ^3J = 6.9 Hz, CH$\underline{Me}$Me), 1.25 (12 H, d, ^3J = 6.9 Hz, CHMe$\underline{Me}$) ppm. $^{13}C\{^1H\}$ NMR (C_6D_6, 100.6 MHz): δ 170.8 ($\underline{C}O_2Me$), 161.8 ($\underline{C}$(O)=CH_2), 147.1 (*o*-$\underline{C}_6H_3{}^iPr_2$), 140.2 (*i*-$\underline{C}_6H_3{}^iPr_2$), 127.5 (*m*-$\underline{C}_6H_3{}^iPr_2$), 124.2 (*p*-$\underline{C}_6H_3{}^iPr_2$), 117.4 (NCH), 112.2 ($C_5H_5$), 88.8 (C(O)=$\underline{C}H_2$), 51.2 (OMe), 42.9 (C(O)$\underline{C}H_2$C(O)), 28.8 ($\underline{C}$HMeMe), 25.6 (CHMe$\underline{Me}$), 23.6 (CH$\underline{Me}$Me) ppm. $^{11}B\{^1H\}$ NMR (C_6D_6, 128.4 MHz): δ 25.2 ppm. IR (NaCl plates, Nujol mull, cm^{-1}): 3275 (w, N–H), 3098 (w), 2784 (w), 2737 (w), 2271 (w), 1939 (w), 1879 (w), 1809 (w), 1736 (s), 1622 (s), 1549 (w), 1264 (w), 1230 (w), 1195 (w), 1173 (w), 1131 (m), 1059 (m), 1014 (s), 964 (m), 932 (m), 894 (w), 802 (s), 748 (s), 713 (m), 644 (s). EI-MS: *m/z* = 737 $[M]^+$ (5%). Anal. found (calcd. for $C_{41}H_{54}BN_3O_3Zr$): C, 66.68 (66.64); H, 7.46 (7.37); N, 5.62 (5.69)%.

*Data for $Cp_2Zr\{NHB(NAr'CH)_2\}(OMe)$(**57**).* ^1H NMR (C_6D_6, 400.1 MHz): δ 7.24 (6 H, s, *m*- and *p*-$C_6\underline{H}_3{}^iPr_2$), 6.00 (2 H, s, NCH), 5.61 (10 H, s, C_5H_5), 4.17 (1 H, s, NH), 3.55 (4 H, sept., ^3J = 6.9 Hz, C$\underline{H}$MeMe), 3.45 (3 H, s, OCH_3), 1.42 (12 H, d, ^3J = 6.9 Hz, CH$\underline{Me}$Me), 1.25 (12 H, d, ^3J = 6.9 Hz, CHMe$\underline{Me}$) ppm. $^{13}C\{^1H\}$ NMR (C_6D_6, 100.6 MHz): δ 147.2 (*o*-$\underline{C}_6H_3{}^iPr_2$), 140.4 (*i*-$\underline{C}_6H_3{}^iPr_2$), 127.2 (*m*-$\underline{C}_6H_3{}^iPr_2$), 124.0 (*p*-$\underline{C}_6H_3{}^iPr_2$), 117.3 (NCH), 111.5 ($C_5H_5$), 61.5 (OMe), 28.7 ($\underline{C}$HMeMe), 25.6 (CHMe$\underline{Me}$), 23.5 (CH$\underline{Me}$Me) ppm. $^{11}B\{^1H\}$ NMR (C_6D_6, 128.4 MHz): δ 25.1 ppm.

Alternative synthesis of $Cp_2Zr\{NHB(NAr'CH)_2\}(OMe)$ (57). To a solution of $Cp_2Zr\{NB(NAr'CH)_2\}(py)$ (**11**, 0.240 g, 0.342 mmol) in toluene (15 mL) was added MeOH (14.5 µL, 0.359 mmol) at 0 °C. The reaction mixture was stirred at RT for 1 h, after which the volatiles were removed under reduced pressure. ^{1}H NMR spectroscopy indicated that $Cp_2Zr\{NHB(NAr'CH)_2\}(OMe)$ (**57**) had formed quantitatively, along with $H_2NB(Ar'CH)_2$ (*ca.* 30%) and was subsequently characterised by ^{1}H, ^{13}C and ^{11}B NMR spectroscopy showing signals consistent with **57** found above.

NMR tube scale synthesis of $Cp_2Zr\{NHB(NAr'CH)_2\}\{OC(CH_2)CH_2CO_2Et\}$ (58) and $Cp_2Zr\{NHB(NAr'CH)_2\}(OEt)$ (59). To a C_6D_6 solution (0.6 mL) of $Cp_2Zr\{NB(NAr'CH)_2\}(py)$ (**11**, 0.008 g, 0.0114 mmol) in an NMR tube equipped with a J. Youngs valve was added $MeCO_2Et$ (1.2 µL, 0.0125 mmol) *via* microsyringe at RT. After 16 h at 60 °C, the volatiles were removed under reduced pressure and the resultant mixture dried *in vacuo* before being redissolved in C_6D_6 (0.6 mL). ^{1}H NMR spectroscopy indicated that $Cp_2Zr\{NHB(NAr'CH)_2\}\{OC(CH_2)CH_2CO_2Et\}$ (**58**) and $Cp_2Zr\{NHB(NAr'CH)_2\}(OEt)$ (**59**) formed in *ca.* 1:1 ratio. Compounds **58** and **59** were subsequently characterised by ^{1}H, ^{13}C and ^{11}B spectroscopy at RT. Compound **59** shows signals consistent with those isolated.

*Data for $Cp_2Zr\{NHB(NAr'CH)_2\}\{OC(CH_2)CH_2CO_2Et\}$ (**58**).* ^{1}H NMR (C_6D_6, 400.1 MHz): δ 7.24 (6 H, s, *m*- and *p*-$C_6\underline{H}_3{}^i Pr_2$), 6.19 (2 H, s, NCH), 5.73 (10 H, s, C_5H_5), 4.89 (1 H, s, NH), 4.00 (2 H, q, ^3J = 7.2 Hz, $OC\underline{H}_2CH_3$), 3.95 (1 H, s, C(O)=C$\underline{H}$H), 3.72 (1 H, s, C(O)=CH$\underline{H}$), 3.45 (4 H, sept., ^3J = 6.9 Hz, C$\underline{H}$MeMe), 2.84 (2 H, s, C(O)C$\underline{H}_2$C(O)), 1.38 (12 H, d, ^3J = 6.9 Hz, CH$\underline{Me}$Me), 1.25 (12 H, d, ^3J = 6.9 Hz, CHMe$\underline{Me}$), 1.02 (3 H, t, ^3J = 7.2 Hz, $OCH_2C\underline{H}_3$) ppm. ^{13}C{^{1}H} NMR (C_6D_6, 100.6 MHz): δ 170.4 ($\underline{C}O_2Et$), 161.9 ($\underline{C}$(O)=CH_2), 147.1 (*o*-$\underline{C}_6H_3{}^i Pr_2$), 140.2 (*i*-$\underline{C}_6H_3{}^i Pr_2$), 127.5 (*m*-$\underline{C}_6H_3{}^i Pr_2$), 124.2 (*p*-$\underline{C}_6H_3{}^i Pr_2$), 117.4 (NCH), 112.2 ($C_5H_5$), 88.7 (C(O)=$\underline{C}H_2$), 60.3 ($O\underline{C}H_2CH_3$), 43.2 (C(O)$\underline{C}H_2$C(O)), 28.8 ($\underline{C}$HMeMe), 25.6 (CHMe$\underline{Me}$), 23.6 (CH$\underline{Me}$Me), 14.3 ($OCH_2\underline{C}H_3$) ppm. ^{11}B{^{1}H} NMR (C_6D_6, 128.4 MHz): δ 25.1 ppm.

Alternative synthesis of $Cp_2Zr\{NHB(NAr'CH)_2\}(OEt)$ (59). To a solution of $Cp_2Zr\{NB(NAr'CH)_2\}(py)$ (**11**, 0.280 g, 0.399 mmol) in toluene (15 mL) was added EtOH (23.5 µL, 0.399 mmol) at 0 °C. The reaction mixture was stirred at RT for 1 h, after which the volatiles were removed under reduced pressure, and the crude product

dissolved in hexane (10 mL) and cooled to 4 °C, resulting in pale yellow, diffraction-quality crystals of **59**. Yield: 0.117 g (44%).

^{1}H NMR (C_6D_6, 400.1 MHz): δ 7.24 (6 H, s, *m*- and *p*-$C_6\underline{H}_3{}^i Pr_2$), 6.16 (2 H, s, NCH), 5.63 (10 H, s, C_5H_5), 4.03 (1 H, s, NH), 3.61 (2 H, q, ^3J = 7.2 Hz, OC$\underline{H}_2$CH$_3$), 3.55 (4 H, sept., ^3J = 6.9 Hz, C$\underline{H}$MeMe), 1.40 (12 H, d, ^3J = 6.9 Hz, CH$\underline{Me}$Me), 1.26 (12 H, d, ^3J = 6.9 Hz, CHMe$\underline{Me}$), 0.92 (3 H, t, ^3J = 7.2 Hz, OCH$_2$C$\underline{H}_3$) ppm. ^{13}C{^{1}H} NMR (C_6D_6, 100.6 MHz): δ 147.2 (*o*-$\underline{C}_6H_3{}^i Pr_2$), 140.4 (*i*-$\underline{C}_6H_3{}^i Pr_2$), 127.2 (*m*-$\underline{C}_6H_3{}^i Pr_2$), 123.9 (*p*-$\underline{C}_6H_3{}^i Pr_2$), 117.3 (NCH), 111.5 ($C_5H_5$), 68.7 (O$\underline{C}H_2CH_3$), 28.7 ($\underline{C}$HMeMe), 25.6 (CHMe$\underline{Me}$), 23.6 (CH$\underline{Me}$Me), 19.7 (OCH$_2\underline{C}H_3$) ppm. ^{11}B{^{1}H} NMR (C_6D_6, 128.4 MHz): δ 25.2 ppm. IR (NaCl plates, Nujol mull, cm^{-1}): 3322 (w, N–H), 3103 (w), 2727 (w), 1932 (w), 1869 (w), 1809 (w), 1708 (w), 1565 (w), 1274 (m), 1249 (m), 1112 (s), 1059 (m), 1011 (m), 964 (w), 903 (m), 793 (s), 748 (s), 704 (w), 647 (s). Anal. found (calcd. for $C_{38}H_{52}BN_3OZr$): C, 67.90 (68.24); H, 7.61 (7.84); N, 6.37 (6.28)%.

Kinetic measurements for the conversion of Cp$_2$Zr{NHB(NAr'CH)$_2$}{OC(CH$_2$)OEt} (54) to Cp$_2$Zr{NHB(NAr'CH)$_2$}{OC(CH$_2$)CH$_2$CO$_2$Et} (58) and Cp$_2$Zr{NHB(NAr'CH)$_2$}(OEt) (59). The general procedure is as follows. In a dry-box, a C_6D_6 solution (0.6 mL) of Cp$_2$Zr{NHB(NAr'CH)$_2$}{OC(CH$_2$)OEt} (**54**, 0.0100 g, 0.0141 mmol) was transferred to an NMR tube fitted with a J. Youngs valve. A blank C_6D_6 sample was added to the NMR probe at RT, locked and shimmed, and the probe heated to the relevant temperature (328, 331, 334, 337, 340 K). After thermal equilibration, the experimental sample replaced the blank sample and an array was set up to record a ^{1}H NMR spectrum (4 scans) every 150 s. The decay of **54**, and the formation of **58** and **59** were calculated by measuring the integral of C_5H_5. First order rate constants were obtained from linear plots of –ln([**54**]/[**54**]$_0$) *vs* time.

Cp$_2$Zr{NHB(NAr'CH)$_2$}{OC(CH$_2$)SMe} (60). To a solution of Cp$_2$Zr{NB(NAr'CH)$_2$}(py) (**11**, 0.260 g, 0.370 mmol) in benzene (15 mL) was added MeC(O)SMe (40.0 μL, 0.444 mmol) at RT. The reaction mixture was stirred at RT for 15 h, after which the volatiles were removed under reduced pressure, and the crude product dissolved in hexane (8 mL) and cooled to –30 °C, resulting in pale red, diffraction-quality crystals of **60**. Yield: 0.190 g (72%).

^{1}H NMR (C_6D_6, 400.1 MHz): δ 7.23 (6 H, s, *m*- and *p*-$C_6\underline{H}_3{}^i Pr_2$), 6.15 (2 H, s, NCH), 5.71 (10 H, s, C_5H_5), 5.13 (1 H, s, NH), 3.96 (1 H, s, C(O)=C$\underline{H}$H), 3.88 (1 H, s, C(O)=CH$\underline{H}$),

3.49 (4 H, sept., ^{3}J = 6.9 Hz, C<u>H</u>MeMe), 1.93 (3 H, s, SCH_3), 1.40 (12 H, d, ^{3}J = 6.9 Hz, CH<u>Me</u>Me), 1.24 (12 H, d, ^{3}J = 6.9 Hz, CHMe<u>Me</u>) ppm. $^{13}C\{^{1}H\}$ NMR (C_6D_6, 100.6 MHz): δ 165.3 (<u>C</u>(O)=CH_2), 147.0 (*o*-<u>C</u>$_6H_3{}^{i}Pr_2$), 140.1 (*i*-<u>C</u>$_6H_3{}^{i}Pr_2$), 127.6 (*m*-<u>C</u>$_6H_3{}^{i}Pr_2$), 124.2 (*p*-<u>C</u>$_6H_3{}^{i}Pr_2$), 117.4 (NCH), 112.4 (C_5H_5), 82.3 (C(O)=<u>C</u>H_2), 28.8 (<u>C</u>HMeMe), 25.6 (CHMe<u>Me</u>), 23.6 (CH<u>Me</u>Me), 15.1 (S<u>Me</u>) ppm. $^{11}B\{^{1}H\}$ NMR (C_6D_6, 128.4 MHz): δ 25.3 ppm. IR (NaCl plates, Nujol mull, cm^{-1}): 3294 (w, N–H), 2720 (w), 2286 (w), 1932 (w), 1872 (w), 1691 (w), 1591 (s), 1274 (m), 1255 (m), 1188 (s), 1140 (w), 1116 (w), 1059 (w), 1011 (s), 970 (m), 932 (m), 888 (m), 793 (s), 748 (s), 710 (m), 679 (s), 644 (m). Anal. found (calcd. for $C_{39}H_{52}BN_3OSZr$): C, 65.64 (65.70); H, 7.45 (7.35); N, 5.91 (5.89)%.

$Cp_2Zr\{NHB(NAr'CH)_2\}\{OC(CH_2)SEt\}$ (61). To a solution of $Cp_2Zr\{NB(NAr'CH)_2\}(py)$ (**11**, 0.330 g, 0.470 mmol) in benzene (15 mL) was added MeC(O)SEt (60.0 μL, 0.564 mmol) at RT. The reaction mixture was stirred at RT for 43 h, after which the volatiles were removed under reduced pressure, and the crude product extracted into hexane (20 mL), and dried *in vacuo*, yielding **61** as a pale yellow solid. Yield: 0.256 g (75%).

^{1}H NMR (C_6D_6, 400.1 MHz): δ 7.23 (6 H, s, *m*- and *p*-$C_6\underline{H}_3{}^{i}Pr_2$), 6.15 (2 H, s, NCH), 5.72 (10 H, s, C_5H_5), 5.08 (1 H, s, NH), 4.03 (1 H, s, C(O)=C<u>H</u>H), 3.97 (1 H, s, C(O)=CH<u>H</u>), 3.49 (4 H, sept., ^{3}J = 6.9 Hz, C<u>H</u>MeMe), 2.47 (2 H, q, ^{3}J = 7.5 Hz, $SC\underline{H}_2CH_3$), 1.40 (12 H, d, ^{3}J = 6.9 Hz, CH<u>Me</u>Me), 1.23 (12 H, d, ^{3}J = 6.9 Hz, CHMe<u>Me</u>), 1.17 (3 H, t, ^{3}J = 7.5 Hz, $SCH_2C\underline{H}_3$) ppm. $^{13}C\{^{1}H\}$ NMR (C_6D_6, 100.6 MHz): δ 163.4 (<u>C</u>(O)=CH_2), 147.0 (*o*-<u>C</u>$_6H_3{}^{i}Pr_2$), 140.1 (*i*-<u>C</u>$_6H_3{}^{i}Pr_2$), 127.6 (*m*-<u>C</u>$_6H_3{}^{i}Pr_2$), 124.2 (*p*-<u>C</u>$_6H_3{}^{i}Pr_2$), 117.4 (NCH), 112.4 (C_5H_5), 84.6 (C(O)=<u>C</u>H_2), 28.8 (<u>C</u>HMeMe), 26.0 ($S\underline{C}H_2CH_3$), 25.6 (CHMe<u>Me</u>), 23.6 (CH<u>Me</u>Me), 14.6 ($SCH_2\underline{C}H_3$) ppm. $^{11}B\{^{1}H\}$ NMR (C_6D_6, 128.4 MHz): δ 25.1 ppm. IR (NaCl plates, Nujol mull, cm^{-1}): 3269 (w, N–H), 2724 (w), 2357 (w), 1951 (w), 1882 (w), 1812 (w), 1717 (w), 1657 (w), 1591 (s), 1559 (m), 1261 (m), 1185 (s), 1138 (w), 1109 (m), 1059 (w), 1017 (s), 960 (m), 938 (m), 891 (m), 812 (s), 748 (s), 704 (w), 656 (s). Anal. found (calcd. for $C_{40}H_{54}BN_3OSZr$): C, 65.95 (66.09); H, 7.61 (7.49); N, 5.92 (5.78)%.

NMR tube scale synthesis of $Cp_2Zr\{NHB(NAr'CH)_2\}\{OC(CH_2)CH_2C(O)SMe\}$ (62) and $Cp_2Zr\{NHB(NAr'CH)_2\}(SMe)$ (63). To an NMR tube equipped with a J. Youngs valve was added a C_6D_6 solution (0.6 mL) of $Cp_2Zr\{NB(NAr'CH)_2\}(OC(CH_2)SMe)$ (**60**,

0.010 g, 0.0140 mmol), and the tube heated to 60 °C for 23h. The volatiles were removed under reduced pressure and the resultant mixture dried *in vacuo* before being redissolved in C_6D_6 (0.6 mL). ^{1}H NMR spectroscopy indicated that $Cp_2Zr\{NHB(NAr'CH)_2\}\{OC(CH_2)CH_2C(O)SMe\}$ (**62**) and $Cp_2Zr\{NHB(NAr'CH)_2\}(SMe)$ (**63**) formed in *ca.* 1:1 ratio. Compound **62** and **63** were subsequently characterised by ^{1}H, ^{13}C and ^{11}B spectroscopy at RT.

*Data for $Cp_2Zr\{NHB(NAr'CH)_2\}\{OC(CH_2)CH_2C(O)SMe\}$ (**62**).* ^{1}H NMR (C_6D_6, 400.1 MHz): δ 7.23 (6 H, s, *m*- and *p*-$C_6\underline{H}_3{}^i Pr_2$), 6.15 (2 H, s, NCH), 5.72 (10 H, s, C_5H_5), 4.88 (1 H, s, NH), 3.95 (1 H, s, C(O)=C$\underline{H}$H), 3.70 (1 H, s, C(O)=CH$\underline{H}$), 3.49 (4 H, sept., ^3J = 6.9 Hz, C$\underline{H}$MeMe), 3.02 (2 H, s, C(O)C$\underline{H}_2$C(O)), 2.02 (3 H, s, SCH_3), 1.37 (12 H, d, ^3J = 6.9 Hz, CH$\underline{Me}$Me), 1.24 (12 H, d, ^3J = 6.9 Hz, CHMe$\underline{Me}$) ppm. ^{13}C{^{1}H} NMR (C_6D_6, 100.6 MHz): δ 195.8 (C(O)SMe), 161.6 ($\underline{C}$(O)=CH_2), 147.0 (*o*-$\underline{C}_6H_3{}^i Pr_2$), 140.2 (*i*-$\underline{C}_6H_3{}^i Pr_2$), 127.5 (*m*-$\underline{C}_6H_3{}^i Pr_2$), 124.2 (*p*-$\underline{C}_6H_3{}^i Pr_2$), 117.4 (NCH), 112.2 ($C_5H_5$), 89.7 (C(O)=$\underline{C}H_2$), 52.2 (C(O)$\underline{C}H_2$C(O)), 28.8 ($\underline{C}$HMeMe), 25.6 (CHMe$\underline{Me}$), 23.6 (CH$\underline{Me}$Me), 11.6 (SMe) ppm. ^{11}B{^{1}H} NMR (C_6D_6, 128.4 MHz): δ 25.1 ppm.

*Data for $Cp_2Zr\{NHB(NAr'CH)_2\}(SMe)$ (**63**).* ^{1}H NMR (C_6D_6, 400.1 MHz): δ 7.23 (6 H, s, *m*- and *p*-$C_6\underline{H}_3{}^i Pr_2$), 6.14 (2 H, s, NCH), 5.51 (10 H, s, C_5H_5), 5.23 (1 H, s, NH), 3.41 (4 H, sept., ^3J = 6.9 Hz, C$\underline{H}$MeMe), 2.31 (3 H, s, SCH_3), 1.39 (12 H, d, ^3J = 6.9 Hz, CH$\underline{Me}$Me), 1.20 (12 H, d, ^3J = 6.9 Hz, CHMe$\underline{Me}$) ppm. ^{13}C{^{1}H} NMR (C_6D_6, 100.6 MHz): δ 146.9 (*o*-$\underline{C}_6H_3{}^i Pr_2$), 140.0 (*i*-$\underline{C}_6H_3{}^i Pr_2$), 127.5 (*m*-$\underline{C}_6H_3{}^i Pr_2$), 124.1 (*p*-$\underline{C}_6H_3{}^i Pr_2$), 117.4 (NCH), 110.7 ($C_5H_5$), 28.8 ($\underline{C}$HMeMe), 25.6 (CHMe$\underline{Me}$), 23.5 (CH$\underline{Me}$Me), 19.1 (SMe) ppm. ^{11}B{^{1}H} NMR (C_6D_6, 128.4 MHz): δ 25.2 ppm.

NMR tube scale synthesis of $Cp_2Zr\{NHB(NAr'CH)_2\}\{OC(CH_2)CH_2C(O)SEt\}$ (64) and $Cp_2Zr\{NHB(NAr'CH)_2\}(SEt)$ (65). To an NMR tube equipped with a J. Youngs valve was added a C_6D_6 solution (0.6 mL) of $Cp_2Zr\{NB(NAr'CH)_2\}(OC(CH_2)SEt)$ (**61**, 0.010 g, 0.0138 mmol), and the tube heated to 75 °C for 23h. The volatiles were removed under reduced pressure and the resultant mixture dried *in vacuo* before being redissolved in C_6D_6 (0.6 mL). ^{1}H NMR spectroscopy indicated that $Cp_2Zr\{NHB(NAr'CH)_2\}\{OC(CH_2)CH_2C(O)SEt\}$ (**64**) and $Cp_2Zr\{NHB(NAr'CH)_2\}(SEt)$ (**65**) formed in *ca.* 1:1 ratio. Compound **64** and **65** were subsequently characterised by ^{1}H, ^{13}C and ^{11}B spectroscopy at RT. Compound **65** shows signals consistent with those isolated below.

*Data for $Cp_2Zr\{NHB(NAr'CH)_2\}\{OC(CH_2)CH_2C(O)SEt\}$ (**64**).* ^{1}H NMR (C_6D_6, 400.1 MHz): δ 7.22 (6 H, s, *m*- and *p*-$C_6\underline{H}_3{}^i Pr_2$), 6.15 (2 H, s, NCH), 5.73 (10 H, s, C_5H_5), 4.89 (1 H, s, NH), 3.96 (1 H, s, C(O)=C$\underline{H}$H), 3.72 (1 H, s, C(O)=CH$\underline{H}$), 3.49 (4 H, sept., ^3J = 6.9 Hz, C$\underline{H}$MeMe), 3.02 (2 H, s, C(O)C$\underline{H}_2$C(O)), 2.72 (2 H, q, ^3J = 7.5 Hz, SC$\underline{H}_2$CH$_3$), 1.37 (12 H, d, ^3J = 6.9 Hz, CH$\underline{Me}$Me), 1.25 (12 H, d, ^3J = 6.9 Hz, CHMe$\underline{Me}$), 1.07 (3 H, t, ^3J = 7.5 Hz, SCH$_2$C$\underline{H}_3$) ppm. ^{13}C{^{1}H} NMR (C_6D_6, 100.6 MHz): δ 195.6 (C(O)SEt), 161.6 (C(O)=CH$_2$), 147.0 (*o*-$C_6H_3{}^i Pr_2$), 140.2 (*i*-$C_6H_3{}^i Pr_2$), 127.5 (*m*-$C_6H_3{}^i Pr_2$), 124.2 (*p*-$C_6H_3{}^i Pr_2$), 117.4 (NCH), 112.2 (C_5H_5), 89.8 (C(O)=CH$_2$), 52.5 (C(O)CH$_2$C(O)), 28.9 (CHMeMe), 25.6 (CHMeMe), 23.5 (SCH$_2$CH$_3$), 23.6 (CHMeMe), 15.1 (SCH$_2$CH$_3$) ppm. ^{11}B{^{1}H} NMR (C_6D_6, 128.4 MHz): δ 25.1 ppm.

Alternative synthesis of $Cp_2Zr\{NHB(NAr'CH)_2\}(SEt)$ (65). To a solution of $Cp_2Zr\{NHB(NAr'CH)_2\}(Cl)$ (**16**, 0.300 g, 0.455 mmol) in THF (15 mL) was added NaSEt (0.047 g, 0.910 mmol) at RT. The reaction mixture was stirred at RT for 16 h, after which the volatiles were removed under reduced pressure, and the crude product dissolved in hexane (10 mL) and cooled to 4 °C, resulting in pale yellow, diffraction-quality crystals of **65**. Yield: 0.196 g (63%).

^{1}H NMR (C_6D_6, 400.1 MHz): δ 7.22 (6 H, s, *m*- and *p*-$C_6\underline{H}_3{}^i Pr_2$), 6.13 (2 H, s, NCH), 5.53 (10 H, s, C_5H_5), 5.03 (1 H, s, NH), 3.41 (4 H, sept., ^3J = 6.9 Hz, C$\underline{H}$MeMe), 2.64 (2 H, q, ^3J = 7.2 Hz, SC$\underline{H}_2$CH$_3$), 1.42 (3 H, t, ^3J = 7.2 Hz, SCH$_2$C$\underline{H}_3$), 1.39 (12 H, d, ^3J = 6.9 Hz, CH$\underline{Me}$Me), 1.22 (12 H, d, ^3J = 6.9 Hz, CHMe$\underline{Me}$) ppm. ^{13}C{^{1}H} NMR (C_6D_6, 100.6 MHz): δ 146.9 (*o*-$C_6H_3{}^i Pr_2$), 140.0 (*i*-$C_6H_3{}^i Pr_2$), 127.5 (*m*-$C_6H_3{}^i Pr_2$), 124.1 (*p*-$C_6H_3{}^i Pr_2$), 117.5 (NCH), 110.7 (C_5H_5), 30.1 (SCH$_2$CH$_3$), 28.8 (CHMeMe), 25.7 (CHMeMe), 23.5 (CH$\underline{Me}$Me), 20.3 (SCH$_2$CH$_3$) ppm. ^{11}B{^{1}H} NMR (C_6D_6, 128.4 MHz): δ 25.0 ppm. IR (NaCl plates, Nujol mull, cm^{-1}): 3291 (w, N–H), 2715 (w), 2363 (w), 2331 (w), 1942 (w), 1584 (w), 1252 (w), 1192 (w), 1147 (w), 1103 (w), 1060 (w), 1024 (m), 964 (m), 935 (w), 897 (m), 818 (w), 789 (s), 767 (m), 745 (s), 655 (s). Anal. found (calcd. for $C_{38}H_{52}BN_3SZr$): C, 66.50 (66.35); H, 7.70 (7.57); N, 6.07 (5.95)%.

Kinetic measurements for the conversion of $Cp_2Zr\{NHB(NAr'CH)_2\}\{OC(CH_2)SEt\}$ (61) to $Cp_2Zr\{NHB(NAr'CH)_2\}\{OC(CH_2)CH_2C(O)SEt\}$ (64) and $Cp_2Zr\{NHB(NAr'CH)_2\}(SEt)$ (65). In a dry-box, a C_6D_6 solution (0.6 mL) of $Cp_2Zr\{NHB(NAr'CH)_2\}\{OC(CH_2)SEt\}$ (**61**, 0.0100 g, 0.0138 mmol) was transferred to an NMR tube fitted with a J. Youngs valve. A blank C_6D_6 sample was added to the NMR

probe at RT, locked and shimmed, and the probe heated to the relevant temperature 340 K. After thermal equilibration, the experimental sample replaced the blank sample and an array was set up to record a ^{1}H NMR spectrum (4 scans) every 200 s. The decay of **61** was calculated by measuring the integral of C_5H_5. Second order rate constants were obtained from linear plots of –1/[**61**] *vs* time.

$Cp_2Zr\{NHB(NAr'CH)_2\}\{OC(CH_2)NMe_2\}$ (66). To a solution of $Cp_2Zr\{NB(NAr'CH)_2\}(py)$ (**11**, 0.280 g, 0.399 mmol) in benzene (15 mL) was added $MeC(O)NMe_2$ (52.0 µL, 0.559 mmol) at RT. The reaction mixture was stirred at RT for 15 h, after which the volatiles were removed under reduced pressure, and the crude product dissolved in hexane (8 mL) and cooled to 4 °C, resulting in pale brown, diffraction-quality crystals of **66**. Yield: 0.122 g (43%).

^{1}H NMR (C_6D_6, 400.1 MHz): δ 7.22 (6 H, s, *m*- and *p*-$C_6\underline{H}_3{}^{i}Pr_2$), 6.14 (2 H, s, NCH), 5.72 (10 H, s, C_5H_5), 4.72 (1 H, s, NH), 3.53 (4 H, sept., ^{3}J = 6.9 Hz, C$\underline{H}$MeMe), 2.96 (2 H, s, C(O)=C$\underline{H}_2$), 2.42 (6 H, s, N$\underline{Me}_2$), 1.40 (12 H, d, ^{3}J = 6.9 Hz, CH$\underline{Me}$Me), 1.24 (12 H, d, ^{3}J = 6.9 Hz, CHMe$\underline{Me}$) ppm. ^{13}C{^{1}H} NMR (C_6D_6, 100.6 MHz): δ 168.1 ($\underline{C}$(O)=CH_2), 147.0 (*o*-$\underline{C}_6H_3{}^{i}Pr_2$), 140.4 (*i*-$\underline{C}_6H_3{}^{i}Pr_2$), 127.5 (*m*-$\underline{C}_6H_3{}^{i}Pr_2$), 124.2 (*p*-$\underline{C}_6H_3{}^{i}Pr_2$), 117.6 (NCH), 112.2 ($C_5H_5$), 62.1 (C(O)=$\underline{C}H_2$), 39.0 (N$\underline{Me}_2$), 28.8 ($\underline{C}$HMeMe), 25.5 (CHMe$\underline{Me}$), 23.6 (CH$\underline{Me}$Me) ppm. ^{11}B{^{1}H} NMR (C_6D_6, 128.4 MHz): δ 25.1 ppm. IR (NaCl plates, Nujol mull, cm^{-1}): 3291 (w, N–H), 2715 (w), 2360 (w), 2322 (w), 1714 (w), 1603 (s), 1274 (w), 1252 (w), 1207 (s), 1138 (w), 1055 (w), 1014 (m), 995 (m), 967(w), 939 (m), 891 (m), 799 (s), 770 (w), 755 (s), 707 (m), 656 (s), 590 (m). Anal. found (calcd. for $C_{40}H_{55}BN_4OZr$): C, 66.94 (67.67); H, 7.76 (7.81); N, 7.67 (7.89)%. Repeated attempts to obtain an elemental analysis with satisfactory % C values failed, presumably due to incomplete combustion of the compound.

NMR tube scale reaction of $Cp_2Zr\{NB(NAr'CH)_2\}(py)$ (11) with MeC(O)Cl. To a C_6D_6 solution (0.6 mL) of $Cp_2Zr\{NB(NAr'CH)_2\}(py)$ (**11**, 0.010 g, 0.0142 mmol) in an NMR tube equipped with a J. Youngs valve was added MeC(O)Cl (1.1 µL, 0.0157 mmol) *via* microsyringe. The ^{1}H NMR spectrum demonstrated conversion to $Cp_2Zr\{NHB(NAr'CH)_2\}Cl$ (**16**) after 24 h at RT, with resonances indentical to those isolated above.

$Cp_2Zr\{NHB(NAr'CH)_2\}\{OC(CHSiMe_3)CH_2CO_2{}^{i}Pr\}$ (69). To a solution of $Cp_2Zr\{NHB(NAr'CH)_2\}(OC(CH_2)O^{i}Pr)$ (**53**, 0.150 g, 0.207 mmol) in benzene (10 mL)

was added $Me_3Si(H)CCO$ (38 µL, 0.269 mmol) at RT. The reaction mixture was stirred at RT for 10 min, after which the volatiles were removed under reduced pressure yielding a yellow solid **69**. Yield: 0.137 g (79%). Diffraction-quality crystals were grown from a saturated hexane solution at 4 °C.

^{1}H NMR (C_6D_6, 400.1 MHz): δ 7.22 (6 H, s, *m*- and *p*-$C_6\underline{H}_3{}^i Pr_2$), 6.11 (2 H, s, NCH), 5.81 (10 H, s, C_5H_5), 5.10 (1 H, sept., ^3J = 6.0 Hz, OC$\underline{H}Me_2$), 4.73 (1 H, s, NH), 4.37 (1 H, s, C$\underline{H}SiMe_3$), 3.50 (4 H, sept., ^3J = 6.9 Hz, C$\underline{H}$MeMe), 2.82 (2 H, s, C(O)C$\underline{H}_2$C(O)), 1.40 (12 H, d, ^3J = 6.9 Hz, CH$\underline{Me}$Me), 1.24 (12 H, d, ^3J = 6.9 Hz, CHMe$\underline{Me}$), 1.13 (6 H, d, ^3J = 6.0 Hz, OCH$\underline{Me}_2$), 0.22 (9 H, s, $SiMe_3$) ppm. ^{13}C{^{1}H} NMR (C_6D_6, 100.6 MHz): δ 170.0 ($\underline{C}O_2Me$), 169.0 ($\underline{C}$(O)=CH($SiMe_3$)), 146.8 (*o*-$\underline{C}_6H_3{}^i Pr_2$), 140.4 (*i*-$\underline{C}_6H_3{}^i Pr_2$), 127.6 (*m*-$\underline{C}_6H_3{}^i Pr_2$), 124.2 (*p*-$\underline{C}_6H_3{}^i Pr_2$), 117.8 (NCH), 112.8 ($C_5H_5$), 93.8 (C(O)=$\underline{C}$H($SiMe_3$)), 67.4 (O$\underline{C}HMe_2$), 45.6 (C(O)$\underline{C}H_2$C(O)), 28.9 ($\underline{C}$HMeMe), 25.5 (CHMe$\underline{Me}$), 23.4 (CH$\underline{Me}$Me), 21.9 (OCH$\underline{Me}_2$), 0.6 ($SiMe_3$) ppm. ^{11}B{^{1}H} NMR (C_6D_6, 128.4 MHz): δ 25.0 ppm. IR (NaCl plates, Nujol mull, cm^{-1}): 3300 (w, N–H), 2724 (w), 2366 (w), 1929 (w), 1866 (w), 1727 (s), 1575 (s), 1321 (w), 1287 (w), 1236 (m), 1195 (w), 1147 (w), 1106 (s), 1059 (w), 1008 (m), 970 (m), 945 (w), 891 (w), 862 (w), 812 (m), 786 (m), 752 (s), 717 (m), 656 (s). EI-MS: *m/z* = 837 $[M]^+$ (1%). Anal. found (calcd. for $C_{46}H_{66}BN_3O_3SiZr$): C, 66.02 (65.84); H, 8.07 (7.93); N, 5.16 (5.01)%.

NMR tube scale reaction of $Cp_2Zr\{NHB(NAr'CH)_2\}\{OC(CH_2)OEt\}$ (54) with $Me_3Si(H)CCO$. To a C_6D_6 solution (0.6 mL) of $Cp_2Zr\{NHB(NAr'CH)_2\}\{OC(CH_2)OEt\}$ (**54**, 0.0100 g, 0.0141 mmol) in an NMR tube equipped with a J. Youngs valve was added $Me_3Si(H)CCO$ (2.0 µL, 0.0169 mmol) *via* microsyringe. The solution left at RT and the reaction monitored by ^{1}H NMR spectroscopy. The product $Cp_2Zr\{NHB(NAr'CH)_2\}\{OC(CHSiMe_3)CH_2CO_2Et\}$ (**70**) was quantitively formed immediately and subsquently characterised by ^{1}H, ^{13}C and ^{11}B spectroscopy at RT.

^{1}H NMR (C_6D_6, 400.1 MHz): δ 7.21 (6 H, s, *m*- and *p*-$C_6\underline{H}_3{}^i Pr_2$), 6.11 (2 H, s, NCH), 5.81 (10 H, s, C_5H_5), 4.74 (1 H, s, NH), 4.37 (1 H, s, C$\underline{H}SiMe_3$), 3.50 (2 H, q, ^3J = 7.0 Hz, OC$\underline{H}_2CH_3$), 3.50 (4 H, sept., ^3J = 6.9 Hz, C$\underline{H}$MeMe), 2.85 (2 H, s, C(O)C$\underline{H}_2$C(O)), 1.39 (12 H, d, ^3J = 6.9 Hz, CH$\underline{Me}$Me), 1.22 (12 H, d, ^3J = 6.9 Hz, CHMe$\underline{Me}$), 1.04 (3 H, t, ^3J = 7.0 Hz, OCH$_2$C$\underline{H}_3$), 0.22 (9 H, s, $SiMe_3$) ppm. ^{13}C{^{1}H} NMR (C_6D_6, 100.6 MHz): δ 170.4 ($\underline{C}O_2Et$), 169.8 ($\underline{C}$(O)=CH($SiMe_3$)), 146.8 (*o*-$\underline{C}_6H_3{}^i Pr_2$), 140.4 (*i*-$\underline{C}_6H_3{}^i Pr_2$), 127.6 (*m*-$\underline{C}_6H_3{}^i Pr_2$), 124.2 (*p*-$\underline{C}_6H_3{}^i Pr_2$), 117.8 (NCH), 112.8 ($C_5H_5$), 94.0 (C(O)=$\underline{C}$H($SiMe_3$)),

60.3 (O<u>C</u>H$_2$CH$_3$), 45.4 (C(O)<u>C</u>H$_2$C(O)), 28.9 (<u>C</u>HMeMe), 25.5 (CHMe<u>Me</u>), 23.3 (CH<u>Me</u>Me), 14.3 (OCH$_2$<u>C</u>H$_3$), 0.6 (SiMe$_3$) ppm. ^{11}B{^{1}H} NMR (C$_6$D$_6$, 128.4 MHz): δ 25.2 ppm.

NMR tube scale reaction of Cp$_2$Zr{NHB(NAr'CH)$_2$}{OC(CH$_2$)SEt} (61) with Me$_3$Si(H)CCO. To a C$_6$D$_6$ solution (0.6 mL) of Cp$_2$Zr{NHB(NAr'CH)$_2$}{OC(CH$_2$)SEt} (**61**, 0.0102 g, 0.0141 mmol) in an NMR tube equipped with a J. Youngs valve was added Me$_3$Si(H)CCO (2.0 µL, 0.0169 mmol) *via* microsyringe. The solution left at RT and the reaction monitored by ^{1}H NMR spectroscopy. The product Cp$_2$Zr{NHB(NAr'CH)$_2$}{OC(CHSiMe$_3$)CH$_2$C(O)SEt} **(71)** was quantitively formed and subsquently characterised by ^{1}H, ^{13}C and ^{11}B spectroscopy at RT.

^{1}H NMR (C$_6$D$_6$, 400.1 MHz): δ 7.22 (6 H, s, *m*- and *p*-C$_6$<u>H</u>$_3$^{i}Pr$_2$), 6.12 (2 H, s, NCH), 5.83 (10 H, s, C$_5$H$_5$), 4.69 (1 H, s, NH), 4.36 (1 H, s, C<u>H</u>SiMe$_3$), 3.51 (4 H, sept., ^3J = 6.9 Hz, C<u>H</u>MeMe), 3.01 (2 H, s, C(O)C<u>H</u>$_2$C(O)), 2.72 (2 H, q, ^3J = 7.5 Hz, SC<u>H</u>$_2$CH$_3$), 1.41 (12 H, d, ^3J = 6.9 Hz, CH<u>Me</u>Me), 1.23 (12 H, d, ^3J = 6.9 Hz, CHMe<u>Me</u>), 1.06 (3 H, t, ^3J = 7.5 Hz, SCH$_2$C<u>H</u>$_3$), 0.21 (9 H, s, SiMe$_3$) ppm. ^{13}C{^{1}H} NMR (C$_6$D$_6$, 100.6 MHz): δ 195.7 (<u>C</u>(O)SEt), 168.3 (<u>C</u>(O)=CH(SiMe$_3$)), 146.8 (*o*-<u>C</u>$_6$H$_3$^{i}Pr$_2$), 140.4 (*i*-<u>C</u>$_6$H$_3$^{i}Pr$_2$), 127.7 (*m*-<u>C</u>$_6$H$_3$^{i}Pr$_2$), 124.2 (*p*-<u>C</u>$_6$H$_3$^{i}Pr$_2$), 117.9 (NCH), 112.8 (C$_5$H$_5$), 95.8 (C(O)=<u>C</u>H(SiMe$_3$)), 54.0 (C(O)<u>C</u>H$_2$C(O)), 28.9 (<u>C</u>HMeMe), 25.6 (CHMe<u>Me</u>), 23.8 (S<u>C</u>H$_2$CH$_3$), 23.4 (CH<u>Me</u>Me), 15.0 (SCH$_2$<u>C</u>H$_3$), 0.6 (SiMe$_3$) ppm. ^{11}B{^{1}H} NMR (C$_6$D$_6$, 128.4 MHz): δ 25.3 ppm.

NMR tube scale reaction of Cp$_2$Zr{NHB(NAr'CH)$_2$}{OC(CH$_2$)NMe$_2$} (66) with Me$_3$Si(H)CCO. To a C$_6$D$_6$ solution (0.6 mL) of Cp$_2$Zr{NHB(NAr'CH)$_2$}{OC(CH$_2$)NMe$_2$} (**66**, 0.0101 g, 0.0141 mmol) in an NMR tube equipped with a J. Youngs valve was added Me$_3$Si(H)CCO (2.0 µL, 0.0169 mmol) *via* microsyringe. The solution left at RT and the reaction monitored by ^{1}H NMR spectroscopy. The product Cp$_2$Zr{NHB(NAr'CH)$_2$}{OC(CHSiMe$_3$)CH$_2$C(O)NMe$_2$} **(72)** was quantitively formed immediately and subsquently characterised by ^{1}H, ^{13}C and ^{11}B spectroscopy at RT.

^{1}H NMR (C$_6$D$_6$, 400.1 MHz): δ 7.20 (6 H, s, *m*- and *p*-C$_6$<u>H</u>$_3$^{i}Pr$_2$), 6.12 (2 H, s, NCH), 5.86 (10 H, s, C$_5$H$_5$), 4.60 (1 H, s, NH), 3.96 (1 H, s, C<u>H</u>SiMe$_3$), 3.54 (4 H, sept., ^3J = 6.9 Hz, C<u>H</u>MeMe), 2.75 (3 H, s, N<u>Me</u>Me), 2.64 (2 H, s, C(O)C<u>H</u>$_2$C(O)), 2.59 (3 H, s, NMe<u>Me</u>), 1.42 (12 H, d, ^3J = 6.9 Hz, CH<u>Me</u>Me), 1.23 (12 H, d, ^3J = 6.9 Hz, CHMe<u>Me</u>), 0.22 (9 H, s, SiMe$_3$) ppm. ^{13}C{^{1}H} NMR (C$_6$D$_6$, 100.6 MHz): δ 169.9 (<u>C</u>(O)=CH(SiMe$_3$)), 169.6

(CONMe$_2$), 146.8 (*o*-C$_6$H$_3$^{i}Pr$_2$), 140.6 (*i*-C$_6$H$_3$^{i}Pr$_2$), 127.4 (*m*-C$_6$H$_3$^{i}Pr$_2$), 124.1 (*p*-C$_6$H$_3$^{i}Pr$_2$), 117.9 (NCH), 112.8 (C$_5$H$_5$), 93.5 (C(O)=CH(SiMe$_3$)), 45.1 (C(O)CH$_2$C(O)), 37.8 (NMeMe), 35.0 (NMeMe), 28.9 (CHMeMe), 25.6 (CHMeMe), 23.4 (CHMeMe), 0.8 (SiMe$_3$) ppm. ^{11}B{^{1}H} NMR (C$_6$D$_6$, 128.4 MHz): δ 25.0 ppm.

NMR tube scale reaction of Cp$_2$Zr{NHB(NAr'CH)$_2$}{OC(CH$_2$)Ph} (52) with Me$_3$Si(H)CCO. To a C$_6$D$_6$ solution (0.6 mL) of Cp$_2$Zr{NHB(NAr'CH)$_2$}{OC(CH$_2$)Ph} (**52**, 0.0105 g, 0.0141 mmol) in an NMR tube equipped with a J. Youngs valve was added Me$_3$Si(H)CCO (2.0 µL, 0.0169 mmol) *via* microsyringe. The solution left at RT and the reaction monitored by ^{1}H NMR spectroscopy. The product Cp$_2$Zr{NHB(NAr'CH)$_2$}{OC(CHSiMe$_3$)CH$_2$C(O)Ph} **(73)** was quantitively formed after 60 h, indicated by ^{1}H NMR spectroscopy and subsquently characterised by ^{1}H, ^{13}C and ^{11}B spectroscopy at RT.

^{1}H NMR (C$_6$D$_6$, 400.1 MHz): δ 8.09 (2 H, m, *o*-C$_6$H$_5$), 7.23 (1 H, m, *p*-C$_6$H$_5$), 7.22 (6 H, overlapping 2 × m, *m*- and *p*-C$_6$H$_3$^{i}Pr$_2$), 7.21 (2 H, m, *m*-C$_6$H$_5$), 6.12 (2 H, s, NCH), 5.88 (10 H, s, C$_5$H$_5$), 4.55 (1 H, s, NH), 3.96 (1 H, s, CHSiMe$_3$), 3.53 (4 H, sept., ^3J = 6.9 Hz, CHMeMe), 3.20 (2 H, s, C(O)CH$_2$C(O)), 1.41 (12 H, d, ^3J = 6.9 Hz, CHMeMe), 1.20 (12 H, d, ^3J = 6.9 Hz, CHMeMe), 0.12 (9 H, s, SiMe$_3$) ppm. ^{13}C{^{1}H} NMR (C$_6$D$_6$, 100.6 MHz): δ 196.9 (C(O)Ph), 170.3 (C(O)=CH(SiMe$_3$)), 146.7 (*o*-C$_6$H$_3$^{i}Pr$_2$), 140.4 (*i*-C$_6$H$_3$^{i}Pr$_2$), 137.8 (*i*-C$_6$H$_5$), 129.3 (*o*-C$_6$H$_5$), 128.3 (*m*-C$_6$H$_5$), 128.2 (*p*-C$_6$H$_5$), 127.6 (*m*-C$_6$H$_3$^{i}Pr$_2$), 124.2 (*p*-C$_6$H$_3$^{i}Pr$_2$), 118.0 (NCH), 112.9 (C$_5$H$_5$), 96.9 (C(O)=CH(SiMe$_3$)), 49.2 (C(O)CH$_2$C(O)), 28.9 (CHMeMe), 25.6 (CHMeMe), 23.4 (CHMeMe), 0.6 (SiMe$_3$) ppm. ^{11}B{^{1}H} NMR (C$_6$D$_6$, 128.4 MHz): δ 25.4 ppm.

Crossover reaction of Cp$_2$Zr{NHB(NAr'CH)$_2$}{OC(CH$_2$)SMe} (60) with Cp$_2$Zr{NHB(NAr'CH)$_2$}(SEt) (65). A C$_6$D$_6$ solution (0.6 mL) of Cp$_2$Zr{NHB(NAr'CH)$_2$}{OC(CH$_2$)SMe} (**60**, 0.0075 g, 0.0105 mmol) and Cp$_2$Zr{NHB(NAr'CH)$_2$}(SEt) (**65**, 0.0072 g, 0.0105 mmol) was transferred to an NMR tube fitted with a J. Youngs valve. The mixture was then heated at 67 °C for 66 h, with ^{1}H NMR integration showing the mixture to be 9.3% **64**, 13.9% **62**, 41.7% **65** and 35.2% **63**.

Cp$_2$Zr{NHB(NAr'CH)$_2$}{OCH$_2$C(=CH$_2$)CH$_3$} (74). To a solution of Cp$_2$Zr{NB(NAr'CH)$_2$}(py) (**11**, 0.250 g, 0.356 mmol) in benzene (15 mL) was added 1,2-epoxy-2-methylpropane (35.0 µL, 0.392 mmol) at RT. The reaction mixture was stirred at 50 °C for 16 h, after which the volatiles were removed under reduced pressure, and the

crude product dissolved in hexane (10 mL) and cooled to –30 °C, resulting in pale yellow, diffraction-quality crystals of **74**. Yield: 0.136 g (55%).

^{1}H NMR (C_6D_6, 400.1 MHz): δ 7.23 (6 H, s, *m*- and *p*-$C_6\underline{H}_3{}^{i}Pr_2$), 6.16 (2 H, s, NCH), 5.66 (10 H, s, C_5H_5), 4.89 (1 H, s, C=C$\underline{H}$H), 4.81 (1 H, s, C=CH$\underline{H}$), 4.22 (1 H, s, NH), 4.00 (2 H, s, OCH_2), 3.53 (4 H, sept., ^{3}J = 6.9 Hz, C$\underline{H}$MeMe), 1.57 (3 H, s, C(=CH_2)C$\underline{H}_3$), 1.40 (12 H, d, ^{3}J = 6.9 Hz, CH$\underline{Me}$Me), 1.26 (12 H, d, ^{3}J = 6.9 Hz, CHMe$\underline{Me}$) ppm. ^{13}C{^{1}H} NMR (C_6D_6, 100.6 MHz): δ 147.2 (*o*-$\underline{C}_6H_3{}^{i}Pr_2$), 146.8 ($\underline{C}$(=$CH_2$)$CH_3$), 140.4 (*i*-$\underline{C}_6H_3{}^{i}Pr_2$), 127.3 (*m*-$\underline{C}_6H_3{}^{i}Pr_2$), 124.0 (*p*-$\underline{C}_6H_3{}^{i}Pr_2$), 117.4 (NCH), 111.7 ($C_5H_5$), 108.5 (C(=$\underline{C}H_2$)$CH_3$), 77.2 (O$\underline{C}H_2$), 28.8 ($\underline{C}$HMeMe), 25.7 (CHMe$\underline{Me}$), 23.6 (CH$\underline{Me}$Me), 19.2 (C(=$CH_2$)$\underline{C}H_3$) ppm. ^{11}B{^{1}H} NMR (C_6D_6, 128.4 MHz): δ 25.3 ppm. IR (NaCl plates, Nujol mull, cm^{-1}): 3299 (w, N–H), 2686 (w), 2357 (w), 2335 (w), 1936 (w), 1869 (w), 1799 (w), 1657 (w), 1565 (w), 1286 (m), 1255 (m), 1141 (s), 1112 (w), 1071 (s), 960 (m), 926 (w), 897 (s), 828 (s), 755 (s), 653 (s). EI-MS: *m/z* = 693 $[M]^+$ (1%). Anal. found (calcd. for $C_{40}H_{54}BN_3OZr$): C, 69.26 (69.14); H, 7.91 (7.83); N, 6.04 (6.05)%.

$Cp_2Zr\{NHB(NAr'CH)_2\}\{OCH_2CH{=}CH_2\}$ (75). To a solution of $Cp_2Zr\{NB(NAr'CH)_2\}$(py) (**11**, 0.150 g, 0.214 mmol) in benzene (15 mL) was added propylene oxide (15.0 µL, 0.214 mmol) at RT. The reaction mixture was stirred at 50 °C for 16 h, after which the volatiles were removed under reduced pressure yielding a red solid **75**. Yield: 0.103 g (71%).

^{1}H NMR (C_6D_6, 400.1 MHz): δ 7.23 (6 H, s, *m*- and *p*-$C_6\underline{H}_3{}^{i}Pr_2$), 6.16 (2 H, s, NCH), 5.77 (1 H, tdd, ^{3}J = 2.0, 6.0, 17.2 Hz, $OCH_2C\underline{H}$=CHH), 5.64 (10 H, s, C_5H_5), 5.09 (1 H, dd, ^{2}J = 2.0, ^{3}J = 17.2 Hz, OCH_2CH=C$\underline{H}$H), 5.00 (1 H, dd, ^{2}J = 2.0, ^{3}J = 10.0 Hz, OCH_2CH=CH$\underline{H}$), 4.22 (1 H, s, NH), 4.11 (2 H, m, O$\underline{C}H_2$CH=CHH), 3.53 (4 H, sept., ^{3}J = 6.9 Hz, C$\underline{H}$MeMe), 1.40 (12 H, d, ^{3}J = 6.9 Hz, CH$\underline{Me}$Me), 1.25 (12 H, d, ^{3}J = 6.9 Hz, CHMe$\underline{Me}$) ppm. ^{13}C{^{1}H} NMR (C_6D_6, 100.6 MHz): δ 147.3 (*o*-$\underline{C}_6H_3{}^{i}Pr_2$), 140.4 (*i*-$\underline{C}_6H_3{}^{i}Pr_2$), 140.3 ($OCH_2\underline{C}H{=}CH_2$), 127.3 (*m*-$\underline{C}_6H_3{}^{i}Pr_2$), 124.0 (*p*-$\underline{C}_6H_3{}^{i}Pr_2$), 117.3 (NCH), 112.7 ($OCH_2CH{=}\underline{C}H_2$), 111.6 ($C_5H_5$), 74.3 (O$\underline{C}H_2$CH=$CH_2$), 28.8 ($\underline{C}$HMeMe), 25.7 (CHMe$\underline{Me}$), 23.6 (CH$\underline{Me}$Me) ppm. ^{11}B{^{1}H} NMR (C_6D_6, 128.4 MHz): δ 25.3 ppm. IR (NaCl plates, Nujol mull, cm^{-1}): 3316 (w, N–H), 2724 (w), 2366 (w), 2331 (w), 1923 (w), 1863 (w), 1799 (w), 1676 (w), 1585 (m), 1277 (m), 1236 (m), 1157 (m), 1097 (s), 1017 (s), 922 (w), 875 (w), 798 (s), 755 (s), 653 (s). EI-MS: *m/z* = 679 $[M]^+$ (1%). Satisfactory elemental analysis could not be obtained.

$Cp_2Zr\{NHB(NAr'CH)_2\}\{O\text{-cyclohex-2,3-ene}\}$ (76). To a solution of $Cp_2Zr\{NB(NAr'CH)_2\}(py)$ (**11**, 0.250 g, 0.356 mmol) in toluene (15 mL) was added cyclohexene oxide (43.3 µL, 0.427 mmol) at RT. The reaction mixture was stirred at 90 °C for 16 h, after which the volatiles were removed under reduced pressure yielding a red solid **76**. Yield: 0.169 g (66%).

^{1}H NMR (C_6D_6, 400.1 MHz): δ 7.24 (6 H, overlapping 2 × m, *m*- and *p*-$C_6\underline{H}_3{}^i Pr_2$), 6.15 (2 H, s, NCH), 5.70 (10 H, s, C_5H_5), 5.58 (1 H, m, 3-cyclohexene), 5.46 (1 H, m, 2-cyclohexene), 4.19 (1 H, m, 1-cyclohexene), 3.72 (1 H, s, NH), 3.58 (4 H, sept., ^3J = 6.9 Hz, C<u>H</u>MeMe), 1.83 (2 H, m, 4-cyclohexene), 1.56 (2 H, m, 6-cyclohexene), 1.43 (12 H, d, ^3J = 6.9 Hz, CH<u>Me</u>Me), 1.26 (12 H, d, ^3J = 6.9 Hz, CHMe<u>Me</u>), 1.20 (2 H, m, 5-cyclohexene) ppm. $^{13}C\{^1H\}$ NMR (C_6D_6, 100.6 MHz): δ 147.3 (*o*-$\underline{C}_6H_3{}^i Pr_2$), 140.7 (*i*-$\underline{C}_6H_3{}^i Pr_2$), 133.3 (2-cyclohexene), 127.2 (3-cyclohexene), 127.1 (*m*-$\underline{C}_6H_3{}^i Pr_2$), 124.0 (*p*-$\underline{C}_6H_3{}^i Pr_2$), 117.4 (NCH), 111.7 ($C_5H_5$), 75.9 (1-cyclohexene), 33.2 (6-cyclohexene), 28.8 (<u>C</u>HMeMe), 25.6 (CHMe<u>Me</u>), 25.5 (4-cyclohexene), 23.8 (CH<u>Me</u>Me), 20.4 (5-cyclohexene) ppm. $^{11}B\{^1H\}$ NMR (C_6D_6, 128.4 MHz): δ 25.5 ppm. IR (NaCl plates, Nujol mull, cm^{-1}): 3282 (w, N–H), 2718 (w), 1923 (w), 1872 (w), 1796 (w), 1644 (w), 1581 (w), 1557 (w), 1251 (m), 1138 (w), 1100 (s), 1005 (s), 967 (m), 932 (w), 884 (w), 796 (s), 748 (s), 698 (w), 644 (s), 590 (m). EI-MS: *m/z* = 719 $[M]^+$ (1%). Anal. found (calcd. for $C_{42}H_{56}BN_3OZr$): C, 69.84 (69.97); H, 7.79 (7.83); N, 5.87 (5.83)%.

$Cp_2Zr\{NHB(NAr'CH)_2\}\{OC(H)=C(H)Ph\}$ (77). To a solution of $Cp_2Zr\{NB(NAr'CH)_2\}(py)$ (**11**, 0.250 g, 0.356 mmol) in toluene (15 mL) was added styrene oxide (40.7 µL, 0.356 mmol) at RT. The reaction mixture was stirred at 90 °C for 2 h, after which the volatiles were removed under reduced pressure yielding a red solid **77**. Yield: 0.190 g (72%).

^{1}H NMR (C_6D_6, 400.1 MHz): δ 7.68 (2 H, d, ^3J = 7.6 Hz, *o*-C_6H_5), 7.31 (2 H, t, ^3J = 7.6 Hz, *m*-C_6H_5), 7.23 (6 H, overlapping 2 × m, *m*- and *p*-$C_6\underline{H}_3{}^i Pr_2$), 7.10 (1 H, t, ^3J = 7.6 Hz, *p*-C_6H_5), 6.46 (1 H, d, ^3J = 6.4 Hz, OC(<u>H</u>)=C(H)), 6.16 (2 H, s, NCH), 5.60 (10 H, s, C_5H_5), 5.32 (1 H, s, NH), 5.15 (1 H, d, ^3J = 6.4 Hz, OC(H)=C(<u>H</u>)), 3.48 (4 H, sept., ^3J = 6.9 Hz, C<u>H</u>MeMe), 1.37 (12 H, d, ^3J = 6.9 Hz, CH<u>Me</u>Me), 1.23 (12 H, d, ^3J = 6.9 Hz, CHMe<u>Me</u>) ppm. $^{13}C\{^1H\}$ NMR (C_6D_6, 100.6 MHz): δ 153.4 (O<u>C</u>(H)=C(H)), 147.0 (*o*-$\underline{C}_6H_3{}^i Pr_2$), 140.0 (*i*-$\underline{C}_6H_3{}^i Pr_2$), 138.7 (*i*-$\underline{C}_6H_5$), 128.2 (*o*-$\underline{C}_6H_5$), 127.9 (*m*-$\underline{C}_6H_5$), 127.6 (*m*-$\underline{C}_6H_3{}^i Pr_2$), 124.8 (*p*-$\underline{C}_6H_5$), 124.2 (*p*-$\underline{C}_6H_3{}^i Pr_2$), 117.4 (NCH), 112.3 ($C_5H_5$), 104.8

(OC(H)=C(H)), 28.8 (CHMeMe), 25.7 (CHMeMe), 23.5 (CHMeMe) ppm. $^{11}B\{^1H\}$ NMR (C_6D_6, 128.4 MHz): δ 25.0 ppm. IR (NaCl plates, Nujol mull, cm^{-1}): 3286 (w, N–H), 2692 (w), 2373 (w), 2281 (w), 1942 (w), 1885 (w), 1815 (w), 1714 (w), 1614 (s), 1559 (s), 1306 (m), 1207 (m), 1166 (m), 1141 (m), 1090 (s), 1074 (w), 1005 (s), 957 (s), 932 (m), 884 (w), 794 (s), 748(m), 694 (m), 655 (s). EI-MS: *m/z* = 741 $[M]^+$ (2%). Anal. found (calcd. for $C_{44}H_{54}BN_3OZr$): C, 71.04 (71.13); H, 7.23 (7.33); N, 5.55 (5.66)%.

NMR tube scale reaction of $Cp_2Zr\{NB(NAr'CH)_2\}(py)$ (11) with propylene sulfide. To a C_6D_6 solution (0.6 mL) of $Cp_2Zr\{NB(NAr'CH)_2\}(py)$ (**11**, 0.0105 g, 0.0141 mmol) in an NMR tube equipped with a J. Youngs valve was added propylene sulfide (2.6 µL, 0.0310 mmol) *via* microsyringe, and the solution heated to 60 °C for 16 h. The products $[Cp_2Zr\{\mu\text{-}N\{B(NAr'CH)_2\}S_2\}]_2$ (**79**) with resonances indentical to those isolated above, and $Cp_2Zr\{NHB(NAr'CH)_2\}\{SCH_2CH{=}CH_2\}$ (**78**), which is analogous to **75** described above, were formed in *ca* 4:1 ratio indicated by ^1H NMR spectroscopy. The compound **78** was subsquently characterised by ^1H NMR at RT.

^1H NMR (C_6D_6, 400.1 MHz): δ 7.23 (6 H, overlapping 2 × m, *m*- and *p*-$C_6H_3{}^iPr_2$), 6.12 (2 H, s, NCH), 5.71 (1 H, m, $SCH_2CH{=}CHH$), 5.54 (10 H, s, C_5H_5), 5.31 (1 H, d, ^3J = 10.4 Hz, $SCH_2CH{=}CHH$), 5.15 (1 H, s, NH), 5.06 (1 H, d, ^3J = 10.4 Hz, $SCH_2CH{=}CHH$), 3.41 (4 H, sept., ^3J = 6.9 Hz, CHMeMe), 3.36 (2 H, m, $SCH_2CH{=}CHH$), 1.39 (12 H, d, ^3J = 6.9 Hz, CHMeMe), 1.22 (12 H, d, ^3J = 6.9 Hz, CHMeMe) ppm.

$[Cp_2Zr\{\mu\text{-}N\{B(NAr'CH)_2\}S_2\}]_2$ (79). $Cp_2Zr\{NB(NAr'CH)_2\}(py)$ (**11**, 0.250 g, 0.356 mmol), ethylene sulfide (47.0 µL, 0.783mmol) and toluene (10 mL) were added to a Rotaflo ampoule with a Teflon valve, which was sealed and heated to 90 °C for 2 h. Upon cooling to RT, the yellow solution was filtered into a Schlenk flask and the volatiles removed under reduced pressure. The resulting yellow solid was then washed with hexane (2 × 5 mL) and dried *in vacuo*, yielding a pale yellow powder **79**. Yield: 0.183g (75%). Diffraction-quality crystals were grown from a saturated benzene solution at RT.

^1H NMR (C_6D_6, 400.1 MHz): δ 7.21 (6 H, overlapping 2 × m, *m*- and *p*-$C_6H_3{}^iPr_2$), 5.98 (2 H, s, NCH), 5.47, 5.45 (5 H, s, C_5H_5), 3.59, 3.51 (2 H, sept., ^3J = 6.9 Hz, CHMeMe), 1.66, 1.48 (6 H, d, ^3J = 6.9 Hz, CHMeMe), 1.32, 1.27 (6 H, d, ^3J = 6.9 Hz, CHMeMe) ppm. $^{13}C\{^1H\}$ NMR (C_6D_6, 100.6 MHz): δ 147.4 (*o*-$C_6H_3{}^iPr_2$), 147.2 (*o*-$C_6H_3{}^iPr_2$), 141.9 (*i*-$C_6H_3{}^iPr_2$), 128.6 (*m*-$C_6H_3{}^iPr_2$), 124.2, 123.9 (*p*-$C_6H_3{}^iPr_2$), 112.0 (NCH), 112.6, 108.8

(C_5H_5), 29.4, 29.0 (CHMeMe), 27.1, 26.4 (CHMeMe), 24.2, 23.0 (CHMeMe) ppm. $^{11}B\{^1H\}$ NMR (C_6D_6, 128.4 MHz): δ 24.8 ppm. IR (NaCl plates, Nujol mull, cm^{-1}): 2724 (w), 2360 (w), 2335 (w), 1584 (w), 1185 (w), 1109 (m), 1021 (w), 983 (w), 929 (w), 884 (w), 796 (s), 758 (m), 723 (w), 644 (w). Anal. found (calcd. for $C_{72}H_{92}B_2N_6S_4Zr_2$): C, 63.13 (62.95); H, 6.87 (6.75); N, 6.06 (6.12)%.

Alternative NMR tube scale synthesis of $[Cp_2Zr\{\mu\text{-}N\{B(NAr'CH)_2\}S_2\}]_2$ (79). A C_6D_6 solution (0.6 mL) of $Cp_2Zr\{NB(NAr'CH)_2\}(py)$ (**11**, 0.0100 g, 0.0141 mmol) and sulfur powder (0.0036 g, 0.0141 mmol) in an NMR tube equipped with a J. Youngs valve was heated to 60 °C for 5 h. The product $[Cp_2Zr\{\mu\text{-}N\{B(NAr'CH)_2\}S_2\}]_2$ (**79**) with resonances is indentical to those isolated above.

5.8 References

1 A. B. Pangborn, M. A. Giardello, R. H. Grubbs, R. K. Rosen and F. J. Timmers, *Organometallics*, 1996, **15**, 1518–1520.

2 C. Kleeberg, *Dalton. Trans.*, 2013, **42**, 8276–8287.

3 L. Weber, I. Domke, W. Greschner, K. Miqueu, A. Chrostowska and P. Baylère, *Organometallics*, 2005, **24**, 5455–5463.

4 L. Weber, J. Kahlert, L. Böhling, A. Brockhinke, H.-G. Stammler, B. Neumann, R. A. Harder, P. J. Low and M. A. Fox, *Dalton. Trans.*, 2013, **42**, 2266–2281.

5 T. J. Hadlington, J. A. B. Abdalla, R. Tirfoin, S. Aldridge and C. Jones, *Chem. Commun.*, 2016, **52**, 1717–1720.

6 R. F. Jordan, *J. Organomet. Chem.*, 1985, **294**, 321–326.

7 P. J. Walsh, F. J. Hollander and R. G. Bergman, *J. Am. Chem. Soc.*, 1988, **110**, 8729–8731.

8 K. C. Jantunen, B. L. Scott and J. L. Kiplinger, *J. Alloys Compd.*, 2007, **444**–**445**, 363–368.

9 E. J. Hawrelak and P. A. Deck, *Organometallics*, 2004, **23**, 9–11.

10 S. Couturier, G. Tainturier and B. Gautheron, *J. Organomet. Chem.*, 1980, **195**, 291–306.

11 K. Kaleta, P. Arndt, A. Spannenberg and U. Rosenthal, *Acta Crystallogr. Sect. E*, 2010, **66**, m1180.

12 T. Nishikawa, A. Ino and M. Isobe, *Tetrahedron*, 1994, **50**, 1449–1468.

13 Z. Yadong and W. Jianxun, *J. Fluor. Chem.*, 1990, 47, 533–535.

14 L. C. Stevenson, DPhil Thesis, University of Oxford, 2015.

15 J. Wang, A. K. Dash, M. Kapon, J.-C. Berthet, M. Ephritikhine and M. S. Eisen, *Chem. – A Eur. J.*, 2002, **8**, 5384–5396.

16 Y. Kita, N. Fu and T. T. Tidwell, in *Encyclopedia of Reagents for Organic Synthesis*, John Wiley & Sons, Ltd, 2001.

17 Z. Otwinowski and W. Minor, *Processing of X-ray Diffraction Data Collected in Oscillation Mode*, Academic press, New York, 1997.

18 A. Altomare, G. Cascarano, G. Giacovazzo, A. Guagliardi, M. C. Burla, G. Polidori and M. Camalli, *J. Appl. Crystallogr.*, 1994, **27**, 435.

19 L. Palatinus and G. Chapuis, *J. Appl. Cryst.*, 2007, **40**, 786–790.

20 P. W. Betteridge, J. R. Cooper, R. I. Cooper, K. Prout and D. J. Watkin, *J. Appl. Cryst.*, 2003, **36**, 1487.

21 M. J. Frisch, G. W. Trucks, H. B. Schlegel, G. E. Scuseria, M. A. Robb, J. R. Cheeseman, G. Scalmani, V. Barone, B. Mennucci, G. A. Petersson, H. Nakatsuji, M. Caricato, X. Li, H. P. Hratchian, A. F. Izmaylov, J. Bloino, G. Zheng, J. L. Sonnenberg, M. Hada, M. Ehara, K. Toyota, R. Fukuda, J. Hasegawa, M. Ishida, T. Nakajima, Y. Honda, O. Kitao, H. Nakai, T. Vreven, J. A. Montgomery Jr., J. E. Peralta, F. Ogliaro, M. J. Bearpark, J. Heyd, E. N. Brothers, K. N. Kudin, V. N. Staroverov, R. Kobayashi, J. Normand, K. Raghavachari, A. P. Rendell, J. C. Burant, S. S. Iyengar, J. Tomasi, M. Cossi, N. Rega, N. J. Millam, M. Klene, J. E. Knox, J. B. Cross, V. Bakken, C. Adamo, J. Jaramillo, R. Gomperts, R. E. Stratmann, O. Yazyev, A. J. Austin, R. Cammi, C. Pomelli, J. W. Ochterski, R. L. Martin, K. Morokuma, V. G. Zakrzewski, G. A. Voth, P. Salvador, J. J. Dannenberg, S. Dapprich, A. D. Daniels, Ö. Farkas, J. B. Foresman, J. V Ortiz, J. Cioslowski and D. J. Fox, *Gaussian 09, Revis. D.01, Gaussian Inc., Wallingford CT*, 2013.

22 A. D. Becke, *J. Chem. Phys.*, 1993, **98**, 5648–5652.

23 J. P. Perdew and Y. Wang, *Phys. Rev. B*, 1992, **45**, 13244–13249.

24 S. Grimme, J. Antony, S. Ehrlich and H. Krieg, *J. Chem. Phys.*, 2010, **132**, 154104–154119.

25 S. Grimme, S. Ehrlich and L. Goerigk, *J. Comput. Chem.*, 2011, **32**, 1456–1465.

26 A. Schäfer, H. Horn and R. Ahlrichs, *J. Chem. Phys.*, 1992, **97**, 2571–2577.

27 F. Weigend and R. Ahlrichs, *Phys. Chem. Chem. Phys.*, 2005, **7**, 3297–3305.

28 A. V Marenich, C. J. Cramer and D. G. Truhlar, *J. Phys. Chem. B*, 2009, **113**, 6378–6396.

29 E. D. Glendening, J. K. Badenhoop, A. E. Reed, J. Carpenter, J. A. Bohmann, C. M. Morales, C. R. Landis and F. Weinhold, *NBO 6.0, Theor. Chem. Institute, Univ. Wisconsin, Madison*.

30 T. A. Keith, *AIMAll (Version 16.10.31), TK Gristmill Software, Overl. Park KS, USA,*.

31 T. Takahashi, Y. Nishihara and T. Ishida, *Chem. Lett.*, 1995, **24**, 159–160.

32 U. Wieser, D. Babushkin and H.-H. Brintzinger, *Organometallics*, 2002, **21**, 920–923.

Appendix

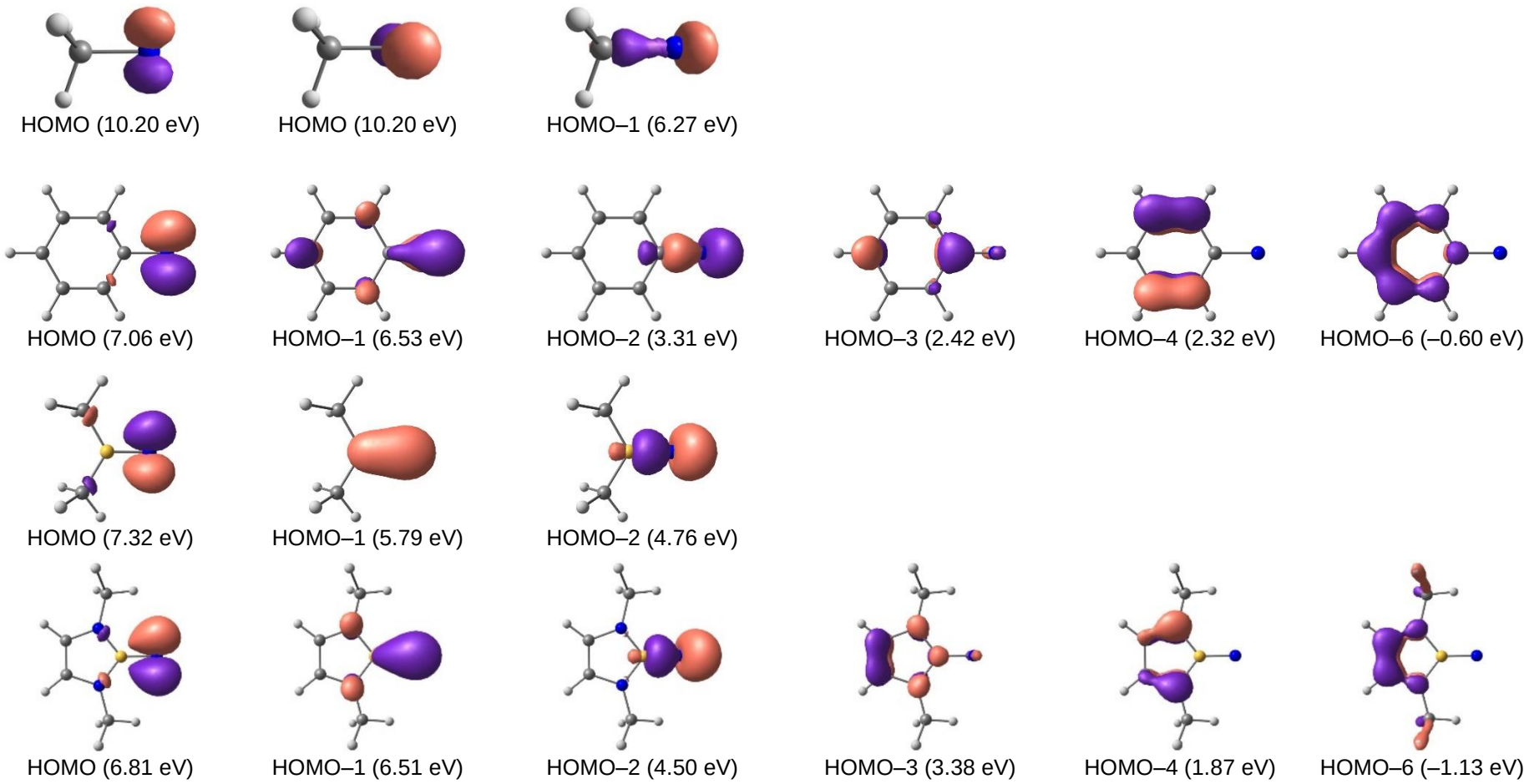

Figure A1. Isosurfaces and energies of molecular orbitals (σ and 2 π) in the model imido-type dianions $[NMe]^{2-}$, $[NPh]^{2-}$, $[NBMe_2]^{2-}$ and $[NB(NMeCH)_2]^{2-}$, along with occupied π-orbitals of the phenyl ring in $[NPh]^{2-}$ and boryl ring in $[NB(NMeCH)_2]^{2-}$. Isosurfaces are drawn at the 0.075 a.u. contour level. Calculations were performed in the geometry of the respective models $CpTi(NR)\{MeC(NMe)_2\}$.[1]

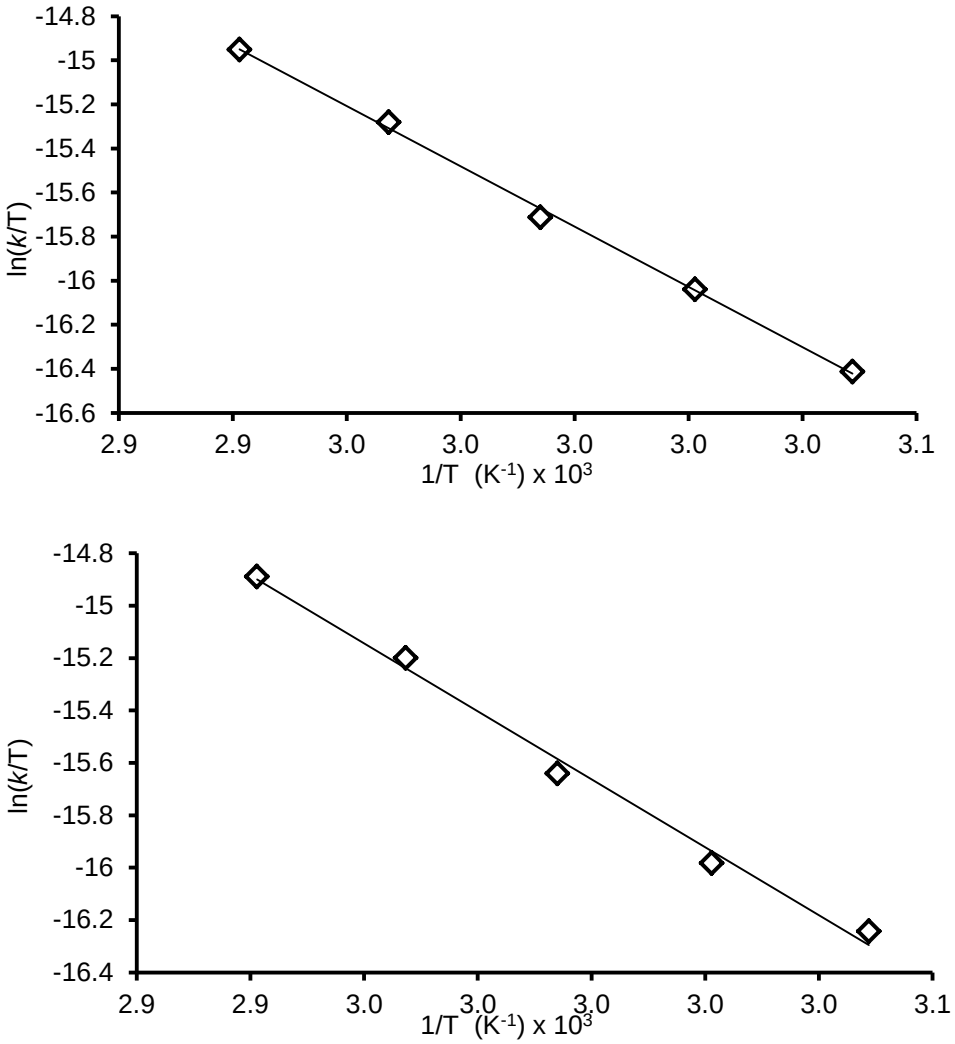

Figure A2. Top: Eyring plot for the conversion of $Cp_2Zr\{NHB(NAr'CH)_2\}\{OC(CH_2)OEt\}$ (**54**) to $Cp_2Zr\{NHB(NAr'CH)_2\}\{OC(CH_2)CH_2CO_2Et\}$ (**58**) and $Cp_2Zr\{NHB(NAr'CH)_2\}(OEt)$ (**59**) in C_6D_6, within one half-life. Activation parameters derived from linear regression analysis (r^2 = 0.997): $\Delta H^{\ddagger}$ = 26.8(0.8) kcal mol^{-1}; $\Delta S^{\ddagger}$ = 1.8(2.0) cal mol^{-1} K^{-1}; $\Delta G_{340}{}^{\ddagger}$ = 26.2(1.0) kcal mol^{-1}. Bottom: Eyring plot for the conversion of $Cp_2Zr\{NHB(NAr'CH)_2\}\{OC(CH_2)OEt\}$ (**54**) to $Cp_2Zr\{NHB(NAr'CH)_2\}\{OC(CH_2)CH_2CO_2Et\}$ (**58**) and $Cp_2Zr\{NHB(NAr'CH)_2\}(OEt)$ (**59**) in C_6D_6 using initial rate measurement. Activation parameters derived from linear regression analysis (r^2 = 0.992): $\Delta H^{\ddagger}$ = 25.8(1.3) kcal mol^{-1}; $\Delta S^{\ddagger}$ = –1.1(4.0) cal mol^{-1} K^{-1}; $\Delta G_{340}{}^{\ddagger}$ = 26.2(1.9) kcal mol^{-1}.

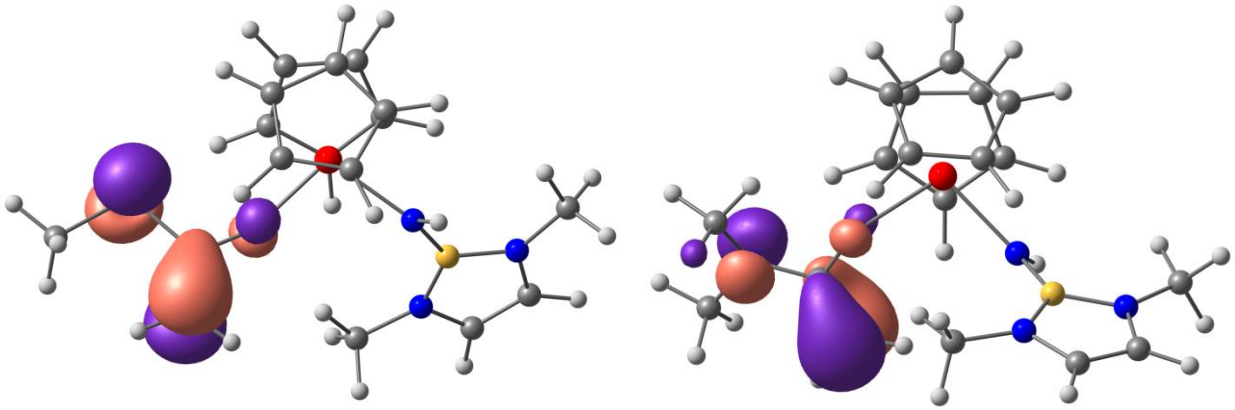

Figure A3. DFT computed HOMO-1 of $Cp_2Zr\{NHB(NMeCH)_2\}\{OC(CH_2)SMe\}$ (**60Q**, left, E = –5.52 eV) and $Cp_2Zr\{NHB(NMeCH)_2\}\{OC(CH_2)NMe_2\}$ (**66Q**, right, E = –5.06 eV). The normalised atomic contributions from C(2p) for the enolate $\underline{C}=CH_2$ and $C=\underline{C}H_2$ carbons are 0.09 and 0.44, respectively for **60Q**, and 0.03 and 0.47 for **66Q**. The HOMO in each case is a ligand-based orbital on $B(NMeCH)_2$.

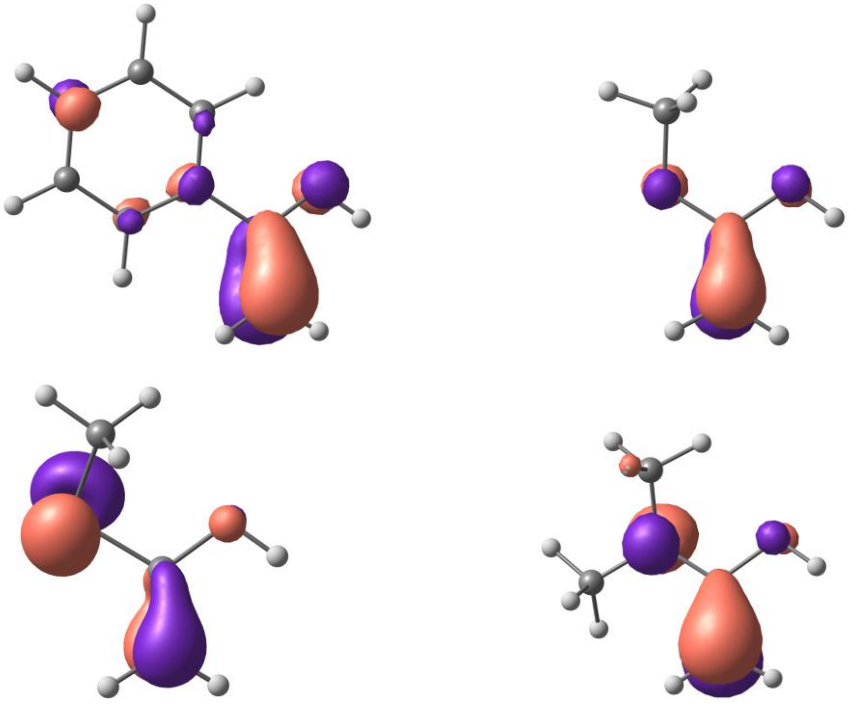

Figure A4. DFT computed HOMO of $PhC(OH)CH_2$ (top-left, E = –6.20 eV), $MeOC(OH)CH_2$ (top-right, E = –6.01 eV), $MeSC(OH)CH_2$ (bottom-left, E = –4.73 eV) and $Me_2NC(OH)CH_2$ (bottom-right, E = –5.44 eV). The normalised atomic contributions from C(2p) for the enolate $\underline{C}=CH_2$ and $C=\underline{C}H_2$ carbons are 0.12 and 0.43, respectively for $PhC(OH)CH_2$, 0.15 and 0.55 for $MeOC(OH)CH_2$, 0.05 and 0.45 for $MeSC(OH)CH_2$ and 0.08 and 0.50 for $Me_2NC(OH)CH_2$.

References

1 B. A. Clough, S. Mellino, A. V Protchenko, M. Slusarczyk, L. C. Stevenson, M. P. Blake, B. Xie, E. Clot and P. Mountford, *Inorg. Chem.*, 2017, **56**, 10794–10814.